NGS TECHNOLOGIES OF RARE DISEASES DIAGNOSIS

EDITED BY: María L. Couce, Emiliano González Vioque and Richard J. Rodenburg

PUBLISHED IN: Frontiers in Genetics and Frontiers in Pediatrics

frontiers Research Topics

ISSN 1664-8714
ISBN 978-2-83250-876-3
DOI 10.3389/978-2-83250-876-3

About Frontiers

Frontiers is more than just an open-access publisher of scholarly articles: it is a pioneering approach to the world of academia, radically improving the way scholarly research is managed. The grand vision of Frontiers is a world where all people have an equal opportunity to seek, share and generate knowledge. Frontiers provides immediate and permanent online open access to all its publications, but this alone is not enough to realize our grand goals.

Frontiers Journal Series

The Frontiers Journal Series is a multi-tier and interdisciplinary set of open-access, online journals, promising a paradigm shift from the current review, selection and dissemination processes in academic publishing. All Frontiers journals are driven by researchers for researchers; therefore, they constitute a service to the scholarly community. At the same time, the Frontiers Journal Series operates on a revolutionary invention, the tiered publishing system, initially addressing specific communities of scholars, and gradually climbing up to broader public understanding, thus serving the interests of the lay society, too.

Dedication to Quality

Each Frontiers article is a landmark of the highest quality, thanks to genuinely collaborative interactions between authors and review editors, who include some of the world's best academicians. Research must be certified by peers before entering a stream of knowledge that may eventually reach the public - and shape society; therefore, Frontiers only applies the most rigorous and unbiased reviews.
Frontiers revolutionizes research publishing by freely delivering the most outstanding research, evaluated with no bias from both the academic and social point of view. By applying the most advanced information technologies, Frontiers is catapulting scholarly publishing into a new generation.

What are Frontiers Research Topics?

Frontiers Research Topics are very popular trademarks of the Frontiers Journals Series: they are collections of at least ten articles, all centered on a particular subject. With their unique mix of varied contributions from Original Research to Review Articles, Frontiers Research Topics unify the most influential researchers, the latest key findings and historical advances in a hot research area! Find out more on how to host your own Frontiers Research Topic or contribute to one as an author by contacting the Frontiers Editorial Office: frontiersin.org/about/contact

NGS TECHNOLOGIES OF RARE DISEASES DIAGNOSIS

Topic Editors:
María L. Couce, Complejo Hospitalario Universitario de Santiago, Spain
Emiliano González Vioque, University Clinical Hospital of Santiago, Spain
Richard J. Rodenburg, Radboud University Medical Centre, Netherlands

Citation: Couce, M. L., Vioque, E. G., Rodenburg, R. J., eds. (2022). NGS Technologies of Rare Diseases Diagnosis. Lausanne: Frontiers Media SA. doi: 10.3389/978-2-83250-876-3

Table of Contents

frontiers | Frontiers in Pediatrics

TYPE Editorial
PUBLISHED 12 November 2022
DOI 10.3389/fped.2022.1032359

OPEN ACCESS

EDITED AND REVIEWED BY
Domingo González-Lamuño,
University of Cantabria, Spain

*CORRESPONDENCE
María L. Couce
maria.luz.couce.pico@sergas.es

SPECIALTY SECTION
This article was submitted to Genetics of Common and Rare Diseases, a section of the journal Frontiers in Pediatrics

RECEIVED 30 August 2022
ACCEPTED 24 October 2022
PUBLISHED 12 November 2022

CITATION
Couce ML and González-Vioque E (2022) Editorial: NGS technologies of rare diseases diagnosis.
Front. Pediatr. 10:1032359.
doi: 10.3389/fped.2022.1032359

Editorial: NGS technologies of rare diseases diagnosis

María L. Couce[1]* and Emiliano González-Vioque[2]

[1]Diagnosis and Treatment Unit of Congenital Metabolic Diseases, Department of Paediatrics, University Clinical Hospital of Santiago de Compostela, IDIS, CIBERER, MetabERN, Santiago de Compostela, Spain, [2]Molecular Genetics Unit, Clinical Biochemistry Service, University Hospital Puerta de Hierro, Madrid, Spain

KEYWORDS

DNA SEQUENCING, exome sequencing, genome sequencing, transcriptome, variants

Editorial on the Research Topic
NGS technologies of rare diseases diagnosis

By Couce ML, González-Vioque E. (2022) Front. Pediatr. 10: 1032359. doi: 10.3389/fped.2022.1032359

Of the estimated 7,000 rare diseases, 80% have a genetic cause (1). Because these diseases can be difficult to recognize based on clinical features alone, genetic testing is critical to help establish diagnosis (2). Genomic sequencing techniques allow the simultaneous analysis of hundreds to thousands of genes in a very short time and at low cost, and offer several strategies to facilitate the diagnosis of patients with suspected genetic disease, including gene panels and clinical exome sequencing (3), whole exome sequencing (WES) (4, 5), and whole genome sequencing (WGS) (6). However, it is becoming increasingly clear that an individual genome cannot be interpreted in isolation (7). WES and WGS data scaling necessitates automation of variant filtering to focus on clinically relevant genomic intervals and/or variants. On the other hand, analytical workflows for rare disease diagnosis involving processing of raw sequencing data, identification of pathogenic variants, and integration of clinical data to achieve robust genetic diagnosis are complex and not fully standardized (8, 9). Assigning pathogenicity to a rare variant identified using a bioinformatic algorithm and establishing a genetic diagnosis can be an extremely challenging process, and may require additional functional studies.

This Special Issue of *Frontiers in Genetics* "NGS Technologies of Rare Diseases Diagnosis" contains 33 studies about prenatal diagnostic technologies, phenotype expansions, added value of gene expression monitoring, and functional studies in the field of rare diseases, particularly those affecting the pediatric population. This collection of articles underscores the recent growth and extensive interest in research on this topic.

Prenatal research studies (Xu et al. (2021), 10) demonstrate the efficacy of cell-free DNA-based noninvasive prenatal screening (NIPS) diagnostic technologies for common trisomies in low-risk and twin pregnancies. However, the authors conclude that NIPS cannot replace invasive prenatal diagnostic techniques, and recommend prenatal diagnosis for fetuses with abnormal ultrasound findings.

Seven original studies have examined how WES can be used to identify genetic variants in rare diseases (Yang et al., Fareed et al., Zhang S et al., Huang et al., Giu et al., Zhang F et al., Yu et al.). The findings of these studies have expanded the variant spectrum of several rare diseases, revealing clearer relationships with clinical phenotypes, improving our understanding of the underlying etiology, and contributing to more rapid genetic diagnosis and subsequent genetic counseling. In their study, Yu et al. examined a fetus with structural brain abnormalities and identified a *de novo*, likely pathogenic variant of *TAOK1* (11). In addition, of the 19 case reports, 16, (Zhang J et al., Nabouli et al., Wang et al., Luo et al., Zhang P et al., Lin et al., Carneiro et al., Andreeva et al., Zhang T et al., Liu et al., Qiao et al., Ji et al., Zhou et al., Li et al., Tang et al., Hu et al.) describe the identification of a new variant, in known genetic diseases. Interestingly, Zaytseva et al. (2022) describe a loss-of-function variant in *ABCC9* that is associated with ventricular fibrillation. And, two of the case reports describe patients with 2 concomitant conditions Su et al. (2021), Kim et al. (2021) describe a case of a 7-year-old boy with two X-linked diseases, Duchenne muscular dystrophy (DMD) and frontometaphyseal dysplasia 1 (FMD1); while Shu et al. report a case of MEGDEL syndrome coinciding with SATB2-associated syndrome. Particularly noteworthy is the case report by Luo et al., which describes a novel frameshift mutation of *α-Actin 1* (ACTN1) in a Chinese family with macrothrombocytopenia and mild bleeding (NM_001130004: c.398_399insTGCG, p.F134AfsX60). This variant was identified in the proband and his mother, but was absent in other unaffected family members. Western blot revealed that expression of α-actin 1 in the proband was decreased markedly indicating that the novel frameshift mutation may induce nonsense-mediated mRNA decay. These findings not only broaden the spectrum of *ACTN1* variants, but also confirmed diagnosis of inherited macrothrombocytopenia, which may facilitate the management and prognosis of the members of the family in question.

The opinion article by Woo et al. (2021) discusses the inclusion of *GBA1* in many NGS analyses for Parkinson's disease, and the importance of considering the effects of the nearby homologous pseudogene. Recombinant alleles in *GBA1* identified in Gaucher disease and Parkinson's disease patients could be missed by relying on NGS analysis alone without Sanger sequencing validation.

Gene expression monitoring was also addressed in this special issue. Villate et al. (12) contribute a brief report on the importance of performing RNA functional assays in order to determine the clinical significance of intronic variants, and to facilitate genetic counseling and clinical management of patients and their relatives. The authors undertook clinical characterization of a novel splice variant in *NSD1* that causes familial Sotos syndrome. Their findings help highlight the importance of using *in silico* prediction tools to detect potential alterations in the splicing process. RNA-seq has emerged as a useful tool in the field of rare diseases, enabling the identification of new disease mechanisms and helping us to better understand the information generated by DNA sequencing.

And finally, functional analysis were included in three original studies (13, 14). Chen et al. (2021) characterized gene variants in Han Chinese patients with hypospadias, identifying 1 *de novo* missense variant loci in *AR gene,* and conducted *in vivo* and *in vitro* functional studies that provide molecular evidence that the consequent p.I817N amino acid change may significantly reduce AR transcriptional function, leading to hypospadias. Shen et al. are the first to describe a *B3GALT6*-dominant variant leading to Ehlers–Danlos disease, and their functional experiments confirm that the R295C variant plays a loss-of-function role, while the elongated variant (p.L170fs*268) may exert a dominant-negative effect. Votsi et al. studied a novel *SPG7* pathogenic variant in a Cypriot family with autosomal recessive spastic ataxia, and performed functional studies showing that the variant does not affect RNA or protein expression or protein localization. However, their findings reveal aberrant mitochondrial morphology, suggesting mitochondrial dysfunction and further demonstrating the pathogenicity of the identified variant.

Conclusion

This special issue provides a useful summary of progress made in the field of NGS technologies applied to genetic medicine, particularly in the area of rare diseases. These approaches have helped improve diagnostic capabilities as well as expanding our knowledge of the molecular basis of these diseases, with important clinical and public health implications. Nonetheless, clinical studies with longer follow-up periods will be necessary to establish recommendations to ensure adequate and earlier diagnosis.

Author contributions

MLC and EGV contributed to the design, writing and editing the paper. All authors contributed to the article and approved the submitted version.

Conflict of interest

The authors declare that the research was conducted in the absence of any commercial or financial relationships that could be construed as a potential conflict of interest.

Publisher's note

References

1. Amberger JS, Bocchini CA, Schiettecatte F, Scott AF, Hamosh A. OMIM.Org: online Mendelian inheritance in man (OMIM(R)), an online catalog of human genes and genetic disorders. *Nucleic Acids Res.* (2015) 43(Database issue): D789–98. doi: 10.1093/nar/gku1205

2. Wright CF, FitzPatrick DR, Firth HV. Paediatric genomics: diagnosing rare disease in children. *Nat Rev Genet.* (2018) 19:325. doi: 10.1038/nrg.2017.116

3. de Castro MJ, González-Vioque E, Barbosa-Gouveia S, Salguero E, Rite S, López-Suárez O, et al. Rapid phenotype-driven gene sequencing with the NeoSeq panel: a diagnostic tool for critically ill newborns with suspected genetic disease. *J Clin Med.* (2020) 9:2362. doi: 10.1038/gim.2016.1

4. Stark Z, Tan TY, Chong B, Brett GR, Yap P, Walsh M, et al. A prospective evaluation of whole-exome sequencing as a first-tier molecular test in infants with suspected monogenic disorders. *Genet Med.* (2016) 18:1090–6. doi: 10.1038/gim.2016.1

5. Australian Genomics Health Alliance Acute Care Flagship, Lunke S, Eggers S, Wilson M, Patel C, Barnett CP, Pinner J, et al., Feasibility of ultra-rapid exome sequencing in critically ill infants and children with suspected monogenic conditions in the Australian public health care system. *JAMA*. (2020) 323: 2503–11. doi: 10.1001/jama.2020.7671

6. French CE, Disease NB, Delon I, Dolling H, Sanchis-Juan A, Shamardina O, et al. Whole genome sequencing reveals that genetic conditions are frequent in intensively ill children. *Intensiv Care Med*. (2019) 45:627–36. doi: 10.1007/s00134-019-05552-x

7. Sweeny K, Ghane A, Legg AM, Huynh HP, Andrews SE. Predictors of genetic testing decisions: a systematic review and critique of the literature. *J Genet Couns*. (2014) 23:263–88. doi: 10.1007/s10897-014-9712-9

8. Ceyhan-Birsoy O, Murry JB, Machini K, Lebo MS, Yu TW, Fayer S, et al. Interpretation of genomic sequencing results in healthy and ill newborns: results from the BabySeq project. *Am J Hum Genet*. (2019) 104:76–93. doi: 10.1016/j.ajhg.2018.11.016

9. Telenti A, Pierce LC, Biggs WH, di Iulio J, Wong EH, Fabani MM, et al. Deep sequencing of 10,000 human genomes. *Proc Natl Acad Sci U S A*. (2016) 113:11901–6. doi: 10.1073/pnas.1613365113

10. Liu Y, Jing X, Xing L, Liu S, Liu J, Jing Cheng J, et al. Noninvasive prenatal screening based on second-trimester ultrasonographic soft markers in low-risk pregnant women. *Front Genet*. (2021) 12:793894. doi: 10.3389/fgene.2021.793894

11. Yu L, Yang C, Shang N, Ding H, Zhu J, Zhu Y, et al. Paternal De Novo variant of *TAOK1* in a Fetus with structural brain abnormalities. *Front Genet*. (2022) 13:836853. doi: 10.3389/fgene.2022.836853

12. Villate O, Maortua H, Tejada MI, Llano-Rivas I. RNA Analysis and clinical characterization of a novel splice variant in the NSD1 gene causing familial sotos syndrome. *Front Pediatr*. (2022) 10:827802. doi: 10.3389/fped.2022.827802

13. Shen F, Yang Y, Zheng Y, Tu M, Zhao L, Luo Z, et al. Mutant B3GALT6 in a Multiplex family: a dominant variant co-segregated with moderate malformations. *Front Genet*. (2022) 13:824445. doi: 10.3389/fgene.2022.824445

14. Votsi C, Ververis A, Nicolaou P, Christou YP, Christodoulou K, Zamba-Papanicolaou E. A novel SPG7 gene pathogenic variant in a Cypriot family with autosomal recessive spastic ataxia. *Front Genet*. (2022) 12:812640. doi: 10.3389/fgene.2021.812640

frontiers in Genetics

CASE REPORT
published: 16 February 2021
doi: 10.3389/fgene.2021.619948

Case Report: Exome Sequencing Identified a Novel Compound Heterozygous Variation in *PLOD2* Causing Bruck Syndrome Type 2

Jing Zhang[1†], *Huaying Hu*[2,3†], *Weihong Mu*[1], *Mei Yu*[1], *Wenqi Chen*[1], *Dongqing Mi*[1], *Kai Yang*[4*] and *Qing Guo*[1*]

[1] Prenatal Diagnosis Center, Shijiazhuang Obstetrics and Gynecology Hospital, Shijiazhuang, China, [2] School of Medicine, Xiamen University, Xiamen, China, [3] Jiaen Genetics Laboratory, Beijing Jiaen Hospital, Beijing, China, [4] Prenatal Diagnosis Center, Beijing Obstetrics and Gynecology Hospital, Capital Medical University, Beijing, China

OPEN ACCESS

Edited by:
María L. Couce,
Complejo Hospitalario Universitario de Santiago, Spain

Reviewed by:
Fulya Taylan,
Karolinska Institutet (KI), Sweden
Liang-Liang Fan,
Central South University, China

***Correspondence:**
Qing Guo
yfguoqing@163.com
Kai Yang
yk19830919@163.com

[†]These authors have contributed equally to this work

Specialty section:
This article was submitted to Genetics of Common and Rare Diseases, a section of the journal Frontiers in Genetics

Received: 21 October 2020
Accepted: 28 January 2021
Published: 16 February 2021

Citation:
Zhang J, Hu H, Mu W, Yu M, Chen W, Mi D, Yang K and Guo Q (2021) Case Report: Exome Sequencing Identified a Novel Compound Heterozygous Variation in PLOD2 Causing Bruck Syndrome Type 2. Front. Genet. 12:619948. doi: 10.3389/fgene.2021.619948

Bruck Syndrome (BRKS) is a rare type of recessive osteogenesis imperfecta (OI) and consists of two subtypes, BRKS1 and BRKS2, which are caused by variations in *FKBP10* and *PLOD2* genes, respectively. In this study, a family that had experienced multiple miscarriages and recurrent fetal skeletal dysplasia was recruited for the purpose of a multiplatform laboratory investigation. Prenatal genetic testing with whole-exome sequencing (WES) identified a compound heterozygous variation in the *PLOD2* gene with two variants, namely c.2038C>T (p.R680*) and c.191_201+3 delATACTGTGAAGGTA (p.Y64Cfs*12). The amino acids affected by the two variants maintained conserved across species. And the result of immunohistochemistry (IHC) indicated that the expression of PLOD2 protein in the proband's osteochondral tissue was significantly decreased. These findings in our study expanded the variation spectrum of *PLOD2* gene, provided solid evidence for the family's counseling in regard to future pregnancies, strongly supported the application of WES in prenatal diagnosis, and might give insight into the understanding of PLOD2 function.

Keywords: *PLOD2* gene, Bruck syndrome type 2, osteogenesis imperfecta, whole-exome sequencing, immunohistochemistry detection

INTRODUCTION

Congenital skeletal dysplasia (SD) often displays severe *in utero* manifestations, which provides clues and challenges for prenatal diagnosis (Offiah, 2015; Liu et al., 2019). First, they can provide evidence for the timely formation of management plans; on the other hand, due to the strong clinical heterogeneity of SDs, it is difficult to accurately judge the prognosis by these indeterminate indications alone (Konstantinidou et al., 2009; Offiah, 2015). Under such circumstances, a meticulously designed strategy of genetic detection would help overcome the setbacks in clinical differential diagnosis (Zhou et al., 2018; Yang et al., 2019).

Osteogenesis imperfecta (OI) is a series of congenital metabolic bone disorders and comprises dozens of conditions ranging from early lethality to mild manifestations (Marini, 2013; Liu et al., 2017). OI is mainly characterized by increasing bone fragility, recurrent fracture, and subsequent growth retardation (Forlino and Marini, 2016; Liu et al., 2017). OI patients also share some extraskeletal symptoms, such as blue sclera, hearing deficits, dentinogenesis imperfecta (DI),

and valvular heart disease (Forlino and Marini, 2016). Bruck syndrome types 1 and 2 (BRKS1, MIM #259450; BRKS2, MIM #609220), caused by biallelic pathogenic variants in the*FKBP10* (MIM *607063) and *PLOD2* (MIM *601865) genes, respectively, are two rare subtypes of OI, mainly characterized by congenital joint contractures and pterygia other than the common OI manifestations (Viuoen et al., 1989). *PLOD2* encodes lysyl hydroxylase 2 (LH2, EC 1.14.11.4), while *FKBP10* encodes the prolyl cis-trans isomerase FKBP65, the activities of which are required in forming mature crosslinks in bone collagen (Bank et al., 1999; Alanay et al., 2010).

To our knowledge, fewer than 20 studies have reported the BRKS2 cases with respect to defects in *PLOD2* (Mumm et al., 2020). Moreover, the genotype-phenotype correlation of BRKS2 is not fully established, owing to the low amount and relatively clustered distribution of constitutional variations in *PLOD2*, the vague structural and functional delineation of the N-terminal of LH2 protein as well as the strong phenotypic variability of BRKS2 (Tham et al., 2018; Mumm et al., 2020). Furthermore, given the commonality of cell signaling pathways between BRKS2 and multiple types of cancers, the in-depth study of corresponding molecules would benefit scientific and clinical understanding in both fields (Guo et al., 2018; Wang et al., 2020).

Thus, we studied a family having experienced multiple abnormal gestations. Prenatal ultrasonography examination and genetic detections were conducted to identify the cause of fetal skeletal dysplasia in the subject family.

CASE PRESENTATION

A 34-year-old woman was first referred to our Center in February 2015 for having experienced multiple abnormal gestations. At that point she was 8 weeks pregnant.

Based on medical records and her personal dictation, we combed through the couple's complete medical history and illustrated in a pedigree diagram (**Figure 1A**). They had eight previous pregnancies in total: In August 2005, missed abortion occurred at the eighth gestational week of their first pregnancy. In October 2006, it was diagnosed that the second pregnancy was an ectopic pregnancy on the left fallopian tube, whereupon transabdominal resection of the left fallopian tube was performed. In October 2007, July 2008, August 2010, and December 2012, the couple went through four missed abortions or miscarriages, all of which occurred between 8 and 16 gestational weeks. In November 2013, the fetus of their seventh pregnancy was diagnosed with thickened nuchal translucency (NT), right abdominal fissure and visceral valgus. Induced labor was performed at 15 weeks of gestation.

In 2015, all indicators of their 8th pregnancy during early pregnancy were normal, including serological screening, NIPT (non-invasive prenatal testing) results. However, at 17th week of gestation, ultrasonic examination revealed that the fetus had extremely short limbs and bowing of long bones (**Figure 1B**). Amniocentesis and subsequent prenatal diagnosis with chromosomal karyotyping and micro array (CMA) were conducted. However, no variation with clinical

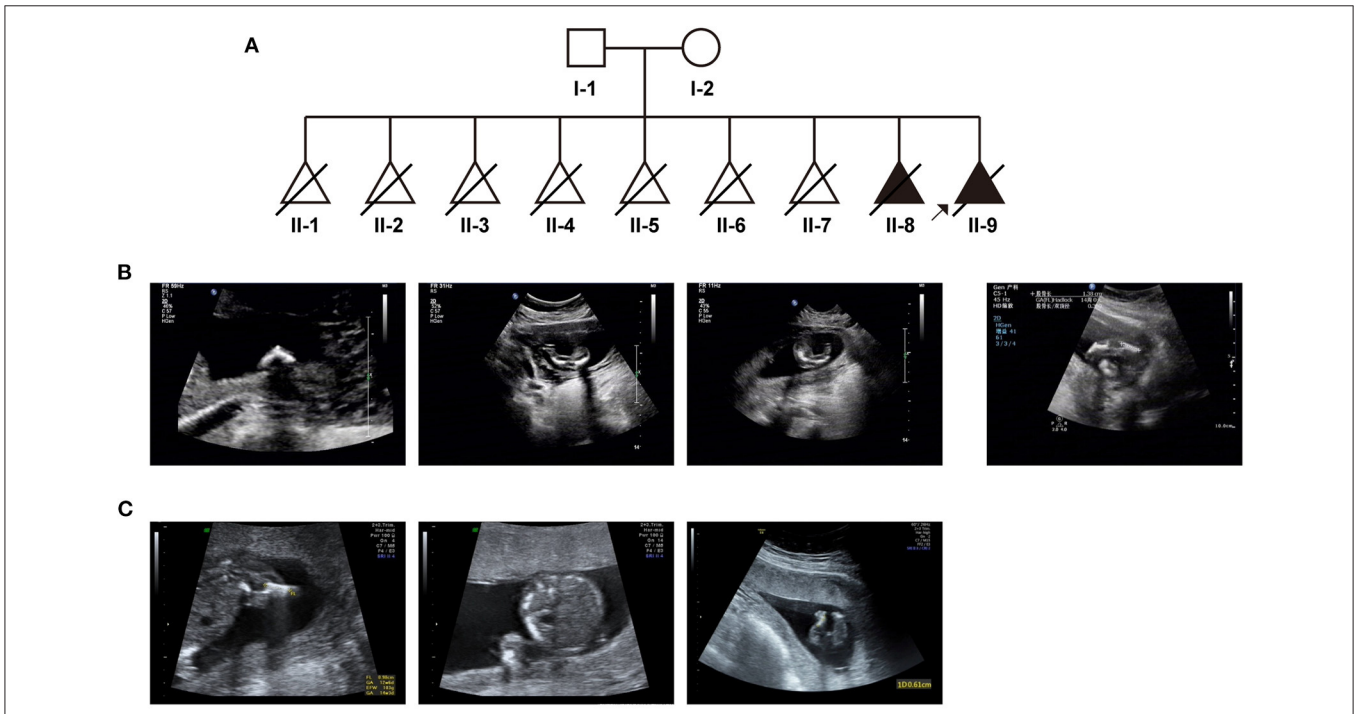

FIGURE 1 | The clinical findings in this case: **(A)** Pedigree diagram of the family with fetal skeletal dysplasia and multiple miscarriages. **(B)** Ultrasonographic indications of the couple's eighth pregnancy. **(C)** Ultrasonographic indications of the couple's most recent (ninth) pregnancy.

significance was identified. The fetus was aborted at 20 gestational weeks.

In April 2018, we performed prenatal diagnosis for their most recent pregnancy at the 16th week of gestation. Ultrasonography indicated that bilateral lower limbs of the fetus were shortened, not excluding the presence of bending (**Figure 1C**). Besides regular prenatal genetic testing as described above, whole-exome sequencing was also introduced after induction.

LABORATORY INVESTIGATIONS

Prenatal genetic testing including karyotyping and CMA (with Cytoscan 750k, Thermo Fisher platform) were performed on the last two adverse pregnancies in 2015 and 2018. Both results of those were normal.

Accordingly, whole-exome sequencing was performed on the skin tissue obtained from the aborted fetus of the last pregnancy. In brief, the enrichment of target-region sequences was performed by means of the Sure Select Human Exon Sequence Capture Kit (Agilent, USA). The sequencing libraries were quantified using the DNA Standards and Primer Premix Kit (Kapa Biosystems, USA), massively parallel-sequenced using the XTEN platform and then massively parallel-sequenced again (Illumina, USA). After sequencing and filtering out the low-quality readings, the high-quality readings were compared to the human genome reference sequence [(hg19/GRC h37)]. The GATK software (Genome Analysis TK3.3.0, https://software.broadinstitute.org/gatk/) and the Verita Trekker® Variants Detection system (Berry Genomics, China) were used to identify single-nucleotide polymorphisms, insertion and deletions, copy-number variants (CNVs), mitochondrial gene variants, and runs of homozygosity. Subsequently, the Enliven® Variants Annotation Interpretation (Berry Genomics, China) system was used to fulfill the annotation and interpretation progress referring to multiple databases [1000g2015aug_eas (https://www.internationalgenome.org/); ExAC_EAS (http://exac.broadinstitute.org); gnomAD_exome_EAS (http://gnomad.broadinstitute.org/); HGMD®: Human Gene Mutation Database (Professional Version 2019.4)]. The suspected pathogenic variant was validated by Sanger sequencing through use of ABI 3730 Automated Sequencer (Applied Biosystems). The mutations were identified by sequence alignment with the NCBI Reference Sequence (NG 011537.1) using Chromas 2.33. WES identified a compound heterozygous variation in the *PLOD2* gene consisting of two variants, namely c.2038C>T (p.R680*) and c.191_201+3delATACTGTGAAGGTA (p.Y64Cfs*12) (NM_000935) (**Figure 2A**). Sanger sequencing revealed that the father carried the heterozygous c.2038C>T variant, while the mother carried c.191_201+3del (**Figure 2A**). The former one was reported by Lyu et al. as a pathogenic variant (Lv et al., 2017), while the latter, which would result in a premature truncated protein, was first reported in this study. According to the variant interpretation criteria by ACMG (Richards et al., 2015), it was classified as pathogenic, with the evidence of PVS1, PM2, PM3, and PP4.

The conservatism of all amino acids effected by detected variants was analyzed using MEGA7 (http://www.megasoftware.net/previousVersions.php) with default parameters. The results showed that the amino acids Y64 and R680 (i.e., the two variants) maintained evolutionary conservatism among species (**Figure 3A**).

Protein modeling was conducted using SWISS-MODEL (https://swissmodel.expasy.org/) and Swiss-Pdb Viewer software (https://spdbv.vital-it.ch/disclaim.html#). PLOD2 protein model of wild type (WT)-6fxm.1.A (Seq Identity:59.26%/GMQE: 0.82/QMEAN: −0.67), p.Y64Cfs*12-6fxm.1.A (Seq Identity:57.80%/GMQE: 0.80/QMEAN: −0.78), and p.R680*-6fxk.1.A (Seq Identity:43.59%/GMQE:0.18/QMEAN: −0.87) were shown (**Figure 3B**). According to the results, these two variants would result in premature truncated peptides, which could cause severe damage to protein function. Immunohistochemistry (IHC) (with Anti-PLOD2/LH2 antibody, ab90088, Abcam, USA) was conducted on the paraffin sections of fetal auricular finger osteochondrocytes of the proband (along with a cartilage tissue sample from an aborted fetus (*PLOD2* wild-type) at similar gestational age as normal control). The results indicated that the expression level of *PLOD2* protein was significantly decreased in the osteochondral tissues of the proband (**Figure 3C**). The low protein expression of *PLOD2* was possibly because c.2038C>T (p.R680*) and c.191_201+3delATACTGTGAAGGTA would be expected to induce non-sensical mediated decay.

DISCUSSION

Recessive forms only account for <10% in OI disorders, yet the list of causative genes has been growing through recent years (Eyre and Weis, 2013). Additionally, with the defects in various proteins involved in bone formation, OIs display a broad range of phenotypic variability (Forlino and Marini, 2016). This promotes the challenge in prenatal diagnosis and management on fetal SDs with similar early manifestations. Therefore, it would appear to be more and more arbitrary to consider the *in utero* limb shortening and bowing of long bones as a collagen-related autosomal dominant condition.

As a rare but typical example of recessive OI, most cases of BRKS are distinguished by congenital joint contractures and pterygia, albeit with several exceptions (Tham et al., 2018; Mumm et al., 2020). Currently, two BRKS subtypes, BRKS1 and BRKS2, with almost identical phenotypes but different pathogenesis are recognized (van der Slot et al., 2003; Alanay et al., 2010). To our knowledge, 25 constitutional mutations in *PLOD2* associating with BRKS2-like phenotypes have been detected in fewer than 20 studies, showing significant C-terminal aggregation (**Figure 2B**; **Supplementary Table 1**) (Mumm et al., 2020). In this study, a compound heterozygous variation in the*PLOD2* gene with two variants, c.2038C>T and c.191_201+3del, was identified and confirmed. The former one, c.2038C>T, was once reported in BRKS2 patient (Lv et al., 2017); while the latter one, c.191_201+3del, was a novelly detected frame-shift variant causing early termination of protein translation. This finding

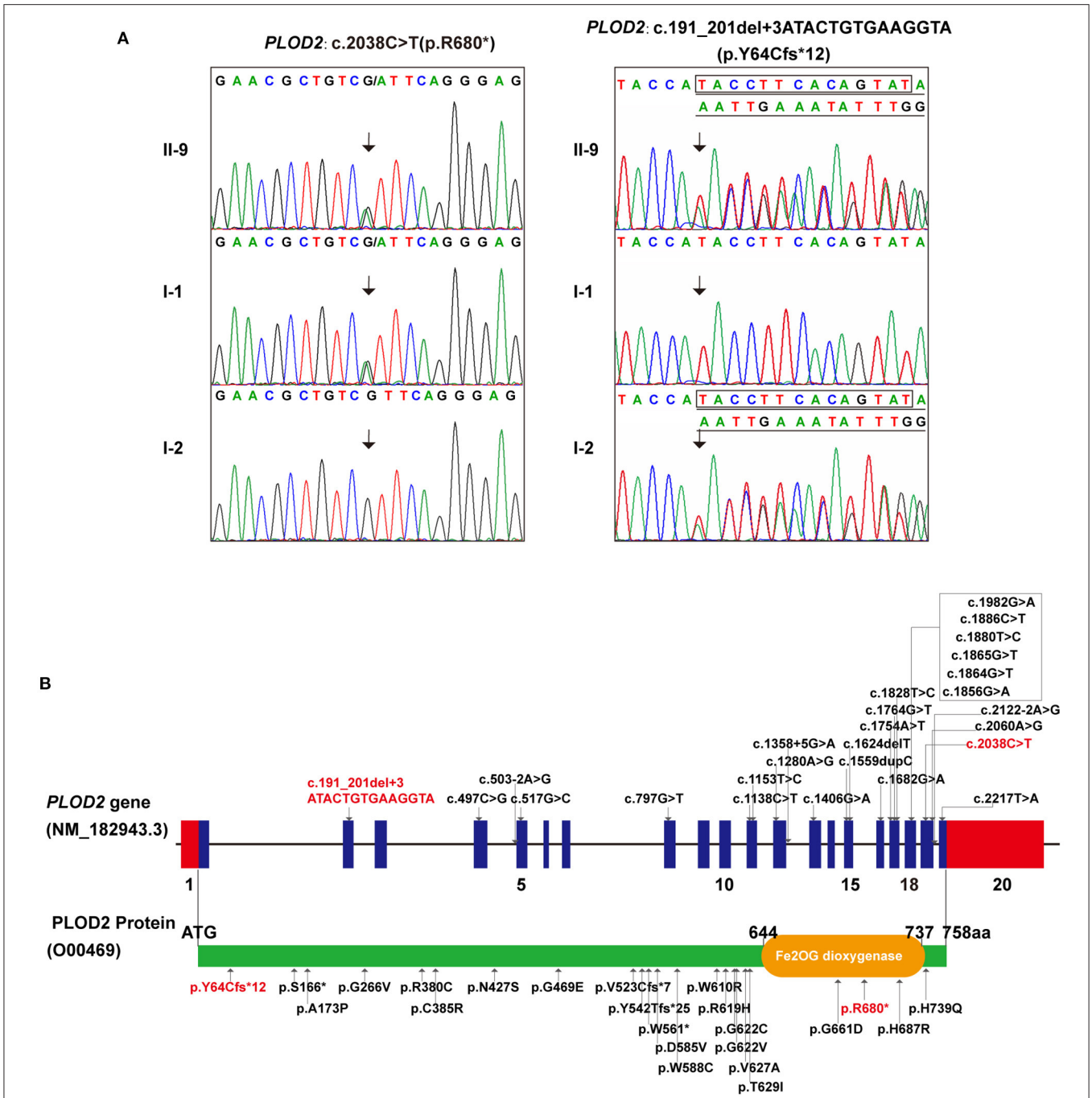

FIGURE 2 | The genetic variations identified in this case: **(A)** The two variants detected in this fetus and his parents (individual no. corresponding to **Figure 1A**). **(B)** All *PLOD2* variants associating with BRKS2-like phenotype in the literature and in this study, illustrated in diagrams of gene and protein. (In this study, red font represents variants).

expanded the variation spectrum of *PLOD2* gene. Additionally, Guo et al. have determined a 2Å crystal structure of the lysyl hydroxylase (LH) domain corresponding to human *PLOD2* amino acids 548–758, which provided sub-molecular insight into how specific variants affect the structure of LH2 (Guo et al., 2018). The genotype-phenotype correlation of *PLOD2* skeletal dysplasia is pending further elucidation along with the identification of more variations, particularly at the N-terminal (Leal et al., 2018).

LH2, cloned by Valtavaara et al. (1997), is encoded by PLOD2 gene, the defect of which is responsible for the onset of BRKS2. LH2 specifically catalyzes the hydroxylation of telopeptide lysyl residues in collagen, which is essential for the

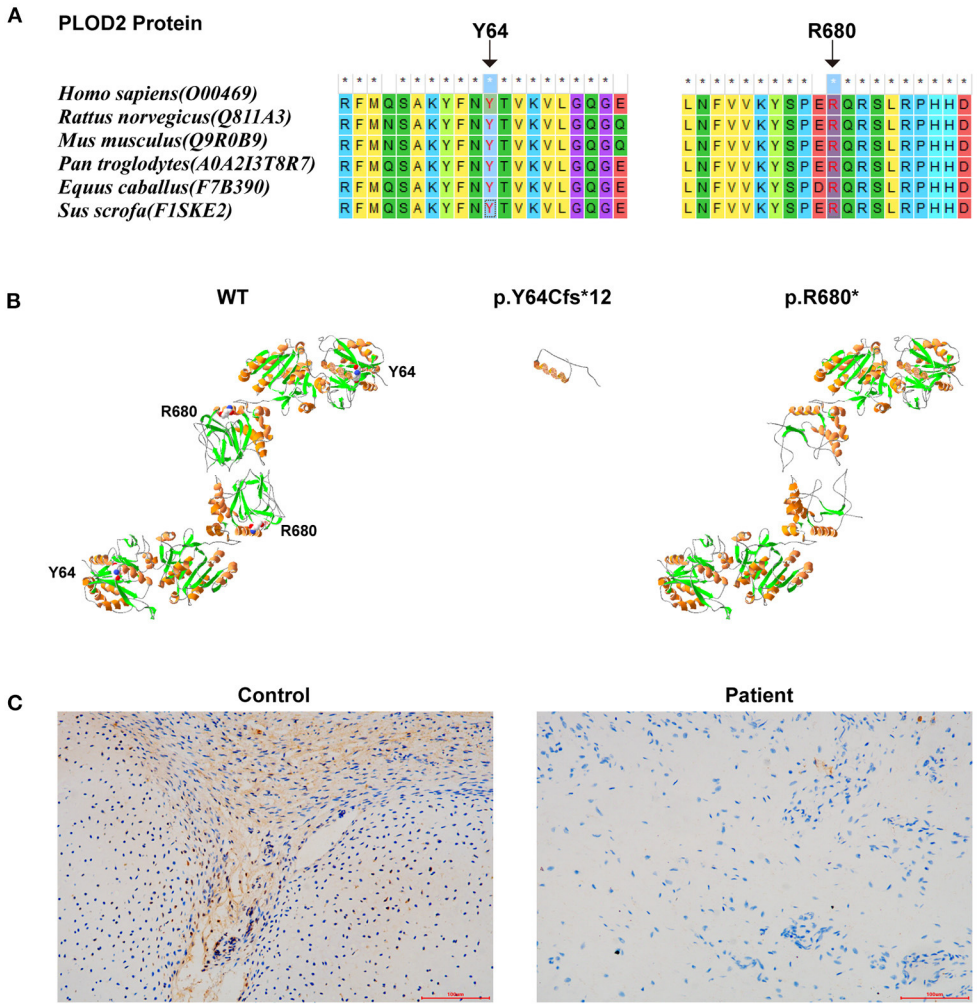

FIGURE 3 | The results of *in silico* analysis and IHC experimentation: **(A)** The conservatism of the two amino acids effected by the two variants. **(B)** The protein models of WT, p.Y64Cfs*12, and p.R680* of *PLOD2* protein model 6fxm.1.A. **(C)** *PLOD2* protein expression in the osteochondrocytes of the proband and control samples, by IHC.

normal crosslinking of bone collagen (Bank et al., 1999; van der Slot et al., 2003). FKBP10, whose deficiency is causative for BRKS1, belongs to a group of proteins termed immunophilins and displays high binding affinity for the immunosuppressant drugs FK506 (Patterson et al., 2000). FKBP10 is thought to function as a collagen chaperone and to assist in collagen folding (Lietman et al., 2014). Subsequently, Chen et al. found that the peptidyl prolyl isomerase activity of FKBP10 positively modulated LH2 enzymatic activity and was critical for the formation of hydroxylysine-aldehyde derived intermolecular collagen crosslinks, which indirectly explained why phenotypes of BRKS1 and BRKS2 were so similar (Chen et al., 2017). LH2 has two splice forms–LH2a (short) and LH2b (long)–resulting from alternative splicing of *PLOD*2, with LH2b containing an additional exon 13 A encoding 21 amino acids (Gjaltema and Bank, 2017). The absence of LH2b has great impact on musculoskeletal tissues, particularly bone, as illustrated by mutations in PLOD2 (Gjaltema and Bank, 2017). LH2 activity is positively correlated with pyridinoline levels, which indicates its important role in the formation of collagen telopeptide-derived pyridinoline crosslinks (van der Slot et al., 2005; Gjaltema and Bank, 2017). In this study, the result of IHC indicated the extremely low expression of *PLOD2* in cartilage tissue of the proband, which should be the result of the variation he carried. Both mutations c.2038C>T (p.R680*) and c.191_201+3delATACTGTGAAGGTA would be possibly expected to induce nonsense mediated mRNA decay (NMD), whereby the low expression level of *PLOD2* could be responsible for the NMD. Further functional experiments are needed to explore the possible mechanism. However, we failed to detect the mRNA-level expression of *PLOD2* due to the degradation of RNA in the fibroblast sample, which is a flaw in our study and needs to be remedied by subsequent functional studies. From another angle, the protein modeling result revealed that both mutations

possibly caused the peptide chain truncation, which clearly affected the dimerization and maturation process and even the presence of the protein. Besides, the evolutionary conservatism of the amino acids affected by the two variants further supported their pathogenicity. However, further functional experiments are necessary, not only to clarify the effect of each variant on the protein itself but also to understand the role of this effect in the overall process of osteogenic differentiation.

In practical terms, diagnostic report in this study was obtained before the fetal pregnancy entered the perinatal period (after 27^{+6} gestational weeks), which was supportive for the application of WES in the field of prenatal diagnosis.

For any future pregnancy of the proband in this study, the recurrent risk of Bruck syndrome 2 condition would be 25%. Given such circumstances, the couple were informed of reproductive options such as prenatal testing and preimplantation genetic diagnosis (PGD). We need to follow up on the outcome of the couple's pregnancy.

CONCLUSION

In summary, this study detected a novel *PLOD2* compound heterozygous variation in a 17-gestation-week fetus with BRKS2 by a multi-platform genetic approach. It clarified the cause of fetal OI in the subject family, provided guidance for any future pregnancy the couple might have and highlighted the value of WES in diagnosis of SD with unclear prenatal indications.

DATA AVAILABILITY STATEMENT

The datasets presented in this study can be found in online repositories. The names of the repository/repositories and accession number(s) can be found at: https://www.ncbi.nlm.nih.gov/, NG 011537.1; http://www.wwpdb.org/, NM_000935.

ETHICS STATEMENT

The studies involving human participants were reviewed and approved by the Research Ethics Committee of the Shijiazhuang Obstetrics and Gynecology Hospital. The patients/participants provided their written informed consent to participate in this study.

AUTHOR CONTRIBUTIONS

QG designed the overall research strategy and supervised the whole process. JZ recruited the case, performed the prenatal counseling, sampling, and part of the genetic experiments. HH performed the other part of the genetic experiments and data analysis. WM and MY performed IHC. WC conducted protein modeling. DM performed prenatal ultrasonic exam. JZ and HH cooperated in the preparation of this manuscript. All authors contributed to the article and approved the submitted version.

ACKNOWLEDGMENTS

We thank the patients and their families for their participation in this study.

SUPPLEMENTARY MATERIAL

The Supplementary Material for this article can be found online at: https://www.frontiersin.org/articles/10.3389/fgene.2021.619948/full#supplementary-material

REFERENCES

Alanay, Y., Avaygan, H., Camacho, N., Utine, G. E., Boduroglu, K., Aktas, D., et al. (2010). Mutations in the gene encoding the RER protein FKBP65 cause autosomal-recessive osteogenesisimperfecta. *Am. J. Hum. Genet*. 86, 551–559. doi: 10.1016/j.ajhg.2010.02.022

Bank, R. A., Robins, S. P., Wijmenga, C., Breslau-Siderius, L. J., Bardoel, A. F. J., Sluijs, H. A. V. D., et al. (1999). Defective collagen crosslinking in bone, but not in ligament or cartilage, in Bruck syndrome: indications for a bone-specific telopeptidelysyl hydroxylase on chromosome 17. *Proc. Natl. Acad. Sci. U.S.A.* 96, 1054–1058. doi: 10.1073/pnas.96.3.1054

Chen, Y., Terajima, M., Banerjee, P., Guo, H., Liu, X., Yu, J., et al. (2017). FKBP65-dependent peptidyl-prolylisomerase activity potentiates the lysyl hydroxylase 2-driven collagen cross-link switch. *Sci. Rep*. 7:46021. doi: 10.1038/srep46021

Eyre, D. R., and Weis, M. A. (2013). Bone collagen: new clues to its mineralization mechanism from recessive osteogenesisimperfecta. *Calcif. Tissue Int*. 93, 338–347. doi: 10.1007/s00223-013-9723-9

Forlino, A., and Marini, J. C. (2016). Osteogenesisimperfecta. *Lancet* 387, 1657–1671. doi: 10.1016/S0140-6736(15)00728-X

Gjaltema, R. A., and Bank, R. A. (2017). Molecular insights into prolyl and lysyl hydroxylation of fibrillar collagens in health and disease. *Crit. Rev. Biochem. Mol. Biol*. 52, 74–95. doi: 10.1080/10409238.2016.1269716

Guo, H. F., Tsai, C. L., Terajima, M., Tan, X., Banerjee, P., Miller, M. D., et al. (2018). Pro-metastatic collagen lysyl hydroxylase dimer assemblies stabilized by Fe(2+)-binding. *Nat. Commun*. 9:512. doi: 10.1038/s41467-018-02859-z

Konstantinidou, A. E., Agrogiannis, G., Sifakis, S., Karantanas, A., Harakoglou, V., Kaminopetros, P., et al. (2009). Genetic skeletal disorders of the fetus and infant: pathologic and molecular findings in a series of 41 cases. *Birth Defects Res. A Clin. Mol. Teratol*. 85, 811–821. doi: 10.1002/bdra.20617

Leal, G. F., Nishimura, G., Voss, U., Bertola, D. R., Astrom, E., Svensson, J., et al. (2018). Expanding the clinical spectrum of phenotypes caused by pathogenic variants in PLOD2. *J. Bone Miner. Res*. 33, 753–760. doi: 10.1002/jbmr.3348

Lietman, C. D., Rajagopal, A., Homan, E. P., Munivez, E., Jiang, M. M., Bertin, T. K., et al. (2014). Connective tissue alterations in Fkbp10-/- mice. *Hum. Mol. Genet*. 23, 4822–4831. doi: 10.1093/hmg/ddu197

Liu, Y., Asan, Ma, D., Lv, F., Xu, X., Wang, J., et al. (2017). Gene mutation spectrum and genotype-phenotype correlation in a cohort of Chinese osteogenesisimperfecta patients revealed by targeted next generation sequencing. *Osteoporos. Int*. 28, 2985–2995. doi: 10.1007/s00198-017-4143-8

Liu, Y., Wang, L., Yang, Y. K., Liang, Y., Zhang, T. J., Liang, N., et al. (2019). Prenatal diagnosis of fetal skeletal dysplasia using targeted next-generation sequencing: an analysis of 30 cases. *Diagn. Pathol*. 14:76. doi: 10.1186/s13000-019-0853-x

Lv, F., Xu, X., Song, Y., Li, L., Asan, Wang, J., et al. (2017). Novel Mutations in PLOD2 Cause Rare Bruck Syndrome. *Calcif. Tissue Int*. 102, 296–309. doi: 10.1007/s00223-017-0360-6

Marini, J. C. (2013). New genes in bone development: what's new in osteogenesis imperfecta. *J Clin. Endocrinol. Metab*. 98, 3095–3103. doi: 10.1210/jc.2013-1505

Mumm, S., Gottesman, G. S., Wenkert, D., Campeau, P. M., Nenninger, A., Huskey, M., et al. (2020). Bruck syndrome 2 variant lacking congenital contractures and involving a novel compound heterozygous PLOD2 mutation. *Bone* 130:115047. doi: 10.1016/j.bone.2019.115047

Offiah, A. C. (2015). Skeletal dysplasias: an overview. *Endocr. Dev*. 28, 259–276. doi: 10.1159/000381051

Patterson, C. E., Schaub, T., Coleman, E. J., and Davis, E. C. (2000). Developmental regulation of FKBP65 an ER-localized extracellular matrix binding-protein. *Mol. Biol. Cell* 11, 3925–3935. doi: 10.1091/mbc.11.11.3925

Richards, S., Aziz, N., Bale, S., Bick, D., Das, S., Gastier-Foster, J., et al. (2015). Standards and guidelines for the interpretation of sequence variants: a joint consensus recommendation of the American College of Medical Genetics and Genomics and the Association for Molecular Pathology. *Genet. Med*. 17, 405–424. doi: 10.1038/gim.2015.30

Tham, E., Grigelionis, G., Hammarsjo, A., and Grigelioniene, G. (2018). Genotype-phenotype correlation of PLOD2 skeletal dysplasias using structural information. *J. Bone Miner. Res*. 33, 1377–1378. doi: 10.1002/jbmr.3460

Valtavaara, M., Papponen, H., Pirttila, A.-M., Helander, H., Hiltunen, K., and Myllyla, R. (1997). Cloning and characterization of a novel human lysyl hydroxylase isoform highly expressed in pancreas and muscle. *J. Biol. Chem*. 272, 6831–6834.

van der Slot, A. J., van Dura, E. A., de Wit, E. C., DeGroot, J., Huizinga, T. W. J., Bank, R. A., et al. (2005). Elevated formation of pyridinoline cross-links by profibrotic cytokines is associated with enhanced lysyl hydroxylase 2b levels. *Biochim. Biophys. Acta* 1741, 95–102. doi: 10.1016/j.bbadis.2004.09.009

van der Slot, A. J., Zuurmond, A. M., Bardoel, A. F., Wijmenga, C., Pruijs, H. E., Sillence, D. O., et al. (2003). Identification of PLOD2 as telopeptidelysyl hydroxylase, an important enzyme in fibrosis. *J. Biol. Chem*. 278, 40967–40972. doi: 10.1074/jbc.M307380200

Viuoen, D., Versfeld, G., and Beighton, P. (1989). Osteogenesisimperfecta with congenital joint contractures (Bruck Syndrome). *Clin. Genet*. 36, 122–126. doi: 10.1111/j.1399-0004.1989.tb03174.x

Wang, X., Guo, J., Dai, M., Wang, T., Yang, T., Xiao, X., et al. (2020). PLOD2 increases resistance of gastric cancer cells to 5-fluorouracil by upregulating BCRP and inhibiting apoptosis. *J. Cancer* 11, 3467–3475. doi: 10.7150/jca.41828

Yang, K., Shen, M., Yan, Y., Tan, Y., Zhang, J., Wu, J., et al. (2019). Genetic analysis in fetal skeletal dysplasias by trio whole-exome sequencing. *Biomed. Res. Int*. 2019, 1–8. doi: 10.1155/2019/2492590

Zhou, X., Chandler, N., Deng, L., Zhou, J., Yuan, M., and Sun, L. (2018). Prenatal diagnosis of skeletal dysplasias using a targeted skeletal gene panel. *Prenat. Diagn*. 38, 692–699. doi: 10.1002/pd.5298

Conflict of Interest: The authors declare that the research was conducted in the absence of any commercial or financial relationships that could be construed as a potential conflict of interest.

frontiers in Genetics

CASE REPORT
published: 26 February 2021
doi: 10.3389/fgene.2021.652381

Case Report: Identification of a Novel *ODAD3* Variant in a Patient With Primary Ciliary Dyskinesia

Rongchun Wang[1,2,3†], *Danhui Yang*[1,2,3†], *Ting Guo*[1,2,3], *Cheng Lei*[1,2,3], *Xu Chen*[1,2,3], *Xi Kang*[1,2,3], *Jie Qing*[1,2,3*] *and Hong Luo*[1,2,3*]

[1] *Department of Pulmonary and Critical Care Medicine, The Second Xiangya Hospital, Central South University, Changsha, China,* [2] *Research Unit of Respiratory Disease, Central South University, Changsha, China,* [3] *Hunan Diagnosis and Treatment Center of Respiratory Disease, Changsha, China*

OPEN ACCESS

Edited by:
Emiliano González Vioque, University Clinical Hospital of Santiago, Spain

Reviewed by:
Fulya Taylan, Karolinska Institutet (KI), Sweden
Ana Westenberger, University of Lübeck, Germany

***Correspondence:**
Hong Luo
drluohong@csu.edu.cn
Jie Qing
qingjie00@csu.edu.cn

[†] *These authors have contributed equally to this work*

Specialty section:
This article was submitted to Genetics of Common and Rare Diseases, a section of the journal Frontiers in Genetics

Received: *12 January 2021*
Accepted: *09 February 2021*
Published: *26 February 2021*

Citation:
Wang R, Yang D, Guo T, Lei C, Chen X, Kang X, Qing J and Luo H (2021) Case Report: Identification of a Novel ODAD3 Variant in a Patient With Primary Ciliary Dyskinesia. Front. Genet. 12:652381. doi: 10.3389/fgene.2021.652381

Background: *ODAD3* encodes a protein of 595 amino acids and contain three highly conserved coiled-coil domains, which is essential for cilia axoneme dynein arm assembly and docking. Primary ciliary dyskinesia (PCD) of *ODAD3* deficiency are rarely reported. Female infertility in PCD related to *ODAD3* variants has not been reported.

Methods: Whole-exome and Sanger sequencing were used to identify the disease-related gene of the patient with PCD in a consanguineous Chinese family. Domain analysis was applied to predict the impact of the variant on ODAD3 protein.

Results: The 35 year-old female patient exhibited chronic sinusitis, diffuse bronchiectasis, dextrocardia and infertility. We identified a novel homozygous variant in *ODAD3*, c.1166_1169dupAGAC, p.(Leu391Aspfs*105) in the PCD patient by exome sequencing and Sanger sequencing. This frameshift variant was predicted to be disease causing by bioinformatics analysis and was also not presented in the current authorized large genetic databases.

Conclusions: Our study enriches the genetic spectrum and clinical phenotypes of *ODAD3* variants in PCD and provide more evidence for future genetic counseling and gene-targeted therapy for this disease.

Keywords: primary ciliary dyskinesia, *ODAD3*, *CCDC151*, sinusitis, bronchiectasis, dextrocardia, infertility

INTRODUCTION

Primary ciliary dyskinesia (PCD, MIM 244400) is a clinically and genetically heterogeneous motile ciliopathy characterized by recurrent upper and lower respiratory infections, subfertility and laterality defect (Mirra et al., 2017). The estimated prevalence of PCD is 1:10 000 to 1:20 000 live-born children (Afzelius and Stenram, 2006). So far, more than 47 genes associated with cilia structure or function dysfunction have been identified causative for PCD (Wallmeier et al., 2020).

ODAD3 (Outer dynein arm docking complex subunit 3; formerly known as *CCDC151*; coiled-coil domain containing 151) encodes a protein of 595 amino acids which contains three highly conserved coiled-coil domains. This protein was initially recognized as a potential ciliome gene due to its expression in

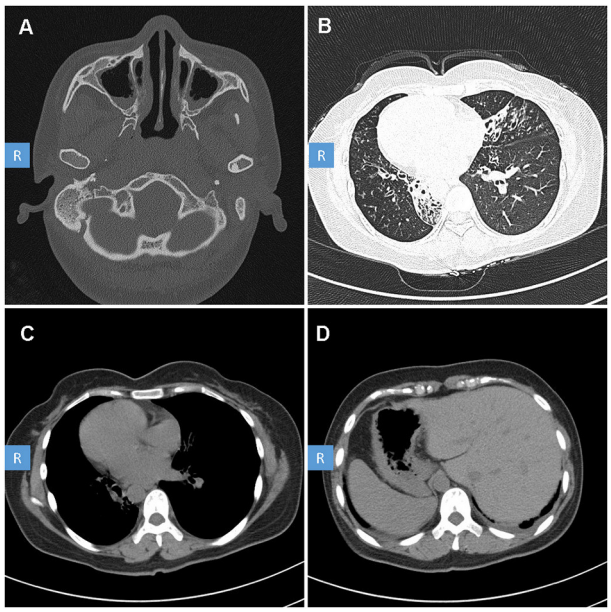

FIGURE 1 | High-resolution computed tomography (HRCT) scan of the patient with PCD. CT scan showed: **(A)** Sinusitis. **(B)** Diffuse bronchiectasis. **(C)** Right-side heart. **(D)** Abdominal organ heterotaxy: liver in the left side, stomach and spleen in the right side.

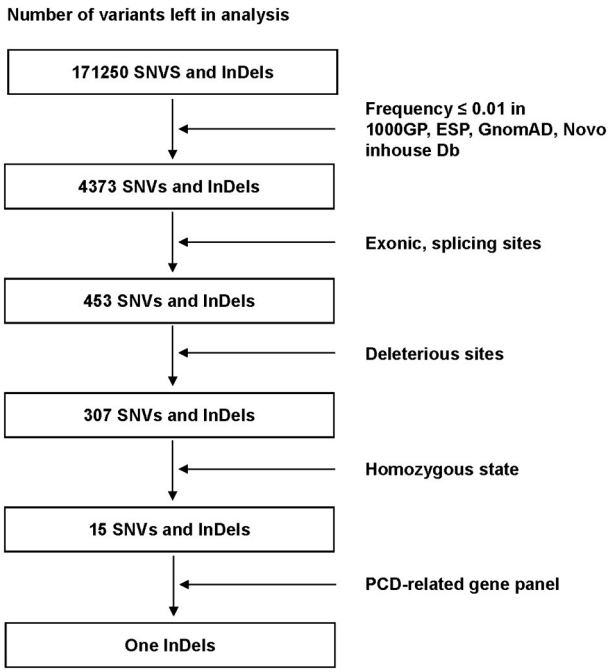

FIGURE 2 | Filter process performed to all variants in the alignment SNVs and InDels. Only one InDels (*ODAD3*, NM_145045.4: c.1166_1169dup) left after all filter steps. SNVs, single-nucleotide variants: InDels, insertions and deletions; 1000GP, 1000 Genomes Project; ESP, Exome Sequencing Project; GnomAD, Genome Aggregation Database; PCD, Primary ciliary dyskinesia.

human ciliary axonemes (Ostrowski et al., 2002) and it is essential for cilia axoneme dynein arm assembly and docking (Hjeij et al., 2014). Up to now, PCD caused by *ODAD3* variants (MIM 616037, CILD30) are rarely reported and female infertility has not been identified in PCD caused by *ODAD3* variants.

In the present study, a novel variant in *ODAD3* was identified in a female PCD patient with infertility from a Chinese consanguineous family.

CASE PRESENTATION

The patient is a 35 year-old female. She was admitted to our hospital because of chronic cough, purulent sputum, nasal congestion for over 30 years and dyspnea for about 5 years. She has been inflicted by recurrent infections of the lower and upper airways since newborn. And he has been married for 10 years but without pregnancy and was diagnosed with infertility. She had no history of drowning, measles, polio, tuberculosis, immunodeficiency, connective tissue disease, etc. Her family members denied any obvious respiratory or other disease history. Physical examination indicated right-side heart sound. High resolution computed tomography of this patient revealed chronic sinusitis (**Figure 1A**), diffuse bronchiectasis (**Figure 1B**), situs inversus: heart dextroversion (**Figure 1C**) and abdominal organs in the reverse location (**Figure 1D**). Lung function test revealed a moderate to severe mixed (restrictive and obstructive) ventilation dysfunction. Her nasal nitric oxide concentration (nNO) (6 nl/min) was far below the reference nNO cutoff value of PCD (77 nl/min) (Leigh et al., 2013).

METHODS

Ethical Compliance

This study was approved by the Review Board of the Second Xiangya Hospital of Central South University in China. Written informed consent was obtained from the patient.

DNA Extraction and Variant Analysis

We extracted genomic DNA from peripheral blood of the proband and healthy control, using a QIAamp DNA Blood Mini Kit (250) (QIAGEN, Valencia, CA). Then we captured the DNA of the proband with the Agilent SureSelect Human All Exon V5 Kit (Agilent, California, USA) and sequenced on Illumina Hiseq 4000 (Illumina Inc., San Diego, USA).

The valid sequencing reads were aligned to the NCBI human reference genome (GRCh37/hg19) by the Burrows Wheeler Aligner software (Li and Durbin, 2010). ANNOVAR is used to do annotation for Variant Call Format file (Wang et al., 2010). We classified the variants as pathogenic, likely pathogenic and uncertain significance, likely benign, benign according to American College of Medical Genomics (ACMG) guidance (Richards et al., 2015).

We filtered single-nucleotide variants (SNVs) and short insertions and deletions (InDels) as follows (**Figure 2**): (1) High-frequency (minor allele frequency > 0.01) variants found in 1000 Genomes Project, Exome Sequencing Project (ESP), Genome Aggregation Database (gnomAD) and Novo inhouse Database,

were excluded. (2) Variants within Exonic, splicing sites were included from subsequent analysis. (3) Bioinformatics programs: Mutation Taster, Polyphen2, SIFT, CADD, and LoFtool were used to predict the possible impacts of SNVs. (4) Homozygous variants were retained to be filtered by a PCD-related gene panel including 47 identified genes (**Supplementary Table 1**). Sanger sequencing was performed in the patient to validate the mutation. The location of the mutation was analyzed by SMART program (http://smart.embl-heidelberg.de). The DNA samples from the patient's parents were not available. The primer sequences were designed as follows: forward, 5′-ATTCTAAGACCGCTGTGT CCC-3′; reverse, 5′ TTGCACAGCAATGTATGGGG-3′.

RESULTS

For the DNA sample of the patient, exome sequencing generated an average of 14.5 Gb data with an ∼99% coverage and a depth of >50×. After alignment and frequency filter, 4,373 non-synonymous variants (SNVs and InDels) were further analyzed and 453 variants in exons or in canonical splice sites (splicing junction 10 bp) were further analyzed. Fifteen SNVs and InDels in homozygous state were left and then filtered by the PCD-related gene panel. Finally, only one homozygous variant, *ODAD3*, NC_000019.9:g.11533477_11533480dup, NM_145045.4: c.1166_1169dupAGAC, NP_659482.3: p.(Leu391Aspfs*105), which caused frameshift insertion, passed the filtration.

This variant was in accord with the hereditary mode from consanguineous family (**Figure 3A**) and was validated via Sanger sequencing (**Figures 3B,C**). According to ACMG guidelines (Richards et al., 2015), this variant was classified into pathogenic (meeting criteria of PVS1, PM2, PM3). The location of the variant is within the third coiled-coil domain of the 595-amino-acid ODAD3 protein (Refseq NP_659482.3) analyzed by SMART program (http://smart.embl-heidelberg.de) (**Figure 3D**).

DISCUSSION AND CONCLUSION

This study describes a female with PCD that carried a novel homozygous variant in the *ODAD3* gene. This patient in our study exhibited chronic sinusitis, bronchiectasis, situs inversus, and infertility. Our case enriches the mutation spectrum and clinical phenotypes of *ODAD3* variants in PCD.

PCD is a motile ciliopathy involving multiple organs or system, especially in respiratory tract. Cilia can be classified into two types according their motility: motile cilia with 9+2 or 9+0 microtube structure and immotile cilia with 9+0 microtube (Satir and Christensen, 2007). Motile cilia has highly conserved cell structure among different species and extensively exists on airway epithelium, germinal center in fetal period, oviduct and sperm flagella (Bayless et al., 2019). The critical pathogenesis of PCD lies in the abnormality of motile cilia structure or function or ciliogenesis, which accounts for ineffective cilia clearance, abnormal left–right asymmetry and subfertility (Bustamante-Marin and Ostrowski, 2017).

To date, a total of seven likely loss-of-function variants in *ODAD3* have been reported in PCD (**Supplementary Table 2**). The reported *ODAD3* variants including three non-sense variants: p.(Gly309 *) (Hjeij et al., 2014); p.(Ser409*) (Hjeij et al., 2014); p.(Glu109*) (Zhang et al., 2019); three frame-shifting variants: p.(Gly56Aspfs*26) (Deng et al., 2020); p.(Lys77Leufs*6) (Mani et al., 2020); p.(His199Argfs*60) (Olm et al., 2019) and one splice site variant: c.244+1G>A (Monies et al., 2019). The only two hitherto reported female patients (10 week and 1 year-old, respectively) did not reach reproductive age. infertility has not been determined in the previously reported patients. However, it means that it was not reported (and probably not even investigated in adult patients) and not that it was not present. Therefore, assessing and reporting infertility in patients affected by PCD is essential, whenever possible. In our study, we detected a novel homozygous variant of *ODAD3*, p.(Leu391Aspfs*105) which was likely to be PCD disease-causing. The patient in our study exhibited typical PCD phenotypes including chronic sinusitis, bronchiectasis, situs inversus and infertility. The frame-shift variant results in an incorrect and premature termination of translation of ODAD3 protein which may undergo non-sense-mediated decay, indicating a loss of function of *ODAD3* in outer dynein arm (ODA) assembly and docking.

Infertility is more common in males than females in PCD (Wallmeier et al., 2020). The prevalence of infertility among PCD females is unclear, partly due to insufficient awareness of clinicians. A cohort study (Vanaken et al., 2017) among PCD reported 61% (22/36) women are considered infertile related with 13 genes such as *CCDC39*, *CCDC40*, *DNAH5,* which affect motile cilia structure. *CCDC39* and *CCDC40*, similar to *ODAD3*, also contain coiled-coil domains and their defects display disorganization of microtubule doublets and central pair in cilia (Becker-Heck et al., 2011; Merveille et al., 2011). *DNAH5* is the ODA component of motile cilia and its defect lead to ciliary dyskinesia (Hornef et al., 2006). These data indicate that those genes impacting motile cilia structure, may related to female infertility. Our study is the first to report infertility in female PCD patient with *ODAD3* deficiency. The frameshift *ODAD3* variant may lead to ODA defects and then impede the oocytes transportation across the oviduct, which finally results in infertility. As there are currently no way for women to test their potentially PCD-related fertility before trying to conceive, it is necessary for clinicians to pay more attention to fertility status of PCD. Fertility counseling and appropriate assisted reproductive technologies should be included in the standard PCD patient care.

Animal models of deficient *ODAD3* demonstrated phenotypes of ciliary dyskinesia and laterality defects similar to human. *Odad3* in vertebrates is homologous to the *Chlamydomonas ODA10* gene which is also associated with cilia outer ODA assembly (Dean and Mitchell, 2013). *ODAD3* is involved in regulating intraflagellar transport (IFT)-dependent dynein arm assembly according to previous research in *drosophila*, zebrafish, and mice (Alsaadi et al., 2014; Hjeij et al., 2014; Jerber et al., 2014). *ODAD3*-knockdown zebrafish had motile ciliary dysfunction in the pronephros and Kupffer's vesicle, and showed abnormal left–right asymmetry (Hjeij et al., 2014). In mice, *Odad3* is expressed

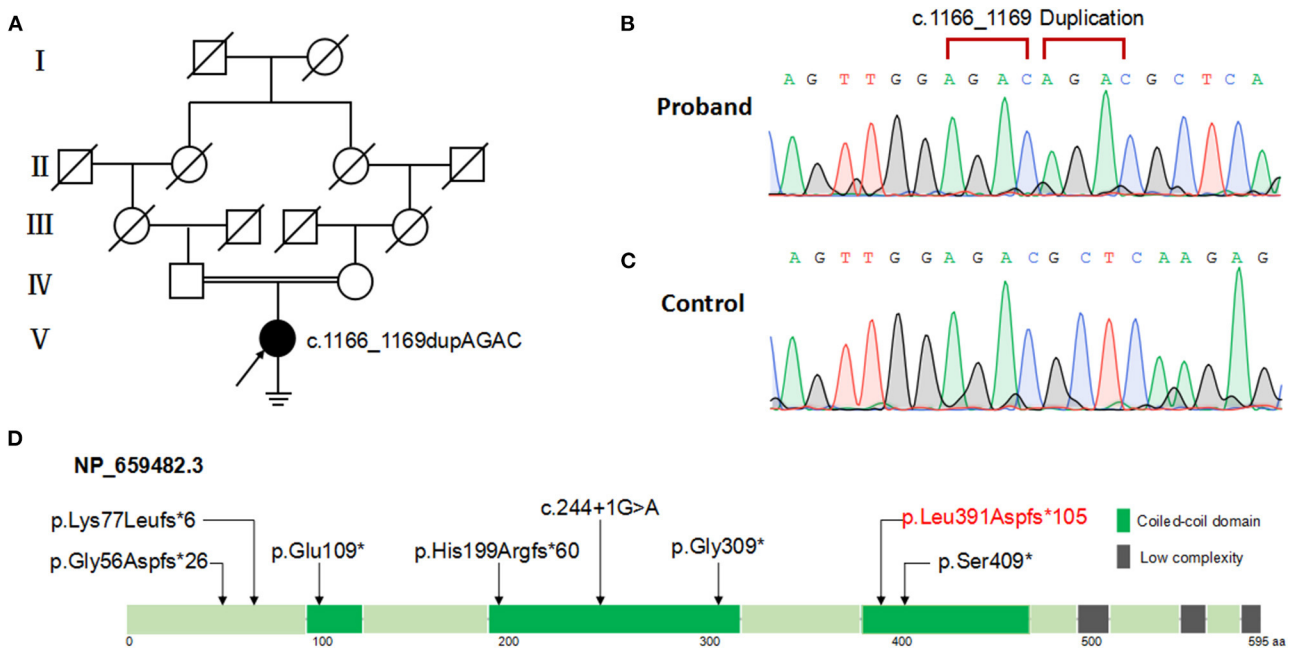

FIGURE 3 | Pedigree and *ODAD3* variants analysis of the patient with PCD. **(A)** Family pedigree of the patient with PCD. Filled symbol represents the affected member, empty symbol represents unaffected members, slashed symbols represent deceased members. Squares, males; circles, females. The patient (V:1) is indicated by a black arrow. **(B)** Patient with *ODAD3* c.1166_1169dupAGAC alleles. **(C)** Normal control with wild-type alleles. **(D)** The location of the mutations is shown within the third coiled-coil domain of the 595-amino-acid ODAD3 protein (Refseq NP_659482.3) model. Green boxes indicate coiled-coil domain; gray boxes indicate low-complexity repeat regions.

in embryonic nodes and ependymal cells, and deficient *Odad3* may result in ciliary dyskinesia and laterality defects (Jerber et al., 2014). Whether *ODAD3* defect leads to infertility in animal remains unknown and need further research to recapture phenotype in human.

In conclusion, combined clinical profile and sequencing data, we suggest that novel homozygous variant of *ODAD3*, p.(Leu391Aspfs*105), is one of the pathogenic cause of PCD. This is also the first report about female infertility in PCD of *ODAD3* deficiency. Our study enriches the genetic spectrum and clinical phenotypes of *ODAD3* variants in PCD and provides more evidence for future genetic counseling and gene-targeted therapy for this disease.

DATA AVAILABILITY STATEMENT

The datasets for this article are not publicly available due to concerns regarding participant/patient anonymity. Requests to access the datasets should be directed to the corresponding author.

ETHICS STATEMENT

The studies involving human participants were reviewed and approved by Review Board of the Second Xiangya Hospital of Central South University in China. The patients/participants provided their written informed consent to participate in this study. Written informed consent was obtained from the individual(s) for the publication of any potentially identifiable images or data included in this article.

AUTHOR CONTRIBUTIONS

HL and JQ designed the study. RW, DY, TG, and CL performed the genetic analysis and bioinformatics evaluations. RW and DY drafted the manuscript. HL, JQ, XC, and XK conducted the clinical evaluations. All authors analyzed the data and approved the final manuscript.

FUNDING

This study was supported by the National Natural Science Foundation of China (81470202, 81770002, 82070003, 81900002), Natural Science Foundation of Hunan Province, China (2020JJ5805), Fundamental Research Funds for Central Universities of Central South University (2020zzts292, 2020zzts281), the Hunan Provincial Innovation Foundation For Postgraduate (CX20200289), the Hunan Province Health Commission Scientific Research Project (B2019159), the Science and Technology Program of Changsha, China (kq1901120), Xiangya Clinical Big Data System Construction Project in Pulmonary Inflammatory Disease of Central South University,

and the National Key Clinical Specialty Construction Projects of China.

ACKNOWLEDGMENTS

We are grateful to the patient and the healthy control for their collaboration. We acknowledge the State Key Laboratory of Medical Genetics of China for technical assistance. We acknowledge Shuizi Ding in Yale University for language editing advice of this manuscript.

SUPPLEMENTARY MATERIAL

The Supplementary Material for this article can be found online at: https://www.frontiersin.org/articles/10.3389/fgene.2021.652381/full#supplementary-material

REFERENCES

Afzelius, B. A., and Stenram, U. (2006). Prevalence and genetics of immotile-cilia syndrome and left-handedness. *Int. J. Dev. Biol.* 50, 571–573. doi: 10.1387/ijdb.052132ba

Alsaadi, M. M., Erzurumluoglu, A. M., Rodriguez, S., Guthrie, P. A., Gaunt, T. R., Omar, H. Z., et al. (2014). Nonsense mutation in coiled-coil domain containing 151 gene (CCDC151) causes primary ciliary dyskinesia. *Hum. Mutat.* 35, 1446–1448. doi: 10.1002/humu.22698

Bayless, B. A., Navarro, F. M., and Winey, M. (2019). Motile cilia: innovation and insight from ciliate model organisms. *Front. Cell Dev. Biol.* 7:265. doi: 10.3389/fcell.2019.00265

Becker-Heck, A., Zohn, I. E., Okabe, N., Pollock, A., Lenhart, K. B., Sullivan-Brown, J., et al. (2011). The coiled-coil domain containing protein CCDC40 is essential for motile cilia function and left-right axis formation. *Nat. Genet.* 43, 79–84. doi: 10.1038/ng.727

Bustamante-Marin, X. M., and Ostrowski, L. E. (2017). Cilia and mucociliary clearance. *Cold Spring Harb. Perspect. Biol.* 9:a028241. doi: 10.1101/cshperspect.a028241

Dean, A. B., and Mitchell, D. R. (2013). Chlamydomonas ODA10 is a conserved axonemal protein that plays a unique role in outer dynein arm assembly. *Mol. Biol. Cell* 24, 3689–3696. doi: 10.1091/mbc.e13-06-0310

Deng, S., Wu, S., Xia, H., Xiong, W., Deng, X., Liao, J., et al. (2020). Identification of a frame shift mutation in the CCDC151 gene in a Han-Chinese family with Kartagener syndrome. *Biosci. Rep.* 40:BSR20192510. doi: 10.1042/BSR20192510

Hjeij, R., Onoufriadis, A., Watson, C. M., Slagle, C. E., Klena, N. T., Dougherty, G. W., et al. (2014). CCDC151 mutations cause primary ciliary dyskinesia by disruption of the outer dynein arm docking complex formation. *Am. J. Hum. Genet.* 95, 257–274. doi: 10.1016/j.ajhg.2014.08.005

Hornef, N., Olbrich, H., Horvath, J., Zariwala, M. A., Fliegauf, M., Loges, N. T., et al. (2006). DNAH5 mutations are a common cause of primary ciliary dyskinesia with outer dynein arm defects. *Am. J. Respir. Crit. Care Med.* 174, 120–126. doi: 10.1164/rccm.200601-084OC

Jerber, J., Baas, D., Soulavie, F., Chhin, B., Cortier, E., Vesque, C., et al. (2014). The coiled-coil domain containing protein CCDC151 is required for the function of IFT-dependent motile cilia in animals. *Hum. Mol. Genet.* 23, 563–577. doi: 10.1093/hmg/ddt445

Leigh, M. W., Hazucha, M. J., Chawla, K. K., Baker, B. R., Shapiro, A. J., Brown, D. E., et al. (2013). Standardizing nasal nitric oxide measurement as a test for primary ciliary dyskinesia. *Ann. Am. Thorac. Soc.* 10, 574–581. doi: 10.1513/AnnalsATS.201305-110OC

Li, H., and Durbin, R. (2010). Fast and accurate long-read alignment with Burrows-Wheeler transform. *Bioinformatics* 26, 589–595. doi: 10.1093/bioinformatics/btp698

Mani, R., Belkacem, S., Soua, Z., Chantot, S., Montantin, G., Tissier, S., et al. (2020). Primary ciliary dyskinesia gene contribution in Tunisia: identification of a major Mediterranean allele. *Hum. Mutat.* 41, 115–121. doi: 10.1002/humu.23905

Merveille, A. C., Davis, E. E., Becker-Heck, A., Legendre, M., Amirav, I., Bataille, G., et al. (2011). CCDC39 is required for assembly of inner dynein arms and the dynein regulatory complex and for normal ciliary motility in humans and dogs. *Nat. Genet.* 43, 72–78. doi: 10.1038/ng.726

Mirra, V., Werner, C., and Santamaria, F. (2017). Primary ciliary dyskinesia: an update on clinical aspects, genetics, diagnosis, and future treatment strategies. *Front. Pediatr.* 5:135. doi: 10.3389/fped.2017.00135

Monies, D., Abouelhoda, M., Assoum, M., Moghrabi, N., Rafiullah, R., Almontashiri, N., et al. (2019). Lessons learned from large-scale, first-tier clinical exome sequencing in a highly consanguineous population. *Am. J. Hum. Genet.* 105:879. doi: 10.1016/j.ajhg.2019.09.019

Olm, M. A. K., Marson, F. A. L., Athanazio, R. A., Nakagawa, N. K., Macchione, M., Loges, N. T., et al. (2019). Severe pulmonary disease in an adult primary ciliary dyskinesia population in Brazil. *Sci. Rep.* 9:8693. doi: 10.1038/s41598-019-45017-1

Ostrowski, L. E., Blackburn, K., Radde, K. M., Moyer, M. B., Schlatzer, D. M., Moseley, A., et al. (2002). A proteomic analysis of human cilia: identification of novel components. *Mol. Cell. Proteomics* 1, 451–465. doi: 10.1074/mcp.M200037-MCP200

Richards, S., Aziz, N., Bale, S., Bick, D., Das, S., Gastier-Foster, J., et al. (2015). Standards and guidelines for the interpretation of sequence variants: a joint consensus recommendation of the American College of Medical Genetics and Genomics and the Association for Molecular Pathology. *Genet. Med.* 17, 405–424. doi: 10.1038/gim.2015.30

Satir, P., and Christensen, S. T. (2007). Overview of structure and function of mammalian cilia. *Annu. Rev. Physiol.* 69, 377–400. doi: 10.1146/annurev.physiol.69.040705.141236

Vanaken, G. J., Bassinet, L., Boon, M., Mani, R., Honore, I., Papon, J. F., et al. (2017). Infertility in an adult cohort with primary ciliary dyskinesia: phenotype-gene association. *Eur. Respir. J.* 50:1700314. doi: 10.1183/13993003.00314-2017

Wallmeier, J., Nielsen, K. G., Kuehni, C. E., Lucas, J. S., Leigh, M. W., Zariwala, M. A., et al. (2020). Motile ciliopathies. *Nat. Rev. Dis. Primers* 6:77. doi: 10.1038/s41572-020-0209-6

Wang, K., Li, M., and Hakonarson, H. (2010). ANNOVAR: functional annotation of genetic variants from high-throughput sequencing data. *Nucleic Acids Res.* 38:e164. doi: 10.1093/nar/gkq603

Zhang, W., Li, D., Wei, S., Guo, T., Wang, J., Luo, H., et al. (2019). Whole-exome sequencing identifies a novel CCDC151 mutation, c.325G>T (p.E109X), in a patient with primary ciliary dyskinesia and situs inversus. *J. Hum. Genet.* 64, 249–252. doi: 10.1038/s10038-018-0540-x

Conflict of Interest: The authors declare that the research was conducted in the absence of any commercial or financial relationships that could be construed as a potential conflict of interest.

frontiers in Pediatrics

CASE REPORT
published: 26 February 2021
doi: 10.3389/fped.2021.628190

Case Report: Co-occurrence of Duchenne Muscular Dystrophy and Frontometaphyseal Dysplasia 1

Jaewon Kim[1†], *Dong-Woo Lee*[1†], *Ja-Hyun Jang*[2], *Myungshin Kim*[3], *Jisook Yim*[3] *and Dae-Hyun Jang*[1*]

[1] Department of Rehabilitation Medicine, College of Medicine, Incheon St. Mary's Hospital, The Catholic University of Korea, Seoul, South Korea, [2] Department of Laboratory Medicine and Genetics, Samsung Medical Center, Sungkyunkwan University School of Medicine, Seoul, South Korea, [3] Department of Laboratory Medicine, College of Medicine, The Catholic University of Korea, Seoul, South Korea

Herein, we present a rare case of co-occurring Duchenne muscular dystrophy (DMD) and frontometaphyseal dysplasia 1 (FMD1), two different X-linked diseases, in a 7-year-old boy. He presented with proximal muscle weakness and elevated creatine phosphokinase levels. A multiplex ligation-dependent probe amplification study of *DMD* revealed the *de novo* duplications of exons 2–37, thereby confirming the diagnosis of DMD. Initial evaluation revealed atypical features, such as facial dysmorphism, multiple joint contractures, and severe scoliosis, at an early age. However, these were overlooked and were assumed to be atypical manifestations of DMD. Then, the patient's maternal cousin was diagnosed with FMD1 with pathogenic missense variant in *FLNA* (NM_001110556.2: c.3557C>T/p.Ser1186Leu). A family genetic test revealed that the patient and his mother had the same pathogenic variant in *FLNA*. The patient's atypical manifestations were considered symptoms of FMD1. Therefore, if one disease does not fully explain the patient's clinical features, an expanded genetic study is needed to detect coincidental disease.

Keywords: Duchenne muscular dystrophy, frontometaphyseal dysplasia 1, X-linked genetic diseases, FLNA gene mutation, genetic disease

OPEN ACCESS

Edited by:
Emiliano González Vioque, University Clinical Hospital of Santiago, Spain

Reviewed by:
Muhammad Jawad Hassan, National University of Medical Sciences (NUMS), Pakistan
Nicolina Cristina Sorrentino, Telethon Institute of Genetics and Medicine (TIGEM), Italy

***Correspondence:**
Dae-Hyun Jang
dhjangmd@naver.com

[†] These authors have contributed equally to this work

Specialty section:
This article was submitted to Genetics of Common and Rare Diseases, a section of the journal Frontiers in Pediatrics

Received: *11 November 2020*
Accepted: *08 February 2021*
Published: *26 February 2021*

Citation:
Kim J, Lee D-W, Jang J-H, Kim M, Yim J and Jang D-H (2021) Case Report: Co-occurrence of Duchenne Muscular Dystrophy and Frontometaphyseal Dysplasia 1. Front. Pediatr. 9:628190. doi: 10.3389/fped.2021.628190

INTRODUCTION

Duchenne muscular dystrophy (DMD) is characterized by progressive muscle weakness and atrophy, and it affects ∼1 in 3,500−5,000 males (1). DMD is caused by pathogenic variants in *DMD* on chromosome Xp21, and over 2,000 pathogenic variants have been determined. Approximately 55–65% of cases are caused by exon deletions, 30% by single-base variants or small deletions or insertions, and 5–15% by exon duplications (2–5). Individuals with this condition usually experience progressive wasting of the skeletal, respiratory, or cardiac muscles, resulting in death due to cardiac or respiratory compromise (6).

Frontometaphyseal dysplasia 1 (FMD1) is a rare genetic disorder caused by pathogenic variants in *FLNA* on chromosome Xq28 and is characterized by various skeletal development abnormalities. Worldwide, only a few dozen patients have been diagnosed with FMD1 to date. This condition has >10 pathogenic variants, with most being single-base variants (7). Herein, we describe a rare case of co-occurring DMD and FMD1, two different X-linked genetic disorders, coincidently diagnosed in one patient.

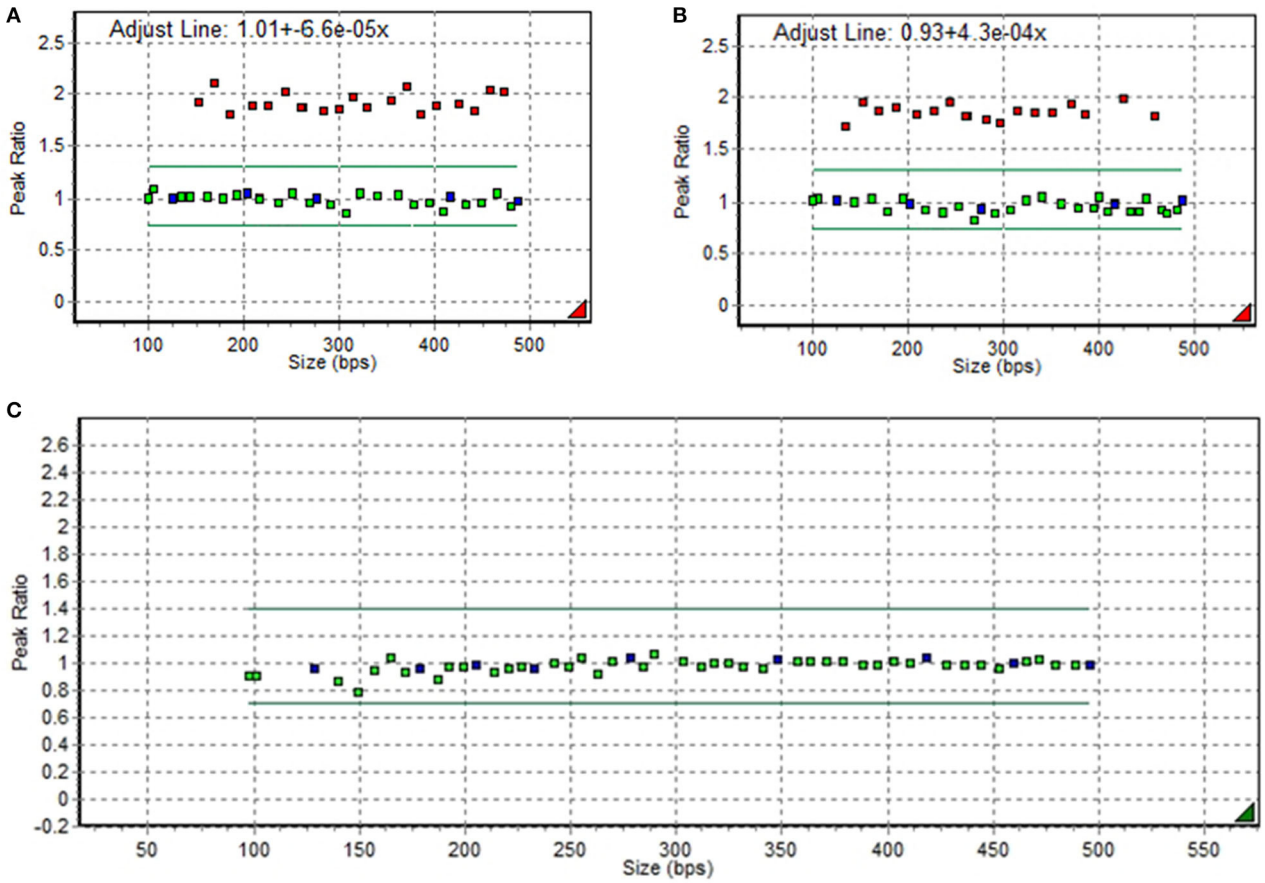

FIGURE 1 | Duplications of exons 2–37 in *DMD* on multiplex ligation-dependent probe amplification electropherogram in the proband **(A,B)** and in his mother **(C)**.

CASE PRESENTATION

A 7-year-old boy visited the neuromuscular disease clinic of our institution with proximal muscle weakness and multiple contractures of the upper and lower limb joints. There was no significant family history. The patient presented with a waddling gait and Gower's sign. However, he could walk independently and go up the stairs with assistance. The manual muscle test showed grade 3/5 for proximal muscles and 4/5 for distal muscles. Whole-spine radiography revealed scoliosis with a Cobb's angle of 25°. According to laboratory tests, the patient's creatine phosphokinase (CPK) level increased to ∼10,000 U/L (reference range, <250 U/L). To check for DMD, a multiplex ligation-dependent probe amplification study of *DMD* was conducted using a kit (MRC Holland, the Netherlands) with two probes (P034-A2 and P035-A1). Results revealed duplications of exons 2–37, which is expected to be out-of-frame (**Figures 1A,B**). Hence, the proband was diagnosed with DMD. The carrier test result of his mother revealed normal *DMD* without any pathogenic variants (**Figure 1C**).

Based on physical examination, the patient showed facial dysmorphism with hypodontia, prominent supraorbital ridge, broad and depressed nasal ridge, and micrognathia. Other than muscular dystrophy, various features, such as multiple joint contractures and facial dysmorphism, were atypical manifestations of DMD. The patient received regular steroid and physical therapy. However, multiple joint contractures worsened over time, and 4 years after diagnosis, at 11 years of age, he started using a wheelchair. The patient was subsequently lost to follow-up.

After 3 years, another 13-year-old boy with an appearance similar to that of the current patient visited the neuromuscular disease clinic of our institution due to multiple contractures and facial dysmorphism. Using multigene panel sequencing for skeletal dysplasia, the patient was diagnosed with FMD1 caused by *FLNA* located at chromosome Xq28. The missense *FLNA* variant, which was previously reported as pathogenic variant was identified (NM_001110556.2: c.3557C>T /p.Ser1186Leu) (8, 9). Based on family history, the two children were identified as maternal cousins.

When the DMD patient was 15 years old, we called up the patient and requested him to visit our neuromuscular disease clinic to assess the pathogenic variant of *FLNA*. His joint contractures and scoliosis had worsened

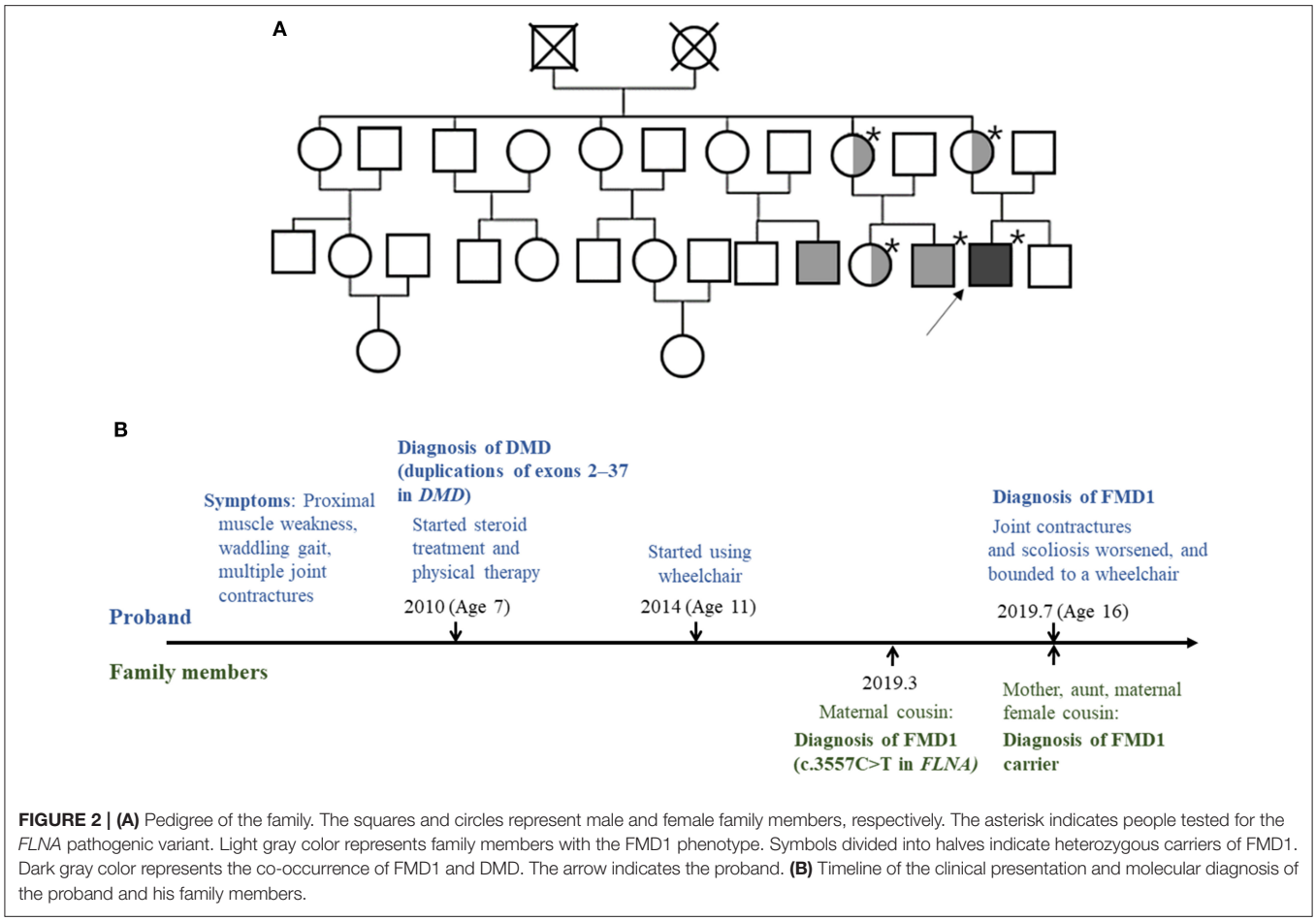

FIGURE 2 | (A) Pedigree of the family. The squares and circles represent male and female family members, respectively. The asterisk indicates people tested for the *FLNA* pathogenic variant. Light gray color represents family members with the FMD1 phenotype. Symbols divided into halves indicate heterozygous carriers of FMD1. Dark gray color represents the co-occurrence of FMD1 and DMD. The arrow indicates the proband. **(B)** Timeline of the clinical presentation and molecular diagnosis of the proband and his family members.

(Cobb's angle increased from 25° to 51°), and he was wheelchair-bound due to progressive weakness, joint contracture, and dyspnea. The strength of both shoulder girdles was graded 2/5; upper limbs, 3/5; proximal lower limbs, 2/5; and distal lower limbs, 3/5, and CPK level was 3,156 U/L.

The patient underwent a Sanger sequencing study for *FLNA*. This study revealed that he had a hemizygous missense variant (NM_001110556.2: c.3557C>T), which is the same variant observed in his cousin. Finally, the patient was diagnosed with FMD1 caused by *FLNA* missense variant (c.3557C>T) inherited from the asymptomatic maternal carrier and, coincidently, DMD caused by *de novo DMD* exons 2–37 duplications.

Through family testing, we found that the proband's mother, aunt, and female cousin also had the same pathogenic heterozygous variant of the *FLNA*. None of them showed definite phenotype of FMD1 (**Figures 2A,B**, **3**).

Since the patient's cousin had Chiari I malformation and syringomyelia, brain and whole-spine magnetic resonance imaging was conducted and Chiari I malformation was detected. Additionally, head computed tomography scan revealed craniosynostosis similar to his cousin.

DISCUSSION

Herein, we report a rare case of co-occurring DMD caused by *DMD* exons 2–37 duplications and FMD1 caused by *FLNA* pathogenic variant (NM_001110556.2: c.3557C>T/p.Ser1186Leu) in a patient. The patient presented with atypical DMD characteristics, such as severe scoliosis, joint contractures, facial dysmorphism, Chiari I malformation, and craniosynostosis. Joint contracture is a common complication of DMD; however, in this case, the patient had developed severe joint contracture at an early age (10).

There have been few cases in which DMD alone induced facial dysmorphism. In a previous case, one patient with DMD presented with facial dysmorphism and craniosynostosis. However, only *DMD* gene-targeted sequencing was conducted, and the presence of other genetic abnormalities was not validated (11). In our case, the presence of multiple contractures and facial dysmorphism, which are not indicative of DMD, was only explained after the diagnosis of FMD1.

This patient presented with two genetic diseases that cause musculoskeletal abnormalities. Hence, whether defective dystrophin and filamin A had interactive or synergic effects was not evaluated in our study but should be considered in the future.

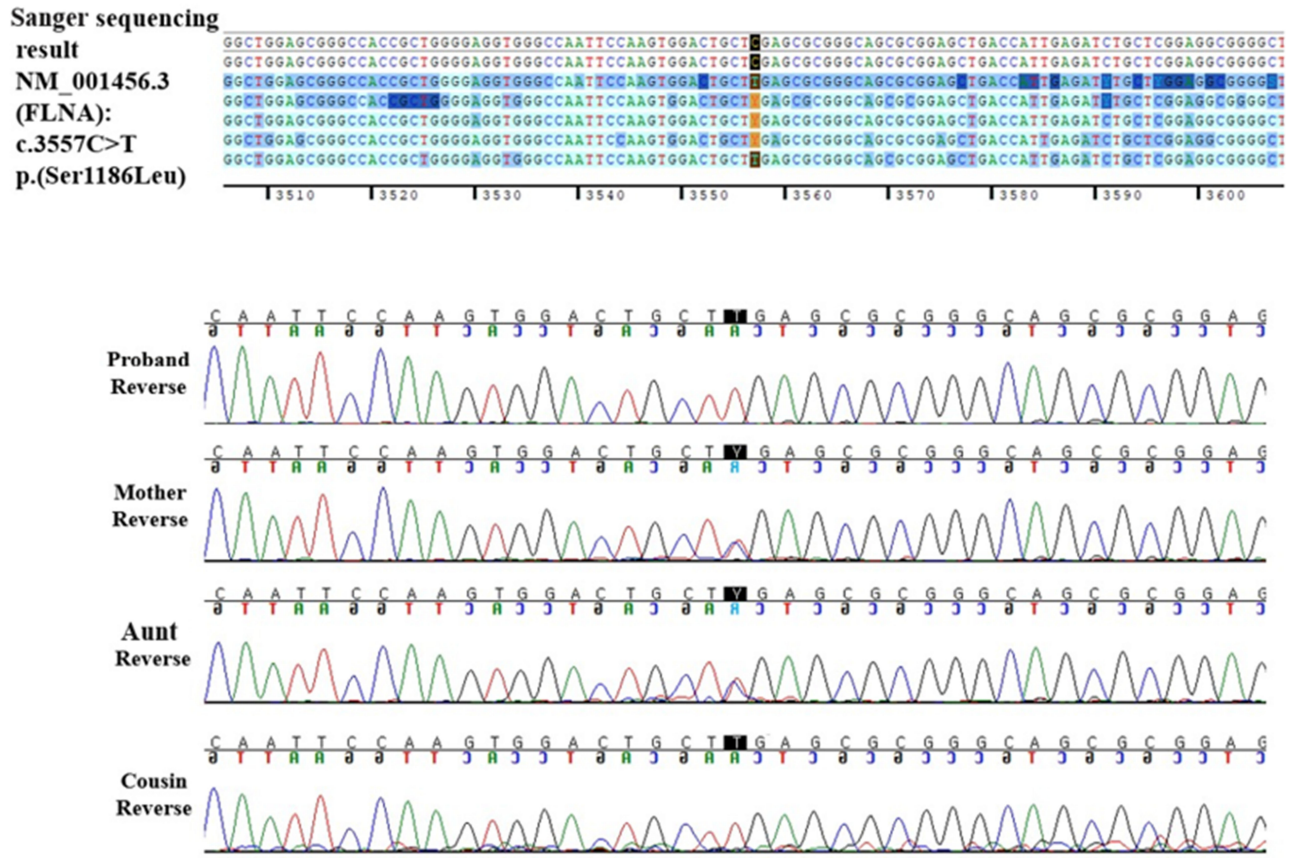

FIGURE 3 | *FLNA* reverse DNA sequencing chromatogram of the proband and his family.

DMD is an X-linked recessive inheritance disorder caused by pathogenic variants in *DMD* that encodes for dystrophin protein, which acts as a connector of the cytoskeleton of muscle fibers and extracellular matrix. These variants help in muscle fiber stabilization during muscle exertion. In the absence of normally functioning dystrophin, progressive muscular damage occurs and regeneration is restricted. Muscle fibers are subsequently transformed into fibrotic or adipose tissues, thus causing pseudohypertrophy (12). In DMD, musculoskeletal complications include progressive muscle degeneration and contracture, resulting in postural compensation or deformities including scoliosis (13). In the later stages, the involvement of cardiac and respiratory muscle becomes apparent. In general, patients require ventilation support during their 20s, and premature death usually occurs during their third or fourth decade of life (14, 15).

FMD1 is a rare genetic disease classified under otopalatodigital syndrome spectrum disorder. It is characterized by skeletal dysplasia, such as multiple joint contractures involving the fingers and/or toes, facial deformity, supraorbital hyperostosis, scoliosis, and sensorineural/conductive hearing loss. The facial features of FMD1 include prominent supraorbital ridge, hypertelorism, and micrognathia (8). In most cases, FMD1 is caused by single-base variants, and all pathogenic variants can maintain the reading frame (9). The *FLNA* comprises 48 exons encoding a 280 kDa filamin A protein. In humans, the filamins are a group of proteins comprising filamins A, B, and C. These proteins are involved in the internal networks of cytoskeleton and filamentous actin rearrangements in the networks in response to mechanical stress. It anchors various transmembrane proteins to the actin cytoskeleton and mediates the signaling processes. Furthermore, filamin A interacts with the glycoprotein-Ibα subunit of the von Willebrand factor receptor, which is associated with cytoskeletal rearrangements, and plays a role in blood vessel and blood clotting (16, 17). Further, filamin C and dystrophin protein were found to have an indirect interaction with each other. However, whether filamin A and dystrophin are correlated or have an interaction with each other is not elucidated (18). Therefore, from a molecular biologic aspect, the presence of these two diseases in one patient is not expected to exert a synergic effect. However, from a clinical aspect, the patient presented with an accelerated deterioration of function, such as gait disturbance, early wheelchair-bound status, severe joint contracture, and scoliosis. If the patient was diagnosed earlier, intensive rehabilitative intervention could have had a positive effect in this case.

TABLE 1 | Pathogenic variants simultaneously found in the X chromosome in patients with DMD.

References	Gender	*DMD* variant	Combined disease	Combined disease gene variant	Clinical manifestation
Takenaka et al. (20)	Male	Exons 46, 47, 50 deletions (inherited)	Fabry disease (inherited)	α-galactosidase A gene c.409delG	Gait disturbance, weakness, CPK↑
Jiang et al. (21)	Female (skewed X-inactivation)	Exons 30–43 deletions (inherited)	X-linked oculo-facio-cardio-dental syndrome (*de novo*)	*BCOR* gene c.1005delC	Muscular hypotonia, weakness, feeding difficulty, CPK↑, congenital anomalies (ASD, cataracts, dental and digital anomalies)
Strmecki et al. (22)	Male	Exons 45–52 deletions (*de novo*)	Hemophilia A (inherited)	Coagulation factor VIII (*F8* gene) Inv22 (distal/type I)	Weakness, CPK↑
Varma et al. (23)	Male	Exons 46–52 deletions (*de novo*)	X-linked myotubular myopathy (inherited)	*MTM1* gene c.1189dupT (p.Tyr397fs)	Weakness, contractures, poor respiratory effort, facial weakness, feeding difficulty
Kim et al. (current case)	Male	Exons 2–37 duplications (*de novo*)	Frontometaphyseal dysplasia 1 (inherited)	*FLNA* gene c.3557C>T (p.Ser1186Leu)	Weakness, gait disturbance, scoliosis, CPK↑, facial dysmorphism, contractures, short stature

CPK, creatine phosphokinase; ASD, atrial septal defect.

The current patient presented with duplications of exons 2–37 in *DMD*, which is an out-of-frame variant, and might have caused DMD (19). In addition, a hemizygous missense variant (NM_001110556.2: c.3557C>T /p.Ser1186Leu) in *FLNA* was previously considered pathogenic, thereby leading to a diagnosis of FMD1.

Until now, there are only a few cases of DMD wherein two or more pathogenic variants occurred simultaneously in the X chromosome. Previous studies have reported Fabry disease (Xq22.1), hemophilia A (Xq28), X-linked myotubular myopathy (Xq28), and oculofaciocardiodental syndrome (Xp11.4) (20–23) (**Table 1**). *DMD* is the largest human gene known to date, of which one of three pathogenic variants occurs as *de novo*. Hence, in some cases, DMD and other pathogenic variants can coexist in the X chromosome (24).

CONCLUSION

Here we report the co-occurrence of DMD and FMD1 in patient, which has not been previously reported to date. Both diseases showed musculoskeletal involvement and X-linked recessive inheritance. DMD occurred *de novo*, and it was incidentally found that FMD1 was a maternal inheritance. In rare cases, two or more genetic disorders can occur concurrently. Therefore, if one disease does not fully explain the patient's clinical features, an expanded genetic study is required to detect coincidental diseases.

DATA AVAILABILITY STATEMENT

The original contributions presented in the study are included in the article/**Supplementary Material**, further inquiries can be directed to the corresponding author.

ETHICS STATEMENT

The studies involving human participants were reviewed and approved by Institutional Review Board, Incheon St. Mary's Hospital. Written informed consent to participate in this study was provided by the participants' legal guardian/next of kin.

AUTHOR CONTRIBUTIONS

JK: acquisition of data, analysis and interpretation of data, and writing. D-WL: acquisition of data and critical revision of manuscript. J-HJ, MK, and JY: analysis and interpretation of data. D-HJ: study concept and design, acquisition of data, analysis and interpretation of data, study supervision, and critical revision of manuscript for intellectual content. All authors: contributed to the article and approved the submitted version.

SUPPLEMENTARY MATERIAL

The Supplementary Material for this article can be found online at: https://www.frontiersin.org/articles/10.3389/fped.2021.628190/full#supplementary-material

REFERENCES

1. Emery AE. Population frequencies of inherited neuromuscular diseases–a world survey. *Neuromuscul Disord.* (1991) 1:19–29. doi: 10.1016/0960-8966(91)90039-U
2. Koenig M, Hoffman EP, Bertelson CJ, Monaco AP, Feener C, Kunkel LM. Complete cloning of the Duchenne muscular dystrophy (DMD) cDNA and preliminary genomic organization of the DMD gene in normal and affected individuals. *Cell.* (1987) 50:509–17. doi: 10.1016/0092-8674(87)90504-6
3. Roberts RG, Gardner RJ, Bobrow M. Searching for the 1 in 2,400,000: a review of dystrophin gene point mutations. *Hum Mutat.* (1994) 4:1–11. doi: 10.1002/humu.1380040102
4. Sitnik R, Campiotto S, Vainzof M, Pavanello RC, Takata RI, Zatz M, et al. Novel point mutations in the dystrophin gene. *Hum Mutat.* (1997) 10:217–22. doi: 10.1002/(SICI)1098-1004(1997)10:3<217::AID-HUMU7>3.0.CO;2-F
5. Hu X, Ray PN, Murphy EG, Thompson M, Worton R. Duplicational mutation at the Duchenne muscular dystrophy locus: its frequency, distribution, origin, and phenotypegenotype correlation. *Am. J. Hum. Genet.* (1990) 46:682
6. Birnkrant DJ, Bushby K, Bann CM, Alman BA, Apkon SD, Blackwell A, et al. Diagnosis and management of Duchenne muscular dystrophy, part 2: respiratory, cardiac, bone health, and orthopaedic management. *Lancet Neurol.* (2018) 17:347–61. doi: 10.1016/S1474-4422(18)30025-5
7. *FLNA Gene*. Available online at: https://ghr.nlm.nih.gov/gene/FLNA (accessed July 13, 2020).
8. Robertson SP, Jenkins ZA, Morgan T, Ades L, Aftimos S, Boute O, et al. Frontometaphyseal dysplasia: mutations in FLNA and phenotypic diversity. *Am J Med Genet A*. (2006) 140:1726–36. doi: 10.1002/ajmg.a.31549
9. Robertson SP, Twigg SR, Sutherland-Smith AJ, Biancalana V, Gorlin RJ, Horn D, et al. Localized mutations in the gene encoding the cytoskeletal protein filamin A cause diverse malformations in humans. *Nat Genet.* (2003) 33:487–91. doi: 10.1038/ng1119
10. Emery AE, Muntoni F, Quinlivan RC. *Duchenne Muscular Dystrophy*. 4th ed. New York, NY: OUP Oxford (2015). p. 29–51.
11. Xu Y, Wang H, Xiao B, Wei W, Liu Y, Ye H, et al. Novel noncontiguous duplications identified with a comprehensive mutation analysis in the DMD gene by DMD gene-targeted sequencing. *Gene.* (2018) 645:113–8. doi: 10.1016/j.gene.2017.12.037
12. Verhaart IEC, Aartsma-Rus A. Therapeutic developments for Duchenne muscular dystrophy. *Nat Rev Neurol.* (2019) 15:373–86. doi: 10.1038/s41582-019-0203-3
13. Bushby K, Finkel R, Birnkrant DJ, Case LE, Clemens PR, Cripe L, et al. Diagnosis and management of Duchenne muscular dystrophy, part 2: implementation of multidisciplinary care. *Lancet Neurol.* (2010) 9:177–89. doi: 10.1016/S1474-4422(09)70272-8
14. Emery AE. The muscular dystrophies. *Lancet.* (2002) 359:687–95. doi: 10.1016/S0140-6736(02)07815-7
15. Van Ruiten H, Bushby K, Guglieri M. State of the art advances in Duchenne muscular dystrophy. *Eur. Med. J.* (2017) 2:90–9.
16. van der Flier A, Sonnenberg A. Structural and functional aspects of filamins. *Biochim Biophys Acta.* (2001) 1538:99–117. doi: 10.1016/S0167-4889(01)00072-6
17. Stossel TP, Condeelis J, Cooley L, Hartwig JH, Noegel A, Schleicher M, et al. Filamins as integrators of cell mechanics and signalling. *Nat Rev Mol Cell Biol.* (2001) 2:138–45. doi: 10.1038/35052082
18. Dalkilic I, Kunkel LM. Muscular dystrophies: genes to pathogenesis. *Curr Opin Genet Dev.* (2003) 13:231–8. doi: 10.1016/S0959-437X(03)00048-0
19. Ling C, Dai Y, Fang L, Yao F, Liu Z, Qiu Z, et al. Exonic rearrangements in DMD in Chinese Han individuals affected with Duchenne and Becker muscular dystrophies. *Hum Mutat.* (2020) 41:668–77. doi: 10.1002/humu.23953
20. Takenaka T, Sakuraba H, Hashimoto K, Fujino O, Fujita T, Tanaka H, et al. Coexistence of gene mutations causing Fabry disease and Duchenne muscular dystrophy in a Japanese boy. *Clin Genet.* (1996) 49:255–60. doi: 10.1111/j.1399-0004.1996.tb03783.x
21. Jiang YH, Fang P, Adesina AM, Furman P, Johnston JJ, Biesecker LG, et al. Molecular characterization of co-occurring Duchenne muscular dystrophy and X-linked oculo-facio-cardio-dental syndrome in a girl. *Am J Med Genet A.* (2009) 149A:1249–52. doi: 10.1002/ajmg.a.32863
22. Strmecki L, Hudler P, Benedik-Dolnicar M, Komel R. *De novo* mutation in DMD gene in a patient with combined hemophilia A and Duchenne muscular dystrophy. *Int J Hematol.* (2014) 99:184–7. doi: 10.1007/s12185-013-1488-4
23. Varma U, Mukherjee D, Hughes I, Sethuraman C, Kamupira S. X-linked myotubular myopathy and Duchenne muscular dystrophy in a preterm infant: a rare combination. *Pediatrics.* (2020) 146:e20182879. doi: 10.1542/peds.2018-2879
24. Cagliani R, Sironi M, Ciafaloni E, Bardoni A, Fortunato F, Prelle A, et al. An intragenic deletion/inversion event in the DMD gene determines a novel exon creation and results in a BMD phenotype. *Hum Genet.* (2004) 115:13–8. doi: 10.1007/s00439-004-1118-6

Conflict of Interest: The authors declare that the research was conducted in the absence of any commercial or financial relationships that could be construed as a potential conflict of interest.

frontiers in Genetics

ORIGINAL RESEARCH
published: 10 May 2021
doi: 10.3389/fgene.2021.661884

Clinical Efficiency of Non-invasive Prenatal Screening for Common Trisomies in Low-Risk and Twin Pregnancies

*Yanfei Xu[1], Pengzhen Jin[1], Yu Lei[2], Yeqing Qian[1,3], Yuqing Xu[1], Miaomiao Wang[1], Jinglei Jin[1], Yixuan Yin[4] and Minyue Dong[1,3,5]**

[1] Department of Reproductive Genetics, Women's Hospital, School of Medicine, Zhejiang University, Hangzhou, China, [2] Department of endocrinology, People's Hospital of Zhejiang Province, Hangzhou, China, [3] Key Laboratory of Reproductive Genetics, Ministry of Education (Zhejiang University), Hangzhou, China, [4] Prenatal Diagnosis Center, Hangzhou Women's Hospital, Hangzhou, China, [5] Key Laboratory of Women's Reproductive Health of Zhejiang Province, Hangzhou, China

To evaluate the clinical efficiency of non-invasive prenatal screening (NIPS) for fetal aneuploidies in low-risk and twin pregnancies, patients who received NIPS in a tertiary university hospital were enrolled, and their clinical data, NIPS results and pregnancy outcomes were collected. Patients were divided into singleton and twin pregnancies, and then those with singleton pregnancies were divided into low- and high-risk pregnancies. Sensitivity, specificity, positive predictive value (PPV) and negative predictive value (NPV) were estimated. Comparisons were made on the clinical efficiency of NIPS between singleton and twin pregnancies, as well as between low- and high-risk pregnancies. Of 66,172 patients enrolled, 59,962 were eligible for analysis. The sensitivity, specificity and NPV were ≥ 99% in singleton and twin pregnancies. The PPVs were 90.4, 56.6, and 13.0% in singleton pregnancies, while 100, 33.3, and 0% in twin pregnancies for trisomy 21 (T21), trisomy 18 (T18) and trisomy 13 (T13), respectively ($P > 0.05$ for all). The PPVs were 97.4 and 90.0% in high-risk pregnancies, while 78.6 and 16.7% in low-risk pregnancies for T21 and T18, respectively ($P < 0.05$ for all). In summary, the performance of NIPS in singleton pregnancies was similar to that in twin pregnancies. NIPS can be recommended for all pregnancies regardless of the risks.

Keywords: non-invasive prenatal screening, twin pregnancy, low-risk pregnancy, trisomy, clinical efficiency

OPEN ACCESS

Edited by:
María L. Couce, Complejo Hospitalario Universitario de Santiago, Spain

Reviewed by:
Yuan Gao, Shandong University, China
Avinash Vijay Dharmadhikari, Columbia University, United States

****Correspondence:***
Minyue Dong
dongmy@zju.edu.cn

Specialty section:
This article was submitted to Genetics of Common and Rare Diseases, a section of the journal Frontiers in Genetics

Received: *31 January 2021*
Accepted: *13 April 2021*
Published: *10 May 2021*

Citation:
Xu Y, Jin P, Lei Y, Qian Y, Xu Y, Wang M, Jin J, Yin Y and Dong M (2021) Clinical Efficiency of Non-invasive Prenatal Screening for Common Trisomies in Low-Risk and Twin Pregnancies. Front. Genet. 12:661884. doi: 10.3389/fgene.2021.661884

INTRODUCTION

In 1997, Lo et al. found the presence of fetal DNA in maternal plasma (Lo et al., 1997). Then cell-free DNA-based non-invasive prenatal screening (NIPS) has been established to detect fetal aneuploidies (Chiu et al., 2011; Ehrich et al., 2011; Palomaki et al., 2011, 2012; Bianchi et al., 2012; Norton et al., 2012). This technology has been widely used and benefited a lot of women (Chandrasekharan et al., 2014). Previous studies have shown that NIPS has high sensitivity and specificity in detecting common fetal trisomies (trisomies 21, 18, and 13) (Ehrich et al., 2011; Bianchi et al., 2012; Porreco et al., 2014; Gil et al., 2017). A recent meta-analysis estimated that the sensitivity of NIPS was more than 99% for trisomy 21 (T21), and more than 97% for trisomy 18 (T18) and trisomy 13 (T13), with a high specificity of more than 99% for these trisomies, even for low-risk pregnancies

(Rezaei et al., 2019). The positive predictive values (PPV) of NIPS was higher for T21 and T18 than for T13, but PPVs vary in different studies (Chiu et al., 2011; Bianchi et al., 2014; Norton et al., 2015; Petersen et al., 2017; van der Meij et al., 2019). Both the ACMG guideline in 2016 and the updated ACOG guideline in 2020 recommend NIPS as the most sensitive and specific screening for T21, T18 and T13 (Gregg et al., 2016; Rose et al., 2020).

However, most studies focused on the NIPS in singleton and high-risk pregnancies, such as pregnancies of advanced maternal age and high-risk standard screening (Chiu et al., 2011; Palomaki et al., 2011, 2012; Norton et al., 2012). The updated ACOG guideline recommends NIPS be offered to all pregnant women regardless of maternal age or risk. Besides, it suggests NIPS be performed in twin pregnancies, and its performance for T21 was encouraging (Rose et al., 2020). However, the performances of NIPS in low-risk and twin pregnancies were not well understood up to now because of the limited positive cases of aneuploidies, especially the limited positive cases of T18 and T13 in low-risk and twin pregnancies. Meanwhile, few studies have compared the low-risk with the high-risk pregnancies on the detective efficiency of NIPS, and a similar problem exists in singleton and twin pregnancies. Thus, the clinical efficacy research of NIPS in low-risk and twin pregnancies is of great significance for the effective application of NIPS at the present stage.

In the current investigation, 66,172 pregnant women were enrolled in a single-centered tertiary university hospital. The first objective was to evaluate the clinical efficiency of NIPS for fetal T21, T18, and T13 in the overall patients. The second objective was to compare the performance between singleton and twin pregnancies, as well as between high- and low-risk pregnancies. This study will contribute to a more comprehensive understanding of the clinical efficiency of NIPS and reduce unnecessary worries for expanding the scope of application.

MATERIALS AND METHODS

Participants and Data Collection

A retrospective single-centered study was conducted in Women's Hospital, Zhejiang University School of Medicine, and 66,172 pregnant women who received NIPS were enrolled from February 2, 2015, to December 31, 2019. This study was approved by the Ethics Committee of Women's Hospital, Zhejiang University School of Medicine, and all the patients provided their informed consent.

Clinical counseling was provided for all the patients before NIPS was provided. Patients with low-risk NIPS were advised to continue the routine prenatal care, and those with high-risk were advised to receive genetic counseling and invasive prenatal diagnosis. The diagnosis of T21, T18, and T13 depends on the karyotyping and physical examination of the newborn. Pregnancy outcomes of all cases were followed up.

The clinical data included gestational age at sampling, maternal age at the expected date of delivery, fetal numbers, results of standard screening, ultrasonography, NIPS risks, karyotypes and pregnancy outcomes, etc. The standard screening included the first or second-trimester screening or the combined screening. The first-trimester screening included the measurement of serum biomarkers with or without nuchal translucency (NT). The abnormalities of ultrasound included: (1) micro-anomalies or soft markers, such as increased NT ($\geq$2.5 mm), fetal choroid plexus cysts, echogenic intracardiac focus (EIF), nasal bone hypoplasia, nasal bone absence, polyhydramnios, oligohydramnios and single umbilical artery (SUA); (2) structural abnormalities, such as fetal hydrops fetalis, cystic hygroma and urinary tract anomalies. A full-time staff followed up pregnancy outcomes, and the information was obtained by questionnaires or phone calls after delivery.

Study Design

In the primary analysis, sensitivity, specificity, PPV and negative predictive value (NPV) were estimated overall. Patients were divided into two groups: singleton and twin pregnancies, and NIPS performance was compared.

In the secondary analysis, singleton pregnancies were divided into three cohorts based on maternal age, results of standard screening and ultrasonography. In each cohort, patients were further divided into high- and low-risk pregnancies. Those with advanced maternal age, high risk of standard screening and abnormal ultrasonography were incorporated into the high-risk pregnancies, and those without the information above were the low-risk pregnancies. The performance was evaluated and comparisons were made.

NIPS

The DNA extraction, library construction and sequencing were performed according to the protocol of the Human Molecular Genetics Guidelines (Jiang et al., 2012; Chen et al., 2013). Two hundred microliter maternal plasma was used for cell-free fetal DNA extraction by BGISP-300 (BGI, Shenzhen, China) and Nucleic Acid Extraction Kit (BGI, Shenzhen, China). End-repair was performed by adding end-repair enzymes, and PCR was used to amplify DNA. The DNA amplification products were quantified by Qubit® 2.0 (Life Tech, Invitrogen, United States) using Qubit™ dsDNA HS Assay Kits (Life Tech, Invitrogen, United States). The volume was calculated according to the concentration of each sample, and samples of the same mass were mixed by pooling. The DNA double strands were thermally denatured after pooling, and then the cyclic buffer and the ligase were added to make DNA circles by the cyclization reaction. DNA circles were used to make DNBs by rolling circle replication (RCR). The concentration of DNBs was quantified by Qubit 2.0 using Qubit™ ssDNA Assay Kits (Life Tech, Invitrogen, United States) and the DNBs concentration in the range of 8–40 ng/μL was considered as appropriate concentration. The DNBs were loaded onto chips and sequenced on the BGISEQ-500 sequencing platform (BGI, Shenzhen, China). Any sample that failed to meet the quality control criteria (**Supplementary Table 1**) was reported as a detection failure.

The sequence from NGS was compared with the reference sequence map of the human genome, and the percentage of each chromosome was calculated by Illumina Sequencing Analysis

Viewer1.9.1 software. The Z value was used to evaluate the actual disease situation of the samples.

Karyotyping

Amniotic fluid or umbilical cord blood samples were collected. The karyotype was analyzed according to the standard of ISCN (2016) through the process of standardized cell culture, filmmaking and G-banding.

Statistical Analysis

The SPSS statistical software package (version 25.0) was used for statistical analysis. For the analysis of sensitivity, specificity, PPV, NPV and the corresponding 95% confidence intervals (CI), Non-parametric Test of One Sample and the Clopper–Pearson method was used. Chi-square test of Crosstabulation, Pearson Chi-Square or Fisher's Exact Test were used where appropriate. A *P*-value of less than 0.05 was considered to be of statistical significance.

RESULTS

Study Participants

Among 66,172 enrolled patients, 4,716 (7.1%) were excluded because of the drop in follow-up. 1,494 (2.3%) were excluded due to the following situations: (1) missing the data of pregnancy outcomes; (2) missing the data of fetal karyotypes; (3) twin pregnancies but one fetus without the data of pregnancy outcomes or karyotypes; (4) newborns died without karyotypes or physical examinations. 59,962 patients were included for analysis (**Figure 1**).

Most previous studies focused on the performance of NIPS in high-risk pregnancies. To respond to the updated ACOG guideline in 2020, we focused on low-risk pregnancies. The proportion of high- and low-risk pregnancies varies with the year was shown in **Figure 2**. High-risk pregnancies had one of the following factors: advanced maternal age, high risk of standard screening, abnormal ultrasonography and personal or family history of aneuploidy. Low-risk pregnancies had none of

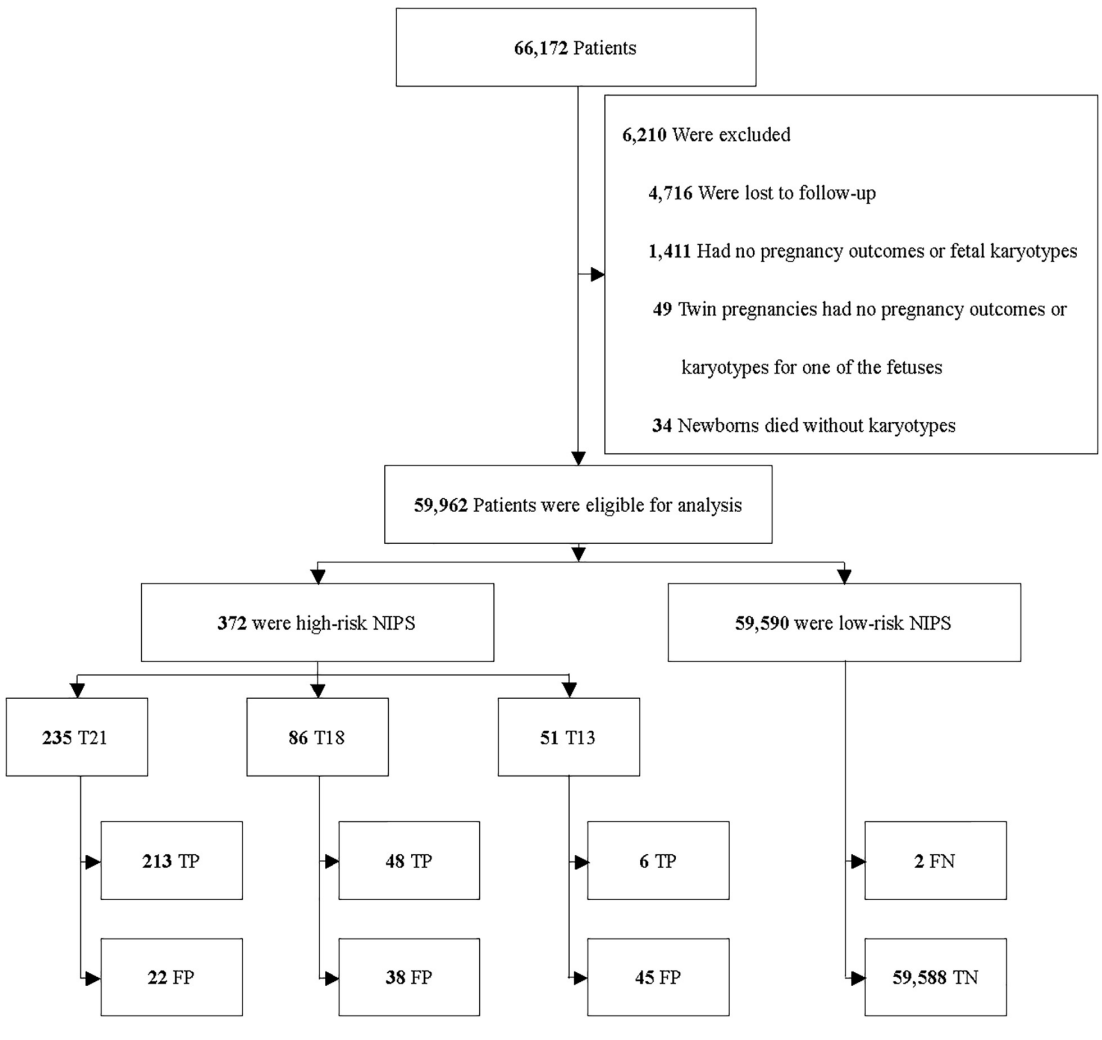

FIGURE 1 | Enrollment and outcomes.

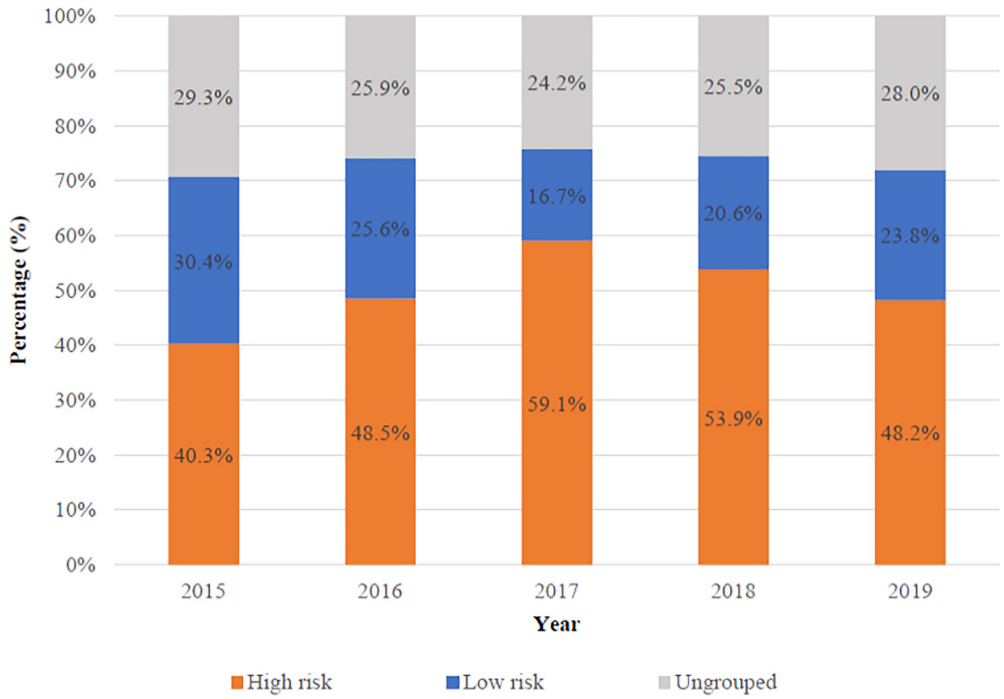

FIGURE 2 | The proportion of high- and low-risk pregnancies varies with the year.

the high-risk factors above. There were 30,405 (50.7%) high-risk and 13,731 (22.9%) low-risk patients in all 59,962 patients, respectively. Besides, 15,826 (26.4%) patients could not be grouped because of missing the complete standard screening data, ultrasonography, or information of maternal age.

The clinical characteristics were presented in **Table 1**. The mean maternal age was 32 years old (range 15–60) at delivery, and the mean gestational age was 17^{+} weeks (range 12–37.4) at sampling. In all, 892 (1.5%) patients underwent karyotyping. Among them, 10 were postnatal testing. For the remaining patients, the pregnancy outcomes were based on the physical examinations of the newborns.

Among 59,962 patients, 269 (1 in 223) carried fetuses of aneuploidies that were confirmed by karyotyping. Among them, 215 were T21, 48 were T18 and six were T13, with a prevalence of 1 in 279 for T21, 1 in 1,249 for T18 and 1 in 9,994 for T13, respectively.

Primary Analysis

Overall Performance

Among the 59,962 patients, 213 were true positive (TP), 22 were false positive (FP) and two were false negative (FN) for T21; 48 were TP, 38 were FP and none was FN for T18; six were TP, 45 were FP and none was FN for T13. The estimated sensitivity, specificity, PPV and NPV were listed in **Table 2**.

Performance in Singleton and Twin Pregnancies

Among the 57,563 women with singleton pregnancies, 206 were TP, 22 were FP and two were FN for T21; 47 were TP, 36 were FP and none was FN for T18; six were TP, 40 were FP and none was FN for T13. Among the 2,399 women with twin pregnancies, seven were TP, none was FP or FN for T21; one was TP, two were FP and none was FN for T18; none was TP, five were FP and none was FN for T13. The detective efficiency and comparisons

TABLE 1 | Clinical characteristics.

Characteristics	Value
No.	59,962
Maternal age (range), years	32 (15–60)
Maternal age < 35 years, no. (%)	33,246 (55.4)
Maternal age ≥ 35 years, no. (%)	22,777 (38.0)
Gestational age (range), weeks	17^{+} (12–37.4)
First trimester (12–13.9 weeks), no. (%)	7,877 (13.1)
Second trimester (14–27.9 weeks), no. (%)	45,087 (75.2)
Third trimester (28–37.4weeks), no. (%)	410 (0.7)
Singleton, no. (%)[§]	57,563 (96.0)
Twin, no. (%)	2,399 (4.0)
IVF-ET, no. (%)	3,951 (6.6)
Spontaneous, no. (%)	49,389 (82.4)
Standard screening for T21 and T18, no. (%)	20,330 (33.9)
High risk	5,373 (9.0)
Low risk	14,957 (24.9)
Abnormal ultrasonography, no. (%)	2,741 (4.6)
Personal or family history of aneuploidy, no. (%)	148 (0.2)
Karyotype analysis, no. (%)	892 (1.5)

[§]145 patients had vanished twin syndromes; IVF-ET, in vitro fertilization and embryo transfer.

TABLE 2 | Overall performance.

NIPS	TP	FP	TN	FN	Sensitivity	Specificity	PPV	NPV
	N				%, (95% CI)			
T21	213	22	59,725	2	99.1 (96.7–99.9)	100 (99.9–100)	90.6 (86.2–94.0)	100 (100–100)
T18	48	38	59,876	0	100 (92.6–100)	99.9 (99.9–100)	55.8 (44.7–66.5)	100 (100–100)
T13	6	45	59,911	0	100 (54.1–100)	99.9 (99.9–99.9)	11.8 (4.4–23.9)	100 (100–100)

PPV, positive predictive value; NPV, negative predictive value.

between the two groups were listed in **Table 3**. Except for the specificity of T13 ($P = 0.03$), there was no statistical difference ($P > 0.05$ for all).

Secondary Analysis

About 96.0% (57,563 in 59,962) of women were singleton, and 97.0% (261 in 269) of T21, T18 and T13 were detected in singleton pregnancies. Of the three cohorts of maternal age, standard screening and ultrasonography in singleton pregnancies, the detective efficiency was estimated and comparisons were made on the clinical efficiency between low- and high-risk pregnancies (**Table 4**).

TABLE 3 | NIPS performance in twin pregnancies.

NIPS	Singleton pregnancies	Twin pregnancies	*P*-value
No.	57,563	2,399	
T21			
TP (n)	206	7	
FP (n)	22	0	
TN (n)	57,333	2,392	
FN (n)	2	0	
Sensitivity,%, (95% CI)	99.0 (96.6–99.9)	100 (59.0–100)	1.00
Specificity,%, (95% CI)	100 (99.9–100)	100 (99.8–100)	1.00
PPV,%, (95% CI)	90.4 (85.8–93.9)	100 (59.0–100)	1.00
NPV,%, (95% CI)	100 (100–100)	100 (99.8–100)	1.00
T18			
TP (n)	47	1	
FP (n)	36	2	
TN (n)	57,480	2,396	
FN (n)	0	0	
Sensitivity,%, (95% CI)	100 (92.5–100)	100 (2.5–100)	*
Specificity,%, (95% CI)	99.9 (99.9–100)	99.9 (99.7–100)	0.66
PPV,%, (95% CI)	56.6 (45.3–67.5)	33.3 (0.8–90.6)	0.58
NPV,%, (95% CI)	100 (100–100)	100 (99.8–100)	*
T13			
TP (n)	6	0	
FP (n)	40	5	
TN (n)	57,517	2,394	
FN (n)	0	0	
Sensitivity,%, (95% CI)	100 (54.1–100)	Cannot be calculated	*
Specificity,%, (95% CI)	99.9 (99.9–100)	99.8 (99.5–99.9)	0.03
PPV,%, (95% CI)	13.0 (4.9–26.3)	0 (0–52.2)	1.00
NPV,%, (95% CI)	100 (100–100)	100 (99.8–100)	*

**The paired groups could not make comparisons.*

The Cohort of Maternal Age

Among the 31,359 patients who were under 35 years old at delivery (low-risk), 101 were TP, 10 were FP and one was FN for T21; 22 were TP, 23 were FP and none was FN for T18; three were TP, 25 were FP and none was FN for T13. Among the 22,324 patients who were 35 years old or older (high-risk), 96 were TP, ten were FP and one was FN for T21; 23 were TP, 12 were FP and none was FN for T18; two were TP, 13 were FP and none was FN for T13. There was no significant difference in detective efficiency between the two groups ($P > 0.05$ for all).

The Cohort of Standard Screening

Among the 14,902 patients who were at low risk of standard screening, 22 were TP, six were FP and one was FN for T21; three were TP, 15 were FP and none was FN for T18; none was TP, ten were FP and none was FN for T13. The incidence was 0.2% (23/14,902) for T21, 0.02% (3/14,902) for T18 and 0% (0/14,902) for T13, respectively. Among the 5,362 patients who were at high risk of standard screening, 38 were TP, one was FP and none was FN for T21; nine were TP, one was FP and none was FN for T18; one was TP, two were FP and none was FN for T13. The incidence was 0.7% (38/5,362) for T21, 0.2% (9/5,362) for T18 and 0.02% (1/5,362) for T13, respectively. The incidence of T21 and T18 was significantly higher in the high-risk than in the low-risk group ($P < 0.01$ for both). Except for the PPV of T21 ($P = 0.02$) and T18 ($P \leq 0.01$), there was no statistical difference ($P > 0.05$) between the two groups.

The Cohort of Ultrasonography

Among the 51,080 patients who had normal ultrasonography (low-risk), 151 were TP, 19 were FP and none was FN for T21; 35 were TP, 35 were FP and none was FN for T18; three were TP, 32 were FP and none was FN for T13. The incidence was 0.3% (151/51,080) for T21, 0.1% (35/51,080) for T18 and 0.01% (3/51,080) for T13, respectively. Among the 2,606 patients who had abnormal ultrasonography (high-risk), 46 were TP, one was FP and two were FN for T21; 11 were TP, none was FP and none was FN for T18; two were TP, six were FP and none was FN for T13. The incidence was 1.8% (48/2,606) for T21, 0.4% (11/2,606) for T18 and 0.1% (2/2,606) for T13, respectively. The incidence of T21, T18 and T13 was higher in the high-risk than in the low-risk group ($P < 0.01$ for T21 and T18; $P = 0.02$ for T13). Except for the NPV of T21 ($P \leq 0.01$), PPV of T18 ($P \leq 0.01$) and specificity of T13 ($P \leq 0.01$), there was no statistical difference ($P > 0.05$) between the two groups.

TABLE 4 | NIPS performance in singleton pregnancies at different risks.

NIPS	Maternal age (years)		Standard screening$^{\Phi}$		Ultrasonography		Low-risk pregnancies$^{\Psi}$
	< 35	≥ 35	Low-risk	High-risk	Normal	Abnormal	
No.	31,359	22,324	14,902	5,362	51,080	2,606	13,731
T21							
TP	101	96	22	38	151	46	19
FP	10	10	6	1	19	1	6
TN	31,247	22,217	14,873	5,323	50,910	2,559	13,706
FN	1	1	1	0	0	2	0
Sensitivity,%, (95% CI)	99.0 (94.7–100)	99.0 (94.4–100)	95.7 (78.1–99.9)	100 (90.7–100)	100 (97.6–100)	95.8 (85.7–99.5)	100 (82.4–100)
Specificity,%, (95% CI)	100 (99.9–100)	100 (99.9–100)	100 (99.9–100)	100 (99.9–100)	100 (99.9–100)	100 (99.8–100)	100 (99.9–100)
PPV,%, (95% CI)	91.0 (84.1–95.6)	90.6 (83.3–95.4)	78.6 (59.0–91.7)	97.4 (86.5–99.9)¶	88.8 (83.1–93.1)	97.9 (88.7–99.9)	76.0 (54.9–90.6)
NPV,%, (95% CI)	100 (100–100)	100 (100–100)	100 (100–100)	100 (99.9–100)	100 (100–100)	99.9 (99.7–100)‡	100 (100–100)
T18							
TP	22	23	3	9	35	11	3
FP	23	12	15	1	35	0	15
TN	31,314	22,289	14,884	5,352	51,010	2,595	13,713
FN	0	0	0	0	0	0	0
Sensitivity,%, (95% CI)	100 (84.6–100)	100 (85.2–100)*	100 (29.2–100)	100 (66.4–100)*	100 (90.0–100)	100 (71.5–100)*	100 (29.2–100)
Specificity,%, (95% CI)	99.9 (99.9–100)	99.9 (99.9–100)	99.9 (99.8–99.9)	100 (99.9–100)	99.9 (99.9–100)	100 (99.9–100)	99.9 (99.8–99.9)
PPV,%, (95% CI)	48.9 (33.7–64.2)	65.7 (47.8–80.9)	16.7 (3.6–41.4)	90.0 (55.5–99.7)‡	50.0 (37.8–62.2)	100 (71.5–100)‡	16.7 (3.6–41.4)
NPV,%, (95% CI)	100 (100–100)	100 (100–100)*	100 (100–100)	100 (99.9–100)*	100 (100–100)	100 (99.9–100)*	100 (100–100)
T13							
TP	3	2	0	1	3	2	0
FP	25	13	10	2	32	6	9
TN	31,331	22,309	14,892	5,359	51,045	2,598	13,722
FN	0	0	0	0	0	0	0
Sensitivity,%, (95% CI)	100 (29.2–100)	100 (15.8–100)*	Cannot be calculated	100 (2.5–100)*	100 (29.2–100)	100 (15.8–100)*	Cannot be calculated
Specificity,%, (95% CI)	99.9 (99.9–99.9)	99.9 (99.9–100)	99.9 (99.9–100)	100 (99.9–100)	99.9 (99.9–100)	99.8 (99.5–99.9)‡	99.9 (99.9–100)
PPV,%, (95% CI)	10.7 (2.3–28.2)	13.3 (1.7–40.5)	0 (0–30.8)	33.3 (0.8–90.6)	8.6 (1.8–23.1)	25.0 (3.2–65.1)	0 (0–33.6)
NPV,%, (95% CI)	100 (100–100)	100 (100–100)*	100 (100–100)	100 (99.9–100)*	100 (100–100)	100 (99.9–100)*	100 (100–100)

*The comparisons were made between the paired groups on the sensitivity, specificity, PPV and NPV. The P-values (two-sided) were marked if there was a statistical significance; $^{\Phi}$the cut-off value was < 1/270 for T21 and < 1/350 for T18 in the low-risk group; the cut-off value was ≥ 1/270 for T21 and ≥ 1/350 for T18 in the high-risk group; $^{\Psi}$patients had no high-risk factors, including maternal age, standard screening, ultrasonography and personal or family history of aneuploidy simultaneously; ¶ P < 0.05; ‡P < 0.01; *the paired groups could not make comparisons.*

Performance in the Low-Risk Pregnancies

Among the 13,731 patients without any high-risk factors, 19 were TP, six were FP and none was FN for T21; 3 were TP, 15 were FP and none was FN for T18; none was TP, nine were FP, and none was FN for T13.

False-Negative Cases

There were two false-negative cases of singleton pregnancies. For case 1, the woman was 29 years old with a body mass index (BMI) of 27.3 and a normal karyotype. She had a low-risk standard screening. NIPS was conducted at the gestational age of 13 weeks. The fetal fraction of DNA was unknown. For case 2, the woman was 39 years old with a BMI of 24.8 and a normal karyotype. NIPS was conducted at the gestational age of 13^{+} weeks. The fetal fraction of DNA was 7%. No other high-risk factors were found before the screening except for the increased NT (3 mm for case 1 and 7.1 mm for case 2). It was confirmed that the karyotype of case 1 was 47, XX, + 21(15)/46, XX(85). Case 2 underwent the prenatal diagnosis because of the abnormal ultrasonography of hydroncus and complete cardiac cushion defect, and the confirmed karyotype was 47, XN, +21.

DISCUSSION

In this retrospectively single-centered study, we found that NIPS had high sensitivity, specificity and NPV for detecting common

fetal trisomies in pregnancies with all risk levels, which was similar to a multicenter prospective study in China (Zhang et al., 2015). The PPV of NIPS was highest for T21 (90.6%), moderate for T18 (55.8%), and relatively low for T13 (11.8%). Our study included singleton and twin pregnancies, as well as pregnancies of all risk levels. We found that the performance of NIPS in singleton pregnancies was similar to that in twin pregnancies. With the higher incidence of T21 and T18 in high-risk pregnancies, the PPV was higher in high-risk than in low-risk pregnancies, but the high sensitivity, specificity and NPV were shown in both high- and low-risk pregnancies. Two false-negative cases of T21 were identified in pregnancies with abnormal ultrasonography, indicating that the pregnancies with abnormal ultrasonography should receive the prenatal diagnosis. The confirmed mosaic T21 indicates that fetal mosaicism is an important cause of false-negative NIPS.

In the current study, the high-risk patients were the main population for NIPS, indicating that NIPS has mainly been applied for or chosen by high-risk pregnant women, and this is inconsistent with the 2020 ACOG guidelines. One reason for this might be that patients who were at high risk would like to choose the NIPS first. The second reason might be the marked increase in pregnant women with advanced maternal age due to the two-child policy in China (Tian et al., 2020). NIPS had a similar performance on sensitivity, specificity, PPV and NPV in different maternal ages in the current observation, and it was consistent with a previous report, but they only analyzed the sensitivity (Dar et al., 2014).

Generally, the incidence of fetal trisomies was higher in the high-risk than in the low-risk pregnancies (Nicolaides et al., 2012). In our study, the incidence of fetal T21 was higher in the high-risk than in the low-risk standard screening, and the same was found for T18 in standard screening and ultrasonography cohorts. The higher incidence might explain the higher PPV in high-risk pregnancies because the PPV is associated with the number of positives cases in the population (Neufeld-Kaiser et al., 2015; Wang et al., 2015). In our study, the PPVs for T21, T18, and T13 were lower than a multicenter prospective study in China (Zhang et al., 2015), and lower than a national study in the Netherlands in which the PPV was 96% for T21, 98% for T18 and 53% for T13, respectively (van der Meij et al., 2019). The possible reason is that the first study was performed begin 2012 when the enrolled cases were mainly high-risk pregnancies. Therefore, they had a higher incidence of aneuploidies (1/155, 1/663, and 1/5,121 for T21, T18, and T13, respectively) and higher PPVs. The second study had a higher follow-up rate than ours, especially for cases with a high-risk NIPS. While in our cohort, some cases that had a high-risk NIPS rejected karyotyping or were lost to follow-up, and these cases might carry fetal trisomies. Considering those, the incidence of trisomies in our cohort may be lower than it was, so as PPV. Even though the higher PPV in high-risk pregnancies, we could not directly conclude that NIPS performs better in high-risk pregnancies because the ability of the test is determined by the precision of the technology and fetal fractions in the maternal blood rather than the incidence of trisomies in the population (Ashoor et al., 2012; Nicolaides et al., 2012). Additionally, the high specificity and NPV in each group of the three cohorts as well as in low-risk pregnancies showed the excellent ability of NIPS in excluding the unaffected pregnancies at any risk levels.

Herein, we proved the high sensitivity of NIPS in singleton and twin pregnancies, which is similar to previous reports (Gil et al., 2015, 2017). Due to the similar performance of NIPS in twin and singleton pregnancies (Fosler et al., 2017; Niemchak et al., 2020), some researchers considered that it could be used as a first-line screening in twin pregnancies (Le Conte et al., 2018; Yu et al., 2019). However, on account of the limited cases of trisomies in twin pregnancies, especially T18 and T13, the performance of NIPS may be unrepresentative and it needs to be further evaluated (Gil et al., 2019).

Two cases of false-negative T21 were identified in pregnancies with abnormal ultrasonography, and it lowed the NPV in this population. These discordant results highlight the irreplaceable status of early ultrasound in prenatal screening strategies (Hui et al., 2017), and NIPS is not a diagnostic test with inevitable false-positive and false-negative results (Allyse and Wick, 2018). More importantly, for those with abnormal ultrasonography, prenatal diagnosis instead of NIPS is essential, which has been issued in a previous study (Beulen et al., 2017), and it has been reported that the rate of pathogenic chromosome abnormalities missed by NIPS in the population of abnormal ultrasonography was 8% (Benachi et al., 2015), which was higher than ours (4%), but we only estimated the common trisomies. Causes of false-negative NIPS include low fetal fraction, which is caused by maternal obesity, multiple gestations causing low fetal fraction per fetus, maternal medical condition or treatment affecting the quality of circulating DNA, certain fetal chromosomal aneuploidies and confined placental mosaicism (Bianchi and Chiu, 2018). In this study, fetal mosaicism was confirmed by the karyotyping, causing the false-negative NIPS of case 1, and a similar finding has been reported in another study (Grati et al., 2014). For case 2, the fetal fraction was 7%, and it was a singleton pregnancy with a BMI of 24.8 and a normal karyotype. Meanwhile, there was no maternal medical condition or treatment during that time. A similar finding has been reported in an obvious study in which placental samples of two false-negative cases of T18 were obtained and both showed low-level confined placental mosaicism of T18 (Zhang et al., 2015). So, confined placental mosaicism may be the cause of false-negative NIPS of case 2.

There are several strengths in this study. Firstly, we assessed the performance of NIPS for common trisomies in a large population with different risk levels. Secondly, we make comparisons of singleton and twin pregnancies and confirmed a similar performance. Thirdly, we make comparisons of low- and high-risk populations in singleton pregnancies, and in which, the analysis was based on a single cohort of maternal age, conventional Down screening, or ultrasonography instead of the combined risk factors (Zhang et al., 2015). This study is the first large-scale retrospective study to assess the performance of NIPS in twin and low-risk pregnancies since the publication of the updated ACOG guideline.

There are also limitations in our study. Firstly, more than 4,400 patients lack information on maternal age, and some did not receive standard and ultrasound screening. So, we could not assess the risk levels of aneuploidy for these patients

accurately. Secondly, we did not enroll cases that had no-call NIPS results and cases that had intrauterine fetal demise or selective termination of pregnancy, but they may be high risk for aneuploidy (Norton et al., 2015). From this point of view, our results may be little different from reality.

CONCLUSION

NIPS has excellent clinical efficiency for common fetal trisomies in the overall patients at different risks, and its performance in singleton pregnancies was similar to that in twin pregnancies. However, NIPS cannot replace the invasive prenatal diagnosis, and fetuses with abnormal ultrasonography should undergo prenatal diagnosis.

DATA AVAILABILITY STATEMENT

The datasets presented in this study can be found in online repositories. The names of the repository/repositories and accession number(s) can be found below: doi: 10.6084/m9.figshare.14407616.

ETHICS STATEMENT

This study was approved by the Ethics Committee of Women's Hospital, Zhejiang University School of Medicine, and all the patients provided their informed consent.

AUTHOR CONTRIBUTIONS

MD and YaX: conception and designing. YaX: statistical analysis and manuscript writing. MD: supervising and manuscript revising. All authors collected the data and approved the final version of the manuscript.

FUNDING

This research was funded by the National Key Research and Development Program of China (2016YFC1000703, and 2018YFC1004900) and the Key Research and Development Program of Zhejiang Province (2019C03025).

ACKNOWLEDGMENTS

We wish to thank Jiong Gao of BGI, who made suggestions and helped revise the manuscript on the manuscript drafting stage.

SUPPLEMENTARY MATERIAL

The Supplementary Material for this article can be found online at: https://www.frontiersin.org/articles/10.3389/fgene.2021.661884/full#supplementary-material

REFERENCES

Allyse, M. A., and Wick, M. J. (2018). Noninvasive prenatal genetic screening using cell-free DNA. *JAMA* 320, 591–592.

Ashoor, G., Syngelaki, A., Wagner, M., Birdir, C., and Nicolaides, K. H. (2012). Chromosome-selective sequencing of maternal plasma cell-free DNA for first-trimester detection of trisomy 21 and trisomy 18. *Am. J. Obstet. Gynecol.* 206:322.e1–5.

Benachi, A., Letourneau, A., Kleinfinger, P., Senat, M. V., Gautier, E., Favre, R., et al. (2015). Cell-free DNA analysis in maternal plasma in cases of fetal abnormalities detected on ultrasound examination. *Obstet. Gynecol.* 125, 1330–1337. doi: 10.1097/aog.0000000000000874

Beulen, L., Faas, B. H. W., Feenstra, I., Van Vugt, J. M. G., and Bekker, M. N. (2017). Clinical utility of non-invasive prenatal testing in pregnancies with ultrasound anomalies. *Ultrasound Obstet. Gynecol.* 49, 721–728. doi: 10.1002/uog.17228

Bianchi, D. W., and Chiu, R. W. K. (2018). Sequencing of circulating cell-free DNA during pregnancy. *N. Engl. J. Med.* 379, 464–473. doi: 10.1056/nejmra1705345

Bianchi, D. W., Parker, R. L., Wentworth, J., Madankumar, R., Saffer, C., Das, A. F., et al. (2014). DNA sequencing versus standard prenatal aneuploidy screening. *N. Engl. J. Med.* 370, 799–808. doi: 10.1056/nejmoa1311037

Bianchi, D. W., Platt, L. D., Goldberg, J. D., Abuhamad, A. Z., Sehnert, A. J., Rava, R. P., et al. (2012). Genome-wide fetal aneuploidy detection by maternal plasma DNA sequencing. *Obstet. Gynecol.* 119, 890–901. doi: 10.1097/aog.0b013e31824fb482

Chandrasekharan, S., Minear, M. A., Hung, A., and Allyse, M. (2014). Noninvasive prenatal testing goes global. *Sci. Transl. Med.* 6:231fs15. doi: 10.1126/scitranslmed.3008704

Chen, S., Lau, T. K., Zhang, C., Xu, C., Xu, Z., Hu, P., et al. (2013). A method for noninvasive detection of fetal large deletions/duplications by low coverage massively parallel sequencing. *Prenat. Diagn.* 33, 584–590. doi: 10.1002/pd.4110

Chiu, R. W., Akolekar, R., Zheng, Y. W., Leung, T. Y., Sun, H., Chan, K. C., et al. (2011). Non-invasive prenatal assessment of trisomy 21 by multiplexed maternal plasma DNA sequencing: large scale validity study. *BMJ* 342:c7401. doi: 10.1136/bmj.c7401

Dar, P. E., Curnow, K. J., Gross, S. J., Hall, M. P., Stosic, M., Demko, Z., et al. (2014). Clinical experience and follow-up with large scale single-nucleotide polymorphism-based noninvasive prenatal aneuploidy testing. *Am. J. Obstet. Gynecol.* 211, 527.e1–527.e17.

Ehrich, M., Deciu, C., Zwiefelhofer, T., Tynan, J. A., Cagasan, L., Tim, R., et al. (2011). Noninvasive detection of fetal trisomy 21 by sequencing of DNA in maternal blood: a study in a clinical setting. *Am. J. Obstet. Gynecol.* 204:11.

Fosler, L., Winters, P., Jones, K. W., Curnow, K. J., Sehnert, A. J., Bhatt, S., et al. (2017). Aneuploidy screening by non-invasive prenatal testing in twin pregnancy. *Ultrasound Obstet. Gynecol.* 49, 470–477. doi: 10.1002/uog.15964

Gil, M. M., Accurti, V., Santacruz, B., Plana, M. N., and Nicolaides, K. H. (2017). Analysis of cell-free DNA in maternal blood in screening for aneuploidies: updated meta-analysis. *Ultrasound Obstet. Gynecol.* 50, 302–314. doi: 10.1002/uog.17484

Gil, M. M., Galeva, S., Jani, J., Konstantinidou, L., Akolekar, R., Plana, M. N., et al. (2019). Screening for trisomies by cfDNA testing of maternal blood in twin pregnancy: update of The Fetal Medicine Foundation results and meta-analysis. *Ultrasound Obstet. Gynecol.* 53, 734–742.

Gil, M. M., Quezada, M. S., Revello, R., Akolekar, R., and Nicolaides, K. H. (2015). Analysis of cell-free DNA in maternal blood in screening for fetal aneuploidies: updated meta-analysis. *Ultrasound Obstet. Gynecol.* 45, 249–266. doi: 10.1002/uog.14791

Grati, F. R., Malvestiti, F., Ferreira, J. C., Bajaj, K., Gaetani, E., Agrati, C., et al. (2014). Fetoplacental mosaicism: potential implications for false-positive and false-negative noninvasive prenatal screening results. *Genet. Med.* 16, 620–624. doi: 10.1038/gim.2014.3

Gregg, A. R., Skotko, B. G., Benkendorf, J. L., Monaghan, K. G., Bajaj, K., Best, R. G., et al. (2016). Noninvasive prenatal screening for fetal aneuploidy, 2016 update: a position statement of the American College of Medical Genetics and Genomics. *Genet. Med.* 18, 1056–1065. doi: 10.1038/gim.2016.97

Hui, L., Hutchinson, B., Poulton, A., and Halliday, J. (2017). Population-based impact of noninvasive prenatal screening on screening and diagnostic testing for fetal aneuploidy. *Genet. Med.* 19, 1338–1345. doi: 10.1038/gim.2017.55

Jiang, F., Ren, J., Chen, F., Zhou, Y., Xie, J., Dan, S., et al. (2012). Noninvasive Fetal Trisomy (NIFTY) test: an advanced noninvasive prenatal diagnosis methodology for fetal autosomal and sex chromosomal aneuploidies. *BMC Med. Genomics* 5:57. doi: 10.1186/1755-8794-5-57

Le Conte, G., Letourneau, A., Jani, J., Kleinfinger, P., Lohmann, L., Costa, J. M., et al. (2018). Cell-free fetal DNA analysis in maternal plasma as screening test for trisomies 21, 18 and 13 in twin pregnancy. *Ultrasound Obstet. Gynecol.* 52, 318–324. doi: 10.1002/uog.18838

Lo, Y. M. D., Corbetta, N., Chamberlain, P. F., Rai, V., Sargent, I. L., Redman, C. W. G., et al. (1997). Presence of fetal DNA in maternal plasma and serum. *Lancet* 350, 485–487.

Neufeld-Kaiser, W. A., Cheng, E. Y., and Liu, Y. J. (2015). Positive predictive value of non-invasive prenatal screening for fetal chromosome disorders using cell-free DNA in maternal serum: independent clinical experience of a tertiary referral center. *BMC Med.* 13:129. doi: 10.1186/s12916-015-0374-8

Nicolaides, K. H., Syngelaki, A., Ashoor, G., Birdir, C., and Touzet, G. (2012). Noninvasive prenatal testing for fetal trisomies in a routinely screened first-trimester population. *Am. J. Obstet. Gynecol.* 207:374.e1–6. doi: 10.1016/j.ajog.2012.08.033

Niemchak, T., Adamski, C., Allen, R., Woods, S., and Monroe, T. (2020). 1057: noninvasive prenatal screening for fetal aneuploidy in twin pregnancies: a clinical laboratory experience. *Am. J. Obstet. Gynecol.* 222:S654.

Norton, M. E., Brar, H., Weiss, J., Karimi, A., Laurent, L. C., Caughey, A. B., et al. (2012). Non-Invasive Chromosomal Evaluation (NICE) study: results of a multicenter prospective cohort study for detection of fetal trisomy 21 and trisomy 18. *Am. J. Obstet. Gynecol.* 207:137.e1–8. doi: 10.1016/j.ajog.2012.05.021

Norton, M. E., Jacobsson, B., Swamy, G. K., Laurent, L. C., Ranzini, A. C., Brar, H., et al. (2015). Cell-free DNA analysis for noninvasive examination of trisomy. *N. Engl. J. Med.* 372, 1589–1597. doi: 10.1056/nejmoa1407349

Palomaki, G. E., Deciu, C., Kloza, E. M., Lambert-Messerlian, G. M., Haddow, J. E., Neveux, L. M., et al. (2012). DNA sequencing of maternal plasma reliably identifies trisomy 18 and trisomy 13 as well as Down syndrome: an international collaborative study. *Genet. Med.* 14, 296–305. doi: 10.1038/gim.2011.73

Palomaki, G. E., Kloza, E. M., Lambert-Messerlian, G. M., Haddow, J. E., Neveux, L. M., Ehrich, M., et al. (2011). DNA sequencing of maternal plasma to detect Down syndrome: an international clinical validation study. *Genet. Med.* 13, 913–920. doi: 10.1097/gim.0b013e3182368a0e

Petersen, A. K., Cheung, S. W., Smith, J. L., Bi, W., Ward, P. A., Peacock, S., et al. (2017). Positive predictive value estimates for cell-free noninvasive prenatal screening from data of a large referral genetic diagnostic laboratory. *Am. J. Obstet. Gynecol.* 217:691.e1–691.e6.

Porreco, R. P., Garite, T. J., Maurel, K., Marusiak, B., Obstetrix Collaborative Research Network Mathias Ehrich, van den Boom, D., et al. (2014). Noninvasive prenatal screening for fetal trisomies 21, 18, 13 and the common sex chromosome aneuploidies from maternal blood using massively parallel genomic sequencing of DNA. *Am. J. Obstet. Gynecol.* 211, e361–e312.

Rezaei, M., Winter, M., Zander-Fox, D., Whitehead, C., Liebelt, J., Warkiani, M. E., et al. (2019). A reappraisal of circulating fetal cell noninvasive prenatal testing. *Trends Biotechnol.* 37, 632–644. doi: 10.1016/j.tibtech.2018.11.001

Rose, N. C., Kaimal, A. J., Dugoff, L., Norton, M. E., and Soc Maternal, F.-M. (2020). Screening for fetal chromosomal abnormalities ACOG practice bulletin summary, number 226. *Obstet. Gynecol.* 136, E48–E69.

Tian, C., Deng, T., Zhu, X., Gong, C., Zhao, Y., Wei, Y., et al. (2020). Evidence of compliance with and effectiveness of guidelines for noninvasive prenatal testing in China: a retrospective study of 189,809 cases. *Sci. China Life Sci.* 63, 319–328. doi: 10.1007/s11427-019-9600-0

van der Meij, K. R. M., Sistermans, E. A., Macville, M. V. E., Stevens, S. J. C., Bax, C. J., Bekker, M. N., et al. (2019). TRIDENT-2: national implementation of genome-wide non-invasive prenatal testing as a first-tier screening test in the netherlands. *Am. J. Hum. Genet.* 105, 1091–1101.

Wang, J. C., Sahoo, T., Schonberg, S., Kopita, K. A., Ross, L., Patek, K., et al. (2015). Discordant noninvasive prenatal testing and cytogenetic results: a study of 109 consecutive cases. *Genet. Med.* 17, 234–236. doi: 10.1038/gim.2014.92

Yu, W., Lv, Y., Yin, S., Liu, H., Li, X., Liang, B., et al. (2019). Screening of fetal chromosomal aneuploidy diseases using noninvasive prenatal testing in twin pregnancies. *Expert Rev. Mol. Diagn.* 19, 189–196. doi: 10.1080/14737159.2019.1562906

Zhang, H., Gao, Y., Jiang, F., Fu, M., Yuan, Y., Guo, Y., et al. (2015). Non-invasive prenatal testing for trisomies 21, 18 and 13: clinical experience from 146 958 pregnancies. *Ultrasound Obstet. Gynecol.* 45, 530–538. doi: 10.1002/uog.14792

Conflict of Interest: The authors declare that the research was conducted in the absence of any commercial or financial relationships that could be construed as a potential conflict of interest.

frontiers in Genetics

ORIGINAL RESEARCH
published: 25 May 2021
doi: 10.3389/fgene.2021.641925

Whole-Exome Sequencing Reveals a Rare Variant of *OTOF* Gene Causing Congenital Non-syndromic Hearing Loss Among Large Muslim Families Favoring Consanguinity

Mohd Fareed[1,2], Varun Sharma[3], Inderpal Singh[4], Sayeed Ur Rehman[5], Gurdarshan Singh[1,2] and Mohammad Afzal[6]*

[1] PK-PD Formulation and Toxicology Division, CSIR Indian Institute of Integrative Medicine, Jammu, India, [2] Academy of Scientific and Innovative Research (AcSIR), Ghaziabad, India, [3] Ancient DNA Laboratory, Birbal Sahni Institute of Palaeosciences, Lucknow, Uttar Pradesh, India, [4] BioinfoRes, Jammu, India, [5] Department of Biochemistry, School of Chemical and Life Sciences, Jamia Hamdard, New Delhi, India, [6] Human Genetics and Toxicology Laboratory, Section of Genetics, Department of Zoology, Aligarh Muslim University, Aligarh, India

OPEN ACCESS

Edited by:
Emiliano González Vioque, University Clinical Hospital of Santiago, Spain

Reviewed by:
Barakat Abdelhamid, Institut Pasteur du Maroc, Morocco
Sofia Gouveia, University Clinical Hospital of Santiago, Spain

***Correspondence:**
Mohd Fareed
m.fareed@iiim.res.in;
mohdfareedk@gmail.com;
fareedgenetics2012@gmail.com

Specialty section:
This article was submitted to Genetics of Common and Rare Diseases, a section of the journal Frontiers in Genetics

Received: *15 December 2020*
Accepted: *02 March 2021*
Published: *25 May 2021*

Citation:
Fareed M, Sharma V, Singh I, Rehman SU, Singh G and Afzal M (2021) Whole-Exome Sequencing Reveals a Rare Variant of OTOF Gene Causing Congenital Non-syndromic Hearing Loss Among Large Muslim Families Favoring Consanguinity. Front. Genet. 12:641925. doi: 10.3389/fgene.2021.641925

Non-syndromic hearing loss (NSHL) is one of the most frequent auditory deficits in humans characterized by high clinical and genetic heterogeneity. Very few studies have reported the relationship between *OTOF* (Locus: DFNB9) and hereditary hearing loss in India. We aimed to decipher the genetic cause of prelingual NSHL in a large affected Muslim consanguineous families using whole-exome sequencing (WES). The study was performed following the guidelines and regulations of the Indian Council of Medical Research (ICMR), New Delhi. The population was identified from Jammu and Kashmir, the Northernmost part of India. Near about 100 individuals were born deaf-mute in the village of 3,000 inhabitants. A total of 103 individuals (with 52 cases and 51 controls) agreed to participate in this study. Our study revealed a rare non-sense homozygous mutation NC_000002.11:g.2:26702224G>A; NM_001287489.2:c.2122C>T; NP_001274418.1:p.(Arg708*) in the 18th exon of the *OTOF* gene. Our study provides the first insight into this homozygous condition, which has not been previously reported in ExAC, 1,000 Genome and genomAD databases. Furthermore, the variant was confirmed in the population cohort (n = 103) using Sanger sequencing. In addition to the pathogenic *OTOF* variant, the WES data also revealed novel and recurrent mutations in *CDH23, GJB2, MYO15A, OTOG*, and *SLC26A4* genes. The rare pathogenic and the novel variants observed in this study have been submitted to the ClinVar database and are publicly available online with the accessions SCV001448680.1, SCV001448682.1 and SCV001448681.1. We conclude that *OTOF*-related NSHL hearing loss is prevalent in the region due to successive inbreeding in its generations. We recommend premarital genetic testing and genetic counseling strategies to minimize and control the disease risk in future generations.

Keywords: hearing disorders, hearing impairment, deaf mutes, autosomal recessive (AR) diseases, cousin marriages, Indian population, Jammu and Kashmir (J and K), genetic counseling

INTRODUCTION

Over 446 million people have disabling hearing loss worldwide. This estimate is projected to accelerate over 630 million by 2,030 and may raise up to 900 million in 2,050 (Olusanya et al., 2019). The global prevalence of prelingual hearing loss is 1 in 500 newborns and is the 4th leading cause of disability among living individuals (Duman and Tekin, 2012). Phenotypically, hereditary hearing loss (HHL) can be classified into syndromic hearing loss (SHL) and non-syndromic hearing loss (NSHL). The NSHL is one of the most frequent sensory deficits in humans characterized by high clinical and genetic heterogeneity. Approximately 90% of NSHL cases from severe to profound congenital deafness exhibit an autosomal-recessive (AR) pattern of inheritance (DFNB forms). The prevalence of prelingual NSHL is approximately 2.7 cases per 1,000 live births (Vona et al., 2015).

Genotype-phenotype correlations help in understanding the mechanistic etiology, progression, and prognosis of the inherited genetic disorder. However, in case of NSHL, the diagnosis becomes more challenging due to high clinical complexity and genetic heterogeneity. The molecular elucidation of such complex disorder with precise genomic approaches can provide genetic origin and functional consequences, which could be better implemented for proper medical investigation, prognostic, and therapeutic targets. To date, a total of 116 NSHL genes have been identified[1]. Out of these, 45 genes for autosomal dominant-NSHL (AD-NSHL), 5 genes for X-linked and about 75 genes are linked with AR-NSHL. The product of these genes has multiple roles in maintaining the normal physiology of the inner ear. Mutation in any of these genes may have a deleterious impact, altering the normal hearing physiology (Shearer et al., 1993).

Hearing loss is a severe disorder but grossly neglected in India. According to World Health Organization (2018) data, the prevalence of auditory deficit in the country is over 63 million (about 6.3%) of the total population. The population of India and other South Asian countries provides much complexity due to the admixture of their genomes during evolutionary timescales (Patterson et al., 2012). To discover genetic variations of the heterogenetic disorder in such an ethnic group and/or geographically isolated population may need highly equipped and rigorous diagnostic approaches. Massive parallel sequencing (MPS) or next-generation sequencing (NGS) technologies provide an opportunity to precisely explore the genetic architecture of the disease, which furthermore could be used as a baseline for medical genetic testing (Shearer et al., 2010). Very few studies have reported the relationship between *OTOF* (Locus: DFNB9) and HHL in India.

Here, we employed the whole-exome sequencing (WES) approach to precisely identify the functional pathogenic mutations causing congenital hearing loss from the Muslim population favoring consanguinity.

[1]http://hereditaryhearingloss.org/

MATERIALS AND METHODS

Study Population

The cohort was selected from the Doda District of Jammu and Kashmir, North India. Approximate 3,000 residents inhabited this village, belonging to the Muslim community favoring consanguinity in their ancestry. To date, in this village, more than 100 individuals were born deaf-mute; some of them migrated to other states (i.e., Punjab, India) and a few to nearby districts. In our preliminary survey, we identified 74 deaf-mute live and 3 deceased cases. **Figure 1** presents the pedigree and inheritance detail of all 77 cases. Out of 74 deaf-mutes, only 52 cases were agreed to participate in the study. A total of 103 individuals aged 20–60 years (with 52 cases and 51 controls) were recruited for this study. WES was performed in 07 samples with 02 cases (i.e., F7 and G8) and 05 controls (i.e., C4, D5, H9, K11, and M12), while the rest ($n = 96$) were subjected to Sanger sequencing to confirm the candidate pathogenic variant.

Sample Collection, DNA Isolation and Quantification

Blood samples were collected using a 21-gage syringe to draw up to a volume of 5 ml in a vacutainer containing Tris-EDTA. For saliva samples, the participants were provided with collection tubes and were asked to provide a 2.5 ml sample. The participants were instructed to spit into the tube up to the red fill line marked on the tube (approximately 2.5 ml), excluding the froth. DNA was extracted using QIAamp DNA Mini Kit 50 (Cat# 51304, Qiagen). The DNA samples were was subjected to QIAXPERT for quantifying the amount of DNA and the purity was checked by measuring the 260/280 nm ratio. DNA samples were also subjected to agarose gel electrophoresis and, after passing through DNA quality check (**Supplementary Table 1**), were proceeded for Library Protocol.

Whole-Exome Sequencing and Bioinformatic Analysis

The WES library was prepared using Agilent-Sure Select XT Reagent Kit, Illumina (ILM) platforms. Biotinylated oligonucleotide capture probes (V5 + UTR), also called baits, that was designed for the human exons was provided with the kit and used to enrich the region of interest (whole exome) by hybridization. The workflow involved shearing of DNA, repairing ends, adenylation of 3' ends, followed by adapter ligation. At each step, the products were purified using AMPure beads. The adapter sequence was added onto the ends of DNA fragments to generate paired-end libraries. The resulting adaptor-ligated library was purified, quantified and hybridized with an exome-specific biotinylated capture library. After hybridization, the targeted molecules were captured on streptavidin beads. The resulting enriched DNA library was multiplexed by adding index tags by amplification, followed by purification. Indexed captured library DNA was assessed to check the quality and quantity of the captured libraries. The sequencing was carried out in Illumina HiSeq X10 to generate 2X–150 bp sequence reads at an average 100− sequencing depth. Only those samples

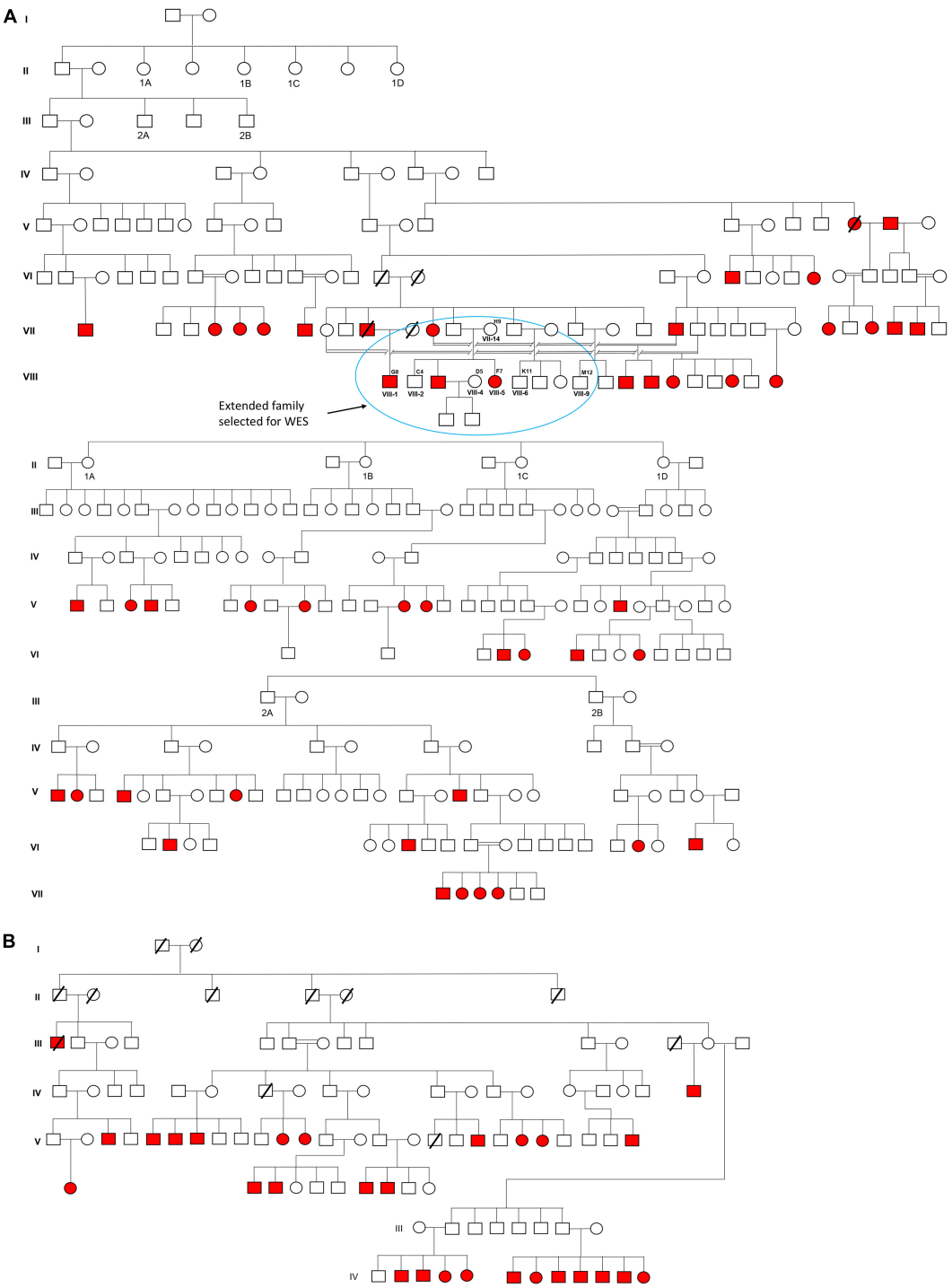

FIGURE 1 | Pedigree and inheritance of deaf-mute syndrome in the families. **(A,B)** are the two large family trees and **(A)** have two sub-family trees expatiated from its first and second generations. The extended family from the first family tree (circled blue) was considered for whole-exome sequencing. The squares and circles represent males and females, respectively, where the cases are presented in red color.

were considered for data processing that surpasses the quality scores (Q30 value) greater than 75% of the sequenced bases. The base quality distribution, base content and the GC content are presented in **Supplementary Figure 1**. The overall alignment percentage (alignment to GRCh37/hg19) in all the samples was greater than 97% (**Supplementary Table 2**). The average coverage and on-target percentage for the samples was around 99 and 90%, respectively (**Supplementary Table 3**). The distribution

of sequencing depth is shown in **Supplementary Figure 2**. The sequencing reads were processed and analyzed using the BROAD Institute's Genome Analysis Toolkit (GATK-Toolkit) (DePristo et al., 2011) and variant calling was performed using the complete human reference genome (hg19, NCBI release GRCh37).

The bioinformatic pipelines (alignment variant calling and variant annotation) used in our study are shown in **Supplementary Figure 3**. All common polymorphisms with a minor allele frequency (MAF) higher than 0.01 were filtered out using several public databases such as 1,000 genomes database (1000 Genomes Project Consortium et al., 2015), Ensembl GRCh37 genome browser (Zerbino et al., 2018), exome aggregation consortium database (ExAC) (Lek et al., 2016), genome aggregation database (gnomAD) (Karczewski et al., 2020), and database of single nucleotide polymorphisms (dbSNP). The ClinVar database was used to check the previously reported mutations and associated phenotypes. Exclusion of intronic, synonymous, inframe insertions/deletions (InDels) and mutations in untranslated regions whereas the missense, non-sense variations and frameshift InDels located in exons or splice sites were prioritized. The remaining variants were then verified in dbSNP and NCBI databases.

In silico Evaluation for the Pathogenicity of Candidate Mutation

The altered amino acid was checked for its evolutionary conservation across different species, including the primates and mammals using the genome browser of the University of California at Santa Cruz (UCSC) (Kent et al., 2002). *In silico* programs including MutationTaster2 (Schwarz et al., 2014), PolyPhen-2 (Adzhubei et al., 2010) and scale-invariant feature transform (SIFT) (Kumar et al., 2009) were used to predict the possible impact of the detected variants.

Audiometric Characteristics

The pulse tone audiometric (PTA) records of the subjects were noted. The hearing level grades were categorized according to WHO and the National Hearing Test (NHT) guidelines viz., normal (<20 dB), mild (20–40 dB), moderate (41–70 dB), severe (71–90 dB), and profound (>90 dB). The average values of both the ears (left and right) were considered to calculate the hearing threshold levels. The age of the individual was also recorded at the time of audiometry.

Co-segregation Analysis

Whole-exome sequencing (at 100X depth) provides sufficient details for the confirmation of the candidate variant. However, Sanger sequencing has also been performed to re-validate/or reconfirm the mutation identified by targeted NGS. Primers (PXL-A0145439) for exon 18 of the *OTOF* gene (reference sequence NM_001287489.2 and Chr2:26669916-26791779 context region in hg19), were manufactured and supplied by Pxlence[2]. The thermal cycler program was set according to the manufacturer's instructions, using the conditions: initial incubation 98°C for 2 min, 98°C for 20 sec, followed by 35 cycles at 60°C for 30 s, 72°C for 40 s, final extension 72°C for 10 min and hold at 4°C. PCR products were confirmed using a 1.7% w/v agarose gel electrophoresis. The PCR products were then processed for cycle sequencing/BigDye terminator assay, followed by Sephadex (column-based) purification. Finally, the PCR products were loaded onto DNA Sequencer (SeqStudio Genetic Analyzer).

[2]https://www.pxlence.com/index.php/

RESULTS

Identification of a Pathogenic Mutation Using Whole-Exome Sequencing

The variants produced from exome-sequencing are presented in **Supplementary Tables 4–6**. WES analysis generated approximately 72,000 genetic variants (including SNPs, insertions and deletions) in each sample. By applying the narrow down filtering approach, the number of probable causative mutations are presented in **Supplementary Tables 7–9**, respectively. The variant filtering strategy used to find out the most promising causative mutation has been presented in **Figure 2**. The most promising causative variants have been presented in **Supplementary Table 10**. After the removal of duplicates and common mutations, the variants were filtered for rare (<1%), evolutionary conserved and functional homozygous recessive mutations using the online GenIO database (an integrated pipeline based on RefGene, NHLBI-ESP, 1,000 Genomes, dbSNP, ClinVar, COSMIC, gnomAD, OMIM and M-CAP databases) following the American College of Medical Genetics and Genomics and the Association of Molecular Pathology (ACMG-AMP) guidelines (Koile et al., 2018). We observed approximately 03 homozygous and 140 heterozygous mutations (likely to be pathogenic, global MAF <0.01) among the two cases (F7 and G8). After the removal of overlapping variants with controls and considering the conserved in evolution (GERP score >0), we thus identified the disease-causing rare variant NC_000002.11:g.2:26702224G > A; NM_001287489.2:c.2122C > T; NP_001274418.1:p.(Arg708*) (rs80356590) in 18th exon of the *OTOF* gene. This *OTOF* variant is very rare and no homozygous variant previously reported in genomAD, ExAC, and 1,000 Genome databases; however, few heterozygous cases have been reported in genomAD. We confirmed the *OTOF* mutation using BAM and VCF files in IGV 2.5.3 software.

The functional consequence (*in silico* validation) of the variant was predicted using Mutation Taster (**Table 1**), which revealed the deleterious consequence homozygous condition by premature terminating the otoferlin protein at 708 amino acid. The substitution of the arginine by a premature stop codon p.(Arg708*) produces a truncated variant of otoferlin remains non-functional in the sensory hair cells, potentially causing profound hearing loss.

In addition to the rare pathogenic *OTOF* variant, the WES data also revealed some novel and rare recurrent genomic mutations in the extended family. The novel variants (not found in ExAC, 1,000 G and genomAD databases) of

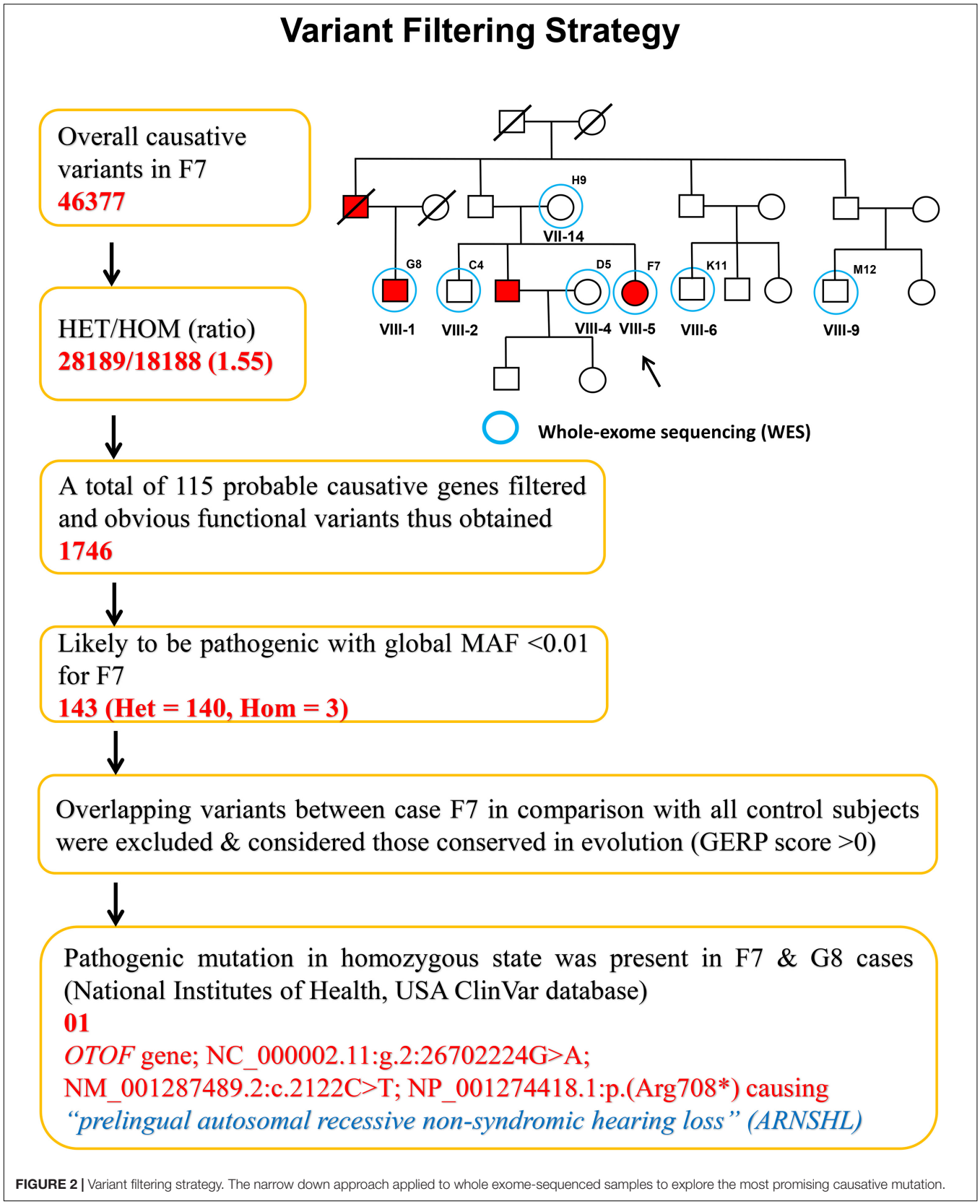

FIGURE 2 | Variant filtering strategy. The narrow down approach applied to whole exome-sequenced samples to explore the most promising causative mutation.

TABLE 1 | Functional evidence of the *OTOF* variant (NC_000002.12:g.2:26702224G > A) by *in silico* evaluation, using Mutation Taster.

Start (aa)	End (aa)	Feature	Details	Impact
1	1963	TOPO_DOM	Cytoplasmic	Lost
792	821	COILED		Lost
947	1052	DOMAIN	C2 3	Lost
1088	1088	CONFLICT	L = P (in Ref. 1; AAD26117 and 2; AAG12992/AAG17468)	Lost
1303	1310	COMPBIAS	Poly-Lys	Lost
1314	1320	COMPBIAS	Poly-Glu	Lost
1479	1577	DOMAIN	C2 4	Lost
1787	1787	CONFLICT	G = S (in Ref. 5; BAG58982)	Lost
1964	1984	TRANSMEM	Helical	Lost
1965	1983	COMPBIAS	Poly-Leu	Lost
1985	1997	TOPO_DOM	Extracellular	Lost

The stop codon insertion by the variant (NM_001287489.2:c.2122C > T) terminates the protein at 708 position (NP_001274418.1:p.Arg708), causing the loss of various functional domains.*

OTOG NM_001292063.2:c.5438T > G; NP_001264198.1: p.(Val1813Gly) and *SLC26A4* NM_000441.2:c.1668T > A NP_000432.1:p.(Tyr556*) and the recurrent variants of *CDH23* NM_022124.6:c.4892C > T NP_071407.4:p.(Ala1631Val), *GJB2* NM_004004.6:c.493C > T NP_003995.2:p.(Arg165Trp), *MYO15A* NM_016239.4:c.5894G > A NP_057323.3:p.(Arg1965His) and others (presented in **Supplementary Table 10**) were observed in heterozygous/or compound heterozygous conditions. The candidate pathogenic (*OTOF*) and the novel variants (*OTOG* and *SLC26A4*) have been submitted to ClinVar database and are publicly available online with the accessions SCV001448680.1, SCV001448682.1, and SCV001448681.1, respectively.

Audiometric and Genotypic Characteristics

All subjects (cases and controls) showed normal clinical features (i.e., no structural and observable phenotypic deformity) other than hearing. The audiometric and genomic characteristics of proband have been presented in **Figure 3**. The normal individuals (control) showed the hearing level in between 0–20 dB at frequencies 0.125, 0.25, 0.5, 1, 2, 3, 4, 6, and 8 kHz. However, the threshold level of deaf-mute subjects falls under a profound (>90 dB) category for the same audio frequencies (**Figure 3A**). The cases F7 (aged 31 years), G8 (aged 25 years) exhibit the characteristics of profound prelingual NSHL. The WES data of cases (F7 and G8) and controls C4 (aged 43 years), D5 (aged 35 years), H9 (aged 60 years), K11 (aged 22 years), and M12 (aged 34 years) have been shown in **Figure 3B**. The cases (F7 and G8) carry a homozygous mutation; among controls, the C4, H9, and M12 possess heterozygous and D5 and K11 are homozygous for the reference allele (carrying no *OTOF* mutation).

Co-segregation Analysis

The family pedigree and *OTOF* segregation with the disease phenotype has been well demonstrated in **Supplementary Figure 4a**. The next generation WES (**Figure 3B**) and Sanger sequencing data (**Supplementary Figure 4B**) provides the evidence for perfect segregation of the *OTOF* variant with the auditory phenotype. The data clearly depicts the autosomal recessive non-syndromic hearing loss (ARNSHL). Further, Sanger sequencing was performed in the remaining 96 samples to reconfirm the mutation pattern of the *OTOF* gene. The genotypic details of the candidate variant of *OTOF* gene for all 103 subjects have been displayed in **Figure 4**. The ancestral lineage of the subjects has a history of consanguineous marriages which determines the existence of the phenotypic spectrum of *OTOF* in the current generation.

DISCUSSION

The results of our study indicate that a non-sense mutation in the *OTOF* gene was terminating the peptide chain and generating a truncated protein variant, which ultimately leads to prelingual neurosensory non-syndromic DFNB9 (OMIM, #601071) hearing loss. The functional evidence of the *OTOF* relationship with DFNB9 impairment has been well established by earlier studies (Roux et al., 2006; Pangršič et al., 2012). The *OTOF*-related NSHL has been previously reported in the populations from India, Pakistan, China, Japan, Altai Republic, Korea, Spain, Turkey, and Iran (Yasunaga et al., 2000; Tekin et al., 2005; Rodríguez-Ballesteros et al., 2008; Choi et al., 2009; Wang et al., 2010; Mahdieh et al., 2012; Ñhurbanov et al., 2016; Kim et al., 2018; Iwasa et al., 2019). In addition to OTOF-related deafness, mutations in the autosomal genes like *CDH23, Claudin14, GJB2, GJB6, MYO6, MYO15A, SLC26A4, TMC1, TMIE, TMPRSS3, TRIOBP, USHIC*, and others are predominant to cause HHL among Indian and Pakistani populations (Yan et al., 2015). It is evident from the previous studies that the mutation spectrum of *GJB2, GJB6, SLC26A4*, and *TMC1* genes was much common in the ethnic groups of eastern and southern parts of India (Padma et al., 2009; Ganapathy et al., 2014; Adhikary et al., 2015; Singh et al., 2018). In the present study, we have also identified the missense/non-sense heterozygous variants in the *OTOG* p.(Val1813Gly), *SLC26A4* p.(Tyr556*) *CDH23* p.(Ala1631Val), *GJB2* p.(Arg165Trp), and *MYO15A* p.(Arg1965His) genes which are predominant to cause deafness among Indian populations.

Otoferlin is a transmembrane vesicular protein (1997 amino acids in humans) encoded by the *OTOF* gene, spanning in the short arm of chromosome 2 (2p23.3). The otoferlin is expressed in the inner hair cells (IHCs) (Liu et al., 2014) and plays a significant role in neuronal synapse and exocytosis (Shin, 2014). The protein consists of six C2 domains (C2A-F), two Ferlin conserved motifs (Fer-1 and Fer-B) and a transmembrane domain (TMD). Using the Treefam database, Schreiber et al. (2014) the close relationship of otoferlin across different species depicts the domains and motifs that were highly conserved (**Figure 5A**). The functional evidence for the high level of protein

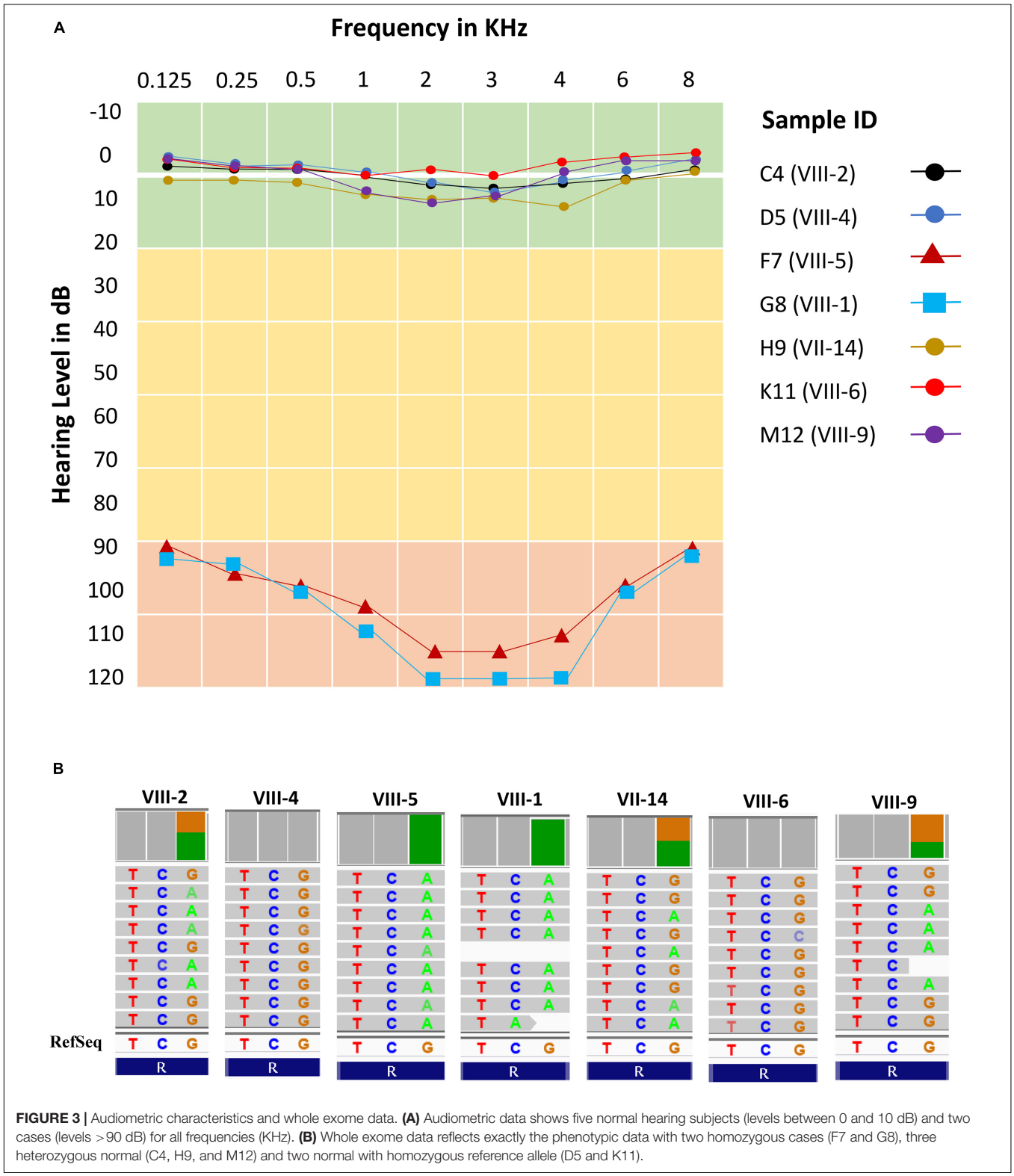

FIGURE 3 | Audiometric characteristics and whole exome data. **(A)** Audiometric data shows five normal hearing subjects (levels between 0 and 10 dB) and two cases (levels >90 dB) for all frequencies (KHz). **(B)** Whole exome data reflects exactly the phenotypic data with two homozygous cases (F7 and G8), three heterozygous normal (C4, H9, and M12) and two normal with homozygous reference allele (D5 and K11).

conservation at the site of *OTOF* mutation (NP_001274418.1:p.Arg708*) in 8 vertebrates has been displayed in **Figure 5B** and **Supplementary Figure 5a** (using UCSC Genome Browser). The mRNA levels in 20 different tissues reveal the *OTOF* in the brain is highly expressed (**Supplementary Figure 5b**). The protein-protein interactions of OTOF using STRING v11.0 confirm the functional involvement in the neuronal synapse, exocytosis and hearing functions (**Figure 5C**; Szklarczyk et al., 2019).

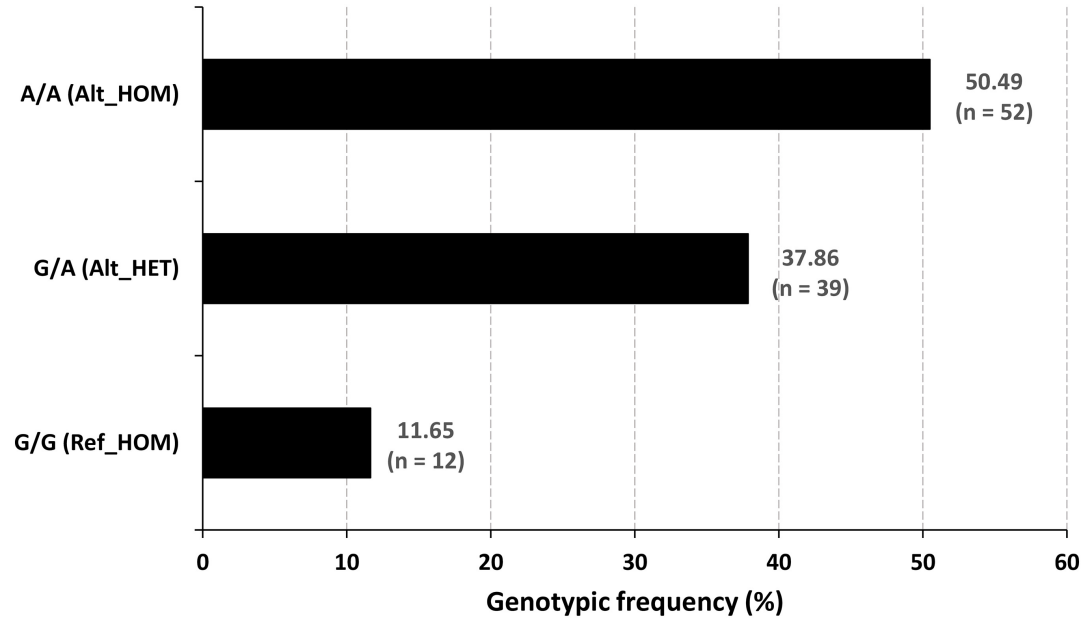

FIGURE 4 | Genotypic frequency of the *OTOF* variant. The mutated homozygotes were the (*n* = 52) cases, and the normal hearing people were the reference homozygotes (*n* = 12) and heterozygous carrier (*n* = 39) genotypes.

The non-sense mutations in the *OTOF* gene producing truncated versions of protein causing DFNB9 deafness has been well-established by the researchers using *in vitro* and *in vivo* models in their experiments (Pangršič et al., 2012; Chatterjee et al., 2015; Hams et al., 2017). In the present study, a similar non-sense mutation (NM_001287489.2:c.2122C > T) results in the protein truncation at p.(Arg708*) eventually altering the normal otoferlin physiology. The truncated otoferlin (N-terminus C2A-C) lacking C2D-F and TMD remain unbound with no membrane fusion or exocytosis, which ultimately halts the neurotransmitter release, causing profound hearing loss. Based upon the substantial evidence from *in silico* testing (**Table 1**) and previously well-established proofs of protein truncation due to different *OTOF* non-sense mutations (Chatterjee et al., 2015; Hams et al., 2017), we propose a schematic model showing the role of otoferlin protein with normal and altered physiology via p.(Arg708*) in the current study (**Figure 6**). The otoferlin held on synaptic vesicles via TMD and C2 domains interact with the presynaptic membrane via SNAREs to execute exocytosis under Ca^{2+} influx. It is evident from the previous studies that missense mutations in C2B and C2C domains have been linked to hearing loss (Mirghomizadeh et al., 2002; Helfmann et al., 2011). N-terminal domains' role provides structural stability to the protein and C-terminal domains (C2D-F) may play a functionally conserved or redundant role in otoferlin physiology (Chatterjee et al., 2015). Our findings predict the otoferlin synthesis stops at 708 amino acid (between C2C and FerB domains), leading to almost half protein (N-terminal with C2A-C domains) lacking the most conserved and functional part (C2D-F with TMD at C-terminus).

Parental consanguinity has been associated with an increased risk of autosomal recessive disorders (Fareed and Afzal, 2017). The consanguineous marriages with the adverse effects have been previously reported from the Muslim populations of Jammu and Kashmir (Fareed and Afzal, 2014a,b, 2016; Fareed et al., 2017). In the present study, the prevalence of prelingual hearing loss was 1 in 30, considerably higher than the global prevalence (Duman and Tekin, 2012), providing the evident consequence of inbreeding in the population. It might be possible that these groups have settled to the northernmost region of India during the evolutionary time frames and unknowingly have undergone marriages within the groups, which ultimately increased the prevalence of the disorder.

CONCLUSION

The present study evaluated the ARNSHL in a tribal family of the Jammu and Kashmir region. The clinical audiometric evaluation and the information gathered from village representatives suggest the profound prelingual NSHL prevailing in the area. WES categorizes the rare pathogenic mutation in the *OTOF* gene p.(Arg708*), which has been well segregated with the disease. *OTOF* plays a significant role in the neuronal synapse in the IHCs of the cochlea. The pathogenic mutation (NC_000002.11:g.2:26702224G > A) is predicted to result in the lack of the most conserved and functional domains.

The global allele frequency of this *OTOF* variant (rs80356590) is 0.00004284 (source: genomAD), which affirms the extremely rare criteria. However, in the present study population, this globally recognized rare variant of *OTOF* turns into a common one because consanguineous marriages were much prevalent in the region, ultimately increasing the risk of such autosomal

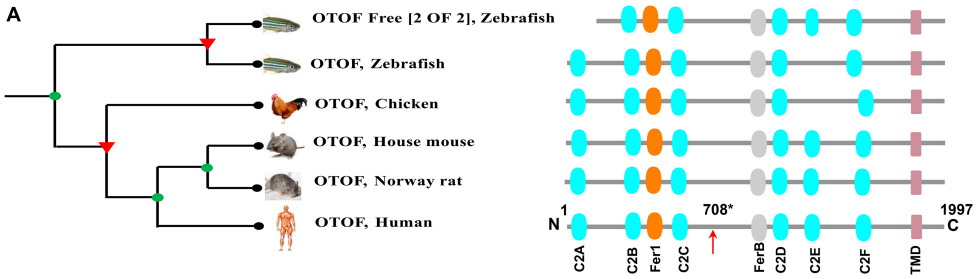

B

NC_000002.12:g.2:26702224G>A, rs80356590
NP_001274418.1:p.(Arg708*)

Homo sapiens	XP_016860827.1	TDRNYFHLPYLERKPCIYIKSWWPD
Macaca mulatta	XP_014967379.2	TDRNYFHLPYLERKPCIYIKSWWPD
Gorilla gorilla	XP_018876157.1	TDRNYFHLPYLERKPCIYIKSWWPD
Equus caballus	XP_023475130.1	TDRNYFHLPYLERKPCIYIKSWWPD
Canis lupus	XP_022260255.1	TDRNYFHLPYLERKPCIYMKSWWPD
Felis catus	XP_023107792.1	TDRNYFHLPYLERKPCIYIKSWWPD
Rattus norvegicus	NP_001263649.1	TDRNYFHLPYLERKPCIYIKSWWPD
Mus musculus	NP_001300696.1	TDRNYFHLPYLERKPCIYIKSWWPD

C

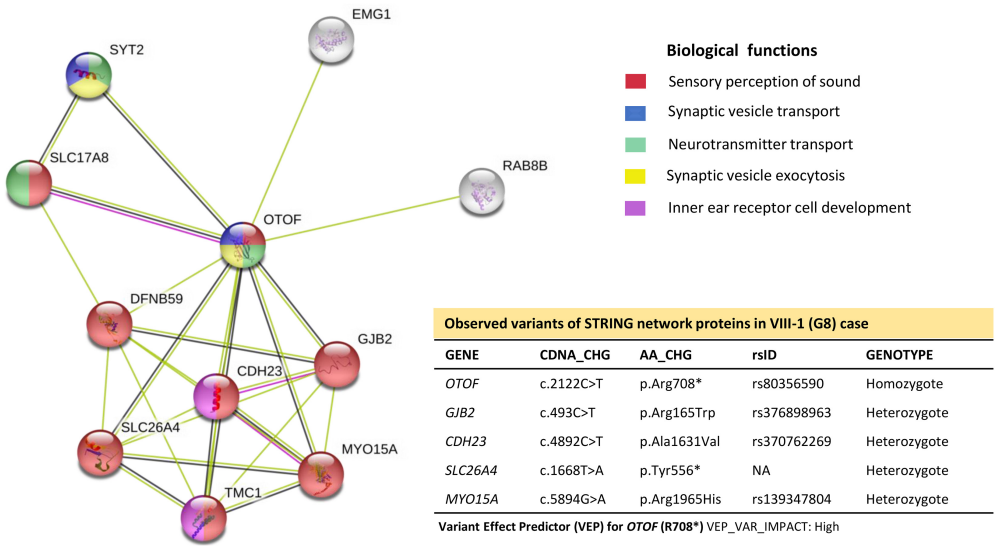

Observed variants of STRING network proteins in VIII-1 (G8) case

GENE	CDNA_CHG	AA_CHG	rsID	GENOTYPE
OTOF	c.2122C>T	p.Arg708*	rs80356590	Homozygote
GJB2	c.493C>T	p.Arg165Trp	rs376898963	Heterozygote
CDH23	c.4892C>T	p.Ala1631Val	rs370762269	Heterozygote
SLC26A4	c.1668T>A	p.Tyr556*	NA	Heterozygote
MYO15A	c.5894G>A	p.Arg1965His	rs139347804	Heterozygote

Variant Effect Predictor (VEP) for *OTOF* (R708*) VEP_VAR_IMPACT: High

FIGURE 5 | The phylogenetic relationship, conservation and association networks of OTOF protein. **(A)** The human OTOF protein domains show high resemblance with mouse and rat except for the chicken and zebrafish, which lacks the C2E domain. Ferlin1, FerlinB and Trans-membrane domains are common among all species. **(B)** The comparison of OTOF for 8 vertebrates shows a highly conserved region (at Arg708 residue) spanning between C2C and FerB domains across different vertebrates. **(C)** Network showing the functional association of *OTOF* using STRING v11.0 (https://stringdb.org/). The proximity of the proteins via threads predicts the association and their role in sensorineural activities. In the present study, exome-data have also identified the additional genomic variants in *CDH23, GJB2, MYO15A, OTOG,* and *SLC26A4* for the current STRING model.

recessive disorder. In summary, our study provides the roadmap and a piece of safeguard advice for clinicians and health care providers to make people familiar with the genetic cause and its increased risk in the context of inbreeding. Identification of such mutations supports better management of such disorders through genetic counseling. Establishing genetic testing facilities will help the appropriate diagnosis and opening new gateways for precision medicine. Familial and premarital screening will help in

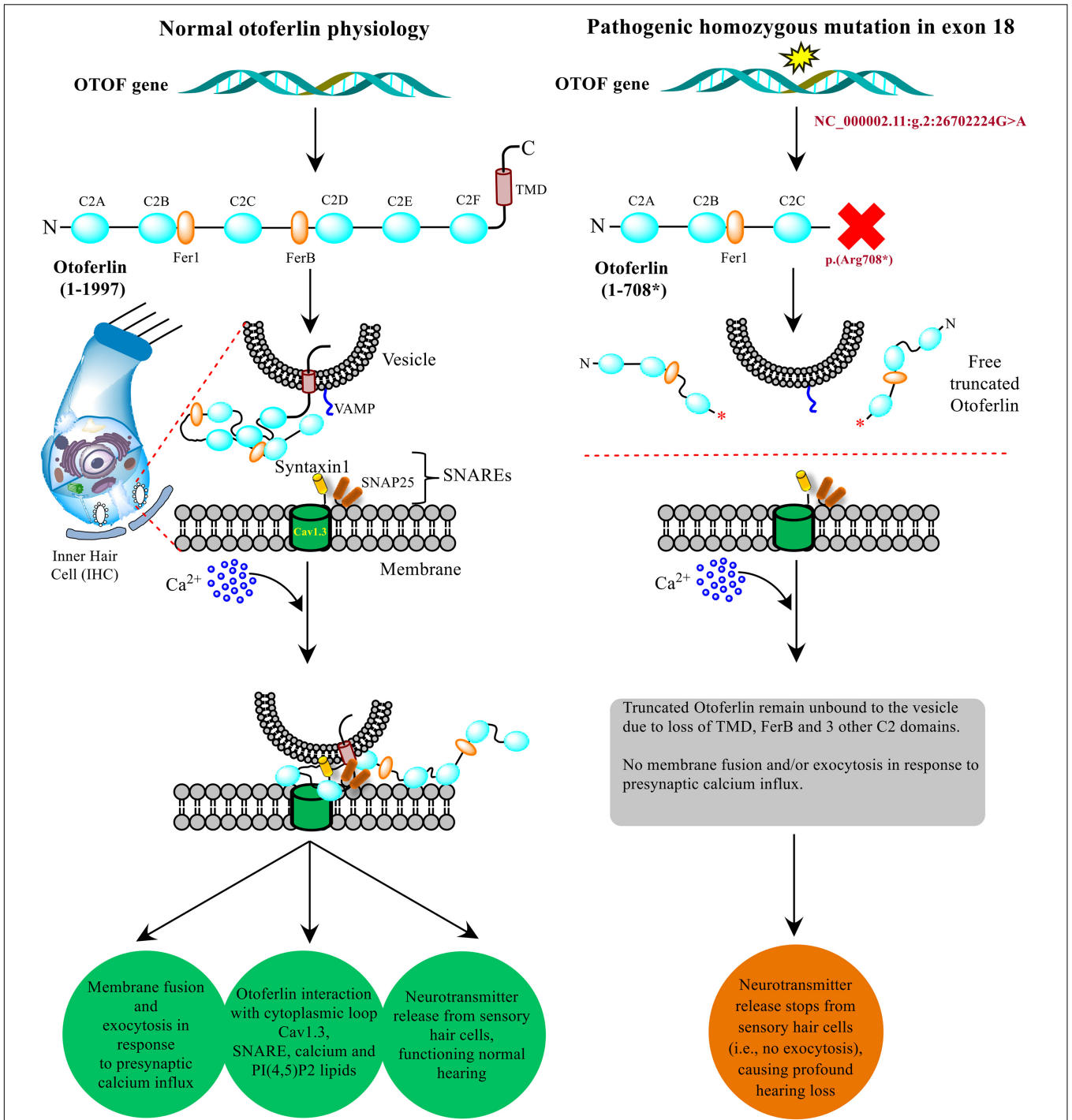

FIGURE 6 | Model presenting the role of OTOF in hearing physiology. The otoferlin expressed in the inner hair cells (IHCs) cochlea typically perform the neuronal synapse and exocytosis. A non-sense mutation brings stop codon (at p. 708*) in between C2C and C2D domains results in a truncated version of the protein, which disrupts the normal function and hearing physiology. The current model was adapted from the previously well-established experimental-based studies (Ramakrishnan et al., 2014; Shin, 2014; Chatterjee et al., 2015; Hams et al., 2017).

controlling the hearing disability in future generations. Further population-wide screening is needed to explore the *OTOF* penetrance and other possible genetic hideouts in NSHL among North Indian populations.

DATA AVAILABILITY STATEMENT

The rare pathogenic and the novel variants observed in this study have been submitted to the ClinVar database and are

publicly available online with the accessions SCV001448680.1, SCV001448682.1, and SCV001448681.1

ETHICS STATEMENT

The studies involving human participants were reviewed and approved by Institutional Ethical Committee (IEC), Jawaharlal Nehru Medical College (JNMC), Aligarh Muslim University, India. The patients/participants provided their written informed consent to participate in this study. All methods were performed following the guidelines and regulations of the Indian Council of Medical Research (ICMR), New Delhi.

AUTHOR CONTRIBUTIONS

MF, VS, IS, SUR, GS, and MA conceived and designed the study. MF analyzed and interpreted the data. MF, VS, SUR, GS, and MA contributed to the drafting and critical review of the manuscript. All authors contributed to the article and approved the submitted version.

ACKNOWLEDGMENTS

We thank the Department of Science and Technology (DST), New Delhi, for financial assistance (File No. DST/INSPIRE/04/2017/001350) to Dr. Mohd Fareed. Special thanks to the Sarpanch (Mr. Mohd Haneef), residents and the participants of the study for their utmost support and cooperation. Thanks to Mr. Shaghaf M. Ansari (Scientist), Information Technology Division of CSIR-IIIM for his help in downloading the data. Thanks to the IPR committee (CSIR-IIIM/IPR/00284) for reviewing and approving the manuscript.

WEB RESOURCES

GenIO, http://bioinformatics.ibioba-mpsp-conicet.gov.ar/GenIO/index.php/

gnomAD, https://gnomad.broadinstitute.org/

Hereditary Hearing Loss, http://hereditaryhearingloss.org/

Mutation Taster, http://www.mutationtaster.org/, https://www.mutationdistiller.org/

NCBI ClinVar, https://www.ncbi.nlm.nih.gov/clinvar/

NCBI dbSNP, https://www.ncbi.nlm.nih.gov/snp/

OMIM, https://www.omim.org/

PolyPhen-2 http://genetics.bwh.harvard.edu/pph2/

SIFT, http://sift.jcvi.org/

STRING, https://stringdb.org/

The Human Gene Mutation Database, http://www.hgmd.cf.ac.uk/ac/index.php/

TreeFam, http://www.treefam.org/family/TF316871

University of California Santa Cruz Genomics Institute Genome Browser, https://genome.ucsc.edu/.

SUPPLEMENTARY MATERIAL

The Supplementary Material for this article can be found online at: https://www.frontiersin.org/articles/10.3389/fgene.2021.641925/full#supplementary-material

REFERENCES

1000 Genomes Project Consortium, Auton, A., Brooks, L. D., Durbin, R. M., Garrison, E. P., Kang, H. M., et al. (2015). A global reference for human genetic variation. *Nature* 526, 68–74. doi: 10.1038/nature15393

Adhikary, B., Ghosh, S., Paul, S., Bankura, B., Pattanayak, A. K., Biswas, S., et al. (2015). Spectrum and frequency of GJB2, GJB6 and SLC26A4 gene mutations among nonsyndromic hearing loss patients in eastern part of India. *Gene* 573, 239–245. doi: 10.1016/j.gene.2015.07.050

Adzhubei, I. A., Schmidt, S., Peshkin, L., Ramensky, V. E., Gerasimova, A., Bork, P., et al. (2010). A method and server for predicting damaging missense mutations. *Nat. Methods* 7, 248–249. doi: 10.1038/nmeth0410-248

Chatterjee, P., Padmanarayana, M., Abdullah, N., Holman, C. L., LaDu, J., Tanguay, R. L., et al. (2015). Otoferlin deficiency in zebrafish results in defects in balance and hearing: rescue of the balance and hearing phenotype with full-length and truncated forms of mouse otoferlin. *Mol. Cell. Biol.* 35, 1043–1054. doi: 10.1128/mcb.01439-14

Choi, B. Y., Ahmed, Z. M., Riazuddin, S., Bhinder, M. A., Shahzad, M., Husnain, T., et al. (2009). Identities and frequencies of mutations of the otoferlin gene (OTOF) causing DFNB9 deafness in Pakistan. *Clin. Genet.* 75, 237–243. doi: 10.1111/j.1399-0004.2008.01128.x

DePristo, M. A., Banks, E., Poplin, R., Garimella, K. V., Maguire, J. R., Hartl, C., et al. (2011). A framework for variation discovery and genotyping using next-generation DNA sequencing data. *Nat. Genet.* 43, 491–498. doi: 10.1038/ng.806

Duman, D., and Tekin, M. (2012). Autosomal recessive nonsyndromic deafness genes: a review. *Front. Biosci.* 17:2213–2236. doi: 10.2741/4046

Fareed, M., and Afzal, M. (2014a). Estimating the inbreeding depression on cognitive behavior: a population based study of child cohort. *PLoS One* 9:e109585. doi: 10.1371/journal.pone.0109585

Fareed, M., and Afzal, M. (2014b). Evidence of inbreeding depression on height, weight, and body mass index: a population-based child cohort study. *Am. J. Hum. Biol.* 26, 784–795. doi: 10.1002/ajhb.22599

Fareed, M., and Afzal, M. (2016). Increased cardiovascular risks associated with familial inbreeding: a population-based study of adolescent cohort. *Ann. Epidemiol.* 26, 283–292. doi: 10.1016/j.annepidem.2016.03.001

Fareed, M., and Afzal, M. (2017). Genetics of consanguinity and inbreeding in health and disease. *Ann. Hum. Biol.* 44, 99–107. doi: 10.1080/03014460.2016.1265148

Fareed, M., Kaisar Ahmad, M., Azeem Anwar, M., and Afzal, M. (2017). Impact of consanguineous marriages and degrees of inbreeding on fertility, child mortality, secondary sex ratio, selection intensity, and genetic load: a cross-sectional study from Northern India. *Pediatr. Res.* 81, 18–26. doi: 10.1038/pr.2016.177

Ganapathy, A., Pandey, N., Srisailapathy, C. R. S., Jalvi, R., Malhotra, V., Venkatappa, M., et al. (2014). Non-syndromic hearing impairment in India: high allelic heterogeneity among mutations in TMPRSS3, TMC1, USHIC, CDH23 and TMIE. *PLoS One* 9:e84773. doi: 10.1371/journal.pone.0084773

Hams, N., Padmanarayana, M., Qiu, W., and Johnson, C. P. (2017). Otoferlin is a multivalent calcium-sensitive scaffold linking SNAREs and calcium channels. *Proc. Natl. Acad. Sci. U.S.A.* 114, 8023–8028. doi: 10.1073/pnas.1703240114

Helfmann, S., Neumann, P., Tittmann, K., Moser, T., Ficner, R., and Reisinger, E. (2011). The crystal structure of the C2A domain of otoferlin reveals an unconventional top loop region. *J. Mol. Biol.* 406, 479–490. doi: 10.1016/j.jmb.2010.12.031

Iwasa, Y.-I., Nishio, S.-Y., Sugaya, A., Kataoka, Y., Kanda, Y., Taniguchi, M., et al. (2019). OTOF mutation analysis with massively parallel DNA sequencing in

2,265 Japanese sensorineural hearing loss patients. *PLoS One* 14:e0215932. doi: 10.1371/journal.pone.0215932

Karczewski, K. J., Francioli, L. C., Tiao, G., Cummings, B. B., Alföldi, J., Wang, Q., et al. (2020). The mutational constraint spectrum quantified from variation in 141,456 humans. *Nature* 581, 434–443. doi: 10.1038/s41586-020-2308-7

Kent, W. J., Sugnet, C. W., Furey, T. S., Roskin, K. M., Pringle, T. H., Zahler, A. M., et al. (2002). The human genome browser at UCSC. *Genome Res.* 12, 996–1006. doi: 10.1101/gr.229102

Kim, B. J., Jang, J. H., Han, J. H., Park, H.-R., Oh, D. Y., Lee, S., et al. (2018). Mutational and phenotypic spectrum of OTOF-related auditory neuropathy in Koreans: eliciting reciprocal interaction between bench and clinics. *J. Trans. Med.* 16:330. doi: 10.1186/s12967-018-1708-z

Koile, D., Cordoba, M., de Sousa Serro, M., Kauffman, M. A., and Yankilevich, P. (2018). GenIO: a phenotype-genotype analysis web server for clinical genomics of rare diseases. *BMC Bioinformatics* 19:25. doi: 10.1186/s12859-018-2027-3

Kumar, P., Henikoff, S., and Ng, P. C. (2009). Predicting the effects of coding non-synonymous variants on protein function using the SIFT algorithm. *Nat. Protoc.* 4, 1073–1081. doi: 10.1038/nprot.2009.86

Lek, M., Karczewski, K. J., Minikel, E. V., Samocha, K. E., Banks, E., Fennell, T., et al. (2016). Analysis of protein-coding genetic variation in 60,706 humans. *Nature* 536, 285–291. doi: 10.1038/nature19057

Liu, H., Pecka, J. L., Zhang, Q., Soukup, G. A., Beisel, K. W., and He, D. Z. Z. (2014). Characterization of transcriptomes of cochlear inner and outer hair cells. *J. Neurosci.* 34, 11085–11095. doi: 10.1523/JNEUROSCI.1690-14.2014

Mahdieh, N., Shirkavand, A., Rabbani, B., Tekin, M., Akbari, B., Akbari, M. T., et al. (2012). Screening of OTOF mutations in Iran: a novel mutation and review. *Int. J. Pediatr. Otorhinolaryngol.* 76, 1610–1615. doi: 10.1016/j.ijporl.2012.07.030

Mirghomizadeh, F., Pfister, M., Apaydin, F., Petit, C., Kupka, S., Pusch, C. M., et al. (2002). Substitutions in the conserved C2C domain of otoferlin cause DFNB9, a form of nonsyndromic autosomal recessive deafness. *Neurobiol. Dis.* 10, 157–164. doi: 10.1006/nbdi.2002.0488

Olusanya, B. O., Davis, A. C., and Hoffman, H. J. (2019). Hearing loss: rising prevalence and impact. *Bull. World Health Organ.* 97, 646–646A. doi: 10.2471/BLT.19.224683

Padma, G., Ramchander, P. V., Nandur, U. V., and Padma, T. (2009). GJB2 and GJB6 gene mutations found in Indian probands with congenital hearing impairment. *J. Genet.* 88, 267–272. doi: 10.1007/s12041-009-0039-5

Pangršič, T., Reisinger, E., and Moser, T. (2012). Otoferlin: a multi-C2 domain protein essential for hearing. *Trends Neurosci.* 35, 671–680. doi: 10.1016/j.tins.2012.08.002

Patterson, N., Moorjani, P., Luo, Y., Mallick, S., Rohland, N., Zhan, Y., et al. (2012). Ancient admixture in human history. *Genetics* 192, 1065–1093. doi: 10.1534/genetics.112.145037

Ramakrishnan, N. A., Drescher, M. J., Morley, B. J., Kelley, P. M., and Drescher, D. G. (2014). Calcium regulates molecular interactions of otoferlin with soluble NSF attachment protein receptor (SNARE) proteins required for hair cell exocytosis. *J. Biol. Chem.* 289, 8750–8766. doi: 10.1074/jbc.M113.480533

Rodríguez-Ballesteros, M., Reynoso, R., Olarte, M., Villamar, M., Morera, C., Santarelli, R., et al. (2008). A multicenter study on the prevalence and spectrum of mutations in the otoferlin gene (OTOF) in subjects with nonsyndromic hearing impairment and auditory neuropathy. *Hum. Mut.* 29, 823–831. doi: 10.1002/humu.20708

Roux, I., Safieddine, S., Nouvian, R., Grati, M., Simmler, M.-C., Bahloul, A., et al. (2006). Otoferlin, defective in a human deafness form, is essential for exocytosis at the auditory ribbon synapse. *Cell* 127, 277–289. doi: 10.1016/j.cell.2006.08.040

Schreiber, F., Patricio, M., Muffato, M., Pignatelli, M., and Bateman, A. (2014). TreeFam v9: a new website, more species and orthology-on-the-fly. *Nucleic Acids Res.* 42, D922–D925. doi: 10.1093/nar/gkt1055

Schwarz, J. M., Cooper, D. N., Schuelke, M., and Seelow, D. (2014). MutationTaster2: mutation prediction for the deep-sequencing age. *Nat. Methods* 11, 361–362. doi: 10.1038/nmeth.2890

Shearer, A. E., DeLuca, A. P., Hildebrand, M. S., Taylor, K. R., Gurrola, J., Scherer, S., et al. (2010). Comprehensive genetic testing for hereditary hearing loss using massively parallel sequencing. *Proc. Natl. Acad. Sci. U.S.A.* 107, 21104–21109. doi: 10.1073/pnas.1012989107

Shearer, A. E., Hildebrand, M. S., and Smith, R. J. (1993). *Hereditary Hearing Loss and Deafness Overview*. Seattle: University of Washington.

Shin, O.-H. (2014). Exocytosis and synaptic vesicle function. *Compr. Physiol.* 4, 149–175. doi: 10.1002/cphy.c130021

Singh, P. K., Sharma, S., Ghosh, M., Shastri, S. S., Gupta, N., and Kabra, M. (2018). Spectrum of GJB2 gene variants in Indian children with non-syndromic hearing loss. *Ind. J. Med. Res.* 147, 615–618. doi: 10.4103/ijmr.IJMR_76_16

Szklarczyk, D., Gable, A. L., Lyon, D., Junge, A., Wyder, S., Huerta-Cepas, J., et al. (2019). STRING v11: protein-protein association networks with increased coverage, supporting functional discovery in genome-wide experimental datasets. *Nucleic Acids Res.* 47, D607–D613. doi: 10.1093/nar/gky1131

Tekin, M., Akcayoz, D., and Incesulu, A. (2005). A novel missense mutation in a C2 domain of OTOF results in autosomal recessive auditory neuropathy. *Am. J. Med. Genet. A* 138, 6–10. doi: 10.1002/ajmg.a.30907

Vona, B., Nanda, I., Hofrichter, M. A. H., Shehata-Dieler, W., and Haaf, T. (2015). Non-syndromic hearing loss gene identification: a brief history and glimpse into the future. *Mol. Cell. probes* 29, 260–270. doi: 10.1016/j.mcp.2015.03.008

Wang, D.-Y., Wang, Y.-C., Weil, D., Zhao, Y.-L., Rao, S.-Q., Zong, L., et al. (2010). Screening mutations of OTOF gene in Chinese patients with auditory neuropathy, including a familial case of temperature-sensitive auditory neuropathy. *BMC Med. Genet.* 11:79. doi: 10.1186/1471-2350-11-79

World Health Organization (2018). *WHO Programme for Ear and Hearing Care*. 1–14. Available online at: https://www.hearingreview.com/wp-content/uploads/2019/02/WHO-2018-Activity-Report.pdf (accessed March 10, 2021).

Yan, D., Kannan-Sundhari, A., Vishwanath, S., Qing, J., Mittal, R., Kameswaran, M., et al. (2015). The genetic basis of nonsyndromic hearing loss in Indian and Pakistani populations. *Genet. Test. Biomarkers* 19, 512–527. doi: 10.1089/gtmb.2015.0023

Yasunaga, S., Grati, M., Chardenoux, S., Smith, T. N., Friedman, T. B., Lalwani, A. K., et al. (2000). OTOF encodes multiple long and short isoforms: genetic evidence that the long ones underlie recessive deafness DFNB9. *Am. J. Hum. Genet.* 67, 591–600. doi: 10.1086/303049

Zerbino, D. R., Achuthan, P., Akanni, W., Amode, M. R., Barrell, D., Bhai, J., et al. (2018). Ensembl 2018. *Nucleic Acids Res.* 46, D754–D761. doi: 10.1093/nar/gkx1098

Ñhurbanov, A. Y., Karafet, T. M., Morozov, I. V., Mikhalskaia, V. Y., Zytsar, M. V., Bondar, A. A., et al. (2016). Whole exome sequencing reveals homozygous mutations in RAI1, OTOF, and SLC26A4 genes associated with nonsyndromic hearing loss in altaian families (South Siberia). *PLoS One* 11:e0153841. doi: 10.1371/journal.pone.0153841

Conflict of Interest: IS was employed by company BioinfoRes, Jammu, India.

The remaining authors declare that the research was conducted in the absence of any commercial or financial relationships that could be construed as a potential conflict of interest.

frontiers in Genetics

CASE REPORT
published: 31 May 2021
doi: 10.3389/fgene.2021.650639

Case Report: Identification of Novel Variants in *ERCC4* and *DDB2* Genes in Two Tunisian Patients With Atypical Xeroderma Pigmentosum Phenotype

*Imen Nabouli[1], Asma Chikhaoui[1], Houcemeddine Othman[2], Sahar Elouej[1,3], Meriem Jones[1,4], Arnaud Lagarde[3], Meriem Ben Rekaya[1], Olfa Messaoud[1], Mohamed Zghal[4], Valerie Delague[3], Nicolas Levy[3,5], Annachiara De Sandre-Giovannoli[3,6], Sonia Abdelhak[1] and Houda Yacoub-Youssef[1]**

[1] Laboratoire de Génomique Biomédicale et Oncogénétique, Institut Pasteur de Tunis, LR16IPT05, Université Tunis ElManar, Tunis, Tunisia, [2] Faculty of Health Sciences, Sydney Brenner Institute for Molecular Bioscience, University of the Witwatersrand, Johannesburg, South Africa, [3] Aix Marseille Univ, INSERM, MMG, U1251, Marseille, France, [4] Service de dermatologie, Hôpital Charles Nicolle, Tunis, Tunisia, [5] Departement of Medical Genetics, Assistance Publique Hôpitaux de Marseille, La Timone Children's Hospital, Marseille, France, [6] Biological Resource Center (CRB-TAC), Assistance Publique Hôpitaux de Marseille, La Timone Children's Hospital, Marseille, France

OPEN ACCESS

Edited by:
Emiliano González Vioque, University Clinical Hospital of Santiago, Spain

Reviewed by:
Liang-Liang Fan, Central South University, China
Wei-Ling Tsou, Wayne State University, United States

***Correspondence:**
Houda Yacoub-Youssef
houda.yacoub@pasteur.utm.tn
orcid.org/0000-0001-5351-4775

Specialty section:
This article was submitted to Genetics of Common and Rare Diseases, a section of the journal Frontiers in Genetics

Received: *07 January 2021*
Accepted: *29 April 2021*
Published: *31 May 2021*

Citation:
Nabouli I, Chikhaoui A, Othman H, Elouej S, Jones M, Lagarde A, Rekaya MB, Messaoud O, Zghal M, Delague V, Levy N, De Sandre-Giovannoli A, Abdelhak S and Yacoub-Youssef H (2021) Case Report: Identification of Novel Variants in ERCC4 and DDB2 Genes in Two Tunisian Patients With Atypical Xeroderma Pigmentosum Phenotype. Front. Genet. 12:650639. doi: 10.3389/fgene.2021.650639

Xeroderma Pigmentosum (XP) is a rare genetic disorder affecting the nucleotide excision repair system (NER). It is characterized by an extreme sensitivity to sunlight that induces cutaneous disorders such as severe sunburn, freckling and cancers. In Tunisia, six complementation groups have been already identified. However, the genetic etiology remains unknown for several patients. In this study, we investigated clinical characteristics and genetic defects in two families with atypical phenotypes originating from the central region in Tunisia. Clinical investigation revealed mild cutaneous features in two patients who develop multiple skin cancers at later ages, with no neurological disorders. Targeted gene sequencing revealed that they carried novel variants. A homozygous variation in the *ERCC4* gene c.1762G>T, p.V588F, detected in patient XP21. As for patient XP134, he carried two homozygous mutations in the *DDB2* gene c.613T>C, p.C205R and c.618C>A, p.S206R. Structural modeling of the protein predicted the identified *ERCC4* variant to mildly affect protein stability without affecting its functional domains. As for the case of DDB2 double mutant, the second variation seems to cause a mild effect on the protein structure unlike the first variation which does not seem to have an effect on it. This study contributes to further characterize the mutation spectrum of XP in Tunisian families. Targeted gene sequencing accelerated the identification of rare unexpected genetic defects for diagnostic testing and genetic counseling.

Keywords: xeroderma pigmentosum, NER defects, skin cancer, ERCC4/XPF, DDB2 gene

INTRODUCTION

Consanguinity plays a relevant role in the emergence of rare genetic diseases especially in North Africa and Middle East countries (Romdhane et al., 2012). Xeroderma pigmentosum (XP) is a rare autosomal recessive disorder characterized by predisposition to cutaneous malignancies. Its prevalence is estimated to 1/250.000 in Europe (Kleijer et al., 2008). However, it is more frequent in North Africa and especially in Tunisia (1/10.000) (Zghal et al., 2005). XP displays a wide clinical and genetic heterogeneity. It results from mutations in eight different genes: *XPA* through *XPG*, which encode Nucleotide Excision Repair (NER) genes, and *XPV* that encodes the Translesion Synthesis (TLS) DNA polymerase eta (Kleijer et al., 2008).

XP prognosis was widely improved due to increased knowledge about the frequent forms of the disease in Tunisia as XP-A, XP-C and XP-V (Ben Rekaya et al., 2009, 2014; Messaoud et al., 2010), Recently, thanks to the use of novel technologies such as high throughput sequencing, extremely rare forms are increasingly being identified as XP-D, XP-E, XP-G (Ben Rekaya et al., 2017; Chikhaoui et al., 2019).

The identification of disease-causing mutations in XP patients has an important impact on patient care, as it provides early dermatological follow up to prevent skin cancers and provides genetic counseling for affected family members. However, genetic diagnosis is difficult to carry out for a disease that shows such genetic heterogeneity. In addition, Sanger sequencing for known recurrent mutations that are common in specific geographic area does not always succeed in finding the genetic causes of atypical forms of the disease.

In this study, we describe clinical features and report novel genetic defects using targeted gene sequencing in two patients with particular forms of XP. One associated to XP-F, phenotype which we identify for the first time in the Tunisian population and the other consists of a double homozygous mutation in the *DDB2* gene associated to XP-E form.

Case Presentation

Clinical Presentation

Patient XP21

Patient XP21 is a 56-year-old woman, second child of healthy first-degree consanguineous parents originating from North-West of Tunisia (**Figure 1A**). When she was 6 years old, she developed achromic maculas on sun-exposed area of her skin. She consulted a doctor at 26, when she developed her fist basal cell carcinoma (BCC). XP21 had a normal psychomotor and mental development with no neurological manifestations. In her last consultation at age 56, when this study was conducted, she had developed several actinic keratosis. Her skin was dry and presented hyperpigmented areas. It is important to note that XP21 did not suffer from acute sunburn reaction nor had any photosensitivity manifestations. In addition, she had a short stature, but no microcephaly or neurological disorders suggestive of Cockayne syndrome were observed (**Table 1**). Only the reported patient and her healthy sister underwent clinical examination in a medical center. As mentioned by the patient, other family members with similar phenotypes came to our attention during the genetic inquiry about familial history, who presented mainly achromic maculas on their sun exposed area and that's in 2 brothers and one sister (**Figure 1A**). Unfortunately, they were out of reach as they lived far from medical centers.

Patient XP134

Patient XP134 was a 15-year old girl born from a consanguineous marriage (**Figure 1B**), with parents originating from the central region of Tunisia. The patient did not show any neurological abnormalities. As she was not protected from UV radiations, she presented an important number of actinic keratosis on sun-exposed areas and numerous squamous cell carcinomas and basal cell carcinomas on the face especially around the nose. She presented few hyperpigmented and hypopigmented patterns macules on her skin (**Table 1**). We tried to reach XP134's sister who was described as having similar clinical manifestations as pigmentation problems on sun exposed area, but she was out of reach. The proband's parents as well.

Genetic Investigations

Sanger Sequencing for Recurrent Mutations

Genetic pre-screening for recurrent and founder mutations observed in Tunisian XP patients was conducted in both patients XP21 and XP134 using Sanger Sequencing. Firstly, the patients were screened for already known mutations that are recurrent in Tunisian population as: p.Arg228* in *XPA* gene, p.Val548AlafsX25 in *XPC* gene and the deletion g.36847_40771del3925 in *POLH* gene. Secondly, we screened the mutations associated with other mild forms of XP with neurological manifestations as: p.Arg683Gln in the *ERCC2* gene (XP-D phenotype), P.Leu778Pro in *ERCC5* gene (XP-G phenotype) and p.Lys381Argfs*2 mutation in *DDB2* gene (XP-E phenotype). None of these mutations was found.

Therefore, samples underwent targeted gene sequencing to cover other genes of the DNA repair pathways.

Targeted Gene Sequencing Results

Through targeted gene sequencing of 87 genes involved in NER pathway, we identified in patient XP21 a novel homozygous missense variation in *ERCC4,* within exon 8, (NM_005236.2 c.1762G>T p.Val588Phe) (**Figure 2A**). Bioinformatic prediction tools (SIFT, POLYPHEN, mutation taster…) indicated that this mutation was pathogenic (**Table 2**). Moreover, through the prediction algorithm of human splicing finder tools, this variation was suggested to create an exonic splicing silencer (ESS) probably altering the splicing process.

Regarding the patient XP134, we found that he carried a double homozygous missense variation in *DDB2* gene in exon 5 (NM_000107.2: c.613T>C p.Cys205Arg) and c.618C>A p.Ser206Arg (rs759622121) (**Figure 2B**). Both variants were not described in any population database (Exac, GnomAD, 1000 Genomes...) and both are predicted to induce pathogenic effects using several prediction tools (SIFT, POLYPHEN, mutation taster…) (**Table 2**). Concerning the ACMG classification (Varsome), both variants were classed as of uncertain significance (class 3). Furthermore, this particular genetic profile was not

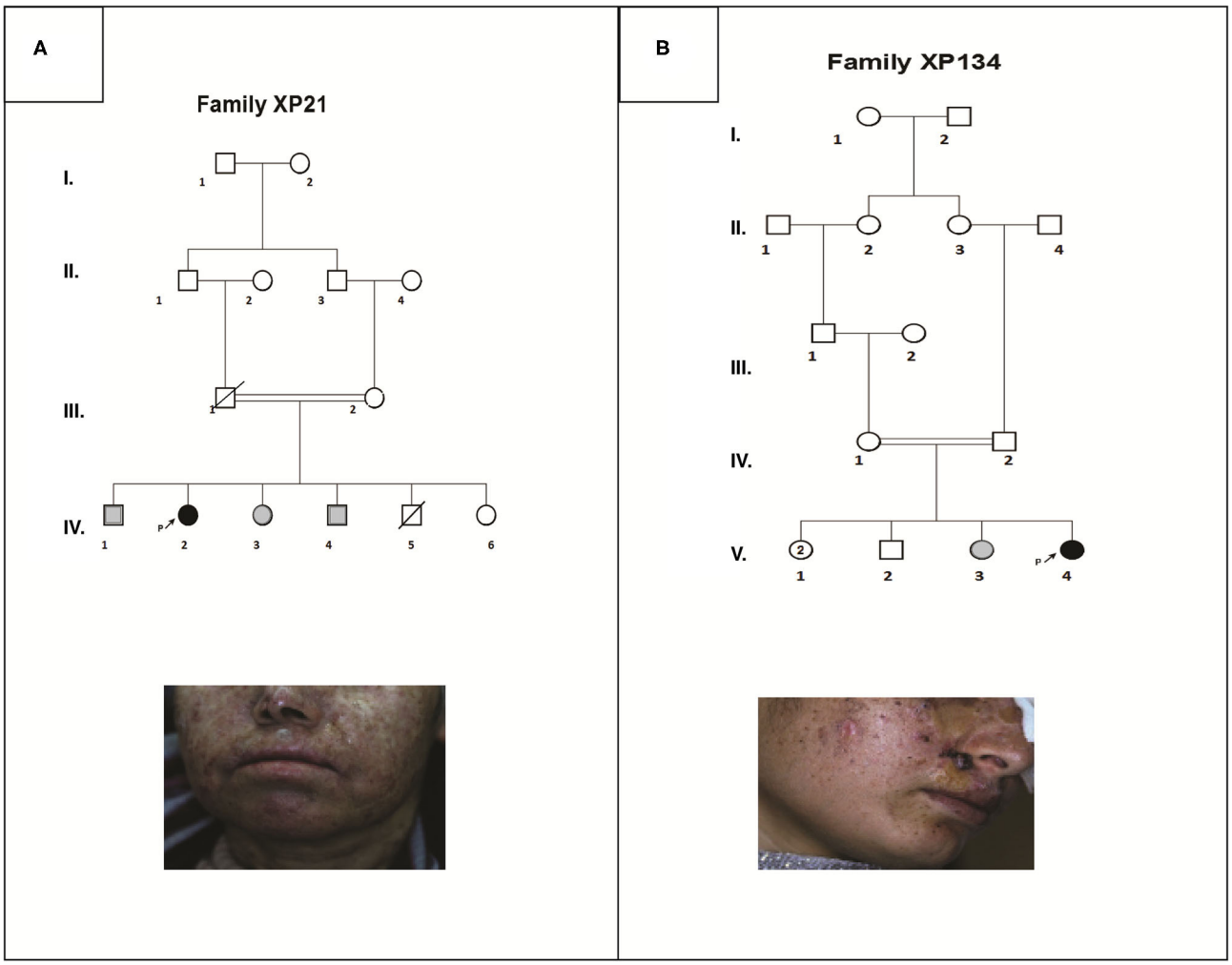

FIGURE 1 | Pedigrees and clinical images describing two XP affected family members (XP21 and XP134) **(A,B)**. Filled symbols represent affected individuals, open symbols represent unaffected individuals, gray symbols are for suspected individuals, the studied pro-band is indicated with an arrow.

previously described in any XP patient. Molecular diagnosis was confirmed by Sanger sequencing for each variation.

Molecular Modeling of the Mutant Protein Structures

Modeling XP-F Mutation

The search for a template using BLAST-based approaches was not able to identify an appropriate template. Therefore, we used a fold recognition based approach for such an end. First, we predicted the repartition of the domains of XPF along the sequence. We found that the segment 374–623 matches a hit with a significant E-value of 7.60e-98 corresponding to a helicase insert domain superfamily in accordance with the functional properties of XPF. We then proceeded to model this domain using a threading approach. pGenTHREADER was able to identify several hits with high confidence values. We selected the PDB entry, 1WP9, which corresponds to the crystal structure of Pyrococcus furiosus Hef helicase domain (PubMed: 15642269) as a template to construct the model. Our initial attempt to predict the structure led to a bad quality model consisting of severe distortions of the rigid secondary structure elements. In fact, the RMSD (Root Mean Square Distance) between the template and the model is of 6 Angstroms. When we inspected the model, we found that the problem is caused by the long exposed loops spanning between the alpha-helices of the protein. We, therefore, proceed by trimming the sequences of these loops (**Supplemental Material**) to keep at least 4 amino acids from the C and N termini ends. Such an approach might be capable of preserving the original properties of the exposed surface of the target protein. The Ramachandran plot confirmed a decent quality of the model with 90% of the dihedral angles are in the favored domain and 7% in the allowed region. Even with such a model, we could not be able to explain the effect of the mutation. Therefore, we inspected the possibility that the predicted structure of the helicase insert domain could establish interdomain contacts in the XPF protein. We proceeded first by predicting the residue-residue contact map using RaprorX (Wang et al., 2017). Indeed,

TABLE 1 | Summary of the clinical examination of XP patients.

	XP21 (XP-F)	XP134-1 (XP-E)
Age at last observation (year)	56	15
Age at onset of first symptoms (year)	6	5
Sex	F	F
Protection level	+	–
Geographical origin	Seliana (North West)	Kairouan (Sbikha)
Photophobia	–	±
Photosensitivity	–	–
Neurologic phenotype	–	–
Language delay	–	–
Sunburn	–	–
Irritation	±	±
Hyperpigmentation	+	+
Hypopigmented macula	–	+
Achromic macula	+	+
Dry skin	+	+
Cheilit	+	±
Age at consultation for skin cancer	26 years old for BCC	15 years old Multiple actinic keratosis, SCC and BCC
Actinic keratosis	+	++
Benign skin neoplasm, internal cancers	–	–

BCC, Basal Cell Carcinoma; SCC, Spino Cell Carcinoma.

the tool predicted a putative interaction of the helicase insert domain with residues 210-216 (EVVEIHV). According to the protein secondary structure prediction, this segment corresponds to a beta-sheet strand (Drozdetskiy et al., 2015). This region is also flanked by two alpha-helices with 6 and 24 residues. The equivalent aligned segment of the template structure corresponds to two helices of 5 and 24 amino acids flanking a beta stand segment interacting with the helicase insert domain.

Therefore, the structure of XPF was modeled in the presence of the 210-216 segment.

The position of V588 (R138 in the structure) corresponds to an alpha-helix (585-LTFVRQ LEIYR-596) rich in charged and polar amino acids. Residues of this helix are exposed to the solvent with only F589 and L591 making part of the hydrophilic core of the protein. We noticed that in the V588 in the wild type protein forms a hydrophobic cluster of residues with F607, A583, and L580. In the case of V588F mutation causes steric clashes with L580 residue due to its large bulky side chain compared to a valine amino acid in the wild type form (**Figure 2C**).

Modeling XP-E Mutation

The two mutations, C205R and S206R are located on a beta sheet that forms one of the blades of the WD40 beta-propeller domain. The mutations are close to the protein-DNA interface which are known to rely on electrostatic forces to stabilize the complex. In order to verify if the two mutations can disrupt the electrostatic properties of the protein-DNA interface, we calculated the pKa for the ionizable side chains at positions 205 and 206 for both the wild type and the mutant forms at physiological pH of 7.4 using PROPKA 3.0 (10.1021/ct100578z). The pKa value of C205 side chain is predicted to be at 8.59. Therefore, this residue is probably deprotonated in the wild type form. Both residues R205 and R206 in the mutant form are positively charged with predicted pKa values of 10.41 and 8.63. To our surprise, the electrostatic potential at the protein DNA interface did not drastically change between the wild type and the mutant forms (**Supplementary Data**). The R205 ionizable group remains exposed to the central cavity of the WD40 beta-propeller domain. The same configuration is also demonstrated by the side chain of C205 residue in the wild type form. However, for R206, the side chain is bulky compared to S206 amino acid in the wild type form. Its relatively long side chain is unable to interact with the deepest most residues forming the interface of two bladders (Residues V225, V245 and T260) which is not the case for S206 in the wild type form (**Figure 2D**).

MATERIALS AND METHODS

Patients

This study was conducted according to the principles of the declaration of Helsinki and has obtained the ethical approval (IPT/LR05/ProjectPCI/22/2012/v2) from the institutional review board of Institut Pasteur de Tunis.

The two patients (XP21 and XP134) referred to dermatology department of Charles Nicolle hospital with clinical features suggestive of XP. Written informed consent was obtained for genetic analysis from patients or their parents.

DNA Extraction, Library Construction, Sequencing, and Data Analysis

Genomic DNA was extracted from peripheral blood. Amplicon libraries were prepared from 1,000 ng of genomic DNA from patients. Custom design of DNA repair disorders' panel was performed using SureDesign (Agilent Technologies Inc.), with probes that cover the exons in 87 genes and 15 bp of the surrounding intronic sequences. Library preparation for NGS was done using the Agilent's HaloPlex^{HS} workflow as a target enrichment method. Massively parallel sequencing was performed on an Ion Torrent PGM (Thermo Fisher Scientific).

The data from the sequencing runs were analyzed using the Torrent Suite v4.0.2 analysis pipeline, and aligned using TMAPv.3. The output variant call format (VCF) file was then annotated using the in-house VarAft software version 2.5, which is available online (http://varaft.eu/index.php) (Desvignes et al., 2018). Sequence variants were compared with data in Exome Variant Server (http://evs.gs.washington.edu/EVS/), 1000 Genomes Project (http://www.1000genomes.org/), or GnomAD (https://gnomad.broadinstitute.org/), including Exome Aggregation Consortium database (ExAC), Cambridge, MA (http://exac.broadinstitute.org). A number of online tools were used to predict the functional impact and pathogenicity of the variants such as MutationTaster (http://www.mutationtaster.org/), PolyPhen (http://genetics.bwh.harvard.edu/pph2/),

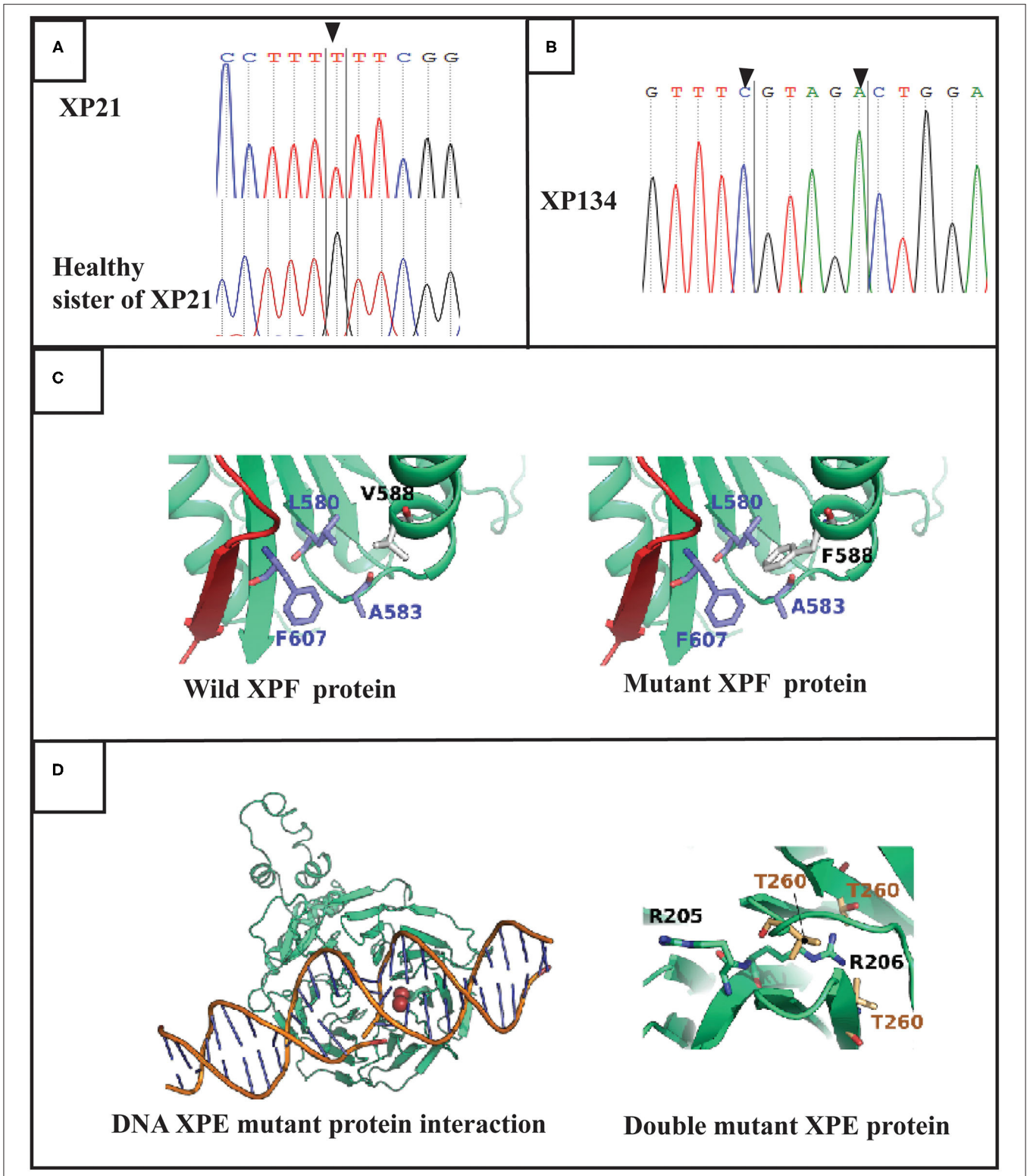

FIGURE 2 | Molecular findings: **(A)** Electropherogram showing the variation in *ERCC4* gene in exon 8 (c.1762 G>T p.V588F) at a homozygous state in the patient XP21. **(B)** Electropherogram showing double variation in *DDB2* gene (c.613 T>C p.C205R and c.618 C>A p.S206R) in exon 5 in XP134 patient. **(C)** Structures of the XPF protein and F588 XPF mutant suggesting a mild distortion in helix domain. **(D)** DNA DDB2 protein interaction for muted DDB2 protein suggestion that R206 affect this process.

TABLE 2 | Prediction scores of the new detected variants in DDB2 and ERCC4 genes.

Gene	Variant	Prediction tools	Score	Significance
DDB2	c.613T>C; p.C205R	Mutation taster	0.99	Disease causing
		Polyphen	1	Probably damaging
		SIFT	2.77	damaging
		M-CAP	0.066	Possibly damaging
		Provean	−6.13	deleterious
		MUpro	−1.40	Decrease stability
DDB2	c.618C>A; p.S206R	Mutation taster	0.99	Disease causing
		Polyphen	1	Probably damaging
		SIFT	2.78	damaging
		M-CAP	0.05	Possibly damaging
		Provean	−2.9	deleterious
		MUpro	−1.05	Decrease stability
ERCC4	c.1762G>T; p.V588P	Mutation taster	0.99	Disease causing
		Polyphen	1	Probably damaging
		SIFT	2.8	damaging
		M-CAP	0.177	Possibly damaging
		Provean	−5.69	deleterious
		MUpro	−1.64	Decrease stability

SIFT (http://sift.bii.a-star.edu.sg/), M-CAP (http://bejerano.stanford.edu/mcap/), Provean (http://provean.jcvi.org/index.php) and MU Pro for protein stability prediction (http://mupro.proteomics.ics.uci.edu/).

Sanger Sequencing

The detected variants with a high prediction score of pathogenicity underwent targeted Sanger sequencing for validation using the following primers: **ERCC4F**: 5′GTAAGATGTCTTCCCTTCGG 3′; **ERCC4R:** 5′CATAAGCAGCATCGTAACGG 3′ and **DDB2F**: 5′ATGGAGCAGTCTGAATGTTC 3′; **DDB2R**: 5′CCACTCCTCTAGACAGG3′) which cover both variants in DDB2 gene. Direct sequencing was performed using Big Dye terminator technology (ABI 3130), and sequences were analyzed using Bioedit packages. Genomic and protein sequence variants are described following the Human Genome Variations Society Guidelines available at https://varnomen.hgvs.org/. *ERCC4* and *DDB2* variants are, respectively, described relative to the transcript reference sequences NM_005236.2 and NM_NM_000107.2. ACMG classification of the variants (Richards et al., 2015) was obtained using Varsome at https://varsome.com.

Protein Modeling

The primary structure of XPF endonuclease was deposited in UiprotKB database under the accession Q92889. The sequence consists of 916 amino acids of which only the structure corresponding to segment 834-916 was solved experimentally. To solve the structure of the region containing the mutation we first searched for conserved domains of the entire sequence. The search for the appropriate template to construct the 3D structure of XPF was performed using the pGenTHREADER program. The sequences of the best hits were then processed and aligned to the target sequence of XPF using 3D-expresso. The resulting alignment was then used to guide the model building process by MODELER (version 9.15). Twenty conformers were generated by the comparative modeling software of which we selected the best model according to the DOPE and the GA341 scores. Finally, the stereochemical quality of the model was assessed by constructing the Ramachandran plot to dress the repartition of the phi/psi angles in the favored, allowed, and non-tolerated dihedral domains.

The XP-E structure was retrieved from the co-crystal complex of PDB code 4E54 (PMID 22822215).

DISCUSSION

XP is a rare autosomal recessive disorder, characterized by ubiquitous defects in the DNA repair system. This disorder is especially characterized by sunburn after brief sun exposure and pigmented macules on sun-exposed skin (Krieger and Berneburg, 2012). Targeted gene panels help to focus on a set of relevant candidate genes within the overlapping phenotypes with similar clinical manifestations, to identify the exact genetic etiology while providing cost and time advantages when compared to classical Sanger sequencing.

About 40% of XP patients do not show sunburn reactions (Bradford et al., 2011). As for XP-E, increased number of freckles in sun-exposed areas seems to be the unique symptom for clinical diagnosis of the disease. These maculae are usually ignored and only the development of primary malignant lesions seems to be the reason leading to clinical consultation. This often results in a late diagnosis of patients with mild XP forms.

We report in the region, the XP-F form which is among the rarest complementation groups of XP. To date, 29 XP-F patients were reported worldwide (Ferri et al., 2020). Most of them are Japanese (Tofuku et al., 2015). XP-F (Omim: #278760) is caused by mutations in *ERCC4* gene. Furthermore, several *ERCC4* mutations were associated to a combined XP/CS phenotype, to XFE progeroid syndrome, Cockayne syndrome, Cerebellar ataxia-dominant phenotype or to Fanconi Anemia disease complementation group Q (Kashiyama et al., 2013; Doi et al., 2018). Although the clinical features of patient XP21 indicated a phenotype of Xeroderma pigmentosum, a moderate form of Fanconi anemia type Q was suspected. This hypothesis was quickly dismissed as patient XP21, and despite her short stature, did not develop internal cancers or neurological disorders. Fertility was not explored as the patient was not married.

The protein XPF consists of 916 amino acids. It forms a heterodimeric complex with ERCC1 and plays the role of structure-specific endonuclease 5' incision during the activation of NER repair system upon UV induced DNA damage (Sijbers et al., 1996; Richards et al., 2015). Twenty-seven variations have been reported thus far in the *ERCC4* gene (Zhou et al., 2017). While most mutations in this gene are located in exon 8, suggesting that it may represent a hotspot mutation site, the variants in this area can lead to different disorders.

Indeed, patient XP21 harbored a novel G to T transversion at position c.1762. In the same exon, other variants as p.R589W give rise to combined XP/CS/FA, Fanconi anemia or mild XP forms. In our study, given the late onset of cutaneous cancer and the lack of associated neurological disorders, we suggest that patient XP21 was affected with a mild XP-F form.

The *ERCC4* endonuclease consists of an N-terminal DNA helicases domain (1-457), a domain containing the nuclease active site (656-813) and a C-terminal containing 2 tandem helix-hairpin-helix (HhH) domain (Manandhar et al., 2015). The previously reported *ERCC4* mutations are widely distributed over the entire length of the protein (Bogliolo et al., 2013; Kashiyama et al., 2013; Zhou et al., 2017; Mori et al., 2018). The novel reported variation in this study is located outside the nuclease active site.

The molecular modeling study suggests that the V588F mutation effect is probably caused by the steric clashes between F588 and L580. The latter amino acid belongs to the beta sheet which holds many of the core residues of the helicase insert domain. Of most importance, the 210-216 segment also belongs to this beta-sheet forming the outermost strand. The steric clash between F588 and L580 could cause a local distortion of the beta sheet. While this might not have a significant effect on the interaction of the helicase insert domain with the DNA, the fact that the 210-216 segment is implicated in the interaction network of the central beta sheet, suggests the cooperative functionality established between modeled helicase insert domain and other segments of the protein might be affected by the mutation.

Xeroderma pigmentosum type E (Omim: # 278740) caused by mutations in the *DDB2* gene. The DDB2 subunit is a component of a complex involved in ubiquitin-mediated proteolysis. Consisting of 427 residues, it plays a major role in DNA-damage recognition (Stoyanova et al., 2009). To date, more than 24 XP-E patients have been reported worldwide (Nichols et al., 1996; Itoh et al., 2000; Vahteristo et al., 2007; Oh et al., 2011; Karagün et al., 2020; Yang et al., 2020) and 17 variations were reported in *DDB2* gene (Yang et al., 2020). None of them is from North African countries except 3 Tunisian patients reported previously by our lab (Ben Rekaya et al., 2017). In this study, we report another novel variation in the Tunisian population emphasizing the complex genetic background of North African population.

It is a double homozygous patient harboring two novel mutations in the same exon of *DDB2* gene, responsible for XP-E, which was never described in XP patients. The emergence of rare autosomal genetic variants is frequent in people with common ethnic origin caused by consanguinity and endogamy. However, the appearance of double variations is an extremely rare event. These double mutations could explain the severe clinical phenotype in XP134 patient.

The DDB2 protein is composed from an N-terminal helix-loop helix segment (101 to 136) followed by a 7-bladed WD40 b propeller domain (residues 137 to 454) (Scrima et al., 2008). It is an ubiquitin ligase component of a multimeric complex involved in the degradation of DNA damage-response proteins (Liu et al., 2009). The two C205R and S206R variants in XP134 are located on a beta sheet that forms one of the blades of the beta-propeller WD40 domain of the DDB2 protein. Mutations close to the protein-DNA interface are known to delay electrostatic forces to stabilize the complex (Scrima et al., 2008), which could explain the severity of the XP134 phenotype compared to previously described XP-E patients (Ben Rekaya et al., 2017).

Our protein modeling study also suggests that the effect of the C205R mutation is not probably responsible for the clinical phenotype since the mutation preserves both, the number of charges carried by the corresponding residue and the electrostatic potential at the protein-DNA interface. Instead, the S206R mutation might have a significant effect on the protein structure. This could be explained by the fact that the mutation causes the R205 positively charged side chain to be buried inside the hydrophobic core of the protein. Such configuration is highly unstable and could cause the local distortion of the protein at the mutation level, but also could have a more severe consequence on the interaction with the damaged DNA.

CONCLUSION

In this report, we further characterize new XP complementation groups emerging in the Tunisian population and in the region. While the mutational findings have improved the understanding of XP phenotype, it is necessary to continue the molecular investigations for other underdiagnosed patients for whom the discovery of genetic etiology will improve the clinical follow up.

DATA AVAILABILITY STATEMENT

The original contributions presented in the study are included in the article/**Supplementary Material**, further inquiries can be directed to the corresponding author/s.

ETHICS STATEMENT

The studies involving human participants were reviewed and approved by Institut Pasteur Tunisia ethical committe. Written informed consent to participate in this study was provided by the participants' legal guardian/next of kin. Written informed consent was obtained from the minor(s)' legal guardian/next of kin for the publication of any potentially identifiable images or data included in this article.

AUTHOR CONTRIBUTIONS

IN did experiments. AC did the analysis, interpretations of data, and drafted the manuscript. HO did *in silico* protein modeling. SE and AL did experiments, analysis, and interpretation of targeted gene sequencing data. MJ and MZ clinical investigation of patients and family members. MR and OM helped in patients pre-screening for known mutations. VD, AD, NL, and SA study

concept and design. AD, SA, and HY-Y critical revision of the manuscript. HY-Y supervision of the study. All authors contributed to the article and approved the submitted version.

FUNDING

This work was supported by the Tunisian Ministry of Public Health, the Ministry of Higher Education and Scientific Research (LR16IPT05), the Projet collaborative interne (PCI_Melanoma, IPT), the RARE-MED project (A* MIDEX Initiative d'Excellence Aix Marseille Université) and the TRIM-RD project (Projet N° 19272) from AFM-Téléthon France.

ACKNOWLEDGMENTS

The authors would like to thank the patients and their families as well as the patients' support group Helping Xeroderma pigmentosum Children (http://www.xp-tunisie.org.tn/) for their collaboration.

SUPPLEMENTARY MATERIAL

The Supplementary Material for this article can be found online at: https://www.frontiersin.org/articles/10.3389/fgene.2021.650639/full#supplementary-material

REFERENCES

Ben Rekaya, M., Laroussi, N., Messaoud, O., Jones, M., Jerbi, M., and Naouali, C. (2014). A founder large deletion mutation in Xeroderma pigmentosum-Variant form in Tunisia: implication for molecular diagnosis and therapy. *Biomed. Res. Int.* 2014:256245. doi: 10.1155/2014/256245

Ben Rekaya, M., Messaoud, O., Talmoudi, F., Nouira, S., Ouragini, H., Amouri, A., et al. (2009). High frequency of the V548A fs X572 XPC mutation in Tunisia: implication for molecular diagnosis. *J. Hum. Genet.* 54, 426–429. doi: 10.1038/jhg.2009.50

Ben Rekaya, M., Naouali, C., Messaoud, O., Jones, M., Bouyacoub, Y., Nagara, M., et al. (2017). Whole Exome Sequencing allows the identification of two novel groups of Xeroderma pigmentosum in Tunisia, XP-D and XP-E: impact on molecular diagnosis. *J. Dermatol. Sci.* 89, 172–180. doi: 10.1016/j.jdermsci.2017.10.015

Bogliolo, M., Schuster, B., Stoepker, C., Derkunt, B., Su, Y., Raams, A., et al. (2013). Mutations in ERCC4, encoding the DNA-repair endonuclease XPF, cause Fanconi anemia. *Am. J. Hum. Genet.* 92, 800–806. doi: 10.1016/j.ajhg.2013.04.002

Bradford, P. T., Goldstein, A. M., Tamura, D., Khan, S. G., Ueda, T., Boyle, J., et al. (2011). Cancer and neurologic degeneration in xeroderma pigmentosum: long term follow-up characterises the role of DNA repair. *J. Med. Genet.* 48, 168–176. doi: 10.1136/jmg.2010.083022

Chikhaoui, A., Elouej, S., Nabouli, I., Jones, M., Lagarde, A., Ben Rekaya, M., et al. (2019). Identification of a ERCC5 c.2333T>C (L778P) variant in two tunisian siblings with mild xeroderma pigmentosum phenotype. *Front. Genet.* 10:111. doi: 10.3389/fgene.2019.00111

Desvignes, J. P., Bartoli, M., Delague, V., Krahn, M., Miltgen, M., Béroud, C., et al. (2018). VarAFT: a variant annotation and filtration system for human next generation sequencing data. *Nucleic Acids Res* 46, W545–w553. doi: 10.1093/nar/gky471

Doi, H., Koyano, S., Miyatake, S., Nakajima, S., Nakazawa, Y., Kunii, M., et al. (2018). Cerebellar ataxia-dominant phenotype in patients with ERCC4 mutations. *J. Hum. Genet.* 63, 417–423. doi: 10.1038/s10038-017-0408-5

Drozdetskiy, A., Cole, C., Procter, J., and Barton, G. J. (2015). JPred4: a protein secondary structure prediction server. *Nucleic Acids Res.* 43, W389–W394. doi: 10.1093/nar/gkv332

Ferri, D., Orioli, D., and Botta, E. (2020). Heterogeneity and overlaps in nucleotide excision repair disorders. *Clin. Genet.* 97, 12–24. doi: 10.1111/cge.13545

Itoh, T., Yamaizumi, M., Linn, S., and Ono, T. (2000). Reinvestigation of the classification of five cell strains of xeroderma pigmentosum group E with reclassification of three of them. *J. Investigative Dermatol.* 114, 1022–1029. doi: 10.1046/j.1523-1747.2000.00952.x

Karagün, E., Eroz, R., Gamsizkan, M., Baysak, S., Eyup, Y., and Ozcan, Y. (2020). Novel mutation identified in the DDB2 gene in patients with xeroderma pigmentosum group–E. *Int. J. Dermatol.* 59, 989–996. doi: 10.1111/ijd.14957

Kashiyama, K., Nakazawa, Y., Pilz, D. T., Guo, C., Shimada, M., Sasaki, K., et al. (2013). Malfunction of nuclease ERCC1-XPF results in diverse clinical manifestations and causes Cockayne syndrome, xeroderma pigmentosum, and Fanconi anemia. *Am. J. Hum. Genet.* 92, 807–819. doi: 10.1016/j.ajhg.2013.04.007

Kleijer, W. J., Laugel, V., Berneburg, M., Nardo, T., Fawcett, H., Gratchev, A., et al. (2008). Incidence of DNA repair deficiency disorders in western Europe: xeroderma pigmentosum, Cockayne syndrome and trichothiodystrophy. *DNA Repair.* 7, 744–750. doi: 10.1016/j.dnarep.2008.01.014

Krieger, L., and Berneburg, M. (2012). "Pigmentary lesions in patients with increased DNA damage due to defective DNA repair," in *Annales de Dermatologie et de Venereologie* (Tübingen: Elsevier), S130-S134. doi: 10.1016/S0151-9638(12)70124-2

Liu, L., Lee, S., Zhang, J., Peters, S. B., Hannah, J., Zhang, Y., et al. (2009). CUL4A abrogation augments DNA damage response and protection against skin carcinogenesis. *Mol. Cell* 34, 451–460. doi: 10.1016/j.molcel.2009.04.020

Manandhar, M., Boulware, K. S., and Wood, R. D. (2015). The ERCC1 and ERCC4 (XPF) genes and gene products. *Gene* 569, 153–161. doi: 10.1016/j.gene.2015.06.026

Messaoud, O., Ben Rekaya, M., Cherif, W., Talmoudi, F., Boussen, H., Mokhtar, I., et al. (2010). Genetic homogeneity of mutational spectrum of group-A xeroderma pigmentosum in Tunisian patients. *Int. J. Dermatol.* 49, 544–548. doi: 10.1111/j.1365-4632.2010.04421.x

Mori, T., Yousefzadeh, M. J., Faridounnia, M., Chong, J. X., Hisama, F. M., Hudgins, L., et al. (2018). ERCC4 variants identified in a cohort of patients with segmental progeroid syndromes. *Hum. Mutation* 39, 255–265. doi: 10.1002/humu.23367

Nichols, A. F., Ong, P., and Linn, S. (1996). Mutations specific to the xeroderma pigmentosum group E Ddb– phenotype. *J. Biol. Chem.* 271, 24317–24320. doi: 10.1074/jbc.271.40.24317

Oh, K.-S., Emmert, S., Tamura, D., Digiovanna, J. J., and Kraemer, K. H. (2011). Multiple skin cancers in adults with mutations in the XP-E (DDB2) DNA repair gene. *J. Investigative Dermatol.* 131:785. doi: 10.1038/jid.2010.352

Richards, S., Aziz, N., Bale, S., Bick, D., Das, S., Gastier-Foster, J., et al. (2015). Standards and guidelines for the interpretation of sequence variants: a joint consensus recommendation of the American College of Medical Genetics and Genomics and the Association for Molecular Pathology. *Genet. Med.* 17, 405–424. doi: 10.1038/gim.2015.30

Romdhane, L., Kefi, R., Azaiez, H., Halim, N. B., Dellagi, K., and Abdelhak, S. (2012). Founder mutations in Tunisia: implications for diagnosis in North Africa and Middle East. *Orphanet J. Rare Dis.* 7:52. doi: 10.1186/1750-1172-7-52

Scrima, A., Konícková, R., Czyzewski, B. K., Kawasaki, Y., Jeffrey, P. D., Groisman, R., et al. (2008). Structural basis of UV DNA-damage recognition by the DDB1-DDB2 complex. *Cell* 135, 1213–1223. doi: 10.1016/j.cell.2008.10.045

Sijbers, A. M., De Laat, W. L., Ariza, R. R., Biggerstaff, M., Wei, Y.-F., Moggs, J. G., et al. (1996). Xeroderma pigmentosum group F caused by a defect in a structure-specific DNA repair endonuclease. *Cell* 86, 811–822. doi: 10.1016/S0092-8674(00)80155-5

Stoyanova, T., Roy, N., Kopanja, D., Raychaudhuri, P., and Bagchi, S. (2009). DDB2 (damaged-DNA binding protein 2) in nucleotide excision repair and DNA damage response. *Cell Cycle* 8, 4067–4071. doi: 10.4161/cc.8.24.10109

Tofuku, Y., Nobeyama, Y., Kamide, R., Moriwaki, S., and Nakagawa, H. (2015). Xeroderma pigmentosum complementation group F: report of a case and review of Japanese patients. *J. Dermatol.* 42, 897–899. doi: 10.1111/1346-8138.12942

Vahteristo, P., Kokko, A., Saksela, O., Aittomäki, K., and Aaltonen, L. A. (2007). Blood-derived gene-expression profiling in unravelling susceptibility to recessive disease. *J. Med. Genet.* 44, 718–720. doi: 10.1136/jmg.2007.051342

Wang, S., Sun, S., Li, Z., Zhang, R., and Xu, J. (2017). Accurate *de novo* prediction of protein contact map by ultra-deep learning model. *PLoS Comp. Biol.* 13:e1005324. doi: 10.1371/journal.pcbi.1005324

Yang, R., Kong, Q., Duan, Y., Li, W., and Sang, H. (2020). Identification of a novel DDB2 mutation in a Chinese Han family with Xeroderma pigmentosum group E:a case report and literature review. *BMC Med. Genet.* 21:67. doi: 10.1186/s12881-020-00997-0

Zghal, M., El-Fekih, N., Fazaa, B., Fredj, M., Zhioua, R., Mokhtar, I., et al. (2005). [Xeroderma pigmentosum. Cutaneous, ocular, and neurologic abnormalities in 49 Tunisian cases]. *La Tunisie Med.* 83, 760–763.

Zhou, E. Y., Wang, H., Lin, Z., Xu, G., Ma, Z., Zhao, J., et al. (2017). Clinical and molecular epidemiological study of xeroderma pigmentosum in China: a case series of 19 patients. *J. Dermatol.* 44, 71–75. doi: 10.1111/1346-8138.13576

Conflict of Interest: The authors declare that the research was conducted in the absence of any commercial or financial relationships that could be construed as a potential conflict of interest.

frontiers in Genetics

ORIGINAL RESEARCH
published: 04 June 2021
doi: 10.3389/fgene.2021.643546

High Genetic Heterogeneity in Chinese Patients With Waardenburg Syndrome Revealed by Next-Generation Sequencing

Sen Zhang[1†], Hongen Xu[2,3†], Yongan Tian[4], Danhua Liu[3], Xinyue Hou[1], Beiping Zeng[4], Bei Chen[5], Huanfei Liu[2], Ruijun Li[2], Xiaohua Li[5], Bin Zuo[5], Ryan Tang[6] and Wenxue Tang[2,3,7]*

[1] School of Basic Medical Sciences, Zhengzhou University, Zhengzhou, China, [2] Precision Medicine Center, Academy of Medical Science, Zhengzhou University, Zhengzhou, China, [3] The Second Affiliated Hospital of Zhengzhou University, Zhengzhou, China, [4] BGI College, Zhengzhou University, Zhengzhou, China, [5] Department of Otology, The First Affiliated Hospital of Zhengzhou University, Zhengzhou, China, [6] Johns Hopkins University, Maryland, MD, United States, [7] Henan Institute of Medical and Pharmaceutical Sciences, Zhengzhou University, Zhengzhou, China

OPEN ACCESS

Edited by:
Emiliano González Vioque, University Clinical Hospital of Santiago, Spain

Reviewed by:
Duangrurdee Wattanasirichaigoon, Mahidol University, Thailand
Chufeng He, Central South University, China

***Correspondence:**
Wenxue Tang
twx@zzu.edu.cn

† These authors have contributed equally to this work and share the first authorship

Specialty section:
This article was submitted to Genetics of Common and Rare Diseases, a section of the journal Frontiers in Genetics

Received: 18 December 2020
Accepted: 23 April 2021
Published: 04 June 2021

Citation:
Zhang S, Xu H, Tian Y, Liu D, Hou X, Zeng B, Chen B, Liu H, Li R, Li X, Zuo B, Tang R and Tang W (2021) High Genetic Heterogeneity in Chinese Patients With Waardenburg Syndrome Revealed by Next-Generation Sequencing. Front. Genet. 12:643546. doi: 10.3389/fgene.2021.643546

Objective: This study aimed to explore the genetic causes of probands who were diagnosed with Waardenburg syndrome (WS) or congenital sensorineural hearing loss.

Methods: A detailed physical and audiological examinations were carried out to make an accurate diagnosis of 14 patients from seven unrelated families. We performed whole-exome sequencing in probands to detect the potential genetic causes and further validated them by Sanger sequencing in the probands and their family members.

Results: The genetic causes for all 14 patients with WS or congenital sensorineural hearing loss were identified. A total of seven heterozygous variants including c.1459C > T, c.123del, and c.959-409_1173+3402del of *PAX3* gene (NM_181459.4), c.198_262del and c.529_556del of *SOX10* gene (NM_006941.4), and c.731G > A and c.970dup of *MITF* gene (NM_000248.3) were found for the first time. Of these mutations, we had confirmed two (c.1459C > T and c.970dup) are *de novo* by Sanger sequencing of variants in the probands and their parents.

Conclusion: We revealed a total of seven novel mutations in *PAX3*, *SOX10*, and *MITF*, which underlie the pathogenesis of WS. The clinical and genetic characterization of these families with WS elucidated high heterogeneity in Chinese patients with WS. This study expands the database of *PAX3*, *SOX10*, and *MITF* mutations and improves our understanding of the causes of WS.

Keywords: *PAX3*, *SOX10*, *MITF*, Waardenburg syndrome, next-generation sequencing, genetic heterogeneity

INTRODUCTION

Waardenburg syndrome (WS) is a congenital developmental disorder, which is mainly characterized by congenital sensorineural hearing loss (SNHL) and abnormal pigmentation of the iris, hair, and skin (manifests as heterochromia iridis and brilliant blue eyes, a white forelock, and premature graying, and hypopigmented skin) (Read and Newton, 1997). WS has an incidence

rate of approximately 1/42,000 births and is responsible for 2–5% of cases of total congenital deafness (Read and Newton, 1997; Nayak and Isaacson, 2003). Four different types of Waardenburg syndrome (WS I∼IV) have been described based on genotypic and phenotypic variations (Read and Newton, 1997; Pingault et al., 2010). WS I is distinguished from WS II by the presence of dystopia canthorum, which is lateral displacement of the inner canthus in each eye; WS III (Klein–Waardenburg syndrome) is similar to WS I except with additional upper limb abnormalities; WS IV (Waardenburg-Shah syndrome) is characterized by general WS features as well as Hirschsprung's disease, a disorder that causes severe blockage of the large intestine. Current research suggests that WS I and WS II are more common than WS III and WS IV (Read and Newton, 1997; Pingault et al., 2010).

Waardenburg syndrome shows a high degree of genetic heterogeneity (Hageman and Delleman, 1977; Read and Newton, 1997; Pingault et al., 2010; Song et al., 2016). Six genes have been linked to this syndrome: paired box 3 (*PAX3*) (Baldwin et al., 1992; Tassabehji et al., 1992; Hoth et al., 1993), melanocyte inducing transcription factor (*MITF*) (Tassabehji et al., 1994), SRY-box transcription factor 10 (*SOX10*) (Pingault et al., 1998; Bondurand et al., 2007), endothelin 3 (*EDN3*) (Edery et al., 1996), endothelin receptor type B (*EDNRB*) (Puffenberger et al., 1994), and snail family transcriptional repressor 2 (*SNAI2*) (Sánchez-Martín et al., 2002). *PAX3* is responsible for WS I and WS III (Baldwin et al., 1992; Tassabehji et al., 1992; Hoth et al., 1993). *SOX10*, *MITF*, and *SNAI2* are associated with WS IV (Tassabehji et al., 1994; Pingault et al., 1998; Sánchez-Martín et al., 2002; Bondurand et al., 2007). *SOX10*, *EDNRB*, and *EDN3* are found to be involved in WS IV (Puffenberger et al., 1994; Edery et al., 1996; Pingault et al., 1998; Bondurand et al., 2007). Although not currently fully understood, all these genes are involved in a complex network in neural crest cells and other derivatives (Read and Newton, 1997; Bondurand et al., 2000; Pingault et al., 2010). The interaction of these genes during the formation and development of melanocytes could be the pathogenesis of WS and other related diseases (Read and Newton, 1997; Bondurand et al., 2000; Pingault et al., 2010).

Diagnosis of WS can be difficult because all features are not present in every patient (Hageman and Delleman, 1977; Newton, 1990; Tamayo et al., 2008; Pingault et al., 2010; Yang et al., 2013). Even within a single family, patients can display different clinical manifestations due to variations in the expressivity of causative genes (Hageman and Delleman, 1977; Newton, 1990; Tamayo et al., 2008; Pingault et al., 2010; Yang et al., 2013). Therefore, genetic testing is an important method for diagnosing this disease and its subtypes (Hageman and Delleman, 1977; Read and Newton, 1997; Pingault et al., 2010; Tang et al., 2015; Song et al., 2016; Wu et al., 2016; Li et al., 2019). To date, ∼400 mutations including missense/nonsense mutations, frameshift mutations, insertions/deletions, and copy number variants (CNVs) have been identified in genes associated with WS (The Human Gene Mutation Database[1]), with most variants in genes *PAX3*, *SOX10*, and *MITF* (Chen et al., 2010; Pingault et al., 2010; Song et al., 2016). Of these variants, ∼100 mutations were identified in Chinese people. Nevertheless, there are still a number of cases unexplained at the molecular level (Pingault et al., 2010; Song et al., 2016). Discovering novel mutations will lead to a better understanding of the genetic causes of WS pathogenesis.

Recently, next-generation sequencing (NGS) has proven to be a potent tool for the identification of pathogenic mutations related to deafness, which can improve the diagnosis of genetic diseases and the detection of mutations in genes associated with different clinical manifestations (Brownstein et al., 2012; Lin et al., 2012; Tang et al., 2012; Li et al., 2019). In this study, WES was used to identify the possible pathogenic mutations of patients with SNHL or WS. A total of seven novel variants in *PAX3*, *SOX10*, and *MITF* were found, and two of them are *de novo* confirmed by Sanger sequencing of variants in the probands and their parents. Our results show that WS in China has a high degree of genetic heterogeneity and extend the mutational spectrum of WS-related genes.

MATERIALS AND METHODS

Patients

From seven Han Chinese families in the Henan province, 14 patients (**Table 1**) and nine unaffected family members were recruited for our study and asked to perform audiological and general physical examinations (**Figure 1**). Furthermore, in family WS04, only WS04-II:1 was recruited because he was adopted and had lost contact with his biological family. Among the seven families, WS01 and WS06 were isolated cases, while the remaining families had multiple affected individuals (**Figure 1**). Photos and blood were collected after informed consent (**Figure 2**). This study was conducted according to the Declaration of Helsinki and approved by the institutional review board of the Medical Ethics Committee of The Second Affiliated Hospital of Zhengzhou University (Approval No. 2018008).

Clinical Investigation

All patients (medical history described by parents) received elaborate physical examinations in their hair color and skin pigmentation, joints, skeletomuscular system, digestion, ophthalmology and otology, and intelligence assessment. Patients also underwent audiological examinations, which included auditory steady-state response (ASSR), auditory brainstem response (ABR), and distortion product otoacoustic emission (DPOAE). Additionally, imageological examinations such as computerized tomography (CT) of the temporal bone and magnetic resonance imaging (MRI) were conducted. The characteristics of the patients are summarized in **Table 1**.

Next-Generation Sequencing-Based Genetic Testing

In this study, WES was applied to identify the potential genetic causes for probands. A standard NGS-based genetic testing, including sample preparation and quantification, library construction, sequencing, and data analyses, was performed as previously described (Pan et al., 2020). Briefly, after library

[1] www.hgmd.cf.ac.uk/

TABLE 1 | Summary of clinical data for patients.

Individual	Gender	Hearing loss	Blue iris	White forelock	Dystopia canthorum	Brown freckles
WS01-II:1	Female	+	−	−	−	−
WS02-I:1	Male	−	+	−	+	−
WS02-II:2	Female	−	−	−	+	−
WS02-III:1	Male	−	+(Unilateral)	−	+	−
WS02-III:2	Male	+	+	−	+	−
WS03-I:2	Female	+	+	−	−	−
WS03-II:1	Female	+	+	−	−	−
WS03-II:2	Female	+	+(Unilateral)	−	−	−
WS04-II:1	Male	+	+	+	−	−
WS05-III:1	Male	−	+	−	−	+
WS05-IV:1	Female	+	+	−	−	−
WS06-II:1	Female	+	−	+	−	−
WS07-I:1	Male	−	−	−	+	−
WS07-II:1	Female	+	+(Unilateral)	−	+	−

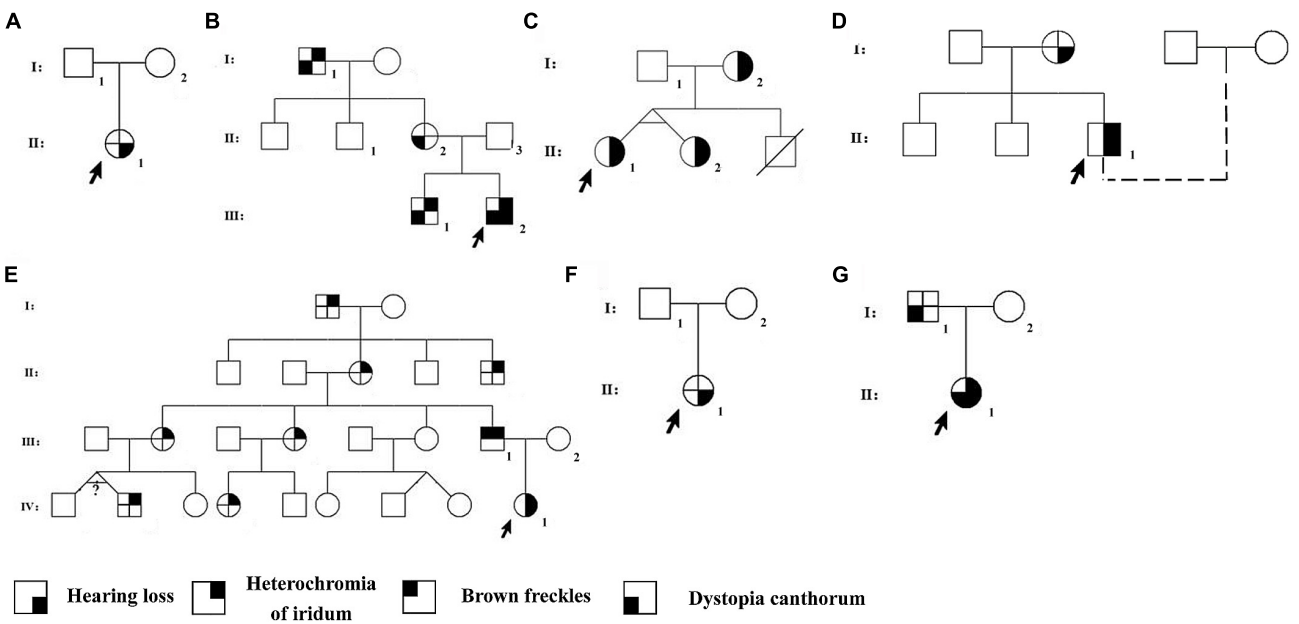

FIGURE 1 | Pedigrees of the Waardenburg syndrome families. Pedigrees of families Individuals with a number assigned participated in the current study. Phenotypes of the rest of the family members were based on the relative's description. The probands were pointed by arrows. **(A)** WS01, **(B)** WS02, **(C)** WS03, **(D)** WS04, **(E)** WS05, **(F)** WS06, and **(G)** WS07.

construction, the resulting libraries were hybridized to the Agilent SureSelect Human All Exon V7. Then, sequencing was carried out on an Illumina HiSeq 4000 sequencer (Illumina Inc., San Diego, CA, United States) to generate paired-end reads of 150 bp.

Data analyses were divided into bioinformatics analysis and variant interpretation. Under the framework of bcbio-nextgen[2], we used the Burrows–Wheeler Aligner (BWA) (version 0.7.17-r1188) (Li, 2013) to align the sequencing reads to the human reference genome (GRCh37); GATK Haplotype Caller software (version 4.1.2) (McKenna et al., 2010) to identify the single nucleotide variants (SNVs) and short indels; DECoN (Fowler et al., 2016) to identify the CNVs; and Vcfanno software (version 0.3.1) (Pedersen et al., 2016) to annotate the VCF files with external database, including Clinvar (Landrum et al., 2018), ExAC (Lek et al., 2016), dbNSFP (Liu et al., 2016), 1,000 Genomes (Auton et al., 2015), and gnomAD (Karczewski et al., 2019). The filtered variants were interpreted following the guidelines of the American College of Medical Genetics and Genomics and the Association for Molecular Pathology (ACMG-AMP) (Richards et al., 2015) and the ClinGen hearing loss expert group's recommendation on variant interpretation (Oza et al., 2018). Copy number analysis was performed from NGS data using DECoN with

[2]https://github.com/bcbio/bcbio-nextgen

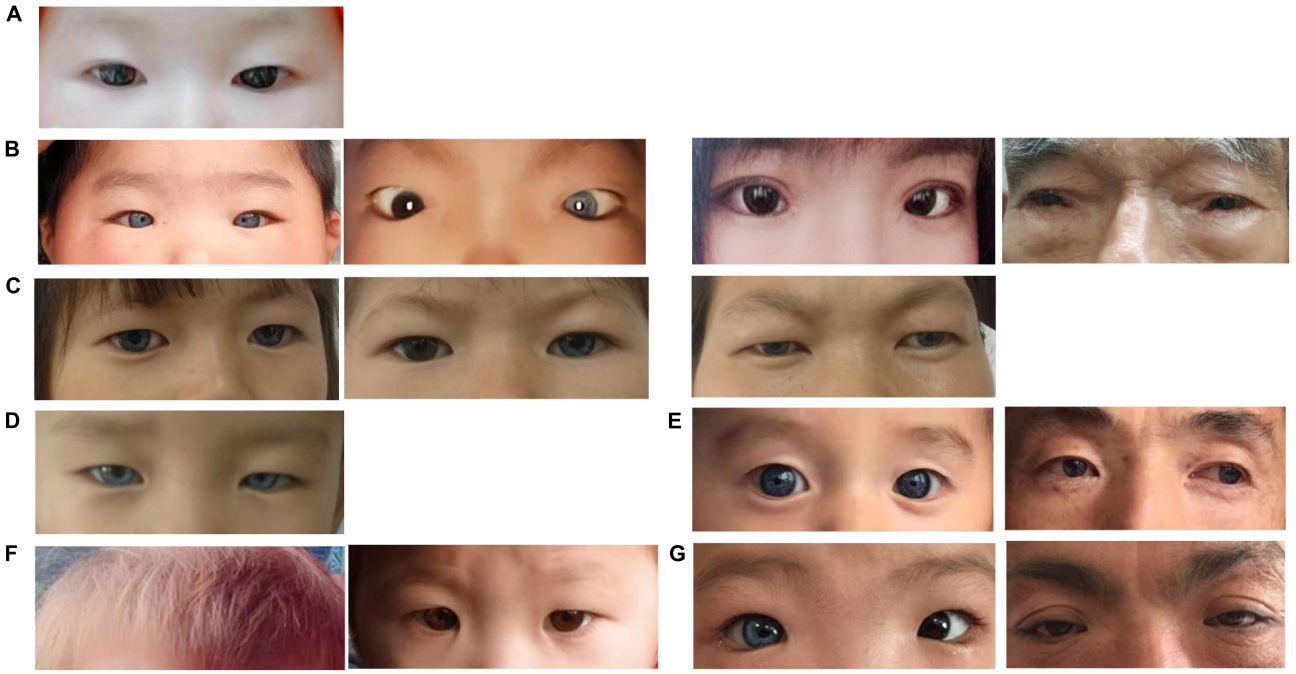

FIGURE 2 | Photographs of affected individuals. **(A)** WS01-II:1 presented normal pigmentation of the iris, hair, and skin, and without dystopia canthorum. **(B)** B1, WS02-III:2; B2, WS02-III:1; B3, WS02-II:2; and B4, WS02-I:1. They all presented dystopia canthorum, while WS02-III:2 has bilateral blue iris and WS02-III:1 has unilateral. **(C)** C1, WS03-II:1; C2, WS03-II:2; and C3, WS03-I:2. They presented bilateral or unilateral blue iris. **(D)** WS04-II:1 presented complete bilateral blue iris. **(E)** E1, WS05-IV:1 presented complete bilateral blue iris. E2, WS05-III:1 presented complete bilateral blue iris and special brown freckles on the face. **(F)** F1, F2, WS06-II:1 presented yellow hair and normal iridis color. **(G)** G1, WS07-II:1 presented unilateral blue iris and dystopia canthorum. G2, WS07-II:1 presented dystopia canthorum.

the bam files from the same enrichment panel and sequencing run. Paternity tests were performed on families WS01 and WS06 since the gene tests had shown mutations occurred *de novo*.

Sanger Sequencing

Sanger sequencing was used to confirm the candidate variants detected by NGS and to conduct co-segregation analyses in family members. The specific primers (**Table 2**) were designed by NCBI Primer-BLAST and synthesized by Sunya Biotech Co., Ltd. (Zhengzhou, China). Conventional PCR was performed for SNVs and short indels detected in families WS01 to WS06. While long-range PCR (LR-PCR) based on nested-PCR and fragments gel-purified were performed for the CNV of patients WS07-I:1 and WS07-II:1. LR-PCR is a traditional approach to obtain CNV breakpoint junction (Woodward et al., 2005; Zhang et al., 2017), for which several primers were designed from both the proximal and the distal breakpoint regions identified, and used in different combinations until an appropriate size product was generated (**Supplementary Figure 1**). After PCR amplification, purification, and quality control, Sanger sequencing was run in a SeqStudio Genetic Analyzer (Thermo Scientific, United States) with a mixture of PCR products and BigDyeTM Terminator v3.1 Cycle Sequencing Kit (Applied Biosystems, Foster City, CA, United States). The sequencing results were analyzed by the SnapGene viewer (**Figure 3**).

RESULTS

Clinical Findings

A total of 14 patients from seven unrelated families were involved in this study. Before genetic testing, patients WS01-II:1 and WS06-II:1 were primarily diagnosed with SNHL, while the other 12 patients were diagnosed with WS. These diagnoses were made by otorhinolaryngologists based on the manifestation of the typical symptom of WS, such as SNHL, abnormal pigmentation, and the presence or absence of dystopia canthorum, musculoskeletal anomalies, and intestinal aganglionosis. After a genetic diagnosis, further examinations were performed on the patients WS01-II:1 and WS06-II:1. We found that the hair color of WS06-II:1 is gray, which was previously ignored, but nothing new with WS01-II:1.

Among all the patients, heterochromia iridum and deafness were the most frequent features. Ten affected individuals (10/14, 71.4%) had blue iris, of which three were heterochromia iridum; nine patients (9/14, 64.3%) had a profound sensorineural hearing impairment; six (6/14, 42.9%) had dystopia canthorum; one (1/14, 7.1%) had facial freckles; two (2/14, 14.3%) had abnormal pigmentation of hair (**Figures 1**, **2**). **Table 1** lists the clinical data of these WS patients.

Members in the same family can have different symptoms. WS03-II:1 and WS03-II:2 are identical twins; one has bilateral blue iris and the other has unilateral. According to his adoptive

TABLE 2 | Primer pairs of the novel mutations of paired box 3 (PAX3), SRY-box transcription factor 10 (SOX10), and melanocyte inducing transcription factor (MITF).

Mutations	Affected family	Forward primer sequence (5′–3′)	Reverse primer sequence (5′–3′)	Product length
PAX3:c.1459C > T	WS01	GCCCAAACCAGTCTGGGTAAAT	GCATGACCTAAAAAGCTGCGT	471 bp
PAX3:c.123del	WS02	AGGACGTATGGAGCCAGTCT	GAGTCCGATGTCGAGCAGTT	351 bp
SOX10:c.198_262del	WS03	TGGTCTTCCAGCCCTATCCA	CAGGCGAGCTGGGCAAG	419 bp
SOX10:c.529_556del	WS04	CAGGGTCTCATTGCCATCCA	CAGGGCCTCACATCTTCCAA	459 bp
MITF:c.731G > A	WS05	GCAAACACTCGTGAATGGCA	CTGAGCAACAAATGCCGGTT	510 bp
MITF:c.970dup	WS06	TTCCCTTATTCCATCCACGGG	TCAGTCCCAGTTCCGAGGTT	186 bp
PAX3:c.959-409_1173+3402del	WS07	GAGCGCGTAATCAGTCTGGG	GGCCACATTTAGGACATGCG	19,658/15,633 bp*
	WS07	AAAATGCACAGACCCTTTCAGCA	TCTGGTTTAGCAACCGCCG	4,998/973 bp*

**The product length of the normal allele and mutated allele is separated by the slash. Reference sequence transcript: PAX3: NM_181459.4; SOX10: NM_006941.4; and MITF: NM_000248.3.*

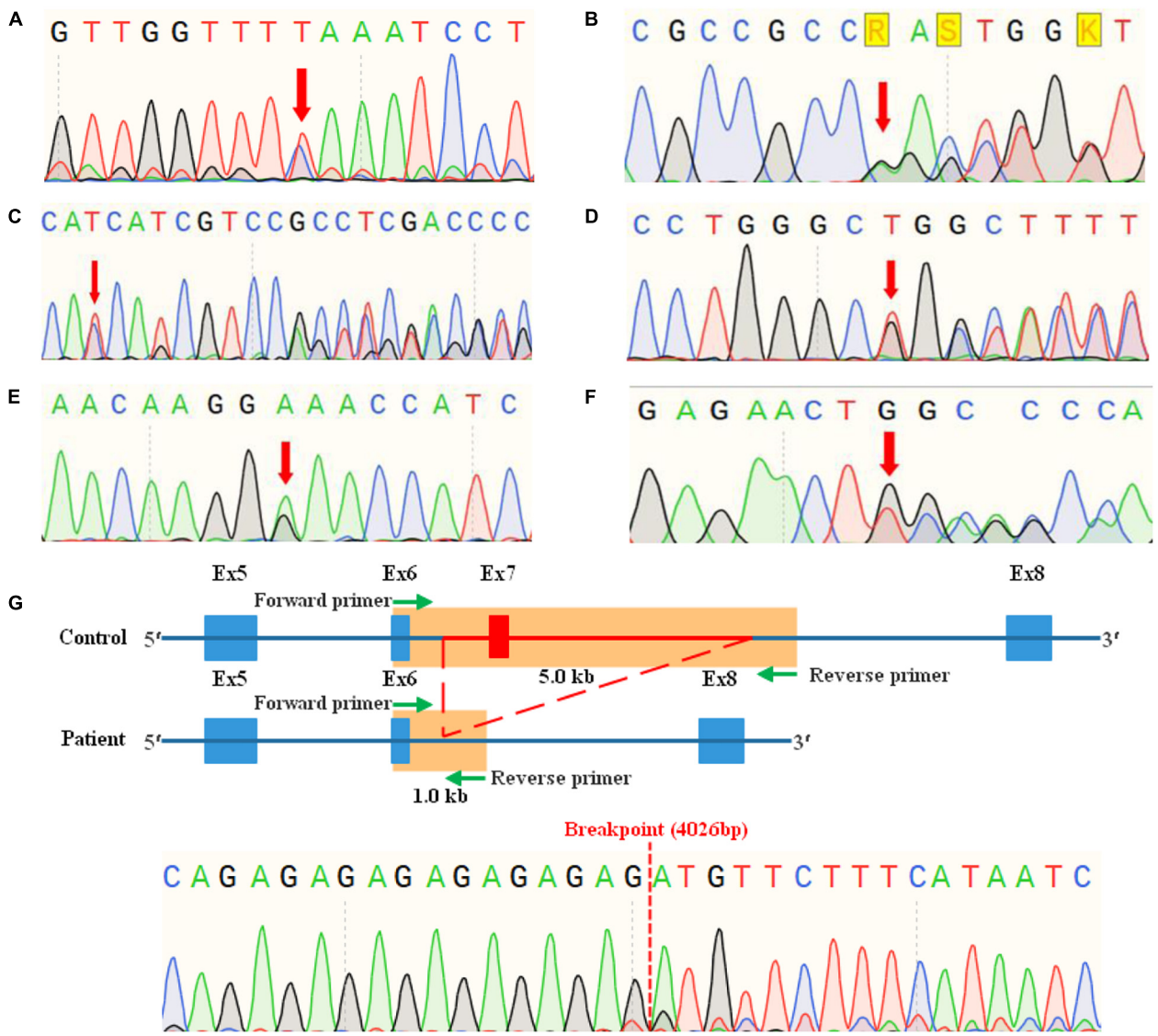

FIGURE 3 | Mutation analyses of Chinese Waardenburg syndrome families WS01 to WS07 by sanger sequencing. **(A)** Heterozygous mutation c.1459C > T of *PAX3* in WS01-II:1. **(B)** Heterozygous mutation c.123del of *PAX3* in WS02-I:1, II:3, III:1, and III:2. **(C)** Heterozygous mutation c.198_262del of *SOX10* in WS03-I:2, II:1, and III:2. **(D)** Heterozygous mutation c.529_556del of *SOX10* in WS04-II:1. **(E)** Heterozygous mutation c.731G > A of *MITF* in WS05-III:3, IV:4. **(F)** Heterozygous mutation c.970dup of *MITF* in WS06-II:1. **(G)** Heterozygous mutation c.959-409_1173+3402del of *PAX3* in WS07-I:1, II:1.

father, WS04-II:1 was born with a white forelock that returned to being black (we were unable to collect pictures of the patient with a white forelock). Across four generations, seven members of the family WS05 had unexpectedly brilliant blue eyes without other WS-related symptoms. However, it is impossible to confirm whether they were affected by the same mutation of the proband (WS05-IV:1) since they refused to provide blood samples.

Molecular Etiology

Whole-exome sequencing was performed in probands of these seven families. For each sample, at least 10 Gbp raw data was generated, with more than 82% of bases having a Phred quality score $Q \geq 30$ (Q30), 99% of the clean reads can map to the human reference genome (GRCh37/hg19), and the average sequencing depth of target regions was 100×, with 95% of target regions having coverage greater than 20× (**Supplementary Table 1**).

In this study, the genetic causes for all recruited patients had been confirmed, which contain a total of seven mutations in *PAX3*, *SOX10*, and *MITF*, respectively (**Table 3**). To our best knowledge, these mutations, including a nonsense mutation, a missense mutation, a CNV, and four frameshift mutations, have not been reported by previous studies or recorded in any public database. Further analysis by Sanger sequencing of patients and their family members shows that all the variants were present in the affected members and absent in the unaffected ones (**Figure 3**), and variants of probands WS01-II:1 and WS06-II:1 are *de novo*. Pathogenicity analysis of variants was according to the standards and guidelines for interpreting genetic variants proposed by the ACMG-AMP. The mutations and pathogenicity analysis were summarized in **Table 3**.

Genotype–Phenotype Correlation

The phenotypes of WS patients with *PAX3* ($n = 7$), *SOX10* ($n = 4$), and *MITF* ($n = 3$) mutations are compared in **Supplementary Table 2**. Among the WS patients who participated in this study, all patients with *SOX10* mutations have hearing loss, while some patients with *PAX3* (3/7) or *MITF* (2/3) have. Similarly, the symptom of the blue iris could be found in all patients with *SOX10* mutations, while it was found in some patients with *PAX3* (4/7) or *MITF* (2/3) variants. Abnormal hair pigmentation is rare in patients with *PAX3* (0/7), *SOX10* (1/4), and *MITF* (1/3) mutations. Previous reports suggested that freckles could be observed only in Chinese WS II patients with *MITF* mutations (Chen et al., 2010; Sun et al., 2016). Indeed, in this study, we found one WS II patient with *MITF* mutation has freckles. Synophridia is only present in WS I patients with *PAX3* mutations.

DISCUSSION

In this study, we had confirmed seven novel heterozygous variants which are the genetic causes of 14 WS patients from seven unrelated families, including c.1459C > T (nonsense), c.123del (frameshift), and c.959-409_1173+3402del (deletion) of *PAX3* (NM_181459.4), c.198_262del (frameshift) and c.529_556del (frameshift) of *SOX10* (NM_006941.4), and c.731G > A (missense) and c.970dup (frameshift) of *MITF* (NM_000248.3) (**Table 3**). Among 14 patients, seven each were classified as WS I and WS II, respectively, based on their phenotypes and genotypes, showing that WS I and WS II were two major WS subtypes (Read and Newton, 1997; Pingault et al., 2010). While mutations in *PAX3* were the major causes for WS I (7/7), *SOX10* (4/7), and *MITF* (3/7) were two major causative genes attributable to WS II. Our findings had extended the mutational spectrum of WS-related genes and revealed high genetic heterogeneity in Chinese WS patients (Yang et al., 2013; Sun et al., 2016; Liu et al., 2020).

To explore the genotype–phenotype correlation, we compared the phenotypes between WS patients with *PAX3*, *SOX10*, and *MITF* mutations (**Supplementary Table 2**). Several reports had shown that the clinical features of WS II caused by *SOX10* and *MITF* mutations were indistinguishable, except that freckle was frequent in WS II probands with *MITF* mutation (Chen et al., 2010; Toriello, 2011; Sun et al., 2016). Indeed, in this study, freckle seems to be unique for patients with *MITF* mutations (1/3) but was absent in those with *PAX3* (0/7) or *SOX10* (0/4) mutations. Dystopia canthorum is a rebarbative but crucial clinical feature, because of its value in distinguishing WS I and WS II, but it is not completely applicable for Chinese WS I patients (Sun et al., 2016; Morimoto et al., 2018; Suzuki et al., 2018; Minami et al., 2019). Herein, we had an interesting finding that the synophridia, even though a minor symptom, was only present in WS patients (5/7) but absent in WS II patients (0/7). Our results may have shown the clinical differences between WS II patients with *SOX10* and *MITF* mutations, and between WS II and WS I. However, gene test is as necessary as clinical investigation for the accurate diagnosis and subtype confirmation (Hageman and Delleman, 1977; Read and Newton, 1997; Pingault et al., 2010; Song et al., 2016; Li et al., 2019).

Mutations in *PAX3*, *SOX10*, and *MITF* were the most common genetic causes for WS and responsible for almost all Chinese WS patients (Chen et al., 2010; Wu et al., 2016; Liu et al., 2020). Beyond that, to date, several WS cases associated with mutations in *ENDRB*, *EDN3*, and *SNAI2* had been reported (Sánchez-Martín et al., 2002; Pingault et al., 2010; Xiong et al., 2015; Somashekar et al., 2019), but the situation is a bit different in Chinese. There were two reported cases of WS type I caused by mutations in the *EDNRB* gene (Cheng et al., 2019; Li et al., 2019), which is different from the cases in other races (WS II or IV) (Pingault et al., 2010; Issa et al., 2017). Of the few reports about WS type II being caused by mutations in the *EDN3* gene, there was no Chinese case reported. Only one research group reported *SNAI2* mutations caused WS within two unrelated WS II patients (Sánchez-Martín et al., 2002), which had been questioned recently (Song et al., 2016; Mirhadi et al., 2020). To understand the differences of WS among different races, we need further research on the pathogenesis of WS and more accurate diagnostic means.

The deficiency of melanocytes, the neural crest (NC) derivatives, is common to various WS types (Bondurand et al., 2000; Pingault et al., 2010; Song et al., 2016), which is responsible for the phenotypes of pigmentation defects and hearing loss (Steel and Barkway, 1989). *PAX3* encodes a DNA-binding transcription factor, consisting of a paired box (PD) encoded by exons 2, 3,

TABLE 3 | Gene variants and pathogenicity analysis of patients.

Family	Affected family members	Variants	Exon	Zygote	Reference	ACMG-AMP classification	ACMG-AMP criteria
WS01	II:1	*PAX3*:c.1459C > T p.Gln487Ter Nonsense	Exon10	Heterozygous	This study	Pathogenic	PVS1, PM2, PP3, and PS2
WS02	I:1; II:2; III:1; III:2	*PAX3*:c.123del p.Gly42AlafsTer68 Frameshift	Exon2	Heterozygous	This study	Pathogenic	PVS1, PM2, PP1, PP3, and PP4
WS03	I:2; II:1; II:2	*SOX10*:c.198_262del p.Lys67AlafsTer45 Frameshift	Exon2	Heterozygous	This study	Pathogenic	PVS1, PM2, PP1, PP3, and PP4
WS04	II:1	*SOX10*:c.529_556del p.Arg177AlafsTer100 Frameshift	Exon3	Heterozygous	This study	Pathogenic	PVS1, PM2, and PP3
WS05	III:1; IV:1	*MITF*:c.731G > A p.Gly244Glu Missense	Exon8	Heterozygous	Steingrímsson et al., 1996 *	Likely Pathogenic	PS3*, PM2, PP1, and PP3
WS06	II:1	*MITF*:c.970dup p.Cys324LeufsTer36 Frameshift	Exon9	Heterozygous	This study	Pathogenic	PVS1, PM2, PS2, and PP3
WS07	I:1; II:1	c.959-409_1173+3402del Deletion	Exon7	Heterozygous	This study	Pathogenic	PVS1, PM2, and PP4

**This mutation was, for the first time, found in humans after being detected and researched by Steingrímsson et al. (1996) in mice, so the criteria "PS3" was given. ACMG-AMP, Association for Molecular Pathology. Reference sequence transcript: PAX3: NM_181459.4; SOX10: NM_006941.4; and MITF: NM_000248.3.*

and 4, the homeodomain (HD) by exons 5 and 6, C-terminal transcriptional activation domain by exons 7 and 8 (Read and Newton, 1997; Wildhardt et al., 2013). It is indispensable in the development of somites, skeletal muscle, and the neural crest cells (NCC) and their derivatives like melanocytes. It can cooperate with *SOX10* to regulate the expression of the *MITF* promoter (Pingault et al., 2010). *PAX3*:c.123del and c.959-409_1173+3402del mutations are predicted to activate the nonsense-mediated mRNA decay (NMD) machinery (Khajavi et al., 2006), thereby resulting in haploinsufficiency, which might be the disease-causing mechanism for WS I. *PAX3*:c.1459C > T mutation is located in the exon 10 and could only influence the isoform *PAX3e* (Wang, 2006), which most likely pathogenic mechanism is haploinsufficiency (Barber et al., 1999).

SRY-box transcription factor 10 encodes a transcription factor that contains an HMG (high mobility group) DNA binding domain and a C-terminal transactivation domain (Chan et al., 2003). In the early development of NC, *SOX10* plays an important role in promoting cell survival and maintaining the multipotency of NC stem cells (Kapur, 1999; Kelsh, 2006; Pingault et al., 2010; Stolt and Wegner, 2010). Besides synergy with *PAX3* to regulate the expression of *MITF*, it also can directly regulate the expression of genes important for melanin synthesis, suggesting the importance for melanocyte differentiation (Bondurand et al., 2000; Lee et al., 2000; Potterf et al., 2000; Verastegui et al., 2000; Jiao et al., 2004; Wegner, 2005; Pingault et al., 2010). It is also crucial for the peripheral nervous system like sensory, sympathetic, and enteric ganglia and along nerves (Bondurand et al., 2000; Pingault et al., 2010). *SOX10*: c.198_262del and c.529_556del are located in the HMG domain and predicted to activate the NMD machinery, resulting in haploinsufficiency.

Melanocyte inducing transcription factor, a basic helix–loop–helix leucine zipper (bHLHZip) protein, is the key transcription factor of melanocyte development. The bHLHZip structure binds DNA by basic domain, dimerizes through HLH domain, and is stabilized via the Zip domain (Hodgkinson et al., 1993; Steingrímsson et al., 1994). The C-terminal of MITF contributes to defining the target genes by a serine-rich transcriptional activation domain. Mice with *MITF* mutations show reduced or absent pigmentation, deafness, and small or absent eyes, etc. (Yasumoto et al., 1995; Bertolotto et al., 1998; Steingrímsson et al., 2004; Pingault et al., 2010). *MITF*:c.970dup is a frameshift mutation and predicted to activate the NMD machinery, leading to haploinsufficiency. *MITF*:c.731G > A (p.Gly244Glu) is the genetic cause of III:1 and IV:1 of family WS05 and might be responsible for the other seven affected individuals (**Figure 1**). We had noticed that only one had hearing loss and blue iris while the other eight only had blue iris in this family, although Song et al. (2016) had suggested that nearly 90% of patients with *MITF* have hearing loss. The Gly244Glu mutation of MITF was found in humans for the first time, while the mouse model with the same mutation ($MITF^{Mi-b}$) had been found by Steingrímsson et al. (1996). The phenotype of $MITF^{Mi-b}$ homozygous animals is mild compared with loss-of-function *mi* alleles. Gly244 would lie at the very beginning of the second helix, close to the protein-DNA interface. The Gly244Glu alteration is at the junction of the loop and helix 2 of the protein. The $MITF^{Mi-b}$ protein largely spares dimerization function, while it is defective in its ability to bind DNA. However, the DNA binding function can be partially compensated by a wild-type partner in the dimer, since $MITF^{Mi-b}$ is capable of forming TFE3 (Transcription factor E3) heterodimeric complexes which had a stronger DNA binding than the $MITF^{Mi-b}$ homodimers. It may explain why the mutation c.731G > A resulting in a less-severe phenotype in the family WS05.

WS has high genetic heterogeneity and highly variable phenotype expressivity (Hageman and Delleman, 1977; Newton, 1990; Read and Newton, 1997; Tamayo et al., 2008; Pingault et al., 2010; Yang et al., 2013; Song et al., 2016), which makes the diagnosis challenging. NGS of numerous genes is allowed in a single test with lower turnaround time, cost, and higher throughput, which makes it ideal for figuring out the exact genetic mechanism (Brownstein et al., 2012;

Tang et al., 2012, 2015). Mutations in *PAX3* are responsible for WS I and WS III in most cases; however, using WES, we had detected a heterozygous nonsense mutation of *PAX3*:c.1459C > T in an SNHL patient (WS01-II:1). To our best knowledge, this is the first mutation found in exon 10 of *PAX3* and results in a premature stop codon, which is very close to the normal ending (487/506) (Boudjadi et al., 2018). We suspect that this is why SNHL is the only symptom of WS01-II:1, even though previous studies argued that there was no correlation between genotype and phenotype of WS caused by *PAX3* mutations (Tassabehji et al., 1995; Boudjadi et al., 2018). Patient WS06-II:1 was also diagnosed with SNHL initially, before being corrected to WS type II after the genetic testing in which a heterozygous *de novo* mutation *MITF*: c.970dup was detected. Besides, the other five families with classic symptoms and clear family histories, these two cases in particular highlight the superiority of NGS in the diagnosis of WS.

In conclusion, the clinical and genetic characteristics of one SNHL patient and six Chinese families of WS had been investigated in this study. Altogether, seven novel pathogenic/likely pathogenic variants in the *PAX3*, *SOX10*, and *MITF* were identified. Our results support that NGS is a useful diagnostic procedure for the diagnosis and subtype differentiation of WS. This report reveals the highly genetic heterogeneity and variable phenotype in Chinese patients with WS and will contribute to a better understanding of the WS by extending the mutational spectrum of WS-related genes.

DATA AVAILABILITY STATEMENT

According to national legislation/guidelines, specifically the Administrative Regulations of the People's Republic of China on Human Genetic Resources (http://www.gov.cn/zhengce/content/2019-06/10/content_5398829.htm, http://english.www.gov.cn/policies/latest_releases/2019/06/10/content_281476708945462.htm), no additional raw data is available at this time. Data of this project can be accessed after an approval application to the Bio-Med Big Data Center, NODE. Please refer to https://www.biosino.org/node/project/detail/OEP001401 for detailed application guidance. The accession code OEP001401 should be included in the application.

ETHICS STATEMENT

The studies involving human participants were reviewed and approved by the institutional review board of the Medical Ethics Committee of The Second Affiliated Hospital of Zhengzhou University. Written informed consent to participate in this study was provided by the participants' legal guardian/next of kin.

AUTHOR CONTRIBUTIONS

WT and HX: study design. BC, HL, RL, XL, and BZu: patient phenotypic analysis and genetic counseling. SZ, YT, XH, BZe, HL, and RL: next−generation sequencing and Sanger sequencing. HX, DL, SZ, and YT: data analysis and variant interpretation. SZ, HX, DL, WT, and RT: writing and review of original draft of the manuscript. RT: language editing of original draft of the manuscript. All authors have read and approved the final manuscript.

FUNDING

This study is funded by the Collaborative Innovation Project of Zhengzhou (Zhengzhou University) (Grant No. 18XTZX12004) and the Medical Science and Technology Projects in Henan (Grant No. SBGJ2018043) to WT, and the Joint Project of Medical Science and Technology Research in Henan Province (Grant No. LHGJ20190317) to HX.

ACKNOWLEDGMENTS

We sincerely thank all the family members for their participation in this study. We also thank the Supercomputing Center of Zhengzhou University for providing computational and storage resources.

SUPPLEMENTARY MATERIAL

The Supplementary Material for this article can be found online at: https://www.frontiersin.org/articles/10.3389/fgene.2021.643546/full#supplementary-material

Supplementary Figure 1 | LR-PCR for the identification of the large deletion, *PAX3*:c.959-409_1173+3402del.

Supplementary Table 1 | Detailed information for quality control of WES data.

Supplementary Table 2 | Phenotypes in patients with *PAX3*, *SOX10*, and *MITF* mutations.

REFERENCES

Auton, A., Abecasis, G. R., Altshuler, D. M., Durbin, R. M., Abecasis, G. R., Bentley, D. R., et al. (2015). A global reference for human genetic variation. *Nature* 526, 68–74. doi: 10.1038/nature15393

Baldwin, C. T., Hoth, C. F., Amos, J. A., da-Silva, E. O., and Milunsky, A. (1992). An exonic mutation in the HuP2 paired domain gene causes Waardenburg's syndrome. *Nature* 355, 637–638. doi: 10.1038/355637a0

Barber, T. D., Barber, M. C., Cloutier, T. E., and Friedman, T. B. (1999). PAX3 gene structure, alternative splicing and evolution. *Gene* 237, 311–319.

Bertolotto, C., Buscà, R., Abbe, P., Bille, K., Aberdam, E., Ortonne, J. P., et al. (1998). Different cis-acting elements are involved in the regulation of TRP1 and TRP2 promoter activities by cyclic AMP: pivotal role of M boxes (GTCATGTGCT) and of microphthalmia. *Mol. Cell. Biol.* 18, 694–702. doi: 10.1128/MCB.18.2.694

Bondurand, N., Dastot-Le Moal, F., Stanchina, L., Collot, N., Baral, V., Marlin, S., et al. (2007). Deletions at the SOX10 gene locus cause Waardenburg syndrome types 2 and 4. *Am. J. Hum. Genet.* 81, 1169–1185. doi: 10.1086/522090

Bondurand, N., Pingault, V., Goerich, D. E., Lemort, N., Sock, E., Caignec, C. L., et al. (2000). Interaction among SOX10, PAX3 and MITF, three genes altered in Waardenburg syndrome. *Hum. Mol. Genet.* 9, 1907–1917. doi: 10.1093/hmg/9.13.1907

Boudjadi, S., Chatterjee, B., Sun, W., Vemu, P., and Barr, F. G. (2018). The expression and function of PAX3 in development and disease. *Gene* 666, 145–157.

Brownstein, Z., Bhonker, Y., and Avraham, K. B. (2012). High-throughput sequencing to decipher the genetic heterogeneity of deafness. *Genome Biol.* 13, 245.

Chan, K. K., Wong, C. K. Y., Lui, V. C. H., Tam, P. K. H., and Sham, M. H. (2003). Analysis of SOX10 mutations identified in Waardenburg-Hirschsprung patients: differential effects on target gene regulation. *J. Cell Biochem.* 90, 573–585. doi: 10.1002/jcb.10656

Chen, H., Jiang, L., Xie, Z., Mei, L., He, C., Hu, Z., et al. (2010). Novel mutations of PAX3, MITF, and SOX10 genes in Chinese patients with type I or type II Waardenburg syndrome. *Biochem. Biophys. Res. Communi.* 397, 70–74. doi: 10.1016/j.bbrc.2010.05.066

Cheng, H.-H., Ling, S.-Q., Zhao, P.-Z., Li, W.-L., and Deng, J. (2019). The heterozygous EDNRB mutation in a Chinese family with Waardenburg syndrome type I. *Int. J. Ophthalmol.* 12, 1507–1509. doi: 10.18240/ijo.2019.09.22

Edery, P., Attié, T., Amiel, J., Pelet, A., Eng, C., Hofstra, R. M., et al. (1996). Mutation of the endothelin-3 gene in the Waardenburg-Hirschsprung disease (Shah-Waardenburg syndrome). *Nat. Genet.* 12, 442–444.

Fowler, A., Mahamdallie, S., Ruark, E., Seal, S., Ramsay, E., Clarke, M., et al. (2016). Accurate clinical detection of exon copy number variants in a targeted NGS panel using DECoN. *Wellcome Open Res.* 1:20. doi: 10.12688/wellcomeopenres.10069.1

Hageman, M. J., and Delleman, J. W. (1977). Heterogeneity in Waardenburg syndrome. *Am. J. Hum. Genet.* 29, 468–485.

Hodgkinson, C. A., Moore, K. J., Nakayama, A., Steingrímsson, E., Copeland, N. G., Jenkins, N. A., et al. (1993). Mutations at the mouse microphthalmia locus are associated with defects in a gene encoding a novel basic-helix-loop-helix-zipper protein. *Cell* 74, 395–404. doi: 10.1016/0092-8674(93)90429-t

Hoth, C. F., Milunsky, A., Lipsky, N., Sheffer, R., Clarren, S. K., and Baldwin, C. T. (1993). Mutations in the paired domain of the human PAX3 gene cause Klein-Waardenburg syndrome (WS-III) as well as Waardenburg syndrome type I (WS-I). *Am. J. Hum. Genet.* 52, 455–462.

Issa, S., Bondurand, N., Faubert, E., Poisson, S., Lecerf, L., Nitschke, P., et al. (2017). EDNRB mutations cause Waardenburg syndrome type II in the heterozygous state. *Hum. Mutat.* 38, 581–593. doi: 10.1002/humu.23206

Jiao, Z., Mollaaghababa, R., Pavan, W. J., Antonellis, A., Green, E. D., and Hornyak, T. J. (2004). Direct interaction of Sox10 with the promoter of murine Dopachrome Tautomerase (Dct) and synergistic activation of Dct expression with Mitf. *Pigment Cell Res.* 17, 352–362. doi: 10.1111/j.1600-0749.2004.00154.x

Kapur, R. P. (1999). Early death of neural crest cells is responsible for total enteric aganglionosis in Sox10(Dom)/Sox10(Dom) mouse embryos. *Pediatr. Dev. Pathol.* 2, 559–569. doi: 10.1007/s100249900162

Karczewski, K. J., Francioli, L. C., Tiao, G., Cummings, B. B., Alföldi, J., Wang, Q., et al. (2019). Variation across 141,456 human exomes and genomes reveals the spectrum of loss-of-function intolerance across human protein-coding genes. *J. bioRxiv* [Preprint] doi: 10.1101/531210bioRxiv:531210

Kelsh, R. N. (2006). Sorting out Sox10 functions in neural crest development. *BioEssays* 28, 788–798. doi: 10.1002/bies.20445

Khajavi, M., Inoue, K., and Lupski, J. R. (2006). Nonsense-mediated mRNA decay modulates clinical outcome of genetic disease. *Eur. J. Hum. Genet.* 14, 1074–1081. doi: 10.1038/sj.ejhg.5201649

Landrum, M. J., Lee, J. M., Benson, M., Brown, G. R., Chao, C., Chitipiralla, S., et al. (2018). ClinVar: improving access to variant interpretations and supporting evidence. *Nucleic Acids Res.* 46, D1062–D1067.

Lee, M., Goodall, J., Verastegui, C., Ballotti, R., and Goding, C. R. (2000). Direct regulation of the Microphthalmia promoter by Sox10 links Waardenburg-Shah syndrome (WS4)-associated hypopigmentation and deafness to WS2. *J. Biol. Chem.* 275, 37978–37983. doi: 10.1074/jbc.M003816200

Lek, M., Karczewski, K. J., Minikel, E. V., Samocha, K. E., Banks, E., Fennell, T., et al. (2016). Analysis of protein-coding genetic variation in 60,706 humans. *Nature* 536, 285–291.

Li, H. (2013). Aligning sequence reads, clone sequences and assembly contigs with BWA-MEM. *ArXiv*[Preprint] arXiv: 1303.3997,

Li, W., Mei, L., Chen, H., Cai, X., Liu, Y., Men, M., et al. (2019). New genotypes and phenotypes in patients with 3 subtypes of Waardenburg Syndrome identified by diagnostic next-generation sequencing. *Neural Plast.* 2019, 1–12. doi: 10.1155/2019/7143458

Lin, X., Tang, W., Ahmad, S., Lu, J., Colby, C. C., Zhu, J., et al. (2012). Applications of targeted gene capture and next-generation sequencing technologies in studies of human deafness and other genetic disabilities. *Hear. Res.* 288, 67–76. doi: 10.1016/j.heares.2012.01.004

Liu, Q., Cheng, J., Lu, Y., Zhou, J., Wang, L., Yang, C., et al. (2020). The clinical and genetic research of Waardenburg syndrome type I and II in Chinese families. *Int. J. Pediatr. Otorhinolaryngol.* 130:109806. doi: 10.1016/j.ijporl.2019.109806

Liu, X., Wu, C., Li, C., and Boerwinkle, E. (2016). dbNSFP v3.0: a one-stop database of functional predictions and annotations for human nonsynonymous and splice-site SNVs. *Hum. Mutat.* 37, 235–241. doi: 10.1002/humu.22932

McKenna, A., Hanna, M., Banks, E., Sivachenko, A., Cibulskis, K., Kernytsky, A., et al. (2010). The genome analysis toolkit: a mapreduce framework for analyzing next-generation DNA sequencing data. *Genome Res.* 20, 1297–1303. doi: 10.1101/gr.107524.110

Minami, S. B., Nara, K., Mutai, H., Morimoto, N., Sakamoto, H., Takiguchi, T., et al. (2019). A clinical and genetic study of 16 Japanese families with Waardenburg syndrome. *Gene* 704, 86–90.

Mirhadi, S., Spritz, R. A., and Moss, C. (2020). Does SNAI2 mutation cause human piebaldism and Waardenburg syndrome? *Am. J. Med. Genet. Part A* 182, 3074–3075. doi: 10.1002/ajmg.a.61887

Morimoto, N., Mutai, H., Namba, K., Kaneko, H., Kosaki, R., and Matsunaga, T. (2018). Homozygous EDNRB mutation in a patient with Waardenburg syndrome type 1. *Auris Nasus Larynx* 45, 222–226. doi: 10.1016/j.anl.2017.03.022

Nayak, C. S., and Isaacson, G. (2003). Worldwide distribution of Waardenburg syndrome. *Ann. Otol. Rhinol. Laryngol.* 112(9 Pt 1), 817–820. doi: 10.1177/000348940311200913

Newton, V. (1990). Hearing loss and Waardenburg's syndrome: implications for genetic counselling. *J. Laryngol. Otol.* 104, 97–103.

Oza, A. M., DiStefano, M. T., Hemphill, S. E., Cushman, B. J., Grant, A. R., Siegert, R. K., et al. (2018). Expert specification of the ACMG/AMP variant interpretation guidelines for genetic hearing loss. *Hum. Mutat.* 39, 1593–1613.

Pan, Z., Xu, H., Tian, Y., Liu, D., Liu, H., Li, R., et al. (2020). Perrault syndrome: clinical report and retrospective analysis. *Mol. Genet. Genomic Med.* 8:e1445.

Pedersen, B. S., Layer, R. M., and Quinlan, A. R. (2016). Vcfanno: fast, flexible annotation of genetic variants. *Genome Biol.* 17:118. doi: 10.1186/s13059-016-0973-5

Pingault, V., Bondurand, N., Kuhlbrodt, K., Goerich, D. E., Préhu, M. O., Puliti, A., et al. (1998). SOX10 mutations in patients with Waardenburg-Hirschsprung disease. *Nat. Genet.* 18, 171–173.

Pingault, V., Ente, D., Dastot-Le Moal, F., Goossens, M., Marlin, S., and Bondurand, N. (2010). Review and update of mutations causing Waardenburg syndrome. *Hum. Mutat.* 31, 391–406. doi: 10.1002/humu.21211

Potterf, S. B., Furumura, M., Dunn, K. J., Arnheiter, H., and Pavan, W. J. (2000). Transcription factor hierarchy in Waardenburg syndrome: regulation of MITF expression by SOX10 and PAX3. *Hum. Genet.* 107, 1–6. doi: 10.1007/s004390000328

Puffenberger, E. G., Hosoda, K., Washington, S. S., Nakao, K., deWit, D., Yanagisawa, M., et al. (1994). A missense mutation of the endothelin-B receptor gene in multigenic Hirschsprung's disease. *Cell* 79, 1257–1266.

Read, A. P., and Newton, V. E. (1997). Waardenburg syndrome. *J. Med. Genet.* 34, 656–665. doi: 10.1136/jmg.34.8.656

Richards, S., Aziz, N., Bale, S., Bick, D., Das, S., Gastier-Foster, J., et al. (2015). Standards and guidelines for the interpretation of sequence variants: a joint consensus recommendation of the american college of medical genetics and genomics and the association for molecular pathology. *Genet. Med.* 17, 405–424.

Sánchez-Martín, M., Rodríguez-García, A., Pérez-Losada, J., Sagrera, A., Read, A. P., and Sánchez-García, I. S. L. U. G. (2002). (SNAI2) deletions in patients with Waardenburg disease. *Hum. Mol. Genet.* 11, 3231–3236.

Somashekar, P. H., Girisha, K. M., Nampoothiri, S., Gowrishankar, K., Devi, R. R., Gupta, N., et al. (2019). Locus and allelic heterogeneity and phenotypic variability in Waardenburg syndrome. *Clin. Genet.* 95, 398–402. doi: 10.1111/cge.13468

Song, J., Feng, Y., Acke, F. R., Coucke, P., Vleminckx, K., and Dhooge, I. J. (2016). Hearing loss in Waardenburg syndrome: a systematic review. *Clin. Genet.* 89, 416–425.

Steel, K. P., and Barkway, C. (1989). Another role for melanocytes: their importance for normal stria vascularis development in the mammalian inner ear. *Development* 107, 453.

Steingrímsson, E., Copeland, N. G., and Jenkins, N. A. (2004). Melanocytes and the microphthalmia transcription factor network. *Annu. Rev. Genet.* 38, 365–411.

Steingrímsson, E., Moore, K. J., Lamoreux, M. L., Ferré-D'Amaré, A. R., Burley, S. K., Sanders Zimring, D. C., et al. (1994). Molecular basis of mouse microphthalmia (mi) mutations helps explain their developmental and phenotypic consequences. *Nat. Genet.* 8, 256–263. doi: 10.1038/ng1194-256

Steingrímsson, E., Nii, A., Fisher, D. E., Ferré-D'Amaré, A. R., McCormick, R. J., Russell, L. B., et al. (1996). The semidominant Mi(b) mutation identifies a role for the HLH domain in DNA binding in addition to its role in protein dimerization. *Embo J.* 15, 6280–6289.

Stolt, C. C., and Wegner, M. (2010). SoxE function in vertebrate nervous system development. *Int. J. Biochem. Cell Biol.* 42, 437–440.

Sun, L., Li, X., Shi, J., Pang, X., Hu, Y., Wang, X., et al. (2016). Molecular etiology and genotype-phenotype correlation of Chinese han deaf patients with type I and type II Waardenburg Syndrome. *Sci. Rep.* 6:35498. doi: 10.1038/srep35498

Suzuki, N., Mutai, H., Miya, F., Tsunoda, T., Terashima, H., Morimoto, N., et al. (2018). A case report of reversible generalized seizures in a patient with Waardenburg syndrome associated with a novel nonsense mutation in the penultimate exon of SOX10. *BMC Pediatr.* 18:171. doi: 10.1186/s12887-018-1139-2

Tamayo, M. L., Gelvez, N., Rodriguez, M., Florez, S., Varon, C., Medina, D., et al. (2008). Screening program for Waardenburg syndrome in Colombia: clinical definition and phenotypic variability. *Am. J. Med. Genet. A* 146a, 1026–1031. doi: 10.1002/ajmg.a.32189

Tang, H. Y., Fang, P., Lin, J. W., Darilek, S., Osborne, B. T., Haymond, J. A., et al. (2015). DNA sequence analysis and genotype-phenotype assessment in 71 patients with syndromic hearing loss or auditory neuropathy. *BMJ Open* 5:e007506.

Tang, W., Qian, D., Ahmad, S., Mattox, D., Todd, N. W., Han, H., et al. (2012). A low-cost exon capture method suitable for large-scale screening of genetic deafness by the massively-parallel sequencing approach. *Genet. Test. Mol. Biomarkers* 16, 536–542. doi: 10.1089/gtmb.2011.0187

Tassabehji, M., Newton, V. E., Liu, X. Z., Brady, A., Donnai, D., Krajewska-Walasek, M., et al. (1995). The mutational spectrum in Waardenburg syndrome. *Hum. Mol. Genet.* 4, 2131–2137.

Tassabehji, M., Newton, V. E., and Read, A. P. (1994). Waardenburg syndrome type 2 caused by mutations in the human microphthalmia (MITF) gene. *Nat. Genet.* 8, 251–255. doi: 10.1038/ng1194-251

Tassabehji, M., Read, A. P., Newton, V. E., Harris, R., Balling, R., Gruss, P., et al. (1992). Waardenburg's syndrome patients have mutations in the human homologue of the Pax-3 paired box gene. *Nature* 355, 635–636.

Toriello, H. V. (2011). Pigmentary anomalies and hearing loss. *Adv. Oto Rhino Laryngol.* 70, 50–55.

Verastegui, C., Bille, K., Ortonne, J. P., and Ballotti, R. (2000). Regulation of the microphthalmia-associated transcription factor gene by the Waardenburg syndrome type 4 gene, SOX10. *J. Biol. Chem.* 275, 30757–30760. doi: 10.1074/jbc.C000445200

Wang, Q. (2006). Functional analysis of alternative isoforms of the transcription factor PAX3 in melanocytes in vitro. *Cancer Res.* 66, 8574–8580. doi: 10.1158/0008-5472.can-06-0947

Wegner, M. (2005). Secrets to a healthy Sox life: lessons for melanocytes. *Pigment Cell Res.* 18, 74–85. doi: 10.1111/j.1600-0749.2005.00218.x

Wildhardt, G., Zirn, B., Graul-Neumann, L. M., Wechtenbruch, J., Suckfüll, M., Buske, A., et al. (2013). Spectrum of novel mutations found in Waardenburg syndrome types 1 and 2: implications for molecular genetic diagnostics. *BMJ Open* 3:e001917.

Woodward, K. J., Cundall, M., Sperle, K., Sistermans, E. A., Ross, M., Howell, G., et al. (2005). Heterogeneous duplications in patients with Pelizaeus-Merzbacher disease suggest a mechanism of coupled homologous and nonhomologous recombination. *Am. J. Hum. Genet.* 77, 966–987. doi: 10.1086/498048

Wu, H., Feng, Y., Jiang, L., Pan, Q., Liu, Y., Liu, C., et al. (2016). Application of a new genetic deafness microarray for detecting mutations in the deaf in China. *PLoS One* 11:e0151909. doi: 10.1371/journal.pone.0151909

Xiong, H. Y., Alipanahi, B., Lee, L. J., Bretschneider, H., Merico, D., Yuen, R. K. C., et al. (2015). RNA splicing. the human splicing code reveals new insights into the genetic determinants of disease. *Science (New York, NY)* 347:1254806. doi: 10.1126/science.1254806

Yang, S., Dai, P., Liu, X., Kang, D., Zhang, X., Yang, W., et al. (2013). Genetic and phenotypic heterogeneity in Chinese patients with Waardenburg syndrome type II. *PLoS One* 8:e77149. doi: 10.1371/journal.pone.0077149

Yasumoto, K., Yokoyama, K., Shibata, K., Tomita, Y., and Shibahara, S. (1995). Microphthalmia-associated transcription factor as a regulator for melanocyte-specific transcription of the human tyrosinase gene. *Mol. Cell. Biol.* 15:1833.

Zhang, L., Wang, J., Zhang, C., Li, D., Carvalho, C. M. B., Ji, H., et al. (2017). Efficient CNV breakpoint analysis reveals unexpected structural complexity and correlation of dosage-sensitive genes with clinical severity in genomic disorders. *Hum. Mol. Genet.* 26, 1927–1941. doi: 10.1093/hmg/ddx102

Conflict of Interest: The authors declare that the research was conducted in the absence of any commercial or financial relationships that could be construed as a potential conflict of interest.

frontiers in Pediatrics

CASE REPORT
published: 18 June 2021
doi: 10.3389/fped.2021.679279

Case Report: Exome Sequencing Identified a Novel Frameshift Mutation of *α-Actin 1* in a Chinese Family With Macrothrombocytopenia and Mild Bleeding

Fang-Mei Luo[1,2†], *Liang-Liang Fan*[2,3†], *Yue Sheng*[2], *Yi Dong*[2] *and Lv Liu*[1*]

[1] Department of Respiratory Medicine, The Second Xiangya Hospital of Central South University, Changsha, China, [2] Department of Cell Biology, The School of Life Sciences, Central South University, Changsha, China, [3] Hunan Key Laboratory of Animal Models for Human Disease, School of Life Sciences, Central South University, Changsha, China

OPEN ACCESS

Edited by:
Emiliano González Vioque, University Clinical Hospital of Santiago, Spain

Reviewed by:
Benedetta Izzi, Istituto Neurologico Mediterraneo Neuromed (IRCCS), Italy
Aniefiok John Udoakang, University of Ghana, Ghana

***Correspondence:**
Lv Liu
docliulv@csu.edu.cn

[†] *These authors have contributed equally to this work*

Specialty section:
This article was submitted to Genetics of Common and Rare Diseases, a section of the journal Frontiers in Pediatrics

Received: *11 March 2021*
Accepted: *17 May 2021*
Published: *18 June 2021*

Citation:
Luo F-M, Fan L-L, Sheng Y, Dong Y and Liu L (2021) Case Report: Exome Sequencing Identified a Novel Frameshift Mutation of α-Actin 1 in a Chinese Family With Macrothrombocytopenia and Mild Bleeding. Front. Pediatr. 9:679279. doi: 10.3389/fped.2021.679279

Inherited macrothrombocytopenia (IMTP) is a rare disorder characterized by a reduced platelet count and abnormally large platelets. The main clinical symptom of IMTP is mild bleeding in some patients. At present, more than 30 genes have been identified in patients with syndromic and non-syndromic IMTP. In this study, a 3-year-old boy and his mother who presented with mild epistaxis and/or gingival bleeding were diagnosed as having IMTP. Wen then selected whole sequencing to explore the genetic lesion of the patients. After data filtering and mutation validation, a novel frameshift mutation (NM_001130004: c.398_399insTGCG, p.F134AfsX60) of *α-actin 1* (*ACTN1*) was identified in the proband and his mother but absent in other unaffected individuals. Previous studies have proven that mutations in *ACTN1* may lead to IMTP with mild to absent bleeding phenotype. The novel mutation, resulting in a truncated protein in exon 4 of the *ACTN1* gene, was absent in the public database, such as 1000G and genomAD. Further Western blot revealed that the expression of α-actin 1 in the proband was decreased overtly, which indicated that the novel frameshift mutation may induce non-sense-mediated mRNA decay. In summary, this study not only broadened the variants spectrum of *ACTN1* gene, which may contribute to the genetic counseling of IMTP, but also confirmed the diagnosis of IMTP, which may help the management and prognosis for the family members.

Keywords: macrothrombocytopenia, mild bleeding, ACTN1 mutation, non-sense-mediated mRNA decay, whole-exome sequencing

INTRODUCTION

Inherited macrothrombocytopenia (IMTP) is an important cause of thrombocytopenia, which is defined as a platelet count of $<150 \times 10^9$/L (1–3). Besides the reduced platelet count, a significant increase in platelet size (>12 fL) is another feature of IMTP (1, 3). As a rare clinical condition, IMTP affects at least 2.7 per 100,000 individuals with mild to absent bleeding phenotype (2, 4). At present, mutations in more than 10 genes including *α-actin 1*(*ACTN1*), *myosin heavy chain 9* (*MYH9*), *tubulin beta class I* (*TUBB*), etc. have been identified in non-syndromic IMTP with autosomal

dominant, recessive, and sex-linked patterns (1, 3). In addition, some syndromes are also typically characterized by low platelet counts and severe bleeding tendency, such as Wiskott-Aldrich syndrome, Bernard-Soulier syndrome, Di George syndrome, and so on (5–7). However, because of varying mutations and clinical manifestations, the IMTP shows obvious heterogeneity, which challenges the clear diagnosis of IMTP and leads to the misdiagnosis as immune thrombocytopenic purpura (8).

In this study, we enrolled a 3-year-old boy and his mother with IMTP and mild epistaxis and/or gingival bleeding. The aim of this study was to explore the genetic lesion of the patients with the help of whole-exome sequencing.

CASE PRESENTATION

A family from central south region of China (Hunan province) including seven persons was investigated in this study (**Figure 1A**). The proband (III-2), a 3-year-old boy, was admitted to our hospital because of mild epistaxis. Blood routine examination of the proband was shown as follows: hemoglobin, 13.0 g/dL; platelet count, 102 $\times$ 10^9/L; mean platelet volume, 12.9 fL; and platelet distribution width, 18.1 fL. *In vitro* platelet aggregation in response to collagen and ristocetin was normal, but adenosine diphosphate (ADP) was slightly reduced (35%). Medical history survey found that the boy (III-2) has suffered from epistaxis several times with unexplained reason. Further family history investigation revealed that the proband's mother (II-1) and grandfather (I-1) have a history of mild epistaxis and gingival bleeding. Blood routine examination of the proband's mother (II-1) also found the reduced platelets (111 $\times$ 10^9/L) count and increased mean platelet volume (12.7 fL) and platelet distribution width (17.7 fL). Peripheral blood smears May-Grünwald Giemsa staining revealed macrothrombocytopenia in the proband and his mother (**Figure 1B**). No other family members showed abnormal blood routine examination and bleeding diathesis. In addition, 200 unrelated, ethnically matched healthy controls were used as internal controls to exclude single-nucleotide polymorphisms (SNPs) in local individuals. These healthy controls (male/female: 100/100, aged 36.7 $\pm$ 8.6 years) lacked IMTP diagnostic features. Each participant underwent thorough examination for clinical diagnosis or exclusion, including general examination such as blood routine examination and peripheral blood smear May-Grünwald Giemsa staining.

We then employed whole-exome sequencing to explore the candidate gene mutation in the proband (III-2). Whole-exome sequencing was conducted at BerryGenomic Institute (Beijing, China) (9). Exomes were captured by Agilent SureSelect Human All Exon V6 kits, and high-throughput sequencing was conducted with an Illumina HiSeq 4000 system. The strategies of data filtering were as follows (9, 10): (a) non-synonymous SNPs or frameshift-causing INDELs with an alternative allele frequency >0.01 in the NHLBI Exome Sequencing Project Exome Variant Server (ESP6500), dbSNP155, the 1000 Genomes Project, the genomAD database, or in-house exome databases of BerryGenomic (2,000 exomes) were excluded; (b) the filtered SNVs and INDELs, predicted by SIFT, Polyphen2, and MutationTaster to be damaging, were remained; (c) the variants belong to pathogenic and likely pathogenic according to American College of Medical Genetics (ACMG) guideline remained (11); (d) cosegregation analysis was conducted in the family.

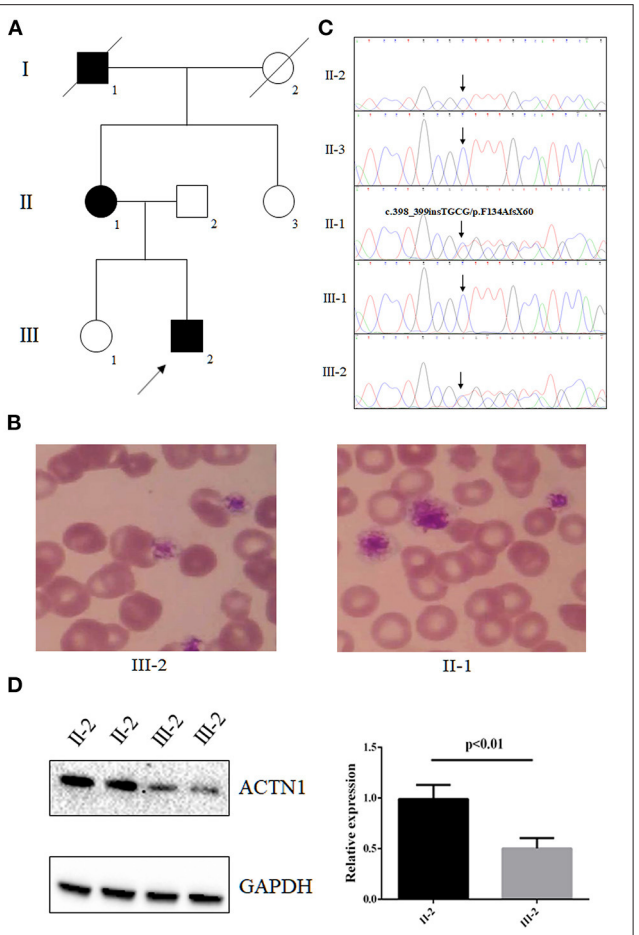

FIGURE 1 | The clinical data and genetic analysis of the family with IMTP and mild bleeding. **(A)** Pedigree of the family. Black circles/squares are affected; white circles/squares are unaffected; slashed symbol is deceased family member. Arrow indicates the proband. **(B)** Blood smears (May-Grünwald Giemsa staining) revealed macrothrombocytopenia in the proband and his mother. **(C)** Sanger DNA sequencing chromatogram demonstrates the heterozygosity for an *ACTN1* frameshift mutation (NM_001130004: c.398_399insTGCG, p.F134AfsX60) in affected members. **(D)** Western blot analysis of the expression of ACTN1 in the proband's platelets.

Whole-exome sequencing yielded 9.98-Gb data. After alignment and single-nucleotide variant calling, 70,145 variants were identified in the proband. Via the aforementioned filtering method and Sanger sequencing validation, a novel frameshift mutation (NM_001130004: c.398_399insTGCG, p.F134AfsX60) of *ACTN1* was identified in the proband and his mother but absent in unaffected individuals (**Figure 1C**). No other potential pathogenic mutation for macrothrombocytopenia-related phenotype was found (**Table 1**). Previous studies have proven that mutations in *ACTN1* may lead to IMTP with mild to absent bleeding phenotype (12, 13). The novel mutation, resulting in a truncated protein in exon 4 of the *ACTN1* gene, was absent in the public database such as 1000G and genomAD, as well as

our 200 healthy controls. Bioinformatics programs predicted that this mutation (NM_001130004: c.398_399insTGCG, p.F134AfsX60) was a pathogenic mutation and located in an evolutionarily conserved site of the α-actin 1 protein. According to ACMG guidelines (11), this mutation was pathogenic (PVS1 + PM2 + PM3). We then further extracted total protein from the platelet of the proband and healthy control (II-2). Western Blot indicated that, compared with the healthy controls, the expression of *ACTN1* was decreased by ∼49% in the heterozygous carrier (**Figure 1D**). These data suggested that the variant (NM_001130004: c.398_399insTGCG, p.F134AfsX60) of *ACTN1* was a loss-of-function mutation and can lead to non–sense-mediated mRNA decay.

DISCUSSION

The human *ACTN1* gene encoding a member of the actin-crosslinking protein named α-actinin is located on chromosome 14q24.1, and it consists of 21 exons spanning ∼3.78 kilobases. α-Actin 1 participates in the organization of the cytoskeleton, thought to be an anchor actin to a variety of intracellular structures and mainly expressed in platelets and megakaryocytes (14). In 2013, six different mutations of *ACTN1* were identified in 13 unrelated families with IMTP, which indicated that *ACTN1* was one of the genetic lesions in IMTP (12). At present, thrombocytopenia caused by pathogenic variants in *ACTN1* gene has been classified to ACTN1-related thrombocytopenia (15). To date, approximately 44 mutations of *ACTN1* have been detected in IMTP patients. Here, we identified a frameshift mutation (NM_001130004: c.398_399insTGCG, p.F134AfsX60) of *ACTN1* in a Chinese family with IMTP. As far as we know, this mutation may be first reported in IMTP patients; our study expanded the variant spectrum of *ACTN1* gene.

The α-actin superfamily consists of four members including ACTN1, ACTN2, ACTN3, and ACTN4, which are responsible for the organization of the cytoskeleton (3, 16). Previous studies have found that *ACTN1* was mainly expressed in platelets and megakaryocytes; the mutated *ACTN1* may lead to a decrease of 50% platelet counts and an increase of 30% in platelet size (12, 17). In our study, the proband and his mother with the novel mutation of *ACTN1* were also presented with macrothrombocytopenia. The novel frameshift mutation (NM_001130004: c.398_399insTGCG, p.F134AfsX60) can lead to the truncation mutation in the N-terminal of ACTN1. According to non–sense-mediated mRNA decay theory (18), the novel mutation may result in the decreased mRNA levels of *ACTN1*. Functional studies further confirmed that the novel mutation may lead to the reduction of *ACTN1* expression, which may affect the organization of the cytoskeleton in platelets and megakaryocytes, finally resulting in macrothrombocytopenia.

Previous studies in Chinese hamster ovary cells revealed that the mutated *ACTN1* may disrupt the normal actin-based cytoskeletal structure (12). The mice with *ACTN1* mutation may present with disorganized actin-based cytoskeleton in megakaryocytes, which may further result in abnormal number and size of platelets (12). In this study, the phenotypes

TABLE 1 | Characteristics of the genetic variants identified for the proband via whole-exome sequencing.

Gene	Transcript	cDNA	Protein	Genotype	dbSNP	ClinVar	ACMG level	OMIM phenotype
CACNB2	NM_201590.2	c.1508C>T	p.S503L	het	rs137886839	Conflicting	Likely pathogenic	Brugada syndrome 4
LIMA1	NM_001113546.1	c.73C>A	p.L25I	het	rs140372565	Association	Likely pathogenic	[Low-density lipoprotein cholesterol level QTL 8]
PNPO	NM_018129.3	c.148G>A	p.E50K	het	rs549477447	Uncertain significance	Likely pathogenic	AR: pyridoxamine 5′-Phosphate oxidase deficiency
COL7A1	NM_000094.3	c.2392G>A	p.G798R	het	rs202237834	Uncertain significance	Likely pathogenic	AD,AR: epidermolysis bullosa dystrophica
IL17RD	NM_017563.4	c.572C>T	p.P191L	het	rs200088377	Likely pathogenic	Likely pathogenic	AD, AR: hypogonadotropic hypogonadism
ARL13B	NM_182896.2	c.568A>G	p.I190V	het	rs193219215	–	Likely pathogenic	AR: Joubert syndrome
C9	NM_001737.4	c.346C>T	p.R116*	het	rs121909592	Pathogenic	Likely pathogenic	C9 deficiency
DNAH11	NM_001277115.1	c.11804C>T	p.P3935L	het	rs72658814	Uncertain significance	Likely pathogenic	AR: ciliary dyskinesia, primary
KCNH2	NM_000238.3	c.2771G>C	p.G924A	het	rs199473009	Uncertain significance	Likely pathogenic	AD: long QT syndrome 2
ACTN1	**NM_001130004.1**	**c.398_399insTGCG**	**p.F134AfsX60**	**het**	**–**	**–**	**Pathogenic**	**AD: bleeding disorder, platelet type**
FANCL	NM_018062.3	c.738dup	p.M247YfsX4	het	–	–	Likely pathogenic	AR: Fanconi anemia

AD, autosomal dominant; AR, autosomal recessive. The MAF of these mutations was <0.01 in ESP6500, dbSNP155, the 1000 Genomes Project, the genomAD database, and in-house exome databases of BerryGenomic. The bold words represent the genetic mutation which was responsible for this family.

of the novel mutation (NM_001130004: c.398_399insTGCG, p.F134AfsX60) carriers (II-1 and III-2) were consistent with mice model and other reported patients, which further confirmed the pathogenicity of this novel mutation (19, 20).

IMTP can easily be misdiagnosed as immune thrombocytopenic purpura, which may further make problems in therapy and management of patients (8). Hence, precise diagnosis is necessary for IMTP patients, especially for the IMTP patients caused by *ACTN1* mutations. A recent study that involved ∼50 *ACTN1* mutation carriers indicated that *ACTN1* mutations lead to a benign form of platelet macrocytosis not always associated with thrombocytopenia (21). Precise diagnosis of *ACTN*1-caused IMTP can provide affected patients and their family members with a good prognosis. In our study, we confirmed the diagnosis of the affected members by whole-exome sequencing and Sanger sequencing, which may aid in the further management and prognosis of the family members. Meanwhile, our study also indicated that whole-exome sequencing combined with Sanger sequencing was an effective method in diagnosis of IMTP.

In summary, by employing whole-exome sequencing, we identified a novel frameshift mutation (NM_001130004: c.398_399insTGCG, p.F134AfsX60) of *ACTN1* in a Chinese family with IMTP and mild epistaxis and/or gingival bleeding. Hence, this study not only broadened the variants spectrum of *ACTN1* gene, which may contribute to the genetic counseling of IMTP, but also confirmed the diagnosis of IMTP, which may help in the management and prognosis of the family members.

DATA AVAILABILITY STATEMENT

The data presented in the study are deposited in the (BioSample) repository, accession number: SAMN18953804, https://www.ncbi.nlm.nih.gov/biosample/18953804.

ETHICS STATEMENT

The studies involving human participants were reviewed and approved by the Second Xiangya Hospital of Central South University, Changsha, China. Written informed consent to participate in this study was provided by the participants' legal guardian/next of kin.

AUTHOR CONTRIBUTIONS

F-ML and LL enrolled the samples and clinical data. YS and YD performed DNA isolation and PCR. F-ML and L-LF wrote the manuscript and revised it. L-LF and LL supported the project. All authors reviewed the manuscript.

FUNDING

This study was supported by National Natural Science Foundation of China (81800220, 82000079, and 82000427) and National Natural Science Foundation of Hunan province (2020JJ5785).

ACKNOWLEDGMENTS

We thank all subjects for participating in this study.

SUPPLEMENTARY MATERIAL

The Supplementary Material for this article can be found online at: https://www.frontiersin.org/articles/10.3389/fped.2021.679279/full#supplementary-material

REFERENCES

1. Gauer RL, Braun MM. Thrombocytopenia. *Am Fam Physician*. (2012) 85:612–22.
2. Favier R, Raslova H. Progress in understanding the diagnosis and molecular genetics of macrothrombocytopenias. *Br J Haematol*. (2015) 170:626–39. doi: 10.1111/bjh.13478
3. Ghosh K, Bhattacharya M, Chowdhury R, Mishra K, Ghosh M. Inherited macrothrombocytopenia: correlating morphology, epidemiology, molecular pathology and clinical features. *Indian J Hematol Blood Transfus*. (2018) 34:387–97. doi: 10.1007/s12288-018-0950-0
4. Savoia A. Molecular basis of inherited thrombocytopenias: an update. *Curr Opin Hematol*. (2016) 23:486–92. doi: 10.1097/MOH.0000000000000269
5. Monteferrario D, Bolar NA, Marneth AE, Hebeda KM, Bergevoet SM, Veenstra H, et al. A dominant-negative GFI1B mutation in the gray platelet syndrome. *N Engl J Med*. (2014) 370:245–53. doi: 10.1056/NEJMoa1308130
6. Grainger JD, Thachil J, Will AM. How we treat the platelet glycoprotein defects; Glanzmann thrombasthenia and Bernard Soulier syndrome in children and adults. *Br J Haematol*. (2018) 182:621–32. doi: 10.1111/bjh.15409
7. Ferrua F, Cicalese MP, Galimberti S, Giannelli S, Dionisio F, Barzaghi F, et al. Lentiviral haemopoietic stem/progenitor cell gene therapy for treatment of Wiskott-Aldrich syndrome: interim results of a non-randomised, open-label, phase 1/2 clinical study. *Lancet Haematol*. (2019) 6:e239–53. doi: 10.1016/S2352-3026(19)30021-3
8. Kanhai D, Mulder R, Ploos van Amstel HK, Schutgens R, Lukens M, Tamminga RYJ. Familial macrothrombocytopenia due to a double mutation in cis in the alpha-actinin 1 gene (ACTN1), previously considered to be chronic immune thrombocytopenic purpura. *Pediatr Blood Cancer*. (2018) 65:e27418. doi: 10.1002/pbc.27418
9. Luo FM, Deng MX, Yu R, Liu L, Fan LL. Case report: chorea-acanthocytosis presents as epilepsy in a consanguineous family with a nonsense mutation of in VPS13A. *Front Neurosci*. (2021) 15:604715. doi: 10.3389/fnins.2021.687435
10. Yu R, Liu L, Li YL, Fan LL. MITF p.Arg217Thr variant identified in a Han Chinese family with Tietz/Waardenburg syndrome. *Biomed Res Int*. (2021) 2021:4381272. doi: 10.1155/2021/4381272
11. Richards S, Aziz N, Bale S, Bick D, Das S, Gastier-Foster J, et al. Standards and guidelines for the interpretation of sequence variants: a joint consensus recommendation of the American College of Medical Genetics and Genomics and the Association for Molecular Pathology. *Genet Med*. (2015) 17:405–24. doi: 10.1038/gim.2015.30
12. Kunishima S, Okuno Y, Yoshida K, Shiraishi Y, Sanada M, Muramatsu H, et al. ACTN1 mutations cause congenital macrothrombocytopenia. *Am J Hum Genet*. (2013) 92:431–8. doi: 10.1016/j.ajhg.2013.01.015
13. Bottega R, Marconi C, Faleschini M, Baj G, Cagioni C, Pecci A, et al. ACTN1-related thrombocytopenia: identification of novel families for phenotypic characterization. *Blood*. (2015) 125:869–72. doi: 10.1182/blood-2014-08-594531

14. Haudek VJ, Slany A, Gundacker NC, Wimmer H, Drach J, Gerner C. Proteome maps of the main human peripheral blood constituents. *J Proteome Res*. (2009) 8:3834–43. doi: 10.1021/pr801085g
15. Boutroux H, David B, Gueguen P, Frange P, Vincenot A, Leverger G, et al. ACTN1-related macrothrombocytopenia: a novel entity in the progressing field of pediatric thrombocytopenia. *J Pediatr Hematol Oncol*. (2017) 39:e515–8. doi: 10.1097/MPH.0000000000000885
16. Murphy AC, Young PW. The actinin family of actin cross-linking proteins - a genetic perspective. *Cell Biosci*. (2015) 5:49. doi: 10.1186/s13578-015-0029-7
17. Yasutomi M, Kunishima S, Okazaki S, Tanizawa A, Tsuchida S, Ohshima Y. ACTN1 rod domain mutation associated with congenital macrothrombocytopenia. *Ann Hematol*. (2016) 95:141–4. doi: 10.1007/s00277-015-2517-6
18. Baker KE, Parker R. Nonsense-mediated mRNA decay: terminating erroneous gene expression. *Curr Opin Cell Biol*. (2004) 16:293–9. doi: 10.1016/j.ceb.2004.03.003
19. Gueguen P, Rouault K, Chen JM, Raguenes O, Fichou Y, Hardy E, et al. A missense mutation in the alpha-actinin 1 gene. (ACTN1) is the cause of autosomal dominant macrothrombocytopenia in a large French family. *PLoS ONE*. (2013) 8:e74728. doi: 10.1371/journal.pone.0074728
20. Vincenot A, Saultier P, Kunishima S, Poggi M, Hurtaud-Roux MF, Roussel A, et al. Novel ACTN1 variants in cases of thrombocytopenia. *Hum Mutat*. (2019) 40:2258–69. doi: 10.1002/humu.23840
21. Faleschini M, Melazzini F, Marconi C, Giangregorio T, Pippucci T, Cigalini E, et al. ACTN1 mutations lead to a benign form of platelet macrocytosis not always associated with thrombocytopenia. *Br J Haematol*. (2018) 183:276–88. doi: 10.1111/bjh.15531

Conflict of Interest: The authors declare that the research was conducted in the absence of any commercial or financial relationships that could be construed as a potential conflict of interest.

frontiers in Genetics

OPINION
published: 21 June 2021
doi: 10.3389/fgene.2021.684067

Next-Generation Sequencing Analysis of *GBA1*: The Challenge of Detecting Complex Recombinant Alleles

*Elizabeth G. Woo, Nahid Tayebi and Ellen Sidransky**

Medical Genetics Branch, National Human Genome Research Institute, National Institutes of Health, Bethesda, MD, United States

Keywords: next-generation sequencing, glucocerebrosidase, Gaucher disease, *GBA1*, pseudogene, genotyping

INTRODUCTION

Gaucher disease (GD) is a rare autosomal recessive lysosomal storage disorder caused by pathologic variants in *GBA1,* the gene encoding the enzyme glucocerebrosidase. Deficiency of glucocerebrosidase leads to the accumulation of the substrates glucocerebroside and glucosylsphingosine in macrophages and neuronal cells. Variants in *GBA1* are a significant genetic risk factor for Define- Parkinson disease (PD) (Sidransky et al., 2009). Both patients with GD and heterozygous carriers are at an increased risk of developing PD, although the exact mechanism of this association is not fully understood (Avenali et al., 2020). An estimated 5–20% of patients with PD carry a *GBA1* mutation, although the frequency varies between populations (Gan-Or et al., 2015). The association of *GBA1* variants with this common complex disorder has led to an increasing interest in analyzing *GBA1* in larger cohorts using next-generation sequencing (NGS) methods (Nalls et al., 2014; Gorostidi et al., 2016; Blauwendraat et al., 2018; Stoker et al., 2020). Challenges arise in using NGS for *GBA1* analysis, however, due to the downstream, highly homologous pseudogene.

GBA1 is located in a gene-rich region on chromosome 1q21 that encompasses seven genes and two pseudogenes within an 85-kb region (Winfield et al., 1997). *GBA1* contains 11 exons and 10 introns over a length of 7.6 kb. Located 16 kb downstream is the shorter (5.7 kb), non-processed pseudogene, *GBAP1* (Horowitz et al., 1989). In the coding regions, *GBAP1* is 96% homologous to the functional gene, increasing to around 98% in the region between intron 8 and the 3′ UTR. However, *GBAP1* lacks a 55-bp segment in exon 9, which is the major exonic difference between the two sequences (Walley and Harris, 1993; Beutler et al., 1995; Tayebi et al., 1996b). *GBA1* has several *Alu* intronic insertions that are not present in *GBAP1*, indicating that evolutionarily, the gene duplication occurred prior to the integration of the *Alu* sequences (Horowitz et al., 1989). The closest downstream gene, located just beyond *GBAP1* is metaxin (*MTX1*), encoding for part of the mitochondrial outer membrane import complex protein 1, which is transcribed convergently to *GBA1* (Long et al., 1996). *MTX1* also has a pseudogene located in the 16-kb region between *GBA1* and *GBAP1* (**Figure 1A**). Several hundred mutations have been identified in *GBA1* including missense mutations, deletions, insertions, splice site mutations, and complex recombinant alleles (Hruska et al., 2008).

The presence of these pseudogenes in this region increases the risk for recombination and the generation of complex alleles, particularly due to the close physical proximity and high homology between *GBA1* and *GBAP1* (Chen et al., 1997). Recombinant alleles can arise from both reciprocal and non-reciprocal recombination, resulting in gene fusions, duplications, and gene conversion alleles (Cormand et al., 2000; Tayebi et al., 2003). These genes can serve as a model to demonstrate the effect of unequal pairing and crossover resulting in recombinant alleles in the genome. Identifying complex alleles poses a significant challenge when relying on NGS analysis.

OPEN ACCESS

Edited by:
María L. Couce, Complejo Hospitalario Universitario de Santiago, Spain

Reviewed by:
Said El Shamieh, Beirut Arab University, Lebanon

***Correspondence:**
Ellen Sidransky
sidranse@mail.nih.gov

Specialty section:
This article was submitted to Human and Medical Genomics, a section of the journal Frontiers in Genetics

Received: *22 March 2021*
Accepted: *27 May 2021*
Published: *21 June 2021*

Citation:
Woo EG, Tayebi N and Sidransky E (2021) Next-Generation Sequencing Analysis of GBA1: The Challenge of Detecting Complex Recombinant Alleles. Front. Genet. 12:684067. doi: 10.3389/fgene.2021.684067

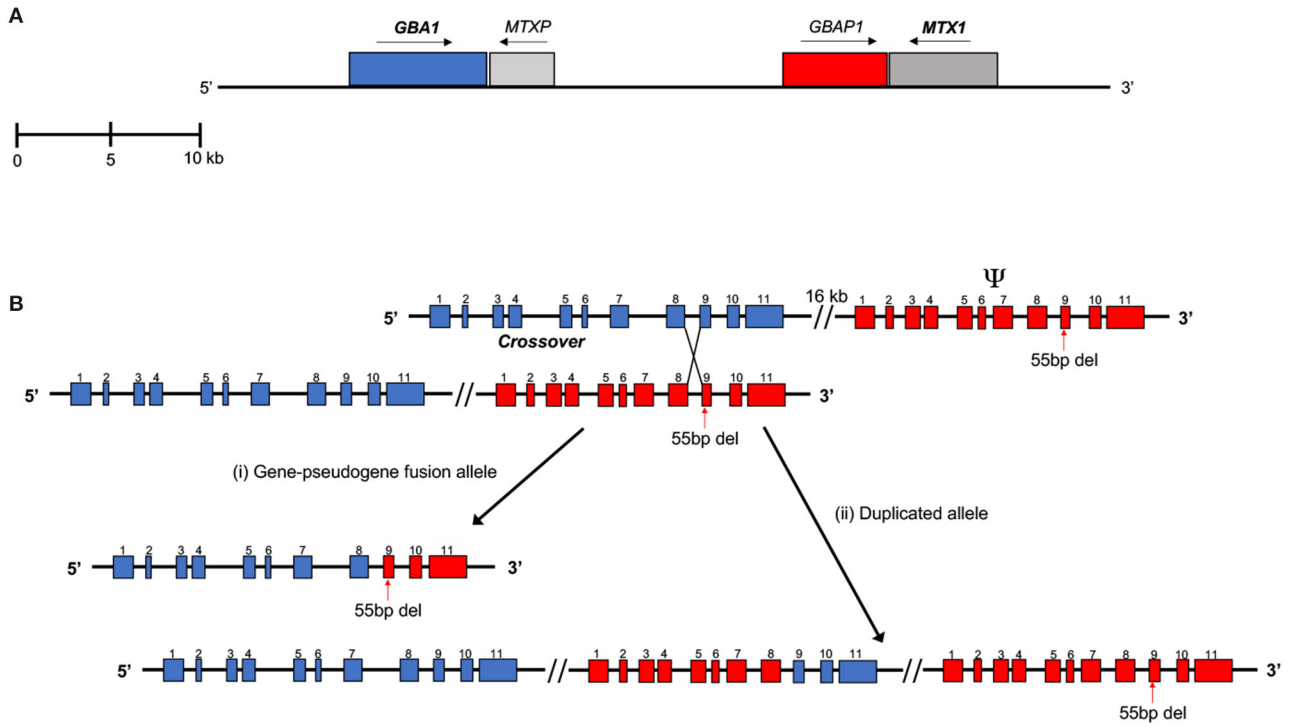

FIGURE 1 | (A) Scaled representation of *GBA1*, *MTX1*, and their highly homologous pseudogenes. *MTXP* lies in the 16 kb region between *GBA1* and *GBAP1*. *MTX1* and *MTXP* are transcribed in the direction opposite to that of *GBA1* and *GBAP1*. **(B)** Example of a reciprocal crossover event, resulting in a (i) gene-pseudogene fusion allele and a (ii) duplicated allele. These recombinant alleles are difficult to detect using next-generation sequencing methods. Sequence reads containing the pseudogene-derived segment (red) of the recombinant alleles may align to the pseudogene instead. This can lead to false negatives and reduce the read depth of *GBA1*. In this example, reads containing the 55 bp deletion from the recombinant alleles may align preferentially to the pseudogene (Adapted in part from Tayebi et al., 2003).

GBA1 GENOTYPING BY CONVENTIONAL MEANS

Previously, PCR-based screening techniques were often used targeting specific panels of 7–10 common *GBA1* pathologic variants (Park et al., 2002). These variants were predicted to account for over 90% of mutant alleles among Ashkenazi Jews, a population with a carrier rate of ∼1 in 14 (Do et al., 2019). However, relying on such panels can miss other mutant alleles, as demonstrated by a 2019 study that fully sequenced *GBA1* in an Ashkenazi Jewish Parkinson disease patient cohort (Ruskey et al., 2019). Sanger sequencing substantially increased variant detection, even in this group, particularly for the common E326K (p.E365K) variant, known to be present in ∼1% of the general population (Lau et al., 1999; Park et al., 2002). This highlights the benefit of sequencing the full *GBA1* gene to detect variants that could be missed using targeted genotyping of selected pathogenic variants. When sequencing *GBA1*, specific primers are required to ensure that functional *GBA1* is being amplified and sequenced rather than the pseudogene (Dandana et al., 2016). For example, primers targeted to the 55-bp pseudogene gap in exon 9 can erroneously misreport patients heteroallelic for a recombination in that region as homozygosity for the second allele (Tayebi et al., 1996b).

NEXT-GENERATION SEQUENCING OF *GBA1*

Next-generation sequencing is able to generate vast amounts of sequence data and has been applied to identify variants in *GBA1*. The use of whole-exome and whole-genome sequencing has increased the discovery rate of these variants. For example, a recent large-scale NGS strategy identified 18 novel *GBA1* variants, as well as a rarely reported complex allele likely to be a Dutch founder allele (Zampieri et al., 2017; den Heijer et al., 2020). One Gaucher diagnostics laboratory relying on NGS run by Centogene (Rostock, Germany) provides an on-line list of their identified *GBA1* variants (CentoLSD™), which now includes over 600 different *GBA1* variants with differing predicted clinical significance (https://www.centogene.com/centolsd.html). Many NGS protocols have utilized short-read sequencing, which can provide data at a relatively low cost and high accuracy but may be less reliable in cases where there are structural variants and repetitive or highly homologous regions (Mandelker et al., 2016; Mantere et al., 2019). If the functional gene is not specifically amplified during library preparation, reads generated by the pseudogene could align with the functional gene, leading to false-positive results, while reads belonging to the functional gene might align to the pseudogene, reducing

read depth and mapping quality (Claes and De Leeneer, 2014). Long range-PCR (LR-PCR) can help to selectively amplify the functional gene (Tayebi et al., 1996a; Jeong et al., 2011). Even after selectively amplifying the functional gene, challenges still remain in the alignment phase, particularly when recombinant alleles contain regions identical to the pseudogene. In an Illumina short-read NGS method for sequencing *GBA1*, Zampieri et al. initially aligned reads to the whole genome, but missed almost all recombinant alleles, which had aligned preferentially to *GBAP1* (Zampieri et al., 2017). After aligning to *GBA1* rather than the whole genome, they were able to identify recombinant variants that had initially been false negatives, except for the 55-bp deletion mutation. Alignment against the whole genome did not significantly affect the mapping quality and coverage of missense mutations unrelated to recombination. Care should therefore be taken not only in the library preparation, but also in data analysis steps of NGS pipelines to sequence *GBA1*.

The introduction of long-read sequencing technology in recent years addressed some limitations of short-read sequencing (Goodwin et al., 2016). The ability to read longer sequences can help to differentiate highly homologous regions. One such technology is the Oxford Nanopore system, which analyzes a single DNA molecule as it passes through a pore (Logsdon et al., 2020). Resulting disruptions to the current are analyzed in real-time to determine the sequence. This strategy has been applied for the detection of *GBA1* variants using the Oxford Nanopore MinION (Leija-Salazar et al., 2019). The authors were able to detect the 55-bp exonic deletion, but not the more common recombinant allele Rec*NciI*. Another study aimed to expand upon this protocol by refining and applying it to the discovery of *GBA1* variants in a PD longitudinal cohort from New Zealand (Graham et al., 2020). They validated the protocol of Leija-Salazar et al. for genotyping *GBA1* and updated the software pipeline, improving accuracy and reducing the computational workload, but were unable to detect any recombinant gene conversion alleles or deletions of >50 bp.

CHALLENGES IN DETECTING RECOMBINANT ALLELES

Accurate and comprehensive NGS analysis of *GBA1* is complicated by complex gene-pseudogene rearrangements and recombination. Recombinant alleles make up a significant proportion of *GBA1* mutations and sites of recombination events have been identified between intron 2 to exon 11 (Hruska et al., 2008). With the high exonic homology between *GBA1* and its pseudogene, there is an increased likelihood of both reciprocal and non-reciprocal recombination (Tayebi et al., 2003). These can result in alleles with multiple exonic point mismatches, such as in Rec*NciI*. In this allele, the site of crossover of chromosomal mispairing between gene and pseudogene occurs within intron 9 and continues to the 3'-UTR of the gene, introducing three exon 10 nucleotide mismatches (Latham et al., 1990). Another frequently described reciprocal recombinant allele, *RecTL,* covers the pseudogene sequence from intron 8 or the beginning of exon 9 [**Figure 1B**(i)] (Zimran and Horowitz, 1994). Reciprocal crossover can also result in a partial duplication of the gene and pseudogene sequence [**Figure 1B**(ii)]. The non-reciprocal exchange of homologous sequence, also known as gene conversion, may also occur. One example is an allele that includes only the 55-bp deletion in exon 9. This is a small, converted gene sequence that resembles the pseudogene. Some polymorphic sequences in *GBAP1* (Martinez-Arias et al., 2001) also been observed. Mostly, homologous recombination events occur in regions of high sequence homology between the gene and pseudogene, such as in introns 8 and 9. Several instances of recombination have occurred as a result of crossover between *MTX* and its pseudogene as well (Tayebi et al., 2003). Quantitative real-time PCR and Southern blot analysis have been used to identify fusions and duplications in patients with recombinant *GBA1* alleles (Velayati et al., 2011).

The complexity of *GBA1* gene rearrangements cannot be sufficiently captured using most current NGS methods. Several recent studies using NGS technology without Sanger sequencing validation have not reported the presence of recombinant alleles, including a recent study performed on more than 3,000 PD cases (den Heijer et al., 2020). Thus, it is likely that the results presented may be an underestimation (Zampieri et al., 2017).

NON-CONVENTIONAL INHERITANCE

Gaucher disease is an autosomal recessive disorder that usually results from the inheritance of a mutant allele from each parent. Increasing evidence suggests this may not always be the case, and that there are important exceptions to the traditional Mendelian pattern of inheritance, such as new mutations or uniparental disomy (Nakka et al., 2019). There have been several reported cases of unrelated patients with type 2 GD with *de novo* or germline mutations on the maternal allele (Saranjam et al., 2013; Hagege et al., 2017). Uniparental disomy of chromosome 1 was reported in a proband with concurrent type 3 GD and Charcot-Marie-Tooth disease, who was homozygous for both L444P (p.L483P) in *GBA1* and S78L in *MPZ* (Benko et al., 2008). There have also been cases of patients with all types of GD carrying more than one *GBA1* mutation on the same allele (Hassan et al., 2018). For example, a common mutant allele in Greece and the Balkans includes both H255Q (p.H255Q) and D409H (p.D448H) together in cis (Vithayathil et al., 2009). These examples of non-conventional inheritance underscore the importance of careful and comprehensive examination of entire coding regions for accurate genotyping. This has important implications for diagnostics and establishing genotype-phenotype correlations. Current NGS technology, however, does not always accurately identify all nucleotide changes and recombinant alleles. As a result, NGS is currently limited in its clinical diagnostic capacity for comprehensive *GBA1* screening, and for now, Sanger sequencing should be used for the most accurate genotyping.

DISCUSSION

Next-generation sequencing allows for unbiased simultaneous analysis of many genes. In addition, it makes it more feasible to

analyze specific genes in larger cohorts for the study of common diseases like Parkinson disease. With the inclusion of *GBA1* in many Parkinson disease NGS analyses, it is important to consider the effects of the nearby homologous pseudogene. Recombinant alleles in *GBA1* have been identified in patients with GD and with PD that might be missed when relying on NGS analysis alone without Sanger sequencing validation.

Challenges exist in short-read NGS methods for sequencing highly homologous regions. The shorter reads cannot be mapped uniquely to the reference genome, especially in cases where there are recombinant alleles aligning to the homologous region. A computational custom scaffold-based approach was recently introduced to improve the detection and phasing of targeted complex variants using short reads (Zeng et al., 2020). This method was able to detect a 55-bp deletion in *GBA1* confirmed by Sanger sequencing. In addition, there is evidence to suggest that the choice of polymerase used could be a factor in the accuracy of NGS variant identification. A recent study performed a large-scale screening of *GBA1* based on an NGS protocol and found a significant number of false negatives due to a polymerase-dependent allelic imbalance (den Heijer et al., 2021). After performing a structured assessment of varied PCR conditions, they found that changing the polymerase used led to the resolution of these false negatives. Allele frequency was unaffected by a change in the other conditions. This raises the possibility that current estimates of variant frequency in populations could be underestimates, due to polymerase-dependent false negatives as well.

Long-read NGS has many advantages, one of which is an improved ability to discriminate functional genes such as *GBA1* from their pseudogenes. An additional advantage is the ability to phase mutations and assign haplotypes. It can also detect intronic SNPs. There are still some limitations, including high costs, low throughput, and high per-base error rates. Long-read NGS also has a limited ability to accurately resolve homopolymers and to detect small insertions and deletions. Importantly, it is still unable to consistently detect recombinant alleles.

The most accurate method for detecting all *GBA1* variants and recombination remains Sanger sequencing. Without validation by Sanger sequencing, the frequencies of *GBA1* variants based on NGS analysis may be underestimated, particularly for complex recombinant alleles. Real-time PCR can also be used to identify recombinant alleles (Velayati et al., 2011). NGS pipelines should be carefully designed in order to capture variants should from the functional gene rather than the pseudogene and attempt to include complex alleles. While long-read sequencing shows promise for increased accuracy of *GBA1* NGS analysis, it is still currently limited in its capacity to recognize recombinant alleles. The shortcomings identified will likely also be pertinent for the analysis of other genes with highly homologous pseudogenes. As sequencing technology continues to rapidly progress, we will likely continue to see improved detection of *GBA1* variants. This has exciting potential for clinical diagnostics and studies of large patient cohorts.

AUTHOR CONTRIBUTIONS

EW: drafted the manuscript and figure. NT: organized the topic, reviewed the literature, and edited the manuscript. ES: conceived of the topic and edited the manuscript. All authors contributed to the article and approved the submitted version.

FUNDING

This work was supported by the Intramural Research Programs of the National Human Genome Research Institute and the National Institutes of Health.

REFERENCES

Avenali, M., Blandini, F., and Cerri, S. (2020). Glucocerebrosidase defects as a major risk factor for Parkinson's Disease. *Front. Aging Neurosci.* 12:97. doi: 10.3389/fnagi.2020.00097

Benko, W. S., Hruska, K. S., Nagan, N., Goker-Alpan, O., Hart, P. S., Schiffmann, R., et al. (2008). Uniparental disomy of chromosome 1 causing concurrent Charcot-Marie-Tooth and Gaucher disease Type 3. *Neurology* 70, 976–978. doi: 10.1212/01.wnl.0000305963.37449.32

Beutler, E., Gelbart, T., Demina, A., Zimran, A., and LeCoutre, P. (1995). Five new Gaucher disease mutations. *Blood Cells Mol. Dis.* 21, 20–24. doi: 10.1006/bcmd.1995.0004

Blauwendraat, C., Bras, J. M., Nalls, M. A., Lewis, P. A., Hernandez, D. G., Singleton, A. B., et al. (2018). Coding variation in GBA explains the majority of the SYT11-GBA Parkinson's disease GWAS locus. *Mov. Disord.* 33, 1821–1823. doi: 10.1002/mds.103

Chen, K. S., Manian, P., Koeuth, T., Potocki, L., Zhao, Q., Chinault, A. C., et al. (1997). Homologous recombination of a flanking repeat gene cluster is a mechanism for a common contiguous gene deletion syndrome. *Nat. Genet.* 17, 154–163. doi: 10.1038/ng1097-154

Claes, K. B., and De Leeneer K. (2014). Dealing with pseudogenes in molecular diagnostics in the next-generation sequencing era. *Methods Mol. Biol.* 1167, 303–315. doi: 10.1007/978-1-4939-0835-6_21

Cormand, B., Diaz, A., Grinberg, D., Chabas, A., and Vilageliu, L. (2000). A new gene-pseudogene fusion allele due to a recombination in intron 2 of the glucocerebrosidase gene causes Gaucher disease. *Blood Cells Mol. Dis.* 26, 409–416. doi: 10.1006/bcmd.2000.0317

Dandana, A., Ben Khelifa, S., Chahed, H., Miled, A., and Ferchichi, S. (2016). Gaucher disease: clinical. biological and therapeutic aspects. *Pathobiology* 83, 13–23. doi: 10.1159/000440865

den Heijer, J. M., Cullen, V. C., Quadri, M., Schmitz, A., Hilt, D. C., Lansbury, P., et al. (2020). A large-scale full GBA1 gene screening in Parkinson's disease in the Netherlands. *Mov. Disord.* 35, 1667–1674. doi: 10.1002/mds.28112

den Heijer, J. M., Schmitz, A., Lansbury, P., Cullen, V. C., Hilt, D. C., Bonifati, V., et al. (2021). False negatives in GBA1 sequencing due to polymerase dependent allelic imbalance. *Sci. Rep.* 11:161. doi: 10.1038/s41598-020-80564-y

Do, J., McKinney, C., Sharma, P., and Sidransky, E. (2019). Glucocerebrosidase and its relevance to Parkinson disease. *Mol. Neurodegener.* 14:36. doi: 10.1186/s13024-019-0336-2

Gan-Or, Z., Amshalom, I., Kilarski, L. L., Bar-Shira, A., Gana-Weisz, M., Mirelman, A., et al. (2015). Differential effects of severe vs mild GBA mutations on Parkinson disease. *Neurology* 84, 880–887. doi: 10.1212/WNL.0000000000001315

Goodwin, S., McPherson, J. D., and McCombie, W. R. (2016). Coming of age: ten years of next-generation sequencing technologies. *Nat. Rev. Genet.* 17, 333–351. doi: 10.1038/nrg.2016.49

Gorostidi, A., Marti-Masso, J. F., Bergareche, A., Rodriguez-Oroz, M. C., Lopez de Munain, A., and Ruiz-Martinez, J. (2016). Genetic mutation analysis of Parkinson's disease patients using multigene next-generation sequencing panels. *Mol. Diagn. Ther.* 20, 481–491. doi: 10.1007/s40291-016-0216-1

Graham, O. E. E., Pitcher, T. L., Liau, Y., Miller, A. L., Dalrymple-Alford, J. C., Anderson, T. J., et al. (2020). Nanopore sequencing of the glucocerebrosidase (GBA) gene in a New Zealand Parkinson's disease cohort. *Parkinsonism Relat. Disord.* 70, 36–41. doi: 10.1016/j.parkreldis.2019.11.022

Hagege, E., Grey, R. J., Lopez, G., Roshan Lal, T., Sidransky, E., and Tayebi, N. (2017). Type 2 Gaucher disease in an infant despite a normal maternal glucocerebrosidase gene. *Am. J. Med. Genet. A.* 173, 3211–3215. doi: 10.1002/ajmg.a.38487

Hassan, S. Y., Lopez, G., Stubblefield, B. K., Tayebi, N., and Sidransky, E. (2018). Alleles with more than one mutation can complicate genotype/phenotype studies in Mendelian disorders: lessons from Gaucher disease. *Mol. Genet. Metab.* 125, 1–3. doi: 10.1016/j.ymgme.2018.06.013

Horowitz, M., Wilder, S., Horowitz, Z., Reiner, O., Gelbart, T., and Beutler, E. (1989). The human glucocerebrosidase gene and pseudogene: structure and evolution. *Genomics* 4, 87–96. doi: 10.1016/0888-7543(89)90319-4

Hruska, K. S., LaMarca, M. E., Scott, C. R., and Sidransky, E. (2008). Gaucher disease: mutation and polymorphism spectrum in the glucocerebrosidase gene (GBA). *Hum. Mutat.* 29, 567–583. doi: 10.1002/humu.20676

Jeong, S. Y., Kim, S. J., Yang, J. A., Hong, J. H., Lee, S. J., and Kim, H. J. (2011). Identification of a novel recombinant mutation in Korean patients with Gaucher disease using a long-range PCR approach. *J. Hum. Genet.* 56, 469–471. doi: 10.1038/jhg.2011.37

Latham, T., Grabowski, G. A., Theophilus, B. D., and Smith, F. I. (1990). Complex alleles of the acid beta-glucosidase gene in Gaucher disease. *Am. J. Hum. Genet.* 47, 79–86.

Lau, E. K., Tayebi, N., Ingraham, L. J., Winfield, S. L., Koprivica, V., Stone, D. L., et al. (1999). Two novel polymorphic sequences in the glucocerebrosidase gene region enhance mutational screening and founder effect studies of patients with Gaucher disease. *Hum. Genet.* 104, 293–300. doi: 10.1007/s004390050957

Leija-Salazar, M., Sedlazeck, F. J., Toffoli, M., Mullin, S., Mokretar, K., Athanasopoulou, M., et al. (2019). Evaluation of the detection of GBA missense mutations and other variants using the Oxford Nanopore MinION. *Mol. Genet. Genomic Med.* 7:e564. doi: 10.1002/mgg3.564

Logsdon, G. A., Vollger, M. R., and Eichler, E. E. (2020). Long-read human genome sequencing and its applications. *Nat. Rev. Genet.* 21, 597–614. doi: 10.1038/s41576-020-0236-x

Long, G. L., Winfield, S., Adolph, K. W., Ginns, E. I., and Bornstein, P. (1996). Structure and organization of the human metaxin gene (MTX) and pseudogene. *Genomics* 33, 177–184. doi: 10.1006/geno.1996.0181

Mandelker, D., Schmidt, R. J., Ankala, A., McDonald Gibson, K., Bowser, M., Sharma, H., et al. (2016). Navigating highly homologous genes in a molecular diagnostic setting: a resource for clinical next-generation sequencing. *Genet. Med.* 18, 1282–1289. doi: 10.1038/gim.2016.58

Mantere, T., Kersten, S., and Hoischen, A. (2019). Long-read sequencing emerging in medical genetics. *Front. Genet.* 10:426. doi: 10.3389/fgene.2019.00426

Martinez-Arias, R., Comas, D., Mateu, E., and Bertranpetit, J. (2001). Glucocerebrosidase pseudogene variation and Gaucher disease: recognizing pseudogene tracts in GBA alleles. *Hum. Mutat.* 17, 191–198. doi: 10.1002/humu.4

Nakka, P., Pattillo Smith, S., O'Donnell-Luria, A. H., McManus, K. F., Team andMe Research, Mountain, J. L., et al. (2019). Characterization of prevalence and health consequences of uniparental disomy in four million individuals from the general population. *Am. J. Hum. Genet.* 105, 921–932. doi: 10.1101/540955

Nalls, M. A., Pankratz, N., Lill, C. M., Do, C. B., Hernandez, D. G., Saad, M., et al. (2014). Large-scale meta-analysis of genome-wide association data identifies six new risk loci for Parkinson's disease. *Nat. Genet.* 46, 989–993. doi: 10.1038/ng.3043

Park, J. K., Tayebi, N., Stubblefield, B. K., LaMarca, M. E., MacKenzie, J. J., Stone, D. L., et al. (2002). The E326K mutation and Gaucher disease: mutation or polymorphism? *Clin. Genet.* 61, 32–34. doi: 10.1034/j.1399-0004.2002.610106.x

Ruskey, J. A., Greenbaum, L., Ronciere, L., Alam, A., Spiegelman, D., Liong, C., et al. (2019). Increased yield of full GBA sequencing in Ashkenazi Jews with Parkinson's disease. *Eur. J. Med. Genet.* 62, 65–69. doi: 10.1016/j.ejmg.2018.05.005

Saranjam, H., Chopra, S. S., Levy, H., Stubblefield, B. K., Maniwang, E., Cohen, I. J., et al. (2013). A germline or de novo mutation in two families with Gaucher disease: implications for recessive disorders. *Eur. J. Hum. Genet.* 21, 115–117. doi: 10.1038/ejhg.2012.105

Sidransky, E., Nalls, M. A., Aasly, J. O., Aharon-Peretz, G., Annesi, E. R., Barbosa, E. R., et al. (2009). Multi-center analysis of glucocerebrosidase mutations in Parkinson disease. *N. Engl. J. Med.* 361, 1651–1661. doi: 10.1056/NEJMoa0901281

Stoker, T. B., Camacho, M., Winder-Rhodes, S., Liu, G., Scherzer, C. R., Foltynie, T., et al. (2020). Impact of GBA1 variants on long-term clinical progression and mortality in incident Parkinson's disease. *J. Neurol. Neurosurg. Psychiatry* 91, 695–702. doi: 10.1136/jnnp-2020-322857

Tayebi, N., Cushner, S., and Sidransky, E. (1996a). Differentiation of the glucocerebrosidase gene from pseudogene by long-template PCR: implications for Gaucher disease. *Am. J. Hum. Genet.* 59, 740–741.

Tayebi, N., Stern, H., Dymarskaia, I., Herman, J., and Sidransky, E. (1996b). 55-base pair deletion in certain patients with Gaucher disease complicates screening for common Gaucher alleles. *Am. J. Med. Genet.* 66, 316–319.

Tayebi, N., Stubblefield, B. K., Park, J. K., Orvisky, E., Walker, J. M., LaMarca, M. E., et al. (2003). Reciprocal and nonreciprocal recombination at the glucocerebrosidase gene region: implications for complexity in Gaucher disease. *Am. J. Hum. Genet.* 72, 519–534. doi: 10.1086/367850

Velayati, A., Knight, M. A., Stubblefield, B. K., Sidransky, E., and Tayebi, N. (2011). Identification of recombinant alleles using quantitative real-time PCR implications for Gaucher disease. *J. Mol. Diagn.* 13, 401–405. doi: 10.1016/j.jmoldx.2011.02.005

Vithayathil, J., Gibney, G., Baxevanis, A. D., Stubblefield, B. K., Sidransky, E., and Tayebi, N. (2009). Glucocerebrosidase mutation H255Q appears to be exclusively in cis with D409H: structural implications. *Clin. Genet.* 75, 503–504. doi: 10.1111/j.1399-0004.2009.01163.x

Walley, A. J., and Harris, A. (1993). A novel point mutation (D380A) and a rare deletion (1255del55) in the glucocerebrosidase gene causing Gaucher's disease. *Hum. Mol. Genet.* 2, 1737–1738. doi: 10.1093/hmg/2.10.1737

Winfield, S. L., Tayebi, N., Martin, B. M., Ginns, E. I., and Sidransky, E. (1997). Identification of three additional genes contiguous to the glucocerebrosidase locus on chromosome 1q21: implications for Gaucher disease. *Genome Res.* 7, 1020–1026. doi: 10.1101/gr.7.10.1020

Zampieri, S., Cattarossi, S., Bembi, B., and Dardis, A. (2017). GBA analysis in next-generation era: pitfalls, challenges, possible solutions. *J. Mol. Diagn.* 19, 733–741. doi: 10.1016/j.jmoldx.2017.05.005

Zeng, Q., Leach, N. T., Zhou, Z., Zhu, H., Smith, J. A., Rosenblum, L. S., et al. (2020). A customized scaffolds approach for the detection and phasing of complex variants by next-generation sequencing. *Sci. Rep.* 10:15060. doi: 10.1038/s41598-020-71471-3

Zimran, A., and Horowitz, M. (1994). RecTL: a complex allele of the glucocerebrosidase gene associated with a mild clinical course of Gaucher disease. *Am. J. Med. Genet.* 50, 74–78. doi: 10.1002/ajmg.1320500116

Conflict of Interest: The authors declare that the research was conducted in the absence of any commercial or financial relationships that could be construed as a potential conflict of interest.

frontiers in Genetics

ORIGINAL RESEARCH
published: 30 June 2021
doi: 10.3389/fgene.2021.673732

Characterization With Gene Mutations in Han Chinese Patients With Hypospadias and Function Analysis of a Novel AR Genevariant

Lifen Chen†, Junqi Wang†, Wenli Lu, Yuan Xiao, Jihong Ni, Wei Wang, Xiaoyu Ma and Zhiya Dong**

Department of Pediatrics, Ruijin Hospital, School of Medicine, Shanghai Jiao Tong University, Shanghai, China

OPEN ACCESS

Edited by:
Emiliano González Vioque, University Clinical Hospital of Santiago, Spain

Reviewed by:
Aline L. Petrin, The University of Iowa, United States
Coriness Piñeyro-Ruiz, University of Puerto Rico, Medical Sciences Campus, Puerto Rico

***Correspondence:**
Xiaoyu Ma
179788825@qq.com
Zhiya Dong
dzy831@126.com

† These authors have contributed equally to this work and share first authorship

Specialty section:
This article was submitted to Genetics of Common and Rare Diseases, a section of the journal Frontiers in Genetics

Received: *28 February 2021*
Accepted: *09 June 2021*
Published: *30 June 2021*

Citation:
Chen L, Wang J, Lu W, Xiao Y, Ni J, Wang W, Ma X and Dong Z (2021) Characterization With Gene Mutations in Han Chinese Patients With Hypospadias and Function Analysis of a Novel AR Genevariant. Front. Genet. 12:673732. doi: 10.3389/fgene.2021.673732

It is estimated that around 10–20% of hypospadias are caused by genetic abnormalities worldwide although the spectrum of associated genes does vary across different ethnicities. The prevalence of hypospadias among the Chinese population has been increasing the last couple of decades. However, the pathogenesis underlying the disease and its associated genetic abnormality remains unclear. Here we performed a genetic analysis of 81 children with karyotype 46, XY and the hypospadias phenotype in order to characterize the genetic components that contribute to the development of hypospadias in Chinese patients. 15 candidate genes, including sex determination genes-*SOX9*, *SRY*, *NR0B1* (*DAX1*), *NR5A1* (*SF1*), *DHH*, sex differentiation genes-*AR*, *SRD5A2*, *MAMLD1*, *INSL3*, and hypospadias-associated genes-*FGF8*, *FGF10*, *BMP4*, *BMP7*, *ATF3*, and *MID1* were screened by using next generation sequencing. A total of 18 patients were found to have mutations identified by PCR and sequencing, including 11 cases of *SRD5A2* genes, 6 cases of *AR* genes, and 1 case of *MID1* gene, respectively. One novel missense mutation p.I817N was discovered in *AR* gene. Further molecular analysis found that subcellular localization of the AR_{I817N} was the same as that of wild type AR_{WT} in the absence or presence of hormone. But it led to 50% reduction in AR-induced transcriptional activity in the presence of either the synthetic androgen R1881 or the natural ligand dihydrotestosterone. Our results indicate that *SRD5A2* and *AR* genes are two top candidate genes associated with 46, XY hypospadias in Chinese patients. Further epidemiological and genetic analysis are still needed to further clarify the pathogenesis of hypospadias in Han Chinese patients.

Keywords: hypospadias, gene mutations, AR, *SRD5A2*, gene function analysis

INTRODUCTION

Hypospadias is one of the most common congenital malformations of the penis (van der Horst and de Wall, 2017; Donaire and Mendez, 2018). It is characterized by a failure of urethral groove closure resulting in an opening on the ventral surface of the penis. The prevalence of hypospadias varies according to ethnical and geographical differences. The reported prevalence in Western countries ranges from 2 to 43 out of 10,000 live births (Springer et al., 2016). In China, the prevalence was

0.7–4.5 from 1996 to 2008, and 5.8 per 10,000 live births in 2010 (Jin et al., 2010), but has increased to 9.3 per 10,000 live births as of 2012 (Li et al., 2012).

Although the exact etiology of hypospadias is unknown, it is agreed upon that environment, endocrine hormones, and genetic factors all play a collective role in the pathogenesis (Carmichael et al., 2012). Environmental factors such as assisted reproductive technology, maternal hypertension during pregnancy, thyroid disease, higher maternal age at delivery, low birth weight, preterm birth, and primiparity have been proposed. Most diagnosed cases of hypospadias are sporadic, but family cluster genetic phenomena do occur (Donaire and Mendez, 2018).

Genetic disruption of male external genital development and urethral growth contribute to 20% of the etiology of hypospadias (Domenice et al., 2000; Gangaher et al., 2016). There are three key pathways in the development of male external genitalia: (a) androgen independent, (b) androgen dependent, and (c) pathways dependent on endocrine and environmental factors (Manson and Carr, 2003). The steroid 5α-reductase 2 (SRD5A2) and androgen receptor (AR) genes are two androgen dependent genes that were widely evaluated in hypospadias. Among the Chinese population, SRD5A2 and AR dysfunction have been discovered in some patients with hypospadias. The AR is an intracellular transcription factor and plays a crucial role in male sex differentiation. In both sporadic and familial hypospadias, AR gene mutations have been discovered. Hypospadias is one of the major phenotypes of partial androgen insensitivity syndrome (PAIS) (Joodi et al., 2019). To date, over 1,000 mutations have been reported in the AR gene, and it is usually included as one of the top genes in the screening panel test for patients with hypospadias. Moreover, not only are their mutations reported in the coding region of AR, but also SNPs located in the promoter region of AR gene were involved in the development and severity of hypospadias (Geller et al., 2014; Pineyro-Ruiz et al., 2020) however, the functional importance of these mutations remains less known. AR gene mutations also lead to several pathological situations such as androgen insensitivity syndrome (AIS), spinal and bulbar muscular atrophy (SBMA), and prostate cancer (Shukla et al., 2016).

To explore the spectrum of genetic abnormality in Chinese hypospadias patients, we performed next generation sequencing (NGS) on 81 patients with hypospadias targeting 15 candidate genes that could potentially cause hypospadias including (1), sex determination genes: sex determining region of Y chromosome (*SRY*), SRY-related high mobility group box gene 9 (*SOX9*), nuclear receptor subfamily 0 group B member 1 (*NR0B1*), nuclear receptor subfamily 5 group A member 1 (*NR5A1*), desert hedgehog (*DHH*) (2), sex differentiation genes: *SRAD5, AR*, mastermind-like domain-containing protein 1 gene (*MAMLD1*), Leydig cell insulin-like 3 (*INSL3*) (3), and hypospadias genes reported by other studies: bone morphogenetic protein gene 4 and 7 (*BMP4* and *7*), fibroblast growth factor 8 and 10 (*FGF8* and *10*), activating transcription factor 3 (*ATF3*), and midline 1 (*MID1*). Multiple mutations were found in these patients, but not in 50 healthy controls. One of 4 identified *AR* missense mutations was *de novo* and functional impairment of AR from this mutation was further explored *in vitro*.

MATERIALS AND METHODS

Patients

Patients with external genital malformations who were followed in the Department of Pediatrics at Ruijin Hospital, Shanghai Jiao Tong University School of Medicine from January 2004 to December 2020 were screened initially. 81 cases with karyotype 46, XY and phenotype of hypospadias were identified and included in this study. Those patients who had syndrome related external genital malformations were excluded. Informed written consent was obtained from all patients' parents or their guardians. In addition, 50 boys without external genital malformation were selected as controls for genetic analysis. The study was approved by the Institutional Review Board (Ethics Committee of Shanghai Jiao Tong University School of Medicine).

Clinical Assessment

Clinical assessment of these patients included the child's birth history, family history, maternal history (exogenous sex hormone exposure or intake history during pregnancy), living environment and possible history of exposure to environmental pollutants. Age, gender, body weight, gonadal developmental status, degree of external genital malformation according to the external masculinization score (EMS), and type of hypospadias were recorded. The measurement of penis length and reference value of Chinese men were performed according to the published study by Fu Chao et al. in 2010 (Fu Chao and Xuliang, 2010). The diagnosis of cryptorchidism in these patients was made according to the study performed by Bao et al. (Bao and Zhang, 2012). External Masculinization Score (EMS, range 0–12) (Ahmed et al., 2000) was used to assess the degree of virilization of the external genitalia. The normal male score is 12 and a smaller score indicates a lower virilization degree. An EMS < 7 is considered ambiguous.

Gonadotropin-Releasing Hormone (GnRH) Agonist Testing and Human Chorionic Gonadotropin (hCG) Stimulation Test

GnRH agonist testing was performed in some patients using intravenous administration of a standard dose of GnRH (2 ug/kg Gonadorelin acetate, maximum dose 100 ug). Blood samples were collected at time points 0, 30, 60 and 90 min after stimulation. Normal test was defined as luteinizing hormone (LH) increases about 3–6 times within 30–45 min, and follicle stimulating hormone (FSH) increases by 20–50% after GnRH injection. Serum LH and FSH were measured by immunoradiometric assay (Abbott, Chicago IL). The hCG stimulation test which was used to evaluate the function of testicular synthetic androgens was performed in some patients with a daily injection of hCG (2,000 U) for 3 days. Serum testosterone (T) and dihydrotestosterone (DHT) were measured using a radioimmunoassay kit (Diagnostic Systems Laboratories, Webster, Tex., United States).

DNA Extraction, PCR and Sequencing

Genomic DNA was extracted from the peripheral whole blood using the FlexiGene DNA Kit (Qiagen GmbH, Hilden, Germany), according to the manufacturer's instructions. 15 genes (FGF8, FGF10, BMP4, BMP7, NR5A1, MAMLD1, SRY, SOX-9, NR0B1, DHH, ATF3, INSL3, MID1, SRD5A2, and AR) according to literature search were selected as candidates for polymerase chain reaction (PCR) and sequencing. Primers targeting all exons of these genes were designed using online tool Primer3[1]. PCRs were performed in a reaction volume of 50 μl containing 20 ng template DNA. A 5 μl aliquot of each PCR was loaded on a 2% agarose gel and visualized by ethidium bromide (Sigma-Aldrich, Beijing, China) staining to confirm the presence of an appropriately sized product. The PCR products were purified using a gel extraction kit (QIAGEN, Mississauga, Ont., Canada) and sequenced in both sense and antisense directions on an Illumina-miseq sequencer (Illumina, United States). DNA fragments were 250–400 bp and the coverage of samples was 80x–3,000x. Positive and negative controls were added to the samples. Sequences generated from all patients were compared with the published reference sequences from the National Center for Biotechnology Information[2]. The mutation was annotated according to HGVS nomenclature[3]. For identified mutation from NGS, purified PCR products were further sequenced and verified by Sanger sequencing on an ABI 700 sequencer (Applied Biosystems PerkinElmer, Foster City, Calif., United States). The ACMG guidelines (Amendola et al., 2016) were used to classify the mutations into five classifications: pathogenic (P), likely pathogenic (LP), variants of uncertain significance (VUS), likely benign (LB), or benign (B).

Site-Directed Mutagenesis and Construction of AR Expression Vectors

The wild type AR expression plasmid (AR_{WT}) (SC114220) was bought from Origene (Rockville, MD). It served as a template to construct the mutant p.I817N (AR_{I817N}) using the QuikChange II site-directed mutagenesis kit (Agilent Genomics, Santa Clara, CA, United States). The primers were ARt2450aF: ccatccactggattaatgctgaagagtagcagtgct andARt2450aR: agcactgctactcttcagcattaatccagtggatgg. Positive clones were selected and sequenced to confirm the site-directed mutation (Du et al., 2009).

Immunofluorescence Staining

The cultured cells were fixed and then followed by overnight incubation with primary antibody anti-AR (Invitrogen). Sections were washed and then incubated with Cy2-anti-mouse and Cy5 anti-rabbit (Jackson Immuno Research, West Grove, PA). Nuclear stating was performed using 4′,6-diamidino-2-phenylindole (DAPI; Molecular Probes, Eugene, OR). Confocal microscopy was performed using a Leica SP2AOBS system (Leica, Wetzlar, Germany) in the Light Microscopy Core Center at the Shanghai Jiao Tong University.

[1]http://primer3.ut.ee/

[2]http://www.ncbi.nlm.nih.gov/

[3]http://www.HGVS.org/varnomen

Western Blot

Cells harvested from cultures were homogenized in cell lysis buffer (Cell Signaling Technology, Danvers, MA). Protein concentration determination and immunoblotting were performed as previously described. Briefly, twenty micrograms of protein were separated by SDS-PAGE, transferred to polyvinylidene difluoride membranes and blotted with primary antibodies and secondary antibodies (Cell Signaling Technology, Danvers, MA). Quantification of the image was performed by scanning densitometry and using NIH Image J 1.54 software (National Institutes of Health, Bethesda, MD).

The Transcription Activity Assay

The transactivation activity of the p.I817N mutated AR and wild-type AR were compared in a reporter gene assay as previously described (Du et al., 2009). In brief, Chinese hamster ovary cells (CHO) were transfected with a total of 100 ng DNA per well, consisting of the expression vector (AR_{WT} or AR_{I817N}) and the Cignal reporter plasmid (QIAGEN, Germantown, MD) using transfection reagent Lipofectarmine 2000 (Invitrogen, Grand Island, NY, United States). Cells were incubated overnight with dihydrotestosterone (DHT; 0.01–30 nM), methyltrienolone (R1881; 0.001–100 nM), and hydroxyflutamide (OHF; 1–5,000 nM) each in triplicate. For OHF treatment, 0.1 nM of R1881 was added 30 min before the addition of OHF to determine the competition binding. Then cells were lysed and luciferase activity assayed using Victor[3] plate reader (Perkinelmer, Waltham, MA).

Statistical Analysis

Statistical analyses were performed using an unpaired, two-tailed *t*-test for comparing between AR_{WT} and AR_{I871N}. The one-way ANOVA was used for comparing cellular responses after R1881 treatment. The clinical data description was not involved in the statistics. Calculations were performed using Graphpad Prism 9 software. Significance was determined using a threshold of $P = 0.05$. All values were reported as mean ± standard error of the mean (SEM) for three independent experiments.

RESULTS

Clinical Findings of Patients With Hypospadias

All 81 patients diagnosed with hypospadias exhibited other features of external genital malformations at variable degrees as listed in **Table 1**. The age of patients ranged from 3 months to 22.2 years and the average age is 6.1 ± 5.1 years old. According to the location of the urethral meatus, hypospadias was classified into four types. Type I was glandular or coronal, type II was shaft (distal, mid and proximal), type III was scrotal and type IV was perineal. The majority of patients (52/81) were found to have severe types (III and IV). 18 (22.2%) patients were raised as female after birth due to obscure external genitalia, short penis, and poor scrotal development like the labia majora. Except for external genital malformation, some children were also accompanied by other abnormalities, such as being small for their

TABLE 1 | Clinical characteristics of 81 patients diagnosed with hypospadias.

Type of hypospadias	I	II	III	IV	Total
Number of cases (%)	9 (11.1%)	14 (17.3%)	31 (38.3%)	27 (33.3%)	81 (100%)
EMS (mean)	7.8	6.9	6.0	5.5	6.2
Other features of ambiguous genitalia					
Micropenis	5 (55.5%)	7 (50%)	24 (77.4%)	13 (48.1%)	49 (60.5%)
Microtesticle	2 (22.2%)	1 (7.1%)	12 (38.7%)	13 (48.1%)	28 (34.6%)
Cryptorchidism	3 (33.3%)	2 (14.3%)	16 (51.6%)	14 (51.9%)	35 (43.2%)
Clubbed penis	0	3 (21.4%)	4 (12.9%)	4 (14.8%)	11 (13.6%)
Poor scrotum	2 (22.2%)	3 (21.4%)	13 (41.9%)	20 (74.1%)	38 (46.9%)
Hydrocele	0	0	3 (9.7%)	3 (11.1%)	6 (7.4%)
Testicular microlithiasis	1 (11.1%)	1 (7.1%)	2 (6.5%)	1 (3.7%)	5 (6.2%)
Epididymal head cyst	0	1 (7.1%)	0	2 (7.4%)	3 (3.7%)
Other associated clinical features					
Inguinal hernia	0	1 (7.1%)	2 (6.5%)	3 (11.1%)	6 (7.4%)
SGA	1 (11.1%)	2 (14.3%)	2 (6.5%)	4 (14.8%)	8 (9.8%)
ASD	0	0	0	5 (18.5%)	5 (6.2%)
Adolescent mammoplasia	0	4 (28.6%)	1 (3.2%)	2 (7.4%)	7 (8.6%)
Positive family history	0	1 (7.1%)	1 (3.2%)	0	2 (24.5%)

EMS, external masculinization score; SGA, small-for-gestational age; ASD, atrial septal defect.

gestational age, inguinal hernia, atrial septal defect and breast development during adolescence. A positive family history was found in 2 children, one of whom had a history of hypospadias in both his father and younger brother, and the other had a cousin diagnosed with hypospadias.

Forty-two cases received GnRH stimulation test as a follow up. Seven patients showed high gonadotrophin dysplasia and the remaining cases had normal response. Fifty-two patients underwent the hCG challenge test, and only five patients had a poor response (the T concentration increased less than 3 times of the baseline value after stimulation). Other patients demonstrated a normal testicular response to hCG.

Identification and Characterization of Nucleotide Substitutions

G banding method was used for karyotype analysis and all children have 46, XY chromosomes. 15 candidate genes were selected for the initial screening using Illumina-miseq sequencing according to previous literatures. All mutations detected in the initial screening by NGS were confirmed by traditional Sanger sequencing. A total of 18 patients were found to have mutations, including 11 cases of SRD5A2 genes, 6 cases of AR genes, and 1 case of MID1 gene. According to ACMG guidelines, these mutations were assessed as pathogenic (P) or likely pathogenic (LP) (**Table 2**). The presence of these mutations was further tested in 50 normal controls to rule out polymorphisms.

Patients With *SRD5A2* Gene Mutations

There were 11 cases identified with SRD5A2 mutations. The age of diagnosis ranged from 4-month to 22-years old. The clinical characteristics are listed in **Table 3**. Among them, 8 patients were seen before puberty (0.3–5.6 years old) and 3 cases were raised as females. There was one case of type II hypospadias that was not accompanied by any other external genital malformations, 7 cases of type III and 3 cases of type IV. The average EMS of these 9 patients was 4.9. The GnRH test was basically normal, but four children underwent hCG stimulation and were found to have increased T/DHT values. Genetic analysis showed 7 heterozygous mutations (p.R227Q/p.R246Q, p.G203S/p.R227Q, p.Y136Ter/p.R227Q, p.N193S/p.R246P, p.L20P/R227, p.N193S/p.F219Sfs*60, and p.G203S/F219fs*60) and 4 homozygous mutations (p.R227Q, p.G203S, p.R246P, p.L20P). 10 of them were reported in the literature. Only p.Y136Ter was a newly identified mutation, where cytosine at position 408 of exon 2 of SRD5A2 gene mutated to adenine causing the stop codon TAA and terminating translation. According to ACMG guidelines, this mutation was assessed as pathogenic (P/PVS1 + PM2 + PM6 + PP3).

Patients With *AR* Gene Mutations

There were 6 cases with an identified AR gene mutation, the clinical phenotype characteristics are shown in **Table 4**. Three children were younger (1.6, 0.3, and 5.9 years old) at the diagnosis and the other three had reached adolescence (14.6, 14.3, and 14.2 years old) before seeking medical care. 4 children were born with a female gender due to poorly developed scrotum-like labia. After comprehensive consideration of chromosomal factors, genitalization of the external genitalia, and psychological acceptance of children and parents, 2 patients were changed to male support, and 2 remained in female support. Three cases of hypospadias were type IV, one cases was type III, and the other two were type II. All abnormalities of AR gene were hemizygous mutations (p.R780W, p.I817N, p.R856H, and p.A871V) and included two gross deletions (Exon 5-8 gross deletion, chX 67716101-67724136, and exon 2 gross deletion chX 67643255-67643407). p.I817N was the newly discovered missense mutation and not found in the 50 normal controls. This site was located at the beginning of exon 7 of the AR gene, and

TABLE 2 | Genotype hypospadias patients with candidate gene abnormities.

Patient ID	Gene	cDNA	Protein	Exon	Rs number	Genotype	Origin	ACMG
1	*SRD5A2*	G680 > A	R227Q	E4	rs9332964	CompoundHet	Mother	P/PS3 + PM1 + PM2 + PM3 + PP4
		G737 > A	R246Q	E5	rs9332967		Father	P/PS3 + PM1 + PM2 + PM3 + PP4
2	*SRD5A2*	G680 > A	R227Q	E4	rs9332964	Hom	Mother/Father	P/PS3 + PM1 + PM2 + PM3 + PP4
3	*SRD5A2*	G607 > A	G203S	E4	rs9332961	CompoundHet	Mother	P/PS3 + PM1 + PM2 + PM3 + PP4
		G680 > A	R227Q	E4	rs9332964		Father	P/PS3 + PM1 + PM2 + PM3 + PP4
4	*SRD5A2*	G607 > A	G203S	E4	rs9332961	Hom	Mother/Father	P/PS3 + PM1 + PM2 + PM3 + PP4
5	*SRD5A2*	C408 > A	Y136Ter	E2	/	CompoundHet	*De novo*	P/PVS1 + PM2 + PM6 + PP3
		G680 > A	R227Q	E4	rs9332964		Mother	P/PS3 + PM1 + PM2 + PM3 + PP4
6	*SRD5A2*	A578 > G	N193S	E5	rs763296857	CompoundHet	Mother	P/PS3 + PM1 + PM2 + PM3 + PP4
		G737 > A	R246Q	E5	rs9332967		Father	P/PS3 + PM1 + PM2 + PM3 + PP4
7	*SRD5A2*	G737 > A	R246Q	E5	rs9332967	Hom	Mother/Father	P/PS3 + PM1 + PM2 + PM3 + PP4
8	*SRD5A2*	C59 > T	L20P	E1	rs761824859	CompoundHet	Mother	LP/PM1 + PM2 + PP3 + PP4 + PP5
		G680 > A	R227Q	E4	rs9332964		Father	P/PS3 + PM1 + PM2 + PM3 + PP4
9	*SRD5A2*	C59 > T	L20P	E1	rs761824859	Hom	Mother/Father	LP/PM1 + PM2 + PP3 + PP4 + PP5
10	*SRD5A2*	A578 > G	N193S	E5	rs763296857	CompoundHet	Father	P/PS3 + PM1 + PM2 + PM3 + PP4
		656delT	F219fs*60	E5	rs61748127		Mother	P/PVS1 + PS3 + PM2 + PM3
11	SRD5A2	G607 > A	G203S	E4	rs9332961	CompoundHet	Father	P/PS3 + PM1 + PM2 + PM3 + PP4
		656delT	F219fs*60	E5	rs61748127		Mother	P/PVS1 + PS3 + PM2 + PM3
12	*AR*	C2338 > T	R780W	E6	/	Hem	Mother	P/PS3 + PM1 + PM2 + PM3 + PP4
13	*AR*	T2450 > A	I817N	E7	/	Hem	*De novo*	LP/PS2 + PM1 + PP3 + PP4
14	*AR*	G2567 > A	R856H	E7	rs9332971	Hem	Mother	P/PS3 + PM1 + PM2 + PM3 + PP4
15	*AR*	C2612 > T	A871V	E8	rs143040492	Hem	Mother	P/PS3 + PM1 + PM2 + PP4 + PP5
16	*AR*	Exon 5-8 gross deletion, chX 67716101-67724136			/	Hem	Mother	P/PVS1 + PM2 + PP3 + PP4
17	*AR*	Exon 2 gross deletion, chX 67643255-67643407			/	Hem	Mother	P/PVS1 + PM2 + PP3 + PP4
18	*MID1*	C2000 > T	P667L	E10	rs147106995	Hom	Mother/Father	LP/PM1 + PM2 + PP3 + PP4

P, pathogenic; LP, likely pathogenic.

TABLE 3 | The clinical features of 11 patients carrying SRD5A2 mutations.

No.	Age at diagnosis	Gender upon diagnosis	Type of hypospadias	Complications			EMS	LH/FSH (mIU/ml)	T/DHT (HCG stimulation before/after)
				Microtesticle	Micropenis	Cryptorchidism			
1	0.6	Male	III	Y	Y	Y	2	0.48/3.94	10/10.5
2	2.7	Male	III	Y	Y	N	6	0.5/1.55	–
3	1.9	Female	III	N	Y	Y	1	2.9/7.76	–
4	12.6	Male	IV	N	Y	N	3	0.1/4.26	81.9/–
5	22.2	Male	II	N	N	N	10	2.6/1.8	–
6	2.7	Male	III	N	Y	N	6	4.21/7.71	–
7	0.9	Male	IV	N	Y	N	6	3.3/2.6	–
8	0.3	Female	IV	Y	Y	N	3	2.19/4.06	25.1/30.5
9	10.9	Female	III	Y	Y	Y	5	0.4/0.35	39.7/64.4
10	5.6	Male	III	N	Y	N	6	< 0.07/0.15	8.3/–
11	5.4	Male	III	N	Y	N	6	0.08/0.54	10.9/10.4

EMS, external masculinization score; LH, Luteinizing Hormone; FSH, Follicle Stimulating Hormone; T, testosterone; DHT, Dihydrotestosterone.

the 245th thymine was mutated to adenine, resulting in the amino acid at position 817 being changed from isoleucine to asparagine. According to ACMG guidelines, this mutation was assessed as likely pathogenic (LP/PS2 + PM1 + PP3 + PP4). Exon 5-8 gross deletion (chX 67716101-67724136) removed 8035bp including the totality of exon 5-8 and exon 2 gross deletion (chX 67643255-67643407) removed 152 bp containing total exon 2 of AR gene, both were assessed as pathogenic (P/PVS1 + PM2 + PP3 + PP4).

Patients With MID1 Mutations

One patient carried a homozygous mutation in the *MID1* gene, p.P667L, which was located in exon 10 of the MID1 gene and was the last amino acid encoded by the gene. MID1 gene mutation

TABLE 4 | The clinical features of 6 patients carrying AR mutations.

No.	Age at diagnosis	Gender upon diagnosis	Type of hypospadias	Complications			EMS	LH/FSH (mIU/ml)	T/DHT (HCG stimulation before/after)
				Microtesticle	Micropenis	Cryptorchidism			
12	1.6	Female	IV	N	N	Y	5	2.26/2.39	–
13	14.6	Female	IV	N	Y	N	3	27.7/6.7	–
14	14.3	Female	II	N	Y	N	6	18.5/8.6	19.6/21.46
15	0.3	Male	II	N	Y	N	4	1.2/0.83	5.83/–
16	5.9	Male	III	N	N	Y	7	9.95/21.93	2.2/3.6
17	14.2	Female	IV	Y	Y	Y	1	0.82/4.63	–

EMS, external masculinization score; LH, Luteinizing Hormone; FSH, Follicle Stimulating Hormone; T, testosterone; DHT, Dihydrotestosterone.

is associated with X-linked Opitz G/BBB syndrome (Fontanella et al., 2008; Preiksaitiene et al., 2015; Maia et al., 2017). The patient with this mutation which was identified in our study only had hypospadias without other symptoms or abnormalities. But according to ACMG guidelines, this mutation was assessed as likely pathogenic (LP/PM1 + PM2 + PP3 + PP4).

Expression and Sub-Cellular Distribution of AR_{I817N}

To determine whether the expression of the AR or the protein stability was affected by this newly identified mutation, site directed mutation was performed using wild type *AR* gene. An immunoblot was performed after incubation of CHO cell line transiently expressing AR_{WT} or AR_{I817N}, respectively, with different concentrations of R1881 or vehicles for 24 h. The protein expression level of AR_{I817N} appeared to be similar at every R1881 concentration (**Figures 1A,B**). These data rule out any severe change in protein stability in the absence or presence of ligand.

To investigate whether the p.I817N mutation of *AR* gene could influence AR expression, we further analyzed the subcellular localization of this mutant in CHO cell line. Cells were transfected with AR_{WT} or AR_{I871N} plasmid DNAs, and the localization of AR protein was examined using confocal microscopy. Both AR_{WT} and AR_{I871N} were predominantly located in the cytoplasm in the absence of hormone (**Figures 2A,B,E**). In the presence of 1nM R1881 both AR_{WT} and AR_{I871N} were translocated in a similar way to the nucleus and displayed a typical punctuate nuclear distribution (**Figures 2C–E**).

Transcriptional Activity of AR_{I817N}

The AR_{I871N} mutation is located in the ligand binding domain (LBD) of the AR, which may play a role in coactivator mediated activation of the transcription. Therefore, functional studies were performed to address whether the AR_{I871N} affects the transcription activation potential of AR. The AR_{I871N} or AR_{WT} expression vector was co-transfected with Cignal reporter in luciferase assay. In dose-response curve, the mutated AR showed reduced ability to induce AR-mediated activation of a reporter gene, compared to wild-type AR assessed by the natural ligand DHT or R188. p.I817N caused a 20∼46% reduction in activity at doses between 1 and 10 nM DHT or 0.1–100 nM R1881 (**Figures 3A,B**). In addition, this was further illustrated by using competitive binding assay with R1881. The mutated AR showed weaker competitive binding than the wild type (**Figure 3C**). These results suggest that p.I817N mutation leads to a decreased sensitivity of the androgen response.

DISCUSSION

The prevalence of hypospadias is increasing in China (Li et al., 2012). To explore the potential contribution of genetic components in these patients, we screened 81 children with karyotype of 46, XY who had hypospadias using NGS of 15 target genes. 18 out of 81 patients were found to have mutations. The identified genetic abnormalities of the novel missense mutation *AR* p.I817N were analyzed. It was also noted that 11 mutations in *SRD5A2* gene, 6 mutations in *AR* gene, and one variant in *MID1* gene in this study were also correlated to abnormal male genital development and hypospadias. The genetic abnormality is 22.2% (18/81) which is higher than reported in the literature which has previously suggested that 10–20% of hypospadias are caused by genetic abnormalities (Carmichael et al., 2012; Kalfa et al., 2019). It supports the hypothesis that hypospadias is a multifactorial disease and is a consequence of combination of both environmental and genetic abnormalities.

Male phenotypic development can be divided into two stages: sex determination and differentiation (Domenice et al., 2000). Genetic mutations in genital differentiation and external genital development can cause hypospadias. Based on previous reports, we have selected 15 genes which are potentially involved in the development of hypospadias. During male sexual development, expression of *SRY* induces a series of gene activation, including its direct downstream gene *SOX9*. They mainly act in the early stage of gender differentiation, and their mutations lead to the development of disorders of sexual development (Harley et al., 2003). *NR5A1* is an important transcription factor in male sexual development and steroid synthesis. INSL3 regulates the expression of steroidogenic factor-1, which is an important regulator in the development of gonads and adrenal glands (Sadeghian et al., 2005). *NR0B1* regulates the early stage of testicular differentiation, and its mutation most often causes adrenal hypoplasia congenita and gonadal dysplasia. *DHH* belongs to Hedgehog secretory signaling molecule family. *DHH* gene mutation can cause 46, XY partial gonadal dysplasia. In this study, 81 patients with hypospadias were screened and

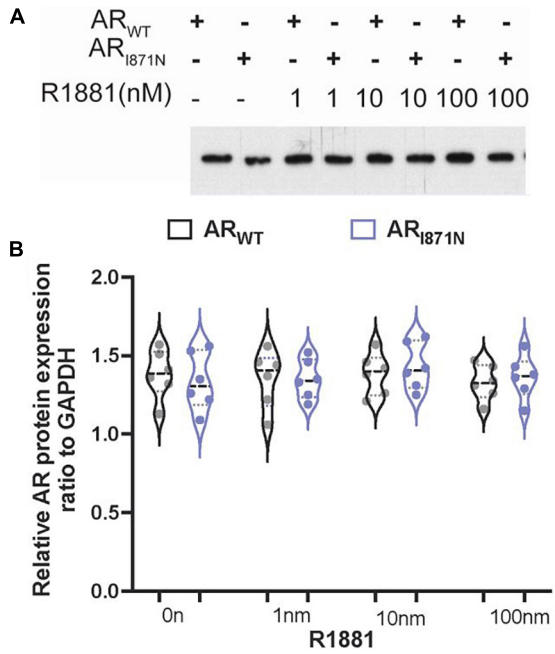

FIGURE 1 | The protein expression of AR_{WT} and AR_{I871N} in transfected cells. **(A)** The expression levels of AR_{WT} and AR_{I871N} were analyzed in cells 24 h post-transfection in the presence of R1881 (1, 10, and 100 nM) or vehicle alone (0.1% DMSO). An amount of 10 ug lysate was subjected to SDS-PAGE and immunoblotting with AR monoclonal antibody. No significant differences of expression were found between AR_{WT} and AR_{I871N}. **(B)** Quantitation the protein expression levels of AR.

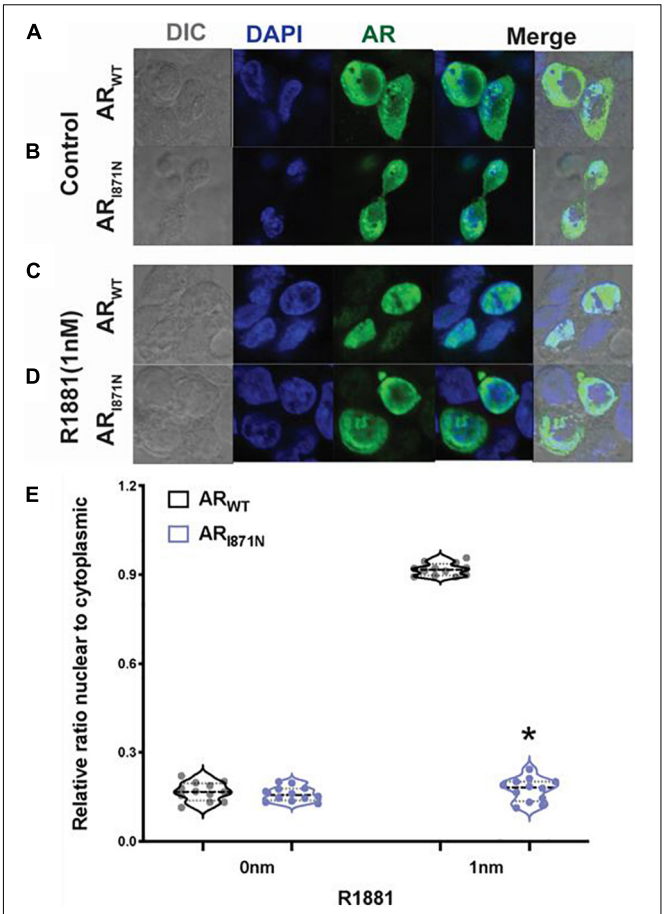

FIGURE 2 | Sub-cellular localization of AR_{WT} and AR_{I871N}. Confocal microscope images of CHO cells transfected with 1 ug of AR_{WT} or AR_{I871N} in the absence of ligand **(A,B)** or in the presence of 1 nM R1881 **(C,D)**. The bars represent 10 μm. **(E)** Quantitation of the ratio of nuclear/cytoplasmic expression of AR. *$P < 0.05$ compared with wild type.

we did not identify any genetic mutations in these six sex determination genes.

Genetic research on hypospadias has focused on identification of causal mutations too. Ethnic variation of genetic contribution of hypospadias has been described in the literature (Beleza-Meireles et al., 2007; van der Zanden et al., 2012). In Chinese patients, mutations or SNPs in *ATF3*, *FGF8*, *FGF10*, *BMP4*, *BMP7,* and *MAMLD1* have been reported. *ATF3* has a regulatory effect on cell growth (Liu et al., 2005; Kalfa et al., 2008). Co-expression and interaction among *FGF8*, *FGF10*, *BMP4,* and *BMP7* participate in the early stage of male genital development (Morgan et al., 2003; Suzuki et al., 2003). *MAMLD1* is a candidate to explore in patients with unexplained 46, XY DSD, as it has been shown to be expressed in fetal Leydig cells around the critical period for sexual development (Chen et al., 2010). The transient knockdown of *MAMLD1* mRNA expression results in significantly reduced testosterone production in mouse Leydig tumor cells and an *NR5A1* target site was found within the *MAMLD1* gene (Ogata et al., 2009). We found *MAMLD1* p.N662S variant in two patients with isolated hypospadias, which were also identified by other hypospadias mutation studies (Kalfa et al., 2012). Based on ACMG guidelines and reference to the ClinVar database, and HGMD databases, the variant was classified into benign (B).

MID1, as a transcriptional regulatory protein, is involved in the development of the mid-segment structure during embryonic development. Opitz syndrome (OS) is a multiple congenital anomaly disorder that shows a wide spectrum of severity and a highly variable expressivity (OMIM 300000) (Opitz, 1987). In male OS patients, mutations have been found to be scattered throughout the entire length of the *MID1* gene suggesting a loss of function mechanism as the basis of this developmental phenotype (Cox et al., 2000). Hypospadias of all grades was found more commonly in males with MID1 mutations than in those without (So et al., 2005). The patient in our study carrying *MID1* variant p. P667L only has isolated hypospadias, this loci was assessed as likely pathogenic. Recently MID1 was found to up-regulate AR protein levels in several prostate cancer cell lines and its expression was negatively regulated by androgen signaling (Kohler et al., 2014). Like the AR gene, MID1 is expressed in the genital tubercle (GT) in human embryos (Pinson et al., 2004). However, If MID1 loss-of-function mutations as seen in OS led to decreased AR protein levels in the GT, this may help explain the urogenital anomalies seen in OS (Winter et al., 2016).

The *SRD5A2* gene encoded 5α-reductase is mainly expressed in male genital and prostate tissues, whose defects cause 46,

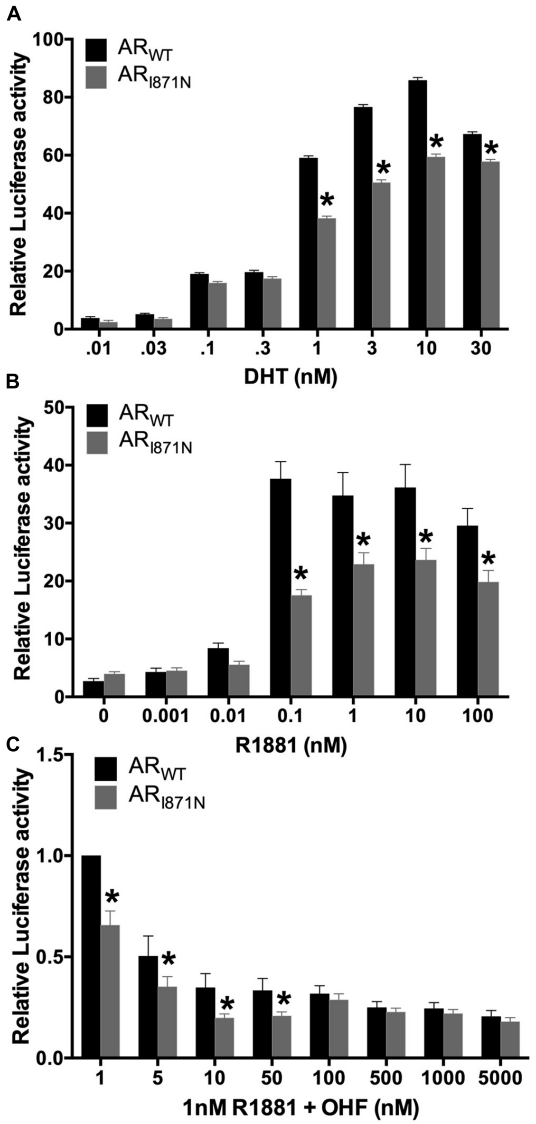

FIGURE 3 | Decreased transactivation activity of AR_{I871N} mutation in reporter gene assay. CHO cells transfected with either AR_{WT} or AR_{I871N}, were exposed to DHT **(A)** or R1881 **(B)** at the different concentrations. In a competitive binding assay, where R1181 competed with the anti-androgen OHF for AR binding sites, the AR_{I871N} mutation showed slightly weaker binding than the wild type **(C)**. Lower activity of AR_{I871N} was observed when it was compared to the wild-type receptor. The experiments were conducted in triplicate. *$P < 0.05$ compared with wild type.

XY DSD due to defects in testosterone metabolism. In this study, 13.6% (11/81) hypospadias is caused by SRAD5 mutation, which takes 61.1% (11/18) genetic etiology of hypospadias. A *de novo* mutation p.Y136Ter leads to a stop codon TAA and terminates the translation of SRD5A2 gene. This loci is assessed as pathogenic. The patient carries compound heterozygote p.Y136Ter/p.R227Q and exhibits type II hypospadias, with no external genital malformations except hypospadias. The EMS score was 10 and hCG stimulation tests showed non-response.

So far, more than 1000 cases of mutations with *AR* defects have been reported in the literature, presenting with a wide variety of phenotypic outcomes. The phenotypes of 46, XY individuals with *AR* gene mutations are categorized as complete androgen insensitivity syndrome (CAIS) or PAIS, respectively, and the more severe forms belong to disorders of sex determination. They range from a complete male-to-female sex reversal in CAIS patients to variable grades of ambiguous genitalia in PAIS patients. Milder forms of PAIS also include male phenotypes with gynecomastia, decreased fertility, or isolated hypospadias. PAIS could be a consequence of partial defect of AR structure or function caused by defects in *AR* gene. In this study, 7.4% (6/81) hypospadias was caused by *AR* mutation, which accounted for 33.3% (6/18) genetic abnormality of hypospadias.

The six mutations of the AR gene were found in 6 patients, of which 3 were previous identified mutation sites (p.R780W, p.R856H, p.A871V). p.I817N was a novel missense mutation. Other two patients have gross deletions of AR gene and both were not reported. All 4 missense mutations were located within the highly conserved carboxy-terminal LBD of the *AR* gene. The LBD domain consists of 12 contiguous alpha helices, most of which are hydrophobic amino acids that form a hydrophobic pocket which in turn binds the androgen ligand through its hydrophobic interaction. Functional impairment after mutation in this region weakens the binding of androgen to the AR protein in the target cell resulting in a decrease in the activity of androgen. It has been reported that p.A871V mutation was associated with a decrease in the binding affinity between AR and androgen by approximately 56%. p.R856H mutation led to changes in AR tertiary structure, resulting in decreased thermal stability and mutual N/C interactions. Large deletions in AR gene have been reported in patients with CAIS (Li et al., 2011; Doehnert et al., 2015), but in our data, two patients were not complete female phenotype (EMS7 and 1).

The p.I817N mutation identified in our study changed thymine to adenine at position 2450 in the *AR* gene. It is located in the LBD region of AR and encodes the first amino acid of exon 7, which is involved in the splicing of amino acid chains during transcription and translation. Conservative analysis of 10 mammalian proteins suggested that this region is highly conserved. The concentration of T in the laboratory test was 9.37 ng/ml, and it was 11.95 ng/ml after hCG challenge. It was significantly higher than the serum T level in boys of the same age. This also supports its molecular diagnosis. *In vitro* functional assay was further utilized and revealed that this mutation led to impaired AR transcriptional activity (20∼46%), decreased sensitivity for androgen ligand, and was responsible to hypospadias observed in the patient.

To exclude the correlation between the identified mutations and clinical manifestations other than hypospadias, we performed Fisher's exact test which was used to compare the incidences of inguinal hernia, SGA, ASD, and puberty breast development in children with and without candidate genes mutations. There were no statistical differences ($P > 0.05$). This study used a candidate gene strategy, there may be unknown gene variation. We cannot rule out the association of these complications with other gene variations.

In conclusion, genetic involvement of hypospadias was explored in 81 Chinese children using NGS. One *de novo* missense mutation loci was identified in AR and further *in vivo* and *in vitro* functional studies provided the molecular evidence that p.I817N amino acid change could cause significant reduction in AR transcriptional function which led to hypospadias. Our results suggest that genetic mutation is one of many factors contributing to the development of hypospadias in Chinese patients as the mutation was not detected in 78% of our patients, but still our data expand the spectrum of mutations in the SRD5A2 gene and AR gene in patients with hypospadias. Recent studies propose that *in utero* exposure to estrogens found in pesticides used in fruits and vegetables as well as in plastic linings can have an anti-androgenic activity (Donaire and Mendez, 2018). Epidemiological and genetic analysis are still needed to further clarify the pathogenesis of hypospadias in Chinese patients.

DATA AVAILABILITY STATEMENT

The data presented in the study are deposited in the China National GeneBank (CNGB) Nucleotide Sequence Archive (CNSA: https://db.cngb.org/cnsa) repository, accession number CNP0001939. The data are also available on request from the corresponding author, ZD and XM to dzy831@126.com and 179788825@qq.com.

ETHICS STATEMENT

The studies involving human participants were reviewed and approved by the Ethics Committee of Shanghai Jiao Tong University School of Medicine. Written informed consent to participate in this study was provided by the participants' legal guardian/next of kin.

AUTHOR CONTRIBUTIONS

LC was responsible for the writing and editing of this manuscript. LC and JW conducted the experiments. WL, YX, JN, and WW elaborated clinical data. XM and ZD were responsible for the editing of this manuscript. All authors contributed to the article and approved the submitted version.

REFERENCES

Ahmed, S. F., Khwaja, O., and Hughes, I. A. (2000). The role of a clinical score in the assessment of ambiguous genitalia. *BJU Int.* 85, 120–124.

Amendola, L. M., Jarvik, G. P., Leo, M. C., McLaughlin, H. M., Akkari, Y., Amaral, M. D., et al. (2016). Performance of ACMG-AMP Variant-Interpretation Guidelines among Nine Laboratories in the Clinical Sequencing Exploratory Research Consortium. *Am. J. Hum. Genet.* 98, 1067–1076. doi: 10.1016/j.ajhg.2016.03.024

Bao, X., and Zhang, W. (2012). Diagnostic Criteria and Treatment for Cryptorchidism in Children. *J. Appl. Clin. Pediatr.* 27, 1847–1848.

Beleza-Meireles, A., Lundberg, F., Lagerstedt, K., Zhou, X., Omrani, D., Frisen, L., et al. (2007). FGFR2. *Eur. J. Hum. Genet.* 15, 405–410. doi: 10.1038/sj.ejhg.5201777

Carmichael, S. L., Shaw, G. M., and Lammer, E. J. (2012). Environmental and genetic contributors to hypospadias: a review of the epidemiologic evidence. *Birth Defects Res. A Clin. Mol. Teratol.* 94, 499–510. doi: 10.1002/bdra.23021

Chen, Y., Thai, H. T., Lundin, J., Lagerstedt-Robinson, K., Zhao, S., Markljung, E., et al. (2010). Mutational study of the MAMLD1-gene in hypospadias. *Eur. J. Med. Genet.* 53, 122–126. doi: 10.1016/j.ejmg.2010.03.005

Cox, T. C., Allen, L. R., Cox, L. L., Hopwood, B., Goodwin, B., Haan, E., et al. (2000). New mutations in MID1 provide support for loss of function as the cause of X-linked Opitz syndrome. *Hum. Mol. Genet.* 9, 2553–2562.

Doehnert, U., Bertelloni, S., Werner, R., Dati, E., and Hiort, O. (2015). Characteristic features of reproductive hormone profiles in late adolescent and adult females with complete androgen insensitivity syndrome. *Sex Dev.* 9, 69–74. doi: 10.1159/000371464

Domenice, S., Arnhold, I. J. P., Costa, E. M. F., and Mendonca, B. B. (2000). "46,XY Disorders of Sexual Development" in *Endotext*. eds L. J. De Groot, G. Chrousos, K. Dungan, K. R. Feingold, A. Grossman, J. M. Hershman, et al. (South Dartmouth).

Donaire, A. E., and Mendez, M. D. (2018). *Hypospadias*. Treasure Island: StatPearls.

Du, X., Rosenfield, R. L., and Qin, K. (2009). KLF15 Is a transcriptional regulator of the human 17beta-hydroxysteroid dehydrogenase type 5 gene. A potential link between regulation of testosterone production and fat stores in women. *J. Clin. Endocrinol. Metab.* 94, 2594–2601. doi: 10.1210/jc.2009-0139

Fontanella, B., Russolillo, G., and Meroni, G. (2008). MID1 mutations in patients with X-linked Opitz G/BBB syndrome. *Hum. Mutat.* 29, 584–594. doi: 10.1002/humu.20706

Fu Chao, L. I., and Xuliang. (2010). Normal penile growth amongst Chinese. *Chin. J. Pediatr. Surg.* 2010, 432–434.

Gangaher, A., Chauhan, V., Jyotsna, V. P., and Mehta, M. (2016). Gender identity and gender of rearing in 46 XY disorders of sexual development. *Indian J. Endocrinol. Metab.* 20, 536–541. doi: 10.4103/2230-8210.183471

Geller, F., Feenstra, B., Carstensen, L., Pers, T. H., van Rooij, I. A., Korberg, I. B., et al. (2014). Genome-wide association analyses identify variants in developmental genes associated with hypospadias. *Nat. Genet.* 46, 957–963. doi: 10.1038/ng.3063

Harley, V. R., Clarkson, M. J., and Argentaro, A. (2003). The molecular action and regulation of the testis-determining factors, SRY (sex-determining region on the Y chromosome) and SOX9 [SRY-related high-mobility group (HMG) box 9]. *Endocr. Rev.* 24, 466–487. doi: 10.1210/er.2002-0025

Jin, L., Ye, R., Zheng, J., Hong, S., and Ren, A. (2010). Secular trends of hypospadias prevalence and factors associated with it in southeast China during 1993-2005. *Birth Defects Res. A Clin. Mol. Teratol.* 88, 458–465. doi: 10.1002/bdra.20673

Joodi, M., Amerizadeh, F., Hassanian, S. M., Erfani, M., Ghayour-Mobarhan, M., Ferns, G. A., et al. (2019). The genetic factors contributing to hypospadias and their clinical utility in its diagnosis. *J. Cell. Physiol.* 234, 5519–5523. doi: 10.1002/jcp.27350

Kalfa, N., Fukami, M., Philibert, P., Audran, F., Pienkowski, C., Weill, J., et al. (2012). Screening of MAMLD1 mutations in 70 children with 46,XY DSD: identification and functional analysis of two new mutations. *PLoS One* 7:e32505. doi: 10.1371/journal.pone.0032505

Kalfa, N., Gaspari, L., Ollivier, M., Philibert, P., Bergougnoux, A., Paris, F., et al. (2019). Molecular genetics of hypospadias and cryptorchidism recent developments. *Clin. Genet.* 95, 122–131. doi: 10.1111/cge.13432

Kalfa, N., Liu, B., Klein, O., Wang, M. H., Cao, M., and Baskin, L. S. (2008). Genomic variants of ATF3 in patients with hypospadias. *J. Urol.* 180, 2183–2188. doi: 10.1016/j.juro.2008.07.066

Kohler, A., Demir, U., Kickstein, E., Krauss, S., Aigner, J., Aranda-Orgilles, B., et al. (2014). A hormone-dependent feedback-loop controls androgen receptor levels by limiting MID1, a novel translation enhancer and promoter of oncogenic signaling. *Mol. Cancer* 13:146. doi: 10.1186/1476-4598-13-146

Li, B. K., Ding, Q., Wan, X. D., and Wang, X. (2011). Clinical and genetic characterization of complete androgen insensitivity syndrome in a Chinese family. *Genet. Mol. Res.* 10, 1022–1031. doi: 10.4238/vol10-2gmr1130

Li, Y., Mao, M., Dai, L., Li, K., Li, X., Zhou, G., et al. (2012). Time trends and geographic variations in the prevalence of hypospadias in China. *Birth Defects Res. A Clin. Mol. Teratol.* 94, 36–41. doi: 10.1002/bdra.22854

Liu, B., Wang, Z., Lin, G., Agras, K., Ebbers, M., Willingham, E., et al. (2005). Activating transcription factor 3 is up-regulated in patients with hypospadias. *Pediatr. Res.* 58, 1280–1283. doi: 10.1203/01.pdr.0000187796.28007.2d

Maia, N., Sa, M. J., Tkachenko, N., Soares, G., Marques, I., Rodrigues, B., et al. (2017). Two Novel Pathogenic MID1 Variants and Genotype-Phenotype Correlation Reanalysis in X-Linked Opitz G/BBB Syndrome. *Mol. Syndromol.* 9, 45–51. doi: 10.1159/000479177

Manson, J. M., and Carr, M. C. (2003). Molecular epidemiology of hypospadias: review of genetic and environmental risk factors. *Birth Defects Res. A Clin. Mol. Teratol.* 67, 825–836. doi: 10.1002/bdra.10084

Morgan, E. A., Nguyen, S. B., Scott, V., and Stadler, H. S. (2003). Loss of Bmp7 and Fgf8 signaling in Hoxa13-mutant mice causes hypospadia. *Development* 130, 3095–3109. doi: 10.1242/dev.00530

Ogata, T., Laporte, J., and Fukami, M. (2009). MAMLD1 (CXorf6): a new gene involved in hypospadias. *Horm. Res.* 71, 245–252. doi: 10.1159/000208797

Opitz, J. M. (1987). G syndrome (hypertelorism with esophageal abnormality and hypospadias, or hypospadias-dysphagia, or "Opitz-Frias" or "Opitz-G" syndrome)–perspective in 1987 and bibliography. *Am. J. Med. Genet.* 28, 275–285. doi: 10.1002/ajmg.1320280203

Pineyro-Ruiz, C., Chorna, N. E., Perez-Brayfield, M. R., and Jorge, J. C. (2020). Severity-Dependent Profile of the Metabolome in Hypospadias. *Front. Pediatr.* 8:202. doi: 10.3389/fped.2020.00202

Pinson, L., Auge, J., Audollent, S., Mattei, G., Etchevers, H., Gigarel, N., et al. (2004). Embryonic expression of the human MID1 gene and its mutations in Opitz syndrome. *J. Med. Genet.* 41, 381–386.

Preiksaitiene, E., Krasovskaja, N., Utkus, A., Kasnauskiene, J., Meskiene, R., Paulauskiene, I., et al. (2015). R368X mutation in MID1 among recurrent mutations in patients with X-linked Opitz G/BBB syndrome. *Clin. Dysmorphol.* 24, 7–12. doi: 10.1097/MCD.0000000000000059

Sadeghian, H., Anand-Ivell, R., Balvers, M., Relan, V., and Ivell, R. (2005). Constitutive regulation of the Insl3 gene in rat Leydig cells. *Mol. Cell. Endocrinol.* 241, 10–20. doi: 10.1016/j.mce.2005.03.017

Shukla, G. C., Plaga, A. R., Shankar, E., and Gupta, S. (2016). Androgen receptor-related diseases: what do we know? *Andrology* 4, 366–381. doi: 10.1111/andr.12167

So, J., Suckow, V., Kijas, Z., Kalscheuer, V., Moser, B., Winter, J., et al. (2005). Mild phenotypes in a series of patients with Opitz GBBB syndrome with MID1 mutations. *Am. J. Med. Genet. A* 132A, 1–7. doi: 10.1002/ajmg.a.30407

Springer, A., van den Heijkant, M., and Baumann, S. (2016). Worldwide prevalence of hypospadias. *J. Pediatr. Urol.* 12, 152.e1–7. doi: 10.1016/j.jpurol.2015.12.002

Suzuki, K., Bachiller, D., Chen, Y. P., Kamikawa, M., Ogi, H., Haraguchi, R., et al. (2003). Regulation of outgrowth and apoptosis for the terminal appendage: external genitalia development by concerted actions of BMP signaling [corrected]. *Development* 130, 6209–6220. doi: 10.1242/dev.00846

van der Horst, H. J., and de Wall, L. L. (2017). Hypospadias, all there is to know. *Eur. J. Pediatr.* 176, 435–441. doi: 10.1007/s00431-017-2864-5

van der Zanden, L. F., van Rooij, I. A., Feitz, W. F., Franke, B., Knoers, N. V., and Roeleveld, N. (2012). Aetiology of hypospadias: a systematic review of genes and environment. *Hum. Reprod. Update* 18, 260–283. doi: 10.1093/humupd/dms002

Winter, J., Basilicata, M. F., Stemmler, M. P., and Krauss, S. (2016). The MID1 protein is a central player during development and in disease. *Front. Biosci.* 21, 664–682. doi: 10.2741/4413

Conflict of Interest: The authors declare that the research was conducted in the absence of any commercial or financial relationships that could be construed as a potential conflict of interest.

frontiers in Genetics

ORIGINAL RESEARCH
published: 02 July 2021
doi: 10.3389/fgene.2021.631221

Whole-Exome Sequencing Identified *CFTR* Variants in Two Consanguineous Families in China

Binyi Yang[1,2,3†], Cheng Lei[1,2,3†], Danhui Yang[1,2,3], Zhiping Tan[4], Ting Guo[1,2,3] and Hong Luo[1,2,3*]*

[1] Department of Pulmonary and Critical Care Medicine, The Second Xiangya Hospital, Central South University, Changsha, China, [2] Research Unit of Respiratory Disease, Central South University, Changsha, China, [3] Hunan Diagnosis and Treatment Center of Respiratory Disease, Changsha, China, [4] Department of Cardiovascular Surgery, Clinical Center for Gene Diagnosis and Therapy, The Second Xiangya Hospital of Central South University, Changsha, China

Background: Cystic fibrosis (CF) is an autosomal recessive disease caused by genetic variants of the cystic fibrosis transmembrane conductance regulator (*CFTR*) gene. It is a common hereditary disease in Caucasians while rare in the Chinese. Until now, only 87 Chinese patients have been reported with molecular confirmations. The variant spectrum and clinical features of Chinese CF patients are obviously different from those of Caucasians.

Materials and Methods: Whole-exome sequencing was applied to analyze the exome of three individuals who have only the typical CF phenotype in the respiratory system from two consanguineous families. The protein domain and structure analysis were applied to predict the impact of the variants. Sanger sequencing was applied to validate the candidate variants.

Results: A previously reported homozygous variant in *CFTR* (NM_000492.4: c.1000C > T, p.R334W) was identified in proband I. A novel homozygous variant in a polymorphic position (NM_000492.4: c.1409T > A, p.V470E) was identified in two individuals in the family II. The novel *CFTR* variant predicted to be disease-causing is the first, to the best of our knowledge, to be reported in *CFTR*. However, *in vitro* validation is still needed.

Conclusion: Our finding expands the variant spectrum of *CFTR*, reveals clearer clinical phenotype distinction and variant spectrum distinction between Chinese and Caucasian CF patients, and contributes to a more rapid genetic diagnosis and future genetic counseling.

Keywords: cystic fibrosis, *CFTR*, bronchiectasis, Chinese, genetic variants, phenotype

OPEN ACCESS

Edited by:
María L. Couce, Complejo Hospitalario Universitario de Santiago, Spain

Reviewed by:
Jeffrey Dennis Calhoun, Northwestern University, United States
Saumel Ahmadi, Washington University in St. Louis, United States

****Correspondence:***
Hong Luo
drluohong@csu.edu.cn
Ting Guo
guotingxy@csu.edu.cn

† These authors have contributed equally to this work

Specialty section:
This article was submitted to Genetics of Common and Rare Diseases, a section of the journal Frontiers in Genetics

Received: *19 November 2020*
Accepted: *12 May 2021*
Published: *02 July 2021*

Citation:
Yang B, Lei C, Yang D, Tan Z, Guo T and Luo H (2021) Whole-Exome Sequencing Identified CFTR Variants in Two Consanguineous Families in China. Front. Genet. 12:631221. doi: 10.3389/fgene.2021.631221

INTRODUCTION

Cystic fibrosis (CF), first reported in 1938, is an inherited autosomal recessive disease involving multiple organs, including the respiratory, digestive, and reproductive systems (Andersen, 1938). Respiratory failure after bronchiectasis and infection is now the main cause of death in CF patients. CF is a common hereditary disease in Caucasians but is rare among Asians, especially the Chinese.

The estimated incidence of the disease in Caucasian population is about 1/3,000, but no more than 100 cases that have been reported in China (Liu et al., 2020). The disease is mainly detected through abnormally high chloride concentrations in sweat and gene sequencing.

Cystic fibrosis is caused by variants of the cystic fibrosis trans-membrane conductance regulator (*CFTR*) gene. CFTR is a chloride and bicarbonate transport protein, encoded by the *CFTR* gene located at the long arm of chromosome 7, which has 27 exons. As *CFTR* is mainly expressed in various glandular tissues, the variants can cause abnormal ion transport and secretory function, subsequently leading to bronchiectasis, pancreatic insufficiency, and fertility dysfunction in males (Ratjen et al., 2015). More than 2,000 different variants have been identified in *CFTR*, and the most recent update from the CFTR2 database[1] recorded a total of 442 variants including 360 CF-causing variants. All variants are divided into six classes according to their mechanisms and pathogenicity. The most prevalent variant in Caucasians, p.F508del, was classified in Class II(Ratjen et al., 2015).

Studies have shown that the clinical phenotypes and variant spectrum of CF patients in China and those of the Caucasian population are very different (Guo et al., 2018). There are approximately 90 Chinese CF patients who have been reported up to now. In recent years, however, as the understanding of CF has deepened and the methods of diagnosis have improved, a growing number of CF patients have been diagnosed and reported in China. Here, we used whole-exome sequencing to analyze the exome of three individuals who have only a typical respiratory system CF phenotype, from two consanguineous families, and found *CFTR* variants including a novel variant in a polymorphic position.

MATERIALS AND METHODS

Ethical Compliance

This study was approved by the Review Board of the Second Xiangya Hospital of Central South University in China. Three patients diagnosed with bronchiectasis from two Chinese consanguineous families participated in the study. Written informed consent was obtained from all participants.

Whole-Exome Sequencing and Variants Filtering

Whole-exome sequencing was performed on three individuals from two consanguineous families. Peripheral blood samples (3–5 ml) from proband I in family I; proband IIa and his brother IIb in family II were obtained with informed consent, respectively. The genomic DNA was extracted from peripheral blood cells by DNeasy blood and tissue kit (QIAGEN # 69506). The exomes of the probands were captured by Agilent Sureselect Human All Exons V6 kit (Agilent, California, United States) and sequencing on Illumina Hiseq X-10 platform (Illumina Inc, San Diego, United States). The single-nucleotide variants (SNVs) and short insertions and deletions (INDELs) were filtered as follow as we describe (**Supplementary Figure 1**): (1) Variants in the 1,000 Genomes Project (1,000G[2]), NHLBI-ESP project[3], and Exome Aggregation Consortium (ExAC[4]) with minor allele frequency (MAF) $\leq$ 0.01 were included. (2) Intergenic, intronic, and untranslated regions and synonymous variants were excluded from subsequent analyses. (3) Bioinformatics analyses (Sift, Polyphen-2, Mutationtaster, MutationAssessor) were used for the remaining variants. (4) The remaining data were flittered by bronchiectasis-related diseases, which include primary ciliary dyskinesia (PCD), cystic fibrosis, and primary immunodeficiency. (5) Runs of homozygosity (ROH) analysis was also performed due to the fact that all probands came from consanguineous families. The ROH analysis was based on the data from whole-exome sequencing data using the Automap algorithm (Quinodoz et al., 2021).

Variant Validation With Sanger Sequencing

Sanger sequencing was used to validate the candidate variants found in whole-exome sequencing. Primers for PCR amplification of fragments with individual variants were designed by Primer Premier 5 software (Premier Biosoft, Palo Alto, CA, United States). The sequences of the primers are listed in **Supplementary Table 1**.

RESULTS

Clinical Summary

Family 1

Proband I was a 14-year-old girl whose parents are consanguineous (**Figure 1**). She had suffered from recurrent coughing and expectoration for 2 years and came to our clinic for 1 day due to acute hemoptysis. Physical examination showed moist rales in both lower lungs. CT (computed tomography) showed inflammation in bilateral maxillary sinus, ethmoid sinus, and sphenoid sinus, bronchiectasis in both lungs, and calcification of the liver (**Figure 2A**). Her nasal nitric oxide concentration (nNO) was 74 parts per billion (ppb). The pulmonary function test indicated that she had severe mixed pulmonary ventilation dysfunction (FEV1% predicted: 48.0%, FEV1/FVC: 80.5%), and the bronchial dilation test was negative. The sputum culture showed infection with *Pseudomonas aeruginosa*. After hemostasis, antibiotic, and expectorant treatment, her symptoms were relieved, and the patient was discharged.

Family 2

Proband IIa was a 17-year-old teenager whose parents are also consanguineous (**Figure 1**). He had been coughing and expectoration repeatedly for 6 years and experiencing

[1]https://cftr2.org

[2]http://www.1000genomes.org

[3]http://evs.gs.washington.edu/EVS/

[4]https://gnomad.broadinstitute.org/

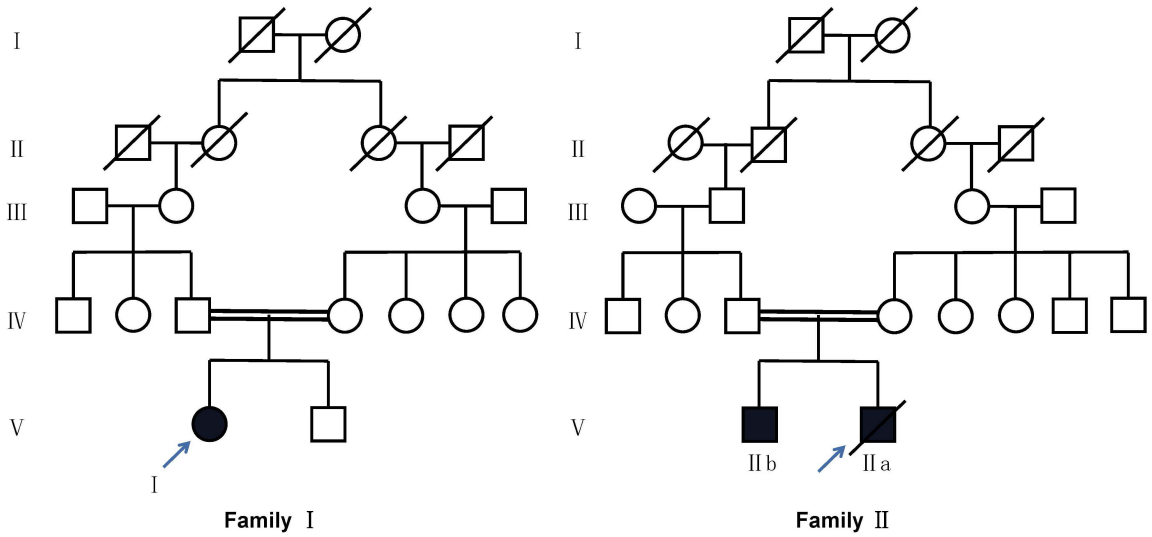

FIGURE 1 | Pedigree of two families with *CFTR* variants. Circles refer to females. Squares refer to male subjects. Solid symbols refer to affected subjects. Crossed-out symbols refer to subjects who have passed away. The arrows indicate the probands.

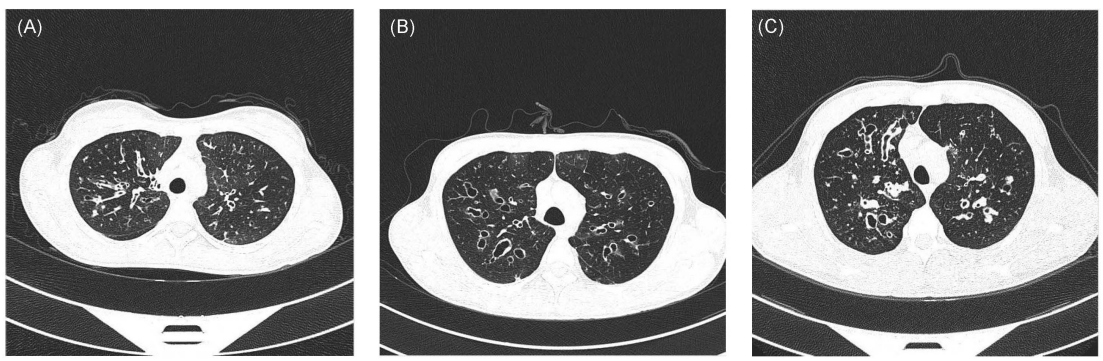

FIGURE 2 | High resolution computed tomography reveals signs of bronchiectasis in all probands [**(A)**, proband I; **(B)**, proband IIa; **(C)**, patient IIb].

shortness of breath for 1 year, and he was admitted to the Respiratory Intensive Care Unit due to suddenly worsening symptoms. Physical examination revealed a barrel chest, some moist rales, and finger clubbing. Arterial blood gas analysis suggested hypercapnic acidosis. Chest radiography suggested bronchiectasis and infection. Color Doppler echocardiography showed mild mitral regurgitation. CT showed chronic inflammation of bilateral maxillary sinuses, an undeveloped sphenoid sinus, and left frontal sinus, along with diffuse bronchiectasis with patchy infection foci (**Figure 2B**). His nasal nitric oxide concentration (nNO) was 159 ppb. The patient was given ventilator and phlegm treatment. The sputum culture was positive for *Pseudomonas aeruginosa*. The cough and expectoration have not improved significantly after changing antibiotics several times. After sputum aspiration under fiberoptic bronchoscopy, the patient's coughing and expectoration decreased, and his condition improved significantly. Soon after, the patient was discharged from the hospital.

IIb is the 5-year-old brother of IIa. His nitric oxide concentration (nNO) was 113 ppb. He had no symptoms except for digital clubbing and the CT suggested sinusitis, bronchiectasis, and calcification of the liver (**Figure 2C**).

Whole-Exome Sequencing Identified Two Variants in *CFTR*

The whole-exome sequencing was performed on three individuals, and the results were listed in **Supplementary Table 2**. Notably, 14.24, 7.09, and 7.25 Gb sequencing data were generated, and more than 99% of the targeted regions were covered, with a depth of more than 10×. Non-synonymous variants occurring in exons or splice sites (splicing junction 10 bp) were selected and analyzed after alignment. After the selection of rare variations (minor allele frequency <1%) related to bronchiectasis, one homozygous variant of cystic fibrosis transmembrane conductance regulator (*CFTR*) was identified in each

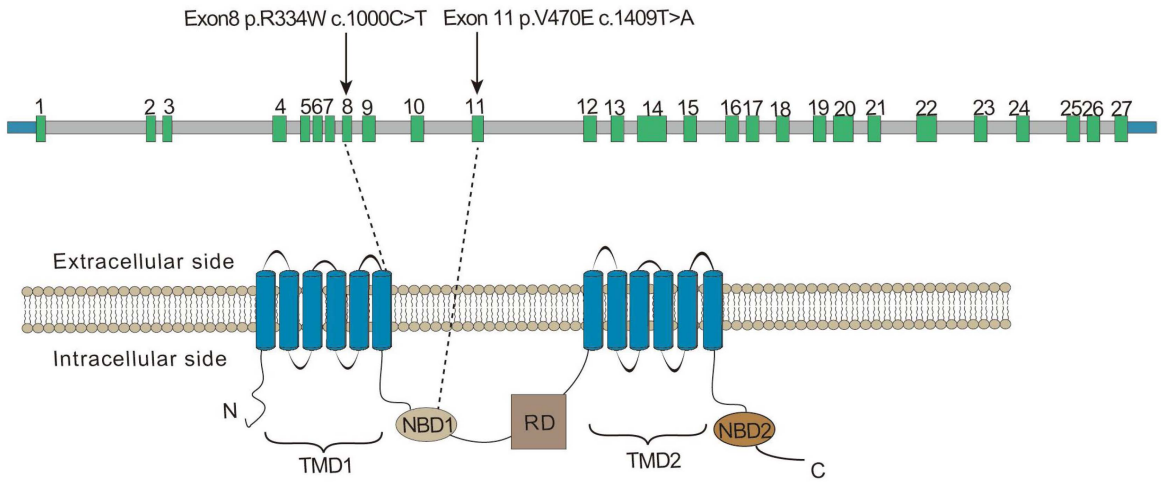

FIGURE 3 | Exon structure of the *CFTR* gene. Domain structure of the CFTR protein. The positions of variant c.1000C > T, p.R334W, and c.1409T > A, p.V470E. TMD, transmembrane domain; NBD, nucleotide binding domain; RD, regulatory (R) domain.

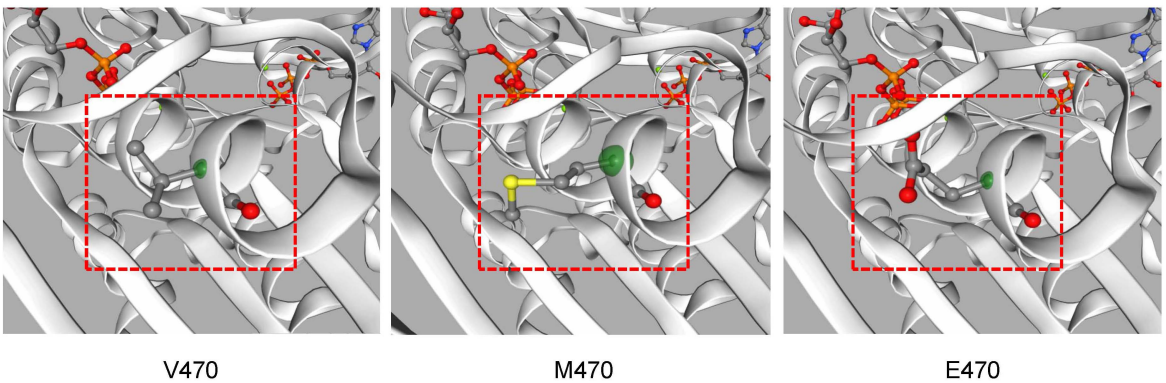

FIGURE 4 | The CFTR protein tertiary structure was predicted by Swiss-model software. Different structures caused by amino acid changes are shown in position 470 of CFTR.

family. The results of our ROH analysis confirmed the homozygous region in chromosome 7 contains the variants of *CFTR*. The detailed results of ROH analysis are shown in **Supplementary Figure 2**.

A homozygous variant of *CFTR*, c.1000C > T, p.R334W, which had been reported to be disease-causing, was found in proband I(Sheppard et al., 1993).

A novel variant of *CFTR*, c.1409T > A, p.V470E was found in proband IIa and IIb. It hadn't been reported before and hadn't been recorded on the Cystic Fibrosis Mutation Database[5]. The novel variant was predicted to be deleterious by SIFT and the CADD (CADD PHRED score = 24.8). Located at the exon 11, the variant may affect the function of the nucleotide binding domains 1 (NBD1) domain after translation (**Figure 3**). Swiss model was also used to predict the protein tertiary structure, the amino acid change from valine to glutamic acid might affect the stability of the helix (**Figure 4**).

[5]http://www.genet.sickkids.on.ca

Sanger Sequencing for Variant Validation of *CFTR*

Sanger sequencing was used to validate the candidate variants identified by whole-exome sequencing, and segregation analyses were performed in both family members. Homozygous variant c.1000C > T, p.R334W in proband I and homozygous variant c.1409T > A, p.V470E in proband IIa and IIb were validated by Sanger sequencing. Sanger sequencing also confirmed that the healthy parents of the probands were all heterozygotes in corresponding positions (**Figure 5**).

DISCUSSION

In this study, whole-exome sequencing was performed to identify 2 variants in *CFTR* in 2 families. The parents of patients in both families are heterozygously married and are close relatives. A novel homozygous variant (c.1409T > A, p.V470E) was found in both patients in family II. It was located in the NBD1 domain

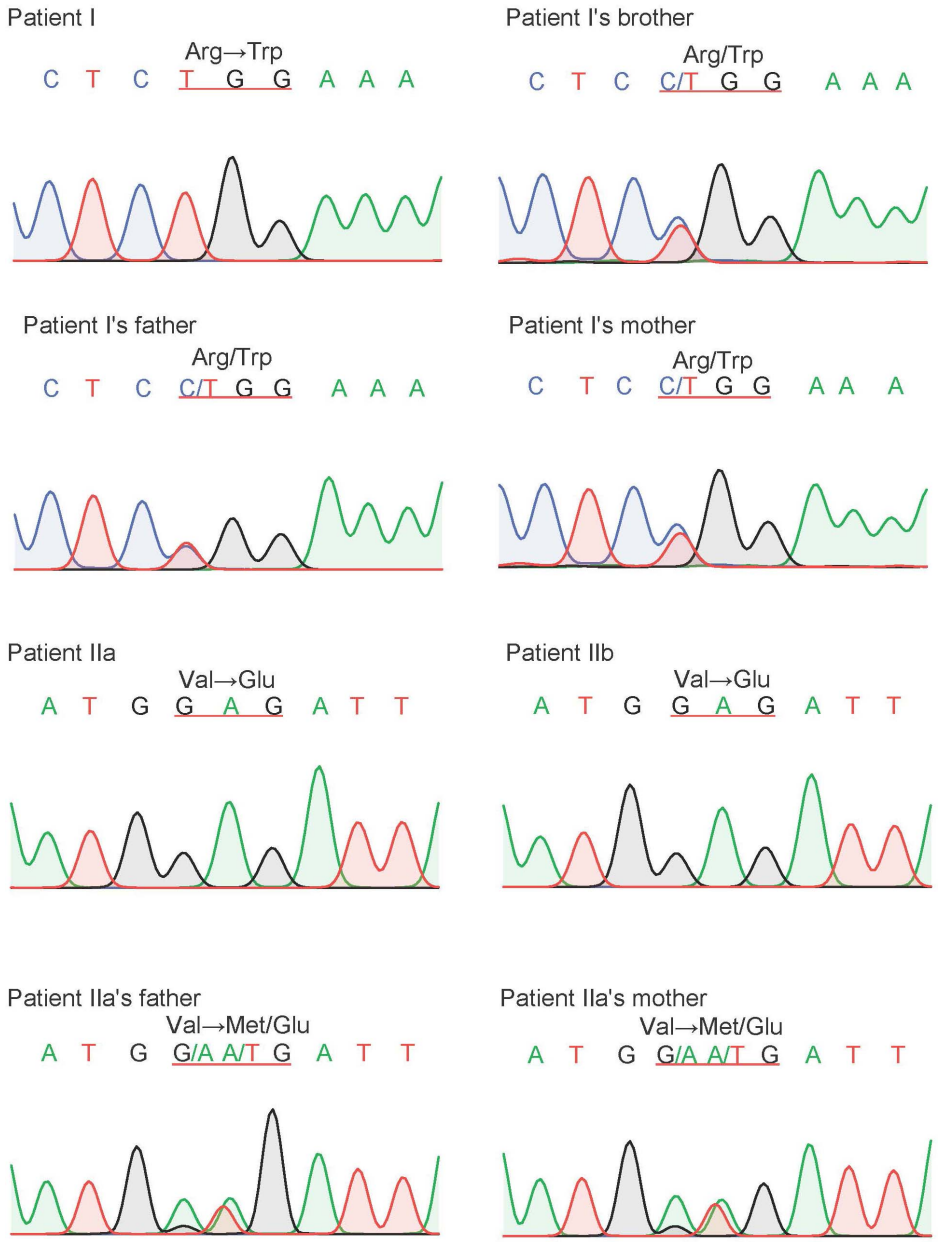

FIGURE 5 | The result of Sanger sequencing of our probands and their family members. The variant of *CFTR*, c.1000C > T, p.R334W, were found in proband I and c.1409T > A, p.V470E were found in proband IIa and IIb. All of our probands are homozygous, and their parents are heterozygotes.

of CFTR and may disturb the structure and function of ATP binding. Another reported homozygous variant (c.1000C > T, p.R334W) found in patient I was considered to be the cause of her respiratory disease.

The novel variant c.1409T > A, p.V470E in exon 11, which may affect the function of the NBD1 domain after translation, was not present in the current Cystic Fibrosis Mutation Database or the Human Gene Mutation Database[6]. Notably, this position is a polymorphic position of M470V (c.1408G > A) variants and is related to bronchiectasis and chronic pancreatitis by affecting structural stability of NBD1 and intrinsic chloride channel activity when it is combined with other variants (Lee et al., 2003; Yang et al., 2018). The V470 allele can reduce the activity of the CFTR protein chloride channel, which might help to reduce the disease damage and decrease the rate of diarrhea, primary sclerosing cholangitis, and prostate cancer (Henckaerts et al., 2009; Qiao et al., 2008). M470 allele is significantly associated with an increasing risk of chronic pancreatitis in both Asian and Caucasian populations (Zhou et al., 2020), which also contributes to a low birth rate through the congenital bilateral

[6]http://www.hgmd.cf.ac.uk/ac/index.php

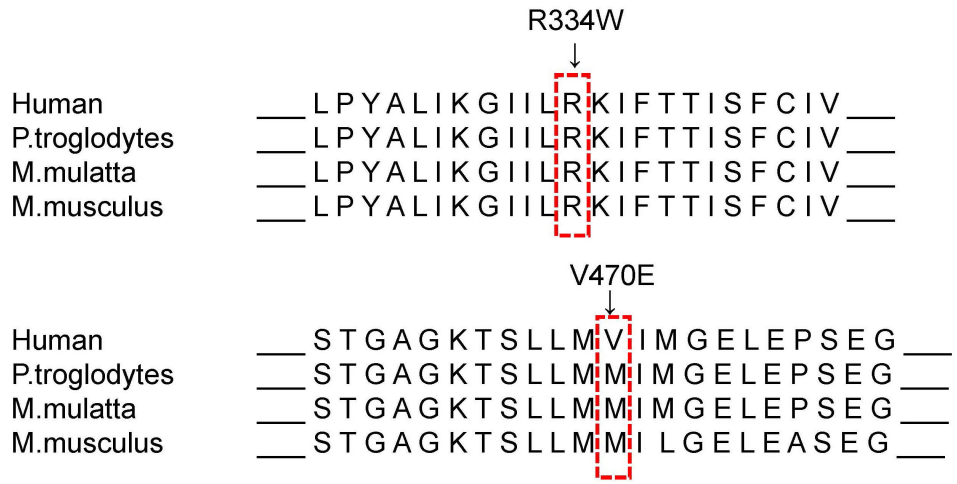

FIGURE 6 | Sequence alignment of mammalian CFTR proteins. The R334 is located in a highly conserved amino acid, and the V470 is located at a variant position according to the MutationTaster.

absence of the vas deferens (CBAVD) (Kosova et al., 2010). The variants in sequence among different races and species well reflect the natural selection during human evolution (Maria Ciminelli et al., 2011; **Figure 6**). The functional difference and species evolution caused by the polymorphic variants at this site also indicate that the variant V470E at this site has a high possibility of affecting the function of CFTR and causing disease. Both patients in family II have the typical cystic fibrosis clinical phenotype, and brother IIb, with no infection or symptoms, still had significant CT imaging findings of bronchiectasis and digital clubbing. This suggested a possible relationship between the variant and cystic fibrosis. According to ACMG guidelines, the novel variant was classified as the variant of uncertain significance (VUS), meeting the following criteria from the ACMG guidelines: PM2, PP1, PP3, and PP4 (Richards et al., 2015). Nevertheless, the phenotype-genotype association is hard to define completely because of the small sample size. *In vitro* validation is still in need for confirmation of this variant's role in cystic fibrosis.

The variant found in proband I was a reported variant c.1000C > T, p.R334W, present in the common Caucasian *CFTR* mutation-screening panels (Gasparini et al., 1991). According to the database of CFTR2, there are 429 recorded data of alleles in this position, and only 40% of patients suffered from pancreatic insufficiency. Like most patients with this site variant, proband I showed no symptoms other than respiratory symptoms such as bronchiectasis and sinusitis. This variant is located in the eighth exon and the sixth transmembrane region, which is close to the gate situated between amino acid residues 337 and 344 (Beck et al., 2008; Gao and Hwang, 2015; **Figure 4**). Because it only affects the conductivity of the channel that decreases the flow of ions, the phenotype of patients is often comparably less severe. The variant was defined as a mild variant (Class IV) based on the pathogenic mechanism and severity of bronchus and pancreas (Ratjen et al., 2015).

The survival rate of CF patients has been greatly improved with the rapid development of treatments. The CFTR potentiator, ivacaftor, the first drug approved to be used in CF patients, is now approved to be used in many class III and class IV variants. Ivacaftor is also effective for the most common pathogenic variant, p.F508del, when combined with corrector lumacaftor. However, patient I in our study has the class IV variant R334W and is not a target of ivacaftor. New research showed that phosphodiesterase (PDE) inhibitors RPL554 (Verona Pharma) can elevate intracellular cAMP in R334W Fisher rat thyroid (FRT) cells. This finding supports the therapeutic potential of RPL554 for CF patients with class III/IV variants including R334W (Turner et al., 2020). In addition, gene and molecular therapy for some mutations is also a research hot spot. At present, the main difficulty is to find a suitable vector (Ratjen et al., 2015).

Cystic fibrosis is the most common and potentially fatal genetic disease in Caucasians, though it is rare in China. Here, we reviewed the 90 cases of Chinese CF patients with DNA sequencing (**Supplementary Table 3**). Like the previous review, only a few patients had pancreas insufficiency and CBVAD, and most patients have been diagnosed with bronchiectasis and lung infections (Shen et al., 2016). According to the results of a sputum culture, chronic infection of *Pseudomonas aeruginosa* was found in 62% of patients. Compared with the low prevalence of ABPA in CF patients in Europe, more than 25% of Chinese CF patients met the criteria for ABPA. Sweat testing has always been the gold standard for CF diagnosis; however, it has only been carried out in hospitals in some large cities. Only 66 of 90 cases had the data of sweat conductivity test. Different from the most common pathogenic variants p.F508del in Europe and America, c.2909G > A (p.G970D) was the most common pathogenic variant in China among all the variants. Research has shown that the *CFTR* variant spectrum of CF patients in China is different from that in Caucasians in Europe and America since some variants, such as c.1766 + 5G > T, only occur in Chinese people (Xu et al., 2017). It is necessary for us to establish

a variant database of Chinese CF patients since most variants in Chinese CF patients have not been present in the common Caucasian *CFTR* mutation-screening panels. For patients with atypical clinical symptoms, it is difficult to make a clear diagnosis at an early stage without sweat tests or genetic testing, explaining the low diagnosis rate of CF in China. In the last decade, the number of reports of cystic fibrosis patients in China has increased significantly, and more cystic fibrosis patients and data will be discovered and reported in the future, after awareness and diagnosis techniques of the disease are improved.

CONCLUSION

Our study used whole-exome sequencing to identify two homozygous variants of *CFTR*, including a novel variant (c.1409T > A, p.V470E) and a reported variant (c.1000C > T, p.R334W), in three individuals from two consanguineous families. The existence of the novel variant (c.1409T > A, p.V470E), which has never been reported, implies the association between the polymorphism of the site and the disease and indicates its changes in human evolution. In addition, our findings in the patient with variant c.1000C > T, p.R334W are the same as that of previous studies that showed that the phenotype identified by this variant is less severe. Although the current functional test and drug experiment for these variants have not achieved decisive results, we do think that they are necessary. Our review of Chinese CF patients also suggests that doctors should pay more attention to the atypical symptoms of Chinese CF patients. Our result expands the variant spectrum of *CFTR* and contributes to a more rapid genetic diagnosis and future genetic counseling.

DATA AVAILABILITY STATEMENT

The data that support the findings of this study are available from the corresponding author upon reasonable request.

ETHICS STATEMENT

The studies involving human participants were reviewed and approved by Review Board of the Second Xiangya Hospital of Central South University in China. Written informed consent to participate in this study was provided by the participants' legal guardian/next of kin. Written informed consent was obtained from the individual(s), and minor(s)' legal guardian/next of kin, for the publication of any potentially identifiable images or data included in this article.

AUTHOR CONTRIBUTIONS

HL and ZT conceived and designed the experiments. BY, CL, and DY performed the experiments and analyzed the data. TG collected samples and the clinical data. BY and CL wrote the manuscript. All authors critically reviewed, revised, and approved the final version of the manuscript.

FUNDING

This study was supported by the National Natural Science Foundation of China (81770002 and 8207003 to HL, 81470445 to ZT, and 81900002 to TG), the Natural Science Foundation of Hunan Province, China (2020JJ5805 to TG), the Hunan Province Health Commission Scientific Research Project (B2019159 to HL), the Science and Technology Program of Changsha, China (kq1901120 to HL), the Xiangya Clinical Big Data System Construction Project in Pulmonary Inflammatory Disease of Central South University, and the National Key Clinical Specialty Construction Projects of China.

ACKNOWLEDGMENTS

We thank the patients for participating in the present study.

SUPPLEMENTARY MATERIAL

The Supplementary Material for this article can be found online at: https://www.frontiersin.org/articles/10.3389/fgene.2021.631221/full#supplementary-material

REFERENCES

Andersen, D. H. (1938). Cystic Fibrosis of the pancrease and its relation to celiac dsease. *Am. J. Dis. Child.* 56, 344–399. doi: 10.1001/archpedi.1938.01980140114013

Beck, E. J., Yang, Y., Yaemsiri, S., and Raghuram, V. (2008). Conformational changes in a pore-lining helix coupled to cystic fibrosis transmembrane conductance regulator channel gating. *J. Biol. Chem.* 283, 4957–4966. doi: 10.1074/jbc.m702235200

Gao, X., and Hwang, T. C. (2015). Localizing a gate in CFTR. *Proc. Natl. Acad. Sci. U. S. A.* 112, 2461–2466. doi: 10.1073/pnas.1420676112

Gasparini, P., Nunes, V., Savoia, A., Dognini, M., Morral, N., Gaona, A., et al. (1991). The search for south European cystic fibrosis mutations: identification of two new mutations, four variants, and intronic sequences. *Genomics* 10, 193–200. doi: 10.1016/0888-7543(91)90500-e

Guo, X., Liu, K., Liu, Y., Situ, Y., Tian, X., Xu, K. F., et al. (2018). Clinical and genetic characteristics of cystic fibrosis in CHINESE patients: a systemic review of reported cases. *Orphanet J. Rare Dis.* 13:224.

Henckaerts, L., Jaspers, M., Van Steenbergen, W., Vliegen, L., Fevery, J., Nuytten, H., et al. (2009). Cystic fibrosis transmembrane conductance regulator gene polymorphisms in patients with primary sclerosing cholangitis. *J. Hepatol.* 50, 150–157. doi: 10.1016/j.jhep.2008.07.033

Kosova, G., Pickrell, J. K., Kelley, J. L., McArdle, P. F., Shuldiner, A. R., Abney, M., et al. (2010). The CFTR Met 470 allele is associated with lower birth rates in fertile men from a population isolate. *PLoS Genet.* 6:e1000974. doi: 10.1371/journal.pgen.1000974

Lee, J. H., Choi, J. H., Namkung, W., Hanrahan, J. W., Chang, J., Song, S. Y., et al. (2003). A haplotype-based molecular analysis of CFTR mutations associated with respiratory and pancreatic diseases. *Hum. Mol. Genet.* 12, 2321–2332. doi: 10.1093/hmg/ddg243

Liu, K., Xu, W., Xiao, M., Zhao, X., Bian, C., Zhang, Q., et al. (2020). Characterization of clinical and genetic spectrum of Chinese patients with cystic fibrosis. *Orphanet J. Rare Dis.* 15:150.

Maria Ciminelli, B., Bombieri, C., Ciccacci, C., Belpinati, F., Pompei, F., Maselli, R., et al. (2011). Anthropological features of the CFTR gene: its variability in an African population. *Ann. Hum. Biol.* 38, 203–209. doi: 10.3109/03014460.2010.507554

Qiao, D., Yi, L., Hua, L., Xu, Z., Ding, Y., Shi, D., et al. (2008). Cystic fibrosis transmembrane conductance regulator (CFTR) gene 5T allele may protect against prostate cancer: a case-control study in Chinese Han population. *J. Cyst. Fibros.* 7, 210–214. doi: 10.1016/j.jcf.2007.07.011

Quinodoz, M., Peter, V. G., Bedoni, N., Royer Bertrand, B., Cisarova, K., Salmaninejad, A., et al. (2021). AutoMap is a high performance homozygosity mapping tool using next-generation sequencing data. *Nat. Commun.* 12:518.

Ratjen, F., Bell, S. C., Rowe, S. M., Goss, C. H., Quittner, A. L., and Bush, A. (2015). Cystic fibrosis. *Nat. Rev. Dis. Primers* 1:15010.

Richards, S., Aziz, N., Bale, S., Bick, D., Das, S., Gastier-Foster, J., et al. (2015). Standards and guidelines for the interpretation of sequence variants: a joint consensus recommendation of the American College of Medical Genetics and Genomics and the Association for Molecular Pathology. *Genet. Med.* 17, 405–424. doi: 10.1038/gim.2015.30

Shen, Y., Liu, J., Zhong, L., Mogayzel, P. J. Jr., Zeitlin, P. L., Sosnay, P. R., et al. (2016). Clinical Phenotypes and Genotypic Spectrum of Cystic Fibrosis in Chinese Children. *J. Pediatr.* 171, 269–276.e1.

Sheppard, D. N., Rich, D. P., Ostedgaard, L. S., Gregory, R. J., Smith, A. E., and Welsh, M. J. (1993). Mutations in CFTR associated with mild-disease-form Cl- channels with altered pore properties. *Nature* 362, 160–164. doi: 10.1038/362160a0

Turner, M. J., Luo, Y., Thomas, D. Y., and Hanrahan, J. W. (2020). The dual phosphodiesterase 3/4 inhibitor RPL554 stimulates rare class III and IV CFTR mutants. *Am. J. Physiol. Lung Cell. Mol. Physiol.* 318, L908–L920.

Xu, J., Yin, Y., Zhang, L., Zhang, J., Yuan, S., and Zhang, H. (2017). Four case reports of Chinese cystic fibrosis patients and literature review. *Pediatr. Pulmonol.* 52, 1020–1028. doi: 10.1002/ppul.23744

Yang, Z., Hildebrandt, E., Jiang, F., Aleksandrov, A. A., Khazanov, N., Zhou, Q., et al. (2018). Structural stability of purified human CFTR is systematically improved by mutations in nucleotide binding domain 1. *Biochim. Biophys. Acta Biomembr.* 1860, 1193–1204. doi: 10.1016/j.bbamem.2018.02.006

Zhou, D., Bai, R., and Wang, L. (2020). The Cystic Fibrosis Transmembrane Conductance Regulator 470 Met Allele Is Associated with an Increased Risk of Chronic Pancreatitis in Both Asian and Caucasian Populations: a Meta-Analysis. *Genet. Test. Mol. Biomarkers* 24, 24–32. doi: 10.1089/gtmb.2019.0199

Conflict of Interest: The authors declare that the research was conducted in the absence of any commercial or financial relationships that could be construed as a potential conflict of interest.

frontiers in Genetics

ORIGINAL RESEARCH
published: 22 July 2021
doi: 10.3389/fgene.2021.676832

A Novel *de novo* Mutation in *EBF3* Associated With Hypotonia, Ataxia, and Delayed Development Syndrome in a Chinese Boy

Yanru Huang[1,2,3†], Libin Mei[1,2,3†], Yangdan Wang[1], Huiming Ye[1,2], Xiaomin Ma[1], Jian Zhang[1], Meijiao Cai[1], Ping Li[1,3], Yunsheng Ge[1*] and Yulin Zhou[1,2*]*

[1] Women and Children's Hospital, School of Medicine, Xiamen University, Xiamen, China, [2] United Diagnostic and Research Center for Clinical Genetics, School of Public Health, Xiamen University, Xiamen, China, [3] Xiamen Key Laboratory of Reproduction and Genetics, Xiamen, China

OPEN ACCESS

Edited by:
María L. Couce, Complejo Hospitalario Universitario de Santiago, Spain

Reviewed by:
Yi Shiau Ng, Wellcome Trust Centre for Mitochondrial Research (WT), United Kingdom
Louise Bicknell, University of Otago, New Zealand

***Correspondence:**
Yulin Zhou
zhou_yulin@126.com
Yunsheng Ge
geyunsheng1979@163.com
Ping Li
lipingxmfy@163.com

† These authors have contributed equally to this work

Specialty section:
This article was submitted to Genetics of Common and Rare Diseases, a section of the journal Frontiers in Genetics

Received: *06 March 2021*
Accepted: *05 July 2021*
Published: *22 July 2021*

Citation:
Huang Y, Mei L, Wang Y, Ye H, Ma X, Zhang J, Cai M, Li P, Ge Y and Zhou Y (2021) A Novel de novo Mutation in EBF3 Associated With Hypotonia, Ataxia, and Delayed Development Syndrome in a Chinese Boy. Front. Genet. 12:676832. doi: 10.3389/fgene.2021.676832

Objective: Global developmental delay has markedly high phenotypic and genetic heterogeneity, and is a great challenge for clinical diagnosis. Hypotonia, ataxia, and delayed development syndrome (HADDS), first reported in 2017, is one type of global development delay. The aim of the present study was to investigate the genetic etiology of a Chinese boy with global developmental delay.

Methods: We combined clinical and imaging phenotyping with trio whole-exome sequencing and Sanger sequencing to the patient and his clinically unaffected parents. A luciferase reporter and immunofluorescence were performed to detect the effect of mutation on transcriptional activity and subcellular localization.

Results: The patient presented with several previously unreported symptoms in the patients with HADDS, including hemangiomas, mild hearing abnormalities and tracheomalacia. A novel *EBF3* c.589A > G missense mutation (p.Asn197Asp, p.N197D) was identified in the patient but not in his parents. By constructing the plasmid and transfecting HEK293T cells, *EBF3*-N197D mutant showed impaired activation of luciferase reporter expression of the p21 promoter, and the mutant affected its entry into the nucleus.

Conclusion: To the best of our knowledge, this is the first report of *EBF3* pathogenic mutation which associated with HADDS in the Chinese population. Our results expand the phenotypes and pathogenic mutation spectrum of HADDS, thus potentially facilitating the clinical diagnosis and genetic counseling of HADDS patients.

Keywords: hypotonia, ataxia, delayed development syndrome, *EBF3*, pathogenic mutation, trio whole-exome sequencing, c.589A > G

INTRODUCTION

Global developmental delay refers to a significant retardation of a child's growth and development relative to its peers (Shevell et al., 2003). It affects cognitive or thinking skills, motor skills, social and emotional, language, and vision.[1] Different individuals present with different levels of severity, thus deterring its clinical diagnosis. The etiology of global developmental delay includes exogenous and genetic (non-metabolic or metabolic) factors (Papavasiliou et al., 2000; Michelson et al., 2011). Advancements in modern biotechnology and genetic testing technology have facilitated

the diagnosis of children with global developmental delay (Srour and Shevell, 2014). Whole-exome sequencing (WES), whole-genome sequencing (WGS), and genome-wide microarrays have facilitated the identification of several candidate genes associated with developmental delays.

Herein, we curated data from one family, which included a boy with global developmental delay, born to non-consanguineous parents with a normal phenotype. The patient presented with motor delay, mental retardation, language delay, fontanelle closure delay, hypotonia, funnel chest, cryptorchidism, hemangioma, and febrile seizures. No obvious microdeletion or microduplication was detected using genome-wide microarray analysis (Affymetrix CytoScan 750K). A novel *EBF3* gene c.589A > G missense mutation was detected in the patient via Trio-WES but not in the parents. To our knowledge, there are no more than 20 cases, who had *de novo* variants in *EBF3* and a distinct neurodevelopmental syndrome, reported worldwide since the disease first reported in 2017 (Chao et al., 2017; Harms et al., 2017; Sleven et al., 2017). Besides, this is the first report about HADDS from China.

MATERIALS AND METHODS

Genomic DNA Extraction and Genome-Wide Copy Number Variation Analysis

Genomic DNA was extracted from peripheral blood leucocytes of the proband and his parents using the QIAamp Blood Mini Kit (QIAGEN, Hilden, Germany) following manufacturer protocol. CMA-SNP array analysis of the prband's DNA was performed using the Affymetrix® CytoScan™ 750K Array (Affymetrix, Santa Clara, CA, United States) following the manufacturer's recommended protocols. When all quality control tests were passed, we analyzed deletions of ≥ 50 kb (marker ≥ 20 kb), repeats of ≥ 100 kb (marker ≥ 20 kb), and homozygous chromosomal fragments of > 5 Mb.

Whole-Exome Sequencing and Bioinformatics Analysis

The genomic DNA of the proband and his parents was digested using segmentase (BGI, Shenzhen, China) into 100–500-bp fragments. Thereafter, 280–320-bp-long fragments were subjected to enrichment, blunting, A-tailing, and adapter ligation, followed by PCR amplification for library preparation. The DNA library thus generated was used to capture and collect DNA from the target exons and adjacent splice sites, using the BGI V4 probe (58.7M). Finally, the MGISEQ-2000 sequencing platform (MGI, Shenzhen, China) was used for PE100 + 100 sequencing. The quality control indicator for the sequencing data was an average effective sequencing depth of ≥ 100 × for the target region, where 95% of the sites had an average depth of 20×.

After the quality control analysis of the raw data, reads were aligned with the UCSC hg19 human reference genome, using BWA to eliminate duplicates. GATK was used to calibrate SNV and INDEL base quality scores and genotype analysis.

Validation by Sanger Sequencing

One pair primers (*EBF3*-7F: CGAAAGTCGCAGCTATTATCAT; *EBF3*-7R: TTAGACTTGATGAATCTGGCATAC) were designed using Oligo 6 to amplify the candidate regions of the mutation in *EBF3* gene (NM_001005463.2) identified by WES. Then, forward and reverse Sanger sequencing were performed using ABI PRISM 3730 gene analyzer (Applied Biosystems, California, United States).

Cell Culture

HEK293T cell line (ATCC, Rockville, MD, United States) was cultured in DMEM medium (GIBCO, Invitrogen Corporation, NY, United States) containing penicillin (final concentration of 100 U/ml, Sigma, St. Louis, MO, United States), streptomycin (final concentration of 100 μg/ml, Sigma, St. Louis, MO, United States) and 10% fetal bovine serum (FBS, Hyclone, Logan, UT, United States).

Expression Analysis

To characterize the effects of the *EBF3* mutation at the cellular level, transient cell transfections were performed in HEK293T cell line with WT or mutated *EBF3* mRNA expressed as fusions to the C-terminus of Flag (pcDNA-Flag-C, Invitrogen Corporation, NY, United States). Mutation was introduced via site-directed mutagenesis (QuickMutation™ Site-Directed Mutagenesis Kit, Beytime, ShangHai, China) with the forward primer 5'-CTAGGATCCATTACAACACAGTCAGCACT-3' and the reverse primer 5'-ATTGAATTCTCTTCTGTTTCATGCCGTAG-3'. All of the inserts were systematically verified by sequencing. The transfection was performed by incubating 2 μg of fusion protein construct using Lipofectamine 3,000 (Thermo Fisher Scientific, Pittsburgh, PA, United States) according to the manufacturer's instructions.

Firefly Luciferase Reporter Gene Assay Kit (Beytime, ShangHai, China) was used to detect the transcriptional activity of *EBF3*-WT and *EBF3*-N197D.

Immunofluorescence was used to detect the subcellular localization and captured by Laser Scanning Confocal Microscopy (Zeiss LSM, Zeiss, Germany).

The scraped cells were transferred to a 1.5 mL precooled microcentrifuge tube with 1 mL precooled PBS. Centrifuge at 4℃, collect cells at 1,000 g for 3 min, remove supernatant as possible with pipet, add 200 μl precooled Buffer A for every 20 μl compacted cell volume (add 1 μl DTT, 10 μl PMSF, and 1 μl protease inhibitor for every 1 mL Buffer A before use), The maximum rotational speed vortex vibrates violently for 15 s, and it is placed on ice for 10–15 min. Add 11 μl precooled Buffer B, swirl vigorously for 15 s at maximum rotating speed, and place on ice for 1 min. The solution was centrifuged at 4°C for 14,000 g for 5 min. At this time, it could be seen that the solution was divided into three layers: The lowest transparent layer, on which was white nucleus precipitate, and then the supernatant. The supernatant is transferred to another clean micro-centrifuge

tube precooled as soon as possible and placed on ice to obtain cytoplasmic protein. The supernatant is packed and stored at –80℃ to avoid repeated freeze-thaw. Insert the tip of a SPAR into the bottom of the centrifuge tube, suck out the bottom liquid and discard it. Add 100 μl of precooled Buffer C to the centrifuge precipitates (add 1 μl of DTT, 10 μl of PMSF, and 1 μl of protease inhibitor for every 1 mL of Buffer C before use). The maximum rotating speed of the vortex vibrated violently for 10 s, and the vortex was placed in an ice bath in a shaker for 40 min, 150 times/min, and then vibrated again for 30 s. The supernatant was centrifuged at 4℃ for 14,000 g for 5 min and transferred into a clean micro-centrifuge tube precooled as soon as possible to obtain nuclear protein. The supernatant was packed and stored at –80℃ to avoid repeated freeze-thaw. At last, the nucleoplasmic distribution of *EBF3*-WT and *EBF3*-N197D was detected by Western blot (Mini-PROTEAN Tetra,® Bio-Rad, United States).

Primary antibodies used were anti-Flag antibody (ab205606), anti-GAPDH antibody (ab8245), Anti-LaminA antibody (ab108595), Goat Anti-Rabbit IgG H&L (HRP) (ab6721), Rabbit Anti-Mouse IgG H&L (HRP) (ab6728), which were purchased from Abcam Company (Abcam, Cambridge, United Kingdom).

RESULTS

The Clinical Phenotypes and Imaging Examination Results of the Patient

The proband, a Chinese boy, was referred to the genetic counseling clinic of our hospital owing to global developmental delay. The patient was the first child and first birth, born through cesarean delivery at 39 weeks. All examinations during pregnance were normal. The proband's birth length was 48 cm (3rd–10th centile); birth weight was 3.2 kg (25th–50th centile); head circumference was 34 cm (25th–50th centile); chest circumference was 32 cm; abdominal circumference was 29 cm. He presented with labored breathing, hypotonia, micropenis, microscrotum, palpable testis in the right inguinal canal, and impalpable left testis. Color ultrasound imaging of the patient's bilateral scrotum, testes, and epididymis at birth elucidated an undescended testis in the left abdominal cavity, and a high mobility of the right testis with minor testicular hydrocele. Significant hypotonia was detected at 5 months. The patient could lift his head only at 10 months and underwent orchiopexy at 10 months. The first febrile seizure occurred at 1 year 2 months of age. The patient is now 1 year 6 months of age, his height is 78 cm ($\leq$1 SD) and weight is 9.5 kg ($\leq$1 SD). He was unsteady when sitting unassisted; could not climb, and could not say dad or mom; had an unclosed fontanelle; presented late teething; and exhibited slight orbital hypertelorism, high nasal bridge, broad nasal tip, deep philtrum, downturned mouth, and myopathic facies (stiff facial expressions) (**Figure 1A**). He also presented with pectus excavatum (**Figure 1B**), motor delay, intellectual disability, hemangiomas (in the palm of the left hand, **Figure 1C**), tracheomalacia, and feeding difficulties.

Brain MRI at 5 months (**Figures 1D,E**) revealed T2 hyperintensity in the bilateral anterior limbs of the internal capsule, suggesting potentially delayed myelination. Furthermore, enlargement of the bilateral lateral ventricles and lateral apertures, mega cisterna magna, bilateral mastoid, and middle ear effusions were observed. Brainstem auditory evoked potentials at 1 year 4 months of age showed prolonged latency of waves I, III, and V, and intervals and amplitudes were normal, suggested damage to the brain stem. No obvious abnormality was found in EEG.

Analysis of the proband's karyotype from peripheral blood lymphocytes (400–500 kb) did not reveal any abnormality. The proband's parents, who were non-consanguineous marriage, had normal clinical assessment, no exposure to toxic or harmful substances during pregnancy, and no family history of genetic diseases.

Genome-Wide Copy Number Variation Analysis

No obvious microdeletion or microduplication was found.

Identification of Candidate Mutations by Whole-Exome Sequencing

High-quality data were obtained through WES. The data of the proband, father, and mother were of 15.5, 14.4, and 15.8 Gb, the coverage of the target region was 99.78, 99.62, and 99.82%, and the average sequencing depth was 119, 131, and 144 reads, respectively. The percentage of the target region with an average sequencing depth of $>$ 10 reads accounted for 98.02, 95.06, and 96.11%, respectively. After filtering variants according to the following criteria: (1) frequency $<$ 1% according to the dbSNP, 1000 Genomes Project, ESP6500, and ExAC database; (2) protein-alteration or on canonical splice-sites; (3) homozygous, heterozygous, or *de novo* mutations; and (4) sequence variants interpreted in accordance with the guidelines of the American College of Medical Genetics and Genomics, and harmful variants were screened in accordance with the proband's phenotype; an *EBF3* heterozygous mutation was detected in the proband but not in his parents.

Validation via Sanger Sequencing

Sanger sequencing was performed to validate this heterozygous mutation in the proband, and the mutation was not observed in the parents' DNA isolated from peripheral blood lymphocytes (**Figure 2A**). The *EBF3* c.589A $>$ G mutation was characterized by a substitution of Asn197 in CDS to Asp (p. Asn197Asp, p.N197D).

There is no record of this variant in the dbSNP, 1000 Genomes Project, ESP6500, and ExAC database. p.N197D is located in a highly conserved domain (**Figure 2B**). Multiple online software, including PolyPhen-2, SIFT, mutationtaster, and revel, predicted that this variant was pathogenic. Based on the ACMG guidelines for interpreting sequence variants, this variant was classified as a likely pathogenic variant. Specific evidences of pathogenicity for this variant includes:

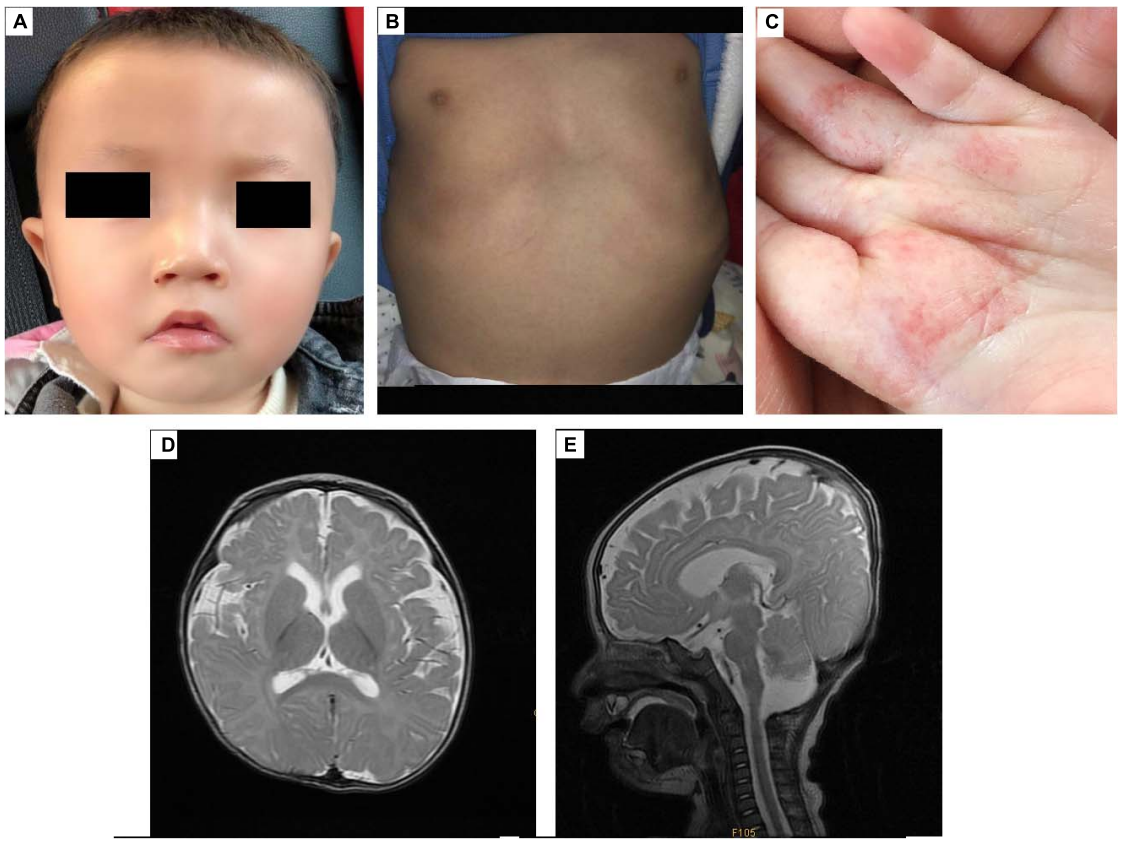

FIGURE 1 | The appearance and MRI results of the patients. **(A)** The patient has an unclosed fontanelle, slight orbital hypertelorism, high nasal bridge, broad nasal tip, deep philtrum, and downturned mouth. **(B)** The patient has pectus excavatum. **(C)** The hemangiomas are in the palm of the left hand. **(D,E)** Brain MRI shows insignificant T2 hyperintensity at the bilateral anterior limbs of the internal capsule, enlargement of the bilateral lateral ventricles and lateral apertures.

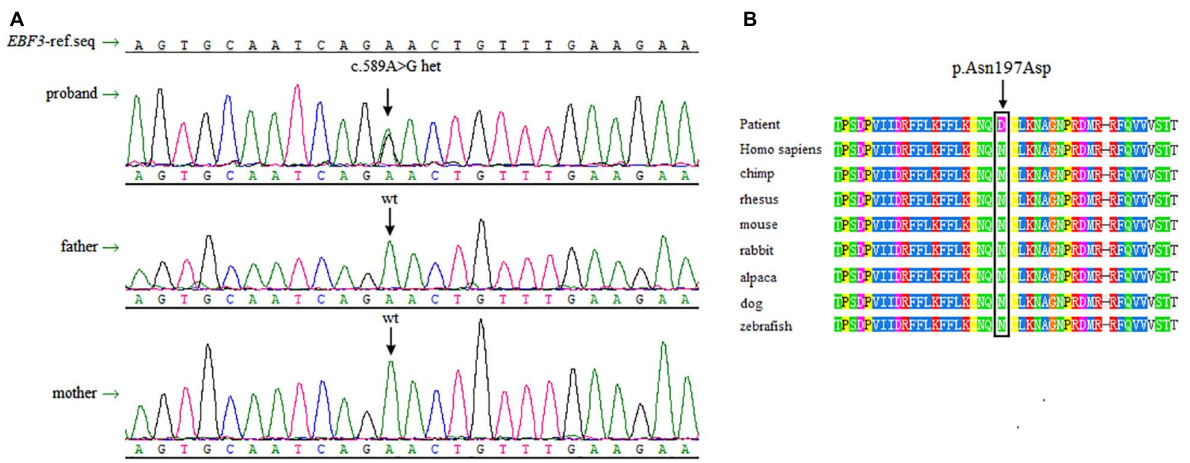

FIGURE 2 | Sanger sequencing data and conservation of the amino acid residues around the mutation sites. **(A)** Sanger sequencing shows a heterozygous mutation of c.589A > G in *EBF3* is present in the proband, whereas both of the parents are wild-type for this variant. **(B)** The box shows the change is located at the conserved leucine residues. The mutated amino acid is highly conserved in 8 species.

(1) PS2, *de novo* (both maternity and paternity confirmed) in a patient with the disease and no family history; (2) PM2, absent from controls (or at extremely low frequency if recessive) in Exome Sequencing Project, 1000 Genomes Project, or Exome Aggregation Consortium; (3) PP3, multiple lines of computational evidence support a deleterious effect on

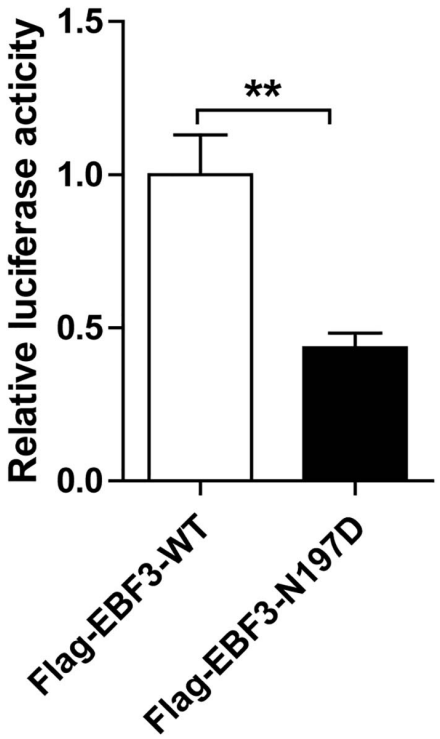

FIGURE 3 | Transcriptional activity of EBF3-N197D mutant in transfected cells. The transcriptional activity of p21 promoter in EBF3-N197D mutant was decreased. Results were mean ± SD for three individual experiments which, for each condition, were performed in triplicate. $^{**}p < 0.01$.

the gene or gene product (conservation, evolutionary, splicing impact, etc.).

The Effects of the EBF3 Mutation at the Cellular Level

To test the transcriptional activity of p21 in *EBF3*-N197D, HEK293T cells were co-transfected with the p21 report plasmid and Flag-*EBF3*-WT or Flag-*EBF3*-N197D, and the luciferase signal was detected. Results were mean ± SD for three individual experiments which, for each condition, were performed in triplicate. In agreement with other studies (Jin et al., 2014; Harms et al., 2017), *EBF3*-N197D mutant showed impaired activation of luciferase reporter expression of the p21 promoter (**Figure 3**). In order to detect the effect of p.N197D mutant on protein localization, HEK293T cells were transfected with Flag-*EBF3*-WT or Flag-*EBF3*-N197D, and the localization of Flag-*EBF3*-WT and Flag-*EBF3*-N197D in HEK293T cells were detected by western blot assay and immunofluorescence assay. As shown in **Figure 4**, in contrast to the WT, the distribution of p.N197D mutant in nucleus was significantly reduced ($p < 0.05$, $p < 0.01$) (**Figures 4A,B**), and the mutant aggregated in the cytoplasm (**Figures 4A,C**) and affected its entry into the nucleus (**Figure 4D**).

DISCUSSION

EBF3, which encodes the early B-cell factor 3, is located in the q26 locus on chromosome 10 (Zardo et al., 2002). The protein is a highly conserved member of the Collier/Olf/EBF (COE) family of transcription factors, and is involved in neuronal differentiation, maturation, and migration. It is a necessary component in the development of the central nervous system (CNS) (Wang et al., 2004; Yamazaki et al., 2004). EBF3 contains a DNA-binding domain (DBD) with a unique zinc-finger-like conformation, an Ig-like/plexins/transcription factors (IPT/TIG) domain, an atypical helix-loop-helix (HLH) domain, and a C-terminal transactivation domain (TAD) (**Figure 5A**; Liberg et al., 2002; Siponen et al., 2010). Structural damage to the DBD potentially decreases the EBF1-like activity of EBF3 owing to haploinsufficiency (the DBD of EBF1 and EBF3 are highly homologous) (Feldhaus et al., 1992; Lukin et al., 2011). Furthermore, *EBF3* mutations potentially lead to the formation of abnormal EBF3-EBF2 heterodimers (EBF2 and EBF3 are highly homologous) (Sleven et al., 2017). *EBF3* p.Arg163Leu and p.Pro177Leu can partially damage the DBD, thus reducing its ability to bind to DNA, while also reducing the transcriptional activity of wild-type EBF3 through dominant negative effects (Lukin et al., 2011; Sleven et al., 2017). However, nonsense variants are predicted to undergo nonsense-mediated mRNA decay *in vivo* (Harms et al., 2017; Sleven et al., 2017). Therefore, *EBF3* mutations may exert their effects through loss of function or dominant negative regulatory mechanisms (Lukin et al., 2011; Chao et al., 2017; Sleven et al., 2017).

Upon validation via trio whole-exome sequencing and Sanger sequencing, we report a novel heterozygous missense mutation, c.589A > G, in *EBF3* in a boy with global developmental delay. JSMOL simulation of the EBF3 protein structure (**Figure 5B**) revealed Asn197 is located proximal to the DNA. Asn is a polar, uncharged amino acid, whereas Asp is a polar, negatively charged amino acid. Therefore, p.Asn197Asp can not only partially damage the DBD, but also affect the ability of EBF3 to recognize DNA, thereby decreasing its DNA-binding ability. Harms et al. (2017) reported that changes in p.Arg209Trp potentially alter Asn197 and reduce the binding affinity between Asn197 and DNA, thereby altering *EBF3*-mediated genetic regulation, inducing the downregulation of wild type *EBF3*, and eventually leading to a series of pathological conditions. The p.Asn197Asp mutation reported herein may directly affect the DNA-binding ability of this protein. In this study, the pathogenicity of the mutation was confirmed by cellular model. p.Lys193Asn, a variation closer to Asn197 (**Figure 5C**), reported by Sleven et al. (2017), could damage the electrostatic network of interactions with the DNA phosphate backbone and the carbonyl oxygen of Ser65, and activate Cd79a transcription. The p.Asn197Asp mutation might also disrupt the electrostatic network. Our study showed that *EBF3*-N197D mutant impaired activation of luciferase reporter expression of the p21 promoter (**Figure 3**) which was consistent with previous studies (Jin et al., 2014; Harms et al., 2017). Besides, the mutant was significantly reduced in nucleus while increased in the cytoplasm which affected its entry into the nucleus (**Figure 4**). These data suggest

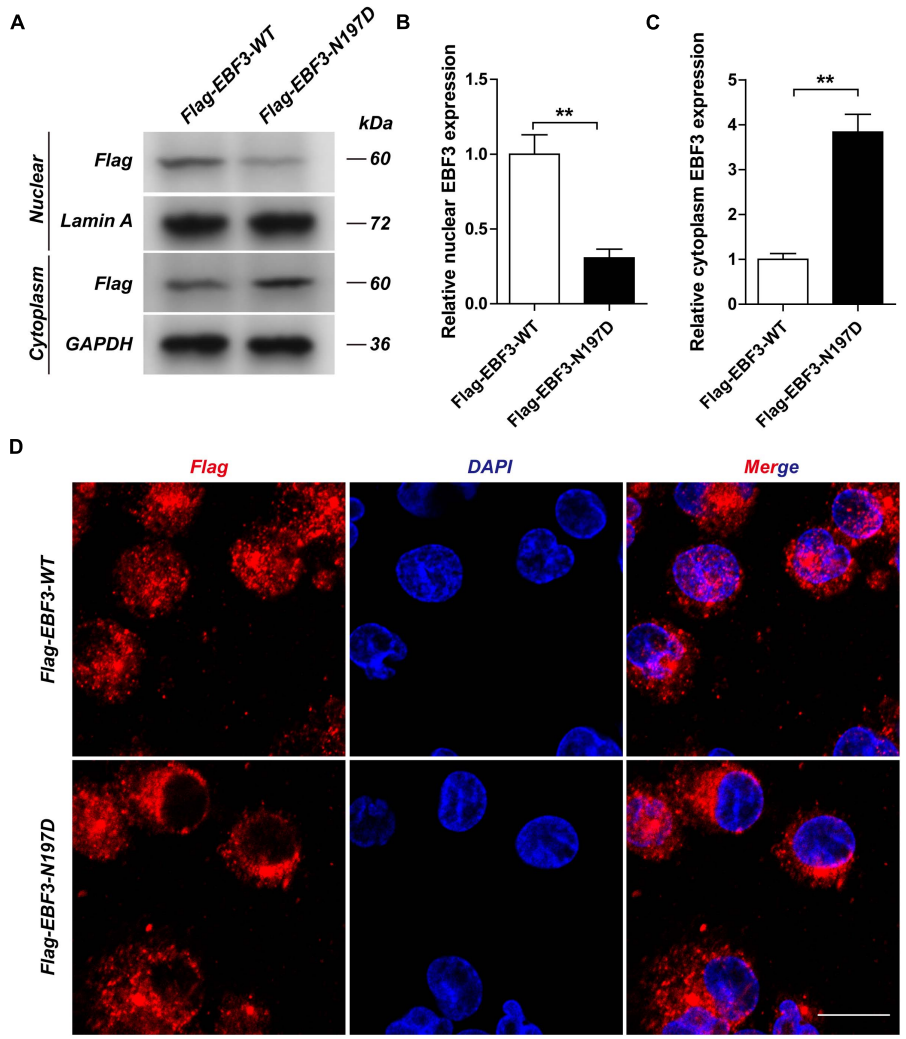

FIGURE 4 | The localization of Flag-EBF3-WT and Flag-EBF3-N197D in HEK293T cells. The distribution of p.N197D mutant was significantly reduced in the nucleus **(A,B)**, and increased in the cytoplasm **(A,C)** and affected its entry into the nucleus **(D)**. Results were mean ± SD for three individual experiments which, for each condition, were performed in triplicate. $^{**}p < 0.01$.

that the decreased affinity between ASN197 and DNA may lead to the reduced nuclear presence of EBF3, thus leading to the decreased expression of reporter genes.

Thus far, 33 mutations of *EBF3* have been reported worldwide, all of which are *de novo* mutations, including missense, frameshift, and nonsense mutations and splice variants (Chao et al., 2017; Harms et al., 2017; Sleven et al., 2017). Its functional heterozygous deletion is associated with developmental defects in the nervous system, eventually leading to hypotonia, ataxia, and delayed development syndrome (HADDS, OMIM #617330) (Chao et al., 2017; Harms et al., 2017; Sleven et al., 2017; Tanaka et al., 2017). HADDS follows an autosomal dominant inheritance. We compared the clinical phenotypes of patients with HADDS previously reported. The common phenotypes shared by these patients include motor delay, hypotonia, intellectual disability, and retardation in language acquisition. Besides the typical HADDS symptoms, our patient presented with an unclosed fontanelle, delayed teething, minimal facial expressions, high nasal bridge, broad nasal tip, deep philtrum, downturned mouth, feeding difficulties, cryptorchidism, micropenis, and pectus excavatum, consistent with the variable symptoms of HADDS, thus providing novel evidence for this syndrome. Furthermore, our patient did not present with ataxia, probably because he was too young for ataxia to be manifested. Although most previously reported patients with HADDS presented with ataxia, this symptom was observed only at a later stage (Lukin et al., 2011; Chao et al., 2017; Harms et al., 2017; Sleven et al., 2017; Tanaka et al., 2017). Moreover, Harms reported that ataxia was absent in a boy aged 1 year 11 months and a 25-year-old female (Harms et al., 2017). The present patient further presented several unusual symptoms including hemangioma, mild hearing abnormalities, and tracheomalacia, which have not been reported. Ebf3-deficient mice reportedly died of respiratory failure due to diaphragmatic relaxation dysfunction within

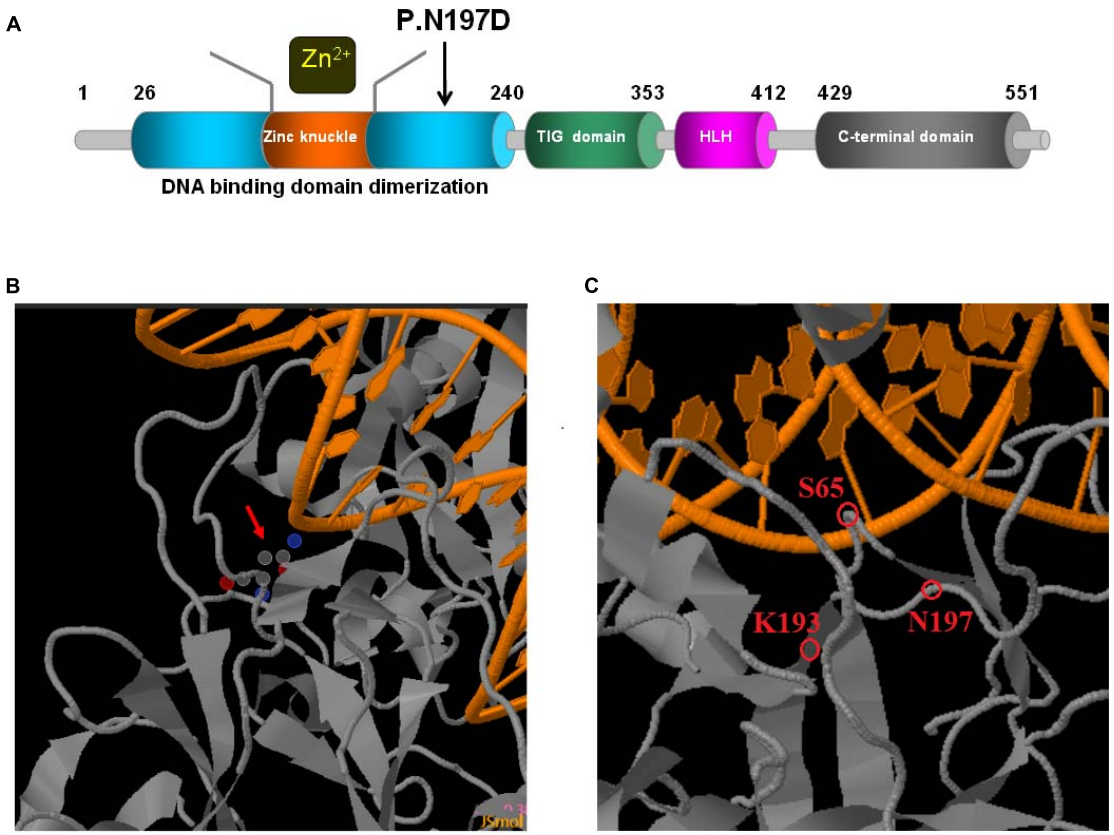

FIGURE 5 | Schematic representations of EBF3 structure. **(A)** The EBF3 protein consists a DNA-binding domain with special zinc knuckle, an Ig-like/plexins/transcription factors domain, an atypical HLH domain, and a C-terminal transactivation domain. The mutant amino acid identified in this study is shown in black arrow. **(B,C)** Close up of DNA-binding interactions of the variant (generated with JSmol). The protein is shown in gray, and the DNA is shown in orange. Asn197 is interacted with DNA. Asn197 is close to Lys193 which participated in the electrostatic network of interactions with the DNA phosphate backbone and the carbonyl oxygen of Ser65.

12 h postpartum (Jin et al., 2014). In the present patient, tracheomalacia may have been caused by hypotonia. However, it remains unclear whether tracheomalacia, and mild hearing abnormalities were truly associated with this condition.

CONCLUSION

We found a novel heterozygous *EBF3* mutation with Trio-WES in a Chinese boy with HADDS. By constructing the plasmid and transfecting HEK293T cells, *EBF3*-N197D mutant showed impaired activation of luciferase reporter expression of the p21 promoter, and the mutant was significantly reduced in nucleus while increased in the cytoplasm which affected its entry into the nucleus. Thus, this mutation was most likely the pathogenic mutation for this individual. This syndrome is yet to be reported in Asia. To the best of our knowledge, this study is the first to report hemangiomas, tracheomalacia, and mild hearing abnormalities in HADDS caused by an *EBF3* mutation. However, only a few cases have been reported and further assessments of a larger number of patients are required to determine whether these symptoms are associated with HADDS. This study further validated the association between *EBF3* pathogenic mutations and HADDS. It provides key information regarding the pathogenic mutation spectrum of HADDS, which will facilitate the clinical diagnosis and genetic counseling of patients with HADDS. More case studies are needed to clarify genotype-phenotype interactions in HADDS.

DATA AVAILABILITY STATEMENT

The datasets presented in this study can be found in online repositories. The names of the repository/repositories and accession number(s) can be found in the article/supplementary material.

ETHICS STATEMENT

This study fully complied with the tenets of the Declaration of Helsinki and has been approved by the Ethics Board of the Women's and Children's Hospital affiliated to Xiamen University, China. Written informed consent to participate in this study was provided by the participants' legal guardian/next of kin.

Written informed consent was obtained from the individual(s), and minor(s)' legal guardian/next of kin, for the publication of any potentially identifiable images or data included in this article.

AUTHOR CONTRIBUTIONS

YH: conceptualization and writing—original draft. LM, YW, HY, XM, and YG: data curation. YH, HY, XM, JZ, MC, and LM: formal analysis. YH and LM: funding acquisition. YH and JZ: methodology. LM: supervision. YG and LM: project administration. YG, PL, and YZ: writing—review and editing. All authors read and approved the final manuscript.

FUNDING

This study was supported by the National Natural Science Foundation of China (Grant No. 31801044) and Young and Middle-aged Personnel Training of Fujian Province (Grant Nos. 2018ZQN90 and 2020GGB064).

ACKNOWLEDGMENTS

We thank the patient and his parents for their participation and support.

REFERENCES

Chao, H. T., Davids, M., Burke, E., Pappas, J. G., Rosenfeld, J. A., and McCarty, A. J. (2017). A syndromic neurodevelopmental disorder caused by de novo variants in EBF3. *Am. J. Hum. Genet.* 100, 128–137.

Feldhaus, A. L., Mbangkollo, D., Arvin, K. L., Klug, C. A., and Singh, H. (1992). BLyF, a novel cell-type- and stage-specific regulator of the B-lymphocyte gene mb-1. *Mol. Cell. Biol.* 12, 1126–1133. doi: 10.1128/mcb.12.3.1126-1133.1992

Harms, F. L., Girisha, K. M., Hardigan, A. A., Kortüm, F., Shukla, A., and Alawi, M. (2017). Mutations in EBF3 disturb transcriptional profiles and cause intellectual disability, ataxia, and facial dysmorphism. *Am. J. Hum. Genet.* 100, 117–127.

Jin, S., Kim, J., Willert, T., Klein-Rodewald, T., Garcia-Dominguez, M., Mosqueira, M., et al. (2014). Ebf factors and MyoD cooperate to regulate muscle relaxation via Atp2a1. *Nat. Commun.* 5:3793.

Liberg, D., Sigvardsson, M., and Akerblad, P. (2002). The EBF/Olf/Collier family of transcription factors: regulators of differentiation in cells originating from all three embryonal germ layers. *Mol. Cell. Biol.* 22, 8389–8397. doi: 10.1128/mcb.22.24.8389-8397.2002

Lukin, K., Fields, S., Guerrettaz, L., Straign, D., Rodriguez, V., and Zandi, S. (2011). A dose-dependent role for EBF1 in repressing non-B-cell-specific genes. *Eur. J. Immunol.* 41, 1787–1793. doi: 10.1002/eji.201041137

Michelson, D. J., Shevell, M. I., Sherr, E. H., Moeschler, J. B., Gropman, A. L., and Ashwal, S. (2011). Evidence report: genetic and metabolic testing on children with global developmental delay: report of the quality standards subcommittee of the american academy of neurology and the practice committee of the child neurology society. *Neurology* 77, 1629–1635. doi: 10.1212/wnl.0b013e3182345896

Papavasiliou, A. S., Bazigou, H., Paraskevoulakos, E., and Kotsalis, C. (2000). Neurometabolic testing in developmental delay. *J. Child Neurol.* 15, 620–622. doi: 10.1177/088307380001500909

Shevell, M., Ashwal, S., Donley, D., Flint, J., Gingold, M., and Hirtz, D. (2003). Practice parameter: evaluation of the child with global developmental delay: report of the quality standards subcommittee of the american academy of neurology and the practice committee of the child neurology society. *Neurology* 60, 367–380. doi: 10.1212/01.wnl.0000031431.81555.16

Siponen, M. I., Wisniewska, M., Lehtiö, L., Johansson, I., Svensson, L., and Raszewski, G. (2010). Structural determination of functional domains in early B-cell factor (EBF) family of transcription factors reveals similarities to Rel DNA-binding proteins and a novel dimerization motif. *J. Biol. Chem.* 285, 25875–25879. doi: 10.1074/jbc.c110.150482

Sleven, H., Welsh, S. J., Yu, J., Churchill, M. E. A., Wright, C. F., and Henderson, A. (2017). De novo mutations in EBF3 cause a neurodevelopmental syndrome. *Am. J. Hum. Genet.* 100, 138–150. doi: 10.1016/j.ajhg.2016.11.020

Srour, M., and Shevell, M. (2014). Genetics and the investigation of developmental delay/intellectual disability. *Arch. Dis. Child.* 99, 386–389. doi: 10.1136/archdischild-2013-304063

Tanaka, A. J., Cho, M. T., Willaert, R., Retterer, K., Zarate, Y. A., Bosanko, K., et al. (2017). De novo variants in EBF3 are associated with hypotonia, developmental delay, intellectual disability, and autism. *Cold Spring Harb. Mol. Case Stud.* 3:a002097. doi: 10.1101/mcs.a002097

Wang, S. S., Lewcock, J. W., Feinstein, P., Mombaerts, P., and Reed, R. R. (2004). Genetic disruptions of O/E2 and O/E3 genes reveal involvement in olfactory receptor neuron projection. *Development* 131, 1377–1388. doi: 10.1242/dev.01009

Yamazaki, H., Sekiguchi, M., Takamatsu, M., Tanabe, Y., and Nakanishi, S. (2004). Distinct ontogenic and regional expressions of newly identified Cajal-Retzius cell-specific genes during neocorticogenesis. *Proc. Natl. Acad. Sci. U. S. A.* 101, 14509–14501. doi: 10.1073/pnas.0406295101

Zardo, G., Tiirikainen, M. I., Hong, C., Misra, A., and Feuerstein, B. G. (2002). Integrated genomic and epigenomic analyses pinpoint biallelic gene inactivation in tumors. *Nat. Genet.* 32, 453–458. doi: 10.1038/ng1007

Conflict of Interest: The authors declare that the research was conducted in the absence of any commercial or financial relationships that could be construed as a potential conflict of interest.

frontiers in Genetics

CASE REPORT
published: 18 August 2021
doi: 10.3389/fgene.2021.726116

Case Report: Identification of a Novel Homozygous Mutation in *GPD1* Gene of a Chinese Child With Transient Infantile Hypertriglyceridemia

Haihua Lin[1], *Youhong Fang*[1], *Lin Han*[2], *Jie Chen*[1], *Jingan Lou*[1] *and Jindan Yu*[1]*

[1] *Department of Gastroenterology, Zhejiang University School of Medicine Children's Hospital, National Center for Clinical Medical Research in Children Health and Disease, National Regional Medical Centre for Children, Hangzhou, China,*
[2] *Running Gene Inc., Beijing, China*

Transient infantile hypertriglyceridemia is a rare autosomal recessive disorder characterized by hypertriglyceridemia, hypohepatia, hepatomegaly, hepatic steatosis and fibrosis in infancy. Mutations in *GPD1* gene are considered the causative factor but the underlying mechanism of this disorder is still enigmatic. To date, only 24 different *GPD1* mutations have been reported in the literature worldwide with transient infantile hypertriglyceridemia or relevant conditions. Here we report a Chinese girl who developed hepatomegaly hepatic steatosis, elevated transaminase and hypertriglyceridemia from the age of 4 months. A novel homozygous variant c.454C>T (p.Q152*) was found in *GPD1* gene by next-generation sequencing. This patient is the 3rd Asian reported with transient infantile hypertriglyceridemia. We summarized the clinical presentations of transient infantile hypertriglyceridemia and also expanded the spectrum of disease-causing mutations in *GPD1*.

Keywords: glycerol-3-phosphate dehydrogenase 1, transient infantile hypertriglyceridemia, hepatomegaly, hypohepatia, hepatic steatosis, next-generation sequencing

OPEN ACCESS

Edited by:
Emiliano González Vioque, University Clinical Hospital of Santiago, Spain

Reviewed by:
Junling Wang, Central South University, China
Mara Marongiu, Institute of Genetic and Biomedical Research, National Research Council (CNR), Italy

***Correspondence:**
Jindan Yu
yjd0610@163.com

Specialty section:
This article was submitted to Genetics of Common and Rare Diseases, a section of the journal Frontiers in Genetics

Received: *16 June 2021*
Accepted: *19 July 2021*
Published: *18 August 2021*

Citation:
Lin H, Fang Y, Han L, Chen J, Lou J and Yu J (2021) Case Report: Identification of a Novel Homozygous Mutation in GPD1 Gene of a Chinese Child With Transient Infantile Hypertriglyceridemia. Front. Genet. 12:726116. doi: 10.3389/fgene.2021.726116

INTRODUCTION

Transient infantile hypertriglyceridemia (HTGTI; OMIM#614480) is a rare disorder with an autosomal recessive pattern of inheritance. Most patients with HTGTI present with transient hypertriglyceridemia, elevated transaminases, early-onset hepatomegaly, persistent fatty liver and hepatic fibrosis. Rare phenotypes include fasting hypoglycemia, kidney disease, obesity, insulin resistance, dermal abnormalities and short stature (Dionisi-Vici et al., 2016; Li et al., 2017). This condition has been considered to be caused by mutations in the *GPD1* gene (OMIM#138420) which encodes the intracellular isomer of glycerol-3-phosphate dehydrogenase 1 (GPD1). A total of 31 mutations in the *GPD1* gene have been reported in Human Gene Mutation Database (HGMD) (Stenson et al., 2017), of which only 24 mutations have been described with HTGTI or associated phenotypes worldwide (Basel-Vanagaite et al., 2012; Joshi et al., 2014; Di Resta et al., 2015; Dionisi-Vici et al., 2016; Dron et al., 2017, 2020; Li et al., 2017, 2018; D'erasmo et al., 2019; Matarazzo et al., 2020). Herein we report a Chinese girl with a hitherto unreported homozygous variant of the *GPD1* gene, who presented with elevated transaminases, massive hepatomegaly, hepatic steatosis and hypertriglyceridemia from the age of 4 months.

CASE PRESENTATION

The patient is a 4-year-old Chinese girl born via cesarean section without remarkable complications. Her weight at birth was 3.15 kg (50th percentile) and her height was 50 cm (50th percentile). Her parents were both healthy and non-consanguineous. Her older brother was physically healthy (**Figure 1A**). The patient has no relevant family history of the disease. No liver dysfunction, hyperlipidemia, or hepatic steatosis has been found in the patient's parents or brother.

The patient suffered from bronchopneumonia at the age of 4 months and 5 days. During this period, liver dysfunction was noticed. After recovering from bronchopneumonia, the patient was referred to our hospital for further examination and treatment due to persistent elevations in liver transaminase. At her physical examination at the age of 4 months, her weight was 5.8 kg (6th percentile) and her height was 61.2 cm (17th percentile). She presented with marked hepatomegaly but splenomegaly. She showed normal growth and psychomotor development. In laboratorial examinations, her results of liver function tests were abnormal. Her alanine aminotransferase (ALT, 107 U/L, reference range (r.r): 0–60 U/L), aspartate aminotransferase (AST, 186 U/L, r.r: 0–60 U/L), γ-glutamyl transpeptidase (γ-GT, 265 U/L, r.r: 0–50 U/L) and total bile acids (18.2 μmol/L, r.r: 0–10 μmol/L) were highly elevated. Blood lipid test also showed elevated triglycerides (TG, 4.39 mmol/L, r.r < 1.7 mmol/L). The levels of total cholesterol, lipoprotein, bilirubin, coagulation test and albumin were within normal limits. Further workups including routine blood test, blood glucose, electrolytes, serum ammonia, lactic acid levels, fatty acids, ceruloplasmin, serological markers for viruses (cytomegalovirus, Epstein-Barr virus, hepatitis virus), toxoplasmosis, thyroid function, creatinine, uric acid, autoimmune serology and immunoglobulin levels, all of which showed normal results. B-mode ultrasound of the liver showed diffuse hepatomegaly with increased echogenicity (**Figure 1B**). Contrast-enhanced abdominal CT suggested significant hepatomegaly with fatty changes (**Figure 1C**). No splenomegaly was observed. The results of echocardiogram showed atrial septal interruption (*Φ* 0.31 cm). No abnormalities were observed in electrocardiogram (ECG), chest radiographs, portal vein and inferior vena cava

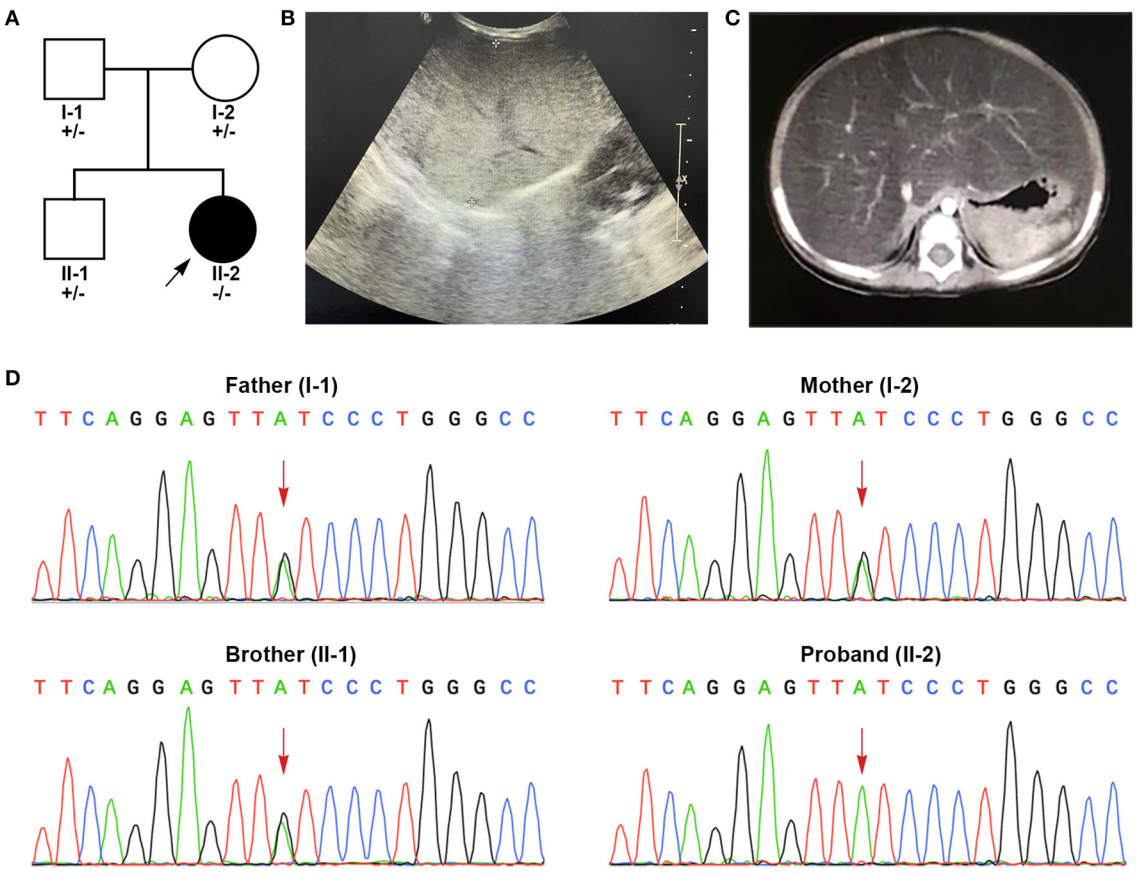

FIGURE 1 | Clinical features and genetic sequencing data of the patient. **(A)** The pedigree of the family. **(B)** B-mode ultrasound demonstrated diffuse hyperechogenicity of the liver with a fine granular pattern. **(C)** Contrast-enhanced CT scan of abdomen shows a significantly enlarged liver with fatty change. **(D)** Sanger sequencing shows that the patient harbored homozygous mutations (c.454C>T, p.Q152*) in exon 6. The patient's parents and brother were all heterozygous for this mutation.

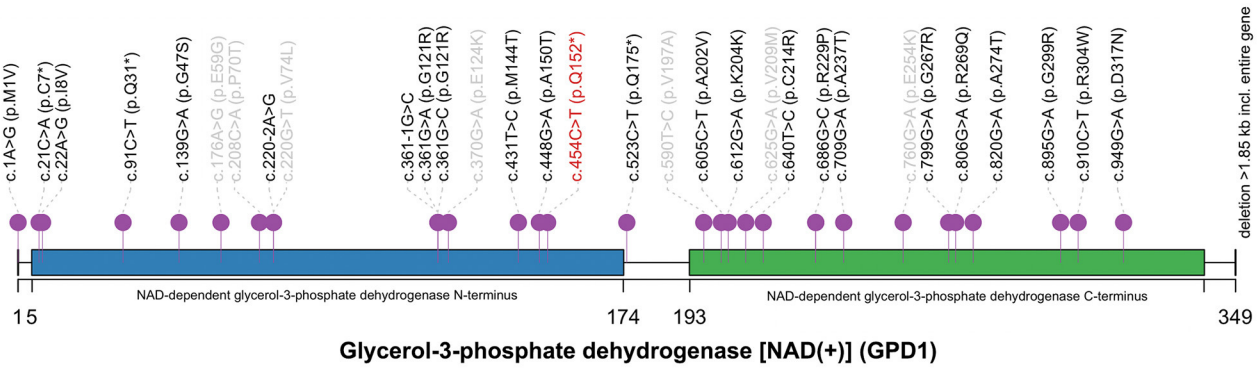

FIGURE 2 | The spectrum of *GPD1* mutations reported in HGMD database. The novel variant c.454C>T (p.Q152*) (red) located in NAD-dependent glycerol-3-phosphoate dehydrogenase N-terminus. Twenty-four mutations relevant to HTGTI are marked in black. Seven mutations not associated with HTGTI are labeled in gray. This spectrum was generated by R with trackViewer: lollipopPlot (Ou and Zhu, 2019).

ultrasonography. Liver biopsy was recommended but her parents refused.

After administrating compound glycyrrhizin tablets (half tablet per day) (Each tablet contains 25 mg glyeyrrhizin, 35 mg monoammonium glycyrrhizinate, 25 mg aminoacetic acid and 25 mg methionine; Minophagen Pharmaceutical Co., Ltd., Japan) for 3 months, her transaminase levels decreased but remained above normal (ALT, 85 U/L; AST, 127 U/L; γ-GT, 258 U/L.). At 3.5 years old, her TG and transaminases were at normal levels and her abdominal ultrasound showed that her liver was smaller in size than before. At the age of 4, her weight was 13 kg (3rd percentile) and her height was 94 cm (3rd percentile). Except for short stature, no other symptoms were presented.

GENETIC ANALYSIS

The patient was suspected with hereditary metabolic liver disease due to a combination of elevated liver transaminases, hypertriglyceridemia and hepatomegaly. Peripheral blood samples of the patient, her parents and her brother were collected and sent to Running Gene Inc. (Beijing, China) for next-generation sequencing (NGS). DNA samples were extracted using the QIAamp DNA Blood Midi Kit (Qiagen, Hilden, Germany) and quantified using Nanodrop spectral analysis (Thermo Fischer Scientific, Inc., Waltham, MA). The patient's genomic DNA was fragmented into 200–300 bp for sequencing library generation by KAPA Library Preparation Kit (#KR0453, Kapa Biosystems, Wilmington, MA). Pooled libraries were screened by the customized xGen Inherited-Diseases-Panel Probe. The captured libraries were sequenced by the Illumina hiseq2500 Analyzers (Illumina, San Diego, CA). Single-nucleotide variants and indels were called and filtered based on multiple databases [ExAC (Lek et al., 2016), gnomAD (Karczewski et al., 2020), 1kGenome (Genomes Project et al., 2015), ESP6000 (Fu et al., 2013), ClinVar (Landrum and Kattman, 2018), and HGMD]. Candidate variants were classified according to the American College of Medical Genetics and Genomics (ACMG) guidelines (Richards et al., 2015). Suspected pathogenic variants were then verified in the proband and her parents by Sanger sequencing.

A pair of homozygous non-sense variant c.454C>T (p.Q152*) was identified in the *GPD1* gene (NM_001257199). The mutated variants of the proband were inherited from her parents, in fact, the same variant was also found in heterozygosis in her parents and her brother, consistent with the pattern of recessive inheritance (**Figure 1D**). This variant, which has not been recorded in any public databases, is novel. Variant c.454C>T altered codon for Glu152 to a termination codon, which may produce a truncated protein or lead to non-sense-mediated mRNA decay (PVS1). This variant is located in N-terminal NAD-dependent glycerol-3-phosphate dehydrogenase (**Figure 2**) (PM1) and absent from controls (ExAC, gnomAD, 1kGenome, ESP6000) (PM2). Multiple software predicted the variant as deleterious [MutationTaster2 (Schwarz et al., 2014), 1.000, disease causing; Ba+Del_addAF (Feng, 2017), 0.625 > cutoff = 0.069, deleterious; CADD (Rentzsch et al., 2019), 35 > 15, damaging; fathmmMKL-inherited (Shihab et al., 2013), 0.927 > 0.5, damaging.] (PP3). Thus, c.454C>T (p.Q152*) is classified as a pathogenic variant (PVS1+PM1+PM2+PP3), according to the ACMG guidelines.

DISCUSSION

GPD1 mutation related to HTGTI was first discovered by Basel-Vanagaite et al. in 10 family members of four highly consanguine Israeli Arab families carrying c.361-1G>C (Basel-Vanagaite et al., 2012). Subsequently, nine articles described extra 30 mutations of *GPD1* gene associated with HTGTI, chylomicronemia syndrome, Brugada syndrome or low HDL cholesterol, respectively. Only six articles worldwide described complete clinical presentation and genetic data of 18 patients with HTGTI or relevant phenotypes, and we summarized them with our current patient (**Table 1**). The mean age of onset was about 10 months, with a median age of 5 months. The gender

TABLE 1 | Clinical and genetic characteristics of *GPD1*-associated 19 HTGTI patients whose data are available.

References	Case	Onset age (m)	Gender (M:F, 11:8)	Mutations in *GPD1* gene	Hypertriglyceridemia (Elevated TG) (18/19)	Last TG	Hypohepatia (Elevated transaminases) (18/19)	Last transaminases	Hepatomegaly (18/18)	Splenomegaly (4/11)	Hepatic steatosis (19/19)	Other features
Present	1	4	F	c.454C>T, p.Q152*	+	−	+	−	+	−	+	TBA elevation; Failure to thrive; Short stature
Li et al. (2017)	2	84	M	c.220-2A>G; c.820G>A, p.A274T	−	−	−	−	NA	NA	+	Short stature; Obesity; Insulin resistance; Dermal abnormalities; EDL
Basel-Vanagaite et al. (2012)	3	1	M	c.361-1G>C, p.I119fs*94	+	↑	+	−	+	NA	+	Vomiting
Basel-Vanagaite et al. (2012)	4	1	M	c.361-1G>C, p.I119fs*94	+	↑	+	↑	+	NA	+	Vomiting; Hepatic fibrosis;
Basel-Vanagaite et al. (2012)	5	4–6	M	c.361-1G>C, p.I119fs*94	+	↑	+	−	+	−	+	Short stature; Hepatic fibrosis
Basel-Vanagaite et al. (2012)	6	At birth	M	c.361-1G>C, p.I119fs*94	+	−	+	↑	+	+	+	Short stature
Basel-Vanagaite et al. (2012)	7	6	F	c.361-1G>C, p.I119fs*94	+	↑	+	↑	+	NA	+	Failure to thrive
Basel-Vanagaite et al. (2012)	8	2.5	F	c.361-1G>C, p.I119fs*94	+	−	+	−	+	−	+	Vomiting
Basel-Vanagaite et al. (2012)	9	7	F	c.361-1G>C, p.I119fs*94	+	−	+	↑	+	+	+	-
Basel-Vanagaite et al. (2012)	10	7	F	c.361-1G>C, p.I119fs*94	+	↑	+	↑	+	+	+	-
Basel-Vanagaite et al. (2012)	11	9	M	c.361-1G>C, p.I119fs*94	+	↑	+	↑	+	−	+	Short stature; Horseshoe kidney
Basel-Vanagaite et al. (2012)	12	3.5	M	c.361-1G>C, p.I119fs*94	+	↑	+	↑	+	−	+	Short stature; Craniocerebral involvement
Dionisi-Vici et al. (2016)	13	12	F	c.361-1G>C, p.I119fs*94	+	−	+	NA	+	NA	+	-
Li et al. (2018)	14	3.5	F	c.523C>T, p.Q175*	+	↑	+	↑	+	-	+	TBA elevation; Portal fibrosis
Dionisi-Vici et al. (2016)	15	5	M	c.640T>C, p.C214R	+	↑	+	↑	+	+	+	Consanguineous parents; TBA elevation; Cirrhosis; Dicarboxylic aciduria
Dionisi-Vici et al. (2016)	16	24	M	c.640T>C, p.C214R	+	↑	+	NA	+	NA	+	Portal and periportal Fibrosis
Joshi et al. (2014)	17	At birth	F	Deletion >1.85 kb including entire *GPD1*; c.686G>C, p.R229P	+	↑	+	NA	+	NA	+	Small head circumference; Failure to thrive; Vomiting
Dionisi-Vici et al. (2016)	18	10	M	c.806G>A, p.R269Q	+	−	+	↑	+	NA	+	Consanguineous parents; Fasting hypoglycemia; Portal and bridging fibrosis
Matarazzo et al. (2020)	19	12	M	c.895G>A, p.G299R	+	−	+	↑	+	−	+	TBA elevation

EDL, elevated dehydroepiandrosterone sulfate and lipoprotein-α levels; NA, not available; TBA, total bile acid; TG, triglyceride; m, months; y, years.

ratio (male to female) is 1.375 (11:8). Common clinical features of *GPD1*-associated patients are hepatic steatosis (100%, 19/19), hepatomegaly (100%, 18/18), hypertriglyceridemia (95%, 18/19), and hypohepatia (elevated liver transaminases) (95%, 18/19). Other phenotypes, including splenomegaly (4/11), fibrosis (6/19), short stature (6/19), vomiting (4/19), elevated total bile acids (4/19), and failure to thrive (3/19), are also involved. The affected individuals tended to vomit and fail to thrive as the first symptoms, but more than half of cases were asymptomatic. A third of patients had a liver biopsy, showing steatosis with varying degrees of fibrosis. Our patient has characteristics of *GPD1* deficiency includes early-onset, elevated ALT and γ-GT levels, hypertriglyceridemia, fatty liver and mild failure to thrive. The clinical manifestations were similar to the 18 patients described in the previous articles (Basel-Vanagaite et al., 2012; Joshi et al., 2014; Dionisi-Vici et al., 2016; Li et al., 2017, 2018; Matarazzo et al., 2020). Although phenotypic studies of *GPD1* mutations have focused on dyslipidemia and secondary hepatic metabolic disorders, the clinical features of patients reported by Dionisi-Vici et al. were slightly different from other reported cases. One patient had recurrent fasting hypoglycemia; the second presented with severe liver disease with intrahepatic cholestasis involving the kidney. A patient with rare phenotypes (obesity, insulin resistance, pimple, acanthosis nigricans, hypertrichosis and short stature) was also reported (Li et al., 2017). Based on the available case reports, the severity of the clinical phenotype of *GPD1* mutation-associated HTGTI is independent of the type and location of the mutation site.

Although hypertriglyceridemia is a significant risk factor for coronary disease, acute pancreatitis and metabolic syndrome (Cullen, 2000; Athyros et al., 2002; Hopkins et al., 2005), all affected individuals had a relatively good medium-term prognosis. According to follow-up data from patients with *GPD1* mutations, in most patients, the TG and liver enzyme indices normalize with age and no specific treatment is required. Furthermore, no clinical evidence of coronary disease or pancreatitis has been reported, nor in the oldest patients (Basel-Vanagaite et al., 2012). Therefore, liver transplant is not recommended for patients with HTGTI. Lipid-lowering drugs are not routinely used because TG levels can be ameliorated without particular treatment. That proves the diagnosis of *GPD1* deficiency is of great significance for the management of the patients. Although no conclusions can be drawn about the risks in adulthood or long-term prognosis, sufficient attention must be given to HTGTI patients during long-term follow-up. Assessment of the growth and development and screening for abnormal indicators such as liver transaminases, total cholesterol, TG, abdominal ultrasound are recommended at follow-up visits.

Located on chromosome 12q13.12, *GPD1* gene encodes glycerol-3-phosphate dehydrogenase 1, a member of the NAD-dependent GPD family. GPD1 is a protein of 37.5 kD size that catalyzes the invertible conversion of dihydroxyacetone phosphate (DHAP) and nicotine adenine dinucleotide (NADH) to glycerol-3-phosphate (G3P) and NAD+ in the cytoplasm, working in the metabolism of carbohydrate and lipid (Menaya et al., 1995; Ou et al., 2006; Basel-Vanagaite et al., 2012). Along with GPD2 (mitochondrial), GPD1 (cytosolic) also forms a glycerol phosphate shuttle which plays an important role in the transport of reducing equivalents from the cytosol to mitochondria, resulting in the reoxidation of NADH formed from glycolysis and the regeneration of NAD+ in the brain and skeletal muscle.

A total of 31 mutations of *GPD1* were reported in HGMD, including 24 mutations associated with HTGTI or relative phenotypes. Of these 24 mutations, only 11 mutations are disease-causing (DM) and 13 are possibly disease-causing (DM?). Including our current novel variant, only four non-sense have been reported in *GPD1* and they are all classified as DM. However, the underlying mechanism of HTGTI caused by *GPD1* mutations is still unknown. Only a few theories have been hypothesized and studied. Since the availability of G3P has been considered as a regulatory factor of TG synthesis, it has been suggested that *GPD1* mutations may cause an increase in the amount of hepatic G3P available for TG synthesis by limiting the conversion of G3P to DHAP, consequently leading to elevated TG (Basel-Vanagaite et al., 2012). Intriguingly, as the conversion is from DHAP to G3P under physiological conditions, it is also possible that DHAP may not be converted to G3P due to the lack of *GPD1*, resulting in a relative surplus of DHAP and a decrease in G3P. This theory has been demonstrated in a mouse model of *GPD1* deficiency (Macdonald and Marshall, 2000). DHAP can be acylated firstly then reduced to 1-acyl-sn-G3P. The acyl DHAP pathway also plays a significant role in the synthesis of glycerides in the liver (Athenstaedt and Daum, 2000; Zheng and Zou, 2001). The pathogenesis of fatty liver in HTGTI patients may be caused by excessive DHAP acylation. *GPD1* mutations lead to increased TG synthesis in the liver, decreased output from the liver, increased inflow of fatty acids into the liver, and impaired hepatic beta-oxidation causing non-alcoholic hepatic steatosis (NASH) (Dionisi-Vici et al., 2016). In two of the studies, *in vitro* functional studies using cell experiments confirmed the pathogenicity of the c.361-1G>C, c.220-2A>G and c.820G>A mutations (Basel-Vanagaite et al., 2012; Li et al., 2017). Only one of the affected individuals described in the above studies has an overweight body mass index, which refutes the role of obesity in the pathophysiology of the development of hepatic steatosis in these individuals. The pathogenesis of each symptom in *GPD1*-associated HTGTI requires more clinical and basic medical research to be explored.

In summary, this study reported a Chinese HTGTI patient and also expanded the spectrum of disease-causing mutations in *GPD1* gene. In future clinical diagnosis, *GPD1* deficiency should be considered if hypertriglyceridemia, elevated liver enzymes, hepatomegaly, hepatic steatosis and fibrosis are present in early infancy. When the cause cannot be determined by traditional clinical examination, NGS is a promising approach to help clinical diagnosis and guide clinical management.

DATA AVAILABILITY STATEMENT

The original contributions presented in the study are included in the article/supplementary materials, further inquiries can be directed to the corresponding author. Genetic sequencing data are available in Sequence Read Archive (SRA) by PRJNA747113.

ETHICS STATEMENT

This study was reviewed and approved by the Research Ethics Committee of The Children's Hospital, Zhejiang University School of Medicine (2020-IRB-166, November 16, 2020). Written informed consent was obtained from the patient's parents for the investigation and publication of this article.

AUTHOR CONTRIBUTIONS

HL analyzed and interpreted the patient data and drafted the manuscript. JC and JL were responsible for guiding the diagnosis and treatment of the patient. LH analyzed sequencing data, produced figures, and made a significant contribution to the manuscript. YF contributed to gathering patient data and was a major contributor in writing the manuscript. HL and LH reviewed the final manuscript. All authors read and approved the final manuscript.

ACKNOWLEDGMENTS

We thank the patient's family for their cooperation. We are also grateful for the warm helps from physicians, nurses, and technicians who supported us.

REFERENCES

Athenstaedt, K., and Daum, G. (2000). 1-Acyldihydroxyacetone-phosphate reductase (Ayr1p) of the yeast Saccharomyces cerevisiae encoded by the open reading frame YIL124w is a major component of lipid particles. *J. Biol. Chem.* 275, 235–240. doi: 10.1074/jbc.275.1.235

Athyros, V. G., Giouleme, O. I., Nikolaidis, N. L., Vasiliadis, T. V., Bouloukos, V. I., Kontopoulos, A. G., et al. (2002). Long-term follow-up of patients with acute hypertriglyceridemia-induced pancreatitis. *J. Clin. Gastroenterol.* 34, 472–475. doi: 10.1097/00004836-200204000-00020

Basel-Vanagaite, L., Zevit, N., Har Zahav, A., Guo, L., Parathath, S., Pasmanik-Chor, M., et al. (2012). Transient infantile hypertriglyceridemia, fatty liver, and hepatic fibrosis caused by mutated GPD1, encoding glycerol-3-phosphate dehydrogenase 1. *Am. J. Hum. Genet.* 90, 49–60. doi: 10.1016/j.ajhg.2011.11.028

Cullen, P. (2000). Evidence that triglycerides are an independent coronary heart disease risk factor. *Am. J. Cardiol.* 86, 943–949. doi: 10.1016/S0002-9149(00)01127-9

D'erasmo, L., Di Costanzo, A., Cassandra, F., Minicocci, I., Polito, L., Montali, A., et al. (2019). Spectrum of mutations and long-term clinical outcomes in genetic chylomicronemia syndromes. *Arterioscler. Thromb. Vasc. Biol.* 39, 2531–2541. doi: 10.1161/ATVBAHA.119.313401

Di Resta, C., Pietrelli, A., Sala, S., Della Bella, P., De Bellis, G., Ferrari, M., et al. (2015). High-throughput genetic characterization of a cohort of Brugada syndrome patients. *Hum. Mol. Genet.* 24, 5828–5835. doi: 10.1093/hmg/ddv302

Dionisi-Vici, C., Shteyer, E., Niceta, M., Rizzo, C., Pode-Shakked, B., Chillemi, G., et al. (2016). Expanding the molecular diversity and phenotypic spectrum of glycerol 3-phosphate dehydrogenase 1 deficiency. *J. Inherit. Metab. Dis.* 39, 689–695. doi: 10.1007/s10545-016-9956-7

Dron, J. S., Wang, J., Low-Kam, C., Khetarpal, S. A., Robinson, J. F., Mcintyre, A. D., et al. (2017). Polygenic determinants in extremes of high-density lipoprotein cholesterol. *J. Lipid Res.* 58, 2162–2170. doi: 10.1194/jlr.M079822

Dron, J. S., Wang, J., Mcintyre, A. D., Iacocca, M. A., Robinson, J. F., Ban, M. R., et al. (2020). Six years' experience with LipidSeq: clinical and research learnings from a hybrid, targeted sequencing panel for dyslipidemias. *BMC Med. Genomics* 13:23. doi: 10.1186/s12920-020-0669-2

Feng, B. J. (2017). PERCH: a unified framework for disease gene prioritization. *Hum. Mutat.* 38, 243–251. doi: 10.1002/humu.23158

Fu, W., O'connor, T. D., Jun, G., Kang, H. M., Abecasis, G., Leal, S. M., et al. (2013). Analysis of 6,515 exomes reveals the recent origin of most human protein-coding variants. *Nature* 493, 216–220. doi: 10.1038/nature11690

Genomes Project, C., Auton, A., Brooks, L. D., Durbin, R. M., Garrison, E. P., Kang, H. M., et al. (2015). A global reference for human genetic variation. *Nature* 526, 68–74. doi: 10.1038/nature15393

Hopkins, P. N., Wu, L. L., Hunt, S. C., and Brinton, E. A. (2005). Plasma triglycerides and type III hyperlipidemia are independently associated with premature familial coronary artery disease. *J. Am. Coll. Cardiol.* 45, 1003–1012. doi: 10.1016/j.jacc.2004.11.062

Joshi, M., Eagan, J., Desai, N. K., Newton, S. A., Towne, M. C., Marinakis, N. S., et al. (2014). A compound heterozygous mutation in GPD1 causes hepatomegaly, steatohepatitis, and hypertriglyceridemia. *Eur. J. Hum. Genet.* 22, 1229–1232. doi: 10.1038/ejhg.2014.8

Karczewski, K. J., Francioli, L. C., Tiao, G., Cummings, B. B., Alfoldi, J., Wang, Q., et al. (2020). The mutational constraint spectrum quantified from variation in 141,456 humans. *Nature* 581, 434–443. doi: 10.1038/s41586-020-2308-7

Landrum, M. J., and Kattman, B. L. (2018). ClinVar at five years: delivering on the promise. *Hum. Mutat.* 39, 1623–1630. doi: 10.1002/humu.23641

Lek, M., Karczewski, K. J., Minikel, E. V., Samocha, K. E., Banks, E., Fennell, T., et al. (2016). Analysis of protein-coding genetic variation in 60,706 humans. *Nature* 536, 285–291. doi: 10.1038/nature19057

Li, J. Q., Xie, X. B., Feng, J. Y., Chen, L., Abuduxikuer, K., Lu, Y., et al. (2018). A novel homozygous mutation in the glycerol-3-phosphate dehydrogenase 1 gene in a Chinese patient with transient infantile hypertriglyceridemia: a case report. *BMC Gastroenterol.* 18:96. doi: 10.1186/s12876-018-0827-6

Li, N., Chang, G., Xu, Y., Ding, Y., Li, G., Yu, T., et al. (2017). Biallelic mutations in GPD1 gene in a Chinese boy mainly presented with obesity, insulin resistance, fatty liver, and short stature. *Am. J. Med. Genet. A* 173, 3189–3194. doi: 10.1002/ajmg.a.38473

Macdonald, M. J., and Marshall, L. K. (2000). Mouse lacking NAD+-linked glycerol phosphate dehydrogenase has normal pancreatic beta cell function but abnormal metabolite pattern in skeletal muscle. *Arch. Biochem. Biophys.* 384, 143–153. doi: 10.1006/abbi.2000.2107

Matarazzo, L., Ragnoni, V., Malaventura, C., Leon, A., Colavito, D., Vigna, G. B., et al. (2020). Successful fenofibrate therapy for severe and persistent hypertriglyceridemia in a boy with cirrhosis and glycerol-3-phosphate dehydrogenase 1 deficiency. *JIMD Rep.* 54, 25–31. doi: 10.1002/jmd2.12125

Menaya, J., Gonzalez-Manchon, C., Parrilla, R., and Ayuso, M. S. (1995). Molecular cloning, sequencing and expression of a cDNA encoding a human liver NAD-dependent alpha-glycerol-3-phosphate dehydrogenase. *Biochim. Biophys. Acta* 1262, 91–94. doi: 10.1016/0167-4781(95)00069-S

Ou, J., and Zhu, L. J. (2019). trackViewer: a Bioconductor package for interactive and integrative visualization of multi-omics data. *Nat Methods* 16, 453–454. doi: 10.1038/s41592-019-0430-y

Ou, X., Ji, C., Han, X., Zhao, X., Li, X., Mao, Y., et al. (2006). Crystal structures of human glycerol 3-phosphate dehydrogenase 1 (GPD1). *J. Mol. Biol.* 357, 858–869. doi: 10.1016/j.jmb.2005.12.074

Rentzsch, P., Witten, D., Cooper, G. M., Shendure, J., and Kircher, M. (2019). CADD: predicting the deleteriousness of variants throughout the human genome. *Nucleic Acids Res.* 47, D886–D894. doi: 10.1093/nar/gky1016

Richards, S., Aziz, N., Bale, S., Bick, D., Das, S., Gastier-Foster, J., et al. (2015). Standards and guidelines for the interpretation of sequence variants: a joint consensus recommendation of the American College of Medical Genetics and Genomics and the Association for Molecular Pathology. *Genet. Med.* 17, 405–424. doi: 10.1038/gim.2015.30

Schwarz, J. M., Cooper, D. N., Schuelke, M., and Seelow, D. (2014). MutationTaster2: mutation prediction for the deep-sequencing age. *Nat. Methods* 11, 361–362. doi: 10.1038/nmeth.2890

Shihab, H. A., Gough, J., Cooper, D. N., Stenson, P. D., Barker, G. L., Edwards, K. J., et al. (2013). Predicting the functional, molecular, and phenotypic consequences of amino acid substitutions using hidden Markov models. *Hum. Mutat.* 34, 57–65. doi: 10.1002/humu.22225

Stenson, P. D., Mort, M., Ball, E. V., Evans, K., Hayden, M., Heywood, S., et al. (2017). The Human Gene Mutation Database: towards a

comprehensive repository of inherited mutation data for medical research, genetic diagnosis and next-generation sequencing studies. *Hum. Genet.* 136, 665–677. doi: 10.1007/s00439-017-1779-6

Zheng, Z., and Zou, J. (2001). The initial step of the glycerolipid pathway: identification of glycerol 3-phosphate/dihydroxyacetone phosphate dual substrate acyltransferases in Saccharomyces cerevisiae. *J. Biol. Chem.* 276, 41710–41716. doi: 10.1074/jbc.M104749200

Conflict of Interest: LH is employed by Running Gene Inc., Beijing, China.

The remaining authors declare that the research was conducted in the absence of any commercial or financial relationships that could be construed as a potential conflict of interest.

Publisher's Note: All claims expressed in this article are solely those of the authors and do not necessarily represent those of their affiliated organizations, or those of the publisher, the editors and the reviewers. Any product that may be evaluated in this article, or claim that may be made by its manufacturer, is not guaranteed or endorsed by the publisher.

frontiers in Pediatrics

CASE REPORT
published: 27 August 2021
doi: 10.3389/fped.2021.728077

Case Report: Diffuse Polymicrogyria Associated With a Novel *ADGRG1* Variant

Fábio Carneiro[1], *Júlia Duarte*[2], *Francisco Laranjeira*[3], *Sofia Barbosa-Gouveia*[4], *María-Luz Couce*[4]* *and Maria José Fonseca*[5]

[1] *Neurology Department, Hospital Garcia de Orta, Almada, Portugal,* [2] *Neuroradiology Department, Hospital Garcia de Orta, Almada, Portugal,* [3] *Biochemical Genetics Unit, Centro de Genética Médica Doutor Jacinto Magalhães, Porto, Portugal,* [4] *Unit of Diagnosis and Treatment of Congenital Metabolic Diseases, Hospital Clínico Universitario de Santiago de Compostela, Instituto de Investigación Sanitaria de Santiago de Compostela, Centro de Investigación Biomédica en Red de Enfermedades Raras, European Reference Network for Rare Hereditary Metabolic Disorders, Santiago de Compostela, Spain,* [5] *Child Development Centre Torrado da Silva, Hospital Garcia de Orta, Almada, Portugal*

Pathogenic variants of the *ADGRG1* gene are associated with bilateral frontoparietal polymicrogyria, defined radiologically by polymicrogyria with an anterior-posterior gradient, pontine and cerebellar hypoplasia and patchy white matter abnormalities. We report a novel homozygous *ADGRG1* variant with atypical features. The patient presented at 8 months of age with motor delay, esotropia, hypotonia with hyporeflexia and subsequently developed refractory epilepsy. At the last assessment, aged 12 years, head control, sitting and language were not acquired. Magnetic resonance imaging revealed diffuse polymicrogyria with relative sparing of the anterior temporal lobes, without an anterior-posterior gradient, diffuse hypomyelination and pontine and cerebellar hypoplasia. A panel targeting brain morphogenesis defects yielded an unreported homozygous *ADGRG1* nonsense variant (dbSNP rs746634404), present in the heterozygous state in both parents. We report a novel *ADGRG1* variant associated with diffuse polymicrogyria without an identifiable anterior-posterior gradient, diffuse hypomyelination and a severe motor and cognitive phenotype. Our case highlights the phenotypic diversity of *ADGRG1* pathogenic variants and the clinico-anatomical overlap between recognized polymicrogyria syndromes.

Keywords: *ADGRG1*, bilateral generalized polymicrogyria, *GPR56*, polymicrogyria, bilateral frontoparietal polymicrogyria, case report

OPEN ACCESS

Edited by:
Enrico Baruffini, University of Parma, Italy

Reviewed by:
Vishal Sondhi, Armed Forces Medical College, Pune, India
Hsi-Hsien Lin, Chang Gung University, Taiwan
Sultan Cingöz, Dokuz Eylul University, Turkey

***Correspondence:**
María-Luz Couce
maria.luz.couce.pico@sergas.es

Specialty section:
This article was submitted to Genetics of Common and Rare Diseases, a section of the journal Frontiers in Pediatrics

Received: *20 June 2021*
Accepted: *04 August 2021*
Published: *27 August 2021*

Citation:
Carneiro F, Duarte J, Laranjeira F, Barbosa-Gouveia S, Couce M-L and Fonseca MJ (2021) Case Report: Diffuse Polymicrogyria Associated With a Novel ADGRG1 Variant. Front. Pediatr. 9:728077. doi: 10.3389/fped.2021.728077

INTRODUCTION

Polymicrogyria (PMG) is a cortical malformation characterized by supernumerary, small gyri with abnormal cortical lamination. PMG syndromes are markedly heterogeneous in etiology and phenotype, including infectious or vascular causes as well as genetically defined multiple congenital anomaly syndromes or inborn errors of metabolism. PMG can also occur in isolation (unilateral or bilateral PMG syndromes), frequently with a genetic etiology (1). Bilateral PMG syndromes are further categorized according to the topographical distribution of the abnormal gyral pattern into bilateral frontoparietal (BFPP), bilateral generalized (BGP), bilateral perisylvian, bilateral posterior or bilateral parasagittal PMG (1).

Autosomal recessive pathogenic variants of *GPR56* or *ADGRG1* (OMIM*604110; henceforth designated as *ADGRG1*), a member of the family of G protein–coupled receptors (GPCRs), were found to be specifically associated with BFPP (2, 3). BFPP is radiologically defined by the presence of PMG with an anterior to posterior gradient, bilateral patchy white matter signal changes and brainstem and cerebellar hypoplasia or dysplasia (3). The clinical phenotype consists of early onset hypotonia with subsequent motor and cognitive developmental delay, seizures and eye abnormalities (strabismus and/or nystagmus) (3). We herein report a novel *ADGRG1* variant causing a generalized PMG pattern and a severe clinical phenotype.

CASE PRESENTATION

The proband is a 12-year-old male, the second-child of consanguineous parents (first degree cousins). The family history is relevant for learning disabilities and motor delay in a paternal aunt and learning disabilities in a paternal uncle. Notably, the patient's older brother by 9 years has no history of developmental delay or learning difficulties.

Gestation and birth were uneventful and in the post-natal period the patient only presented neonatal jaundice (maximal bilirubin dosing 12.4 mg/dL) treated with phototherapy.

Global development was reportedly normal until 6 months of age, when hypotonia and failure to achieve motor milestones were first noticed and the patient was referred to our Child Neurology outpatient clinic (**Figure 1**). On first assessment, at 8 months of age, the general examination showed mild dysmorphic features (almond eyes, long philtrum and low-set ears) without other relevant findings. Neurological examination revealed bilateral alternating esotropia and predominantly upper limb and axial hypotonia with diminished reflexes. We found a significant delay in psychomotor development, cephalic control was not present and the patient was unable to sit. There was poor social interaction, only few vocalizations and no hand manipulation. The initial magnetic resonance imaging (MRI) at 9 months revealed diffuse polymicrogyria without an identifiable anterior-posterior gradient, diffuse hypomyelination, thin corpus callosum, supratentorial ventriculomegaly and pontine and cerebellar hypoplasia, affecting both cerebellar vermis and hemispheres. There were no abnormalities on the electroencephalogram (EEG). The patient underwent an evaluation for chromosomal abnormalities, fragile-X mutation, imprinting disorders, mitochondrial DNA and ATPase 6 mutations, comprehensive blood, urine and cerebrospinal fluid (CSF) metabolic screening and muscle biopsy with assessment of respiratory chain enzymatic activity, which were all normal. There was no evidence of systemic disease on echocardiogram, liver, renal and spleen ultrasounds.

At 14 months, the patient developed focal seizures with impaired consciousness (behavioral arrest and eye deviation) initially responsive to valproate. The EEG showed predominantly frontal spikes and spike-waves, within a normal background.

The patient progressed very slowly and was able to maintain cephalic control and an unaided sitting position at 21 months. He was able to maintain eye contact, smile and produce elementary sounds, but language was not present.

At 2.5 years, however, there was significant motor and cognitive regression with loss of cephalic control and unsupported sitting ability and poorer interaction. Simultaneously, a gradual worsening of epilepsy was observed, with the appearance of multiple seizure types including epileptic spasms, atonic, myoclonic and tonic-clonic bilateral seizures. The EEG showed slow background activity with multifocal, anterior or centro-parietal predominant, spikes and spike-waves. The patient was subsequently treated with several anti-epileptics including vigabatrin, levetiracetam, topiramate, clonazepam, and perampanel, with partial control of seizures, but without significant motor and cognitive improvement. Serial neurological examinations consistently showed bilateral alternating esotropia, horizontal nystagmus and flaccid tetraparesis, without pyramidal or cerebellar signs. Visual and auditory evoked-potentials revealed prolonged conduction times bilaterally. Repeat MRI at 11 years of age (**Figure 2**) was globally consistent with the above-mentioned features.

Genetic analysis with a next-generation sequencing panel targeting brain morphogenesis defects yielded a homozygous *ADGRG1* nonsense variant (rs746634404), caused by a nucleotide change [(NM_001145771.2: c.1504C>T) (NP_005673.3: p.Arg502Ter)] in exon 12. This variant is not present homozygously in GnomAD. Segregation analysis through Sanger sequencing confirmed the presence of the variant in the homozygous state in the patient and revealed that both parents were heterozygous carriers (**Figure 3A**). The variant is located in the seven-transmembrane (7TM) domain of the *ADGRG1* protein, which binds to a heterotrimeric G-protein complex and initiates downstream signaling (**Figures 3B,C**). The reported allele is rare in the population [GnomAD frequency: $f = 0.0000119$; European (Non-Finnish): $f = 0.00000881$]. *In silico* analysis was performed using two different algorithms to predict the pathogenicity of the variant. DANN (4) (Deleterious Annotation of genetic variants using Neural Networks) is a pathogenicity scoring methodology based on neural networks, with values ranging from 0 to 1 (where 1 represents variants predicted to be most damaging). MutationTaster (5) employs a Bayes classifier to predict the disease potential of an alteration, based on evolutionary conservation, splice-site, mRNA, protein and regulatory features. The reported variant was predicted as "damaging" by DANN (DANN score: 0.9983) and as "disease causing" by MutationTaster. Finally, the level of evidence of pathogenicity was classified as "very strong" according to American College of Medical Genetics criteria (6), as the nonsense variant was identified in a gene for which loss-of-function is a known mechanism of disease.

DISCUSSION

We report a novel *ADGRG1* truncating variant, presenting with atypically diffuse PMG and hypomyelination and a severe clinical phenotype.

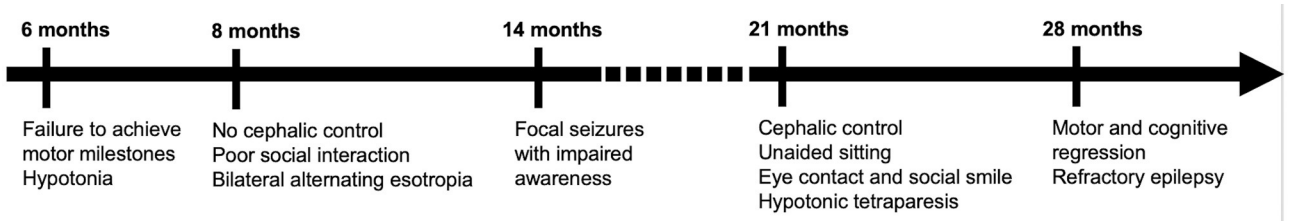

FIGURE 1 | Timeline of symptoms and signs.

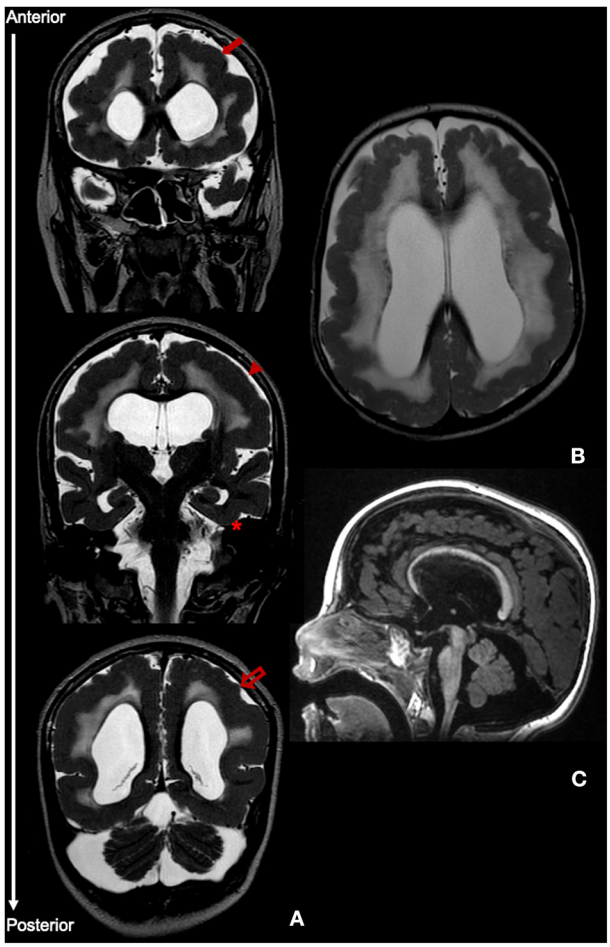

FIGURE 2 | MRI findings at age 11 years. **(A)** Coronal T2-weighted images showing PMG without an anterior-posterior gradient of involvement, including frontal cortex (closed arrow), parietal cortex (arrowhead) and occipital cortex (open arrow). There is relative sparing of the temporal lobes (asterisk). **(B)** Axial T2 image displaying diffuse white matter hypomyelination. **(C)** Sagittal T1 image highlighting pontine and cerebellar hypoplasia.

At the time of publication, *ADGRG1* pathogenic variants have been described in a total of 77 patients from 47 pedigrees and 34 different corresponding variants (2, 3, 7–20). In all reported cases, *ADGRG1* variants were associated with a typical anatomical BFPP distribution, i.e., either a restricted frontoparietal PMG or an anterior-posterior gradient of cortical malformation. However, in our case a gradient of involvement was not identified. Complete or near-complete involvement of the entire cerebral cortex without any region of maximal involvement or any gradient of severity is the hallmark of BGP (21, 22). Relative sparing of the interhemispheric or temporal gyri has been described occasionally and is present in our patient. Considering other associated imaging features, patchy white matter signal changes or white matter volume reduction are most commonly associated with BFPP while more diffuse white matter involvement is present in more than 50% of BGP patients (22). The most distinguishing feature, however, is the presence of brainstem and cerebellar involvement in BFPP, also identified in our patient, and typically absent in BGP. Therefore, we believe that the anatomical distribution of cortical and non-cortical dysgenesis in our case mostly conforms to a severe and diffuse form of the BFPP syndrome.

Clinically, BFPP presents as a pseudomyopathic pattern, with hypotonia developing in the first year of life and occasionally being identified at birth (13). This initial clinical phenotype and imaging pattern is frequently suggestive of congenital muscular dystrophies of the "cobblestone complex" (13). The initial course of disease in our patient mimicked this pattern, but similarly to previously reported cases the muscle biopsy was normal and thus channeled the investigation away from this group of diseases. Following the pseudomyopathic presentation, the clinical course of BFPP is also considerably homogeneous in the cases reported in literature. **Table 1** describes the frequency of clinical features associated with BFPP described in the reported cases.

Cognitive and motor delay are universal features, although their severity is variable between cases. While the majority of patients (79.3%) had severe cognitive impairment with language restricted to only a few words, motor impairment was reportedly milder. Indeed, most patients (81.6%) were able to walk, either with or without support, although gait is frequently described as "unsteady" or ataxic. Gait acquisition was delayed in almost all cases (13, 20). On the other hand, there was a total of nine cases without gait acquisition, originating from six different variants in seven pedigrees, of which five variants were either frameshift or nonsense (14, 20). In our case, also a nonsense variant, motor impairment was abnormally severe, since the patient was unable to walk, sit or achieve cephalic control. To our knowledge, there are only two reports sharing this severe

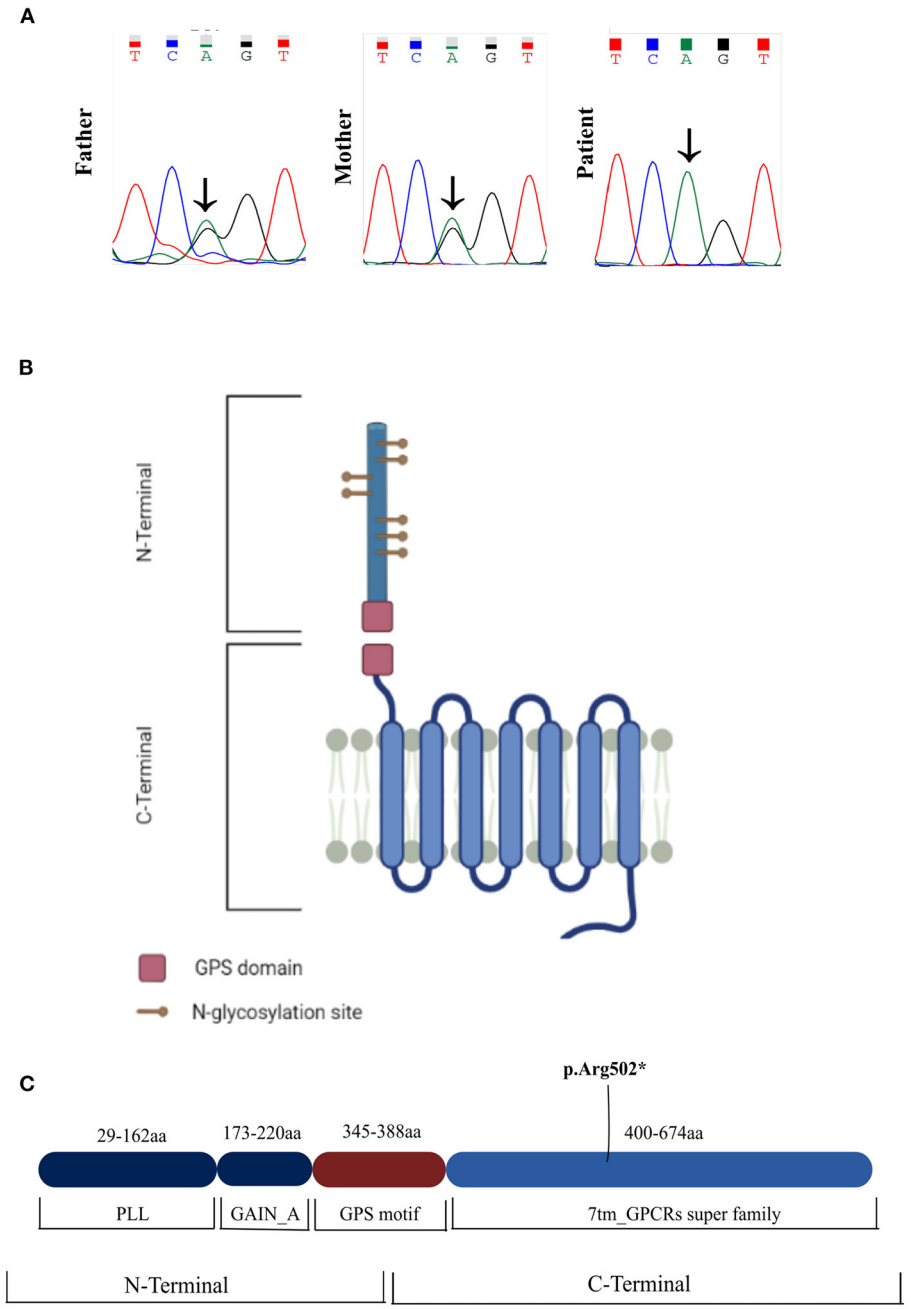

FIGURE 3 | (A) Sanger sequencing chromatograms of the patient and parents. The patient is a homozygous carrier of the nonsense variant c.1504C>T. The variant was present in the heterozygous state in both parents. **(B,C)** Schematic of the ADGRG1 protein, showcasing the novel variant in the 7TM domain of the protein (p.Arg502*). 7TM, 7 transmembrane domain; GAIN, GPCR-Autoproteolysis-INducing domain; GPS, GPCR proteolysis site motif; PLL, Pentraxin/Laminin/neurexin/sex-hormone-binding-globulin-Like domain.

phenotype. One is curiously of a Portuguese patient described by Santos-Silva et al. though the two cases do not share the same variant (14). The other report, by Cauley et al. describes a family with severe motor and cognitive delay, where the typical imaging phenotype of BFPP was present in association with Joubert-like features (7). The patients were found to have an additional pathogenic variant in *KIAA0556* by exome sequencing, with both variants interacting to create a more severe and complex phenotype. Pyramidal signs and ataxia are also common (75.9 and 92.6%), although pyramidal signs were absent in our patient and ataxia was impossible to ascertain due to the severity of motor impairment. Other common clinical manifestations in

TABLE 1 | Clinical features of reported BFPP cases (2, 3, 8–20).

Clinical feature	*n* (%)
Motor impairment	
Able to walk	40 (81.6)
Age at walking in years, median (IQR)	3.5 (3.0)
Unable to walk	9 (18.4)
Missing	25
Cognitive impairment	
Severe	46 (79.3)
Moderate	11 (18.9)
Mild	1 (1.7)
Missing	16
Cerebellar signs	
Present	50 (92.6)
Absent	4 (7.4)
Missing	18
Pyramidal signs	
Present	44 (75.9)
Absent	14 (24.1)
Missing	16
Oculomotor findings	
Present	59 (92.1)
Strabismus	25 (59.5)
Nystagmus	6 (14.3)
Strabismus + nystagmus	10 (23.8)
Other[a]	1 (2.4)
Missing	17
Absent	5 (7.9)
Missing	10
Head circumference	
Normal	57 (85.1)
Microcephaly	6 (9.0)
Macrocephaly	4 (5.9)
Missing	7
Seizures	
Present	60 (88.2)
Age at onset in years, median (IQR)	3.0 (3.0)
Refractory	36 (60.0)
Missing	13
Absent	8 (11.8)
Missing	6

[a]*Macular pigmentary changes; IQR, interquartile range.*

BFPP and present in this case are epilepsy (88.2% of patients described in the literature, being drug-refractory in 60% of those) and oculomotor dysfunction (92.1% of reported cases, most commonly strabismus). In short, the clinical picture present in our case is in accordance to BFPP, although the severity of motor impairment is atypical.

Could this severe phenotype be more in line with BGP? In the study by Leventer et al. (22), BGP patients were more likely to present with global developmental delay, intellectual disability, spastic quadriplegia, seizure onset at younger age, and hearing and cortical visual impairment, when compared to other PMG syndromes. Interestingly, the reported severity of cognitive and motor delay was also variable, with mild impairment in some cases, although severe phenotypes similar to our patient were reported (21). Thus, there seems to be considerable clinical overlap between BFPP and BGP in both the type and severity of clinical manifestations.

Several hypotheses can be proposed to explain the atypical clinical features in our case. First, they may result from the unique molecular characteristics of the gene product associated with the pathogenic variant. Physiologically, the ADGRG1 protein is a GPCR that binds extracellular matrix proteins (most notably collagen type III) and undergoes agonist-induced conformational changes. This, in turn, promotes release of the α subunit of the heterotrimeric G-protein complex from the 7TM domain of ADGRG1 and initiates downstream signaling via interaction with various cytosolic effector proteins. Even though other pathogenic variants of the surrounding 7TM region (such as the L487P, E496K, and R565W variants) do not present this particular phenotype (8, 12, 18), it is possible that subtle variations in the mutated protein impair different downstream signaling cascades, thereby resulting in varied phenotypic expressions. In our particular case, the severity of the clinical phenotype can also be interpreted in the context of an epileptic encephalopathy since there was motor and cognitive regression occurring simultaneously with epilepsy decompensation. Another hypothesis is the co-existence of additional pathogenic variants of genes involved in brain morphogenesis, as highlighted by the recent report from Cauley et al.

CONCLUSIONS

We report a novel *ADGRG1* truncating variant associated with generalized PMG without an anterior-posterior gradient, diffuse hypomyelination and a severe motor phenotype. Clinical and radiological features of BFPP were also present, highlighting the clinical-anatomical overlap between recognized PMG syndromes and the phenotypic diversity of *ADGRG1* pathogenic variants.

DATA AVAILABILITY STATEMENT

The original contributions presented in the study are included in the article/supplementary materials, further inquiries can be directed to the corresponding author/s.

ETHICS STATEMENT

The studies involving human participants were reviewed and approved by Ethics Committee of Clinical Research of Galicia (2015/410). Written informed consent to participate in this study was provided by the participants' legal guardian/next of kin.

AUTHOR CONTRIBUTIONS

FC and MF contributed to conception and design of the study. SB-G and M-LC performed the genetic experiments and data analysis. FC wrote the first draft of the manuscript. FC and SB-G designed the figures. All authors contributed to clinical care of the patient, manuscript revision, read, and approved the submitted version.

FUNDING

This work was supported by Foundation of Health Research Institute of Santiago de Compostela, Spain.

ACKNOWLEDGMENTS

The authors thank Sofia de Melo Araújo for assistance with proofreading and language editing.

REFERENCES

1. Barkovich AJ, Guerrini R, Kuzniecky RI, Jackson GD, Dobyns WB. A developmental and genetic classification for malformations of cortical development: update 2012. *Brain.* (2012) 135:1348–69. doi: 10.1093/brain/aws019
2. Chang BS, Piao X, Bodell A, Basel-Vanagaite L, Straussberg R, Dobyns WB, et al. Bilateral frontoparietal polymicrogyria: clinical and radiological features in 10 families with linkage to chromosome 16. *Ann Neurol.* (2003) 53:596–606. doi: 10.1002/ana.10520
3. Piao X, Chang BS, Bodell A, Woods K, Benzeev B, Topcu M, et al. Genotype-phenotype analysis of human frontoparietal polymicrogyria syndromes. *Ann Neurol.* (2005) 58:680–7. doi: 10.1002/ana.20616
4. Quang D, Chen Y, Xie X. DANN: a deep learning approach for annotating the pathogenicity of genetic variants. *Bioinformatics.* (2015) 31:761–3. doi: 10.1093/bioinformatics/btu703
5. Schwarz JM, Cooper DN, Schuelke M, Seelow D. MutationTaster2: mutation prediction for the deep-sequencing age. *Nat Methods.* (2014) 11:361–2. doi: 10.1038/nmeth.2890
6. Richards S, Aziz N, Bale S, Bick D, Das S, Gastier-Foster J, et al. Standards and guidelines for the interpretation of sequence variants: a joint consensus recommendation of the American College of Medical Genetics and Genomics and the Association for Molecular Pathology. *Genet Med.* (2015) 17:405–24. doi: 10.1038/gim.2015.30
7. Cauley ES, Hamed A, Mohamed IN, Elseed M, Martinez S, Yahia A, et al. Overlap of polymicrogyria, hydrocephalus, and Joubert syndrome in a family with novel truncating mutations in ADGRG1/GPR56 and KIAA0556. *Neurogenetics.* (2019) 20:91–8. doi: 10.1007/s10048-019-00577-2
8. Sawal H, Harripaul R, Mikhailov A, Vleuten K, Naeem F, Nasr T, et al. Three mutations in the bilateral frontoparietal polymicrogyria gene GPR56 in Pakistani intellectual disability families. *J Pediatr Genet.* (2018) 07:060–6. doi: 10.1055/s-0037-1612591
9. Piao X, Basel-Vanagaite L, Straussberg R, Grant PE, Pugh EW, Doheny K, et al. An autosomal recessive form of bilateral frontoparietal polymicrogyria maps to chromosome 16q12.2-21. *Am J Hum Genet.* (2002) 70:1028–33. doi: 10.1086/339552
10. Piao X, Hill SS, Bodell A, Chang BS, Basel-Vanagaite L, Straussberg R, et al. G protein-coupled receptor-dependent development of human frontal cortex. *Science (80-).* (2004) 303:2033–6. doi: 10.1126/science.1092780
11. Harbord MG, Boyd S, Hall-Craggs MA, Kendall B, McShane MA, Baraitser M. Ataxia, developmental delay and an extensive neuronal migration abnormality in 2 siblings. *Neuropediatrics.* (1990) 21:218–21. doi: 10.1055/s-2008-1071501
12. Luo R, Yang HM, Jin Z, Halley DJJ, Chang BS, MacPherson L, et al. A novel GPR56 mutation causes bilateral frontoparietal polymicrogyria. *Pediatr Neurol.* (2011) 45:49–53. doi: 10.1016/j.pediatrneurol.2011.02.004
13. Bahi-Buisson N, Poirier K, Boddaert N, Fallet-Bianco C, Specchio N, Bertini E, et al. GPR56-related bilateral frontoparietal polymicrogyria: further evidence for an overlap with the cobblestone complex. *Brain.* (2010) 133:3194–209. doi: 10.1093/brain/awq259
14. Santos-Silva R, Passas A, Rocha C, Figueiredo R, Mendes-Ribeiro J, Fernandes S, et al. Bilateral frontoparietal polymicrogyria: a novel GPR56 mutation and an unusual phenotype. *Neuropediatrics.* (2015) 46:134–8. doi: 10.1055/s-0034-1399754
15. Borgatti R, Marelli S, Bernardini L, Novelli A, Cavallini A, Tonelli A, et al. Bilateral frontoparietal polymicrogyria (BFPP) syndrome secondary to a 16q12.1-q21 chromosome deletion involving GPR56 gene. *Clin Genet.* (2009) 76:573–6. doi: 10.1111/j.1399-0004.2009.01262.x
16. Fujii Y, Ishikawa N, Kobayashi Y, Kobayashi M, Kato M. Compound heterozygosity in GPR56 with bilateral frontoparietal polymicrogyria. *Brain Dev.* (2014) 36:528–31. doi: 10.1016/j.braindev.2013.07.015
17. Desai NA, Udani V. GPR56 -related polymicrogyria. *J Child Neurol.* (2015) 30:1819–23. doi: 10.1177/0883073815583335
18. Parrini E, Ferrari AR, Dorn T, Walsh CA, Guerrini R. Bilateral frontoparietal polymicrogyria, Lennox-Gastaut syndrome, and GPR56 gene mutations. *Epilepsia.* (2009) 50:1344–53. doi: 10.1111/j.1528-1167.2008.01787.x
19. Öncü-Öner T, Ünalp A, Porsuk-Doru I, Agilkaya S, Güleryüz H, Saraç A, Ergüner B, et al. Gpr56 homozygous nonsense mutation p.r271* associated with phenotypic variability in bilateral frontoparietal polymicrogyria. *Turk J Pediatr.* (2018) 60:229. doi: 10.24953/turkjped.2018.03.001
20. Quattrocchi CC, Zanni G, Napolitano A, Longo D, Cordelli DM, Barresi S, et al. Conventional magnetic resonance imaging and diffusion tensor imaging studies in children with novel GPR56 mutations: further delineation of a cobblestone-like phenotype. *Neurogenetics.* (2013) 14:77–83. doi: 10.1007/s10048-012-0352-7
21. Chang BS, Piao X, Giannini C, Cascino GD, Scheffer I, Woods CG, et al. Bilateral generalized polymicrogyria (BGP): a distinct syndrome of cortical malformation. *Neurology.* (2004) 62:1722–8. doi: 10.1212/01.WNL.0000125187.52952.E9
22. Leventer RJ, Jansen A, Pilz DT, Stoodley N, Marini C, Dubeau F, et al. Clinical and imaging heterogeneity of polymicrogyria: a study of 328 patients. *Brain.* (2010) 133:1415–27. doi: 10.1093/brain/awq078

Conflict of Interest: The authors declare that the research was conducted in the absence of any commercial or financial relationships that could be construed as a potential conflict of interest.

Publisher's Note: All claims expressed in this article are solely those of the authors and do not necessarily represent those of their affiliated organizations, or those of the publisher, the editors and the reviewers. Any product that may be evaluated in this article, or claim that may be made by its manufacturer, is not guaranteed or endorsed by the publisher.

frontiers in Pediatrics

CASE REPORT
published: 31 August 2021
doi: 10.3389/fped.2021.725231

Case Report: Clinical Features of a Chinese Boy With Epileptic Seizures and Intellectual Disabilities Who Carries a Truncated *NUS1* Variant

Pingli Zhang[1†], *Di Cui*[2†], *Peiyuan Liao*[1], *Xiang Yuan*[1], *Nuan Yang*[1], *Yuanyuan Zhen*[1], *Jing Yang*[1*] and *Qikun Huang*[1*]

[1] Department of Pediatrics, Qilu Hospital (Qingdao), Cheeloo College of Medicine, Shangdong University, Qingdao, China, [2] Running Gene Inc., Beijing, China

OPEN ACCESS

Edited by:
Emiliano González Vioque, University Clinical Hospital of Santiago, Spain

Reviewed by:
Wang Jiaping, Peking University First Hospital, China
Qifei Li, Boston Children's Hospital and Harvard Medical School, United States
Maria Virginia Soldovieri, University of Molise, Italy

***Correspondence:**
Qikun Huang
huangqikun2021@163.com
Jing Yang
dryangyang@163.com

[†] These authors have contributed equally to this work

Specialty section:
This article was submitted to Genetics of Common and Rare Diseases, a section of the journal Frontiers in Pediatrics

Received: 15 June 2021
Accepted: 02 August 2021
Published: 31 August 2021

Citation:
Zhang P, Cui D, Liao P, Yuan X, Yang N, Zhen Y, Yang J and Huang Q (2021) Case Report: Clinical Features of a Chinese Boy With Epileptic Seizures and Intellectual Disabilities Who Carries a Truncated NUS1 Variant. Front. Pediatr. 9:725231. doi: 10.3389/fped.2021.725231

The mental retardation-55 with seizures (MRD55) is a rare genetic disease characterized by developmental delay, intellectual disability, language delay and multiple types of epileptic seizures. It is caused by pathogenic variants of the *NUS1* gene, which encodes Nogo-B receptor (NgBR), a necessary subunit for the glycosylation reactions in mammals. To date, 25 disease-causing mutations of *NUS1* have been reported, which are responsible for various diseases, including dystonia, Parkinson's disease, developmental and epileptic encephalopathy as well as congenital disorder of glycosylation. In addition, only 9 of these mutations were reported with detailed clinical features. There are no reports about Chinese cases with MRD55. In this study, a novel, *de novo* pathogenic variant of *NUS1* (c.51_54delTCTG, p.L18Tfs*31) was identified in a Chinese patient with intellectual disability and epileptic seizures. This pathogenic variant resulted in truncated NgBR proteins, which might be the cause of the clinical features of the patient. Oxcarbazepine was an effective treatment for improving speech and movement of the patient, who consequently presented with no seizure. With this novel pathogenic variant found in *NUS1*, we expand the genotype spectrum of MRD55 and provide valuable insights into the potential genotype-phenotype correlation.

Keywords: whole-exome sequencing, *NUS1*, epilepsy, MRD55, ID

INTRODUCTION

The mental retardation-55 with seizures (MRD55, OMIM 617831) is a rare genetic disease characterized by developmental delay, intellectual disability, language delay and multiple types of epileptic seizures (1). It is caused by pathogenic variants of the *NUS1* gene, which encodes Nogo-B receptor (NgBR) (2). NgBR is a conserved subunit of the dehydrodolichyl diphosphate synthase (DDS) complex, which promotes cisprenyltransferase (cis-PTase) activity and is necessary for the glycosylation reactions in mammals (3). To date, 25 disease-causing mutations of *NUS1* have been reported (according to the Human Mutation Database), nine of which were reported with detailed clinical phenotypes. These nine pathogenic variants, however, are associated with four various diseases, including dystonia (4), Parkinson's disease (5, 6), developmental and epileptic encephalopathy (1, 6–8), and congenital disorder of glycosylation (3). Thus, it seems that different pathogenic variants cause distinct diseases. In addition, cases with genotypes and detailed clinical

features are limited. Additional cases are needed for a better understanding of the relationship between MRD55 and the associated pathogenic variants.

Here, we report the clinical and molecular characterization of the first Chinese MRD55 patient, who displayed intellectual disability and epileptic seizures, and had a novel, *de novo* pathogenic variant of *NUS1* (c.51_54delTCTG, p.L18Tfs*31). With this novel pathogenic variant found in *NUS1*, we expanded the genotype spectrum of MRD55.

METHODS

Case Presentation

Our patient was the first child to non-consanguineous, healthy parents. He was born full-term *via* cesarean delivery, G1P1, with no asphyxia. The birth parameters included weight 3.0 kg ($Z = -0.925$), length 50.0 cm ($Z = 0.004$), and head circumference (HC) 38.0 cm ($Z = 1.299$). There was no abnormality in the perinatal period, and neither of his parents had a related family history. He could roll over, sit, call his parents and walk independently at the ages of 3, 6, 12, and 16 months, respectively. When the patient was 3 years old, he presented with unstable standing, involuntary movement of the limbs, abnormal posture and dance-like movements when he was emotionally agitated or fatigued. During this period, the patient was conscious and occasionally experienced sudden falls or involuntary squatting, with no binocular upward gaze, perioral bruising, or limb stiffness. The whole duration lasted approximately several seconds to several hours, which could be relieved spontaneously after the patient rested. The results of brain magnetic resonance imaging (MRI) were normal whereas video electroencephalogram (EEG) revealed slow and spiny-slow waves in the bilateral frontopolar, frontal, and anterior temporal regions during the sleeping period. The diagnosis of epilepsy was confirmed, and he was treated with Depakine (6 mg/kg/day) for a month. The treatment was not effective, and the patient continued to have seizures and unsteady standing in a variable frequency. The patient gradually developed occasional instability in the walking gait. He did not have any malformations or autistic feature but presented with a moderate intellectual disability at the age of 4 years and 7 months. The scores of full-scale intelligence quotient (FIQ), performance intelligence quotient (PIQ) and verbal intelligence quotient (VIQ) were 48, 47, and 61, respectively, as tested by Korean-Wechsler Preschool and Primary Scale of Intelligence (K-WPPSI). He was not given any treatment this time. At the age of 6 years, the patient suffered convulsions. The symptoms included unconsciousness, rolled-up left eye, stiff upper limbs and cyanotic lips. The duration of each convulsion was ∼5 min, and the patient was admitted to the hospital for "paroxysmal dyskinesias." The following abnormalities were detected in the video EEG: paroxysmal hypertonic 2–3 Hz slow waves interspersed with spikes were found in each conductor, especially in the frontal region. No other abnormality was identified from the blood or urine test, metabolic profiling analyses (amino-acid and acyl-arnitine profiles) or MRI scans (cervical, thoracic and lumbar spine). The patient was treated with madopar (2.1 mg/kg/day, Q12h) for a month, but did not improve. He still walked unsteadily and sometimes stood unsteadily. The treatment was discontinued. After 15 months, when the patient was 7 years and 3 months old, convulsions occurred during the quiet sleep. The symptoms were similar to those described before. Physical examination was performed, and the results were all normal except for the video EEG. The background activity was slow, with slow wave emitted in the left frontopolar during sleep. Meantime, the Gesell developmental scales were performed, and the results indicated a developmental stage of 2 years old. The patient was given oxcarbazepine (40 mg/kg/d) and sensory integration training. The treatment was effective, and the patient consequently did not have seizures. His speech and movement improved. However, he still presented with an unsteady walking gait, slow and slurred communication and poor numeracy. He was unable to add or subtract within ten digits of recognizable numbers. Additionally, his logic and comprehension were poor.

Genetic Analysis

The peripheral blood of the patient was collected and sent to Running Gene Inc. (Beijing, China) for whole-exome sequencing (WES) to identify the causal gene. Briefly, DNA was isolated and fragmented to build a DNA library by using the KAPA Library Preparation Kit (Illumina, Inc., USA). Then, the library was sequenced using an Illumina HiSeq X10 platform (Illumina, San Diego, USA) using a 150-bp paired-end reads according to the standard manual. The sequencing data was filtered and aligned with the human reference genome (GRCh37/hg19) by using the BWA Aligner (http://bio-bwa.sourceforge.net/). and variants were annotated by ANNOVAR (annovar.openbioinformatics.org/en/latest/). The candidate causal genes thereby discovered were then confirmed *via* Sanger sequencing.

RESULTS

A novel variant c.51_54delTCTG (p.L18Tfs*31) of *NUS1* (NM_138459.3) was identified in the patient *via* WES analysis (**Figure 1A**). This *de novo* (PS2) heterozygous deletion in exon 1 introduces a premature terminator and results in a truncated protein with 31 miscoded amino acids (**Figure 1B**). The truncated protein consists of 18 correctly encoded amino acids, constituting part of the transmembrane domain 1 (TM1). Other functional domains (TM2, TM3, the *cis*-IPTase domain and the RXG motif) are expected to be deleted, resulting in the loss of function (PVS1). This vatiant is absent from the controls (1000 Genomes, ExAC, gnomAD, and CNGB) (PM2). Thus, variant c.51_54delTCTG is classified as a pathogenic variant of *NUS1* according to the standard of American College of Medical Genetics (9), and was predicted to cause MRD55. No other pathogenic variant was identified in genes that may be associated with the developmental delay and epileptic encephalopathy of our patient.

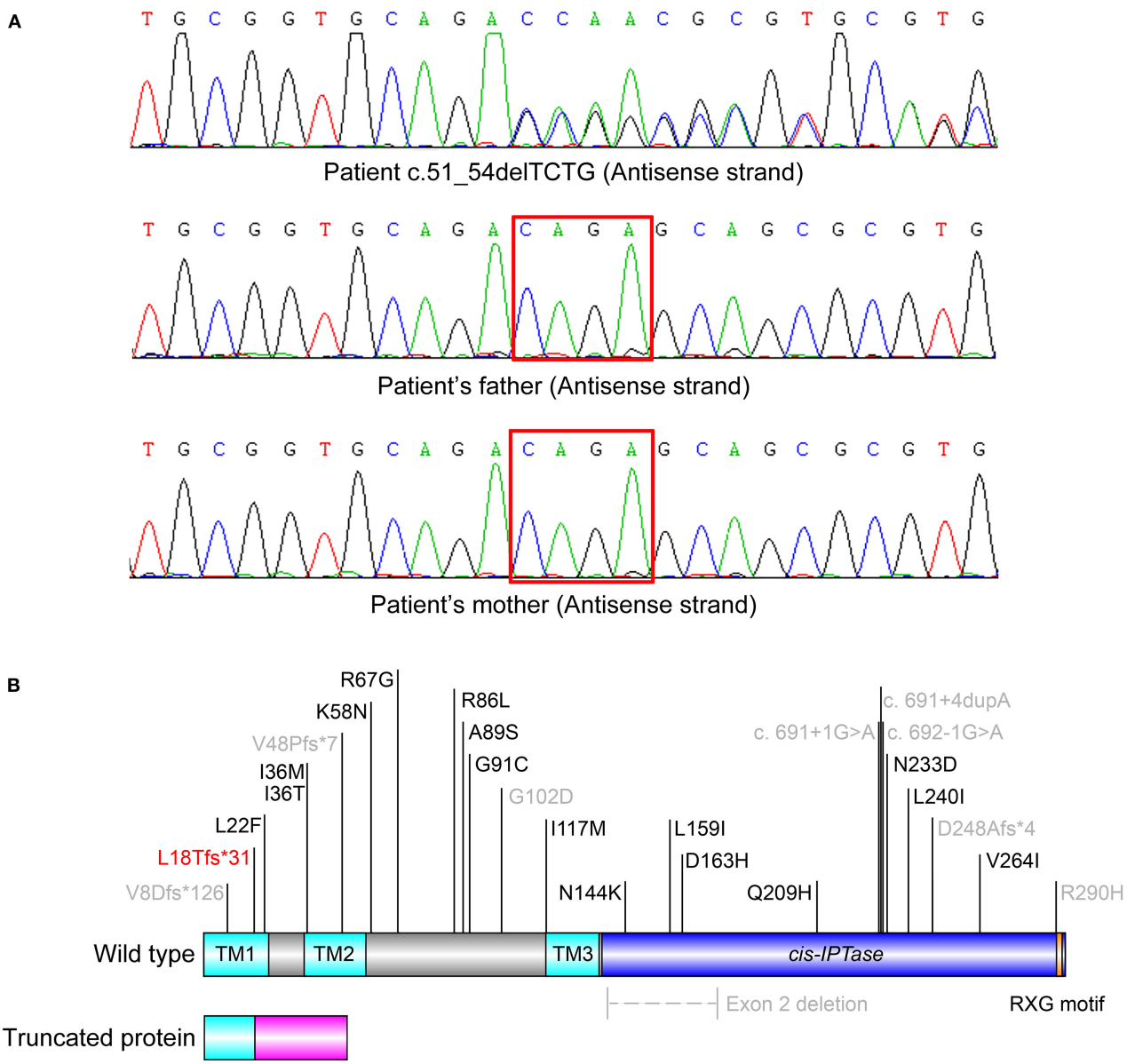

FIGURE 1 | (A) *De novo* heterozygous variants of c.51_54delTCTG in the patient. **(B)** Scheme of the reported disease-causing mutations of *NUS1*. The transmembrane (TM) 1 (AA 1-23), TM2 (AA 35-56) and TM3 (AA 117-135) domains are colored in cyan. The *cis-IPTase* domain (AA 136-293) is colored in blue. The RXG motif (AA 290-292), which is crucial for the prenyltransferase activity, is colored in orange. The 31 miscoded amino acids of the truncated protein are colored in magenta. The pathogenic variant reported in this study is colored in red and those reported with detailed clinical features are colored in gray. **(C)** Alignment of the NUS1 proteins of various species. Residues G102 and R290 (indicated in blue boxes) are highly conserved.

TABLE 1 | Clinical features of individuals with *NUS1* pathogenic variants.

Origin	This study	Fraiman et al.	Araki et al.	Araki et al.	Araki et al.	Araki et al.	Araki et al.	Wirth et al.	Den et al.	Den et al.	Guo et al.	Hamdan et al.	Hamdan et al.	Hamdan et al.	Park et al.	Park et al.
Individuals	1	2	3	4	5	6	7	8	9	10	11	12	13	14	15	16
Pathogenic variant (ACMG classification)	c.51_54delTCT, G.p.L18Tfs*31 (PVS1 + PS2 + PM2, Pathogenic)	c.692-1G>A splice (PVS1 + PS2 + PM2, Pathogenic)	c.22_23insA, p.V8Dfs*126 (PVS1 + PM 2 + PP1, Pathogenic)	c.22_23insA, p.V8Dfs*126 (PVS1 + PM 2 + PP1, Pathogenic)	c.22_23insA, p.V8Dfs*126 (PVS1 + PM 2 + PP1, Pathogenic)	c.22_23insA, p.V8Dfs*126 (PVS1 + PM 2 + PP1, Pathogenic)	c.22_23insA, p.V8Dfs*126 (PVS1 + PM 2 + PP1, Pathogenic)	c.305G>A, p.G102D (PS2 + PM2 + PP3, Likely pathogenic)	c.691+1G>A, splice (PVS1 + PS2 + PS3 + PM 2, Pathogenic)	c.691+1G>A, splice (PVS1 + PS2 + PS3 + PM 2, Pathogenic)	c.691+4dupA, splice (PVS1 + PS2 + PS3 + PM 2, Pathogenic)	c.743delA, p.D248Afs*4 (PVS1 + PS2 + PM2, Pathogenic)	c.128_141dup14, p.V48Pfs*7 (PVS1 + PS2 + PM 2, Pathogenic)	exon 2 deletion, 1.3 kb (PVS1 + PS2 + PM2, Pathogenic)	c.869G>A, p.R290H (PS3+PM2, Likely pathogenic)	c.869G>A, p.R290H (PS3+PM2, Likely pathogenic)
Zygote type/Inheritance	Het/*De novo*	Het/*De novo*	Het/N/A	Het/Paternal	Het/ N/A	Het/maternal	Het/maternal	Het/*De novo*	Het/*De novo*	Het/*De novo*	Het/*De novo*	Het/*De novo*	Het/*De novo*	Het/*De novo*	Hom/Parents	Hom/Parents
Disease	MRD55	MRD55	Parkinson's disease	MRD55 without ID	MRD55	MRD55	MRD55	Dystonia	MRD55	MRD55	Parkinson's disease	MRD55	MRD55	MRD55	CDG1AA	CDG1AA
Gender	Male	Male	Male	Female	Male	Female	Female	Male	Female	Male	Female	Male	Male	Female	Male	Male
Age	7 years 3 months	31 years	77 years	44 years	42 years	17 years	15 years	28 years	17 years	59 years	26 years	8 years 9 months	15 years	29 years	Deceased at 29 months	4 years
Ethnicity	Chinese Korean	N/A	Japanese	Japanese	Japanese	Japanese	Japanese	N/A	Japanese	Japanese	Chinese Han	N/A	French-Canadian	Caucasian	Czechs	Czechs
Family history	–	–	–	Two daughters	N/A	Mother	Mother	–	Elder brother (febrile seizures)	N/A	N/A	N/A	N/A	N/A	Brother (patient 10)	Brother (patient 9)
Birth weight	3.0 kg	N/A	N/A	N/A	N/A	N/A	N/A	N/A	2.826 kg	3.5 kg	N/A	N/A	N/A	N/A	N/A	N/A
Birth length	50.0 cm	N/A	N/A	N/A	N/A	N/A	N/A	N/A	N/A	56.0 cm	N/A	N/A	N/A	N/A	N/A	N/A
Age of onset	3 years	13 years	N/A	N/A	N/A	N/A	N/A	7 years	9 months	8 years	16 years	12 months	10 months	2.5 years	11 months	7 months
Seizures	Atonic seizures, tonic-clonic seizures, focal seizers, tonic seizers,	Tonic-clonic seizures	–	Clonic seizures	Absence seizures, Tonic-clonic seizures	Absence seizures	Absence seizures	–	Febrile seizure at 9 months, generalized tonic-clonic convulsion without fever at 14 months, status epilepticus at 6 years 3 months	Loss of consciousness without convulsion at 8 years	N/A	Generalized myoclonic epilepsy, convulsive epilepsy, nocturnal jerks	Myoclonic absences with behavioral arrest, facial and palpebral myoclonus	Myoclonic absences with behavioral arrest and eyelid flutters, as well as limb myoclonus	Tonic-clonic seizures, refractory epilepsy and recurrent attacks of "status epilepticus"	Refractory epilepsy, severe seizure
Frequency of seizures	in an irregular number	N/A	N/A	N/A	N/A	N/A	N/A	N/A	Seizure-free since 6 years of age	N/A	N/A	N/A	5 times a day, lasting 5–10 s	1–2 times a week	N/A	N/A
EEG	Spiny slow wave and slow wave, paroxysmal hypertonic 2–3 HZ slow waves interspersed with spikes, slow background and slow wave emission	Spikes and polyspikes-waves, sometimes with slow spike-wave complexes	Normal	Normal	Slow rhythm (5–7 Hz), Generalized ~3 Hz spike and wave complexes	Generalized ~3 Hz spike and wave complexes	Slow rhythm (7–8 Hz), Generalized ~3 Hz spike and wave complexes	N/A	3-Hz, diffuse, spike-and-slow-wave, complexed with 7-Hz, slow wave background	8–9 Hz slow α rhythm background with no epileptiform activity	N/A	Bifrontal epileptiform activity	Diffuse background slowing, with rhythmic, bifrontal, high-amplitude theta discharges	Generalized spike-wave and poly-spike wave activity	N/A	N/A
Effective medicines for seizures	Oxcarbazepine	Levetiracetam	Zonisamide, Clonazepam	Valproic acid, Clonazepam	Valproic acid, Clonazepam	Valproic acid	Valproic acid	N/A	Valproic acid was effective for seizures, Normal lessened 3-Hz, diffuse, spike-and-slow wave complexes	Myoclonus lessened with 50 mg baclofen	N/A	Levetiracetam	N/A	Relatively well-controlled with a combination of valproic acid, lamotrigine and clonazepam	N/A	N/A

(Continued)

TABLE 1 | Continued

Origin	This study	Fraiman et al.	Araki et al.	Araki et al.	Araki et al.	Araki et al.	Araki et al.	Wirth et al.	Den et al.	Den et al.	Guo et al.	Hamdan et al.	Hamdan et al.	Hamdan et al.	Park et al.	Park et al.
Brain MRI	Normal	Thickening of the corpus callosum	Cerebellar atrophy	Suspected cerebellar atrophy	Cerebellar atrophy	Suspected cerebellar atrophy	Cerebellar atrophy	Normal	Normal at 20 months, slight cerebellaratrophy at 14 years	Normal	Normal	Normal (2 years 3 months)	Normal (8 years)	Normal	N/A	Severe cortical atrophy
ID	Moderate	Mild to moderate	–	–	Mild	Mild	Moderate	Mild	Mild to moderate	Moderate	N/A	Moderate	Moderate	Mild	Yes	N/A
Language delay	Yes	N/A	N/A	N/A	N/A	N/A	N/A	N/A	Mild (speaking two-word sentences at 2 years)	Yes	-	Yes	Mild	-	N/A	N/A
Developmental delay	Yes	N/A	N/A	N/A	N/A	N/A	N/A	N/A	Mild psychomotor delay	–	N/A	Yes	Yes	Mild motor delay	Yes	N/A
Ataxia	Yes	Mild	Yes	Yes	Yes	Yes	Yes	–	Yes	Yes	N/A	Yes	–	–	N/A	N/A
Autism	–	N/A	N/A	N/A	N/A	N/A	N/A	N/A	–	–	N/A	N/A	Yes	N/A	N/A	N/A
Scoliosis	–	N/A	N/A	N/A	N/A	N/A	N/A	N/A	Yes (operation at 15 years of age)	Yes	N/A	N/A	N/A	N/A	Yes, congenital	Yes, congenital
Hypotonia	–	N/A	N/A	N/A	N/A	N/A	N/A	Segmental non progressive dystonia of upper limbs	–	–	N/A	N/A	N/A	N/A	Severe	Severe
Dysmorphic features	–	N/A	–	–	–	–	–	N/A	–	–	N/A	N/A	–	N/A	Microcephaly	Microcephaly
Additional features	–	Psychosis	Resting and intention tremor, Myoclonus	Resting and intention tremor	Intention tremor	Intention tremor	Resting and intention tremor, Myoclonus	Myoclonus, tremor	Dysgraphia due to tremulous myoclonus of bilateral extremities	Eye pursuits were saccadic, hyperkinesia volitionelle-like movement, cortical myoclonus	Parkinson's disease, asymmetric onset, bradykinesia, resting tremor in limbs, mild gait difficulties	–	–	Eye pursuits were saccadic, but saccades were normal	Histophathological examination of autopsy tissue revealed non-specific neuronal loss in brain cortex and cerebellum	No

PVS1, null variant (non-sense, frameshift, canonical ±1 or 2 splice sites, initiation codon, single or multi-exon deletion) in a gene where loss of function (LOF) is a known mechanism of disease; PS2, de novo (both maternity and paternity confirmed) in a patient with the disease and no family history; PM2, absent from controls (or at extremely low frequency if recessive) in Exome Sequencing Project, 1000 Genomes or ExAC; PP1. Co-segregation with disease in multiple affected family members in a gene definitively known to cause the disease; PP3, Multiple lines of computational evidence support a deleterious effect on the gene or gene product; MRD55, mental retardation-55 with seizures; CDG1AA, congenital disorder of glycosylation type Iaa; ID, intellectual disability; N/A Not available, Not assessed; Het, Heterozygous; Hom, Homozygous.

DISCUSSION

MRD55 is a rare congenital disease characterized by developmental delay, intellectual disability, language delay and multiple types of seizures (1). It was first reported in three unrelated patients, who presented with onset of myoclonic seizures and carried heterozygous, *de novo* pathogenic variants of the *NUS1* gene (1). The diagnostic criterion for this disorder

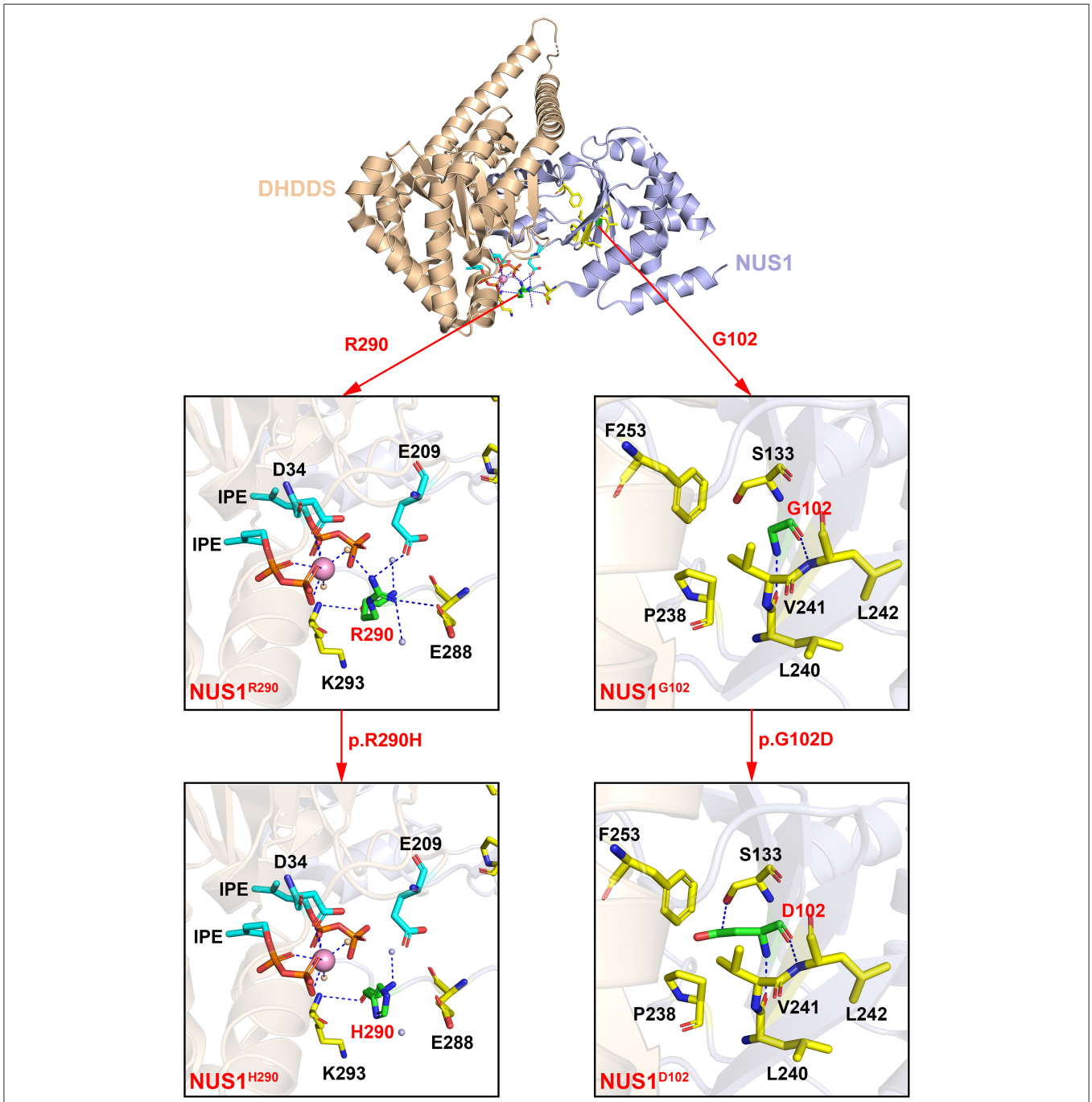

FIGURE 2 | The crystal structure of the human NgBR/DHDDS complex (PDB code: 6W2L). Shown are the cartoon representation of the wildtype NgBR/DHDDS structure and the G102, R290 mutants. The DHDDS and NgBR subunits of the heterodimer are colored in wheat and light blue, respectively. Residues G102, R290 and their pathogenic variants D102, H290 are shown in green sticks. D34, S133, E209, P238, L240, V241, L242, F253, E288, E293 and two IPEs are shown in sticks and highlighted in cyan (DHDDS subunit) and yellow (NgBR subunit). The water molecules of DHDDS and NgBR are colored in orange and light blue, respectively. The metal ion Mg^{2+} is colored in pink. All the structural figures were generated using PyMOL (http://www.pymol.org).

were established. Considering the epileptic seizures, moderate intellectual disability and the identified pathogenic *NUS1* variant, the patient was diagnosed with MRD55.

NUS1 encodes Nogo-B receptor, which consists of 293 amino acids and regulates cis-PTase activity (3). It interacts with the dehydrodolichyl diphosphate synthase complex subunit (DHDDS), forming a biological functional heteromer (the DDS complex). DDS is essential for the biosynthesis of dolichol monophosphate (Dol-P), which is utilized as a sugar carrier during protein glycosylation in the endoplasmic reticulum (ER) (3, 10–12). Therefore, the protein encoded by pathogenic *NUS1* variants might lack the proper function, and thus the regulation of protein glycosylation is disrupted and disease ensue.

To date, 25 disease-causing mutations of *NUS1* have been reported (**Figure 1B**), nine of which are described with detailed clinical phenotypes (**Table 1**) (1, 3–8). It is interesting that ten pathogenic variants, including the one reported in our study, are responsible for four different diseases, including dystonia, Parkinson's disease, CDG1AA and MRD55. Phenotypes are diverse, patients present with seizures (13/16), intellectual disability (ID, 12/16), language delay (5/16), developmental delay (6/16), ataxia (10/16), scoliosis (4/16) and hypotonia (3/16). Autism and dysmorphic features are rare, which are only found in one MRD55 (1) and two CDG1AA patients (3), respectively. All the *NUS1* pathogenic variants carried by MRD55 patients are truncated variants (frameshift, splicing and exon deletion), suggested to cause MRD55 features *via* a mechanism of haploinsufficiency (1). Two heterozygous variants have been detected in patients with Parkinson's disease. One had the splicing-site variant c.691+4dupA, which generates an aberrant spliced mRNA, leading to a significant reduction in the NUS1 level (5). The other one carries the frameshift variant c.22_23insA, which is barely expressed in human embryonic kidney (HEK) cells 293 cells, indicating a similar reduction in NUS1 level (6). In the patients with dystonia and CDG1AA, the missense variants p.G102D (heterozygous) and p.R290H (homozygous) were observed, respectively. G102 and R290 are phylogenetically highly conserved (**Figure 1C**), and their substitutions are expected to impair the function of NUS1.

G102 is located on the β-sheet of the NUS1 protein, directly binding to residues L240 and L242, as shown in the crystal structure of the human NgBR/DHDDS complex (**Figure 2**, the right side). The substitution of G102 with D102 forms an interaction between D102 and S133. Additionally, the side chain of D102 highly repels residues P238, V241 and F253, and thus the protein structure of the protein destroyed, impairing the protein function.

R290 is located on the contact surface of the NgBR/DHDDS complex. The coordination sphere of R290 includes residues from NgBR (E288 and K293), residues from DHDDS (D34 and E209), two IPEs, and three water molecules (**Figure 2**, the left side). When residue R290 is substituted, its interactions with E209, E288 and the three water molecules are lost. One of the three water molecules mediates and interaction between R290 and Mg^{2+}. The interaction between residues R290 (NgBR) and E209 (DHDDS) contributes to the formation of the heterodimer. Therefore, the substitution of R290 with H290 has a great impact on the structure and function of the protein complex. In addition, the pathogenic variant p.R290H is homozygous, which is expected to cause a more dramatic reduction in NgBR activity, resulting in more severe clinical symptoms.

It is noteworthy that a heterozygous *NUS1* frameshift variant has been identified in 5 familial patients with different clinical features (6). Three patients had ID and absent seizures, and could be diagnosed with typical MRD55. One patient only presented with clonic seizures, and another one displayed Parkinsonism without epilepsy. Why these five patients presented with distinct phenotypes is unknown. We can only speculate that NUS1 pathogenic variants as well as epigenetic, and/or environmental factors interact with each other to produce the specific phenotypes.

The number of cases with the *NUS1* pathogenic variants is still too low to draw a genotype/phenotype correlation, especially given that the *NUS1* pathogenic variants can cause different diseases. The molecular mechanisms underlying the effects of the *NUS1* pathogenic variants in patients who presented with different diseases are unknown. Additional cases and functional studies are needed for a better understanding of *NUS1* gene and related diseases.

CONCLUSION

In this study, we reported a Chinese MRD55 patient with detailed clinical phenotypes. The *de novo* variant of *NUS1* identified by WES was novel and was concluded to be responsible for the clinical presentation of the patient. With this novel pathogenic variant found in *NUS1*, we expanded the genotype spectrum associated with the MRD55 phenotype and provided the potential for a better understanding of the relationship between this rare disease and the pathogenic variants.

DATA AVAILABILITY STATEMENT

The raw data supporting the conclusions of this article will be made available by the authors, without undue reservation, to any qualified researcher.

ETHICS STATEMENT

The studies involving human participants were reviewed and approved by The Ethics Committee of Shandong University Qilu Hospital (Qingdao). Written informed consent was obtained from the individual(s), and minor(s)' legal guardian/next of kin, for the publication of any potentially identifiable images or data included in this article.

AUTHOR CONTRIBUTIONS

PZ, JY, and QH cared for the patient, collected the clinical data of the patient and drafted the clinical portion of the manuscript. DC analyzed the results of WES and wrote the extra part of the manuscript. XY applied the clinical tests on patients. PL assisted the clinical test and recorded the clinical information. YZ and NY

summarized characteristics of reported cases. PZ, DC, JY, and QH finally revised the manuscript. All authors read and approved the submitted version.

FUNDING

This study was supported by Shandong Provincial Natural Science Foundation Project (ZR2020MH196). The funding bodies had no roles in the design of the study, the collection, analysis, or interpretation of the data, or writing the manuscript.

ACKNOWLEDGMENTS

We thank all colleagues in our department for their clinical assist. We thank Running Gene Inc. for their technical support.

REFERENCES

1. Hamdan FF, Myers CT, Cossette P, Lemay P, Spiegelman D, Laporte AD. High rate of recurrent *de novo* mutations in developmental and epileptic encephalopathies. *Am J Hum Genet.* (2017) 101:664–85. doi: 10.1016/j.ajhg.2017.09.008
2. Miao RQ, Gao Y, Harrison KD, Prendergast J, Acevedo LM, Yu J, et al. Identification of a receptor necessary for Nogo-B stimulated chemotaxis and morphogenesis of endothelial cells. *Proc Natl Acad Sci USA.* (2006) 103:10997–1002. doi: 10.1073/pnas.0602427103
3. Park EJ, Grabińska KA, Guan Z, Stránecký V, Hartmannová H, Hodanová K, et al. Mutation of Nogo-B receptor, a subunit of cis-prenyltransferase, causes a congenital disorder of glycosylation. *Cell Metab.* (2014) 20:448–57. doi: 10.1016/j.cmet.2014.06.016
4. Wirth T, Tranchant C, Drouot N, Keren B, Mignot C, Cif L, et al. Increased diagnostic yield in complex dystonia through exome sequencing. *Parkinsonism Relat Disord.* (2020) 74:50–6. doi: 10.1016/j.parkreldis.2020.04.003
5. Guo JF, Zhang L, Li K, Mei JP, Xue J, Chen J, et al. Coding mutations in NUS1 contribute to Parkinson's disease. *Proc Natl Acad Sci USA.* (2018) 115:11567–72. doi: 10.1073/pnas.1809969115
6. Araki K, Nakamura R, Ito D, Kato K, Iguchi Y, Sahashi K, et al. NUS1 mutation in a family with epilepsy, cerebellar ataxia, and tremor. *Epilepsy Res.* (2020) 164:106371. doi: 10.1016/j.eplepsyres.2020.106371
7. Den K, Kudo Y, Kato M, Watanabe K, Doi H, Tanaka F, et al. Recurrent NUS1 canonical splice donor site mutation in two unrelated individuals with epilepsy, myoclonus, ataxia and scoliosis - a case report. *BMC Neurol.* (2019) 19:253. doi: 10.1186/s12883-019-1489-x
8. Fraiman P, Maia-de-Oliveira JP, Moreira-Neto M, Godeiro-Junior C. Psychosis in NUS1 de novo mutation: new phenotypical presentation. *Clin Genet.* (2021) 99:475–76. doi: 10.1111/cge.13867
9. Richards S, Aziz N, Bale S, Bick D, Das S, Gastier-Foster J, et al. Standards and guidelines for the interpretation of sequence variants: a joint consensus recommendation of the American College of Medical Genetics and Genomics and the Association for Molecular Pathology. *Genet Med.* (2015) 17:405–24. doi: 10.1038/gim.2015.30
10. Harrison KD, Park EJ, Gao N, Kuo A, Rush JS, Waechter CJ, et al. Nogo-B receptor is necessary for cellular dolichol biosynthesis and protein N-glycosylation. *EMBO J.* (2011) 30:2490–500. doi: 10.1038/emboj.2011.147
11. Grabińska KA, Edani BH, Park EJ, Kraehling JR, Sessa WC. A conserved C-terminal RXG motif in the NgBR subunit of cis-prenyltransferase is critical for prenyltransferase activity. *J Biol Chem.* (2017) 292:17351–61. doi: 10.1074/jbc.M117.806034
12. Edani BH, Grabińska KA. Structural elucidation of the cis-prenyltransferase NgBR/DHDDS complex reveals insights in regulation of protein glycosylation. *Proc Natl Acad Sci USA.* (2020) 117:20794–802. doi: 10.1073/pnas.2008381117

Conflict of Interest: DC was employed by the company Running Gene Inc.

The remaining authors declare that the research was conducted in the absence of any commercial or financial relationships that could be construed as a potential conflict of interest.

Publisher's Note: All claims expressed in this article are solely those of the authors and do not necessarily represent those of their affiliated organizations, or those of the publisher, the editors and the reviewers. Any product that may be evaluated in this article, or claim that may be made by its manufacturer, is not guaranteed or endorsed by the publisher.

frontiers in Pediatrics

CASE REPORT
published: 01 October 2021
doi: 10.3389/fped.2021.713458

Case Report: Progressive Cholestasis: Severe Phenotype of MEGDEL Syndrome With SATB2-Associated Syndrome

Yajie Su[1,2], *Hui Zhang*[2], *Huijun Wang*[3], *Bingbing Wu*[4], *Jiao Yang*[2], *Wenhao Zhou*[1,3,4*] and *Long Li*[2*]

[1] Department of Neonatology, Children's Hospital of Fudan University, Shanghai, China, [2] Department of Neonatology, Children's Hospital of Xinjiang Uygur Autonomous Region, Urumqi, China, [3] Shanghai Key Laboratory of Birth Defects, Pediatrics Research Institute, Shanghai, China, [4] Center for Molecular Medicine, Children's Hospital of Fudan University, Shanghai, China

MEGDEL syndrome and *SATB2*-associated syndrome (SAS) are both rare congenital disorders with poor prognoses caused by gene mutations. We present the case of a 2-day-old girl with an unexplained abnormal liver function, feeding problem, and dystonia. Using next-generation sequencing, we identified two novel mutations in *SERAC1* and a mutation in *SATB2*. Now, she is 15 months old and has the characteristics of SAS, such as downslanting palpebral fissures and delayed primary dentition. Besides the typical phenotypes of MEGDEL syndrome, such as hypertonia, failure to thrive, deafness, and motor regression, she has progressive cholestasis and is prone to high serum lactate after rehabilitation training and hypoglycemia with low ketone under starving conditions. These phenotypes substantially differ from the transient liver function abnormalities and hypoglycemia reported in the literature.

Keywords: MEGDEL syndrome, SATB2-associated syndrome, phenotype, next-generation sequencing, follow-up

OPEN ACCESS

Edited by:
Emiliano González Vioque, University Clinical Hospital of Santiago, Spain

Reviewed by:
Nida Mirza, Sri Aurobindo Institute of Medical Science, India
Baoheng Gui, The Second Affiliated Hospital of Guangxi Medical University, China

***Correspondence:**
Wenhao Zhou
zhouwenhao@fudan.edu.cn
Long Li
lilong65@126.com

Specialty section:
This article was submitted to Genetics of Common and Rare Diseases, a section of the journal Frontiers in Pediatrics

Received: *23 May 2021*
Accepted: *03 September 2021*
Published: *01 October 2021*

Citation:
Su Y, Zhang H, Wang H, Wu B, Yang J, Zhou W and Li L (2021) Case Report: Progressive Cholestasis: Severe Phenotype of MEGDEL Syndrome With SATB2-Associated Syndrome. Front. Pediatr. 9:713458. doi: 10.3389/fped.2021.713458

INTRODUCTION

MEGDEL syndrome (3-methylglutaconic acidemia, deafness, encephalopathy, and Leigh-like syndrome) is a rare specific mitochondrial disorder due to mutations in the *SERAC1* gene (NM_032861), which is an autosomal recessive inherited disorder (1). The *SERAC1* gene encodes for a phosphatidylglycerol remodeler that is essential for mitochondrial functions and intracellular cholesterol trafficking (2). The *SATB2*-associated syndrome (SAS) is a recently described syndrome caused by mutaion of *SATB2* gene (NM_015265). It's an autosomal dominantly inherited disorder which characterized by developmental delay with absent or limited speech, behavioral problems, dysmorphic features, and craniofacial abnormalities, including palatal and dental abnormalities (3).

We describe a rare disease progression and a severe phenotype of progressive cholestasis of a girl from birth to 15 months, who was compound heterozygous for *SERAC1* of MEGDEL syndrome and had a mutation in *SATB2* of *SATB2*-associated syndrome.

CASE DESCRIPTION

A female infant was born at 38+ 5/7 weeks gestational age to a 38-year-old mother who had gestational anemia, which was supplemented with oral iron, and gestational diabetes, which

was controlled with diet. The mother has a healthy 6-year-old girl but also had a spontaneous abortion and an artificial abortion due to embryo death. The mother's brother had a history of epilepsy and had passed away.

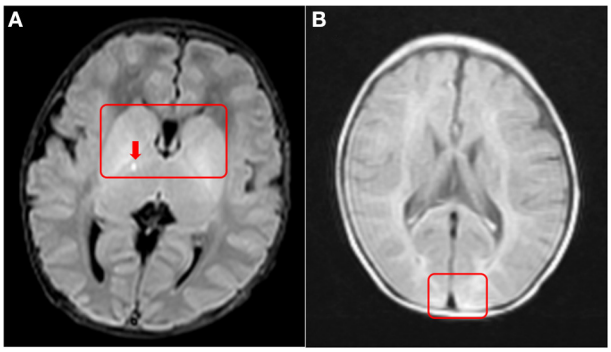

FIGURE 1 | Brain MRI at 10 days and 3 months of age. **(A)** T2W: Red boxes indicate a high signal of basal ganglia, swelling of bilateral lenticular nucleus; Red arrows indicate an abnormal signal point of posterior branch of right internal capsule. **(B)** T2W: Red boxes indicate white matter of occipital lobe has high signal, and the boundary of gray and white matter is not clear.

The infant's birth weight, head circumference, and length were 2,830 g (10–25th percentile), 33 cm (25–50th percentile), and 48 cm (10–25th percentile), respectively, with a normal Apgar score. However, she had mild blepharoptosis and there was a 3 cm cleft palate from the palate to the uvula. On day of life (DOL) 2, the infant vomited milk twice accompanied by weakness in sucking. A few hours later, she went into convulsions that involved rowing movements of the limbs. Her blood glucose was 0.7 mmol/L and blood gas analysis revealed anion gap metabolic acidosis (24.69 mmol/L). After providing glucose (8 mg/kg/min) and phenobarbital (10 mg/kg) injection treatment, the convulsions did not occur again, but she became somnolent, developed an unexplained abnormal liver function, and an aggravating increase in serum lactate (16.4 mmol/L). The infant was immediately transferred to our tertiary neonatal intensive care unit (NICU) center on DOL 3 for further newborn care.

The infant's serum lactate was normal on DOL 4 after giving intravenous fluids and nasogastric feeding. Blood glucose was

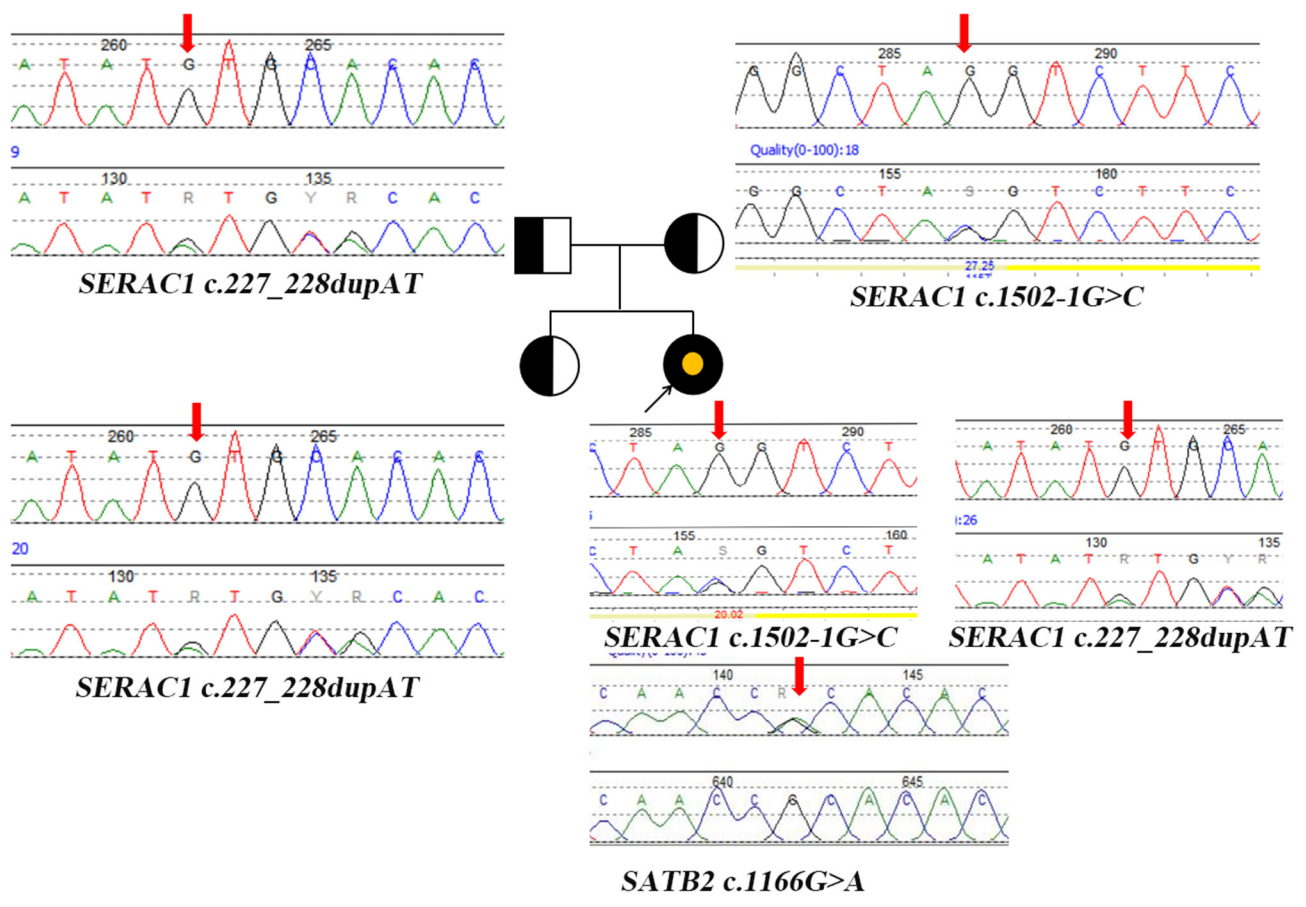

FIGURE 2 | Pedigree diagram and genetic characterization of the family with *SERAC1* and *SATB2*. Parents and sisters are heterozygous carriers of the *SERAC1* gene; The yellow point represents the mutation of *SATB2* gene. Heterozygous mutation (c.227-228dupAT) in *SERAC1* was found in the patient, her father and her healthy sister. Heterozygous mutation (c.1502-1G>C) in *SERAC1* was found in the patient and her mother. Heterozygous mutation (c.1166G>A) in *SATB2* was only found in the patient; Red arrow indicate location of mutation.

normal on DOL 6 without intravenous fluids. The problems during hospitalization were poor neonatal sucking, reduced movements, and unexplained elevated liver enzymes (gamma-glutamyltransferase (GGT) 1,373 mmol/L, total bile acids (TBA) 58.2 μmol/L, aspartate aminotransferase (AST) 132 U/L,prothrombin time (PT) 46.1s, albumin 26.57 g/L) with normal stool color and abdominal ultrasound. In addition, magnetic resonance imaging (MRI) showed high signals on T2 and FLAIR, where the lenticular nucleus was swollen on both sides. There were multiple hyperintensity patches on the dorsal side of the brainstem and posterior limb of the internal capsule near the anterior and posterior horns of the right lateral ventricle (**Figure 1**). Evoked otoacoustic emission test was not passed on both ears.

Blood tandem mass spectrometry (MS/MS) showed an increase in tyrosine 227.85 μM (25–225 μM). Urine gas chromatography-mass spectrometry (GC/MS) showed an increase in oxalate 57.78 (0–33), 3-methylglutaconic aciduria 4.35 (0–1), and 3-(4-hydroxyphenyl) lactic acid 1122.49 (0–20). Next-generation sequencing and Sanger sequencing detected two compound heterozygotes of *SERAC1* (c.1502-1G>C(likely pathogenic) from the maternal side, c.227-228dupAT(pathogenic) from the paternal side) and a *de novo* variant of *SATB2* (c.1166G>A) (likely pathogenic) (**Figure 2**). The quality control of WES data analysis and procedure of variant annotation refers to pipeline version 2 of Children's Hospital of Fudan University (4). We classified the pathogenicity of the identified variants according to the ACMG guideline, the details showed in (**Supplementary Table 1**).

On DOL 17, the infant was discharged from hospital with a nasogastric tube. After symptomatic treatment, the high GGT at admission had dropped to 264 mmol/L and the PT returned to normal (16.2 s). She experienced slow weight gain and increasing TBA, which was unmanageable by drugs after discharge. When she was 3 months old, there was a continuous mild increase in methionine (Met) for 2 months. After providing Met-free formula milk, the level of Met reduced to normal, and her motor development improved. When she was 12 months old, she had a high fever of 39°C. Afterward, her gross and fine motor regressed to the level of 5 months. Now, she is 15 months old with four primary teeth and has completed a cleft palate repair surgery in order to improve her nutritional status. When she was discharged

TABLE 1 | Follow-up of the infant from birth to 15 months of age.

Age	0 d	3 d	17 d	3 m	6 m	9 m	12 m	15 m
Event	Born	NICU	Discharge	Rehabilitation training	Intravenous injection of levocarnitine	Free-Met milk powder	High fever of 39°C+first primary teeth	Cleft palate repair surgery
Weight (g)	2,830 (<25th)	2,630 (<25th)	2,780 (<25th)	4.5 (<5th)	5,500 (<2th)	6,200 (<2th)	7,000 (<2th)	7,800 (<5th)
Height (cm)	48 (<25th)	48 (<25th)	48 (<25th)	53 (<2th)	61 (<2th)	67 (<10th)	72 (<25th)	77 (<50th)
Feeding	Oral feeding	Intravenous fluids and nasogastric feeding	Oral+nasogastric feeding	Oral feeding formula milk	Oral feeding formula milk	Supplementary food+free-Met formula milk (2 months)	Supplementary food+formula milk	Supplementary food+ formula milk
Bile acid (μmol/L)	\	58.20	36.31	149.31	492.20	526.67	386.54	325.7
Lactate (mmol/L)	\	9.25	2.03	2.10	1.90	2.70	5.82	3.60
Others	\	Metabolic acidosis, elevated liver enzymes	Elevated liver enzymes	Elevated liver enzymes	Elevated liver enzymes, cholesterol (3.3 mmol/L)	Hypoglycemia with low ketone	Cholesterol (2.49 mmol/L)	\
	\	aEEG:Intermittent low amplitude in both hemispheres (10–15 μV)	Abdominal CT: the density of liver parenchyma was reduced. The bilateral renal pelvis was slightly dilated	MRI:T2 showed a lower signal of white matter	\	Indexes related to islet function were normal	\	\
Central Nervous System	Normal	Poor neonatal suck+severe hypotonia	Poor neonatal suck and swallow reflexes+ hypertonia	Hypertonia, delayed motor development (1-month)	Hypertonia, delayed gross motor development (4-month), delayed fine motor development (3-month)	Poor swallow reflexes, hypertonia, delayed gross motor development (8-month), delayed fine motor development (6-month)	Poor swallow reflexes, hypertonia, psychomotor regression (5-month)	Poor swallow reflexes, hypertonia, psychomotor regression (5-month)

NICU, neonatal intensive care unit; Met, methionine; aEEG, amplitude-integratedelectroencephalography; MRI, magnetic resonance imaging; CT, computed tomography.

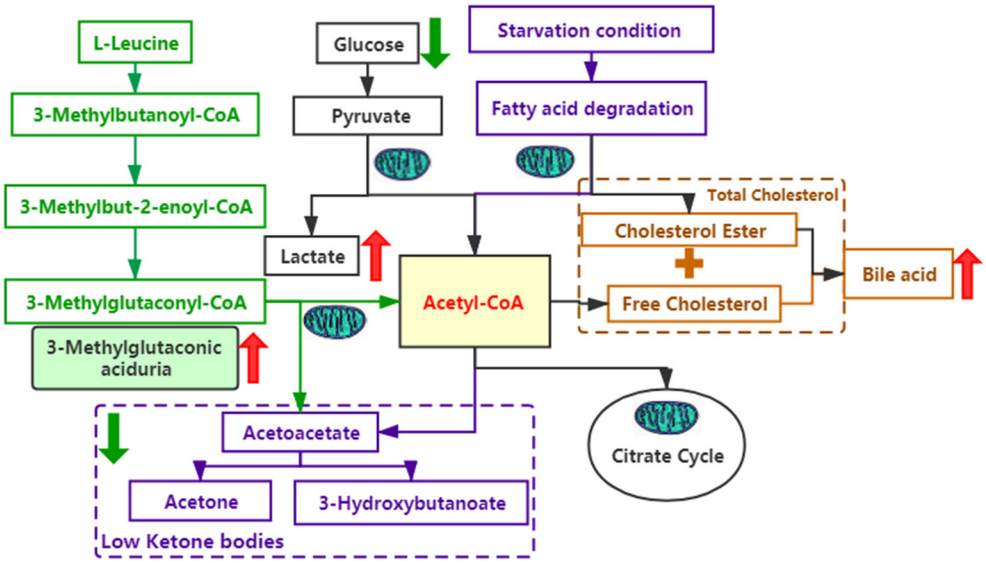

FIGURE 3 | Several metabolic pathways involved in this case. The green font represents the leucine metabolic pathway; the purple font represents the fatty acid metabolic pathway; the black font represents the glucose metabolic pathway; and the yellow font represents the cholesterol metabolic pathway. The red arrows indicate an increase, whereas the green arrows indicate a decrease.

from the hospital in the first time, the GGT were maintained between 430 and 470 mmol/L, the AST were maintained between 62 and 87 U/L and albumin were maintained between 31.4 and 36.9 g/L. In addition, PT (15.1 s) and international normalized ratio (1.31) was slightly elevated at 12 months of age. Only bile acids were continuously increasing. Because she had normal stool color, normal skin color, and normal abdominal ultrasound, we excluded the extrahepatic biliary atresia and choledochal cyst and did not perform liver biopsy. She is susceptible to higher serum lactate after rehabilitation training and hypoglycemia with low ketone under starving conditions (**Table 1**).

DISCUSSION

When a newborn demonstrates an unexplained feeding problem and a high anion gap metabolic acidosis, doctors will change the direction of diagnosis and treatment to inherited metabolic diseases, especially because in this case, the infant had dystonia, an abnormal MRI, and increased liver enzymes and serum lactate. Even though the MS/MS presented an increased level of 3-methylglutaconic aciduria, we still cannot present a diagnosis because of the various phenotypes present in the neonatal period.

The infant carries two variants of *SERAC1* (c.1502-1G>C from the maternal side, c.227-228dupAT from the paternal side), neither of which have been reported before (http://www.hgmd.cf.ac.uk). She has the typical phenotypes of 3-methylglutaconic acidemia, deafness, and Leigh-like syndrome (present with bilateral basal ganglia lesions on brain MRI) (5). She still has progressive cholestasis and is susceptible to high serum lactate after rehabilitation training and hypoglycemia with low ketone under starving conditions. These phenotypes are substantially different from the transient liver function abnormalities and hypoglycemia reported in the literature (6).

As we know, *SERAC1* encodes for a phosphatidylglycerol remodeler that is essential for mitochondrial functions and intracellular cholesterol trafficking. Although there is no medicine that can completely treat the disease. When the diagnosis is clear, we should give *baclofen* (10 mg, bid), *trihexyphenidyl hydrochloride* (2 mg, bid) to improve her hypertonia and *coenzyme Q10* (30 mg/d), *L-carnitine*(1 g,bid), *vitamin B1* (100 mg/d), and *vitamin E* (100 mg/d) to improve mitochondrial functions. Due to the influence of pandemic of COVID-19, she didn't go to the hospital in time and was not treated until 5 months after birth. But her parents thought there was not obvious effect after treatment and did not adhere to the standard treatment. Here, we try to explain its function through the metabolic pathways (**Figure 3**). On one hand, mutations in *SERAC1* cause leucine degradation barriers, which, in turn, cause an increase of 3-methylglutaconic aciduria; on the other hand, under glucose deficiency or starvation, fatty acids are oxidized in the liver to produce ketone bodies as energy for the brain. In the process of amino acid metabolism, fatty acid metabolism, and glycolysis, mitochondria are required to participate in the key production of Acetyl-CoA (7). Therefore, low ketone hypoglycemia not only occurs when fatty acid metabolism is abnormal (8) but also when mitochondrial function is abnormal. In the cholesterol metabolism pathway, impaired SERAC1 activity leads to deficiency of PG36:1 and increases free cholesterol (9), which is the main substance for the synthesis of bile acids.

Many syndromes have the phenotype of developmental delay. We were unable to complete the intelligence test because of the patient's deafness and we could not distinguish whether the

delayed psychomotor development was caused by mutations in SERAC1 or SATB2 or a combination of the two genes. However, the characteristics of downslanting palpebral fissures, cleft palate, and delayed primary dentition are consistent with phenotypes of SAS because SATB2 is expressed in upper-layer neurons, neural crest progenitors of the jaw, osteoblasts, odontoblasts, and other dental progenitor cells (10). We listed the phenotypes of the two diseases in **Supplementary Table 2.**

Strengths and Limitations

We followed-up the case for 15 months and presented a complete process of disease development. These findings extended the phenotype spectrum of the two diseases and provided new insights into such rare diseases. Although medicine of muscle relaxant and antioxidant play roles in symptomatic treatment, the child was not given timely and standardized treatment, which might aggravate her delayed motor development. In addition, MEGDEL syndrome has the phenotype of cholestasis, but we cannot determine whether it is a severe phenotype of MEGDEL syndrome or the superposition of the two rare syndromes.

CONCLUSION

We identified two novel variants of *SERAC1* and a *de novo* variant of *SATB2* in a newborn. The case showed typical and specific phenotypes of these two rare diseases, especially the progressive cholestasis and high serum lactate after rehabilitation training and hypoglycemia with low ketone under starving conditions. The article presented a serious phenotype and disease progression, and summarized the metabolic pathways of abnormal indicators in the infant. We hope to enlighten our pediatric colleagues by providing more information on such rare diseases.

DATA AVAILABILITY STATEMENT

The original contributions presented in the study are included in the article/**Supplementary Materials**, further inquiries can be directed to the corresponding author/s.

ETHICS STATEMENT

The studies involving human participants were reviewed and approved by The People's Hospital of Xinjiang Uygur Autonomous Region (#2017008). Written informed consent to participate in this study was provided by the participants' legal guardian/next of kin.

AUTHOR CONTRIBUTIONS

YS and HZ conceptualized and designed the study, drafted the initial manuscript, and reviewed and revised the manuscript. HW, JY, and BW collected data, carried out the initial analyses, and reviewed and revised the manuscript. LL and WZ designed the data collection instruments, coordinated and supervised data collection, and critically reviewed the manuscript. All authors approved the final manuscript as submitted and agree to be accountable for all aspects of the work.

ACKNOWLEDGMENTS

Thank you to the family of the patient to provide the information.

SUPPLEMENTARY MATERIAL

The Supplementary Material for this article can be found online at: https://www.frontiersin.org/articles/10.3389/fped.2021.713458/full#supplementary-material

REFERENCES

1. Finsterer J, Scorza FA, Fiorini AC, Scorza CA. MEGDEL syndrome. *Pediatr Neurol.* (2020) 110:25–9. doi: 10.1016/j.pediatrneurol.2020.03.009
2. Wortmann SB, Vaz FM, Gardeitchik T, Vissers LE, Renkema GH, Schuurs-Hoeijmakers JH, et al. Mutations in the phospholipid remodeling gene SERAC1 impair mitochondrial function and intracellular cholesterol trafficking and cause dystonia and deafness. *Nat Genet.* (2012) 44:797–802. doi: 10.1038/ng.2325
3. Zarate YA, Fish JL. SATB2-associated syndrome: mechanisms, phenotype, and practical recommendations. *Am J Med Genet A.* (2017) 173:327–37. doi: 10.1002/ajmg.a.38022
4. Lin Y, Xinran D, Xiaomin P, Xiang C, Bingbing W, Huijun W, et al. Evaluation of turn around time and diagnostic accuracy of the next generation sequencing data analysis pipeline version 2 of Children's Hospital of Fudan University. *Chinese J Evidence-Based Pediatr.* (2018) 2:118–23. doi: 10.3969/j.issn.1673-5501.2018.02.008
5. Gerards M, Sallevelt SC, Smeets HJ. Leigh syndrome: resolving the clinical and genetic heterogeneity paves the way for treatment options. *Mol Genet Metab.* (2016) 117:300–12. doi: 10.1016/j.ymgme.2015.12.004
6. Wortmann SB, de Brouwer APM, Wevers RA, Morava E. SERAC1 deficiency. In: Adam MP, Ardinger HH, Pagon RA, Wallace SE, Bean LJH, Mirzaa G, et al., editors. *GeneReviews(®).* Seattle, WA: University of Washington; Initial Posting (2020).
7. Pietrocola F, Galluzzi L, Bravo-San Pedro JM, Madeo F, Kroemer G. Acetyl coenzyme A: a central metabolite and second messenger. *Cell Metab.* (2015) 21:805–21. doi: 10.1016/j.cmet.2015.05.014
8. Talley JT, Mohiuddin SS. *Biochemistry, Fatty Acid Oxidation. StatPearls.* Treasure Island, FL: StatPearls Publishing (2021).
9. Roeben B, Schüle R, Ruf S, Bender B, Alhaddad B, Benkert T, et al. SERAC1 deficiency causes complicated HSP: evidence from a novel splice mutation in a large family. *J Med Genet.* (2018) 55:39–47. doi: 10.1136/jmedgenet-2017-104622
10. Zarate YA, Bosanko KA, Caffrey AR, Bernstein JA, Martin DM, Williams MS, et al. Mutation update for the SATB2 gene. *Hum Mutat.* (2019) 40:1013–29. doi: 10.1002/humu.23771

Conflict of Interest: The authors declare that the research was conducted in the absence of any commercial or financial relationships that could be construed as a potential conflict of interest.

frontiers in Genetics

ORIGINAL RESEARCH
published: 23 December 2021
doi: 10.3389/fgene.2021.793894

Noninvasive Prenatal Screening Based on Second-Trimester Ultrasonographic Soft Markers in Low-Risk Pregnant Women

Yunyun Liu[1,2], Xiaosha Jing[1,2], Lingling Xing[1,2], Sha Liu[1,2], Jianlong Liu[1,2], Jing Cheng[1,2], Cechuan Deng[1,2], Ting Bai[1,2], Tianyu Xia[1,2], Xiang Wei[1,2], Yuan Luo[1,2], Quanfang Zhou[1,2], Qian Zhu[1,2] and Hongqian Liu[1,2]**

[1]Medical Genetics Department/Prenatal Diagnostic Center, West China Second University Hospital, Sichuan University, Chengdu, China, [2]Key Laboratory of Birth Defects and Related Diseases of Women and Children, Ministry of Education, Sichuan University, Chengdu, China

OPEN ACCESS

Edited by:
Emiliano González Vioque, University Clinical Hospital of Santiago, Spain

Reviewed by:
Thomas Liehr, Friedrich Schiller University Jena, Germany
Matthew Hoi Kin Chau, The Chinese University of Hong Kong, China

***Correspondence:**
Qian Zhu
zhuqian_2009@163.com
Hongqian Liu
hongqian.liu@163.com

Specialty section:
This article was submitted to Genetics of Common and Rare Diseases, a section of the journal Frontiers in Genetics

Received: 12 October 2021
Accepted: 25 November 2021
Published: 23 December 2021

Citation:
Liu Y, Jing X, Xing L, Liu S, Liu J, Cheng J, Deng C, Bai T, Xia T, Wei X, Luo Y, Zhou Q, Zhu Q and Liu H (2021) Noninvasive Prenatal Screening Based on Second-Trimester Ultrasonographic Soft Markers in Low-Risk Pregnant Women. Front. Genet. 12:793894. doi: 10.3389/fgene.2021.793894

Background: We aimed to assess the clinical application of noninvasive prenatal screening (NIPS) based on second-trimester ultrasonographic soft markers (USMs) in low-risk pregnant women.

Methods: Data of pregnant women between April 2015 and December 2019 were retrospectively analyzed. Pregnant women [age at expected date of confinement (EDC) of <35 years; low risks for trisomy 21 (T21) and trisomy 18 (T18) based on maternal serum screening; presenting second-trimester USMs (7 types)] who successfully underwent NIPS and had available follow-up information were included in our study. Cases with positive NIPS results were prenatally diagnosed. All patients were followed up for 6 months to 2 years after NIPS, and their clinical outcomes were obtained. Subgroup analyses were performed according to the different USMs.

Results: NIPS suggested that among a total of 10,023 cases, 37 (0.37%) were at high risk of aneuploidy, including 4 T21, 6 trisomy 13 (T13), and 27 sex chromosome abnormalities (SCA). Ten cases with aneuploidy (0.10%) were confirmed by prenatal diagnosis, consisting of two T21 and eight SCA. The eight fetuses with SCA consisted of one monosomy X, two XXY, one XXXY, one XXX, one XYY, and two mosaicisms. T21 was detected in one fetus with absent or hypoplastic nasal bone and one fetus with echogenic intracardiac focus (EICF). SCA was detected in five fetuses with EICF, two fetuses with multiple soft markers, and one fetus with echogenic bowel. The positive rate of chromosomal aneuploidy was significantly higher in fetuses with absent or hypoplastic nasal bone (6.25 vs. 0.10%, $p = 0.017$), echogenic bowel (3.7 vs. 0.10%, $p = 0.029$), and multiple soft markers (0.678 vs. 0.10%, $p = 0.045$) than in the total fetuses. The positive predictive values (PPVs) of NIPS in these three groups were 100%, 50%, and 100%, respectively. EICF accounted for 93.25% (9,346/10,023) of the study population, whereas the PPV of NIPS was only 20%.

Conclusion: NIPS is an advanced screening test for low-risk pregnant women. In the 10,023 pregnant women sampled, SCA were more common than autosomal trisomy, and

EICF was the most frequent USM but the least predictive aneuploidy. Further aneuploidy evaluation is suggested for low-risk pregnant women whose ultrasound indicates absent or hypoplastic nasal bone, echogenic bowel, or multiple soft markers. NIPS can serve as a second-line complementary screening for these women.

Keywords: noninvasive prenatal screening, ultrasonographic soft markers, trisomy 21 (Down syndrome), sex chromosome abnormality, positive predictive value, aneuploidy

INTRODUCTION

With the rapid development of ultrasound technology for application in the first and second trimesters, an increasing number of small ultrasound markers have been discovered, that is, ultrasonographic soft markers (USMs). USMs have a special ultrasonic feature; some USMs disappear naturally in later pregnancy stages or after delivery, whereas others may persist even after birth. USMs are closely associated with fetal chromosomal abnormalities and adverse pregnancy outcomes. The association between nuchal translucency thickness and Down syndrome was first reported in the 1980s (Benacerraf et al., 1985). Since then, diverse ultrasound anomalies have been reported to be associated with trisomy 21 (T21) (Nyberg and Souter, 2001), such as echogenic intracardiac focus (EICF), absent or hypoplastic nasal bone, and mild pyelectasis. Nevertheless, several studies have shown that USMs increase the incidence of invasive prenatal puncture surgery (Ahman et al., 2014). Lee et al. (2007) also found that the detection and interpretation of USMs were correlated to an increase in maternal anxiety and unnecessary amniocentesis.

Moreover, in the relevant laws, regulations, norms, or corresponding guidelines of China, there are currently no clear provisions on how to handle USMs. Article 17 of the Law of the People's Republic of China on Maternal and Infant Health Care (revised on August 30, 2018 and effective as of August 30, 2018) stipulates that if doctors find or suspect fetal abnormalities after prenatal examination, prenatal diagnosis should be made for pregnant women. Article 20 of the Measures for the Implementation of Law of the Peoples Republic of China on Maternal and Infant Health Care (promulgated on June 20, 2001) stipulates that if a fetus is abnormal or has suspicious malformations, doctors should make a prenatal diagnosis; however, USMs do not necessarily indicate fetal abnormalities or malformations. To further confirm aneuploidy, most Chinese doctors refer to the consensus issued by the American College of Obstetricians and Gynecologists (ACOG) (American College of Obstetricians and Gynecologists' Committee on Practice Bulletins-Obstetrics et al., 2020) and the Society for Maternal-Fetal Medicine (SMFM) (Prabhu et al., 2021). ACOG Practice Bulletin 226 (American College of Obstetricians and Gynecologists' Committee on Practice Bulletins-Obstetrics et al., 2020) states that if aneuploidy testing shows a low-risk result, then no further risk assessment is needed for fetus exhibiting particular USMs such as EICF, choroid plexus cyst, mild pyelectasis, or short femur length. The Society for Maternal–Fetal Medicine (SMFM) (Prabhu et al., 2021) also suggests that fetuses with negative maternal serum screening results for EICF, echogenic bowel, and shortened long bones need no further aneuploidy evaluation. However, only few studies have examined the applicability of these two guidelines for pregnant women in China and the residual risks of NIPS in these women.

Currently, maternal serum screening and NIPS are the major prenatal screening programs for evaluating the risk of aneuploidy. Lo et al. (1997) reported the presence of circulating cell-free fetal DNA (cffDNA) in maternal plasma and serum, which has been rapidly and widely used for prenatal screening owing to its high sensitivity and high positive predictive value (PPV). However, the traditional maternal serum screening method cannot assess the risk of sex chromosome aneuploidy (SCA). Except for Turner syndrome, in which structural anomalies are easily observed, the clinical features of other types of SCA are often undetectable in prenatal ultrasound examinations. Unless SCA is detected by invasive prenatal diagnosis, most fetuses with SCA are not diagnosed until birth or puberty. NIPS *via* massive parallel sequencing enables the detection of fetal SCA. Therefore, NIPS can simultaneously detect the risk of trisomy and SCA.

For the identification of birth defects and for health and economic considerations, prenatal screening methods are applied in China, including maternal serum screening, NIPS, and ultrasound examination. Prenatal screening is usually performed in the following order: first-trimester ultrasound (to detect nuchal translucency, NT), first-trimester serum screening, second-trimester serum screening, and second-trimester ultrasound. According to the relevant regulations in China, NIPS is recommended for pregnant women at intermediate risk based on maternal serum screening. These women are subjected to NIPS at relatively late pregnancy weeks. In contrast, some pregnant women choose NIPS for direct evaluation of fetal aneuploidy after understanding the difference between maternal serum screening and NIPS; these women undergo NIPS at relatively early gestational weeks. Prenatal diagnosis is recommended for pregnant women at high risk based on maternal serum screening and high risk of NIPS, as well as those with advanced age at delivery and an indication of abnormal fetal structure in ultrasound examination.

Previous studies have shown that NIPS has a good ability in detecting aneuploidy, including T21 and SCA, in high-risk populations (Bianchi et al., 2014; Garshasbi et al., 2020). However, the application of NIPS for detecting fetal aneuploidy has not been extensively studied in pregnant women at low risk based on maternal serum screening and follow-up ultrasound indicating USMs. Therefore, we retrospectively reviewed the data of pregnant women who underwent maternal serum screening and NIPS in the Prenatal

Diagnosis Center of West China Second University Hospital of Sichuan University. Pregnant women who had low risk for T21 or trisomy 18 (T18) based on maternal serum screening and second-trimester ultrasound and successfully underwent NIPS were included in our study.

The aims of the present study were (1) to assess the clinical application of NIPS in the second trimester in a retrospective cohort of pregnant women with USMs and at low risk for common chromosomal abnormalities according to maternal serum screening; (2) to determine the USMs possessing a strong predictive value in the study population; and (3) to determine the feasibility of recommending the screening method that we designed in clinical genetic counseling from the perspective of health economics.

MATERIALS AND METHODS

Study Population

We retrospectively analyzed the data of pregnant women who underwent maternal serum screening, NIPS, and prenatal diagnosis at the Prenatal Diagnosis Center of West China Second University Hospital of Sichuan University, Chengdu, Sichuan Province, China from April 2015 to December 2019. The inclusion criteria were as follows: (1) age at the expected date of confinement (EDC) of less than 35 years; (2) low risk for T21 and T18 based on maternal serum screening; (3) indication of USMs according to second-trimester ultrasound; and (4) NIPS case. The exclusion criteria were as follows: (1) no NIPS results, including failure during cell-free DNA (cfDNA) extraction and low fetal fraction; (2) no clinical pregnancy outcome, including termination of pregnancy, miscarriage, high-risk NIPS cases who declined further prenatal diagnosis, and cases lost to follow-up.

Pretest counseling was performed by trained clinical geneticists. All patients signed an informed consent form for genetic investigation. The test results were used for research with informed consent from the patients or legal guardians.

MATERNAL SERUM SCREENING

This procedure was described in our previous study (Deng et al., 2019; Bai et al., 2021). Risks of fetal T21 and T18 were obtained based on maternal serum screening, and patients were divided into three groups: the low-risk, intermediate-risk, and high-risk groups. A risk value of <1 in 1,000 indicated low risk for T21, and a risk value of <1 in 1,000 suggested low risk for T18. The risk value of the intermediate-risk group was 1/271–1/1,000 for T21 and 1/351–1/1,000 for T18. The risk value of the high-risk group was ≥1/270 for T21 and ≥1/350 for T18.

First-Trimester and Second-Trimester Ultrasound Examination

First-trimester ultrasound examination for NT and second-trimester ultrasound examination for fetal anomalies were performed in the Department of Diagnostic Ultrasound of West China Second University Hospital, Sichuan University, and other allied hospitals or affiliated hospitals that have medical business cooperation with West China Second Hospital of Sichuan University, following the guidelines of the International Society of Ultrasound in Obstetrics and Gynecology (Salomon et al., 2011). The diagnosis of second-trimester USMs was confirmed by a second experienced ultrasonographer. The following seven types of second-trimester USMs were included in this study: EICF, mild pyelectasis (dilatation of the renal pelvis ≥4 mm), single umbilical artery, mild ventriculomegaly (10 mm and <12 mm), absent or hypoplastic nasal bone (absent or <2.5 mm), echogenic bowel, and short femur length (*Z*-score, −2 to −4).

Noninvasive Prenatal Screening

Peripheral blood (8–10 ml) was collected from each pregnant woman and then placed into Cell-free BCT tubes (Streck Inc., Omaha, NE, United States). The upper plasma was isolated from the blood samples after being centrifuged twice within 72 h. Fifty microliters of cfDNA was isolated from 1,200 μl of plasma using a DNA extraction kit (Hangzhou Berry Gene Diagnostic Technology Co., Ltd., Hangzhou, China) according to the manufacturer's instruction. The obtained DNA concentration ranged from 0.05 ng/μl to 0.6 ng/μl. Next, 20 μl of cfDNA libraries was constructed by end filling and adapter ligation, and qPCR analysis was performed to verify whether the concentration and quality of cfDNA libraries were satisfactory. The cfDNA libraries were subjected to massive parallel sequencing using the NextSeq CN500 high-throughput sequencing kit (Illumina) on a NextSeq CN500 platform (Illumina), generating approximately 5 million raw data with 36-bp reads (Liu et al., 2021).

Sequencing reads were uniquely mapped to the hg19 human reference genome. The *Z*-score values of the 24 chromosomes were further calculated using normalized chromosome representation and GC correction (Liu et al., 2021). The fetal autosomal trisomy status was determined based on *Z*-scores (normal range, $-3 < Z < 3$). A high risk of NIPS was defined as a *Z*-score of greater than 3 for chromosome 21, 18, or 13. A *Z*-score value of chromosome 21, 18, or 13 ranging from −3 to 3 indicated a low risk of NIPS. The method for calculating the *Z*-score value of chromosomes X and Y was described in our previous study (Bai et al., 2021).

All participants were given an NIPS test report on the estimated fetal risk of T21, T18, and trisomy 13 (T13) and a supplementary report if a high risk of SCA was suspected. The test was considered a failure if unqualified total cfDNA concentration was obtained twice or if the fetal fraction was twice calculated to be <4%.

Invasive Prenatal Diagnosis

For pregnant women at high risk of NIPS, clinical counselling was offered by clinical geneticists, and further invasive prenatal diagnosis to determine chromosomal abnormalities was recommended.

Amniocentesis or cordocentesis was performed in the late second trimester or early third trimester, and chromosomal

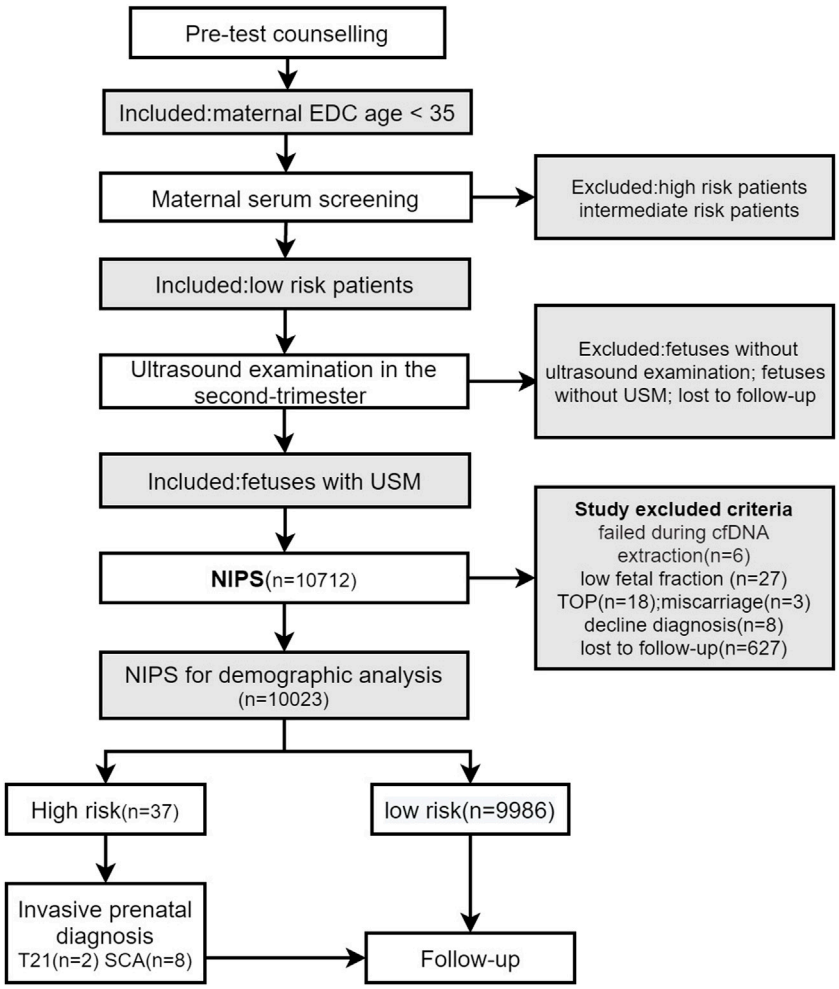

FIGURE 1 | EDC, expected date of confinement; USM, ultrasonographic soft markers; NIPS, noninvasive prenatal screening; TOP, termination of pregnancy.

microarray analysis (CMA), copy number variation sequencing (CNV-Seq), or karyotyping was conducted to detect fetal aneuploidy and other fetal chromosome abnormalities, in accordance with previously published studies (Wang et al., 2018; Deng et al., 2019; Hu et al., 2021). Furthermore, all samples were subjected to quantitative fuorescence polymerase chain reaction (QF-PCR) for chromosomes 21, 18, 13, X, and Y, and if the short tandem repeat markers were abnormal, enumeration was performed by fluorescence *in situ* hybridization.

The pregnant women were subjected to clinical follow-up assessments *via* telephone communication and review of medical records from 6 months to 2 years after undergoing NIPS. We also collected data on circumstances before birth, including prenatal diagnosis results, situations of high-risk NIPS cases who declined further prenatal diagnosis, and developmental details diagnosed by pediatricians after birth.

Statistical Analysis

SPSS Statistics software version 19.0 (SPSS Inc., Chicago, IL, United States) was used for statistical analysis. Comparisons between groups were determined using chi-square test or Fisher's exact test. Statistical significance was set at $p < 0.05$.

RESULTS

Study Participants

This was a retrospective study. A total of 143,067 pregnant women underwent NIPS at our hospital between April 2015 and December 2019. A total of 10,023 pregnant women who met the inclusion criteria were included, and retrospective analysis was performed. The study flow diagram is shown in **Figure 1**.

The maternal age ranged from 16 to 34 years. The median maternal weight was 58.80 kg (range, 37–97 kg), and the median maternal height was 159.00 cm (range, 140–177 cm). The study population predominantly originated from China. A total of 99.60% (9,983/10,023) of the pregnancies were singleton pregnancies, and 1.14% (114/10,023) of the pregnant women conceived with assisted reproductive technology (without Pre-implantation Genetic Testing for Aneuploidy). The demographic

TABLE 1 | Demographic characteristics of the 10,023 patients.

Characteristic	*N* (%)
Mean maternal age (range), years	26.75 (16–34)
<35 years	10,023 (100%)
Median maternal weight (range), kg	58.80 (37–97)
Median maternal height (range), cm	159.00 (140–177)
Gestational age (range), weeks	24 (14–28)
Race or ethnic group, *n* (%)	
Asian	10,023 (100%)
Singleton pregnancy, *n* (%)	9,983 (99.60%)
Twin pregnancy, *n* (%)	40 (0.40%)
ART pregnancy, *n* (%)	114 (1.14%)

ART, assisted reproductive technology.

characteristics of the pregnant women included in this study are shown in **Table 1**.

EICF was the most common USM present in 9,346 cases (93.25%), followed by multiple soft markers in 295 cases (2.94%) and mild pyelectasis in 166 cases (1.66%).

Numerical Abnormality of Chromosomes in the Fetus

The overall prevalence of high risk of chromosomal aneuploidy (NIPS-positive results) in the fetuses was 0.37% (37/10,023). Among the 37 cases, 10 fetuses (27.03%) had a high risk of autosomal trisomy, including 4 fetuses at high risk of T21 and 6 fetuses at high risk of T13, and 27 fetuses (72.97%) had a high risk of SCA.

Finally, two cases were confirmed to have T21, and eight fetuses were diagnosed with SCA *via* invasive prenatal diagnosis. As shown in **Table 2**, among the eight fetuses with SCA, one had monosomy X, two had XXY, one had XXXY, one had XXX, one had XYY, and two had mosaicisms. SCA was detected in two pregnant women with multiple soft markers. Among fetuses with EICF, one T21 and five SCA cases were detected. One T21 case was detected in a fetus with absent or hypoplastic nasal bone, and one SCA was detected in a fetus with echogenic bowel. The other 27 cases showed false-positive results for NIPS, as confirmed by prenatal diagnosis. These cases consisted of 2 fetuses at high risk of NIPS for T21, 6 at high-risk of NIPS for T13, and 19 at high-risk of NIPS for SCA. A false-positive NIPS result for chromosomal aneuploidy was detected in 24 fetuses with EICF, one fetus with mild pyelectasis, one fetus with mild ventriculomegaly, and 1 fetus with echogenic bowel.

Clinical Test Results for NIPS in the Study Population

All NIPS-positive cases were confirmed by prenatal diagnosis and then followed up. No false-negative results were observed in any of the NIPS-negative cases. Thus, the rate of false-negative results for NIPS for T21, T18, T13, and SCA was 0% in this study. The sensitivity, specificity, positive predictive value (PPV), and negative predictive value of NIPS, respectively, were as follows: for T21: 100% (95% CI: 19.79–100%), 99.98% (95% CI: 99.92–99.99%), 50.00% (95% CI: 9.19–90.81%), 100% (95% CI: 99.95–100%); for SCA: 100% (95% CI: 59.77–100%), 99.81% (95% CI: 99.70–99.88%), 29.63% (95% CI: 14.50–50.34%), and 100% (95% CI: 99.95–100%). Among the cases with high risk for T13 as detected by NIPS, there were no true positive cases, resulting in a very low PPV. The clinical test performance of NIPS is outlined in **Table 3**.

Characteristics of Aneuploidy Among Fetuses With Ultrasonographic Soft Markers

In the study population, the rates of true-positive results for T21 and SCA as confirmed by prenatal diagnosis were 0.02% and 0.08%, respectively. The rate of true-positive results for chromosomal aneuploidy was significantly higher in fetuses with absent or hypoplastic nasal bone (6.25% vs. 0.10%, p = 0.017), echogenic bowel (3.7% vs. 0.10%, p = 0.029), and multiple soft markers (0.678% vs. 0.10%, p = 0.045) than in the total fetuses.

In the multiple soft markers and absent or hypoplastic nasal bone groups, NIPS had a PPV of 100% for aneuploidy, and this value reached 50% in the echogenic bowel group. EICF was the most common and abundant USM, accounting for 93.25% (9,346/10,023) of the study population. In contrast, NIPS had

TABLE 2 | Numerical abnormality of chromosomes in the fetus.

Ultrasound category	*n*	High risk of NIPS no	True Positive Validated by Invasive Prenatal diagnosis							Total
			T21	45,X	47,XXY	48,XXXY	47,XXX	47,XYY	Mosaicism	
Multiple soft markers	295	2	—	1	—	1	—	—	—	2
EICF	9,346	30	1		2		1	1	1[a]	6
Mild pyelectasis	166	1	—	—	—	—	—	—	—	0
SUA	117	0	—	—	—	—	—	—	—	0
Mild ventriculomegaly	40	1	—	—	—	—	—	—	—	0
Absent or hypoplastic nasal bone	16	1	1	—	—	—	—	—	—	1
Echogenic bowel	27	2	—	—	—	—	—	—	1[b]	1
Short femur length	16	0	—	—	—	—	—	—	—	0
Total	10,023	37	2 (0.02%)				8 (0.08%)			10 (0.10%)

EICF,echogenic intracardiac focus; SUA, single umbilical artery; T21:trisomy 21.

[a]*NIPS result: high risk of 45,X; diagnosis result: mos 45,X/46,XY, confirmed by FISH: 45,X [15]/46,XY [85].*

[b]*NIPS result: high risk of 47,XXX; diagnosis result: mos 47,XXX/46,XX, confirmed by FISH: 47,XXX [77]/46,XX [23].*

TABLE 3 | Clinical test performance of NIPS.

Variable	T21 (n = 10,023)	T13 (n = 10,023)	SCA (n = 10,023)	Total (n = 10,023)
Having fetal aneuploidy	—	—	—	—
Test positive for aneuploidy	100.00 (2/2)	0	100.00 (8/8)	100.00 (10/10)
Test negative for aneuploidy	0.00 (0/2)	0	0.00 (0/8)	0.00 (0/10)
Not having fetal aneuploidy	—	—	—	—
Test positive for aneuploidy	0.02 (2/10,021)	0.06 (6/10,023)	0.19 (19/10,015)	0.27 (27/10,013)
Test negative for aneuploidy	99.98 (10,019/10,021)	99.94 (10,017/10,023)	99.81 (9,996/10,015)	99.73 (9,986/10,013)
Sensitivity (95% CI), %	100 (19.79–100)	—	100 (59.77–100)	100 (65.55–100)
Specificity (95% CI), %	99.98 (99.92–99.99)	99.94 (99.86–99.98)	99.81 (99.70–99.88)	99.73 (99.60–99.82)
Positive predictive value (95% CI), %	50.00 (9.19–90.81)	0 (0–48.32)	29.63 (14.50–50.34)	27.03 (14.37–44.39)
Negative predictive value (95% CI), %	100 (99.95–100)	100 (99.95–100)	100 (99.95–100)	100 (99.95–100)
False positive rate (95% CI), %	50.00 (9.19–90.81)	100 (51.68–100)	70.37 (49.66–85.50)	72.97 (55.61–85.63)
False negative rate (95% CI), %	0 (0–0.05)	0 (0–0.05)	0 (0–0.05)	0 (0–0.05)

T21, trisomy 21; SCA, sex chromosome aneuploidy. Data are in percentages with raw numbers shown in parentheses. Statistical analysis shows 95% confidence intervals in parentheses.

TABLE 4 | Characteristics of aneuploidy among the fetuses with USM.

Ultrasound category	*n*	High risk of NIPS, *n*	Diagnosis validated aneuploidy						*p*-Value
			TP	FP	PR(%)	PPV(%)	FPR(%)	FNR(%)	
Multiple soft markers	295	2	2	0	0.678	100	0	0	0.045[a]
EICF	9,346	30	6	24	0.064	20	80	0	—
Mild pyelectasis	166	1	0	1	0	0	100	0	—
SUA	117	0	—	—	—	—	—	—	—
Mild ventriculomegaly	40	1	0	1	0	0	100	0	—
Absent or hypoplastic nasal bone	16	1	1	0	6.25	100	0	0	0.017[b]
Echogenic bowel	27	2	1	1	3.7	50	50	0	0.029[c]
Short femur length	16	0	—	—	—	—	—	—	—
Total	10,023	37	10	27	0.10[d]	27.03[e]	72.97	0	—

EICF, echogenic intracardiac focus; SUA, single umbilical artery; T21, trisomy 21; TP, true positive; FP, false positive; PR, positive rate; PPV, positive predictive value; FPR, false-positive rate; FNR, false-negative rate.

[a]*Positive rate: Multiple soft markers group vs. Total population,* p = *0.045.*

[b]*Positive rate: Absent or hypoplastic nasal bone group vs. Total population,* p = *0.017.*

[c]*Positive rate: Echogenic bowel group vs. Total population,* p = *0.029.*

[d]*The value is 0.59 if the study population excluded the EICF group.*

[e]*The value is 50 if the study population excluded the EICF group.*

only 20% PPV and 80% false-positive rate in the EICF group. No positive cases were found in the mild and mild ventriculomegaly groups. The results are listed in **Table 4**.

Among the 10 clinically confirmed aneuploidy cases, two pregnant women had a history of spontaneous abortion. Six pregnant women (60%) were selected for prenatal diagnosis with CNV-Seq after positive results for NIPS was obtained. The *Z*-scores of NIPS were >5 in confirmed T21 cases, and the *Z*-scores of X chromosomes were >7 in confirmed Klinefelter syndrome cases. The two pregnant women whose fetus were prenatally diagnosed with mosaicisms chose to give birth. The detailed clinical information is presented in **Table 5**.

Clinical Follow-Up Outcomes of Noninvasive Prenatal Screening-Negative Cases

The pregnancy outcomes of NIPS-negative pregnant women and fetuses are shown in **Table 6**. There were 9,752 normal fetuses, accounting for 97.66% of the total NIPS-negative population. There were 234 abnormal cases, accounting for 2.34% of the total NIPS-negative population, among which the fetus with height less than the standard value 2 SD, with weight less than the standard value 2SD, or both, accounted for 1.08% of the total birth population. Preterm births at less than 37 gestational weeks accounted for 0.39%, followed by congenital heart disease. Fetuses delivered by pregnant women with negative NIPS results were evaluated by senior pediatricians, and they reported no T21, T18, T13, SCA, or related abnormalities during neonatal examination and follow-up of this study population.

DISCUSSION

USMs are of great importance in clinical practice. They are often transient and nonpathological, but may indicate an increased risk of underlying fetal aneuploidy (Hu et al., 2021). In fact, USMs can

TABLE 5 | Clinical details of the 10 cases with fetal aneuploidy and positive NIPS.

No	Maternal age	Conception (spontaneous/ IVF)	Spontaneous abortion history (Y/N)	Result of maternal serum screening (risk of T21/T18)		USM in second trimester	NIPS positive results	NIPS *Z*-scores	Diagnosis methods	Diagnosis results	Comfirm test	Outcomes
1	29	Spontaneous	Y	1/2,493	1/22,378	EICF	T21	Chr21 12.3	CNV-seq	T21	QF-PCR	TOP
2	25	Spontaneous	N	1/1,496	1/70,695	Absent or hypoplastic nasal bone	T21	Chr21 5.14	CNV-seq	T21	QF-PCR	TOP
3	29	Spontaneous	N	1/6,312	1/35,176	EICF	ChrY+	ChrX –5.91 ChrY 105.41	CNV-seq	47,XYY	FISH	Born
4	28	Spontaneous	N	1/5,221	1/50,000	EICF	ChrX+	ChrX 3.66 ChrY –1.47	CMA	47,XXX	FISH	TOP
5	27	Spontaneous	N	1/13,737	1/100,000	EICF	ChrX+(Y)	ChrX 8.2 ChrY 76.09	CNV-seq	47,XXY	FISH	TOP
6	29	Spontaneous	N	1/50,000	1/50,000	EICF	ChrX-	ChrX –9.52 ChrY 6.02	CNV-seq	Mos 45,X/46,XY	FISH	Born
7	28	Spontaneous	N	1/50,000	1/50,000	EICF	ChrX+(Y)	ChrX 7.14 ChrY 88.36	CMA	47,XXY	FISH	TOP
8	27	IVF	Y	1/22,057	1/100,000	Echogenic bowel	ChrX+	ChrX 10.16 ChrY 0.17	CNV-seq	Mos 47,XXX/ 46,XX	FISH	Born
9	30	Spontaneous	N	1/11,734	1/97,085	Multiple soft markers (EICF, mild pyelectasis)	ChrX+(Y)	ChrX 12.28 ChrY 57.67	CMA	48,XXXY	FISH	TOP
10	30	Spontaneous	N	1/1,002	1/98,851	Multiple soft markers (EICF,SUA)	ChrX-	ChrX –7.63 ChrY 0.73	CMA	45,X	FISH	TOP

IVF, in vitro *fertilization; USM, ultrasonographic soft markers; EICF, echogenic intracardiac focus; SUA, single umbilical artery; T21, trisomy 21; Chr,chromosome; CNV-seq, copy number variation sequencing; CMA, chromosomal microarray analysis; FISH, fluorescence* in situ *hybridization; TOP, termination of pregnancy.*

TABLE 6 | Pregnancy outcomes in 9,986 women with negative NIPS.

Pregnant outcomes	*n*	Percentage (%)	Remarks
Normal after birth	9,752	97.66	—
Abnormalities	234	2.34	—
Premature delivery (<37 weeks)	39	0.39	—
Neonatal death	6	0.06	Congenital hypopnea syndrome (1 case), congenital heart disease (2 cases), leukemia (1 case), and death from choking on milk (2 cases)
Developmental delay	108	1.08	Height < standard value − 2 SD level or weight < standard value − 2 SD level
Language development delay	5	0.05	—
Congenital heart disease	25	0.25	Including aortic stenosis, tetralogy of Fallot, and atrial septal defect
Autism	2	0.02	—
Harelip	1	0.01	—
Thalassemia	4	0.04	—
Epilepsy	2	0.02	—
Favism	3	0.03	—
Allergy	8	0.08	Milk and egg allergy
Dystonia	5	0.05	1 had low muscle tone and 4 had high muscle tone
Polydactyly	2	0.02	—
Albinism	1	0.01	—
Angioma	8	0.08	—
Congenital valgus deformity of foot	1	0.01	—
Dysplasia of the ear canal and abnormal hearing	11	0.11	Ear canal development malformation (5), and hearing abnormality (6)
Funnel chest	1	0.01	—
Mediastinal tumor of thoracic cavity	1	0.01	—
Langerhans cell histiocytosis	1	0.01	—
Total	9,986	100	—

increase the detection rate of malformations by 4% (Boyd et al., 1998). However, the detection of USMs cause stress in pregnant women, and the depressive symptoms may persist until delivery (Ahman et al., 2010; Nevay et al., 2016). Previous studies have shown that USMs, such as EICF, thickened nuchal fold, and mild pyelectasis were commonly repeated in subsequent pregnancies, providing deeper insights into the genetic predisposition and recurrence of USMs (Ginsberg et al., 2017). In particular, the interpretation of abnormal results and clinical genetic consultation in pregnant women who have had USMs and undergone NIPS may also cause confusion for them and the clinicians. When ACOG and SMFM guidelines are used for genetic counseling, the residual risk in pregnant women in China must be elucidated. Moreover, large-scale studies of the clinical application of NIPS in pregnant women at low risk based on maternal serum screening and second-trimester ultrasound are required. Thus, we designed this study to explore the potential application of NIPS for USM-based detection of fetal aneuploidy in low-risk pregnant women, as well as to formulate a feasible strategy for aneuploidy detection.

The positive rate of aneuploidy was 0.1% (range: 0.064%–6.25%), which suggests a residual risk for aneuploidy of approximately 0.1% in our study population if no further aneuploidy evaluation is conducted. The positive rate of aneuploidy was lower than that reported in previous studies (Norton et al., 2015; Garshasbi et al., 2020; Margiotti et al., 2020). Selection bias might be attributable to this difference. There were several other possible reasons: (1) In our study, we selected patients with age at EDC of <35 years and those with low risk for T21 and T18 based on maternal serum screening, leading to a reduction in the overall background aneuploidy risk in this study population. (2) Several pregnant women whose age at EDC was close to but did not reach 35 years as well as several pregnant women whose maternal serum screening results were very close to the cutoff value may have been more inclined to opt for prenatal diagnosis directly. (3) In the second trimester, T18 and T13 are more likely to show structural abnormalities than T21, and the group of pregnant women who preferred prenatal diagnosis were excluded from our study population.

The mean gestational age in our study was 24 weeks, with a range of 14–28 weeks, and there were differences in the routine timings of NIPS, which is usually performed in the late first trimester or early second trimester (van der Meij et al., 2019). Detailed sonographic anatomical scanning is usually performed at 22–25 weeks of gestation in China. Our study population was pregnant women who underwent NIPS after second-trimester ultrasound examination; thus, the mean gestational age was the second trimester of pregnancy. Previous studies showed that the percentage of fetal fraction significantly increased with increasing gestational age (Hou et al., 2019). Therefore, the detection results of NIPS were credible.

In our study, the sensitivity of NIPS for both T21 and SCA reached 100%, and the specificity was >99.7%. Compared with direct prenatal diagnosis, NIPS delays the diagnosis of aneuploidy, but it can effectively screen fetal aneuploidy. No false-negative cases were found in our study after long-term follow-up (false-negative rate: 0). In addition, false-positive results are a serious issue in NIPS. In our study, 27 false-positive cases were identified. Considering that the cfDNA sample used for NIPS was derived from placenta, and not fetal DNA, the main cause of these false-positive results may be confined placental mosaicism. Other possible causes include

vanishing twin syndrome, maternal copy number variants, cancer, previous organ or bone marrow transplantation, medical conditions, or treatment affecting the quality of circulating DNA (Snyder et al., 2015; Bianchi and Chiu, 2018).

In the absence or hypoplastic nasal bone group, a case of T21 was confirmed, with a positive rate of 6.25% (1/16). The highest incidence of T21 was found in fetuses with absent or hypoplastic nasal bone, followed by that in fetuses with EICF. In our study, the PPV of NIPS for T21 was 100% in fetuses in the absent or hypoplastic nasal bone group, which was consistent with the data reported by Du et al. (2018). A previous study has also reported absent or hypoplastic nasal bone as one of the most prominent USMs in the second trimester (Agathokleous et al., 2013).

Isolated EICF was the most common USM in our study. The true-positive rates of T21 and SCA in the EICF group were much lower than those in the other groups. Only one T21 and five SCA cases were confirmed by prenatal diagnosis. This was consistent with previous findings (Agathokleous et al., 2013) that EICF had low positive likelihood ratio values for T21. According to ACOG (Committee on Practice Bulletins-Obstetrics; Committee on Genetics; Society for Maternal-Fetal Medicine. 2020) and SMFM (Prabhu et al., 2021), if isolated EICF is detected, no further risk assessment is needed in pregnant women at low risk based on maternal serum screening. Furthermore, NIPS is a good option for evaluating fetal aneuploidy if the mother demands further aneuploidy assessment. In our total study population, the aneuploidy positive rate and PPV of NIPS were reanalyzed after removing the EICF group, which increased the values to 0.59% and 50%, respectively.

However, large-scale studies focusing on the correlations between the prevalence of SCAs and USM in fetuses in low-risk populations have rarely been published in the literature. In our study, the highest incidence of SCAs was found in fetuses with echogenic bowel (3.7%), followed by those with multiple soft markers (0.68%). In previous studies, echogenic bowel was associated with fetal aneuploidy, congenital infections (mainly congenital CMV infection), structural anomalies (D'Amico et al., 2021; Ronin et al., 2017), the incidence of intrauterine growth restriction and intrauterine fetal demise (Mailath-Pokorny et al., 2012), and Zellweger syndrome (Aydemir et al., 2014). In previous studies, multiple soft markers were associated with a high incidence of chromosomal abnormalities (Wang et al., 2018; Hu et al., 2021). Our study found that the PPV of NIPS and the positive rate of SCAs in multiple soft marker groups were higher than those in the total population.

According to previous studies, *Z*-scores are considered to be correlated with NIPS accuracy (Tian et al., 2018; Zheng et al., 2020). In the current study, the *Z*-scores of NIPS were >5 for T21, and the *Z*-scores of X chromosomes were >7 for Klinefelter syndrome. Thus, in clinical genetic counseling with ultrasound, in addition to different types of USMs, we can also focus on the *Z*-scores of NIPS. Hu et al. (2021) and Wang et al. (2018) showed a correlation between the presence of USMs and the risk of pathogenic copy number variations (pCNVs), particularly in short femur length and multiple soft markers. Furthermore, prenatal diagnosis is recommended for detecting pCNVs in pregnant women with USMs and NIPS positivity. Chromosomal microarray analysis and CNV-Seq are also applicable to these cases.

In follow-up, we found that 17.78% (8/45) of women with positive NIPS results rejected further aneuploidy evaluation. Moreover, in pregnant women with negative results for NIPS, the preterm birth rate was 0.39%, and the proportion of infants with height or weight less than the standard value −2 SD was 1.08% of the overall population. The genetic disorders thalassemia and favism were also identified. Although NIPS can identify fetuses with abnormal chromosome numbers, it is not useful for detecting several monogenic diseases and autosomal recessive genetic disorders. Therefore, pregnant women with a family history of relevant genetic disorders should be fully informed of the scope and limitations of NIPS during genetic counseling.

The large sample size was a considerable strength of our study. Moreover, we performed subgroup analyses of different types of USMs and conducted an in-depth investigation of the applicability of NIPS in fetuses with different types of USMs in a low-risk population. Our findings offer more comprehensive genetic counseling for clinicians when facing a certain type of USMs.

However, our study also had several limitations. First, the distribution of the different types of fetal USMs varied considerably. The number of absent or hypoplastic nasal bone and short femur length cases was relatively small, which might have led to selection bias. Second, the karyotype results remained unknown for cases who had positive results for NIPS but rejected further aneuploidy evaluation, as well as for those who had termination of pregnancy and miscarriage, which might have caused bias in data analysis. Third, the gestational weeks at the time of second-trimester ultrasound were not recorded, and thus we could not incorporate this variable in our analysis.

CONCLUSION

Our study suggests that NIPS is an advanced screening test for pregnant women with age at EDC younger than 35 years, a low risk of maternal serum screening, and second-trimester USMs. In our study population, SCA was more common than autosomal trisomy, whereas EICF was the most frequent USM, but the least predictive of aneuploidy. If second-trimester ultrasound indicates absent or hypoplastic nasal bone, echogenic bowel, or multiple USMs, further aneuploidy evaluation is recommended, and NIPS can be used as a viable second-line complementary screening method.

DATA AVAILABILITY STATEMENT

The data analyzed in this study is subject to the following licenses/restrictions: The data for this article are not publicly available because of privacy concerns. Requests to access these datasets should be directed to QZ, zhuqian_2009@163.com; HL, hongqian.liu@163.com.

ETHICS STATEMENT

The studies involving human participants were reviewed and approved by the Institutional Ethics Committee of Sichuan

University. Written informed consent to participate in this study was provided by the participants' legal guardian/next of kin.

AUTHOR CONTRIBUTIONS

YL, QZ, and HL designed the concept and the experiment method of the research. YL wrote the main paper. QZ and HL supervised the project, had given valuable advices on the proceeding of this work, and revised the manuscript. XJ, LX, SL, JL, JC, CD, TB, TX, XW, and YL contributed to the experiments. YL, XJ, LX, and QZ contributed to the follow-up affairs. All authors discussed the results and commented on the manuscript at all stages.

ACKNOWLEDGMENTS

We thank the patients and family members who participated in this research program.

REFERENCES

Agathokleous, M., Chaveeva, P., Poon, L. C. Y., Kosinski, P., and Nicolaides, K. H. (2013). Meta-analysis of Second-Trimester Markers for Trisomy 21. *Ultrasound Obstet. Gynecol.* 41, 247–261. doi:10.1002/uog.12364

Åhman, A., Axelsson, O., Maras, G., Rubertsson, C., Sarkadi, A., and Lindgren, P. (2014). Ultrasonographic Fetal Soft Markers in a Low-Risk Population: Prevalence, Association with Trisomies and Invasive Tests. *Acta Obstet. Gynecol. Scand.* 93, 367–373. doi:10.1111/aogs.12334

Åhman, A., Runestam, K., and Sarkadi, A. (2010). Did I Really Want to Know This? Pregnant Women's Reaction to Detection of a Soft Marker during Ultrasound Screening. *Patient Educ. Couns.* 81, 87–93. doi:10.1016/j.pec.2009.12.011

American College of Obstetricians and Gynecologists' Committee on Practice Bulletins-ObstetricsCommittee on GeneticsSociety for Maternal-Fetal Medicine (2020). Screening for Fetal Chromosomal Abnormalities: ACOG Practice Bulletin Summary, Number 226. *Obstet. Gynecol.* 136, 859–867. doi:10.1097/AOG.0000000000004107

Aydemir, O., Kavurt, S., Esin, S., Kandemir, O., Bas, A. Y., and Demirel, N. (2014). Fetal Echogenic Bowel in Association with Zellweger Syndrome. *J. Obstet. Gynaecol. Res.* 40, 1799–1802. doi:10.1111/jog.12379

Bai, T., Liu, S., Liu, J., Jing, X., Deng, C., Xia, T., et al. (2021). Performance of Noninvasive Prenatal Screening in Twin Pregnancies: a Retrospective Study of 5469 Twin Pregnancies. *J. Maternal-Fetal Neonatal Med.* 1, 1–9. doi:10.1080/14767058.2021.1903860

Benacerraf, B. R., Barss, V. A., and Laboda, L. A. (1985). A Sonographic Sign for the Detection in the Second Trimester of the Fetus with Down's Syndrome. *Am. J. Obstet. Gynecol.* 151, 1078–1079. doi:10.1016/0002-9378(85)90385-0

Bianchi, D. W., and Chiu, R. W. K. (2018). Sequencing of Circulating Cell-free DNA during Pregnancy. *N. Engl. J. Med.* 379 (5), 464–473. doi:10.1056/NEJMra1705345

Bianchi, D. W., Parker, R. L., Wentworth, J., Madankumar, R., Saffer, C., Das, A. F., et al. (2014). DNA Sequencing versus Standard Prenatal Aneuploidy Screening. *N. Engl. J. Med.* 370, 799–808. doi:10.1056/NEJMoa1311037

Boyd, P., Chamberlain, P., and Hicks, N. (1998). 6-year Experience of Prenatal Diagnosis in an Unselected Population in Oxford, UK. *Lancet* 352, 1577–1581. doi:10.1016/s0140-6736(98)03202-4

D'Amico, A., Buca, D., Rizzo, G., Khalil, A., Silvi, C., Makatsariya, A., et al. (2021). Outcome of Fetal Echogenic Bowel: A Systematic Review and Meta-analysis. *Prenatal Diagn.* 41, 391–399. doi:10.1002/pd.5638

Deng, C., Zhu, Q., Liu, S., Liu, J., Bai, T., Jing, X., et al. (2019). Clinical Application of Noninvasive Prenatal Screening for Sex Chromosome Aneuploidies in 50,301 Pregnancies: Initial Experience in a Chinese Hospital. *Sci. Rep.* 9, 7767. doi:10.1038/s41598-019-44018-4

Du, Y., Ren, Y., Yan, Y., and Cao, L. (2018). Absent Fetal Nasal Bone in the Second Trimester and Risk of Abnormal Karyotype in a Prescreened Population of Chinese Women. *Acta Obstet. Gynecol. Scand.* 97, 180–186. doi:10.1111/aogs.13263

Garshasbi, M., Wang, Y., Hantoosh Zadeh, S., Giti, S., Piri, S., and Reza Hekmat, M. (2020). Clinical Application of Cell-free DNA Sequencing-Based Noninvasive Prenatal Testing for Trisomies 21, 18, 13 and Sex Chromosome Aneuploidy in a Mixed-Risk Population in Iran. *Fetal Diagn. Ther.* 47, 220–227. doi:10.1159/000501014

Ginsberg, Y., Khatib, N., Weiner, Z., Beloosesky, R., and Bronshtein, M. (2017). The Recurrence of Sonographic 'soft Markers': Ominous Sign or 'just' Genetics? *Prenat Diagn.* 37, 469–472. doi:10.1002/pd.5034

Hou, Y., Yang, J., Qi, Y., Guo, F., Peng, H., Wang, D., et al. (2019). Factors Affecting Cell-free DNA Fetal Fraction: Statistical Analysis of 13,661 Maternal Plasmas for Non-invasive Prenatal Screening. *Hum. Genomics* 13 (1), 62. doi:10.1186/s40246-019-0244-0

Hu, T., Tian, T., Zhang, Z., Wang, J., Hu, R., Xiao, L., et al. (2021). Prenatal Chromosomal Microarray Analysis in 2466 Fetuses with Ultrasonographic Soft Markers: a Prospective Cohort Study. *Am. J. Obstet. Gynecol.* 224, e1–e1516. doi:10.1016/j.ajog.2020.10.039

Lee, M. J., Roman, A. S., Lusskin, S., Chen, D., Dulay, A., Funai, E. F., et al. (2007). Maternal Anxiety and Ultrasound Markers for Aneuploidy in a Multiethnic Population. *Prenat. Diagn.* 27, 40–45. doi:10.1002/pd.1618

Liu, S., Liu, H., Liu, J., Bai, T., Jing, X., Xia, T., et al. (2021). Follow-up in Patients with Non-invasive Prenatal Screening Failures: A Reflection on the Choice of Further Prenatal Diagnosis. *Front. Genet.* 12, 666648. doi:10.3389/fgene.2021.666648

Lo, Y. M., Corbetta, N., Chamberlain, P. F., Rai, V., Sargent, I. L., Redman, C. W., et al. (1997). Presence of Fetal DNA in Maternal Plasma and Serum. *Lancet* 350, 485–487. doi:10.1016/S0140-6736(97)02174-0

Mailath-Pokorny, M., Klein, K., Klebermass-Schrehof, K., Hachemian, N., and Bettelheim, D. (2012). Are Fetuses with Isolated Echogenic Bowel at Higher Risk for an Adverse Pregnancy Outcome? Experiences from a Tertiary Referral center. *Prenat Diagn.* 32, 1295–1299. doi:10.1002/pd.3999

Margiotti, K., Cesta, A., Dello Russo, C., Cima, A., Barone, M. A., Viola, A., et al. (2020). Cell-free DNA Screening for Sex Chromosomal Aneuploidies in 9985 Pregnancies: Italian Single Experience. *BMC Res. Notes* 13, 167. doi:10.1186/s13104-020-05009-1

Nevay, D. L., Hippman, C., Inglis, A., Albert, A., and Austin, J. (2016). Impact of Increased Risk for Fetal Aneuploidy on Maternal Mood: a Prospective Longitudinal Study. *Acta Obstet. Gynecol. Scand.* 95, 1120–1128. doi:10.1111/aogs.12951

Norton, M. E., Jacobsson, B., Swamy, G. K., Laurent, L. C., Ranzini, A. C., Brar, H., et al. (2015). Cell-free DNA Analysis for Noninvasive Examination of Trisomy. *N. Engl. J. Med.* 372, 1589–1597. doi:10.1056/NEJMoa1407349

Nyberg, D. A., and Souter, V. L. (2001). Sonographic Markers of Fetal Trisomies: Second Trimester. *J. Ultrasound Med.* 20, 655–674. doi:10.7863/jum.2001.20.6.655

Prabhu, M., Kuller, J. A., and Biggio, J. R. (2021). Society for Maternal-Fetal Medicine Consult Series #57: Evaluation and Management of Isolated Soft Ultrasound Markers for Aneuploidy in the Second Trimester. *Am. J. Obstet. Gynecol.* 225, B2–B15. doi:10.1016/j.ajog.2021.06.079

Ronin, C., Mace, P., Stenard, F., Loundou, A., Capelle, M., Mortier, I., et al. (2017). Antenatal Prognostic Factor of Fetal Echogenic Bowel. *Eur. J. Obstet. Gynecol. Reprod. Biol.* 212, 166–170. doi:10.1016/j.ejogrb.2017.01.060

Salomon, L. J., Alfirevic, Z., Berghella, V., Bilardo, C., Hernandez-Andrade, E., Johnsen, S. L., et al. (2011). Practice Guidelines for Performance of the Routine Mid-trimester Fetal Ultrasound Scan. *Ultrasound Obstet. Gynecol.* 37, 116–126. doi:10.1002/uog.8831

Snyder, M. W., Simmons, L. E., Kitzman, J. O., Coe, B. P., Henson, J. M., Daza, R. M., et al. (2015). Copy-number Variation and False Positive Prenatal

Aneuploidy Screening Results. *N. Engl. J. Med.* 372 (17), 1639–1645. doi:10.1056/NEJMoa1408408

Tian, Y., Zhang, L., Tian, W., Gao, J., Jia, L., and Cui, S. (2018). Analysis of the Accuracy of Z-Scores of Non-invasive Prenatal Testing for Fetal Trisomies 13, 18, and 21 that Employs the Ion Proton Semiconductor Sequencing Platform. *Mol. Cytogenet.* 11, 49. doi:10.1186/s13039-018-0397-x

van der Meij, K. R. M., Sistermans, E. A., Macville, M. V. E., Stevens, S. J. C., Bax, C. J., Bekker, M. N., et al. (2019). TRIDENT-2: National Implementation of Genome-wide Non-invasive Prenatal Testing as a First-Tier Screening Test in the Netherlands. *Am. J. Hum. Genet.* 105 (6), 1091–1101. doi:10.1016/j.ajhg.2019.10.005

Wang, J., Chen, L., Zhou, C., Wang, L., Xie, H., Xiao, Y., et al. (2018). Identification of Copy Number Variations Among Fetuses with Ultrasound Soft Markers Using Next-Generation Sequencing. *Sci. Rep.* 8, 8134. doi:10.1038/s41598-018-26555-6

Zheng, Y., Wan, S., Dang, Y., Song, T., Chen, B., and Zhang, J. (2020). Clinical Experience Regarding the Accuracy of NIPT in the Detection of Sex Chromosome Abnormality. *J. Gene Med.* 22, e3199. doi:10.1002/jgm.3199

Conflict of Interest: The authors declare that the research was conducted in the absence of any commercial or financial relationships that could be construed as a potential conflict of interest.

frontiers in Genetics

ORIGINAL RESEARCH
published: 13 January 2022
doi: 10.3389/fgene.2021.812640

A Novel *SPG7* Gene Pathogenic Variant in a Cypriot Family With Autosomal Recessive Spastic Ataxia

Christina Votsi[1], *Antonis Ververis*[1], *Paschalis Nicolaou*[1], *Yiolanda-Panayiota Christou*[2], *Kyproula Christodoulou*[1*†] *and Eleni Zamba-Papanicolaou*[3†]

[1]Neurogenetics Department, The Cyprus Institute of Neurology and Genetics, Nicosia, Cyprus, [2]Neurobiology Department, The Cyprus Institute of Neurology and Genetics, Nicosia, Cyprus, [3]Neuroepidemiology Department, The Cyprus Institute of Neurology and Genetics, Nicosia, Cyprus

The *SPG7* gene encodes the paraplegin protein, an inner mitochondrial membrane—localized protease. It was initially linked to pure and complicated hereditary spastic paraplegia with cerebellar atrophy, and now represents a frequent cause of undiagnosed cerebellar ataxia and spastic ataxia. We hereby report the molecular characterization and the clinical features of a large Cypriot family with five affected individuals presenting with spastic ataxia in an autosomal recessive transmission mode, due to a novel *SPG7* homozygous missense variant. Detailed clinical histories of the patients were obtained, followed by neurological and neurophysiological examinations. Whole exome sequencing (WES) of the proband, *in silico* gene panel analysis, variant filtering and family segregation analysis of the candidate variants with Sanger sequencing were performed. RNA and protein expression as well as *in vitro* protein localization studies and mitochondria morphology evaluation were carried out towards functional characterization of the identified variant. The patients presented with typical spastic ataxia features while some intrafamilial phenotypic variation was noted. WES analysis revealed a novel homozygous missense variant in the *SPG7* gene (c.1763C > T, p. Thr588Met), characterized as pathogenic by more than 20 *in silico* prediction tools. Functional studies showed that the variant does not affect neither the RNA or protein expression, nor the protein localization. However, aberrant mitochondrial morphology has been observed thus indicating mitochondrial dysfunction and further demonstrating the pathogenicity of the identified variant. Our study is the first report of an *SPG7* pathogenic variant in the Cypriot population and broadens the spectrum of *SPG7* pathogenic variants.

Keywords: Cypriot family, novel missense variant, paraplegin, spastic ataxia, *SPG7* gene

OPEN ACCESS

Edited by:
Emiliano González Vioque, University Clinical Hospital of Santiago, Spain

Reviewed by:
Guido Primiano, Agostino Gemelli University Polyclinic (IRCCS), Italy
Andrea Legati, IRCCS Carlo Besta Neurological Institute Foundation, Italy

****Correspondence:***
Kyproula Christodoulou
roula@cing.ac.cy

†These authors have contributed equally to this work and share senior authorship

Specialty section:
This article was submitted to Genetics of Common and Rare Diseases, a section of the journal Frontiers in Genetics

Received: *10 November 2021*
Accepted: *20 December 2021*
Published: *13 January 2022*

Citation:
Votsi C, Ververis A, Nicolaou P, Christou Y-P, Christodoulou K and Zamba-Papanicolaou E (2022) A Novel SPG7 Gene Pathogenic Variant in a Cypriot Family With Autosomal Recessive Spastic Ataxia. Front. Genet. 12:812640. doi: 10.3389/fgene.2021.812640

INTRODUCTION

Hereditary cerebellar ataxias (HCA) and hereditary spastic paraplegias (HSP) comprise two groups of genetically and clinically heterogeneous disorders with more than 70 genes and loci reported for each group (Parodi et al., 2018). Pure and complex clinical forms for both groups as well as a considerable overlap have been described (Tesson et al., 2015; Bereznyakova and Dupre, 2018). Recent advancements in genetic diagnosis such as the use of next generation sequencing (NGS), enabled the association of new genes with

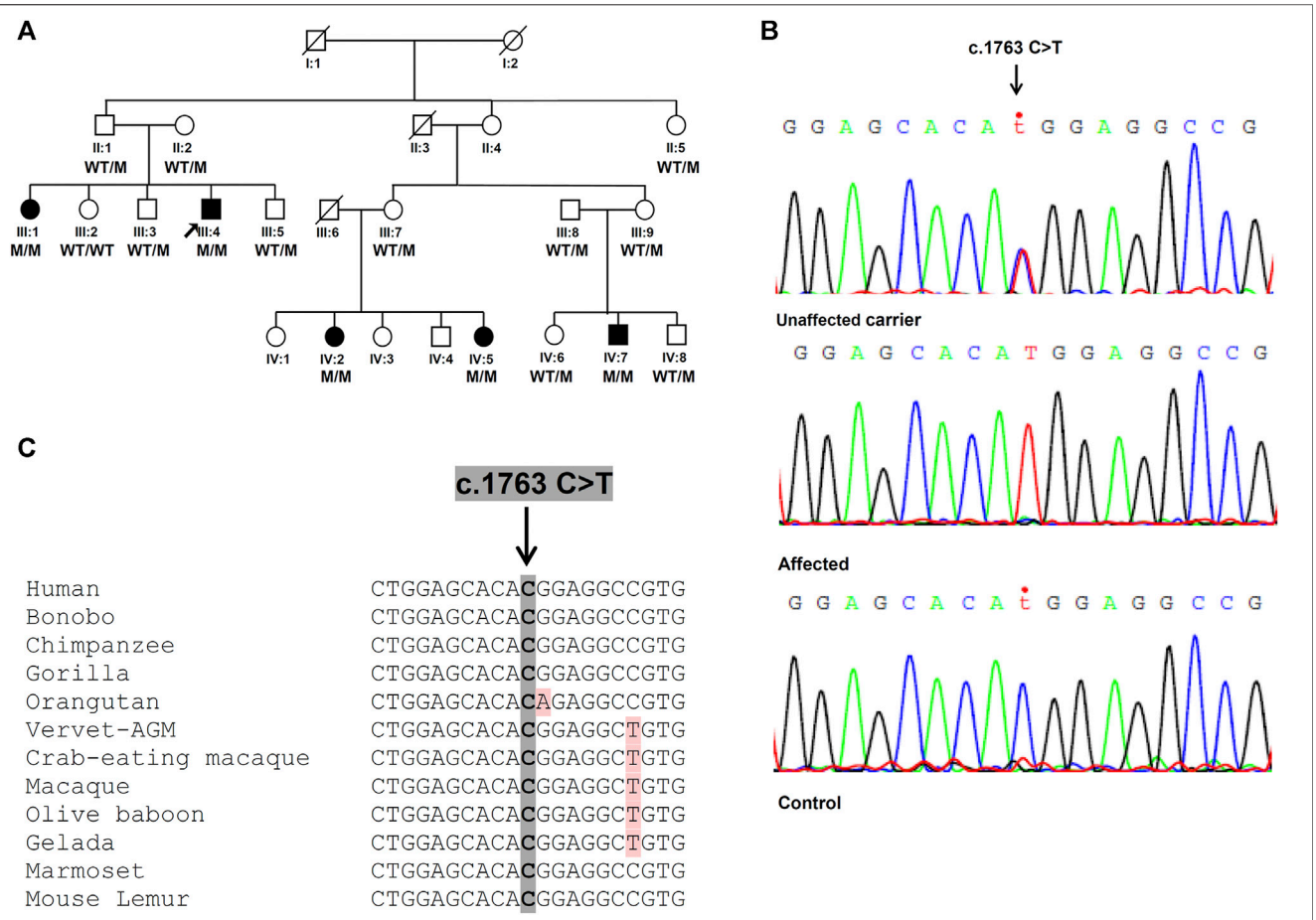

FIGURE 1 | Identification of the *SPG7* novel variant. **(A)** Family pedigree with segregation analysis (WT, wild-type, M, mutant). The arrow indicates the proband. **(B)** Sanger sequencing electropherograms. Unaffected carrier = II:1, affected = III:4 and control = non-related healthy individual. **(C)** Conservation of identified variant. The DNA sequence of the *SPG7* gene region encompassing the identified variant (c.1763C > T; p.Thr588Met) is highly conserved in various mammals.

these disorders and added to the phenotypic expansion of known genes. Therefore, the existing overlap has been strengthened and the new concept of spastic ataxia (SA) spectrum has been defined (Parodi et al., 2018).

Several genes initially classified as HSP or HCA have now been considered as SA genes. The *SPG7* gene with more than 100 reported pathogenic variants, was initially linked to pure and complicated HSP with cerebellar atrophy, and now represents a frequent cause of undiagnosed cerebellar ataxia and SA (Lallemant-Dudek and Durr, 2020). It encodes the paraplegin protein, a member of the ATPases AAA family that is located in the inner mithochondrial membrane and is implicated in other mitochondrial proteins processing (Wedding et al., 2014). Functional studies aiming at understanding the pathogenetic mechanisms of identified variants have linked the protein to mtDNA homeostasis (Wedding et al., 2014).

We hereby describe the genetic investigation of a large Cypriot family with five affected individuals presenting with SA. Whole exome sequencing enabled the identification of a novel homozygous missense variant in the *SPG7* gene. We also provide detailed clinical descriptions of all affected individuals and highlight some intrafamilial phenotypic variation.

MATERIALS AND METHODS

Samples

A four-generation family with 24 members and five patients (two males, three females) in two generations (**Figure 1A**) was included in the study. The grandparents originate from the same village; however, no relationship has been reported. Detailed clinical histories were obtained from all patients and they were subjected to neurological and neurophysiological evaluation by the CING neurologists. Brain MRI has been performed only at the early stages of the disease for three patients (III:4, IV:5, and IV:7). Blood samples were obtained from individuals II:1, II:2, II:5, III:1, III:2, III:3, III:4, III:5, III:7, III:8, III:9, IV:1, IV:2, IV:5, IV:6, IV:7, and IV:8. DNA was extracted from all available samples using standard salting out procedures.

Ethics Statement

This study has been approved by the Cyprus National Bioethics Committee (ΕΕΒΚ/ΕΠ/2013/09 and ΕΕΒΚ/ΕΠ/2013/28). Written informed consent was obtained from all study participants. Written informed consent was obtained from the individuals for the publication of any potentially identifiable images or data included in this article.

Molecular Analyses

Whole Exome Sequencing and Variant Filtering

WES was carried out on the proband as described previously (Votsi et al., 2014), followed by variant filtering: a preliminary filtering excluding variants with a minor allele frequency < 0.05 in 1,000 genomes, ExAC (Exome Aggregation Consortium) and EVS (Exome Variant Server) control databases was initially performed. Further *in silico* analysis focused on a gene panel encompassing HCA and HSP genes. Filtering criteria such as the expected genotype (homozygous/heterozygous), the coverage (>20x), the percentage of the alternative allele (>30%), the severity and the effect prediction according to Sift, Condel and Polyphen tools, were applied in order to prioritize the most significant variants to be further investigated for family segregation, with Sanger sequencing. Pathogenicity prediction was performed for a single novel pathogenic variant cosegregating with the disease in the family. Twenty one additional *in silico* tools or algorithms (including the widely used CADD, PROVEAN, Mutation Taster, DANN and other) provided by the VarCards database (Li et al., 2018) were used.

Sanger Sequencing

Primers amplifying the sequence encompassing the selected novel candidate variant, were designed by us. Amplification products were sequenced in both directions using the Big Dye Terminator v1.1 Cycle Sequencing kit [Applied Biosystems (ABI), California, United States]. Sequence traces were automatically compared with the normal region sequences as listed in the GenBank database using the Seqscape software (ABI).

Cell Lines

Lymphoblastoid cell lines (LCLs) were previously established using the standard Epstein Barr virus (EBV) infection procedure, for a couple of patients and independent control individuals after informed consent. They were cultured in RPMI 1640 medium (Biosera, Nuaille, France), supplemented with 10% FBS (ThermoFisher, Massachusetts, United States), and 50 U/ml of Penicillin/Streptomycin (Biosera).

Human SH-SY5Y were cultured in Dulbecco's Modified Eagle's medium (Biosera) supplemented with 10% FBS, 2 mM Glutamine (ThermoFisher), 50 U/ml Penicillin and 50 mg/ml Streptomycin.

All cell lines were kept at 37°C in 5% CO_2.

RNA Analysis

Total RNA was extracted from patients and independent control individuals LCLs, using the RNeasy Mini Kit (Qiagen, Hilden, Germany). cDNA was synthesized using the Protoscript First Strand cDNA Synthesis Kit (New England Biolabs, Ipswich, MA, United States). The synthesized strands were used as substrates for RNA expression studies and cloning of the *SPG7* gene. Three independent real-time PCR experiments of three technical replicates for each sample, using TaqMan probes for the *SPG7* (Hs00275795_m1) and two housekeeping genes [*GAPDH* (Hs99999905_m1) and *B2M* (Hs00187842_m1)] were performed using the QuantStudio 7 Flex instrument (ABI). The QuantStudio Real-Time PCR software was used for data analysis and the Student's *t*-test was used for the statistical analysis of the independent experiments derived values. A p-value < 0.05 was set as a threshold for statistical significance.

Plasmid Construction and Cell Transfection

The cDNA samples of a control individual and the proband were used as templates in order to amplify the wild-type (WT) and mutant *SPG7* ORFs, respectively. Appropriate primers sets containing specific restriction sites in order to insert the amplified fragments into the p-EGFP-N1 vector were designed by us and are available upon request. Sanger sequencing was employed in order to confirm that all plasmid constructs have been free of any new nucleotide changes in the *SPG7* cDNA. SH-SY5Y cell lines were then transfected with these constructs with the use of Lipofectamine 3000 (ThermoFisher) following the manufacturer's instructions. Cells were harvested 48 h after transfection for protein extraction.

Protein Analysis

In order to perform expression studies, protein was extracted from the patients' and controls' LCLs as well as the transfected SH-SY5Y cells as described previously (Ververis et al., 2020). After running in an SDS-PAGE polyacrylamide gel, proteins were transferred to Hybond-P hydrophobic polyvinylidene difluoride (PVDF) membranes (Millipore, Germany). Membranes were blocked for 3 h (LCLs) or 1 h (SH-SY5Y) in 5% non-fat dry milk in phosphate buffered saline (PBS)/Tween, at room temperature, followed by overnight incubation at 4°C with the primary antibodies for the protein of interest and a housekeeping control [rabbit anti-SPG7 (Sigma Aldrich Taufkirchen, Germany)/1:6,500 for LCLs, rabbit anti-GFP (Proteintech, Illinois, United States)/1:5,000 for SH-SY5Y, mouse anti-β-ACTIN (Sigma-Aldrich)/1:4,000 for LCLs, mouse anti-vinculin (7F9) (Santa Cruz Biotechnology, Heidelberg, Germany)/1:1,000 for SH-SY5Y]. The next day membranes were washed 3 × 10 min in PBS/Tween and incubated with the appropriate secondary antibodies for 1 hour. Three washes followed and proteins signals were visualised using the LumiSensor Chemiluminescent HRP Substrate Kit (Genscript, New Jersey, United States), in a UVP BioSpectrum Imaging System (UVP, California, United States). Three independent experiments were carried out for each case. The ImageJ 1.51j8 software was used for data analysis.

Immunofluorescence

SH-SY5Y cells were grown on coverslips. After 24 h they were transiently transfected with the pEGFP-N1 $SPG7^{WT}$ and mutant constructs with the use of Lipofectamine 3000 (ThermoFisher) following the manufacturer's instructions. After 48 h, cells were fixed for 10 min at RT with 4% w/v paraformaldehyde in PBS, permeabilised with Methanol for 10 min at −20°C and quenched

TABLE 1 | Clinical features of the patients.

Patient	III:1	III:4	IV:2	IV:5	IV:7
Gender	Female	Male	Female	Female	Male
Age at onset	46	16	23	25	17
First symptom(s)	Unst/GD	Unst/GD	Unst/GD	Unst/GD	Unst/GD
Age at examination	48	32	45	39	18
Mean follow up duration	30	38	11	12	32
Gait	Ataxic-spastic	Ataxic-spastic	Ataxic-spastic	Ataxic-spastic	Ataxic-spastic
Muscle weakness	LL, facial	LL, facial	LL, UL, facial	LL, UL	LL, Facial
Muscle wasting	–	–	–	–	–
Muscle tone UL	Increased	Normal	Normal	Normal	Normal
Muscle tone LL	Increased	Increased	Increased	Increased	Increased
Tendon reflexes	Brisk	Brisk	Brisk	Brisk	Brisk
Extensor plantar reflex	Bilateral	Bilateral	Bilateral	Bilateral	Bilateral
Cerebellar signs	Dysmetria and DDK	Dysmetria and DDK	Dysmetria and DDK	Dysmetria and DDK	Dysmetria and DDK
Dysarthria	+++	++	++	++	++
Dysphagia	++	–	–	–	–
Nystagmus	+	+	+	+	+
Sensory deficit	–	+[a]	–	–	–
Skeletal abnormalities	–	Pes cavus	–	–	Pes cavus
Ophthalmological signs	PEO	PEO and diplopia	Diplopia	–	PEO and diplopia
Optic Atrophy	–	+	–	–	–
Extrapyramidal symptoms	–	–	–	–	–
Peripheral Neuropathy	+	–	–	+	–
Dementia/Psychosis	–	–	–	–	–
Cognitive impairment	–	–	–	–	–
Bladder disturbance	UI	Mild UI	–	UI	–
Hearing loss	–	–	–	–	–
Respiratory difficulties	+++	–	–	–	–
Brain MRI findings	Not available	CA	Not available	CA	CA

[a]*Slightly reduced vibration and proprioception; CA, cerebellar atrophy; DDK, dysdiadochokinesia; LL, lower limbs; PEO, progressive external ophthalmoplegia; Unst/GD, Unsteadiness/ Gait Difficulties; (–), absent; (+), mild (or active); (++), moderate; (+++), severe; UL, upper limbs; UI, urinary incontinence*

for 10 min at RT with 50 mM NH_4Cl in PBS. Cell mitochondria were stained using the AIF antibody (Cell Signaling Technology, Leiden, Netherlands) and nuclei using Hoechst 33342 (ThermoFisher). Coverslips were mounted with Dako Fluorescent Mounting Medium (Agilent, California, United States). Images were captured with a Zeiss fluorescent microscope using the Axiovision software. Colocalization index was quantified by Manders' coefficient using Coloc2 plugin for ImageJ, and two-tailed *t* test was used to assess the *p* value. Mitochondrial morphology parameters were assessed with the use of a macro titled "mitochondrial morphology," developed by the Chu Lab for ImageJ as previously described (Dagda et al., 2009). One-way ANOVA analysis was conducted for the statistical evaluation of the mitochondrial morphology parameters.

RESULTS

Clinical Picture

The proband (III:4) developed balance difficulties during secondary school (16 years old) and by the age of 31 he presented spastic paraparesis. His elder sister (III:1) had a disease onset much later at 46, whereas the younger son of their cousin (IV:7) had an early onset, at 17. The two affected cousins (IV:2 and IV:5) had an onset between 23–25. All patients initially presented with gait unsteadiness and impaired balance which gradually deteriorated. They developed spasticity in the lower limbs, ataxic spastic gait and lower limb proximal weakness (**Table 1**). Dysarthria, bilateral nystagmus, dysmetria and dysdiadochokinesia, as well as bilateral extensor plantar reflex and clonus were observed in all patients. Progressive external ophthalmoplegia (PEO), pes cavus foot deformity, urinary incontinence and upper limbs weakness at advanced stage with facial weakness, double vision and mild neuropathy were also observed in some of the patients (**Table 1**). Patient III:1 also suffers from abdominal pains and gastrointestinal hemorrhages for many years, but most probably these derive from a non-neurological disease. Electrophysiological evaluation of the patients with nerve conduction studies revealed sensory-motor axon neuropathy in two patients (III:1, IV:5). Somatosensory evoked potentials examinations were within normal limits in the majority of the patients. Bilateral optic pathway dysfunction in patients III:4 and IV:7 has been indicated at advanced stages of the disease through visual evoked potentials examination. Brain MRI at the early stages of the disease (performed on three patients) revealed cerebellar atrophy. Muscle biopsy performed on the proband at the early stages of the disease, revealed a normal mitochondria number and structure. Overall, the progression of the disease was slow and the patients became wheel-chair bound on average 20 years after the disease onset. The first clinical impression had been recessive cerebellar ataxia with spasticity and more recently it has been redefined to SA.

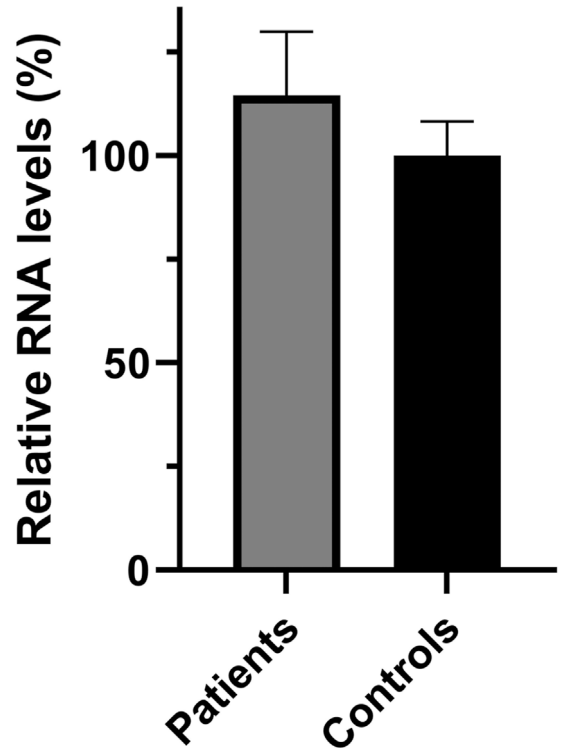

FIGURE 2 | Relative *SPG7* mRNA expression levels in lymphoblastoid cell lines derived from patients and control individuals. qPCR revealed that the *SPG7* gene expression has no significant difference between the patients (average 114%) and the controls (set to 100%), $p > 0.05$. Values were obtained after normalization with the *GAPDH* and *B2M* housekeeping genes. Data are represented as the mean of three independent triplicate experiments ± SD.

Genetic Analysis

A total of 71,696,896 reads, an average coverage of >20x for 92% of the target regions and 43.500 variants were identified through WES of the proband. After initial exclusion of variants with a minor allele frequency >0.05 in public databases, further analysis considering the HSP/HCA genes panel, enabled a significant reduction of the candidate variants to nine (**Supplementary Table S1**). Further evaluation considering the genotype, the variant consequence and severity, resulted in the identification of the single homozygous missense variant c.1763C > T, p.Thr588Met in the *SPG7* gene (**Figure 1B**), which has been also confirmed with family segregation analysis. Nucleotide and protein position of the reported variant are based on RefSeq accession numbers NM_003119.2 and NP_003110.1. This is a novel variant neither registered in gnomAD (gnomad.broadinstitute.org/), ExAC, 1,000 genomes, the ClinVar nor the LOVD databases. It has been also excluded from more than 200 control Cypriot chromosomes using Sanger sequencing. This variant results in the replacement of a neutral by a hydrophobic amino acid, and is located in the conserved peptidase M41 domain (**Figure 1C**) where many other missense pathogenic variants have been described. It is predicted to affect the protein function causing deleterious consequences. High pathogenicity scores thus enabling the characterizations "deleterious" or "damaging" which denote the most severe possible effects, resulted from 20 prediction algorithms or tools which are based either on single or diverse annotation methods. These included the Sift (0.001), the Provean (−4.94), the CADD (34), the DANN (0.999), the MutationTaster (1.0), the FATHMM (−1.72), the LRT (0.0), and other scores.

RNA and Protein Expression Studies

In addition to the pathogenicity prediction results for the novel *SPG7* c.1763C > T variant, we investigated a possible effect on the RNA and protein expression. To compare the expression of $SPG7^{WT}$ and $SPG7^{T588M}$, RNA and protein extracts derived from two available patients and three control individuals LCLs were used. qRT-PCR lead to the observation of similar expression levels between the patients and controls (**Figure 2**) thus excluding any effect of the variant on the RNA expression levels in this tissue. Western blot analysis using an anti-SPG7 antibody also did not indicate a significant difference between patient and control (**Figure 3A**). To further investigate if this was a tissue specific result we also performed protein expression studies using an

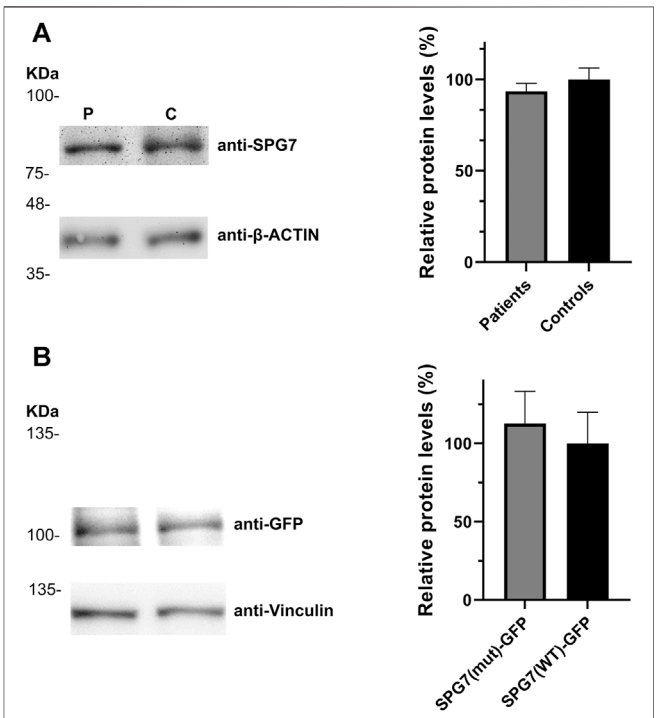

FIGURE 3 | Relative SPG7 protein expression levels in cells expressing the wild-type and the pathogenic variant. **(A)** Western blot using an anti-SPG7 antibody revealed similar protein expression between the group of patients with spastic ataxia (average 94%) and the group of control individuals (set to 100%) lymphoblastoid cell lines. Values were obtained after normalization with the β-actin housekeeping protein. Data are represented as the mean of three independent experiments ± SE. **(B)** Western blot using an anti-GFP antibody revealed similar SPG7-GFP protein expression in SH-SY5Y cells, transfected with the p-EGFP-N1 constructs expressing $SPG7^{T588M}$-GFP (average 113%) or $SPG7^{WT}$-GFP (set to 100%). Values were obtained after normalization with the vinculin housekeeping protein. Data are represented as the mean of three independent experiments ± SE.

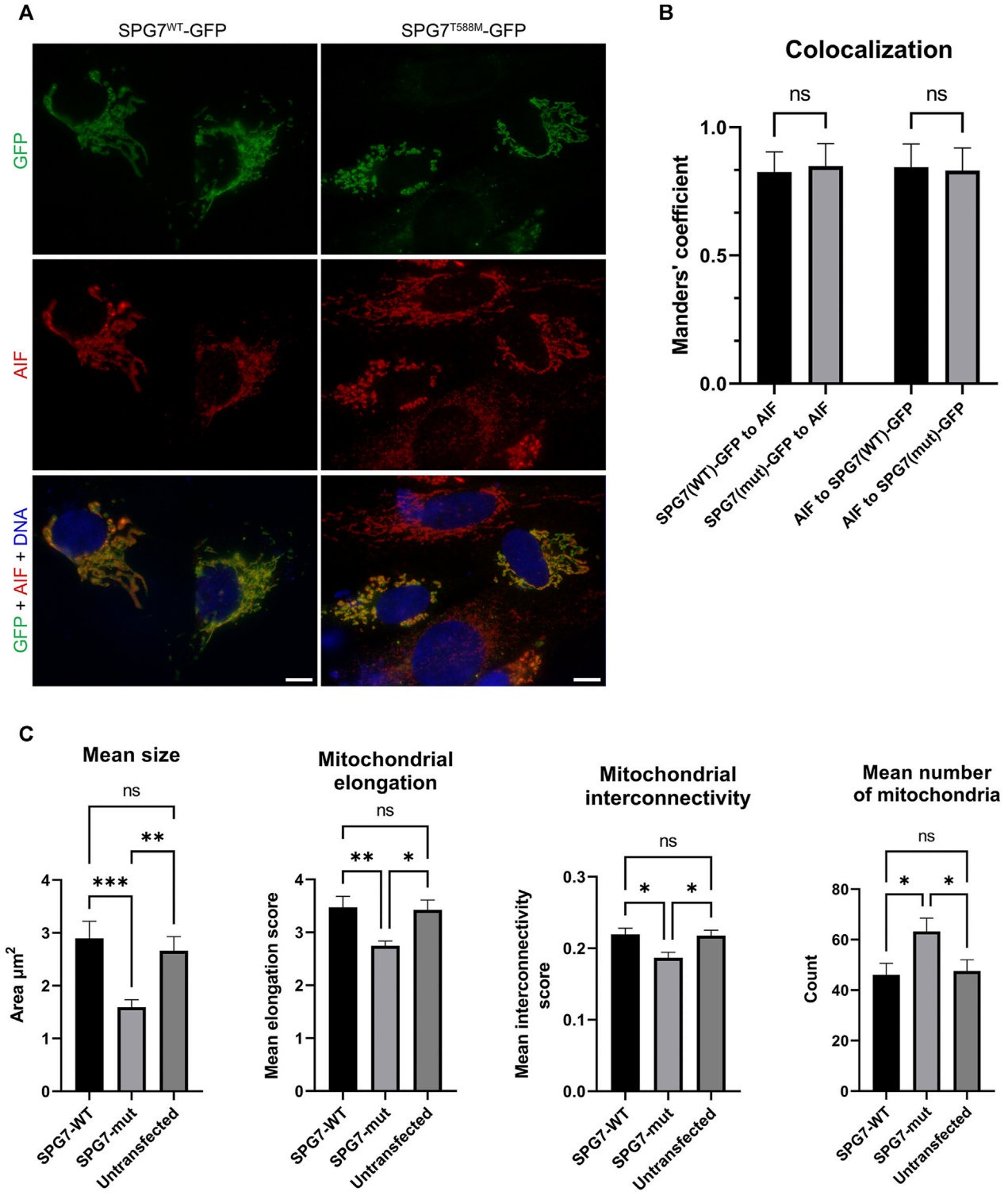

FIGURE 4 | Intracellular localization of SPG7^{WT}-GFP and SPG7^{T588M}-GFP and mitochondrial morphology assessment. **(A)** SPG7^{T588M}-GFP retains colocalization with mitochondria, in similar fashion with SPG7^{WT}-GFP. Green color represents the SPG7-GFP, red color represents mitochondria and blue color represents the nuclei. Scale bars are 10 µm. **(B)** Graph displaying Manders' coefficient quantification (fraction SPG7^{WT}-GFP or SPG7^{T588M}-GFP colocalizing with AIF, and vice versa) calculated from at least 20 fluorescence microscopy images for each isoform. Error bars are given by the SD and $n > 30$ for each condition. **(C)** Graphs displaying morphological characteristics of mitochondria: size, elongation, interconnectivity and number, in WT (SPG7^{WT}-GFP) and mutant (SPG7^{T588M}-GFP) transfected SH-SY5Y cells as well as in untransfected cells, calculated from at least 20 fluorescence microscopy images for each condition. Error bars are given by the SEM and $n > 30$ cells for each condition (* refers to $p < 0.05$, ** to $p < 0.01$, and *** to $p < 0.001$ statistical significance, while ns corresponds to non-significant for the comparisons shown).

in vitro model, the human derived neuroblastoma SH-SY5Y cell lines that had been transfected with the p-EGFP-N1 constructs expressing $SPG7^{WT}$ and $SPG7^{T588M}$. Similar to the LCLs, western blot analysis using an anti-GFP antibody (thus detecting only the exogenous SPG7), did not indicate any significant difference between the expression of the mutant and the WT SPG7 in these cells (**Figure 3B**).

Protein Localization and Mitochondrial Morphology

We also performed immunofluorescence experiments using the transfected SH-SY5Y cells, in order to investigate the localization of the $SPG7^{WT}$ and $SPG7^{T588M}$ proteins and assess the mitochondrial morphology of mutant and WT cells by evaluating four well documented parameters (Dagda et al., 2009; Wiemerslage and Lee, 2016). The resulting data showed that the mutant protein retains its localization to mitochondria similar to the WT (**Figures 4A,B**), thus indicating that possibly the novel variant does not affect protein localization. Regarding mitochondrial morphology, it has been observed that mitochondria in mutant cells were smaller and less elongated with a low degree of interconnectivity (**Figures 4A,C**), which are typical signs of a dysfunctional mitochondrial network. In contrast, mitochondria in WT cells were longer, elongated and interconnected ($p < 0.05$; **Figures 4A,C**), indicating a healthy mitochondrial network. Furthermore, the mitochondria mean number of mutant cells (**Figure 4C**) was significantly higher compared to the WT, and that accompanied by a smaller mitochondrial size indicates mitochondrial fragmentation.

DISCUSSION

We hereby describe the clinical picture and the genetic investigation of a large Cypriot family with SA. Before the advent of WES, the family had been extensively studied and excluded in the past (more than 15 years ago) for linkage to HCA genes and loci (guided from the first clinical impression and that period relevant literature), as well as pathogenic variants previously reported in the Cypriot population (Nicolaou et al., 2008; Zamba-Papanicolaou et al., 2009; Votsi et al., 2014).

It is widely accepted that the advent of NGS strategies, including the targeted sequencing panels, the WES and the whole-genome sequencing (WGS), improved dramatically the genetic diagnosis of clinically and genetically heterogeneous diseases such as the HCAs and HSP. NGS has also enabled the identification of many novel genes and variants (Coutelier et al., 2018; Elert-Dobkowska et al., 2019; Krygier and Mazurkiewicz-Bełdzińska, 2021; Sahin and Saat, 2021). Through a WES approach followed by *in silico* targeted gene analysis, the present study describes the first identification of a pathogenic variant in the *SPG7* gene in the Cypriot population. The successful efficacy of this approach in the study of HCAs and HSPs has been well documented (Coutelier et al., 2018; Sahin and Saat, 2021; Saputra and Kumar, 2021). Compared to other diagnostic approaches such as the classic Sanger sequencing based on phenotype-oriented gene prioritization, or even the NGS gene targeted panel sequencing, the exome targeted capture has several advantages. Gene prioritization based on phenotypic presumptions is abolished, and there is no need to redesign a panel in case new HCA or HSP genes are published. Moreover, in the context of the HCA and HSP heterogeneity, a broader range of genes must be allowed to be tested, including genes linked with other types of transmission or other neurological diseases which have overlapping features with HCA or HSP. This approach captures variants in genes associated with various transmission modes or variants that would not be identified by a typical HCA or HSP panel. However, it might be more expensive than a targeted panel analysis with a relatively lower coverage provided. The major limitation of both the targeted panel and WES compared to the WGS approach, which provides longer reads, has been their inability to detect repeat expansions, deep intronic variants or CNVs (Coutelier et al., 2018; Krygier and Mazurkiewicz-Bełdzińska, 2021; Saputra and Kumar, 2021). Therefore, for undiagnosed patients excluded from small scale variants through gene panel analysis or WES, the use of WGS could be a promising option. Thus far, WGS has contributed to discovering ataxia (Cortese et al., 2019) and other disease novel tandem repeat expansions (Bahlo et al., 2018; Kim et al., 2019) and is expected to identify additional new ataxia-causative expansions in the future. Further advances in NGS techniques and bioinformatics analysis are promising towards better detecting pathogenic variants and expansions even from the analysis of short-read data.

Pathogenic variants in the *SPG7* gene had been initially linked to pure and complicated HSP, whereas lately they have been considered as frequent causes of undiagnosed cerebellar ataxia and SA cases. In the United Kingdom, *SPG7* variants have been reported as the fourth more common cause of the genetic ataxias in general and the second of the recessive ataxias (Hewamadduma et al., 2018). A variety of variants including several missense, frameshift, nonsense, small insertions, deletions, duplications, macro deletions and splice site variants have been described. More recently, a deep intronic heterozygous cryptic splice variant has been reported to cause SA in combination with a heterozygous missense variant, thus suggesting the re-examination of existing cases characterized as dominant *SPG7* variants (Verdura et al., 2020).

The core clinical presentation of the Cypriot family patients is similar to other described cases. The majority of their features correspond to >50% of the worldwide described cases (Hewamadduma et al., 2018). However, within the family some phenotypic differences were observed, with the age of onset being the most significant. It has been reported that the localization of a mutation in relation to the different functional domains of the protein affects the age of onset. More specifically, homozygous mutations in the M41 peptidase domain have been correlated to an earlier disease onset compared to mutations in a non-functionally assigned domain (Hewamadduma et al., 2018). This novel missense *SPG7* c.1763C > T variant is located within the M41domain, and is associated with a variable age of disease onset (ranging from 16–46 years). Patient III:1 had a very later age of onset compared to the other patients, and the two males had an earlier onset compared to the other females. Moreover, only patient III:1 presents with respiratory difficulties and dysphagia, as well as a more severe cerebellar dysarthria. Additional symptoms which are

not common for all the patients such as optic atrophy, sensory deficit, pes cavus deformity, facial weakness, double vision, peripheral neuropathy and urinary incontinence have been recorded. Moreover, PEO is present in 3/5 patients, and it has been referred as one of the rare findings in the majority of described *SPG7* cohorts (Hewamadduma et al., 2018; Verdura et al., 2020). To our knowledge, similar phenotypic differences in patients sharing an identical *SPG7* pathogenic variant, have been observed, mostly between different families and more rarely between members of the same family (Van Gassen et al., 2012; Hewamadduma et al., 2018). Such differential phenotypic expression could be attributed to the contribution of other genetic, epigenetic or environmental factors.

The identified novel *SPG7* variant has been predicted to cause deleterious consequences with almost all the prediction tools. There are many possible effects of a missense variant including protein folding, stability and flexibility alterations, binding processes prevention, subcellular localization and expression alterations. One or a combination of such effects might cause an abnormal protein function (Zhang et al., 2012). To investigate the possible expression and subcellular localization alterations, we employed the patient/control derived LCLs (only for expression) and the *in vitro* model neuroblastoma SH-SY5Y cell lines. The SH-SY5Y cell lines is a well-established model that has been used for the investigation of various neurodegenerative disorders, including ataxia and spastic paraplegia types (Bolinches-Amoros et al., 2014; Wagner et al., 2019; Morani et al., 2020). However, to our knowledge, this is the first time that they are employed for the study of an *SPG7* relevant disease. Furthermore, there are no other reports for the investigation of the effect of missense *SPG7* variants in LCLs. There are limited reports for differential expression in other cells, in most of which a missense variant was in compound heterozygosity with another type of variant and therefore its contribution (if any) was not clear. Increased RNA and protein expression was observed in muscle cells of a group of patients carrying *SPG7* compound heterozygous variants (nonsense and missense) (Pfeffer et al., 2014). Increased protein expression was also identified in olfactory neurosphere-derived cells, isolated from patients carrying the common missense p.Ala510Val variant in compound heterozygosity with other variants (Wali et al., 2020), whereas decreased protein expression was identified in fibroblasts of a patient heterozygous for a missense variant and a deep intronic cryptic splice variant (Verdura et al., 2020). Another study reported paraplegin accumulation in post-mortem cerebellar and cerebral cortex neurites of a patient homozygous for the common p.Ala510Val variant; however, it was not clear whether this observation was due to the protein overexpression or mislocalization (Thal et al., 2015). Our experimental data indicate that the reported variant does not affect the expression of either the RNA or the protein in both tested cell lines. Localization of the mutant protein remains unaffected as well.

Aberrant mitochondrial morphology representing an unhealthy mitochondrial network has been detected in cells expressing $SPG7^{T588M}$, thus indicating mitochondrial dysfunction and further supporting the predicted pathogenicity of the reported variant. Similar mitochondrial morphology, accompanied by additional types of mitochondrial dysfunction that have been associated with neurodegeneration (including decreased mitochondrial membrane potential, reduced mitochondrial mass, reduced oxidative phosphorylation, reduced ATP content, diminished cellular proliferation and increased mitochondrial oxidative stress) were identified in the olfactory neurosphere-derived cells mentioned above (Wali et al., 2020). Mitochondria defects associated with neurodegeneration have also been described through studies in other cell and animal models lacking paraplegin (Atorino et al., 2003; Ferreirinha et al., 2004; Pareek et al., 2018). In contrast, increased mitochondrial mass and enhanced networks which are referred as typical for a mitochondrial disorder, have been identified in fibroblasts of patients carrying compound heterozygous variants (with at least one of the two being nonsense in the three patients) (Pfeffer et al., 2014).

Based on our findings, we hypothesize that the currently reported *SPG7* variant consequences on the tested cell lines mitochondrial network, are not relevant with protein expression alterations or mislocalization. Other mechanism(s) such as the protein folding, stability and flexibility changes, and protein interaction alterations or a combination of these, might affect protein's normal function, thus leading to the observed dysfunctional mitochondrial network and perhaps to other dysfunction(s) that remain unknown.

In conclusion, our study is the first report of an *SPG7* pathogenic variant in the Cypriot population. It is a novel variant that broadens the spectrum of *SPG7* pathogenic variants and evidently causes mitochondrial dysfunction. It also provides detailed clinical features of the patients, thus indicating intrafamilial differences, and enabling comparisons with other reported cases. Our findings also further support the usefulness of WES followed by *in silico* targeted gene analysis as a powerful diagnostic tool in the study of clinically and genetically heterogeneous diseases such as the HCAs and HSPs, as well as the suitability of the SH-SY5Y cells for the functional investigation of *SPG7* variants.

DATA AVAILABILITY STATEMENT

The datasets for this article are not publicly available due to concerns regarding participant/patient anonymity. Requests to access the datasets should be directed to the corresponding author.

ETHICS STATEMENT

The studies involving human participants were reviewed and approved by The Cyprus National Bioethics Committee. The patients/participants provided their written informed consent to participate in this study.

AUTHOR CONTRIBUTIONS

CV and KC designed and conceived the study; Experimental studies, data acquisition, data analysis and interpretation were

carried out by CV (molecular analysis and part of functional analysis) and AV (functional analysis); CV drafted the manuscript; AV, YC, and KC revised the manuscript; PN and KC contributed in data interpretation; YC and EZ-P performed the clinical characterization; KC supervised the study; All authors read and approved the final manuscript.

FUNDING

This work was partly supported by Norway grants and the Cyprus Institute of Neurology and Genetics.

ACKNOWLEDGMENTS

The authors thank the patients and family members for their participation in this study.

SUPPLEMENTARY MATERIAL

The Supplementary Material for this article can be found online at: https://www.frontiersin.org/articles/10.3389/fgene.2021.812640/full#supplementary-material

REFERENCES

Atorino, L., Silvestri, L., Koppen, M., Cassina, L., Ballabio, A., Marconi, R., et al. (2003). Loss of M-AAA Protease in Mitochondria Causes Complex I Deficiency and Increased Sensitivity to Oxidative Stress in Hereditary Spastic Paraplegia. *J. Cel Biol* 163, 777–787. doi:10.1083/jcb.200304112

Bahlo, M., Bennett, M. F., Degorski, P., Tankard, R. M., Delatycki, M. B., and Lockhart, P. J. (2018). Recent Advances in the Detection of Repeat Expansions with Short-Read Next-Generation Sequencing. *F1000Res* 7, 736. doi:10.12688/f1000research.13980.1

Bereznyakova, O., and Dupré, N. (2018). Spastic Ataxias. *Handb Clin. Neurol.* 155, 191–203. doi:10.1016/B978-0-444-64189-2.00012-3

Bolinches-Amoros, A., Molla, B., Pla-Martin, D., Palau, F., and Gonzalez-Cabo, P. (2014). Mitochondrial Dysfunction Induced by Frataxin Deficiency Is Associated with Cellular Senescence and Abnormal Calcium Metabolism. *Front. Cel. Neurosci.* 8, 124. doi:10.3389/fncel.2014.00124

Cortese, A., Simone, R., Sullivan, R., Vandrovcova, J., Tariq, H., Yau, W. Y., et al. (2019). Biallelic Expansion of an Intronic Repeat in RFC1 Is a Common Cause of Late-Onset Ataxia. *Nat. Genet.* 51, 649–658. doi:10.1038/s41588-019-0372-4

Coutelier, M., Hammer, M. B., Stevanin, G., Monin, M.-L., Davoine, C.-S., Mochel, F., et al. (2018). Efficacy of Exome-Targeted Capture Sequencing to Detect Mutations in Known Cerebellar Ataxia Genes. *JAMA Neurol.* 75, 591–599. doi:10.1001/jamaneurol.2017.5121

Dagda, R. K., Cherra, S. J., 3rd, Kulich, S. M., Tandon, A., Park, D., and Chu, C. T. (2009). Loss of PINK1 Function Promotes Mitophagy through Effects on Oxidative Stress and Mitochondrial Fission. *J. Biol. Chem.* 284, 13843–13855. doi:10.1074/jbc.M808515200

Elert-Dobkowska, E., Stepniak, I., Krysa, W., Ziora-Jakutowicz, K., Rakowicz, M., Sobanska, A., et al. (2019). Next-Generation Sequencing Study Reveals the Broader Variant Spectrum of Hereditary Spastic Paraplegia and Related Phenotypes. *Neurogenetics* 20, 27–38. doi:10.1007/s10048-019-00565-6

Ferreirinha, F., Quattrini, A., Pirozzi, M., Valsecchi, V., Dina, G., Broccoli, V., et al. (2004). Axonal Degeneration in Paraplegin-Deficient Mice Is Associated with Abnormal Mitochondria and Impairment of Axonal Transport. *J. Clin. Invest.* 113, 231–242. doi:10.1172/JCI20138

Hewamadduma, C. A., Hoggard, N., O'malley, R., Robinson, M. K., Beauchamp, N. J., Segamogaite, R., et al. (2018). Novel Genotype-Phenotype and MRI Correlations in a Large Cohort of Patients with SPG7 Mutations. *Neurol. Genet.* 4, e279. doi:10.1212/NXG.0000000000000279

Kim, A., Kumar, K. R., Davis, R. L., Mallawaarachchi, A. C., Gayevskiy, V., Minoche, A. E., et al. (2019). Increased Diagnostic Yield of Spastic Paraplegia with or without Cerebellar Ataxia through Whole-Genome Sequencing. *Cerebellum* 18, 781–790. doi:10.1007/s12311-019-01038-0

Krygier, M., and Mazurkiewicz-Bełdzińska, M. (2021). Milestones in Genetics of Cerebellar Ataxias. *Neurogenetics* 22, 225–234. doi:10.1007/s10048-021-00656-3

Lallemant-Dudek, P., and Durr, A. (2020). Clinical and Genetic Update of Hereditary Spastic Paraparesis. *Revue Neurologique* 177, 550–556. doi:10.1016/j.neurol.2020.07.001

Li, J., Shi, L., Zhang, K., Zhang, Y., Hu, S., Zhao, T., et al. (2018). VarCards: An Integrated Genetic and Clinical Database for Coding Variants in the Human Genome. *Nucleic Acids Res.* 46, D1039–D1048. doi:10.1093/nar/gkx1039

Morani, F., Doccini, S., Chiorino, G., Fattori, F., Galatolo, D., Sciarrillo, E., et al. (2020). Functional Network Profiles in ARSACS Disclosed by Aptamer-Based Proteomic Technology. *Front. Neurol.* 11, 603774. doi:10.3389/fneur.2020.603774

Nicolaou, P., Georghiou, A., Votsi, C., Middleton, L. T., Zamba-Papanicolaou, E., and Christodoulou, K. (2008). A Novel c.5308_5311delGAGA Mutation in Senataxin in a Cypriot Family with an Autosomal Recessive Cerebellar Ataxia. *BMC Med. Genet.* 9, 28. doi:10.1186/1471-2350-9-28

Pareek, G., Thomas, R. E., and Pallanck, L. J. (2018). Loss of the Drosophila M-AAA Mitochondrial Protease Paraplegin Results in Mitochondrial Dysfunction, Shortened Lifespan, and Neuronal and Muscular Degeneration. *Cell Death Dis* 9, 304. doi:10.1038/s41419-018-0365-8

Parodi, L., Coarelli, G., Stevanin, G., Brice, A., and Durr, A. (2018). Hereditary Ataxias and Paraparesias: Clinical and Genetic Update. *Curr. Opin. Neurol.* 31, 462–471. doi:10.1097/WCO.0000000000000585

Pfeffer, G., Gorman, G. S., Griffin, H., Kurzawa-Akanbi, M., Blakely, E. L., Wilson, I., et al. (2014). Mutations in the SPG7 Gene Cause Chronic Progressive External Ophthalmoplegia through Disordered Mitochondrial DNA Maintenance. *Brain* 137, 1323–1336. doi:10.1093/brain/awu060

Sahin, I., and Saat, H. (2021). Hereditary Spastic Paraplegia: New Insights into Clinical Variability and Spasticity-Ataxia Phenotype, and Novel Mutations. *Acta Neurol. Belg.* [Epub ahead of print]. doi:10.1007/s13760-021-01779-y

Saputra, L., and Kumar, K. R. (2021). Challenges and Controversies in the Genetic Diagnosis of Hereditary Spastic Paraplegia. *Curr. Neurol. Neurosci. Rep.* 21, 15. doi:10.1007/s11910-021-01099-x

Tesson, C., Koht, J., and Stevanin, G. (2015). Delving into the Complexity of Hereditary Spastic Paraplegias: How Unexpected Phenotypes and Inheritance Modes Are Revolutionizing Their Nosology. *Hum. Genet.* 134, 511–538. doi:10.1007/s00439-015-1536-7

Thal, D., Züchner, S., Gierer, S., Schulte, C., Schöls, L., Schüle, R., et al. (2015). Abnormal Paraplegin Expression in Swollen Neurites, τ- and α-Synuclein Pathology in a Case of Hereditary Spastic Paraplegia SPG7 with an Ala510Val Mutation. *Int. J. Mol. Sci.* 16, 25050–25066. doi:10.3390/ijms161025050

Van Gassen, K. L. I., Van Der Heijden, C. D. C. C., De Bot, S. T., Den Dunnen, W. F. A., Van Den Berg, L. H., Verschuuren-Bemelmans, C. C., et al. (2012). Genotype-Phenotype Correlations in Spastic Paraplegia Type 7: A Study in a Large Dutch Cohort. *Brain* 135, 2994–3004. doi:10.1093/brain/aws224

Verdura, E., Schlüter, A., Fernández-Eulate, G., Ramos-Martín, R., Zulaica, M., Planas-Serra, L., et al. (2020). A Deep Intronic Splice Variant Advises Reexamination of Presumably Dominant SPG7 Cases. *Ann. Clin. Transl Neurol.* 7, 105–111. doi:10.1002/acn3.50967

Ververis, A., Dajani, R., Koutsou, P., Aloqaily, A., Nelson-Williams, C., Loring, E., et al. (2020). Distal Hereditary Motor Neuronopathy of the Jerash Type Is Caused by a Novel SIGMAR1 c.500A>T Missense Mutation. *J. Med. Genet.* 57, 178–186. doi:10.1136/jmedgenet-2019-106108

Votsi, C., Zamba-Papanicolaou, E., Middleton, L. T., Pantzaris, M., and Christodoulou, K. (2014). A NovelGBA2Gene Missense Mutation in Spastic Ataxia. *Ann. Hum. Genet.* 78, 13–22. doi:10.1111/ahg.12045

Wagner, M., Osborn, D. P. S., Gehweiler, I., Nagel, M., Ulmer, U., Bakhtiari, S., et al. (2019). Bi-allelic Variants in RNF170 Are Associated with Hereditary Spastic Paraplegia. *Nat. Commun.* 10, 4790. doi:10.1038/s41467-019-12620-9

Wali, G., Kumar, K. R., Liyanage, E., Davis, R. L., Mackay-Sim, A., and Sue, C. M. (2020). Mitochondrial Function in Hereditary Spastic Paraplegia: Deficits in SPG7 but Not

SPAST Patient-Derived Stem Cells. *Front. Neurosci.* 14, 820. doi:10.3389/fnins.2020.00820

Wedding, I. M., Koht, J., Tran, G. T., Misceo, D., Selmer, K. K., Holmgren, A., et al. (2014). Spastic Paraplegia Type 7 Is Associated with Multiple Mitochondrial DNA Deletions. *PloS one* 9, e86340. doi:10.1371/journal.pone.0086340

Wiemerslage, L., and Lee, D. (2016). Quantification of Mitochondrial Morphology in Neurites of Dopaminergic Neurons Using Multiple Parameters. *J. Neurosci. Methods* 262, 56–65. doi:10.1016/j.jneumeth.2016.01.008

Zamba-Papanicolaou, E., Koutsou, P., Daiou, C., Gaglia, E., Georghiou, A., and Christodoulou, K. (2009). High Frequency of Friedreich's Ataxia Carriers in the Paphos District of Cyprus. *Acta Myol* 28, 24–26.

Zhang, Z., Miteva, M. A., Wang, L., and Alexov, E. (2012). Analyzing Effects of Naturally Occurring Missense Mutations. *Comput. Math. Methods Med.* 2012, 805827. doi:10.1155/2012/805827

Conflict of Interest: The authors declare that the research was conducted in the absence of any commercial or financial relationships that could be construed as a potential conflict of interest.

Publisher's Note: All claims expressed in this article are solely those of the authors and do not necessarily represent those of their affiliated organizations, or those of the publisher, the editors and the reviewers. Any product that may be evaluated in this article, or claim that may be made by its manufacturer, is not guaranteed or endorsed by the publisher.

frontiers in Genetics

CASE REPORT
published: 18 January 2022
doi: 10.3389/fgene.2021.771756

Fetal Congenital Heart Disease Caused by Compound Heterozygous Mutations in the *DNAH9* Gene: A Case Report

Tao Zhang[1,2†], *Hua Yuan*[1,2†], *Hongdan Zhu*[1,2], *Yuyi Ying*[1,2], *Jinlong Ding*[1,2], *Haigang Ding*[1,2], *Xiaoliang Shi*[1,2], *Yao He*[1,2], *Haitao Pan*[1,2*] *and Yongxing Zhong*[1,2*]

[1]*Shaoxing Maternity and Child Health Care Hospital, Shaoxing, China,* [2]*Obstetrics and Gynecology Hospital of Shaoxing University, Shaoxing, China*

OPEN ACCESS

Edited by:
Emiliano González Vioque, University Clinical Hospital of Santiago, Spain

Reviewed by:
Gillian Blue, The Children's Hospital at Westmead, Australia
Lauren Jeffries, Yale University, United States

***Correspondence:**
Haitao Pan
panhaitao@sxfby.com
Yongxing Zhong
zhongyongxing@sxfby.com

†*These authors have contributed equally to this work*

Specialty section:
This article was submitted to Genetics of Common and Rare Diseases, a section of the journal Frontiers in Genetics

Received: *07 September 2021*
Accepted: *20 December 2021*
Published: *18 January 2022*

Citation:
Zhang T, Yuan H, Zhu H, Ying Y, Ding J, Ding H, Shi X, He Y, Pan H and Zhong Y (2022) Fetal Congenital Heart Disease Caused by Compound Heterozygous Mutations in the DNAH9 *Gene: A Case Report. Front. Genet. 12:771756. doi: 10.3389/fgene.2021.771756*

Background: Fetal congenital heart disease (CHD) is the most common congenital defect, with an incidence of 0.6–0.8%, accounting for 30–50% of infant congenital disease deaths. The pathogenesis of CHD is still unclear, so an active and effective prenatal diagnosis is very important for the prevention and control of CHD. Herein, a Chinese CHD patient with rare compound heterozygous mutations in the *DNAH9* gene was reported, and the 3D structure and functional changes of *DNAH9* protein were predicted.

Case presentation: A 23-year-old pregnant woman came to our hospital for prenatal diagnosis at 27 weeks of gestation. Both she and her partner were unaffected. Fetal CHD was detected by ultrasound screening. Copy number variation sequencing (CNV-seq) revealed an 81 kb deletion at chr17p12 (11,486,795–11,568,385), including exons 1–15 of *DNAH9* gene, which plays a key role in cardiac development. Then, whole exome sequencing (WES) was used and identified a nonsense mutation (c.10975C>T) in *DNAH9*, which resulted in the mutation of amino acid 3,659 from glutamine to termination. The 3D mutant protein structures were predicted using SWISS-MODEL and showed structural changes from functional β-sheet and α-helix to termination, respectively.

Conclusion: We describe a case of fetal CHD caused by *DNAH9* mutations and provide an effective diagnostic technique for identifying intragenic deletions. This diagnostic process can be implicated in prenatal diagnosis of CHD.

Keywords: congenital heart disease, DNAH9 gene, copy number variation sequencing, whole exome sequencing, 3D structure

Abbreviations: ACMG, American College of Medical Genetics and Genomics; CHD, Congenital heart disease; CNV-seq, Copy number variation sequencing; *DNAH9*, *dynein axonemal heavy chain 9*; WES, Whole exome sequencing.

INTRODUCTION

Congenital heart diseases (CHD) are the most common birth defects, which can severely affect human health, accounting for 2–8% of newborn children (Hoffman et al., 2004; Lambrechts et al., 2005). The clinical manifestations and severity of CHD are widely variable. Mild cases, such as some small ventricular septal defects, can self-close after birth. Severe cases, such as most instances of tetralogy of Fallot (TOF), seriously affect the function and structure of the heart, with a high mortality. CHD is often accompanied by multiple organ malformations, which is one of the main causes of neonatal death (Pediatric Cardiac Genomics Consortium et al., 2013; Egbe et al., 2014). Traditional thought is that CHD is the combined result of environmental and genetic factors, in which environmental factors are dominant (Kalisch-Smith et al., 2020). However, with the development of technologies, it has been found that the incidence of CHD is significantly higher in monozygotic twins, or when patients have family history of CHD or consanguinity. A variety of chromosomal aberrations is often associated with different types of CHD. It is now highly suggested that genetic factors play an important role in the pathogenesis of CHD (Van der Bom et al., 2011). In particular, the invention and application of chromosome microarray technology (CMA) and high-throughput sequencing technology provide a strong basis for elucidating the extremely important role of genetic factors in the occurrence of CHD (Charron et al., 2010; Rehm, 2013; Aburawi et al., 2015).

Monogenic inherited disease refers to disease caused by a single gene abnormality, also known as Mendelian genetic disease. Monogenic disease can be divided into autosomal dominant or recessive, X-chromosome dominant or recessive genetic diseases. The incidence rate of any individual monogenic disease is not high, but the overall incidence rate of all monogenic diseases combined is 4–5%. This kind of genetic disease can also be seen in various CHD, which can be an isolated CHD phenotype (such as in *GATA4* and *NKX2.5* gene mutations (Winston et al., 2012)) or a part of complex syndrome, such as Noonan syndrome or Holt-Oram syndrome.

DNAH9 gene associated primary ciliary dyskinesia 40 is characterized by chronic respiratory tract infection, visceral translocation and infertility (Fassad et al., 2018; Loges et al., 2018). Most of the patients with primary ciliary dyskinesia have congenital respiratory diseases. From early childhood, patients will have repeated respiratory infections. However, the respiratory compromise of primary ciliary dyskinesia type 40 is relatively light, and usually does not develop into serious lung disease. About 50% of patients with primary ciliary dyskinesia have mirror image inversion of internal organs, and some patients have been reported to have severe congenital heart malformations.

In this study, we reported the case of a Chinese fetal proband, who presented with fetal CHD by ultrasound screening. Copy number variation sequencing (CNV-seq) revealed an 81 kb deletion at chr17p12, including a deletion of exons 1–15 in *DNAH9*. Then, whole exome sequencing (WES) revealed a nonsense mutation (c.10975C>T) in *DNAH9* on the other allele. This base mutation resulted in the codon of amino acid 3,659 from glutamine to termination. To predict the changes of 3D protein structure, we used SWISS-MODEL and PyMO and revealed these two mutations changed functional β-sheet and α-helix structures, respectively.

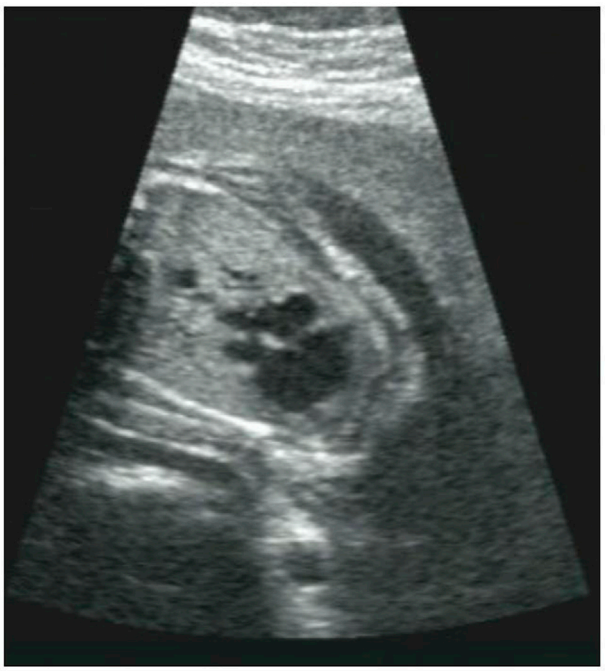

FIGURE 1 | The fetus with congenital heart disease. Ultrasound scans of the fetus showed abnormal heart development, a single ventricle, pulmonary artery stenosis and situs inversus.

MATERIALS AND METHODS

Sample Collection

The study was approved by the institutional ethics committee of Shaoxing Maternity and Child Health Care Hospital. The family members had signed informed consent documents. Parental consent was obtained for collecting the prenatal fetal cord venous blood at 27 weeks of pregnancy. Peripheral blood samples also were collected from proband's parents.

Copy-Number Variation Sequencing and Whole Exome Sequencing

Genomic DNA was extracted from the proband and parental blood using a DNEasy Blood and Tissue Kit (Qiagen, Hilden, Germany) according to the manufacturer's procedures, respectively. For WES, the genomic DNA of the proband was enriched for coding exons using Agilent SureSelect Low Input Reagent Kit and sequenced on Illumina HiSeq X Ten platform. The sequencing data captured 99.75% of coding regions across 35,519,957 bp length of 25,701 genes in total. The average sequence depth is 180.347X and 97.87% of targeted regions

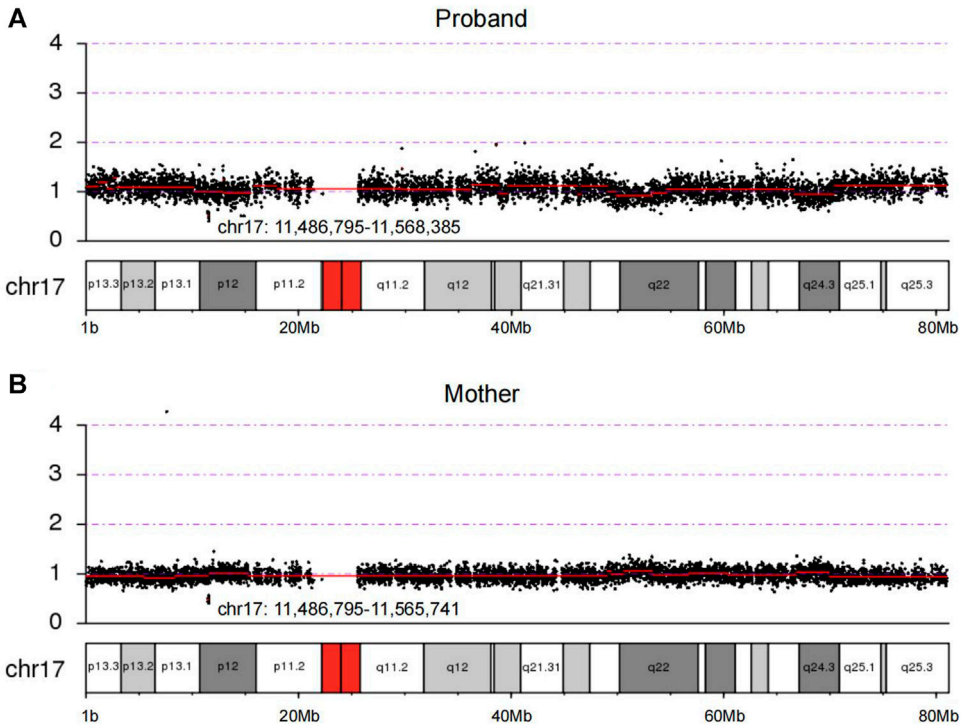

FIGURE 2 | The loss of heterozygosity at 17p12 in the proband and the mother were detected by CNV-seq. **(A)** Copy number of chromosome 17 in the proband by sequencing. **(B)** Copy number of chromosome 17 in the proband's mother by sequencing. The chr17:11,486,795–11,568,385 and chr17:11,486,795–11,565,741 showed in **(A)** and **(B)** were regions of deletion in the proband and her mother, respectively.

with average depth >20X. For CNV-seq, the genomic DNA was fragmented using Hieff NGS® Fast-Pace™ DNA Fragmentation Reagent and prepared for the PCR-free library by Hieff NGS® Complete Adapter Kit for Illumina®.

Data Analysis

The AfterQC (Chen et al., 2017) was used to evaluate the sequencing quality of the original sequencing data, and the low quality and contaminated reads were removed. After data were aligned to human reference hg19 by BWA software (Li and Durbin, 2010), the single nucleotide variants (SNV) and indels in genome were called by using the GATK software (Mckenna et al., 2010). Then, we used 1000 Genomes database (1000 human genome dataset), Genome AD (Genome Aggregation Database dataset) 2.1.1, and ExAC (The Exome Aggregation Consortium dataset) to screen the SNV and indels and the OMIM, HGMD, and Clinvar databases to filter the reported mutations. dbNSFP database was used to predict the pathogenicity of missense mutation and splice mutation. All mutation sites were classified by ACMG genetic variation classification criteria and guidelines. Finally, Sanger sequencing method was used to verify all possible pathogenic sites.

Protein Structure Prediction

The protein sequence with 4,486 amino acid residues of *DNAH9* was download from NCBI (NP_001363.2). The wild-type and mutant-type 3D structure of the *DNAH9* protein was predicted using SWISS-MODEL web server (https://swissmodel.expasy.org/) (Waterhouse et al., 2018). The best model was selected based on QMEANDisCo global score. The final predicted structure was visualized using PyMOL program (https://pymol.org/).

RESULTS

Clinical Features

At 31 weeks of gestation, the parents were fully informed of severe fetal deformity and the significance of the compound *DNAH9* mutations. The parents strongly requested the induction of labor. With the approvement of the institutional ethics committee of Shaoxing Maternity and Child Health Care Hospital, the pregnancy was terminated for fetal anomalies. The parents and other families were in normal physical condition, without any family history of genetic diseases. Prior to the proband, her mother had two histories of adverse pregnancies: 1) At 26 weeks of gestation, pregnancy was terminated due to the discovery of fetal single chamber heart and 2) at the third month of another pregnancy, spontaneous abortion occurred. Her mother's menstruation was irregular in the period of 30–40 days.

There was no early pregnancy reaction, no exposure to poison or radioactive substances, and no history of folic acid supplementation in early pregnancy. At 9 weeks of gestation, her mother came to our hospital for ultrasound examination and

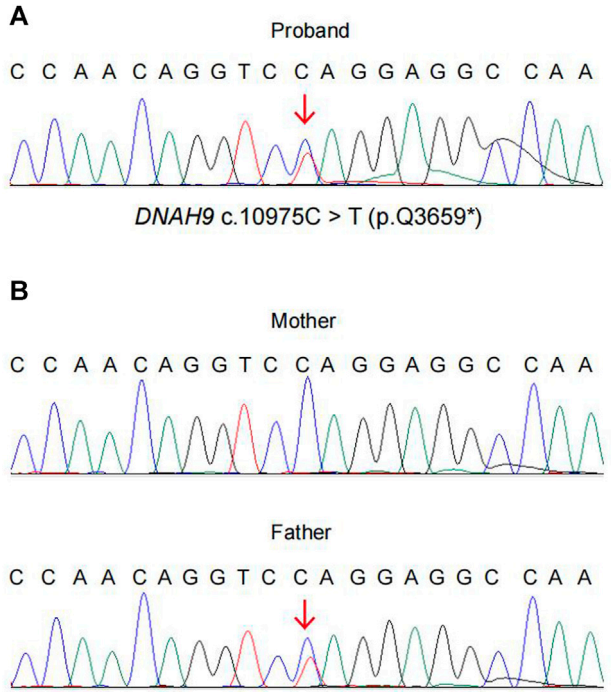

FIGURE 3 | The evidence of the heterozygous nonsense mutation c.10975C> T (p.Q3659*) in the *DNAH9* gene. WES and sanger sequencing verified the heterozygous mutation *DNAH9* c.10975C> T in the proband **(A)** and her parents **(B)**.

found the normal gestational sac and gestational age. At 15 weeks of gestation, her mother came to our hospital for routine prenatal examination and found the normal physical condition, low risk value of non-invasive prenatal testing (NIPT), and normal range of OGTT. However, at 27 weeks of gestation, the result of ultrasound examination showed fetal cardiac abnormalities include single ventricle, pulmonary artery stenosis and visceral inversion (**Figure 1**). More detailed tests were carried out 2 days later and confirmed that the proband had no ventricular septal structure. CDFI showed mild left atrioventricular regurgitation. Because of the continuous histories of adverse pregnancy outcomes, the parents hoped to clarify the genetic factors and guide the next birth.

Molecular Analysis

Using CNV-seq, we identified an 81 kb deletion at chr17p12 (11,486,795–11,568,385) in the fetus (**Figure 2A**). This deletion region includes 1–15 exons of the *DNAH9* gene. After verified in her parents by CNV-seq, it is found that the mother had a 79 kb deletion at chr17p12 (11,486,795–11,565,741) (**Figure 2B**). The result implied the deletion at chr17p12 of the fetus was inherited from her mother. Moreover, we also performed the WES in the fetus and revealed another mutation at c.10975C>T (p.Q3659*) in the exon 57 of *DNAH9* gene (**Figure 3A**). Subsequently, sanger sequencing was used to verify this nonsense mutation in all family members and showed c.10975C>T *DNAH9* mutation

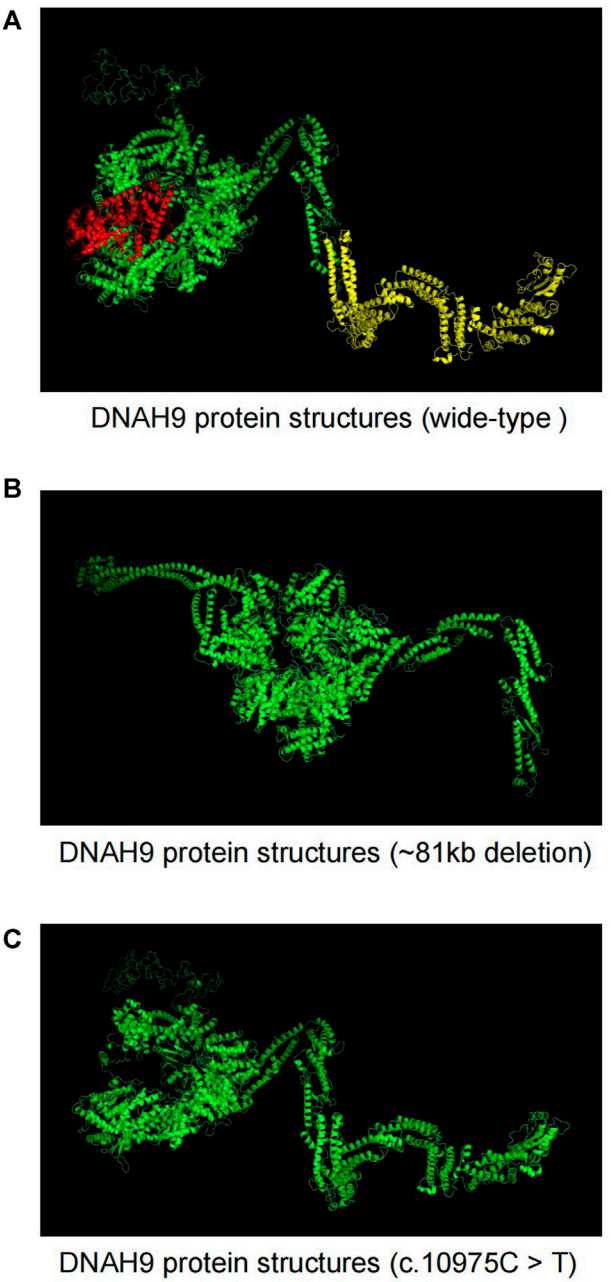

FIGURE 4 | The Effects of *DNAH9* mutations on protein structure. **(A)** The wide-type structure of DNAH9 protein predicted by SWISS-MODEL. The yellow and red parts were modelled using exon 1–15 in *DNAH9* and amino acid residues from glutamine at position 3,659 to end. The mutant protein structures showed in **(B)** and **(C)** upon an 81 kb deletion at chr17p12 (11,486,795–11,568,385) or c.10975C> T mutation in *DNAH9*, respectively.

was inherited from her father (**Figure 3B**). According to the American College of Medical Genetics and Genomics (ACMG) guidelines (Richards et al., 2015), both the 81 kb deletion at chr17p12 and c.10975C>T in *DNAH9* gene were predicted to be pathogenic mutations because of the evidence chain (PVS1+PM2+PP3).

Effect of Mutations on Protein Structures

We used SWISS-MODEL web server (Waterhouse et al., 2018) to predict changes of DNAH9 protein structures when there were mutations in the sequence (**Figure 4A**). The deletion of 1–15 exons in *DNAH9* gene will alter the 3D structure on β-sheet (**Figure 4B**), while the c.10975C>T (p.Q3659*) mutation will change the 3D structure from α-helix to termination (**Figure 4C**). The combination of these structural changes would alter the conformation of the DNAH9 protein and affect the protein stability and binding facility.

DISCUSSION

Fetal CHD has become the most important birth defect type in China, accounting for the majority neonatal non-infectious diseases. However, the accuracy rate of prenatal diagnosis was only 36% by investigating 309 participants with CHD, including post-natal and fetal termination (Friedberg et al., 2009). The prenatal diagnosis rate of left ventricular outflow tract obstruction, transposition of great arteries and anomalous pulmonary venous drainage was the lowest. The traditional technology, ultrasound is the most effective non-invasive way of diagnosing CHD in fetal cases. However, because of the small meridian of the fetal heart, complex blood circulation, difficulties of capturing the fetal variable blood flow and the limitation of ultrasound itself, not all fetal CHD can be diagnosed by ultrasound in the prenatal setting. Although MRI can overcome shortcomings of the small field of vision and poor contrast of soft-tissue, the malformations of CHD patients are sometimes not limited to the heart. Additionally, many CHDs are accompanied by genetic changes, including chromosome aberration, single gene genetic defects, multi gene genetic defects and so on. Therefore, it is of great and urgent practical significance to make early and accurate prenatal genetic diagnosis of CHD in fetal cases by using next-generation sequencing technology.

Previous studies have proved that CMA is an effective tool to detect fetal genomic imbalances, including abnormalities of chromosome number and copy number variations (Xia et al., 2018). However, the price of CMA is relatively expensive. Copy number variation sequencing (CNV-seq), is a technology by using next-generation sequencing technology, can detect CNVs with high resolution in the whole genome. Compared with CMA, it can increase different sequencing depth to obtain more accurate information, and has the advantages of more flexible, fast, accurate and low operation cost (Duan et al., 2013). Moreover, CNV-seq technology has been applied to the genetic diagnosis of fetal CHD, recently (Zhu et al., 2016). In our study, we found that the proband had a loss of heterozygosity of 81 kb at 17p12 (11,486,795–11,568,385) by high-resolution CNV-seq. This deletion was within *DNAH9* gene. Then the parent's samples were verified by CNV-seq, and found her mother was a carrier of this deletion.

The loss of heterozygosity in *DNAH9* alone should not cause CHD. To search for other potential genetic defects, WES and sanger sequencing of the proband and the parents were further performed and found one heterozygous nonsense mutation of *DNAH9* gene (c.10975C>T) in the proband inherited from her father. This mutation resulted in termination of translation at amino acid 3,659. With additional clinical evaluation, these two mutations meet ACMG criteria for classification as pathogenic of *DNAH9* mutations in this case.

In summary, through the combined application of high-through sequencing technologies (CNV-seq and WES), we established a probable cause of the couple's poor pregnancy outcomes. The proband had compound heterozygous mutations, the deletion of 81 kb at 17p12 (11,486,795–11,568,385) and *DNAH9* c.10975C>T (p.Q3659*), inherited from each carrier parent. In addition, our results showed that the combination of CNV-seq and WES is an effective approach to prenatal diagnosis.

DATA AVAILABILITY STATEMENT

The datasets for this article are not publicly available due to concerns regarding participant/patient anonymity. Requests to access the datasets should be directed to the corresponding authors.

ETHICS STATEMENT

The studies involving human participants were reviewed and approved by the Institutional Ethics Committee of Shaoxing Maternity and Child Health Care Hospital Hospital. Written informed consent to participate in this study was provided by the participants' legal guardian/next of kin.

AUTHOR CONTRIBUTIONS

TZ and YZ conceived and designed the experiments. HP performed the experiments, HY, YH, XS and HZ contributed new materials, YY, JD and HD analyzed the data and wrote the paper. All authors read and improved the manuscript.

FUNDING

This work was supported by the National Natural Science Foundation of China (82071729), the China Postdoctoral Science Foundation (2020M681336), the Zhejiang Provincial Natural Science Foundation of China (LY19H040002), the Science Technology Department of Zhejiang Province, China (LGF21H040003, LGF21H040004, LGF19H040004, LGD20H040001) and the Health Commission of Zhejiang Province, China (2021KY375, 2021KY1156, 2019RC296, 2019KY717, 2021KY1154, 2021KY1157, 2019KY229, 2019KY230); the Science Technology Department of Shaoxing, China (2020A13032, 2020A13037, 2018C30042, 2018C30043, 2018C30044, 2018C30048, 2020A13034, 2020A13035).

REFERENCES

Aburawi, E. H., Aburawi, H. E., Bagnall, K. M., and Bhuiyan, Z. A. (2015). Molecular Insight into Heart Development and Congenital Heart Disease: An Update Review from the Arab Countries. *Trends Cardiovasc. Med.* 25, 291–301. doi:10.1016/j.tcm.2014.11.007

Charron, P., Arad, M., Arbustini, E., Basso, C., Bilinska, Z., Elliott, P., et al. (2010). European Society of Cardiology Working Group OnGenetic Counselling and Testing in Cardiomyopathies: a Position Statement of the European Society of Cardiology Working Group on Myocardial and Pericardial Diseases. *Eur. Heart J.* 31, 2715–2726. doi:10.1093/eurheartj/ehq271

Chen, S., Huang, T., Zhou, Y., Han, Y., Xu, M., and Gu, J. (2017). AfterQC: Automatic Filtering, Trimming, Error Removing and Quality Control for Fastq Data. *BMC Bioinformatics* 18, 80. doi:10.1186/s12859-017-1469-3

Duan, J., Zhang, J.-G., Deng, H.-W., and Wang, Y.-P. (2013). Comparative Studies of Copy Number Variation Detection Methods for Next-Generation Sequencing Technologies. *PLoS One* 8, e59128. doi:10.1371/journal.pone.0059128

Egbe, A., Ho, D., Lee, S., Uppu, S., and Srivastava, S. (2014). Prevalence of Congenital Anomalies in Newborns with Congenital Heart Disease Diagnosis. *Ann. Pediatr. Card.* 7, 86–91. doi:10.4103/0974-2069.132474

Fassad, M. R., Shoemark, A., Legendre, M., Hirst, R. A., Koll, F., Le Borgne, P., et al. (2018). Mutations in Outer Dynein Arm Heavy Chain DNAH9 Cause Motile Cilia Defects and Situs Inversus. *Am. J. Hum. Genet.* 103, 984–994. doi:10.1016/j.ajhg.2018.10.016

Friedberg, M. K., Silverman, N. H., Moon-Grady, A. J., Tong, E., Nourse, J., Sorenson, B., et al. (2009). Prenatal Detection of Congenital Heart Disease. *J. Pediatr.* 155, 26–31.e21. doi:10.1016/j.jpeds.2009.01.050

Hoffman, J. I. E., Kaplan, S., and Liberthson, R. R. (2004). Prevalence of Congenital Heart Disease. *Am. Heart J.* 147, 425–439. doi:10.1016/j.ahj.2003.05.003

Kalisch-Smith, J. I., Ved, N., and Sparrow, D. B. (2020). Environmental Risk Factors for Congenital Heart Disease. *Cold Spring Harb Perspect. Biol.* 12, 1. doi:10.1101/cshperspect.a037234

Lambrechts, D., Devriendt, K., Driscoll, D. A., Goldmuntz, E., Gewillig, M., Vlietinck, R., et al. (2005). Low Expression VEGF Haplotype Increases the Risk for Tetralogy of Fallot: a Family Based Association Study. *J. Med. Genet.* 42, 519–522. doi:10.1136/jmg.2004.026443

Li, H., and Durbin, R. (2010). Fast and Accurate Long-Read Alignment with Burrows-Wheeler Transform. *Bioinformatics* 26, 589–595. doi:10.1093/bioinformatics/btp698

Loges, N. T., Antony, D., Maver, A., Deardorff, M. A., Güleç, E. Y., Gezdirici, A., et al. (2018). Recessive DNAH9 Loss-Of-Function Mutations Cause Laterality Defects and Subtle Respiratory Ciliary-Beating Defects. *Am. J. Hum. Genet.* 103, 995–1008. doi:10.1016/j.ajhg.2018.10.020

Mckenna, A., Hanna, M., Banks, E., Sivachenko, A., Cibulskis, K., Kernytsky, A., et al. (2010). The Genome Analysis Toolkit: A MapReduce Framework for Analyzing Next-Generation DNA Sequencing Data. *Genome Res.* 20, 1297–1303. doi:10.1101/gr.107524.110

Pediatric Cardiac Genomics ConsortiumGelb, B., Brueckner, M., Chung, W., Goldmuntz, E., Kaltman, J., et al. (2013). The Congenital Heart Disease Genetic Network Study: Rationale, Design, and Early Results. *Circ. Res.* 112, 698–706. doi:10.1161/CIRCRESAHA.111.300297

Rehm, H. L. (2013). Disease-Targeted Sequencing: A Cornerstone in the Clinic. *Nat. Rev. Genet.* 14, 295–300. doi:10.1038/nrg3463

Richards, S., Aziz, N., Bale, S., Bick, D., Das, S., Gastier-Foster, J., et al. (2015). Standards and Guidelines for the Interpretation of Sequence Variants: A Joint Consensus Recommendation of the American College of Medical Genetics and Genomics and the Association for Molecular Pathology. *Genet. Med.* 17, 405–424. doi:10.1038/gim.2015.30

Van Der Bom, T., Zomer, A. C., Zwinderman, A. H., Meijboom, F. J., Bouma, B. J., and Mulder, B. J. M. (2011). The Changing Epidemiology of Congenital Heart Disease. *Nat. Rev. Cardiol.* 8, 50–60. doi:10.1038/nrcardio.2010.166

Waterhouse, A., Bertoni, M., Bienert, S., Studer, G., Tauriello, G., Gumienny, R., et al. (2018). SWISS-MODEL: Homology Modelling of Protein Structures and Complexes. *Nucleic Acids Res.* 46, W296–W303. doi:10.1093/nar/gky427

Winston, J. B., Schulkey, C. E., Chen, I.-B. D., Regmi, S. D., Efimova, M., Erlich, J. M., et al. (2012). Complex Trait Analysis of Ventricular Septal Defects Caused by Nkx2-5 Mutation. *Circ. Cardiovasc. Genet.* 5, 293–300. doi:10.1161/circgenetics.111.961136

Xia, Y., Yang, Y., Huang, S., Wu, Y., Li, P., and Zhuang, J. (2018). Clinical Application of Chromosomal Microarray Analysis for the Prenatal Diagnosis of Chromosomal Abnormalities and Copy Number Variations in Fetuses with Congenital Heart Disease. *Prenatal Diagn.* 38, 406–413. doi:10.1002/pd.5249

Zhu, X., Li, J., Ru, T., Wang, Y., Xu, Y., Yang, Y., et al. (2016). Identification of Copy Number Variations Associated with Congenital Heart Disease by Chromosomal Microarray Analysis and Next-Generation Sequencing. *Prenat Diagn.* 36, 321–327. doi:10.1002/pd.4782

Conflict of Interest: The authors declare that the research was conducted in the absence of any commercial or financial relationships that could be construed as a potential conflict of interest.

frontiers in Genetics

ORIGINAL RESEARCH
published: 19 January 2022
doi: 10.3389/fgene.2021.768342

Clinical Characteristics and Genetic Analysis of a Family With Birt-Hogg-Dubé Syndrome and Congenital Contractural Arachnodactyly

*Jiayong Qiu[1], Yao Lou[1], Yingwei Zhu[1], Min Wang[1], Huifang Peng[2], Yingying Hao[3], Hongwei Jiang[2] and Yimin Mao[1]**

[1]Department of Respiratory Medicine, The First Affiliated Hospital, and College of Clinical Medicine of Henan University of Science and Technology, Luoyang, China, [2]Department of Endocrinology, The First Affiliated Hospital, and College of Clinical Medicine of Henan University of Science and Technology, Luoyang, China, [3]Department of Radiation Oncology, The First Affiliated Hospital, and College of Clinical Medicine of Henan University of Science and Technology, Luoyang, China

OPEN ACCESS

Edited by:
María L. Couce,
Complejo Hospitalario Universitario de Santiago, Spain

Reviewed by:
Laura Schmidt,
National Cancer Institute at Frederick, United States
Elzbieta Radzikowska,
National Institute of Tuberculosis and Lung Diseases, Poland

***Correspondence:**
Yimin Mao
yimin6107@sina.com

Specialty section:
This article was submitted to Genetics of Common and Rare Diseases, a section of the journal Frontiers in Genetics

Received: 31 August 2021
Accepted: 23 December 2021
Published: 19 January 2022

Citation:
Qiu J, Lou Y, Zhu Y, Wang M, Peng H, Hao Y, Jiang H and Mao Y (2022) Clinical Characteristics and Genetic Analysis of a Family With Birt-Hogg-Dubé Syndrome and Congenital Contractural Arachnodactyly. Front. Genet. 12:768342. doi: 10.3389/fgene.2021.768342

Background: Birt-Hogg-Dubé (BHD) syndrome and congenital contractural arachnodactyly (CCA) or Beals-Hecht syndrome are clinically rare autosomal dominant genetic diseases. In this study, we describe an extremely rare family with BHD syndrome and CCA.

Objective: To investigate the clinical and genetic characteristics of a family with BHD syndrome and CCA.

Methods: We describe the clinical characteristics, family history, and clinical manifestations of the patient's family members. The patient underwent a blood test, computed tomography (CT) of the chest, color Doppler ultrasound of the abdomen and heart, and digital radiography of the hands. Whole exome sequencing was performed on his family members.

Results: Two years ago, the male proband developed chest tightness and shortness of breath that was accompanied by an irritating cough as well as repeated (four times) spontaneous pneumothorax. The chest CT indicated spontaneous pneumothorax on the right side and cyst and bullae in both lungs. He had no kidney tumors or skin lesions. His son had a history of pulmonary bullae and experienced spontaneous pneumothorax twice. The proband, his mother, and his son were all born with a hand deformity. The sequencing results demonstrated that both the proband and his son had heterozygous variations of the folliculin (FLCN) gene c.1015C > T (p. Gln339Ter) and fibrillin-2 (FBN2) gene c.3485G > A (p. Cys1162Tyr), which are associated with BHD syndrome and CCA, respectively.

Abbreviations: ACMG, American College of Medical Genetics and Genomics; ANCA, Anti-Neutrophil Cytoplasmic Antibodies; BHD syndrome, Birt-Hogg-Dubé Syndrome; BHS, Beals Hecht Syndrome; CCA, Congenital contractural arachnodactyly; CT, Computed Tomography; DR, Digital Radiography; FLCN, Folliculin; FBN2, Fibrillin two gene; HGMD, The Human Gene Mutation Database; MFS, Marfan syndrome; OMIM, Online Mendelian Inheritance in Man; UTR, Untranslated Region; WES, Whole Exome Sequencing.

Conclusion: For patients with chest tightness, shortness of breath, recurrent spontaneous pneumothorax, and congenital hand deformity without inducement, genetic testing should be carried out as soon as possible to make a clear diagnosis, which can then guide treatment and genetic counseling.

Keywords: birt-hogg-dubé syndrome, congenital contractual arachnodactyly, FLCN, FBN2, whole exome sequencing

INTRODUCTION

Birt-Hogg-Dubé (BHD) syndrome is a rare autosomal dominant genetic disease. Folliculin (FLCN), located on chromosome 17p11.2, is its causative gene. Its common features include multiple fibrofolliculoma, bullae (spontaneous pneumothorax), and kidney tumors (Black et al., 2020). Phenotypically, this condition is highly variable. Even in the same family, affected individuals may exhibit any combination of skin, lung, or kidney manifestations of varying severities (Daccord et al., 2020). Regardless, spontaneous pneumothorax is usually the first manifestation of BHD syndrome (Johannesma et al., 2015), maybe the only one (Xing et al., 2017). In FLCN mutation carriers, skin manifestations usually appear in the fourth decade and gradually increase and become more obvious with age (Iwabuchi et al., 2018). Compared to lung cysts/pneumothorax, the renal manifestations of BHD syndrome occur later (Pavlovich et al., 2005).

Congenital contractural arachnodactyly (CCA) or Beals-Hecht syndrome is a rare autosomal dominant connective tissue disease; it is associated with the disease-causing fibrillin-2 (FBN2) gene. The main clinical features of CCA are spider fingers (toes), flexion fingers, major joint contractures, scoliosis, pectus excavatum, and helix shrinkage (Aivaz et al., 2015). In this paper, we report an extremely rare family with BHD syndrome and CCA.

MATERIALS AND METHODS

Clinical Characteristics of the Family

We describe the clinical characteristics, family, and clinical manifestations of the patient's family members. Family history: the patient's parents were married but not intermarried, and both were deceased. The father had no history of symptomatic pneumothorax or hand malformations, while the mother had congenital hand malformations and no history of symptomatic pneumothorax. The patient had two brothers (one has three daughters, one has one son and one daughter) and one sister, and none of these people had no history of symptomatic pneumothorax or hand malformations. The second brother had hemiplegia, and the sister died of cerebral infarction at the age of 40. The patient's unmarried son had congenital hand malformations, a history of bullae, and spontaneous pneumothorax twice in the local hospital. His son's condition improved after drainage, and he was physically fit. While the patient denied a history of other familial diseases, his family is considered to have a familial hereditary disease, possibly BHD syndrome.

Blood tests, computed tomography (CT) of the chest, color Doppler ultrasound of the abdomen and heart, rheumatism-related indicators, and digital radiography (DR) of the hands were performed on the patient's family. Blood samples from the patient and his son were sent to the Henan Rare Disease Research Center for genetic sequencing.

The study was approved by the hospital ethics committee (2021-03-B024), and the family members signed informed consent forms.

Whole Exome Sequencing (WES)

With their full notification and informed consent, 3 ml of peripheral blood from the patient and his son was drawn and sent to a third-party company for WES. First, the DNA was fragmented, and the library prepared. Then, the Agilent V6 probe was used to hybridize and capture the DNA from the entire exome as well as part of the untranslated region. Finally, the high-throughput sequencing platform was used to detect mutations. Pathogenic genes of single-gene genetic diseases that had been identified in the Online Mendelian Inheritance in Man (June 2019) were analyzed. Please refer to the American College of Medical Genetics and Genomics (ACMG) for standards and guidelines on the interpretation of genetic variations and their grades. Separate clinical analyses of different samples were performed, including clinical symptom matching and disease recommendations.

RESULTS

A Rare Family's Characteristics

In the past 2 years, a 55-year-old male patient had chest tightness, shortness of breath, and an irritating cough without obvious triggers. He was repeatedly admitted to the hospital for spontaneous pneumothorax (four times in total).

Physical examination: body temperature, heart rate, and blood pressure were stable, except for shortness of breath. No abnormal findings on skin or mucous membranes upon examination. Weak breathing sounds in the right lung and thick breathing sounds in the left lung. No dry or wet rales were heard. Upon percussion, the right lung made drum-like sounds, while the left lung was voiceless. The heart and abdominal examinations found no abnormalities, but the fingers had bilateral deformities and asymmetries, along with incomplete extension. The patient

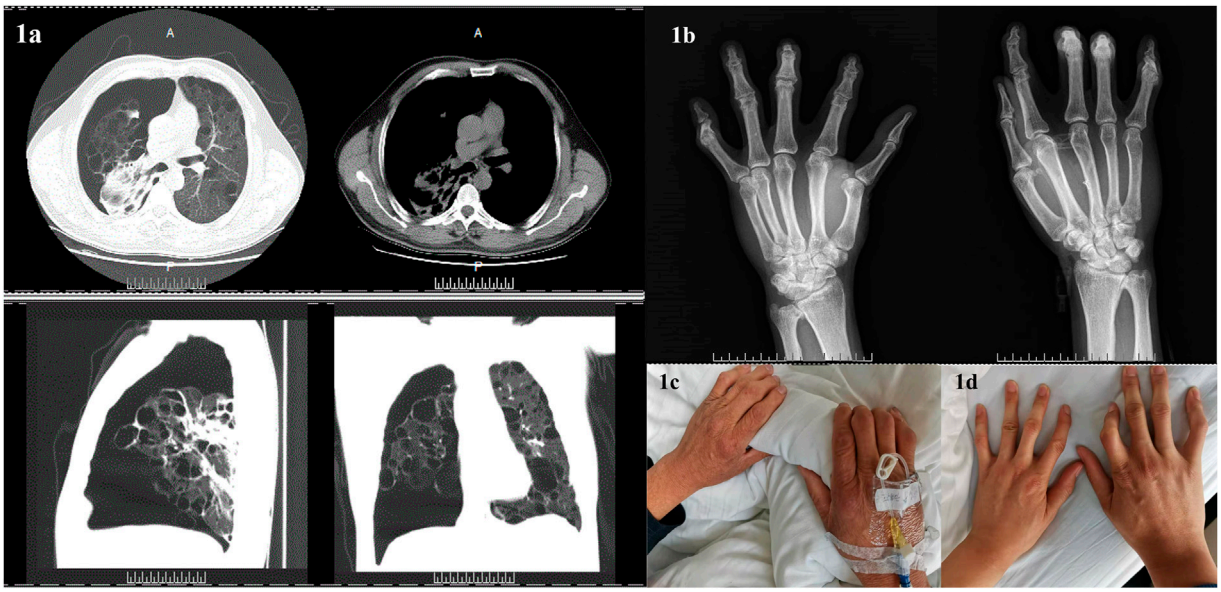

FIGURE 1 | Clinical characteristics of the patient and family members. **(A)**: Computed tomography of the patient's chest indicated spontaneous pneumothorax on the right side and cyst and bullae in both lungs. **(B)**: Digital radiography in both patient's hands revealed changes in both hands and wrists, suggesting degenerative changes or chronic inflammatory lesions. **(C)**: The patient's hands. **(D)**: The hands of the patient's son.

had a history of hypertension for over a month, and his blood pressure was as high as 180/120 mmHg. His blood pressure was lowered via oral administration of amlodipine besylate, valsartan, and bisoprolol fumarate, and it was controllable. The patient had no bad habits of tobacco or alcohol.

Patient's blood tests: blood routine, liver and kidney function, and rheumatism-related indicators (including antinuclear antibody profile, anti-neutrophil cytoplasmic-related antibodies, rheumatoid factor, and high-sensitivity C-reactive protein) were normal.

Chest CT revealed: spontaneous pneumothorax on the right side and cyst and bullae in both lungs (**Figure 1A**). A thoracic surgeon was consulted and asked to provide closed thoracic drainage to promote lung recruitment. The DR in both hands indicated changes in both the hands and wrists, suggesting degenerative changes or chronic inflammatory lesions (**Figure 1B**). Both the patient and his son had a history of hand deformities and pulmonary bullae formation (see **Figures 1C,D**, respectively, for photographs of the patient's and his son's hands). No abnormalities were found with the abdominal and cardiac color Doppler ultrasounds. No manifestations of kidney tumors or skin lesions. Pulmonary function test was not performed due to pneumothorax and bullae.

Following treatment, part of the patient's lung re-expanded, the pneumothorax improved, and air bubbles were still visible in the closed thoracic drainage bottle after the chest tube was intermittently clamped. He was transferred to thoracic surgery for thoracoscopic right lung volume reduction, pleural adhesion cauterization, and pleural fixation. His postoperative recovery was good. No spontaneous pneumothorax recurred during regular telephone and Outpatient follow-up.

Family WES Results

The WES results revealed that the proband and the son had heterozygous variants of the FLCN gene c.1015C > T (p. Gln339Ter) and FBN2 gene c.3485G > A (p. Cys1162Tyr) (**Figure 2**). A heterozygous nonsense mutation was detected in the exon region of the FLCN gene c.1015C > T, resulting in an amino acid change: p. Gln339Ter. The mutation site is reported as a pathogenic variant in the Human Gene Mutation Database (HGMD) but is not included in the ClinVar database. Using the ACMG guidelines, the variant was judged to be pathogenic (PVS1 + PM2 + PP5). A heterozygous missense mutation was also found in the exon region of the FBN2 gene c.3485G > A, resulting in an amino acid change: p. Cys1162Tyr. This mutation is not included in either the HGMD Professional database or the ClinVar database. However, according to the ACMG guidelines, the variant was judged to be potentially pathogenic (PM1 + PM2 + PM5 + PP3).

The FLCN-gene-associated disease is BHD syndrome, an autosomal dominant genetic disease. The proband and son are consistent with the phenotype of this disease. The FBN2 gene-associated disease is CCA, an autosomal dominant genetic disease. The proband, mother, and son are phenotypically consistent with this disease (see **Figure 3** for the genealogical tree). Consequently, the final diagnosis was BHD syndrome and CCA.

DISCUSSION

In this study, we report for the first time an extremely rare family with BHD syndrome and CCA. This combination has not been reported in China or abroad until now. Compared to Caucasians,

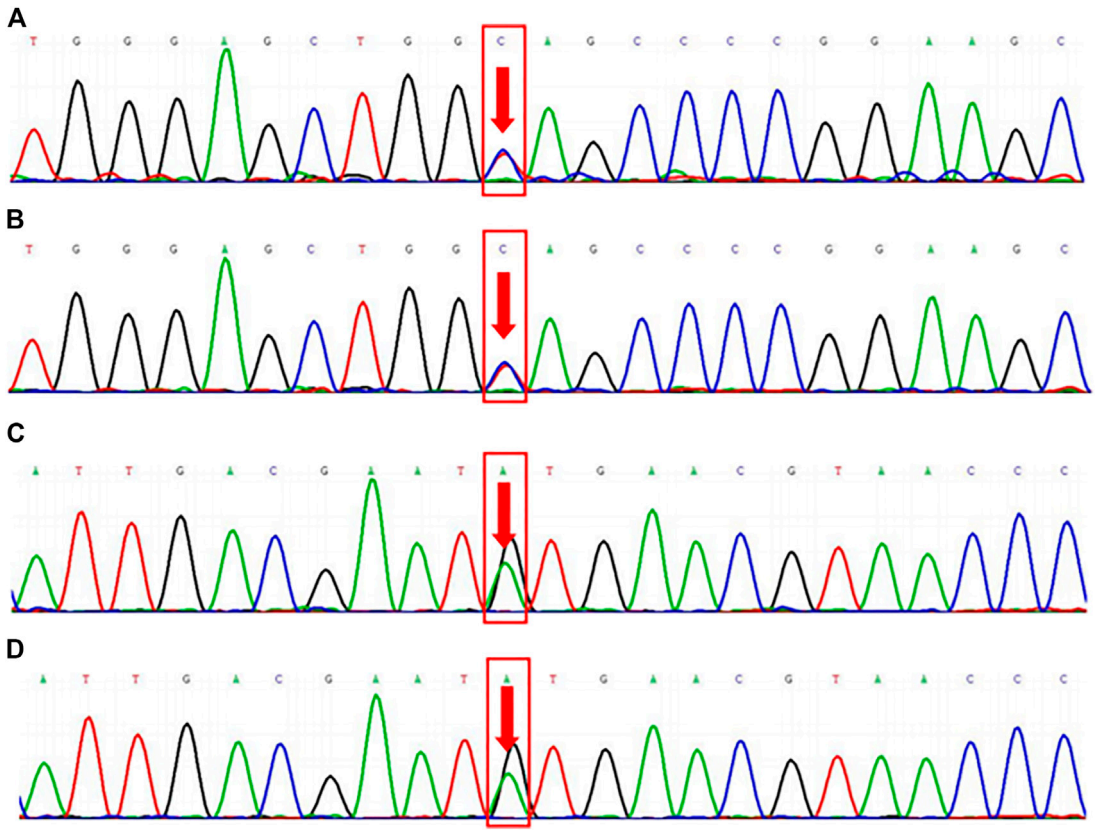

FIGURE 2 | Family whole exome sequencing results. FLCN gene c.1015C > T (p. Gln339Ter) mutation sequencing results in the proband (2a, heterozygous mutation) and his son (2b, heterozygous mutation). FBN2 gene c.3485G > A (p. Cys1162Tyr) mutation sequencing results in the proband (2c, heterozygous mutation) and his son (2d, heterozygous mutation).

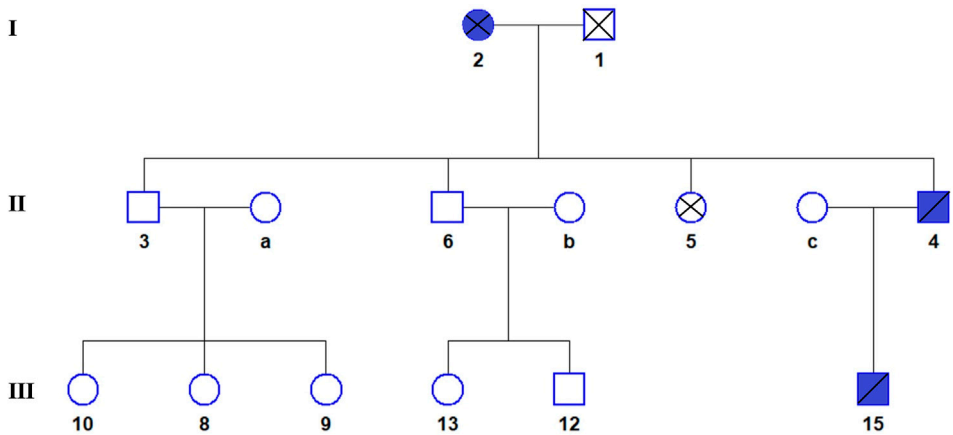

FIGURE 3 | The genealogical tree of Birt-Hogg-Dubé syndrome and congenital contractural arachnodactyly. Blue indicates the patient. The proband (4), his son (15), and his mother (2) all have BHDS and CCA.

Asians with BHD syndrome have a lower incidence of skin and kidney manifestations but a higher rate of pneumothorax recurrence (Park et al., 2017). Indeed, the risk of pneumothorax in BHD patients is 50 times higher than the general population (Kennedy et al., 2016). Pulmonary cysts, multiple and bilateral, occur in 80–100% of patients with BHD syndrome, and 76% of them have pneumothorax. BHD syndrome is one of the most common causes of familial spontaneous

pneumothorax (Liu et al., 2020). Thus, a family history of pneumothorax is an important clue that suggests a BHD diagnosis (Gupta et al., 2016). The pulmonary manifestations of BHD syndrome need to be distinguished from other diffuse cystic lung diseases, such as lymphangioleiomyomatosis, Langerhans cell histiocytosis, and lymphocytic interstitial pneumonia (Cui et al., 2016). Unlike other cystic lung diseases, BHD disease does not cause progressive lung function loss or chronic respiratory insufficiency (Liu et al., 2020). According to the literature, the prevalence of renal involvement in BHD patients ranges from 6.5 to 34% (Kunogi et al., 2010). Furuya et al. (Furuya et al., 2016) found that 25.8% of BHD patients have renal damage, especially renal cell carcinoma, the most common histology in chromophobe renal cell carcinoma (43.6%), and all patients with renal involvement also have lung cysts. Kidney cancer is the most serious manifestation of BHD syndrome.

The skin manifestations of BHD syndrome include fibrofolliculoma, trichodiscoma, and perifollicular fibroma. These three types are papules that are between 2 and 4 mm, flesh-colored or light gray-white, and smooth dome-shaped. They are commonly found on the face, neck, and trunk (Aivaz et al., 2015). The most common skin manifestation of BHD syndrome is fibrofolliculoma, where their numbers can range from two to more than 100. Fibrofolliculoma is rare and unique to BHD syndrome and can be diagnosed using needle biopsies (Tong et al., 2018). This patient's family currently has no skin or kidney manifestations, but they require regular review and follow-ups.

The diagnosis of BHD disease needs to be combined with family history and clinical and/or skin histopathological criteria. Its management mainly includes early pleurodesis in the case of pneumothorax, regular kidney imaging for tumor detection, and diagnostic tests to find BHD syndrome among the patient's relatives (Gupta et al., 2016). For patients diagnosed with BHD syndrome, follow-ups should be initiated, with special attention to the condition of the kidneys. Currently, pneumothorax is usually treated symptomatically, and electrocoagulation, laser, and curettage are generally used for treating skin lesions.

In this family, both the proband and his son had recurrent spontaneous pneumothorax. First, we must be alert to the possibility of familial pneumothorax. After a clear diagnosis, kidney tumors and skin lesions should be ruled out. If corresponding symptoms occur, seek medical attention in time. It is recommended to screen the genetic locus in members of the subject's blood-related family, establish a follow-up plan for carriers as soon as possible, and conduct genetic counseling in situations involving fertility. At present, this disease has no special treatment and should be tracked via regular follow-ups.

The main clinical features of CCA are spider finger (toe), flexion finger, major joint contracture, scoliosis, pectus excavatum, and helix shrinkage (Xu et al., 2020). Marfan syndrome (MFS) is a rare autosomal dominant multi-system disease, and it is manifested via bone, eye, skin, and cardiovascular symptoms (Verstraeten et al., 2016). CCA and MFS have many common clinical features, including the so-called Marfan-like appearance, which consists of a tall, slender, and weak appearance as well as skeletal features that include spider fingers, bipedal deformities, pectus excavatum, and kyphosis (Inbar-Feigenberg et al., 2014). However, most patients with CCA have helix shrinkage, flexion contracture, and muscle hypoplasia (Lavillaureix et al., 2017). MFS and CCA are two similar syndromes that are caused by mutations in genes FBN1 and FBN2, respectively (Frédéric et al., 2009). They are difficult to distinguish based on clinical symptoms alone (Gupta et al., 2004); the best way to differentiate them is via genetic testing.

The clinical manifestations of CCA patients are different, involving the heart, bones, lens, and other parts, requiring individualized treatment for the patients. Flexion contractures of the large joints of the extremities often do not require targeted treatment, while hand joint contractures can loosen joints and skin grafts to improve appearance and function. Kyphosis and scoliosis deformity can be corrected by surgery if it affects life. Severe heart deformities often require early surgical treatment, and regular follow-up monitoring is required for non-severe ones (Yin et al., 2020). The proband, mother, and son in this family all have congenital hand deformities with mild symptoms and do not affect normal functions. Since the mother of the proband also has hand deformities, and because the mother is deceased, it is recommended to send samples from the maternal relatives of the proband for screening at this site and establish a follow-up plan for carriers as soon as possible. Genetic counseling when there is a need for fertility.

CONCLUSION

WES is currently the gold standard for diagnosing these two familial genetic diseases. For patients with chest tightness, shortness of breath, recurrent spontaneous pneumothorax, and congenital hand deformity without inducement, genetic sequencing should be carried out as soon as possible to make a clear diagnosis, which can guide treatment and genetic counseling. Lifelong follow-up after the diagnosis is made to control the patient's progress in time and reduce complications.

Declarations

Ethical Approval and Consent to participate The study was approved by the hospital ethics committee (2021-03-B024), and the family members signed informed consent forms.

Consent for publication Subject agrees.

Availability of data and materials None.

Competing interests None.

Funding Natural Science Foundation of Henan Province (182300410365).

Science and Technology Project of Henan Province (202102310047).

Medical science and technology Project of Henan Province (2018020285).

The scientific and technological achievements transfer and transformation project of Henan sub-center of SCA (2018105).

Authors' contributions Yimin Mao and Hongwei Jiang designed the study, performed the research. Jiayong Qiu and Yao Lou analysed data and wrote the paper. Huifang Peng collected the data. All authors discussed the results and revised the manuscript.

DATA AVAILABILITY STATEMENT

The data analyzed in this study is subject to the following licenses/restrictions: none. Requests to access these datasets should be directed to jiayong5201@163.com.

ETHICS STATEMENT

The studies involving human participants were reviewed and approved by the Ethics Committee of the First Affiliated Hospital of Henan University of Science and Technology (2021-03-B024).

The patients/participants provided their written informed consent to participate in this study. Written informed consent was obtained from the individual(s), and minor(s)' legal guardian/next of kin, for the publication of any potentially identifiable images or data included in this article.

AUTHOR CONTRIBUTIONS

YM and HJ designed the study, performed the research. JQ and YL analysed data and wrote the paper. HP collected the data. All authors discussed the results and revised the manuscript.

REFERENCES

Aivaz, O., Berkman, S., Middelton, L., Linehan, W. M., DiGiovanna, J. J., and Cowen, E. W. (2015). Comedonal and Cystic Fibrofolliculomas in Birt-Hogg-Dube Syndrome. *JAMA Dermatol.* 151 (7), 770–774. doi:10.1001/jamadermatol.2015.0215

Black, M., Wei, X. J., Sun, W., Simms, A., Negron, R., Hagiwara, M., et al. (2020). Adult Rhabdomyoma Presenting as Thyroid Nodule on fine-needle Aspiration in Patient with Birt-Hogg-Dubé Syndrome: Case Report and Literature Review. *Diagn. Cytopathology* 48 (6), 576–580. doi:10.1002/dc.24413

Cui, H., Tian, X., Wang, H., Zhao, J., Huang, H., Zhang, W., et al. (2016). Diffuse Cystic Lung Diseases: Diagnostic Considerations. *Semin. Respir. Crit. Care Med.* 37 (3), 457–467. doi:10.1055/s-0036-1580690

Daccord, C., Cottin, V., Cottin, V., Prévot, G., Uzunhan, Y., Mornex, J. F., et al. (2020). Lung Function in Birt-Hogg-Dubé Syndrome: a Retrospective Analysis of 96 Patients. *Orphanet J. Rare Dis.* 15 (1), 120. doi:10.1186/s13023-020-01402-y

Frédéric, M. Y., Monino, C., Marschall, C., Hamroun, D., Faivre, L., Jondeau, G., et al. (2009). TheFBN2gene: New Mutations, Locus-specific Database (Universal Mutation DatabaseFBN2), and Genotype-Phenotype Correlations. *Hum. Mutat.* 30 (2), 181–190. doi:10.1002/humu.20794

Furuya, M., Yao, M., Tanaka, R., Nagashima, Y., Kuroda, N., Hasumi, H., et al. (2016). Genetic, Epidemiologic and Clinicopathologic Studies of Japanese Asian Patients with Birt-Hogg-Dubé Syndrome. *Clin. Genet.* 90 (5), 403–412. doi:10.1111/cge.12807

Gupta, N., Sunwoo, B. Y., and Kotloff, R. M. (2016). Birt-Hogg-Dubé Syndrome. *Clin. Chest Med.* 37 (3), 475–486. doi:10.1016/j.ccm.2016.04.010

Gupta, P. A., Wallis, D. D., Chin, T. O., Northrup, H., Tran-Fadulu, V. T., Towbin, J. A., et al. (2004). FBN2 Mutation Associated with Manifestations of Marfan Syndrome and Congenital Contractural Arachnodactyly. *J. Med. Genet.* 41 (5), e56. doi:10.1136/jmg.2003.012880

Inbar-Feigenberg, M., Meirowitz, N., Nanda, D., Toi, A., Okun, N., and Chitayat, D. (2014). Beals Syndrome (Congenital Contractural Arachnodactyly): Prenatal Ultrasound Findings and Molecular Analysis. *Ultrasound Obstet. Gynecol.* 44 (4), 486–490. doi:10.1002/uog.13350

Iwabuchi, C., Ebana, H., Ishiko, A., Negishi, A., Mizobuchi, T., Kumasaka, T., et al. (2018). Skin Lesions of Birt-Hogg-Dubé Syndrome: Clinical and Histopathological Findings in 31 Japanese Patients Who Presented with Pneumothorax And/or Multiple Lung Cysts. *J. Dermatol. Sci.* 89 (1), 77–84. doi:10.1016/j.jdermsci.2017.10.014

Johannesma, P. C., Reinhard, R., Kon, Y., Sriram, J. D., Smit, H. J., van Moorselaar, R. J. A., et al. (2015). Prevalence of Birt-Hogg-Dubé Syndrome in Patients with Apparently Primary Spontaneous Pneumothorax. *Eur. Respir. J.* 45 (4), 1191–1194. doi:10.1183/09031936.00196914

Kennedy, J. C., Khabibullin, D., and Henske, E. P. (2016). Mechanisms of Pulmonary Cyst Pathogenesis in Birt-Hogg-Dube Syndrome: The Stretch Hypothesis. *Semin. Cel Develop. Biol.* 52, 47–52. doi:10.1016/j.semcdb.2016.02.014

Kunogi, M., Kurihara, M., Ikegami, T. S., Kobayashi, T., Shindo, N., Kumasaka, T., et al. (2010). Clinical and Genetic Spectrum of Birt-Hogg-Dube Syndrome Patients in Whom Pneumothorax And/or Multiple Lung Cysts Are the Presenting Feature. *J. Med. Genet.* 47 (4), 281–287. doi:10.1136/jmg.2009.070565

Lavillaureix, A., Heide, S., Chantot-Bastaraud, S., Marey, I., Keren, B., Grigorescu, R., et al. (2017). Mosaic Intragenic Deletion of FBN2 and Severe Congenital Contractural Arachnodactyly. *Clin. Genet.* 92 (5), 556–558. doi:10.1111/cge.13062

Liu, Y., Xing, H., Huang, Y., Meng, S., and Wang, J. (2020). Familial Spontaneous Pneumothorax: Importance of Screening for Birt-Hogg-Dubé Syndrome. *Eur. J. Cardiothorac. Surg.* 57 (1), 39–45. doi:10.1093/ejcts/ezz171

Park, H. J., Park, C. H., Lee, S. E., Lee, G. D., Byun, M. K., Lee, S., et al. (2017). Birt-Hogg-Dube Syndrome Prospectively Detected by Review of Chest Computed Tomography Scans. *PLoS One* 12 (2), e0170713. doi:10.1371/journal.pone.0170713

Pavlovich, C. P., Grubb, R. L., 3rd, Hurley, K., Glenn, G. M., Toro, J., Schmidt, L. S., et al. (2005). Evaluation and Management of Renal Tumors in the Birt-Hogg-Dubé Syndrome. *J. Urol.* 173 (5), 1482–1486. doi:10.1097/01.ju.0000154629.45832.30

Tong, Y., Schneider, J. A., Coda, A. B., Hata, T. R., and Cohen, P. R. (2018). Birt-Hogg-Dubé Syndrome: A Review of Dermatological Manifestations and Other Symptoms. *Am. J. Clin. Dermatol.* 19 (1), 87–101. doi:10.1007/s40257-017-0307-8

Verstraeten, A., Alaerts, M., Van Laer, L., and Loeys, B. (2016). Marfan Syndrome and Related Disorders: 25 Years of Gene Discovery. *Hum. Mutat.* 37 (6), 524–531. doi:10.1002/humu.22977

Xing, H., Liu, Y., Jiang, G., Li, X., Hou, Y., Yang, F., et al. (2017). Clinical and Genetic Study of a Large Chinese Family Presented with Familial Spontaneous Pneumothorax. *J. Thorac. Dis.* 9 (7), 1967–1972. doi:10.21037/jtd.2017.06.69

Xu, P., Li, R., Huang, S., Sun, M., Liu, J., Niu, Y., et al. (2020). A Novel Splicing Mutation in the FBN2 Gene in a Family with Congenital Contractural Arachnodactyly. *Front. Genet.* 11, 143. doi:10.3389/fgene.2020.00143

Yin, Y. B., Hou, C. M., and Tian, W. (2020). Reports on Two Families of Congenital Contracture Spider finger Deformities and Literature Review[J]. *Chin. J. Bone Jt.* 9 (03), 20–24.

Conflict of Interest: The authors declare that the research was conducted in the absence of any commercial or financial relationships that could be construed as a potential conflict of interest.

Publisher's Note: All claims expressed in this article are solely those of the authors and do not necessarily represent those of their affiliated organizations, or those of the publisher, the editors and the reviewers. Any product that may be evaluated in this article, or claim that may be made by its manufacturer, is not guaranteed or endorsed by the publisher.

frontiers in Genetics

CASE REPORT
published: 26 January 2022
doi: 10.3389/fgene.2022.807515

Case Report: Novel MFSD8 Variants in a Chinese Family With Neuronal Ceroid Lipofuscinoses 7

Yimeng Qiao[1†], Yang Gu[2†], Ye Cheng[1], Yu Su[1], Nan Lv[2], Qing Shang[2] and Qinghe Xing[1,3*]*

[1]*Institutes of Biomedical Sciences and Children's Hospital, Fudan University, Shanghai, China,* [2]*Children's Hospital of Zhengzhou University and Henan Children's Hospital, Zhengzhou, China,* [3]*Shanghai Center for Women and Children's Health, Shanghai, China*

Neuronal ceroid lipofuscinoses (NCLs) are among the most common progressive encephalopathies of childhood. Neuronal ceroid lipofuscinosis 7 (CLN7), one of the late infantile-onset NCLs, is an autosomal recessive disorder caused by mutations in the *MFSD8* gene on chromosome 4q28. Almost all reported mutations of *MFSD8* in CLN7 patients were SNVs. However, we report a 4-year-old boy with CLN7 harboring compound heterozygous mutations in the *MFSD8* gene, including one novel two-nucleotide deletion c.136_137delAT (p. M46Vfs*22) and one whole gene deletion of *MFSD8* confirmed by Sanger sequencing, genomic quantitative PCR and CNV-seq. Therefore, for nonconsanguineous CLN7 patients with homozygous mutations in the *MFSD8* gene, genetic counseling staff should focus on the possibility of whole gene deletion. This is one case report describing a whole gene deletion in a Chinese patient with CLN7, suggesting the diagnosis of CLN7 should be based on clinical suspicion and genetic testing.

Keywords: neuronal ceroid lipofuscinoses, CLN7, MFSD8, whole gene deletion, mutation

OPEN ACCESS

Edited by:
María L. Couce, Complejo Hospitalario Universitario de Santiago, Spain

Reviewed by:
James A. Poulter, University of Leeds, United Kingdom
Stefano Castellana, Home for Relief of Suffering (IRCCS), Italy

***Correspondence:**
Qinghe Xing
qhxing@fudan.edu.cn
Qing Shang
sqing1965@163.com

[†]These authors have contributed equally to this work

Specialty section:
This article was submitted to Genetics of Common and Rare Diseases, a section of the journal Frontiers in Genetics

Received: *02 November 2021*
Accepted: *06 January 2022*
Published: *26 January 2022*

Citation:
Qiao Y, Gu Y, Cheng Y, Su Y, Lv N, Shang Q and Xing Q (2022) Case Report: Novel MFSD8 Variants in a Chinese Family With Neuronal Ceroid Lipofuscinoses 7. Front. Genet. 13:807515. doi: 10.3389/fgene.2022.807515

INTRODUCTION

Neuronal ceroid lipofuscinoses (NCLs), among the most common progressive encephalopathies of childhood, with ages of onset ranging from birth to adulthood (Williams et al., 2006; Jalanko and Braulke, 2009), are a clinically and genetically heterogeneous group of neurodegenerative disorders (Schulz et al., 2013; Zare-Abdollahi et al., 2019). NCLs are ultrastructurally characterized by the intracellular accumulation of autofluorescent lipopigment storage material in different patterns (Goebel and Wisniewski, 2004). Patients developing such disorders may suffer from cognitive impairment (HP:0100543), motor deterioration (HP:0002333), progressive visual loss (HP:0000529), and uncontrolled seizures (HP:0001250) (Goebel and Wisniewski, 2004; Mole et al., 2005). NCLs are historically classified into four major subtypes based on the age of onset: infantile, late infantile, juvenile, and adult (Butz et al., 2020). To date, thirteen causal genes have been identified in different subtypes (Kohan et al., 2011; Chartier et al., 2021). One gene can be involved in different clinical forms, and conversely, one clinical form can be due to different genes (Mole et al., 2019).

Neuronal ceroid lipofuscinosis 7 (CLN7; OMIM: 610951) is an autosomal recessive disorder caused by mutations in the *MFSD8* gene on chromosome 4q28 (Kousi et al., 2009). *MFSD8* (NP_001358525) encodes a 518-amino acid integral lysosomal transmembrane protein that includes twelve membrane-spanning domains with cytosolic N- and C-terminal domains (Siintola et al., 2007). More than 40 different *MFSD8* mutations, including missense, nonsense or Indel mutations,

have been detected, causing an accumulation of cellular glycoproteins and lipoproteins, ultimately resulting in cellular degeneration and the occurrence of CLN7 (McBride et al., 2018).

To date, next-generation sequencing (NGS), which enables fast and cost-effective generation of genome-scale sequence data with exquisite resolution and accuracy, has been increasingly used as a diagnostic tool in the clinic (Xuan et al., 2013; Sawyer et al., 2016). Technologies including target NGS panel (Panel), clinical exome sequencing (CES), whole exome sequencing (WES), CNV-seq and whole genome sequencing (WGS) have greatly improved the diagnosis rate for inherited diseases (Xue et al., 2015; Monlong et al., 2018).

We report one case of a 4-year-old boy with CLN7 who presented with global developmental delay (GDD) (HP: 0001263), sleeping disturbance (HP:0002360), and ataxia (HP: 0001251) with no ocular abnormalities (HP:0000478) and who harbored novel compound heterozygous mutations in *MFSD8* (c.136_137delAT, p. M46Vfs*22, inherited from the mother and one whole gene deletion, inherited from the father). This is the first report of two severe *MFSD8* trans-mutations associated with CLN7 in a Chinese family.

METHODS AND MATERIALS

Subjects and Clinical Assessment

Four members of a nonconsanguineous Chinese family with one individual affected by GDD were recruited for this study. Magnetic resonance imaging (MRI) and the 24-h video electroencephalogram (EEG) were performed on the proband and an additional three non-affected family members. The Psychiatric Class B scale and the Sign-significant relations were used to assess the developmental characteristics of the proband. After obtaining written informed consent, peripheral venous blood samples were collected from the four family members. A statement of informed consent was obtained from the parents of all subjects under the age of 18 after full explanation of the procedure. The research protocol was reviewed and approved by the ethics committee of Henan Children's Hospital in accordance with the Declaration of Helsinki.

Whole Exome Sequencing and CNV-seq

Total genomic DNA was extracted from peripheral blood with the QIAamp® DNA Blood Mini Kit (QIAGEN, Hilden, Germany) according to the manufacturer's protocol. A NanoDrop spectrophotometer was used to measure DNA purity and concentration. The method of WES and CNV-seq was previously described (Gao et al., 2019).

For WES-seq, DNA libraries were prepared using xGen Exome Research Panel v1.0 (Integrated DNA Technologies, Inc., Coralville, IA, United States) according to manufacturer's protocol. Sequencing was performed on Illumina HiSeq2500 platform to a mean per-sample depth of 100×. After sequencing, the reads were mapped to the hg19 human reference genome using Burrows-Wheeler Aligner and variants were called using the Genome Analysis Toolkit (GATK). SAMtools and Pindel were subjected to call SNVs and Indels, respectively. The variants with minor allele frequency >1% in dbSNP, NHLBI exome sequencing project (ESP1), ExAC database, the 1,000 genomes project database, and 200 in-house controls were removed. The pathogenicity of the variants was predicted using the Sorting Intolerant From Tolerant (SIFT), Polymorphism Phenotyping v2 (PolyPhen-2), Combined Annotation Dependent Depletion (CADD) and Mutation Taster. Each variant identified in a known neurodevelopmental disease gene as selected from OMIM (4 August 2021) could be considered as potential disease-causing variants according to the guidelines of the American College of Medical Genetics and Genomics (ACMG). Possible pathogenic genes were identified based on heredity models, deleterious variants and clinical phenotypes.

For CNV-seq, more than 1 μg genomic DNA was broken into 200–300 bp fragments for library preparation and sequenced on the Illumina HiSeq 2,500 (Illumina, San Diego, United States). Raw data were analyzed by fastp v0.18.1 software, and clean data were then subjected to human reference genome (hg19) analysis using BWA. After PCR duplications were removed by Picard MarkDuplicates, the mixture-hidden Markov model (*m*-HMM) approach was applied to estimate the window-based copy number change points and copy number states. An in-house pipeline was used to map and call CNVs larger than 100 kb. Candidate CNVs were annotated by analyzing the genes contained in the CNVs and the CNV intervals themselves with the databases Decipher v11.8, ClinVar, ClinGen, and OMIM. Then the candidate CNVs were filtered with normal frequency databases DGV v107 and ISCA. Interpretation of constitutional CNV was based on annotation information and frequency database (less than 0.5%) according to ACMG as reported previously.

Sanger Sequencing

The candidate disease-causing variants were confirmed by Sanger sequencing. Amplification was performed using the following primers: 5′-GTTCTAGGGATTGGTTGCACA -3′ (forward) and 5′- TGCTGTCATCAAGTAGAGCATG-3′ (reverse). Parent and sibling samples, where available, were also analyzed by Sanger sequencing to determine if the origin of the variant was paternal, maternal, or *de novo*.

Genomic Quantitative PCR

Deletions in *MFSD8* were validated by qPCR using ABI Quant Studio six Flex (Thermo Fisher). We designed two pairs of primers within the *MFSD8* gene (**Supplementary Table S1**). qPCR was carried out in a total volume of 10 μL containing 5 μL of TB Green® Premix Ex Taq™ (Tli RNaseH Plus) (TaKaRa Biotechnology, Dalian, China), 0.2 μL ROX Reference Dye II, 0.4 μM of each primer and 20 ng of genomic DNA. All samples were run in triplicate. Thermal cycling conditions were 95°C for 30 s, followed by 40 cycles at 95°C for 5 s and 60°C for 30 s. The *ALB* gene was selected as the control amplicon. The dosage of each amplicon relative to *ALB* and normalized to the mother's DNA was determined using the $2^{-\Delta\Delta Ct}$ method.

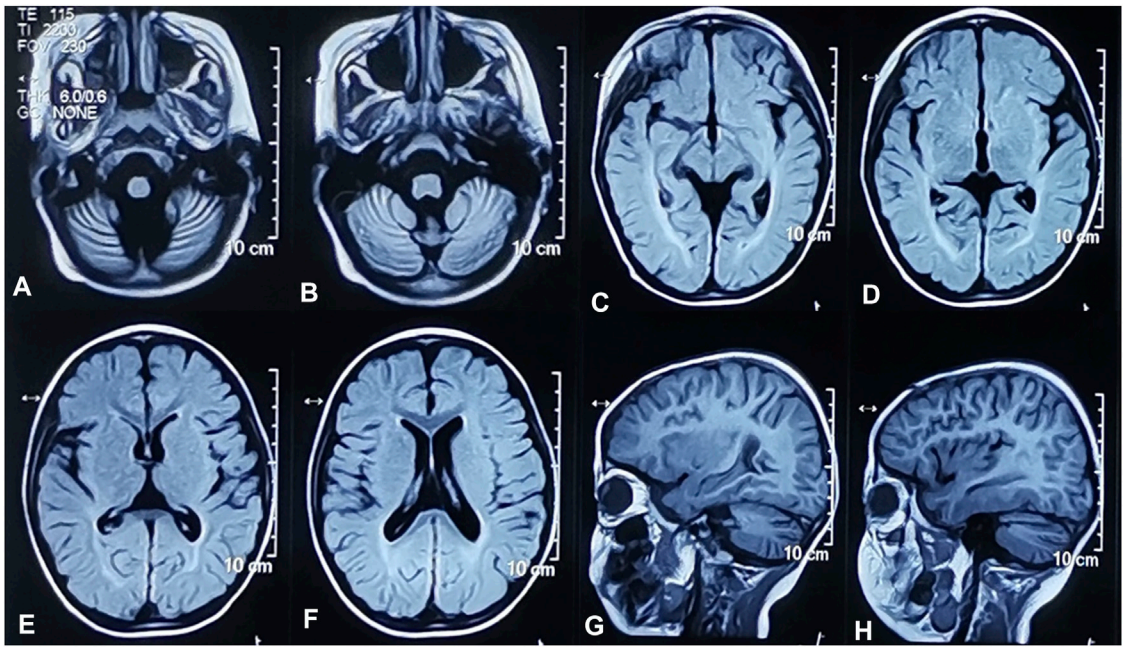

FIGURE 1 | Brain MRI of the proband. Widened cerebellum sulci. Axial T2-weighted FLAIR image **(A,B)**. Abnormal signals of white matter near the posterior horn of bilateral lateral ventricles. Axial T2-weighted FLAIR images **(C,D)**. Widened bilateral cerebral hemispheres sulci. Axial T2-weighted FLAIR image **(E,F)**. Widened bilateral cerebral hemispheres and cerebellar sulci. Sagittal T1-weighted images **(G,H)**.

RESULTS

Case Description

The proband, a 4-year-old boy, was born after an uneventful pregnancy and delivery, with nonconsanguineous marriage of his parents. He was born at the gestation period of 36 weeks plus 5 days with a birth weight of 3,500 g. The patient suffered jaundice approximately 1 month after birth and received blue light radiation and oral medication. He presented some phenotypes, such as cognitive impairment, motor deterioration, expressive language delay (HP:0002474), sleeping disturbance, and ataxia (HP:0001251), with no ocular abnormalities. His lower limbs were prone to involuntary tremors and he would fall when tired or frightened. On physical and neurological examinations at admission, he had a weight of 18.3 kg, a height of 105 cm, and a head circumference of 49.5 cm. The MRI of the brain showed bilateral widening of the cerebral hemispheres and cerebellar sulci and abnormal white matter signals in the posterior horns of both sides of the ventricle (**Figure 1**). The 24-h video EEG showed abnormal activity: widespread sharp waves, sharp slow waves, and pointed slow wave emission. Slow waves were discharged from the tip of his right forehead during sleep. According to the Psychiatric Class B scale, at the age of four, his exercise and social adaptation were equivalent to 12 months, and his intelligence was equivalent to only 11 months. The development score showed the mental index (MI) < 44 points and the developmental quotient (DQ) < 44 points. The Sign-significant relation (S-S) also indicated language developmental delay. Due to these clinical and laboratory findings, he was diagnosed with GDD.

Genetic Analyses

The average coverage for exome sequencing of the proband was approximately 100×, and the mean sequencing depth of the deletion region (chr4:128846736 -128976763) at 4q28.2 was 46×, respectively. After a step-by-step bioinformatics analysis containing base calling, variant annotation, and biological function prediction, only a novel homozygous mutation in *MFSD8* (NM_001371596.2: c.136_137delAT, p. M46Vfs*22) was identified as being responsible for the boy's phenotype. The AT deletion caused a frameshift mutation with a change in amino acids from 46 to 68 and introduced a new terminating TAA codon at position 69. According to ACMG guidelines, the c.136_137delAT (p. M46Vfs*22) variant is classified as "likely pathogenic (LP)" (one PVS1: LOF mutation + one PM2: the frequency of all normal population databases is less than 0.0005). Sanger sequencing revealed that the mother was a heterozygous c.136_137delAT carrier and that the father was a non-carrier (**Figure 2**). These data support the view that one mutation was inherited from the mother and another was *de novo*. To further investigate whether the proband's GDD phenotype was related to the deletion of the paternal genome, we performed qPCR using primers to amplify exon 11—intron 11 (F1R1) and exon 12 (F2R2) of *MFSD8* (NM_001371596.2). Deletions were validated in the proband and his father. Furthermore, we conducted CNV-seq and detected a deletion of approximately 130 kb (chr4:128846736–128976763) at 4q28.2 and confirmed that the identified deletion was paternal,

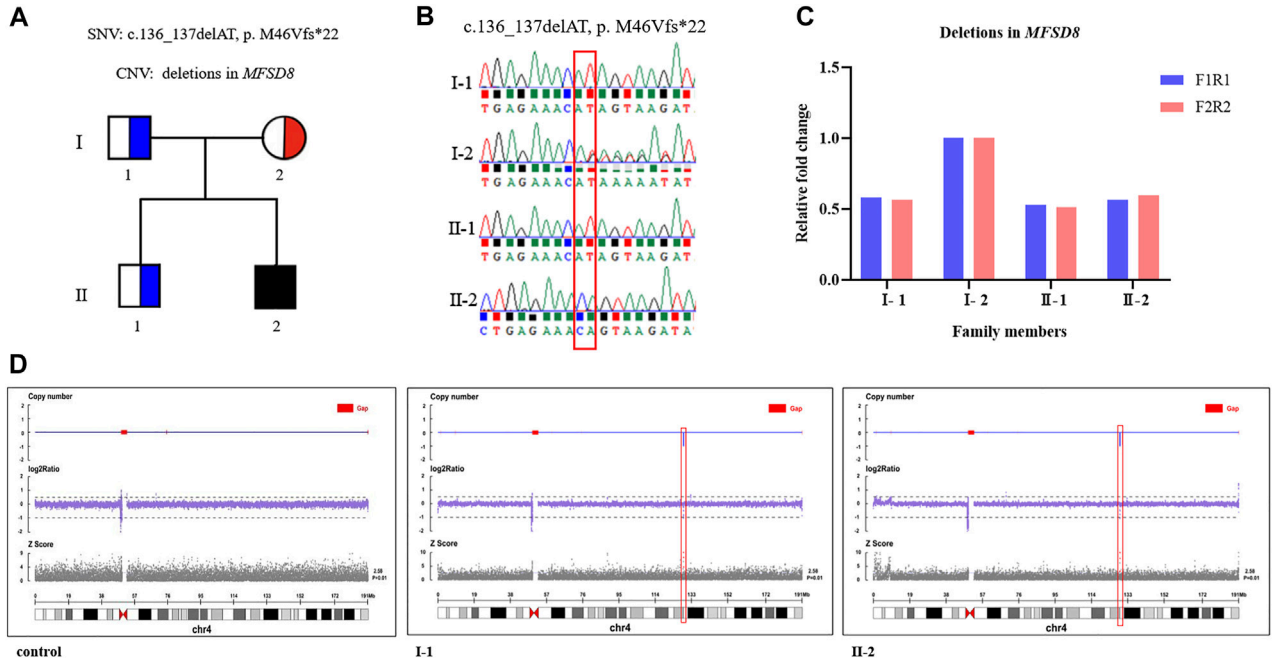

FIGURE 2 | Compound heterozygous variants were identified by WES and CNV-seq. **(A)** A Chinese family with CLN7 and *MFSD8* mutations. The black filled-in square represents the proband (c.136_137delAT, p. M46Vfs*22, and whole *MFSD8* deletion), the blue half-filled squares represent the heterozygous carriers of the *MFSD8* deletions, and the red half-filled circle represents the heterozygous carrier of a novel two-nucleotide deletion (c.136_137delAT, p. M46Vfs*22). **(B)** Sanger sequencing validated the c.136_137delAT (p. M46Vfs*22) variant in the family. **(C)** Deletions in *MFSD8* were confirmed by qPCR. **(D)** CNV-seq detected an ~130 kb deletion at 4q28.2 in both the father and proband.

indicating that both the father and proband were heterozygous for the whole *MFSD8* deletion (**Figure 2**). As far as we know, the identified ~130 kb deletion is not present in our homemade exome database, which contains 200 samples, or in public databases. In addition, according to the ACMG guidelines for sequence variants, the deletion was classified as "pathogenic". All of the above results indicated that the compound heterozygous variants were very likely to be the genetic cause of the proband's GDD phenotype.

DISCUSSION

GDD is an underdiagnosed condition, likely due to its heterogeneous etiology, presentation, and course (Vasudevan and Suri, 2017; Belanger and Caron, 2018). CLN7 is initially diagnosed as GDD and remains a devastating pediatric disease for which there are currently no cures (McBride et al., 2018; Kohlschutter et al., 2019). Although treatments may be useful to slow or even halt disease progression, few therapies are unlikely to reverse the disease (Specchio et al., 2021). In this work, we identified a 4-year-old boy with CLN7 harboring compound heterozygous mutations in *MFSD8* (c.136_137delAT and one whole gene deletion).

The etiology of CLN7 was due to mutations in the *MFSD8* gene. As a member of the major facilitator superfamily of active transport proteins, the MFSD8 protein posits transport solutes across the lysosomal membrane to aid in the digestion and clearance of cellular biomolecules, although the exact function of MFSD8 remains elusive (Sharifi et al., 2010). Human Gene Mutation database (HGMD), indicates that more than 40 mutations have been reported in association with CLN7, among which 30 mutations are nonsense or missense, five mutations are splicing, while six are small indel mutations. Because CLN7 exhibits a variable spectrum of clinical manifestations and the genetic variants may have different effects on the presence and function of the MFSD8, the explanation for the phenotypic variability most likely resides in the genotype of the patients. Non-functional variants result in severe clinical features of CLN7 while dysfunctional variants with residual activity may result in a markedly attenuated presentation. To the best of our knowledge, our case is the first report describing an ~130 kb deletion at 4q28.2 in a Chinese patient with CLN7. The deleted region contained *MFSD8* and *ABHD18* genes (**Figure 3**). Despite the ubiquitous expression of *ABHD18*, the characteristics and function of *ABHD18* are still unknown. *MFSD8* is the causative gene of CLN7, which supports the conclusion that the severe phenotype seen in this patient was attributable to biallelic null variants leading to non-production of MFSD8. This finding will give us a better understanding of the pathogenicity of *MFSD8* and provide new insight into how *MFSD8* works and functions to cause CLN7.

MFSD8 plays an important role during growth and development, not only in humans but also in other animals. In fact, animals such as Japanese macaques and mice with mutations in the *MFSD8* gene had similar symptoms to humans with *MFSD8* mutations. Japanese macaques with a homozygous frameshift mutation in the *MFSD8* gene ($MFSD8^{-/-}$) display progressive neurological deficits, including visual impairment, tremors, incoordination, ataxia and impaired balance (McBride et al., 2018). Homozygous *MFSD8* (tm1a/tm1a)

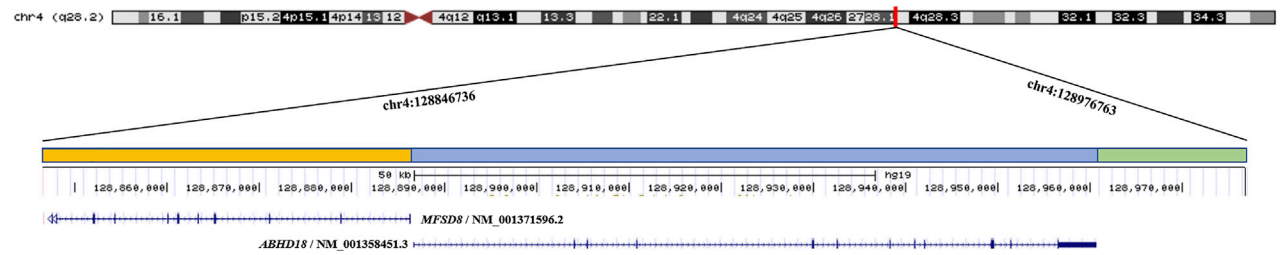

FIGURE 3 | The ~130 kb (chr4:128846736 - 128976763) deletion identified by CNV-seq extends from *MFSD8* to *ABHD18* at 4q28.2 in the proband. The orange bar represents the deletion region of *MFSD8*, the blue bar represents the deletion region of *ABHD18*, and the green bar indicates the deletion region without any known gene.

mice biochemically resembled human CLN7 patients, showing signs of the accumulation of autofluorescent material in the brain and peripheral tissues (Damme et al., 2014).

NCLs are characterized by decreased cognitive impairment, motor deterioration, progressive visual loss, and uncontrolled seizures (Mole et al., 2005). Our case carried two severe trans-mutations (one frameshift deletion and one whole gene deletion) without ocular abnormalities, which provides more evidence for the genotype-phenotype model in which a combination of a severe and mild variant cause nonsyndromic macular dystrophy with central cone involvement, and two severe mutations cause variant late-infantile neuronal ceroid lipofuscinosis (Roosing et al., 2015).

Autosomal recessive disorders such as CLN7 have been associated with homozygous or compound heterozygous mutations. In our report, no definite diagnosis could be given to the 4-year-old boy with GDD until WES was conducted. Initially, when focusing only on the c.136_137delAT (p. M46Vfs*22), the two-nucleotide deletion was thought to be homozygous, which seemed to fit the recessive inheritance pattern in consanguineous families. However, this conclusion was determined to be incorrect when the deletions were verified by qPCR. This uncommon compound heterozygous mutation composed of one two-nucleotide deletion inherited from the mother and one large mutation inherited from the father reminds us of the important role of WES accompanied by CNV-seq in clinical diagnosis. With the correct explanation for causing CLN7, appropriate medical genetic counseling can be given to this family. Therefore, for patients exhibiting homozygous mutations in *MFSD8*, medical staff should focus on the whole *MFSD8* gene deletion.

In summary, the clinical manifestation of movement disorders in patients with CLN7 has not been fully elucidated. Here, whole *MFSD8* gene deletion has been found to underlie CLN7. The uncommon compound heterozygous *MFSD8* mutations in this family show further heterogeneity of CLN7 at the DNA level. The increasing recognition of different mutations may provide insight into the unknown mechanisms involved in the development of CLN7.

DATA AVAILABILITY STATEMENT

The datasets presented in this study can be found in online repositories. The names of the repository/repositories and accession number(s) can be found in the article/**Supplementary Material**.

ETHICS STATEMENT

Written informed consent was obtained from the individual(s), and minor(s)' legal guardian/next of kin, for the publication of any potentially identifiable images or data included in this article.

AUTHOR CONTRIBUTIONS

QX and QS conceived and designed the study. YG and NL recruited subjects and sorted out clinical information. YQ performed the laboratory work. YQ, YC, and YS performed data and statistical analysis. YQ, YG, and YC drafted the manuscript, QX and QS revised the manuscript critically for important intellectual content. All authors contributed and critically reviewed the final version of the manuscript. All authors have read and approved the final manuscript.

FUNDING

This work was supported by the Shanghai Municipal Commission of Science and Technology Research Project (19JC1411001), the National Natural Science Foundation of China (31972880, 31611130035, 31371274), the National Key Research and Development Plan for Stem Cell and Transformation Research (2017YFA0104202), the collaborative innovation center project construction for Shanghai women and children's health (No. 15GWZK0401).

ACKNOWLEDGMENTS

We thank all participants involved in this study and all authors.

SUPPLEMENTARY MATERIAL

The Supplementary Material for this article can be found online at: https://www.frontiersin.org/articles/10.3389/fgene.2022.807515/full#supplementary-material

REFERENCES

Bélanger, S. A., and Caron, J. (2018). Evaluation of the Child with Global Developmental Delay and Intellectual Disability. *Paediatr. Child. Health* 23 (6), 403–410. doi:10.1093/pch/pxy093

Butz, E. S., Chandrachud, U., Mole, S. E., and Cotman, S. L. (2020). Moving towards a new era of Genomics in the Neuronal Ceroid Lipofuscinoses. *Biochim. Biophys. Acta (Bba) - Mol. Basis Dis.* 1866 (9), 165571. doi:10.1016/j.bbadis.2019.165571

Chartier, S., Boutaud, L., Le Guillou, E., Alby, C., Billon, C., Millischer, A. E., et al. (2021). Prenatal-onset of Congenital Neuronal Ceroid Lipofuscinosis with a Novel CTSD Mutation. *Birth Defects Res.* 113, 1324–1332. doi:10.1002/bdr2.1950

Damme, M., Brandenstein, L., Fehr, S., Jankowiak, W., Bartsch, U., Schweizer, M., et al. (2014). Gene Disruption of Mfsd8 in Mice Provides the First Animal Model for CLN7 Disease. *Neurobiol. Dis.* 65, 12–24. doi:10.1016/j.nbd.2014.01.003

Gao, C., Wang, X., Mei, S., Li, D., Duan, J., Zhang, P., et al. (2019). Diagnostic Yields of Trio-WES Accompanied by CNVseq for Rare Neurodevelopmental Disorders. *Front. Genet.* 10, 485. doi:10.3389/fgene.2019.00485

Goebel, H. H., and Wisniewski, K. E. (2004). Current State of Clinical and Morphological Features in Human NCL. *Brain Pathol.* 14 (1), 61–69. doi:10.1111/j.1750-3639.2004.tb00499.x

Jalanko, A., and Braulke, T. (2009). Neuronal Ceroid Lipofuscinoses. *Biochim. Biophys. Acta (Bba) - Mol. Cel Res.* 1793 (4), 697–709. doi:10.1016/j.bbamcr.2008.11.004

Kohan, R., A. Cismondi, I., M. Oller-Ramirez, A., Guelbert, N., Tapia Anzolini, V., Alonso, G., et al. (2011). Therapeutic Approaches to the challenge of Neuronal Ceroid Lipofuscinoses. *Curr. Pharm. Biotechnol.* 12 (6), 867–883. doi:10.2174/138920111795542633

Kohlschütter, A., Schulz, A., Bartsch, U., and Storch, S. (2019). Current and Emerging Treatment Strategies for Neuronal Ceroid Lipofuscinoses. *CNS Drugs* 33 (4), 315–325. doi:10.1007/s40263-019-00620-8

Kousi, M., Siintola, E., Dvorakova, L., Vlaskova, H., Turnbull, J., Topcu, M., et al. (2009). Mutations in CLN7/MFSD8 Are a Common Cause of Variant Late-Infantile Neuronal Ceroid Lipofuscinosis. *Brain* 132 (Pt 3), 810–819. doi:10.1093/brain/awn366

McBride, J. L., Neuringer, M., Ferguson, B., Kohama, S. G., Tagge, I. J., Zweig, R. C., et al. (2018). Discovery of a CLN7 Model of Batten Disease in Non-human Primates. *Neurobiol. Dis.* 119, 65–78. doi:10.1016/j.nbd.2018.07.013

Mole, S. E., Anderson, G., Band, H. A., Berkovic, S. F., Cooper, J. D., Kleine Holthaus, S.-M., et al. (2019). Clinical Challenges and Future Therapeutic Approaches for Neuronal Ceroid Lipofuscinosis. *Lancet Neurol.* 18 (1), 107–116. doi:10.1016/S1474-4422(18)30368-5

Mole, S. E., Williams, R. E., and Goebel, H. H. (2005). Correlations between Genotype, Ultrastructural Morphology and Clinical Phenotype in the Neuronal Ceroid Lipofuscinoses. *Neurogenetics* 6 (3), 107–126. doi:10.1007/s10048-005-0218-3

Monlong, J., Girard, S. L., Meloche, C., Cadieux-Dion, M., Andrade, D. M., Lafreniere, R. G., et al. (2018). Global Characterization of Copy Number Variants in Epilepsy Patients from Whole Genome Sequencing. *Plos Genet.* 14 (4), e1007285. doi:10.1371/journal.pgen.1007285

Roosing, S., van den Born, L. I., Sangermano, R., Banfi, S., Koenekoop, R. K., Zonneveld-Vrieling, M. N., et al. (2015). Mutations in MFSD8, Encoding a Lysosomal Membrane Protein, Are Associated with Nonsyndromic Autosomal Recessive Macular Dystrophy. *Ophthalmology* 122 (1), 170–179. doi:10.1016/j.ophtha.2014.07.040

Sawyer, S. L., Hartley, T., Dyment, D. A., Beaulieu, C. L., Schwartzentruber, J., Smith, A., et al. (2016). Utility of Whole-exome Sequencing for Those Near the End of the Diagnostic Odyssey: Time to Address Gaps in Care. *Clin. Genet.* 89 (3), 275–284. doi:10.1111/cge.12654

Schulz, A., Kohlschutter, A., Mink, J., Simonati, A., and Williams, R. (2013). NCL Diseases - Clinical Perspectives. *Biochim. Biophys. Acta* 1832 (1), 1801–1806. doi:10.1016/j.bbadis.2013.04.008

Sharifi, A., Kousi, M., Sagné, C., Bellenchi, G. C., Morel, L., Darmon, M., et al. (2010). Expression and Lysosomal Targeting of CLN7, a Major Facilitator Superfamily Transporter Associated with Variant Late-Infantile Neuronal Ceroid Lipofuscinosis. *Hum. Mol. Genet.* 19 (22), 4497–4514. doi:10.1093/hmg/ddq381

Siintola, E., Topcu, M., Aula, N., Lohi, H., Minassian, B. A., Paterson, A. D., et al. (2007). The Novel Neuronal Ceroid Lipofuscinosis Gene MFSD8 Encodes a Putative Lysosomal Transporter. *Am. J. Hum. Genet.* 81 (1), 136–146. doi:10.1086/518902

Specchio, N., Ferretti, A., Trivisano, M., Pietrafusa, N., Pepi, C., Calabrese, C., et al. (2021). Neuronal Ceroid Lipofuscinosis: Potential for Targeted Therapy. *Drugs* 81 (1), 101–123. doi:10.1007/s40265-020-01440-7

Vasudevan, P., and Suri, M. (2017). A Clinical Approach to Developmental Delay and Intellectual Disability. *Clin. Med.* 17 (6), 558–561. doi:10.7861/clinmedicine.17-6-558

Williams, R. E., Aberg, L., Autti, T., Goebel, H. H., Kohlschütter, A., and Lönnqvist, T. (2006). Diagnosis of the Neuronal Ceroid Lipofuscinoses: an Update. *Biochim. Biophys. Acta (Bba) - Mol. Basis Dis.* 1762 (10), 865–872. doi:10.1016/j.bbadis.2006.07.001

Xuan, J., Yu, Y., Qing, T., Guo, L., and Shi, L. (2013). Next-generation Sequencing in the Clinic: Promises and Challenges. *Cancer Lett.* 340 (2), 284–295. doi:10.1016/j.canlet.2012.11.025

Xue, Y., Ankala, A., Wilcox, W. R., and Hegde, M. R. (2015). Solving the Molecular Diagnostic Testing Conundrum for Mendelian Disorders in the Era of Next-Generation Sequencing: Single-Gene, Gene Panel, or Exome/genome Sequencing. *Genet. Med.* 17 (6), 444–451. doi:10.1038/gim.2014.122

Zare-Abdollahi, D., Bushehri, A., Alavi, A., Dehghani, A., Mousavi-Mirkala, M., Effati, J., et al. (2019). MFSD8 Gene Mutations; Evidence for Phenotypic Heterogeneity. *Ophthalmic Genet.* 40 (2), 141–145. doi:10.1080/13816810.2019.1592200

Conflict of Interest: The authors declare that the research was conducted in the absence of any commercial or financial relationships that could be construed as a potential conflict of interest.

frontiers in Pediatrics

BRIEF RESEARCH REPORT
published: 02 February 2022
doi: 10.3389/fped.2022.827802

RNA Analysis and Clinical Characterization of a Novel Splice Variant in the *NSD1* Gene Causing Familial Sotos Syndrome

Olatz Villate[1], *Hiart Maortua*[2,3], *María-Isabel Tejada*[3,4,5] *and Isabel Llano-Rivas*[3]*

[1] *Pediatric Oncology Group, Biocruces Bizkaia Health Research Institute, Barakaldo, Spain,* [2] *Neurodegenerative Diseases Group, Biocruces Bizkaia Health Research Institute, Barakaldo, Spain,* [3] *Genetics Service, Hospital Universitario Cruces-Osakidetza, Barakaldo, Spain,* [4] *Biocruces Bizkaia Health Research Institute, Barakaldo, Spain,* [5] *Spanish Consortium for Research on Rare Diseases (CIBERER), Madrid, Spain*

OPEN ACCESS

Edited by:
Emiliano González Vioque, University Clinical Hospital of Santiago, Spain

Reviewed by:
Gerald Bradley Schaefer, University of Arkansas for Medical Sciences, United States
Laurel Willig, Children's Mercy Hospital, United States
Kenneth Myers, McGill University, Canada

***Correspondence:**
Isabel Llano-Rivas
isabel.llanorivas@osakidetza.eus

Specialty section:
This article was submitted to Genetics of Common and Rare Diseases, a section of the journal Frontiers in Pediatrics

Received: *02 December 2021*
Accepted: *10 January 2022*
Published: *02 February 2022*

Citation:
Villate O, Maortua H, Tejada MI and Llano-Rivas I (2022) RNA Analysis and Clinical Characterization of a Novel Splice Variant in the NSD1 Gene Causing Familial Sotos Syndrome. Front. Pediatr. 10:827802. doi: 10.3389/fped.2022.827802

Background: Sotos syndrome is an autosomal dominant disorder characterized by overgrowth, macrocephaly, distinctive facial features and learning disabilities. Haploinsufficiency of the nuclear receptor SET domain-containing protein 1 (*NSD1*) gene located on chromosome 5q35 is the major cause of the syndrome. This syndrome shares characteristics with other overgrowth syndromes, which can complicate the differential diagnosis.

Methods: Genomic DNA was extracted from peripheral blood samples of members of the same family and targeted exome analysis was performed. *In silico* study of the variant found by next-generation sequencing was used to predict disruption/creation of splice sites and the identification of potential cryptic splice sites. RNA was extracted from peripheral blood samples of patients and functional analyses were performed to confirm the pathogenicity.

Results: We found a novel c.6463 + 5G>A heterozygous *NSD1* gene pathogenic variant in a son and his father. Molecular analyses revealed that part of the intron 22 of *NSD1* is retained due to the destruction of the splicing donor site, causing the appearance of a premature stop codon in the NSD1 protein.

Conclusions: Our findings underline the importance of performing RNA functional assays in order to determine the clinical significance of intronic variants, and contribute to the genetic counseling and clinical management of patients and their relatives. Our work also highlights the relevance of using *in silico* prediction tools to detect a potential alteration in the splicing process.

Keywords: next-generation sequencing, *NSD1*, Sotos syndrome, molecular analysis, RNA, splicing mutation

INTRODUCTION

Sotos syndrome (OMIM #117550) is a rare autosomal dominant disorder characterized by overgrowth (increased height, macrosomia, and macrocephaly), characteristic facial features and learning and intellectual disabilities (1). Other associated clinical features include scoliosis, seizures, renal and cardiac anomalies (2, 3).

Sotos Syndrome is caused by heterozygous pathogenic variants in the nuclear receptor SET domain-containing protein 1 (*NSD1*) gene located on 5q35. *NSD1* encodes a histone methyltransferase that catalyzes the transfer of methyl groups to lysine residues of histone tails (4). The overall prevalence of this syndrome is estimated at 1 in 14,000 (5). More than 95% of the cases arise from *de novo* mutations and familial cases of Sotos syndrome account for about 5% of the diagnoses (6–8).

This syndrome shares characteristics with other overgrowth syndromes, which can complicate the differential diagnosis. The greatest phenotypic overlap is between Sotos and Weaver syndromes (5, 6). The clinical features of post-natal overgrowth, advanced bone age, and intellectual disability particularly in the context of mild facial dysmorphism can make it difficult to distinguish between these syndromes (6).

Targeted exome sequencing has become a powerful and useful method to diagnose patients with suspected overgrowth disorders (9). After performing next generation sequencing (NGS) studies, different novel variants of uncertain significance (VUS) can be detected in the studied patients so it is crucial to characterize their biological impact and determine their pathogenicity. In the case of variants that have been shown by bioinformatics programs to alter the splicing process, functional approaches such as RT-PCR analysis of patient-derived RNA or minigene splicing assays can be used to assess the effect of these variants on mRNA splicing (10, 11). The relevance of reclassification of splice variants classified as VUS lies in the fact that the patient needs to follow precise medical management, in accordance with the international guidelines (12, 13).

In this study, we report one novel intronic *NSD1* variant in two members of the same family. Clinical, familial and molecular data, together with our experimental RNA functional assays, have provided a pathogenicity characterization of the *NSD1* variant.

MATERIALS AND METHODS

Patients

A Spanish boy and his father were recruited. This study was conducted in full accordance with the World Medical Association Declaration of Helsinki (version 2008) and the additional requirements. Informed consent approved by the clinical ethical committee of Cruces University Hospital (Spain) was obtained prior to genetic testing.

Next Generation Sequencing Studies and Sanger Validation

Genomic DNA was extracted from peripheral blood and targeted exome analysis was performed in the Institute of Genomic Medicine (IMEGEN, Valencia, Spain). The analysis of the genes associated with overgrowth syndromes included: *AKT1*, *APC2*, *CDC45*, *CDC6*, *CDKN1C*, *CDT1*, *DICER1*, *DIS3L2*, *DNMT3A*, *EED*, *EZH2*, *FBN1*, *GMNN*, *GPC3*, *GPC4*, *H19*, *HERC1*, *IGF2*, *MCM5*, *MYO5A*, *NFIX*, *NSD1*, *OFD1*, *ORC1*, *ORC4*, *ORC6*, *PIK3CA*, *PTEN*, *RNF135*, *SETD2* and *SUZ12*. For this purpose, the exonic regions of interest were captured using the kit xGen Exome Panel v1.0 (IDT) and pair-end libraries were generated. Ultrasequencing was performed on the NextSeq 500 sequencing system platform (Illumina). Bioinformatics analysis of the data was done using Data Genomics Exon Pipeline software (version v1). Subsequently, the results were interpreted and prioritized. Changes with a number of readings >20 and with a frequency greater than 30% were considered variants. The variants detected were analyzed in four different databases (Exome Aggregation Consortium, 1000 Genomes, Human Gene Mutation Database and Exome Variant Server) and *in silico* prediction programs (SIFT, Polyphen-2, and MutationTaster-2). Conventional Sanger sequencing in genomic DNA validated candidate variant. Primers used were NSD1gF 5′-ACCCATTGCCACGGAAGAAA-3′ and NSD1gR 5′-CAC CGCTGTCCCATTCTTCA-3′.

Splicing *in silico* Analyses

In silico study of the variant found by NGS was used to predict disruption/creation of splice sites and the identification of potential cryptic splice sites. The following online programs were used: NNsplice (http://www.fruitfly.org/seq_tools/splice.html) and Human Splicing Finder (http://www.umd.be/HSF/).

RT-PCR and cDNA Analysis

cDNA was obtained using Superscript RT II enzyme (Invitrogen, Carlsbad, CA, USA) from 500 ng of total RNA extracted from peripheral blood in a volume of 20 μl. cDNA was amplified and sequenced to identify potential splicing variants. Primers used for cDNA amplification and identification of splice variants were: NSD1cF 5′-CCAAAGAATCAACCCATTGC-3′ and NSD1cR 5′-GATTGCTCTGCCAGGTGAGT-3′. Primers for new splice variant sequencing were: NSD1svF 5′-AGCAGGTTGATGCCA AAATC-3′ and NSD1svR 5′-CTCTGCCAGGTGAGTGCTT-3′.

RESULTS

Patients

The proband was a 3-year-old male patient being the second child of a non-consanguineous Spanish couple. He presented with plagiocephaly, asymmetric facies, high palate with decreased posterior palatal movement and uvula slightly deviated to the left. Prominent chin and prominent forehead were also present. Ear pinnae were well implanted. Chest and abdomen did not show alterations and no scoliosis was observed. Size was 111.5 cm (>p99 +3.3 SDS), height 23 kg (p99, +2.3 SDS) and head circumference 54 cm (>p99, +2.5 DS). Full limbs, symmetrical, with large hands and feet and thumbs of the four extremities wide (**Figure 1A**). Smooth skin, no spots, no asymmetric overgrowths and no alterations of subcutaneous tissue were noticed. Psychomotor development considered within normality except for delayed speech, language articulation problems, with

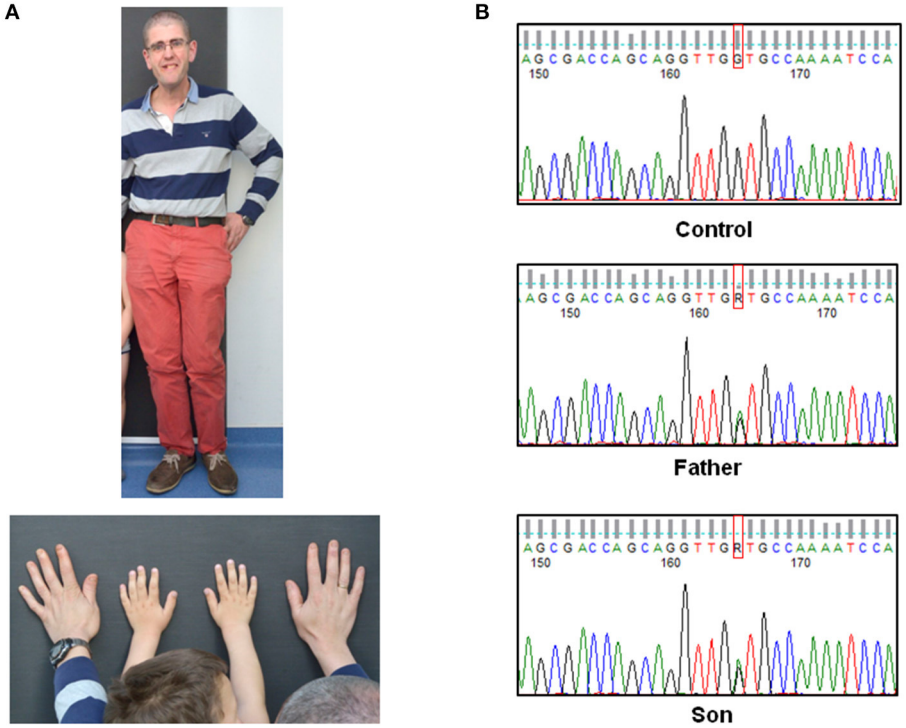

FIGURE 1 | Physical characteristics of the patients and confirmation of the *NSD1* gene variant. **(A)** Photographs of the two patients showing large hands in both of them and macrocephaly, facial asymmetry and tall height in the father. **(B)** Electropherogram of the genomic sequence obtained by Sanger sequencing confirming the *NSD1* variant identified by targeted exome sequencing in the patients. The control did not present the variant.

communicative intention. No seizures. Features were shared with his 43-year-old father presenting with tall stature (184 cm, p84 +1.02 SDS), macrocephaly, facial asymmetry (**Figure 1A**) and velopalatine insufficiency. Intelligence was normal-low and he had no seizures. Paternal grandfather, deceased, seemed to present with macrocephaly and facial features similar to the father.

Targeted Exome Analysis

Father's DNA was used for Next Generation Sequencing studies. In total 94.8% of the region of interest (coding region of the selected genes) was covered at least 20X. A heterozygous change was detected in intron 22 of the *NSD1* gene c.6463 + 5G>A (NM_022455.4). This change was not previously described and it was considered a variant of uncertain significance. In total 100% of the region of interest of the *NSD1* gene was covered with a depth greater than 20X. The coding region of this gene was covered with an average depth of 93.4X. The presence of this variant was validated in the father and his son by Sanger Sequencing (**Figure 1B**) and was not identified in the healthy sister of the proband.

In silico Analyses

The Human Splicing Finder program predicted an alteration of the donor site indicating a probable disruption of splicing in intron 22. The NNsplice program predicted that the score for the donor splice site changes from a high value of 0.80 in the wild type sequence to a low value of 0.23 in the mutated sequence indicating that the donor consensus sequence is weakened. The next donor splice site in the mutated sequence in the intron 22 was predicted to be 120 bp far from the first one indicating that the variant could induce the retention of part of the intron (**Figure 2A**).

Molecular Characterization of the New Variant

To perform the functional studies, RNA samples were obtained from the father, the son and two healthy controls. *NSD1* transcripts were first analyzed by PCR in two controls. Only one band corresponding to the size of the normal transcript was observed and it was confirmed by sequencing (**Figure 2B**). Subsequently, the same study was performed on cDNA obtained from RNA from the father and the son and the results showed two bands, the band corresponding to the normal transcript and an additional one 120 bp longer than the normal one (**Figure 2B**). The two bands obtained in each case were sequenced. Sequencing confirmed that 120 bp of the intron were retained as predicted by *in silico* analysis. The retention of 120 bp has a potential impact on the protein as a premature stop codon is produced and a PHD finger and a C5HCH domain are affected in the mutated protein (**Figure 3**). This alteration confirms the pathogenicity of the variant.

DISCUSSION

In this study, we have combined molecular, clinical and functional analysis of two patients of the same family suspected of having an overgrowth syndrome. Our main aim was to contribute to the molecular and clinical classification of the variant of uncertain significance detected in *NSD1*.

The variant found in *NSD1* by targeted exome sequencing was mapped in the position +5 of the intron 22. It is well known that the GT dinucleotide at the 5′ end of an intron (positions + 1 and + 2) is highly conserved in human genes (> 98%) and critical for RNA splicing (14). These alterations are nearly systematically classified as pathogenic or probably pathogenic. In the position +5 of the 5′ splice sites the guanine is the most frequently nucleotide found, reaching 78% conservation among over 180,000 human 5′ splice sites (14) and it has been shown that disease-associated alterations are very often detected at this nucleotide (15). The variants at this position are usually classified as VUS so functional studies are required to determine their pathogenicity. Our results support the relevant role of intronic position + 5 in normal splicing and agree with previous studies showing that this position seems particularly prone to aberrant splicing when altered (10, 16). Moreover, we observed a good concordance between *in silico* programs used to predict splicing alterations and the results of the molecular assays for this variant located at the + 5 position.

To identify more disease causing variants in overgrowth syndromes there is a need to extend the studies to intronic variants. Due to the size of intronic regions, identifying deep intronic variants that affect splicing is challenging. The recent applications of whole-genome sequencing (WGS) to clinical screening studies enable the investigation of non-coding variation and identification of pathogenic deep intronic variants that lie >100 bp away from the nearest canonical splice sites (17).

In the Human Gene Mutation Database Professional 2020.4, 564 mutations have been reported in *NSD1*, 461 of them associated to Sotos Syndrome. The c.6463 + 5G>A variant is not reported in HGMD and our patients are the first ones described with this change. It is worthy to note that 24 splice variants are described as responsible for Sotos Syndrome phenotype and only one of them is mapped in position +5 of the splice site (18). This could suggest that functional studies are not being performed on variants at positions other than +1 and +2, which are necessary to confirm the diagnosis and provide correct genetic counseling. Of the 24 splice variants described in HGMD, 21 of them affect positions +1, +2, −1 and −2. The Human Splicing Finder program predicts in these variants an alteration of the donor or acceptor site depending on the position, indicating that most probably

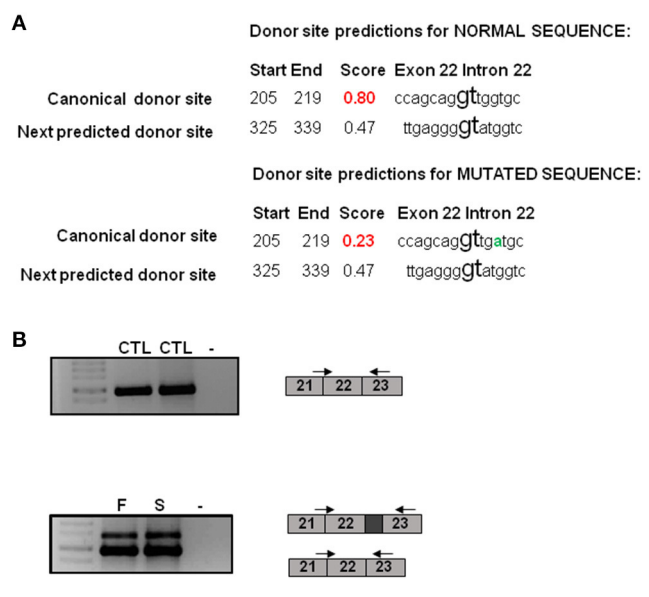

FIGURE 2 | Molecular characterization of the *NSD1* variant. **(A)** Bioinformatics analysis of the c.6463 + 5G>A variant. NNsplice program predicts that the score for the donor splice site changes from a high value of 0.80 in the wild type sequence to a low value of 0.23 in the mutated sequence. The next donor splice site in the mutated sequence in the intron 22 is predicted to be 120 bp far from the first one. The variant change is represented in green. **(B)** RT-PCR analysis reveals an additional band in the father and the son in comparison to controls. This band is 120 bp longer than the other one. CTL, control; F, father; S, son.

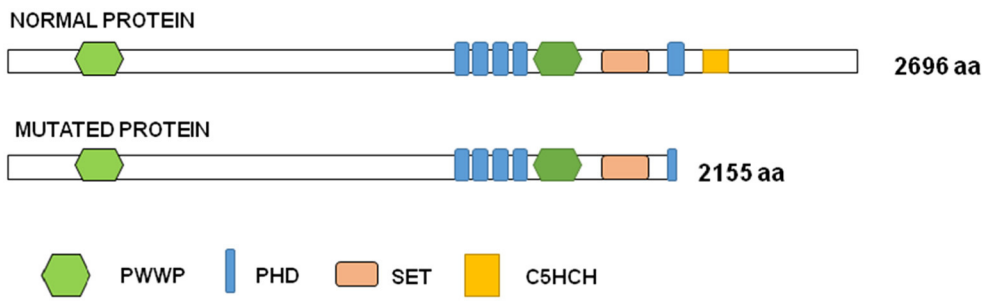

FIGURE 3 | Graph representation of NSD1 protein. Functional domains are represented in colors in the normal and in the mutated proteins: PWWP (proline-tryptophan-proline-tryptophan) is represented in green, PHD (plant homeodomain finger) in blue, SET (SU[VAR]3–9,E[Z], trithorax) in orange and C5HCH (Cys-His-rich domain) in yellow.

affect the splicing process. The variant previously described at position +5, c.4378 + 5G>C, according to bioinformatics analysis causes an alteration of the wild type donor site, most probably affecting splicing. There is also a splice variant described at position −5, c.6152-5T>G, and it is predicted to alter the wild type acceptor site, most probably affecting splicing. The last variant described that is not in the canonical positions is found at position +33, c.3796 + 33A>T, and in this case, the Human Splicing Finder prediction considers no significant impact on splicing signals. The NSD family members, consisting of NSD1, NSD2 and NSD3 are methyltransferases implicated in multiple diseases (19). We have shown that the variant found in *NSD1* has a potential impact on the protein causing a shortening and affecting C5HCH and PHD finger domains due to the appearance of a premature stop codon. NSD1 binds upstream of the bone morphogenetic protein 4 promoter, enforces H3K36 methylation levels within this region, and thus promotes bone morphogenetic protein 4 transcription (20). It has been shown that the PHD5-C5HCH domains of the NSD1 protein might have chromatin targeting ability and that Sotos syndrome mutations within these domains seem to alter the normal function of NSD1 (19). This would confirm the pathogenicity of the variant present in the two patients.

CONCLUSIONS

Our findings underline the importance of performing RNA splicing assays in order to determine the clinical significance of intronic variants, and contribute to the genetic counseling and clinical management of patients and their relatives. Our work also contributes to highlight the relevance of using *in silico* prediction tools to detect a potential alteration in the splicing process.

DATA AVAILABILITY STATEMENT

The original contributions presented in the study are included in the article/supplementary materials, further inquiries can be directed to the corresponding author/s.

ETHICS STATEMENT

The studies involving human participants were reviewed and approved by Clinical Ethical Committee of Cruces University Hospital (Spain). Written informed consent to participate in this study was provided by the participants' legal guardian/next of kin. Written informed consent was obtained from the individual(s), and minor(s)' legal guardian/next of kin, for the publication of any potentially identifiable images or data included in this article.

AUTHOR CONTRIBUTIONS

OV and HM performed the bioinformatics and molecular analyses. M-IT directed the project granted and reviewed the manuscript. IL-R carried out the clinical characterization of patients. OV and IL-R conceived the study, supervised it, and wrote the manuscript. All authors have read and approved the final manuscript.

FUNDING

This work was supported by grant CIBERER17-TRASL7-02 from CIBERER (Spanish Consortium for Research on Rare Diseases).

ACKNOWLEDGMENTS

We would like to thank the family for their cooperation and for consenting to the publication of this manuscript.

REFERENCES

1. Sotos JF, Dodge PR, Muirhead D, Crawford JD, Talbot NB. Cerebral gigantism in childhood: a syndrome of excessively rapid growth with acromegalic features and a nonprogressive neurologic disorder. *N Engl J Med.* (1964) 271:109–16. doi: 10.1056/NEJM196407162710301
2. Foster A, Zachariou A, Loveday C, Ashraf T, Blair E, Clayton-Smith J, et al. The phenotype of Sotos syndrome in adulthood: a review of 44 individuals. *Am J Med Genet.* (2019) 181:502–8. doi: 10.1002/ajmg.c.31738
3. Tatton-Brown K, Douglas J, Coleman K, Baujat G, Cole TRP, Das S, et al. Genotype-phenotype associations in sotos syndrome: an analysis of 266 individuals with NSD1 aberrations. *Am J Med Genet.* (2005) 77:193–204. doi: 10.1086/432082
4. Rayasam GV. NSD1 is essential for early post-implantation development and has a catalytically active SET domain. *EMBO J.* (2003) 22:3153–63. doi: 10.1093/emboj/cdg288
5. Tatton-Brown K, Rahman N. Sotos syndrome. *Eur J Hum Genet.* (2007) 15:264–71. doi: 10.1038/sj.ejhg.5201686
6. Manor J, Lalani SR. Overgrowth syndromes—evaluation, diagnosis, and management. *Front Pediatr.* (2020) 8:574857. doi: 10.3389/fped.2020.574857
7. Waggoner DJ, Raca G, Welch K, Dempsey M, Anderes E, Ostrovnaya I, et al. NSD1 analysis for Sotos syndrome: Insights and perspectives from the clinical laboratory. *Genet Med.* (2005) 7:524–33. doi: 10.1097/01.GIM.0000178503.15559.d3
8. Laccetta G, Moscuzza F, Michelucci A, Guzzetta A, Lunardi S, Lorenzoni F, et al. Novel missense mutation of the NSD1 gene associated with overgrowth in three generations of an italian family: case report, differential diagnosis, and review of mutations of NSD1 gene in familial sotos syndrome. *Front Pediatr.* (2017) 5:236. doi: 10.3389/fped.2017.00236
9. Kim Y-M, Lee Y-J, Park JH, Lee H-D, Cheon CK, Kim S-Y, et al. High diagnostic yield of clinically unidentifiable syndromic growth disorders by targeted exome sequencing. *Clin Genet.* (2017) 92:594–605. doi: 10.1111/cge.13038
10. Piñero TA, Soukarieh O, Rolain M, Alvarez K, López-Köstner F, Torrezan GT, et al. MLH1 intronic variants mapping to + 5 position of splice donor sites lead to deleterious effects on RNA splicing. *Fam Cancer.* (2020) 19:323–36. doi: 10.1007/s10689-020-00182-5
11. Villate O, Ibarluzea N, Fraile-Bethencourt E, Valenzuela A, Velasco EA, Grozeva D, et al. Functional analyses of a novel splice variant in the CHD7 gene, found by next generation sequencing, confirm its pathogenicity in a Spanish patient and diagnose him with CHARGE syndrome. *Front Genet.* (2018) 9:7. doi: 10.3389/fgene.2018.00007
12. Agiannitopoulos K, Pepe G, Papadopoulou E, Tsaousis GN, Kampouri S, Maravelaki S, et al. Clinical utility of functional RNA analysis for the reclassification of splicing gene variants in hereditary cancer. *Cancer Genomics Proteomics.* (2021) 18:285–94. doi: 10.21873/cgp.20259
13. Truty R, Ouyang K, Rojahn S, Garcia S, Colavin A, Hamlington B, et al. Spectrum of splicing variants in disease genes and the ability of RNA analysis

to reduce uncertainty in clinical interpretation. *Am J Med Genet.* (2021) 108:696–708. doi: 10.1016/j.ajhg.2021.03.006
14. Sahashi K, Masuda A, Matsuura T, Shinmi J, Zhang Z, Takeshima Y, et al. *In vitro* and *in silico* analysis reveals an efficient algorithm to predict the splicing consequences of mutations at the 5′ splice sites. *Nucleic Acids Res.* (2007) 35:5995–6003. doi: 10.1093/nar/gkm647
15. Krawczak M, Thomas NST, Hundrieser B, Mort M, Wittig M, Hampe J, et al. Single base-pair substitutions in exon-intron junctions of human genes: nature, distribution, and consequences for mRNA splicing. *Hum Mutat.* (2007) 28:150–8. doi: 10.1002/humu.20400
16. Buratti E, Chivers M, Královičová J, Romano M, Baralle M, Krainer AR, et al. Aberrant 5′ splice sites in human disease genes: mutation pattern, nucleotide structure and comparison of computational tools that predict their utilization. *Nucleic Acids Res.* (2007) 35:4250–63. doi: 10.1093/nar/gkm402
17. Qian X, Wang J, Wang M, Igelman AD, Jones KD Li Y, Wang K, et al. Identification of deep-intronic splice mutations in a large cohort of patients with inherited retinal diseases. *Front Genet.* (2021) 12:647400. doi: 10.3389/fgene.2021.647400
18. Stenson PD, Mort M, Ball EV, Evans K, Hayden M, Heywood S, et al. The Human Gene Mutation Database: towards a comprehensive repository of inherited mutation data for medical research, genetic diagnosis and next-generation sequencing studies. *Hum Genet.* (2017) 136:665–77. doi: 10.1007/s00439-017-1779-6
19. He C, Li F, Zhang J, Wu J, Shi Y. The methyltransferase NSD3 has chromatin-binding motifs, PHD5-C5HCH, that are distinct from other NSD (Nuclear Receptor SET Domain) family members in their histone H3 recognition. *J Biol Chem.* (2013) 288:4692–703. doi: 10.1074/jbc.M112.426148
20. Lucio-Eterovic AK, Singh MM, Gardner JE, Veerappan CS, Rice JC, Carpenter PB. Role for the nuclear receptor-binding SET domain protein 1 (NSD1) methyltransferase in coordinating lysine 36 methylation at histone 3 with RNA polymerase II function. *Proc Natl Acad Sci U S A.* (2010) 107:16952–7. doi: 10.1073/pnas.1002653107

Conflict of Interest: The authors declare that the research was conducted in the absence of any commercial or financial relationships that could be construed as a potential conflict of interest.

Publisher's Note: All claims expressed in this article are solely those of the authors and do not necessarily represent those of their affiliated organizations, or those of the publisher, the editors and the reviewers. Any product that may be evaluated in this article, or claim that may be made by its manufacturer, is not guaranteed or endorsed by the publisher.

frontiers in Genetics

CASE REPORT
published: 22 February 2022
doi: 10.3389/fgene.2022.743472

Case Report: Two New Cases of Autosomal-Recessive Hypertrophic Cardiomyopathy Associated With *TRIM63*-Compound Heterozygous Variant

*Sofiya Andreeva[1†], Olga Chumakova[2†], Elena Karelkina[3], Viktoriya Lebedeva[3], Tamara Lubimtseva[3], Andrey Semenov[3], Alexey Nikitin[4], Gleb Speshilov[5], Alexandra Kozyreva[1], Polina Sokolnikova[1], Sergey Zhuk[1], Yuliya Fomicheva[1], Olga Moiseeva[3] and Anna Kostareva[1,6]**

[1]Institute of Molecular Biology and Genetics and World-Class Research Centre for Personalized Medicine, Almazov National Medical Research Centre, Saint Petersburg, Russia, [2]Central State Medical Academy of Department of Presidential Affairs, City Clinical Hospital #17, Moscow, Russia, [3]Institute of Heart and Vessels, Almazov National Medical Research Centre, Saint Petersburg, Russia, [4]Pulmonology Research Institute, Federal Medical-Biological Agency of Russia, Moscow, Russia, [5]Laboratory of Genotyping, N. F. Gamaleya National Research Center, Moscow, Russia, [6]Department of Women's and Children's Health and Center for Molecular Medicine, Karolinska Institute, Solna, Sweden

Hypertrophic cardiomyopathy (HCM) is one of the most common hereditary diseases, and it is associated with fatal complications. The clinical heterogeneity of HCM requires risk prediction models to identify patients at a high risk of adverse events. Most HCM cases are caused by mutations in genes encoding sarcomere proteins. However, HCM is associated with rare genetic variants with limited data about its clinical course and prognosis, and existing risk prediction models are not validated for such patients' cohorts. *TRIM63* is one of the rare genes recently described as a cause of HCM with autosomal-recessive inheritance. Herein, we present two cases of HCM associated with *TRIM63*-compound heterozygous variants in young male sportsmen. They demonstrated progressively marked hypertrophy, advanced diastolic dysfunction, a significant degree of fibrosis detected by magnetic resonance imaging, and clear indications for implantable cardioverter-defibrillator. One of the cases includes the first description of *TRIM63*-HCM with extreme hypertrophy. The presented cases are discussed in light of molecular consequences that might underlie cardiac and muscle phenotype in patients with mutations of *TRIM63*, the master regulator of striated muscle mass.

Keywords: hypertrophic cardiomyopathy, *TRIM63*, MuRF1, compound heterozygote, extreme hypertrophy, diastolic dysfunction

OPEN ACCESS

Edited by:
María L. Couce, Complejo Hospitalario Universitario de Santiago, Spain

Reviewed by:
James William McNamara, Royal Children's Hospital, Australia
Andreas Perrot, Charité Universitätsmedizin Berlin, Germany

****Correspondence:***
Anna Kostareva
anna.kostareva@ki.se

†These authors have contributed equally to this work and share first authorship

Specialty section:
This article was submitted to Genetics of Common and Rare Diseases, a section of the journal Frontiers in Genetics

Received: *18 July 2021*
Accepted: *14 January 2022*
Published: *22 February 2022*

Citation:
Andreeva S, Chumakova O, Karelkina E, Lebedeva V, Lubimtseva T, Semenov A, Nikitin A, Speshilov G, Kozyreva A, Sokolnikova P, Zhuk S, Fomicheva Y, Moiseeva O and Kostareva A (2022) Case Report: Two New Cases of Autosomal-Recessive Hypertrophic Cardiomyopathy Associated With TRIM63-Compound Heterozygous Variant. Front. Genet. 13:743472. doi: 10.3389/fgene.2022.743472

INTRODUCTION

Hypertrophic cardiomyopathy (HCM) is the most common cardiovascular hereditary disease, and it is characterized by cardiac hypertrophy that cannot be explained solely by abnormal loading conditions (Ommen et al., 2020). The history of genetic research in HCM goes back to 3 decades, and up to date, over 450 causative mutations in at least 20 genes encoding for sarcomeric and myofilament-related proteins have been described (Geisterfer-Lowrance et al., 1990; Wolf, 2019).

Mutations in *MYBPC3* and *MYH7* are the most frequent genetic cause of HCM and attributed to more than 50% of all HCM cases. Other HCM causal mutations have been identified in TNNT2, TNNI3, and genes encoding for structural proteins (Sabater-Molina et al., 2018; Teekakirikul et al., 2019). However, in 30–40% of the cases, the origin of the disease still remains unclear despite extensive genetic testing using targeted gene panels (Wolf, 2019; Salazar-Mendiguchía et al., 2020). In the case of HCM associated with rare causative genes, the existing risk prediction models may not be accurate enough because they have not been validated for this particular population. Therefore, collecting clinical and genetic data of patient groups with the rare genetic background of HCM may facilitate the development of more accurate and personalized risk stratification algorithms.

TRIM63 (tripartite motif 63) is a gene only recently described in association with HCM (Chen et al., 2012; Salazar-Mendiguchía et al., 2020). *TRIM63* encodes muscle-specific RING-finger protein 1 (MuRF1), a member of ubiquitin ligases subfamily, such as MuRF-2 and MuRF-3.

In skeletal myocytes, upregulation of MuRF1 underlies a broad spectrum of muscle atrophy conditions (Peris-Moreno et al., 2020). In cardiac myocytes, overexpression of MuRF1 enhances susceptibility to heart failure in response to pressure overload, and its activation prevents cardiac hypertrophy (Arya et al., 2004; Willis et al., 2009). MuRF1 targets include sarcomere contractile, structural proteins, and signaling molecules (Witt et al., 2005; Polge et al., 2011; Chen et al., 2012; Maejima et al., 2014; Polge et al., 2018; Higashikuse et al., 2019; Bulatov et al., 2018). The involvement of *TRIM63* in various pathological processes has been documented in several experimental and functional studies (Chen et al., 2012; Su et al., 2014; Olivé et al., 2015; Salazar-Mendiguchía et al., 2020).

The original study of Chen et al. revealed three *TRIM63* variants in five unrelated probands among 302 probands with HCM. Additionally, they identified two loss of function variants (p.Ala48Val and p.Ile130Met) and one protein-truncation variant (p.Gln247*) detected in the heterozygous state. Experimental cellular and animal studies demonstrated the reduced colocalization of MuRF1 with alfa-actinin at the Z-disk level, impaired auto-ubiquitination, and depressed ubiquitination and proteasome degradation of substrates (Chen et al., 2012).

Later, the role of p.Gln247* as a single causative variant leading to HCM was challenged due to its relatively frequent detection in healthy European subjects and observation of its clinical phenotype only in the cases of compound heterozygosity or homozygous variants (Płoski et al., 2014). Su et al. found rare variants in MuRF1 and MuRF2 encoding genes in the healthy population but with a much lower frequency than in HCM. Moreover, carriers of these variants had greater maximum left ventricular wall thickness than non-carriers. Hence, rare variants in MuRF1 and MuRF2 encoding genes were associated with higher penetrance and more severe clinical manifestations of HCM, especially when coincided with other sarcomeric mutations, therefore being considered by the authors as modifiers in HCM. It is important to note that all detected rare variants were heterozygous (Su et al., 2014).

The final clarification of the *TRIM63* inheritance pattern became possible after studying 4,867 index cases with HCM (Salazar-Mendiguchía et al., 2020). *TRIM63* sequencing and subsequent familial evaluation revealed that only homozygous

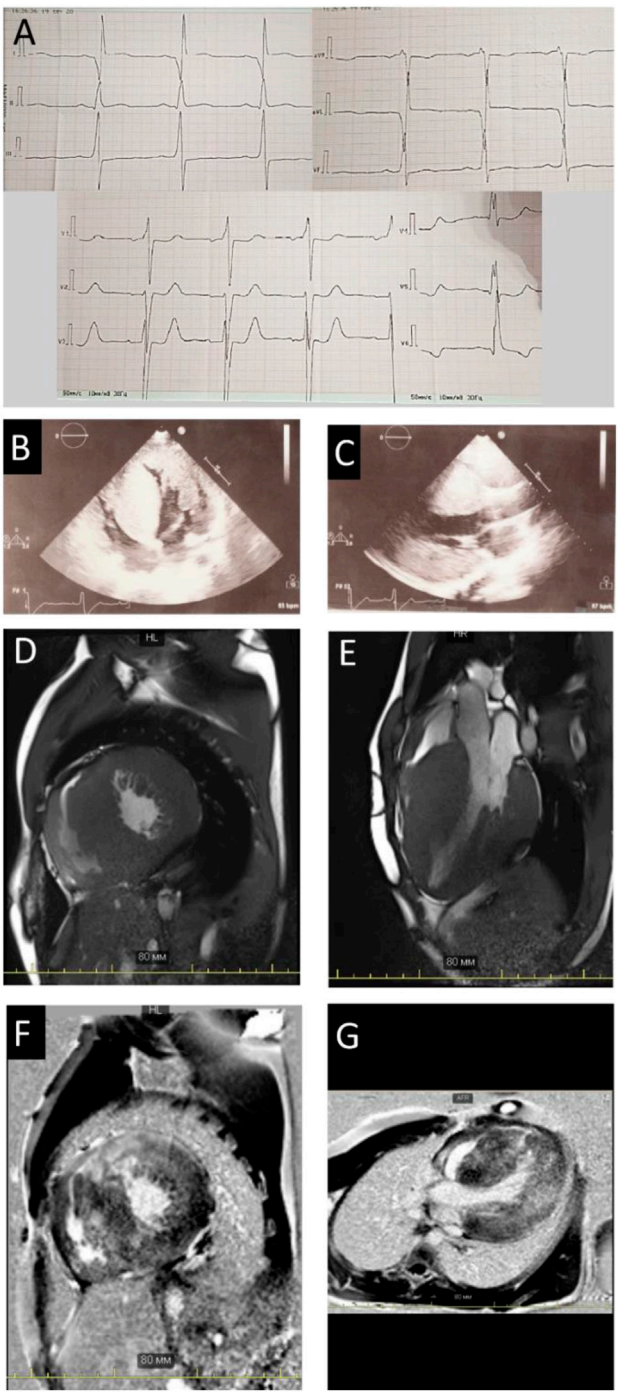

FIGURE 1 | Instrumental findings in Patient 1. Electrocardiogram **(A)** and echocardiography picture correspondence to four-chamber **(B)** view and long-axis view **(C)** illustrated severe hypertrophy. Cardiac MRI images in the short **(D)** and long **(E)** axes, demonstrating wall hypertrophy, limited cavity volume, and late gadolinium enhancement **(F,G)**.

TABLE 1 | Dynamics of echocardiography data in Patient 1.

Parameter/age of examination	19 years old	23 years old	25 years old
LA, mm	46	50	48
LA volume, ml	68	60	126
LA volume index, ml/m^2	30	26	43
RA, mm	44*46	40*45	44*52
Septum, mm	48	50	50
PW, mm	18	37	45
RWT	0.76	1.54	2.0
LV mass, g	1,129	2017	2,900
LV mass index, g/m^2	495	878	988
LV EDD, mm	47	48	48
LV ESD, mm	31	29	27
LV EDV, ml	120	151	105
LV ESV, ml	42	63	28
SV, ml	78	88	77
EDVi, ml/m^2	52.6	65.7	35.7
ESVi, ml/m^2	18.4	27.4	9.5
RV WT, mm	9	11	11
RV, mm	28	29	42
EF, % (Simpson)	65	58	70
GL strain, %	—	-	-
TAPSE, cm	>1.6	2.2	>1.6
ePASP, mmHg	18–23	ND	35
Diastolic dysfunction, type	III	II	II
E/A ratio	2.02	1.7	1.82
LVOT PGmax, mmHg	10.68 at rest. Without increase after Valsalva maneuver	84 at rest	37 at rest during sinus rhythm, 97 during extrasystole
RVOT PGmax, mmHg	—	39	—
Mitral regurgitation	—	Mild	Mild
SAM of the MV	—	+	-

EDV, end-diastolic volume; EDVi, end-diastolic volume index; EF, left ventricle ejection fraction; ESVi, end-systolic volume index; ePASP, estimated pulmonary artery systolic pressure; GL strain, global longitudinal strain; LA, left atrium; LV EDD, left ventricle end-diastolic dimension; LV EDV, left ventricle end-diastolic volume; LV ESD, left ventricle end-systolic dimension; LV ESV, left ventricle end-systolic volume; LVOT PGmax, left ventricle outflow tract maximum pressure gradient; PW, posterior wall; RA, right atrium; RV, right ventricle; RVOT PGmax, right ventricle outflow tract maximum pressure gradient; RV WT, right ventricle wall thickness; RWT, relative wall thickness; SAM of the MV, the systolic anterior motion of the mitral valve; SV, stroke volume; TAPSE, tricuspid annular plane systolic dysfunction.

and compound heterozygous carriers developed full clinical phenotype of the disease (15 patients with HCM and one with restrictive cardiomyopathy), while heterozygous individuals demonstrated mild or almost no phenotype. These data strongly support the hypothesis that *TRIM63* causes HCM with autosomal-recessive inheritance (Salazar-Mendiguchía et al., 2020).

Herein, we present two cases of *TRIM63*-associated HCM due to compound heterozygous mutations along with results of a 5-year follow-up.

CASE DESCRIPTION

Patient 1

A nineteen-year-old male patient was hospitalized due to ECG and echocardiography abnormalities detected during scheduled examination for military enlistment. The patient denied any chest pain, dyspnea, palpitations, headache, dizziness, or syncope. His medical history was notable for hypertension (maximum blood pressure of 140/90 mmHg), without antihypertensive therapy. His exercise tolerance was high, and he had been performing weightlifting for several years. The patient had normal childhood development and demonstrated normal intelligence. He denied smoking and alcohol abuse and did not have a family history of sudden cardiac death (SCD) or early cardiovascular diseases. Physical examination revealed increased body mass index—25 kg/m^2 and prominent hypertrophy of upper limb muscles. ECG and Holter monitoring demonstrated sinus rhythm, signs of biventricular hyperthrophy (Cornell voltage criteria is about 50 mm, R wave in ^{1}V 10 mm), and prolonged QT interval (QTc up to 563 ms on Holter) (**Figure 1A**). Echocardiography showed extreme asymmetric left ventricular (LV) concentric hypertrophy with a predominant increase of interventricular septum (up to 48 mm) without left ventricle outflow tract obstruction (LVOT), right ventricle (RV) hypertrophy, mild left atrium dilatation, and restrictive type of diastolic dysfunction without signs of pulmonary hypertension (**Table 1**; **Figures 1B,C**).

Stress-echocardiography excluded dynamic obstruction of LVOT (maximum pressure gradient 19 mmHg upon exertion). According to the European model "HCM Risk-SCD Calculator," the 5-year risk of SCD was estimated as 3.6%. Therefore, an implantable cardioverter-defibrillator (ICD) implantation was not indicated, and the patient was discharged on metoprolol succinate (25 mg daily). Two years later, he noticed brief episodes of palpitations

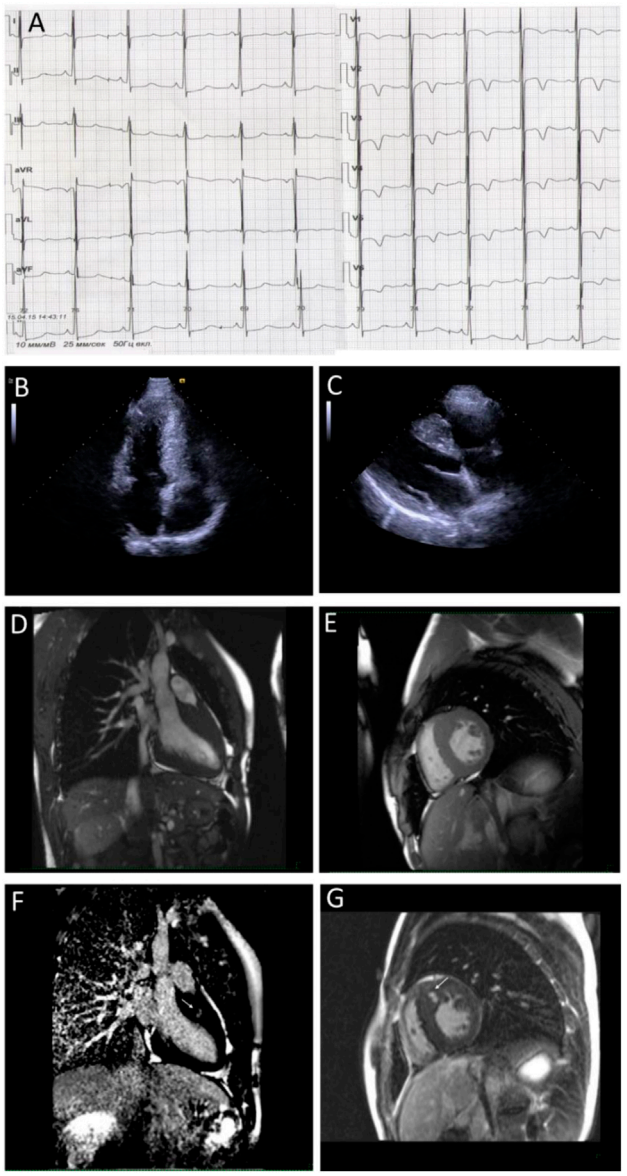

FIGURE 2 | Instrumental findings of Patient 2. Electrocardiogram demonstrates voltage criteria of left ventricle hypertrophy and secondary repolarization changes **(A)**. Echocardiogram correspondence to four-chamber **(B)** and long-axis view **(C)** and MRI images in the long **(D)** and short-axis view **(E)** confirm wall hypertrophy. Arrows indicate the late gadolinium enhancement phenomenon **(F,G)** in the basal anteroseptal segment.

resulting in clinical re-evaluation at the age of 23. Echocardiography documented an increase in LV and RV wall thickness (up to 50 and 11 mm, resp.), mitral valve systolic anterior motion, and LVOT and RV outflow tract obstruction at rest (**Table 1**; **Figure 1** B,C). According to magnetic resonance imaging (MRI), circularly intramurally late gadolinium enhancement (LGE) was documented (**Figures 1D–G**; **Supplementary Table S1**). Re-evaluation of the 5-year risk of SCD resulted in a 4.94% probability, a dual-chamber ICD was implanted, and metoprolol therapy was continued.

During the next 2 years, a progressive increase in myocardial mass, predominantly due to posterior wall thickness, was observed (**Table 1**). Holter monitoring demonstrated multiple single and paired polymorphic ventricular extrasystoles and episodes of non-sustained polymorphic ventricular tachycardia but no appropriate ICD discharges.

To uncover the molecular background of the disease, targeted genetic testing was performed using a SureSelect panel of 108 cardiomyopathy-associated genes for Patient 1 (**Supplementary Table S2**), and no disease-related variants were detected. A subsequent whole-exome sequencing for Patient 1 was performed as described previously using a SureSelect Human All Exon V6 r2 (60 Mbp) target enrichment kit (Agilent Technologies, Santa Clara, CA, United States) with an Illumina HiSeq instrument and SBSv4 chemistry (Vershinina et al., 2020). Data curation, alignment strategy, variant calling, and filtering were performed according to GATK BestPractice recommendation using hg19 reference and annotated with ANNOVAR as previously published (Jorholt et al., 2020). Raw sequencing data are deposited at the SRA database under the reference number SRR16609854. Data interpretation was performed according to the guidelines of the American College of Medical Genetics (ACMG) (Richards et al., 2015). This resulted in the detection of two variants in the TRIM63 gene (NM_032588: c.T115G:p.C39G and NM_032588:c.481_482del: p.S161CfsTer8) in compound heterozygous form (**Figure 3A**; **Table 2**). The first variant, C39G, is newly described, absent in all available databases, and currently, according to ACMG, classified as a variant of unknown significance. A second variant, S161CfsTer8, has been described in a patient with HCM, reported in the GnomAD database (rs540072010), while being classified as a variant of unknown significance according to ACMG has been reported in ClinVar as pathogenic. No pathogenic or likely pathogenic variants or variants of unknown significance were detected in the genes causing storage diseases. Unfortunately, the parental DNA was not available for the analysis due to the parental refusal to participate in genetic analysis and *de novo*/inherited status of the variants remained unknown (**Figure 3B**).

Patient 2

A fifteen-year-old male, a professional soccer player, was examined due to the first syncope that occurred during a sports activity. Conventional ECG revealed ST-segment elevation and T wave inversions up to 6 mm in all precordial, I, and aVL limb leads; signs of severe LV hypertrophy (Sokolow–Lyon index was 66 mm); and borderline QTc interval (480 msec) (**Figure 2A**). Echocardiography demonstrated asymmetric LV hypertrophy with a maximal wall thickness of 16 mm in basal and middle anteroseptal segments without LVOT obstruction at rest and after the exercise stress test (**Figures 2B,C**). The cardiac MRI using gadolinium enhancement demonstrated fibrosis, but Holter monitoring did not reveal ventricular arrhythmia or conduction abnormalities (**Figures 2D–G**). His body mass index and physical and intellectual development were normal, and no signs of peripheral

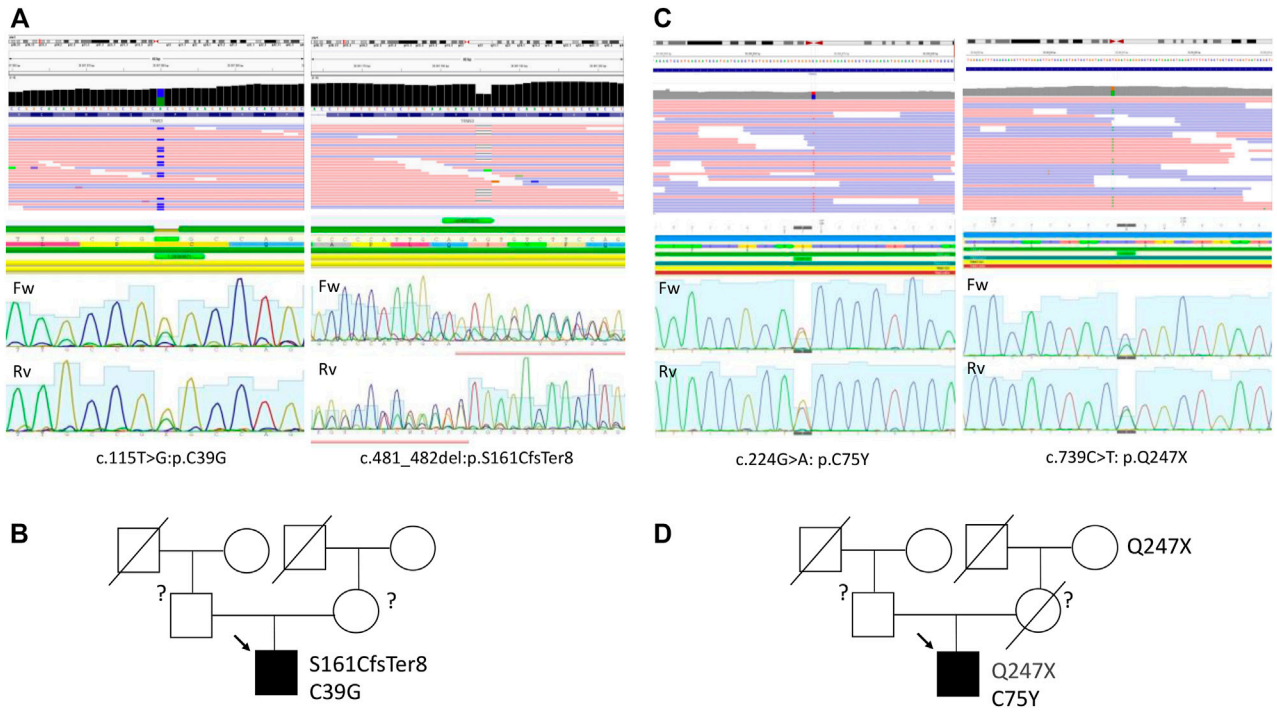

FIGURE 3 | Sequencing data and pedigree of Patient 1 **(A,B)** and Patient 2 **(C,D)**.

TABLE 2 | Genetic variants in *TRIM63* gene of Patient 1 and Patient 2.

Patient	Pathogenicity		Gene	Position GRCh37 and nomenclature	rs	MAF,%
	ACMG	ClinVar				
1	VUS	—	*TRIM63*	Chr1: 26393871:A>C NM_032588: c.T115G:p.C39G	—	—
	VUS	Pathogenic	*TRIM63*	Chr1: 26387675:ACT>A NM_032588:c.481_482del:p.S161CfsTer8	rs540072010	0.004
2	VUS	Likely pathogenic	*TRIM63*	Chr1: 26384973G>A NM_032588: c.739C>T: p.Q247X	rs14839503	0.07
	VUS	—	*TRIM63*	Chr1: 26392867C>T NM_032588: c.224G>A: p.C75Y	rs200811483	0.01

ACMG, American College of Medical Genetics; MAF, minor allele frequency; VUS, variant of unknown significance.

myopathy were noted. The family history was free from SCD episodes, and parental ECG and echocardiography were normal. Over the next 9 years, the patient has been involved in active sport despite restrictive recommendations and remained asymptomatic. Echocardiography detected the progressive increase in septal and anterior wall thickness without LVOT obstruction and decreased LV cavity, and the appearance of LV diastolic dysfunction with mild enlargement of the left atrium was observed (**Table 3**). According to the ESC calculator, the estimated 5-year risk of SCD was high (7.8%) despite unremarkable Holter monitoring, but the patient refused the ICD implantation and remained only on metoprolol therapy.

A targeted sequencing using 176 cardiomyopathy-associate gene panel (**Supplementary Table S3**) resulted in the detection of two variants in the TRIM63 gene (NM_032588: c.739C>T: p.Q247X and NM_032588: c.224G>A: p.C75Y) in compound heterozygous form (**Table 2**; **Figure 3C**), and raw sequencing data are deposited at SRA database under the reference number SRR16946091. Both variants are present in GnomAD, have been previously reported in association with HCM in compound heterozygous form, and, according to ACMG, are classified as a variant of unknown significance. Similar to the previous case, no potentially causative variants were detected in the genes causing storage diseases. The parental DNA was not available for the analysis as the contact to the patient's parents was lost and he was brought up solely by his maternal grandmother. However, the Q247X variant was confirmed to be present in the maternal grandmother with no clinical and echocardiography signs of HCM (**Figure 3D**).

DISCUSSION AND CONCLUSION

The presented cases describe the clinical phenotype of *TRIM63*-associated HCM and extend our knowledge on rare genetic forms of one of the most common inherited human disorders. While HCM remains the most common genetically predicted cardiovascular disease, the vast majority of the cases are linked to the variants in eight sarcomeric genes (*MYBPC3*, *MYH7*, *ACTC*, *TTNI3*, *TTNT2*, *TPM1*, *MYL2*, and *MYL3*) with a clear predominance of *MYH7* and *MYBPC3* variants. Therefore, most clinical algorithms and guidelines are developed using these cohorts of patients (Ho et al., 2018; Lorenzini et al., 2020). Rare genetic forms of HCM account for only 1–2% of the cases (Lopes and Elliott, 2014). However, despite the small number of patients with rare variants, their total number makes up almost one-third of all patients with sarcomeric mutations (Ingles et al., 2019). Currently, it is not clear to what extent the common guidelines and recommendations are valid for these rare genetic groups of HCM. It is generally accepted that HCM associated with sarcomere gene mutations has a worse prognosis than non-sarcomeric forms of the disease (Ho et al., 2018; Marstrand et al., 2020). However, several exceptions exist, such as HCM, associated with *PRKAG2* gene mutations (Ahamed et al., 2020). Thus, such rare clinical variants are waiting for more cases reported along with broader clinical and prospective descriptions.

One of the rare HCM genetic variants is a form of the disease associated with the *TRIM63* gene. It has been described recently and represents one of the rare forms of autosomal-recessive or compound heterozygous form of HCM (Salazar-Mendiguchía et al., 2020). Despite the small number of cases reported by now, several characteristic features of the disease could distinguish this form from the "classical" sarcomeric phenotype. These specific characteristics include the relatively rapid increase in LV free wall thickness, the appearance of diastolic dysfunction from II to III grades with mild atria enlargements, and normal or borderline estimated pulmonary artery systolic pressure. For example, Patient 1 had extreme hypertrophy (septum up to 56 mm), progressing mainly due to posterior wall and RV wall thicknesses, shaping LVOT and RV outflow tract dynamic obstruction. To the best of our knowledge, it is the first report of *TRIM63*-associated HCM with such high magnitude hypertrophy (Chen et al., 2012; Su et al., 2014; Olivé et al., 2015; Salazar-Mendiguchía et al., 2020).

The diastolic dysfunction up to restrictive phenotype was already reported in *TRIM63*-mutation carriers by other authors (Olivé et al., 2015; Salazar-Mendiguchía et al., 2020). While not rare in some forms of HCM, restrictive phenotype had a malign prognosis in pediatric and adult patients with HCM (Maskatia et al., 2012; Li et al., 2020). In *TRIM63*-associated HCM, restrictive dysfunction could reflect the altered molecular interaction of MuRF1 with titin (Higashikuse et al., 2019). There is a MuRF1-binding site in titin adjacent to the titin kinase domain. Mutations of this region lead to hypertrophy and diastolic dysfunction in the medaka fish experimental model and Japanese patients with HCM associated with *TRIM63* (Higashikuse et al., 2019). In addition, mutations of the titin MuRF1-binding site lead to the expression shift to the stiffer titin isoforms, increased titin binding to MuRF1, and enhanced titin degradation through ubiquitination. Thus, MuRF1–titin interaction contributed to sarcomeric protein turnover and titin isoforms switch, determining muscle compliance and diastolic function (Higashikuse et al., 2019).

The development of systolic dysfunction has been reported as a distinct feature of *TRIM63*-associated cardiomyopathies (Salazar-Mendiguchía et al., 2020). Thus, Salazar-Mendiguchiá et al. demonstrated that *TRIM63*-homozygous HCM patients have significant degrees of the LGE phenomenon and progressed to LV systolic dysfunction more often than in the typical HCM, thereby representing a subgroup of increased risk of adverse events (Salazar-Mendiguchía et al., 2020). However, despite the marked degree of fibrosis reflected by LGE on MRI in both cases, no systolic dysfunction was noted in our patients. Possibly, this could be explained by the relatively young patient age, and a thorough follow-up within the next years will shed light on the frequency of systolic dysfunction in patients with *TRIM63*-associated cardiomyopathies and marked fibrosis.

MuRF1 tissue distribution raises the question of whether *TRIM63* mutations can cause skeletal myopathy. Olivé et al. reported a male patient with cardiac and skeletal myosin aggregate myopathy carrying the combination of homozygous *TRIM63* null-mutation and heterozygous *TRIM54* (encoding MuRF3) mutation (Olivé et al., 2015). Clinically, it presented as proximal muscle weakness and HCM with atrial flutter. Electron microscopy of muscle biopsy revealed, apart from I-bands and Z-discs disorganization, myosin-associated proteins aggregates and abnormal microtubules distribution in skeletal muscle cells. The latter demonstrated the possibility that MuRF1 and MuRF3 regulate not only sarcomere protein degradation but also spatial organization of the microtubules. However, whether the presence of both *TRIM63* and *TRIM54* variants or the homozygous *TRIM63* variant itself contributed to myopathic phenotype remains unclear (Olivé et al., 2015). Later, Jokela et al. described female patient with mild clinical symptoms of skeletal myopathy along with creatine kinase elevation and severe cardiac hypertrophy (in the absence of other diseases capable of producing the observed degree of hypertrophy) in association with *TRIM63*-homozygous variant alone (Jokela et al., 2019). Given that, the remarkable muscle hypertrophy of upper limbs observed in both patients potentially could reflect pseudohypertrophy due to the myopathic process. Of note, both patients performed sport and had, similar to the case presented by Olive et al., marked muscular hypertrophic phenotype (Olivé et al., 2015). Of note, Patient 1, who did sport with the prevalence of static load, displayed more severe hypertrophy. However, this notion needs further attention and deeper functional studies, including neuromyography and muscle MRI.

Our study has several important limitations. One of them is an inability to perform a genetic test on the parental DNA and identify whether three of four described variants are *de novo* or inherited.

TABLE 3 | Dynamics of echocardiography data in Patient 2

Parameter/age of examination	15 years old	19 years old	22 years old
LA, mm	39	45	47
LV volume, ml	60	61	68
LA volume index, ml/m^2	33	32	36
RA volume, ml	49	51	63
RA volume index, ml/m^2	27	27	34
Septum, mm	16	24	27
PW, mm	11	11	11
RWT	0.48	0.46	0.44
LV mass, g	335	—	—
LV mass index, g/m^2	184	—	—
LV EDD, mm	46	48	50
LV ESD, mm	30	—	23
LV EDV, ml	114 (Teicholz)	71	79
LV ESV, ml	50 (Teicholz)	19	24
SV, ml	64	52	55
EDVi, ml/m^2	62.6	37.8	42.0
ESVi, ml/m^2	27.5	10.1	12.8
RV WT, mm	4	4	4
RV, mm	25	26	31
EF, %	57	69	70
GL strain, %	19.3	20	—
TAPSE, cm	—	—	—
ePASP, mmHg	11	—	24
Diastolic dysfunction, type	No	No	II
E/A ratio	1.53	1.4	1.6
LVOT PGmax, mmHg	4	7	7
RVOT PGmax, mmHg	—	—	—
Mitral regurgitation	mild	mild	mild
SAM of the MV	No	No	No

EDV, end-diastolic volume; EDVi, end-diastolic volume index; EF, left ventricle ejection fraction; ESVi, end-systolic volume index; ePASP, estimated pulmonary artery systolic pressure; GL strain, global longitudinal strain; LA, left atrium; LV EDD, left ventricle end-diastolic dimension; LV EDV, left ventricle end-diastolic volume; LV ESD, left ventricle end-systolic dimension; LV ESV, left ventricle end-systolic volume; LVOT PGmax, left ventricle outflow tract maximum pressure gradient; PW, posterior wall; RA, right atrium; RV, right ventricle; RVOT PGmax, right ventricle outflow tract maximum pressure gradient; RV WT, right ventricle wall thickness; RWT, relative wall thickness; SAM of the MV, systolic anterior motion of the mitral valve; SV, stroke volume; TAPSE, tricuspid annular plane systolic dysfunction.

Another important limitation is an inability to verify in both cases if two detected variants belong to the same or different alleles. In light of the recently published data on the polygenic impact of many genetic variants into HCM, the role of these and other concomitant variants in the genes not yet described in connection to the observed phenotype cannot be excluded and may need further elucidation.

In summary, we have described two new patients with HCM due to the compound heterozygous *TRIM63* variants. Both patients presented with marked progressed myocardial hypertrophy and diastolic dysfunction from II to III grades and demonstrated clear indications for ICD implantation according to the accepted risk prediction models. Further data collecting regarding rare cases of compound *TRIM63* variants associated with inherited cardiac pathology will allow developing a more personalized approach in this rare cardiac disorder.

DATA AVAILABILITY STATEMENT

The datasets presented in this study can be found in online repositories. The names of the repository/repositories and accession number(s) can be found in the article/**Supplementary Material**.

ETHICS STATEMENT

Ethical review and approval were not required for the study on human participants in accordance with the local legislation and institutional requirements. Written informed consent to participate in this study was provided by the participants' legal guardian/next of kin. Written informed consent was obtained from the individual(s) and minor(s)' legal guardian/next of kin, for the publication of any potentially identifiable images or data included in this article.

AUTHOR CONTRIBUTIONS

AK, OM, and PS contributed to the conception and design of the study, analysis, interpretation of the data, and drafting of the manuscript. SA and OC contributed to the study concept and research design and wrote the manuscript. TL, AS, VL, and YF took part in the analysis and interpretation of data and have been involved in revising the manuscript critically. AN and GS took part in the analysis and interpretation of the data. EK, SZ, YF, and AnK conducted the experiments and performed the analysis and interpretation of the data. All authors have read and agreed to the published version of the manuscript.

FUNDING

This work was financially supported by the Ministry of Science and Higher Education of the Russian Federation (Agreement no. 075-15-2020-901).

SUPPLEMENTARY MATERIAL

The Supplementary Material for this article can be found online at: https://www.frontiersin.org/articles/10.3389/fgene.2022.743472/full#supplementary-material

REFERENCES

Ahamed, H., Balegadde, A. V., Menon, S., Menon, R., Ramachandran, A., Mathew, N., et al. (2020). Phenotypic Expression and Clinical Outcomes in a South Asian PRKAG2 Cardiomyopathy Cohort. *Sci. Rep.* 10, 20610. doi:10.1038/s41598-020-77124-9

Arya, R., Kedar, V., Hwang, J. R., McDonough, H., Li, H.-H., Taylor, J., et al. (2004). Muscle Ring Finger Protein-1 Inhibits PKCε Activation and Prevents Cardiomyocyte Hypertrophy. *J. Cel Biol* 167, 1147–1159. doi:10.1083/jcb.200402033

Bulatov, E., Zagidullin, A., Valiullina, A., Sayarova, R., and Rizvanov, A. (2018). Small Molecule Modulators of RING-Type E3 Ligases: MDM and Cullin Families as Targets. *Front. Pharmacol.* 9, 450. doi:10.3389/fphar.2018.00450

Chen, S. N., Czernuszewicz, G., Tan, Y., Lombardi, R., Jin, J., Willerson, J. T., et al. (2012). Human Molecular Genetic and Functional Studies Identify TRIM63 , Encoding Muscle RING Finger Protein 1, as a Novel Gene for Human Hypertrophic Cardiomyopathy. *Circ. Res.* 111, 907–919. doi:10.1161/CIRCRESAHA.112.270207

Geisterfer-Lowrance, A. A. T., Kass, S., Tanigawa, G., Vosberg, H.-P., McKenna, W., Seidman, C. E., et al. (1990). A Molecular Basis for Familial Hypertrophic Cardiomyopathy: A β Cardiac Myosin Heavy Chain Gene Missense Mutation. *Cell* 62, 999–1006. doi:10.1016/0092-8674(90)90274-i

Higashikuse, Y., Mittal, N., Arimura, T., Yoon, S. H., Oda, M., Enomoto, H., et al. (2019). Perturbation of the titin/MURF1 Signaling Complex Is Associated with Hypertrophic Cardiomyopathy in a Fish Model and in Human Patients. *Dis. Model. Mech.* 12, dmm041103. doi:10.1242/dmm.041103

Ho, C. Y., Day, S. M., Ashley, E. A., Michels, M., Pereira, A. C., Jacoby, D., et al. (2018). Genotype and Lifetime Burden of Disease in Hypertrophic Cardiomyopathy: Insights from the Sarcomeric Human Cardiomyopathy Registry (SHaRe). *Circulation* 138, 1387–1398. doi:10.1161/CIRCULATIONAHA.117.033200

Ingles, J., Goldstein, J., Thaxton, C., Caleshu, C., Corty, E. W., Crowley, S. B., et al. (2019). Evaluating the Clinical Validity of Hypertrophic Cardiomyopathy Genes. *Circ. Genomic Precision Med.* 12, e002460. doi:10.1161/CIRCGEN.119.002460

Jokela, M., Baumann, P., Huovinen, S., Penttilä, S., and Udd, B. (2019). Homozygous Nonsense Mutation p.Q274X in TRIM63 (MuRF1) in a Patient with Mild Skeletal Myopathy and Cardiac Hypertrophy. *J. Neuromuscul. Dis.* 6, 143–146. doi:10.3233/JND-180350

Jorholt, J., Formicheva, Y., Vershinina, T., Kiselev, A., Muravyev, A., Demchenko, E., et al. (2020). Two New Cases of Hypertrophic Cardiomyopathy and Skeletal Muscle Features Associated with ALPK3 Homozygous and Compound Heterozygous Variants. *Genes* 11, 1201. doi:10.3390/genes11101201

Li, S., Wu, B., Yin, G., Song, L., Jiang, Y., Huang, J., et al. (2020). MRI Characteristics, Prevalence, and Outcomes of Hypertrophic Cardiomyopathy with Restrictive Phenotype. *Radiol. Cardiothorac. Imaging* 2, e190158. doi:10.1148/ryct.2020190158

Lopes, L. R., and Elliott, P. M. (2014). A Straightforward Guide to the Sarcomeric Basis of Cardiomyopathies. *Heart* 100, 1916–1923. doi:10.1136/heartjnl-2014-305645

Lorenzini, M., Norrish, G., Field, E., Ochoa, J. P., Cicerchia, M., Akhtar, M. M., et al. (2020). Penetrance of Hypertrophic Cardiomyopathy in Sarcomere Protein Mutation Carriers. *J. Am. Coll. Cardiol.* 76, 550–559. doi:10.1016/j.jacc.2020.06.011

Maejima, Y., Usui, S., Zhai, P., Takamura, M., Kaneko, S., Zablocki, D., et al. (2014). Muscle-Specific RING finger 1 Negatively Regulates Pathological Cardiac Hypertrophy through Downregulation of Calcineurin A. *Circ. Heart Fail.* 7, 479–490. doi:10.1161/CIRCHEARTFAILURE.113.000713

Marstrand, P., Han, L., Day, S. M., Olivotto, I., Ashley, E. A., Michels, M., et al. (2020). Hypertrophic Cardiomyopathy with Left Ventricular Systolic Dysfunction. *Circulation* 141, 1371–1383. doi:10.1161/CIRCULATIONAHA.119.044366

Maskatia, S. A., Decker, J. A., Spinner, J. A., Kim, J. J., Price, J. F., Jefferies, J. L., et al. (2012). Restrictive Physiology Is Associated with Poor Outcomes in Children with Hypertrophic Cardiomyopathy. *Pediatr. Cardiol.* 33, 141–149. doi:10.1007/s00246-011-0106-6

Olivé, M., Abdul-Hussein, S., Oldfors, A., González-Costello, J., van der Ven, P. F. M., Fürst, D. O., et al. (2015). New Cardiac and Skeletal Protein Aggregate Myopathy Associated with Combined MuRF1 and MuRF3 Mutations. *Hum. Mol. Genet.* 24, 6264. doi:10.1093/hmg/ddv311

Ommen, S. R., Mital, S., Burke, M. A., Day, S. M., Deswal, A., Elliott, P., et al. (2020). 2020 AHA/ACC Guideline for the Diagnosis and Treatment of Patients with Hypertrophic Cardiomyopathy. *Circulation* 142 (25), 558–631. doi:10.1161/CIR.0000000000000937

Peris-Moreno, D., Taillandier, D., and Polge, C. (2020). MuRF1/TRIM63, Master Regulator of Muscle Mass. *Int. J. Mol. Sci.* 21 (18), 6663. doi:10.3390/ijms21186663

Płoski, R., Pollak, A., Müller, S., Franaszczyk, M., Michalak, E., Kosinska, J., et al. (2014). Does p.Q247X in TRIM63 Cause Human Hypertrophic Cardiomyopathy? *Circ. Res.* 114, e2–5. doi:10.1161/CIRCRESAHA.114.302662

Polge, C., Heng, A. E., Jarzaguet, M., Ventadour, S., Claustre, A. S., Combaret, L., et al. (2011). Muscle Actin Is Polyubiquitinylated *In Vitro* and *In Vivo* and Targeted for Breakdown by the E3 Ligase MuRF1. *FASEB j.* 25, 3790–3802. doi:10.1096/fj.11-180968

Polge, C., Cabantous, S., Deval, C., Claustre, A., Hauvette, A., Bouchenot, C., et al. (2018). A Muscle-specific MuRF1-E2 Network Requires Stabilization of MuRF1-E2 Complexes by Telethonin, a Newly Identified Substrate. *J. Cachexia, Sarcopenia Muscle* 9, 129–145. doi:10.1002/jcsm.12249

Richards, S., Aziz, N., Bale, S., Bick, D., Das, S., Gastier-Foster, J., et al. (2015). Standards and Guidelines for the Interpretation of Sequence Variants: a Joint Consensus Recommendation of the American College of Medical Genetics and Genomics and the Association for Molecular Pathology. *Genet. Med.* 17, 405–424. doi:10.1038/gim.2015.30

Sabater-Molina, M., Pérez-Sánchez, I., Hernández del Rincón, J. P., and Gimeno, J. R. (2018). Genetics of Hypertrophic Cardiomyopathy: A Review of Current State. *Clin. Genet.* 93, 3–14. doi:10.1111/cge.13027

Salazar-Mendiguchía, J., Ochoa, J. P., Palomino-Doza, J., Domínguez, F., Díez-López, C., Akhtar, M., et al. (2020). Mutations in TRIM63 Cause an Autosomal-Recessive Form of Hypertrophic Cardiomyopathy. *Heart* 106, 1342–1348. doi:10.1136/heartjnl-2020-316913

Su, M., Wang, J., Kang, L., Wang, Y., Zou, Y., Feng, X., et al. (2014). Rare Variants in Genes Encoding MuRF1 and MuRF2 Are Modifiers of Hypertrophic Cardiomyopathy. *Int. J. Mol. Sci.* 15, 9302–9313. doi:10.3390/ijms15069302

Teekakirikul, P., Zhu, W., Huang, H. C., and Fung, E. (2019). Hypertrophic Cardiomyopathy: An Overview of Genetics and Management. *Biomolecules* 9, 878. doi:10.3390/biom9120878

Vershinina, T., Fomicheva, Y., Muravyev, A., Jorholt, J., Kozyreva, A., Kiselev, A., et al. (2020). Genetic Spectrum of Left Ventricular Non-Compaction in Paediatric Patients. *Cardiology* 145, 746–756. doi:10.1159/000510439

Willis, M. S., Schisler, J. C., Li, L., Rodri´guez, J. E., Hilliard, E. G., Charles, P. C., et al. (2009). Cardiac Muscle Ring finger-1 Increases Susceptibility to Heart Failure *In Vivo*. *Circ. Res.* 105, 80–88. doi:10.1161/CIRCRESAHA.109.194928

Witt, S. H., Granzier, H., Witt, C. C., and Labeit, S. (2005). MURF-1 and MURF-2 Target a Specific Subset of Myofibrillar Proteins Redundantly: Towards Understanding MURF-Dependent Muscle Ubiquitination. *J. Mol. Biol.* 350, 713–722. doi:10.1016/j.jmb.2005.05.021

Wolf, C. M. (2019). Hypertrophic Cardiomyopathy: Genetics and Clinical Perspectives. *Cardiovasc. Diagn. Ther.* 9, S388–S415. doi:10.21037/cdt.2019.02.01

Conflict of Interest: The authors declare that the research was conducted in the absence of any commercial or financial relationships that could be construed as a potential conflict of interest.

Publisher's Note: All claims expressed in this article are solely those of the authors and do not necessarily represent those of their affiliated organizations, or those of the publisher, the editors, and the reviewers. Any product that may be evaluated in this article, or claim that may be made by its manufacturer, is not guaranteed or endorsed by the publisher.

frontiers in Genetics

CASE REPORT
published: 03 March 2022
doi: 10.3389/fgene.2022.831133

Case Report: Next-Generation Sequencing Identified a Novel Pair of Compound-Heterozygous Mutations of *LPL* Gene Causing Lipoprotein Lipase Deficiency

Yakun Li[1†], *Man Hu*[1†], *Lin Han*[2†], *Lifang Feng*[1], *Luhong Yang*[1], *Xiaoqian Chen*[1], *Tingting Du*[1], *Hui Yao*[1] *and Xiaohong Chen*[1*]

[1]Department of Endocrinology and Metabolism, Wuhan Children's Hospital, Tongji Medical College, Huazhong University of Science and Technology, Wuhan, China, [2]Running Gene Inc., Beijing, China

Lipoprotein lipase deficiency (LPLD) is a rare disease characterized by the accumulation of chylomicronemia with early-onset. Common symptoms are abdominal pain, hepatosplenomegaly, eruptive xanthomas and lipemia retinalis. Serious complications include acute pancreatitis. Gene *LPL* is one of causative factors of LPLD. Here, we report our experience on an asymptomatic 3.5-month-old Chinese girl with only milky blood. Whole-exome sequencing was performed and identified a pair of compound-heterozygous mutations in *LPL* gene, c.862G>A (p.A288T) and c.461A>G (p.H154R). Both variants are predicted "deleterious" and classified as "likely pathogenic". This study expanded the *LPL* mutation spectrum of disease LPLD, thereby offering exhaustive and valuable experience on early diagnosis and proper medication of LPLD.

Keywords: LPL gene, lipoprotein lipase deficiency (LPLD), familial hyperchylomicronemia syndrome (FCS), hyperlipoproteinemia, whole-exome sequencing (WES)

OPEN ACCESS

Edited by:
Emiliano González Vioque, University Clinical Hospital of Santiago, Spain

Reviewed by:
Georges Nemer, Hamad bin Khalifa University, Qatar
Hayato Tada, Kanazawa University, Japan

***Correspondence:**
Xiaohong Chen
cxhdaifu@163.com

[†]*These authors share first authorship*

Specialty section:
This article was submitted to Genetics of Common and Rare Diseases, a section of the journal Frontiers in Genetics

Received: *08 December 2021*
Accepted: *31 January 2022*
Published: *03 March 2022*

Citation:
Li Y, Hu M, Han L, Feng L, Yang L, Chen X, Du T, Yao H and Chen X (2022) Case Report: Next-Generation Sequencing Identified a Novel Pair of Compound-Heterozygous Mutations of LPL Gene Causing Lipoprotein Lipase Deficiency. Front. Genet. 13:831133. doi: 10.3389/fgene.2022.831133

1 INTRODUCTION

Lipoprotein lipase deficiency (LPLD, OMIM #238600), also called familial hyperchylomicronemia syndrome (FCS) or type 1 hyperlipoproteinemia, is characterized by uncontrolled accumulation of chylomicronemia (Chait and Eckel, 2019). The frequency of LPLD is approximately 1 per million in the most populations (Brahm and Hegele, 2015), except that it is much more common in the province of Quebec, Canada due to founder effect (Gagne et al., 1989). This condition is a rare hereditary disorder with which patients usually developed signs or symptoms before the age of 10 (early-onset), with 25% presenting symptoms by the first year of life (Burnett et al., 1993). Clinical manifestations of LPLD include recurrent abdominal pain, acute pancreatitis, hepatosplenomegaly, eruptive xanthomas and lipemia retinalis. Acute pancreatitis is the most serious consequence of severe hypertriglyceridemia, with a mortality rate of 2–5% (Lowenfels et al., 2009; Omdal et al., 2011). Neurological features such as depression and intellectual decline have also been reported in patients with LPLD. Fortunately, these symptoms can be remedied after blood lipid levels normalize.

In LPLD patients, lipoprotein lipase (LPL) is usually malfunctional or absent. The measurement of LPL enzyme activity in an assay system is an approach to establish the diagnosis but it is not routinely available. Since homozygous or a pair of compound-heterozygous variants in lipoprotein lipase protein gene (*LPL*, OMIM #609708) is the causative factor, the current mainstream approach

to diagnosing LPLD is to detect biallelic pathogenic variants in *LPL* gene. According to Human Gene Mutation Database (HGMD) professional version (Stenson et al., 2017), a total of 214 disease-causing mutations (DM) in *LPL* have been reported to be associated with LPLD or relevant phenotypes. Analysis of the distribution of mutations and expanding the mutation spectrum are necessary for further diagnosis and research on LPLD. Herein, we report the clinical, biochemical and genetic findings of a 3.5-month-old Chinese girl diagnosed with LPLD, who carries a pair of compound-heterozygous *LPL* variants including a novel one. We expanded the spectrum of *LPL* mutations associated with LPLD. We also summarized, illustrated and analyzed mutations reported worldwide.

2 METHODS

This research was approved by the Ethics Committee of Wuhan Children's Hospital (No.2017020). The patient's guardians were informed with a written consent for the investigation and publication of this study.

2.1 Clinical Data Collection

Clinical information of the patient was collected from official medical records and follow-up visits. Physical and biochemical examinations were performed in each visit, including lipid blood test, complete blood count (CBC), blood gas analysis, blood ammonia assay, blood lactic acid, blood sugar, coagulogram, antibody testing, urine organic acids (OAU) test. Abdominal and pelvic CT scanning, chest and abdominal X-ray imaging, brain MRI, brain magnetic resonance angiography (MRA), abdominal color doppler flow imaging (CDFI) and electroencephalogram (EEG) were performed. Blood amino acid and acylcarnitine profile was also analyzed by tandem mass spectrometry.

2.2 Whole-Exome Sequencing

Peripheral blood of the patient and her parents were collected and sent to Running Gene Inc. (Beijing, China) for whole-exome sequencing (WES). Genomic DNA samples were extracted using Blood DNA Kit V2 (#CW2553, Cowin Bio., Taizhou, China). Qubit dsDNA HS Assay Kit (#Q32851, Invitrogen, Carlsbad, CA) was used to determine concentrations. Gel electrophoresis were also performed for quality control. Qualified DNA samples were fragmented into 200–300 bp by sonication and then processed for DNA libraries preparation according to the manufacturer's protocol of KAPA LTP Library Preparation Kit (#KR0453, Kapa Biosystems, Wilmington, MA), which includes four standard steps: end-repair, A-tailing, adapter ligation and library amplification. Cleanups during each steps were carried out with Agencourt AMPure XP reagent (#A63882, Beckman Coulter, Brea, CA). Evaluation of prepared libraries were performed using Qubit dsDNA HS Assay Kit. Capture probes hybridized to pooled DNA libraries using the Agilent SureSelectXT2 Target Enrichment System (Agilent, Santa Clara, CA). Target fragments (exome) were fished out by hybridization with Dynabeads® MyOne™ Streptavidin T1 (#65601, Invitrogen). Purifications were performed using Agencourt AMPure XP reagent. Final libraries were evaluated by Qubit dsDNA HS Assay Kit. DNA libraries were sequenced on the Illumina NovaSeq 6000 platform as paired-end 150-bp reads.

Raw data of WES were stored as FASTQ format and processed by Fastp (Chen et al., 2018) for quality control. Qualified reads were aligned to human genome reference sequence (GRCh37/hg19) using Burrows-Wheeler Alignment (BWA) (Li and Durbin, 2009). Consensus single nucleotide polymorphisms (SNPs) and insertions and deletions (indels) were called by Genome Analysis Toolkit (GATK) (Van der Auwera et al., 2013). After quality control, called variants were annotated based on several public databases, such as 1kGenome (Genomes Project et al., 2015), ExAC (Lek et al., 2016), gnomAD (Karczewski et al., 2020), ESP6500 (Fu et al., 2013), ClinVar (Landrum et al., 2020), HGMD and in-house databases. Annotated variants were then filtered based on their relationship with disease and pathogenicity. The pathogenicity of candidate variants were predicted by multiple *in silico* algorithms, including MutationTaster2 (Schwarz et al., 2014), SIFT (Sim et al., 2012), Provean (Choi and Chan, 2015), Polyphen-2 (HDIV and HVAR) (Adzhubei et al., 2013), LRT (Chun and Fay, 2009), FATHMM (Shihab et al., 2013) and Mutpred2 (Pejaver et al., 2020). Variants were also classified based on American College of Medical Genetics and Genomics (ACMG) guidelines (Richards et al., 2015). Candidate variants, also including mutations in *PLIN1* gene (familial partial lipodystrophy type IV) and *SAR1B* gene (chylomicron retention disease), were then sent to Sanger for validation. Likely pathogenic variants were finally selected on the basis of their relationship to the disease, allele frequency in controls, pattern of segregation with disease, pattern of inheritance and predicted pathogenicity.

3 RESULTS

3.1 Clinical Presentation

A 3.5-month-old Chinese girl admitted to our hospital due to her pneumonia with fever and vomiting, but we found her blood with milky appearance during blood routine examination. She is the second child of her non-consanguineous parents (G2P2). She was born by caesarean section in the 40th gestational weeks, with a birth weight of 3.8 kg (90 percentile) and a birth height of 50 cm (50 percentile). She was under breast-fed and her mom's blood lipids were in the normal range (**Supplementary Table 1**). No abnormalities were found during pregnancy and delivery. No relevant medical history or family history was reported.

3.2 Physical Examinations

Her weight was 6 kg (25 percentile) and height was 63 cm (50 percentile) at the age of 3.5 months. A hemangioma-like red rash (1.0 × 1.0 cm) were identified on her right hypochondrium. The rash was excluded from eruptive xanthomas by dermatologists. Her liver is present 1.5 cm below the costal margin. No abnormalities found on her facial appearance, psychomotor development or muscular tension. No other relevant signs or symptoms were reported.

TABLE 1 | Biochemical examinations of blood lipid and lipoprotein levels.

Patient age	CHOL (mmol/L)		TG (mmol/L)		HDL (mmol/L)		LDL (mmol/L)		ApoA1 (g/L)		ApoB (g/L)	
3m16d	12.58	↑	67.84	↑	0.73	↓	0.24	↓	0.7	↓	0.27	↓
3m19d	5.79	↑	15.61	↑	0.35	↓	1.86	-	0.91	↓	1.86	↑
3m23d	6.74	↑	10.11	↑	0.27	↓	4.26	↑	NA		NA	
4m21d	3.89	-	9.41	↑	0.25	↓	< 0.315	↓	NA		NA	
Discharged												
6m14d	11.31	↑	74.10	↑	0.22	↓	0.11	↓	0.82	↓	0.38	↓
6m17d	6.09	↑	20.75	↑	0.34	↓	0.57	↓	0.74	↓	0.78	-
8m	6.14	↑	7.28	↑	0.30	↓	0.42	↓	0.88	↓	0.97	-
11m	6.10	↑	19.14	↑	0.44	↓	1.27	↓	0.94	↓	1.05	-
1y4m	4.20	-	3.94	↑	0.61	↓	2.69	-	0.86	↓	0.98	-
1y7m	4.73	-	2.20	↑	0.60	↓	3.05	↑	0.89	↓	1.49	↑
1y10m	4.50	-	3.53	↑	0.65	↑	3.07	↑	0.87	↓	1.20	-
2y1m	4.69	-	1.49	↑	0.83	↑	3.41	↑	1.20	-	1.09	-
2y5m	3.50	-	0.66	-	1.63	-	1.72	-	1.59	-	0.48	-
Reference	2.8–5.7		0.32–1.46		0.9–1.74		1.55–2.86		1.1–1.95		0.45–1.4	

ApoA1, apolipoprotein A-1; ApoB, apolipoprotein B; CHOL, cholesterol; HDL, high density lipoprotein; LDL, low density lipoprotein; LP (a), lipoprotein (a); TG, triglyceride; TG: 1 mol/L = 88.5 mg/dl.

3.3 Laboratorial Examinations

Lipid blood test revealed elevated blood triglycerides (TG) and cholesterols (CHOL) levels as well as decreased levels of low-density lipoproteins (LDL), high-density lipoproteins (HDL), apolipoprotein A1 (ApoA1) and apolipoprotein B (ApoB) (**Table 1**). Normal results were shown by other biochemical examinations mentioned above.

Abdominal and pelvic CT scanning with and without contrast presented peripancreatic effusion which indicates the occurrence of pancreatitis. Chest and abdominal X-ray imaging showed increased lung texture. Blood amino acid and acylcarnitine profile analysis revealed decreased levels of multiple amino acids (methionine, leucine, valine, glycine, glutamine and threonine), which may be caused by malnutrition. No clinically significant abnormalities were identified by brain MRI, MRA, abdominal CDFI and EEG.

3.4 Genetic Analysis

WES was applied to support the diagnosis. We identified a pair of compound-heterozygous variants, c.862G>A (p.A288T) and c.461A>G (p.H154R), in *LPL* gene (NM_000237, NP_000228) and validated them by Sanger sequencing (**Figure 1C**). Variant c.862G>A (chr8:19813438) is a missense, which leads to an alteration of protein sequence (p.A288T) (**Figure 1D**). The variant is located in a well-established functional domain (N-terminal lipase) (PM1). It is absent from controls or at extremely low frequencies (ESP6500, 0; ExAC, 4.12E-05; gnomAD, 5.97E-05; 1kGenome, 2.00E-04) (PM2_supporting). Variant c.862G>A has been detected *in trans* with pathogenic mutation c.836T>G (p.L279R) (PM3) (Ma et al., 1994). Multiple lines of computational evidence support the variant will cause a deleterious effect on its products (MutationTaster2, score = 1.000, disease causing; SIFT, score = 0.001 < cutoff = 0.05, damaging; Provean, score = −3.71 < −2.5, deleterious; Polyphen-2, HDIV score = 0.986 > 0.957, HVAR score = 0.933 > 0.909, probably damaging; LRT, deleterious; FATHMM, score = −3.17 < −1.5, damaging; Mutpred2, score = 0.923 > 0.7, pathogenic, gain of phosphorylation) (PP3). Phenotypes of the patient are specific for LPLD (PP4). This variant has been recorded in dbSNP (rs1800011) and reported as likely disease-causing mutation (DM?) in multiple unrelated LPLD patients with the same phenotype according to HGMD database (PS4_moderate and PP5) (Ma et al., 1994; Rodrigues et al., 2016; Jin et al., 2018; Tada et al., 2019). Thus, c.862G>A (p.A288T) is classified as "likely pathogenic" (PS4_moderate+PM1+PM2_supporting+PM3+PP3+PP4+PP5) according to the ACMG guidelines.

Variant c.461A>G (chr8:19810852) is also a missense, resulting in an amino acid change from histidine to arginine (p.H154R) (**Figure 1D**). This variant is a novel one, which has not been reported in any cases before. It is located in a functional domain, N-terminal lipase domain (PM1) and is absent from controls (gnomAD, ExAC, dbSNP, 1kGenome) (PM2_supporting). It has been detected *in trans* with likely pathogenic mutation c.862G>A (PM3). Multiple lines of *in silico* algorithms predicted the variant deleterious (MutationTaster2, score = 1.000, disease causing; SIFT, score = 0.001 < 0.05, damaging; Provean, score = −7.65 < −2.5, deleterious; Polyphen-2, HDIV score = 0.983 > 0.957, HVAR score = 0.962 > 0.909, probably damaging; LRT, deleterious; FATHMM, score = −3.36 < −1.5, damaging; Mutpred2, score = 0.875 > 0.7, pathogenic, loss of catalytic residue) (PP3). Phenotypes of the patient are specific for LPLD (PP4). His154 is highly conserved across species (**Figure 1E**). Therefore, novel variant c.461A>G (p.H154R) is classified as "likely pathogenic" (PM1+PM2_supporting+PM3+PP3+PP4).

3.5 Treatment and Prognosis

The patient was admitted to hospital due to fever and vomiting with extremely high levels of TG and CHOL in the blood (**Table 1**). Anti-infective and symptomatic treatment was applied (**Figure 2**). Two days later, her symptoms of fever and vomiting disappeared, with a dramatic drop of TG and CHOL levels. Then, bezafibrate (10 mg/kg/d, bid) (60 mg/d) and levocarnitine (167 mg/kg/d, bid) (1 g/d) were administrated to

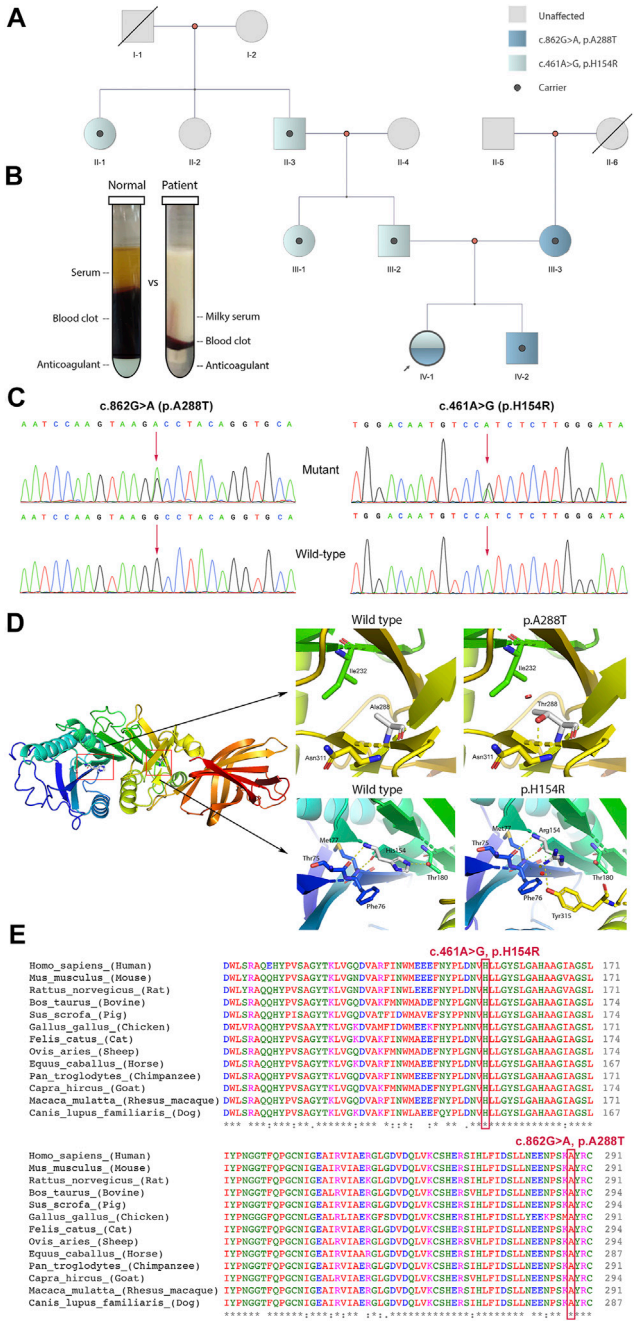

FIGURE 1 | Clinical and genetic information of the patient. **(A)** Pedigree analysis of this family. **(B)** Blood fractionations (set for 24 h) between control and the patient. **(C)** Sanger sequencing of variants c.862G>A and c.461A>G with corresponding wild-types. **(D)** Three-dimensional protein model of lipoprotein lipase. Polar contacts (yellow dash line) between His154 and Arg180 lost and new interactions between His154 and Tyr315 appeared after H154R alteration. With A288T variant, a new repulsion formed between Thr288 and Ile232 (red cylinder). **(E)** Multiple alignments of LPL protein sequence across 13 species. Mutation sites His154 and Ala288 are labelled by a red rectangular. *in the last row indicates amino acid in this site is "highly conserved".

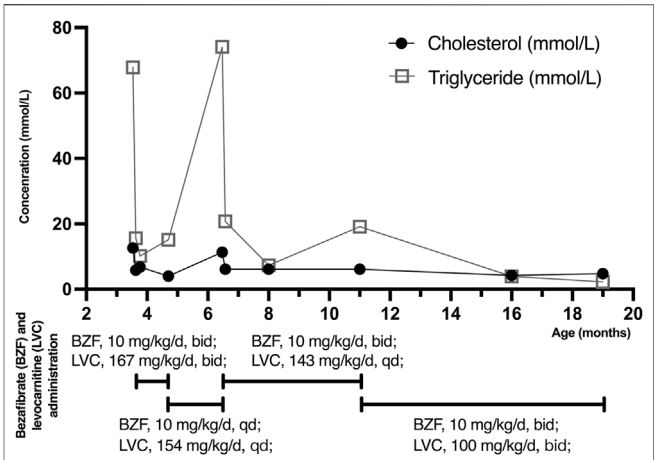

FIGURE 2 | Cholesterol (CHOL) and triglyceride (TG) levels with bezafibrate (BZF) and levocarnitine (LVC) administration. The patient was admitted to hospital with high levels of CHOL (12.58 mmol/L) and TG (67.84 mmol/L) at the age of 3 months and 16 days. Three days later, her CHOL and TG levels plummeted due to bezafibrate and levocarnitine administration. The levels kept decreasing until she was discharged. Her parents reduced the dose without professional medical advice, resulting in a severe relapse (a sharp increased TG level at the age of 6 months and 14 days). The dose of medications was then adjusted and CHOL and TG levels of the patient finally declined to normal and almost normal. (TG: 1 mol/L = 88.5 mg/dl).

enhance lipoprotein lipase activity and promote the β-oxidation of fatty acids, thereby reducing TG levels. As the patient gains weight, the dose of medications changed. During the treatment, TG and CHOL levels continued to decrease towards normal. Her apoprotein levels also recovered. Her LDL level increased and HDL level declined (still out of reference values). However, after discharge, her parents reduced the dose to a half (bezafibrate, 30 mg/d; levocarnitine, 0.5 g/d) without professional medical advice, resulting in a serious relapse (a sharp rise in TG levels at the age of 6 months and 14 days). The dose of bezafibrate was then adjusted to 60 mg/d (9 mg/kg/d, bid). Four and a half months later (the age of 11 months), the dose of bezafibrate and levocarnitine was adjusted to 100 mg/d (10 mg/kg/d, bid) and 1 g/d (100 mg/kg/d, bid), respectively. The patient's blood lipid levels finally fluctuated to nearly normal.

4 DISCUSSION

The *LPL* gene, located on chromosome 8p21.3, encodes the lipoprotein lipase which is the key enzyme of triglyceride metabolism. LPL has both triglyceride lipase and phospholipase activities in the physiological condition. It acts mainly as a triglyceride lipase with very low phospholipase activity (McCoy et al., 2002). LPL catalyzes the hydrolysis of TGs to remove lipids from circulating TG-rich lipoproteins, specifically chylomicrons and very-low-density lipoproteins

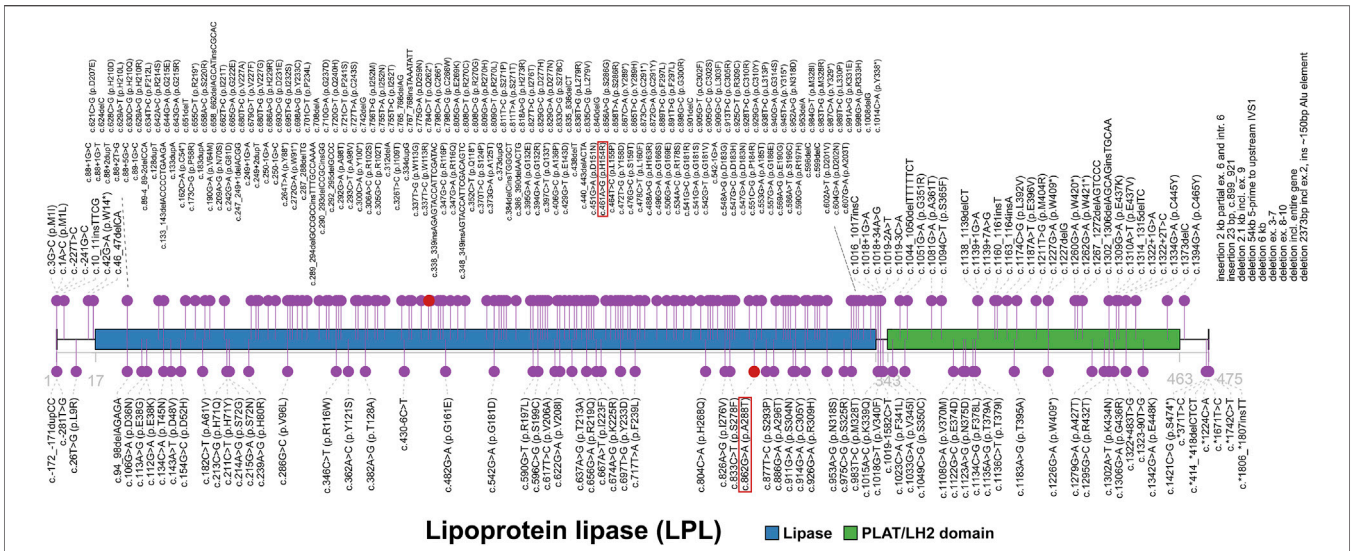

FIGURE 3 | The spectrum landscape of mutations in *LPL* gene. Lipoprotein lipase (1-475) consists of lipase (17-338) and polycystin-1, lipoxygenase, alpha-toxin or lipoxygenase homology (PLAT/LH2) domain (343-463). A total of 287 mutations and polymorphisms of *LPL* gene were reported in HGMD. Disease-causing mutations (DMs) are marked in the top. Other non-DMs and polymorphisms are marked in the bottom. Two variants identified in our case are highlighted in red square.

(VLDL), and thereby plays a critical role in lipid utilization and storage (Weinstock et al., 1995; Lutz et al., 2001; Pingitore et al., 2016). Lipoprotein lipase consists of two domains, lipase domain (17-338) and polycystin-1, lipoxygenase, alpha-toxin or lipoxygenase homology (PLAT/LH2) domain (343-463) (**Figure 3**). Same as the majority of mutations, both current variants are located on lipase domain, indicating the importance of its function and integrity. Mutations in *LPL* gene reduce or eliminate the activity of lipoprotein lipases. The absence of fully functional LPL disrupts the normal breakdown of TGs, preventing adequate clearance of circulating TG-rich lipoproteins. This impaired TG hydrolysis contributes to severely elevated TG levels (usually >16.95 mmol/L [1500 mg/dl]) in plasma (Chait and Eckel, 2019). Moreover, TGs accumulates in the blood vessels and tissues, resulting in pancreatitis, hepatosplenomegaly, eruptive xanthomas and other uncommon symptoms. Although variants in *LPL* gene usually caused lipase deficiency, the enzyme has been found overactivated in some cases, associating with lower TG levels (Smith et al., 2010). In this patient, two missense mutations resulted in reduced activity of LPL rather than complete deficiency, as bezafibrate effectively enhanced the activity of lipoprotein lipase.

There are totally 287 mutations and polymorphisms of *LPL* gene in HGMD (**Figure 3**), including 214 (74.6%) DM, 58 DM? 3 disease-associated polymorphisms (DP), 8 disease-associated polymorphisms with additional functional evidence (DFP) and 4 *in vitro* or *in vivo* functional polymorphisms (FP). Of these, all of 214 DMs were reported to cause LPLD or associated phenotypes clearly. In terms of the type of variants, HGMD collected 118 missense, 44 small insertion/deletion (41 frameshift and 3 inframe), 18 splice (16 canonical), 18 nonsense, 9 large insertion/deletion (>21 bp), 2 regulatory, 3 noncoding and 2 initiation. Missense mutations account for more than half (118/214, 55.1%) of all DMs and are a common mechanism of LPLD, thereby enhancing the likelihood that the two variants reported here cause disease.

Common clinical features of LPLD include recurrent abdominal pain, acute pancreatitis, hepatosplenomegaly, eruptive xanthomas and lipemia retinalis. Some of these symptoms can be fatal for the patient, but none occurred in our patient. We attribute this to the early detection. The combination of results from biochemical examinations and genetic sequencing provides a clear direction for clinical diagnosis. More importantly, it has also led to early diagnosis and proper intervention. For LPLD patients, palliative treatment and medical nutrition therapy are commonly given depending on symptoms. Blood lipid-lowering medicines such as bezafibrate are usually administrated to negatively regulate blood lipid concentrations (Bezafibrate Infarction Prevention, 2000). The maintenance of plasma TGs at less than 11.30 mmol/L (1000 mg/dl) could prevent severe complications such as severe pancreatitis, further preventing the high morbidity and mortality rate (Garg and Rustagi, 2018). In the current case, the concentrations of plasma TGs and CHOL in the patient sharply declined under the action of bezafibrate and levocarnitine. Since this early and proper administration of drugs, the patient's lipid levels are maintained at a normal level while severe complications did not occur. Meanwhile, medium-chain TGs are also recommended for daily diet, as they could be absorbed directly into the portal vein independent on chylomicrons (Burnett et al., 1993).

In summary, this study reported a novel pair of variants in *LPL* gene causing LPLD in a 3.5-month-old Chinese girl. The novel

variant, c.461A>G (p.H154R), further expended the disease-causing mutation spectrum of LPL deficiency. *LPL* mutations reported in HGMD were also reviewed and further analyzed. Missense mutations and mutations located in lipase domain account for the majority. Genetic screening can provide conclusive evidence for diagnosing LPLD. Our study and review are supportive for the early diagnosis and proper treatment of patients with LPLD in the future.

DATA AVAILABILITY STATEMENT

The datasets presented in this study can be found in online repositories. The names of the repository/repositories and accession number(s) can be found in Sequence Read Archive (SRA) database, PRJNA761861.

ETHICS STATEMENT

The studies involving human participants were reviewed and approved by Medical Ethics Committee of Wuhan Children's Hospital (No.2017020). Written informed consent to participate in this study was provided by the participants' legal guardian/next of kin. Written informed consent was obtained from the individual(s) for the publication of any potentially identifiable images or data included in this article.

AUTHOR CONTRIBUTIONS

HY and XC conceived this study. YL, MH, LY, LF, XC, TD, and XC cared the patient and collected the clinical data of the patient. LH interpreted genetic data and contributed to the manuscript. HY and XC supervised the study. All authors read and approved the final manuscript.

FUNDING

This research was funded by Wuhan Municipal Health Commission (Grant number: WX20B13).

ACKNOWLEDGMENTS

We are grateful for the patient and her family. We also thank the staff in Running Gene Inc. (Beijing, China) who performed professional genetic sequencing and analysis.

SUPPLEMENTARY MATERIAL

The Supplementary Material for this article can be found online at: https://www.frontiersin.org/articles/10.3389/fgene.2022.831133/full#supplementary-material

REFERENCES

Adzhubei, I., Jordan, D. M., and Sunyaev, S. R. (2013). Predicting Functional Effect of Human Missense Mutations Using PolyPhen-2. *Curr. Protoc. Hum. Genet.* 76 (1) 7.20.1–7.20.41. doi:10.1002/0471142905.hg0720s76

Bezafibrate Infarction Prevention Study (2000). Secondary Prevention by Raising HDL Cholesterol and Reducing Triglycerides in Patients with Coronary Artery Disease. *Circulation* 102, 21–27. doi:10.1161/01.cir.102.1.21

Brahm, A. J., and Hegele, R. A. (2015). Chylomicronaemia-current Diagnosis and Future Therapies. *Nat. Rev. Endocrinol.* 11, 352–362. doi:10.1038/nrendo.2015.26

Burnett, J. R., Hooper, A. J., and Hegele, R. A. (1993). "Familial Lipoprotein Lipase Deficiency," in *GeneReviews((R))*. Editors M. P. Adam, H. H. Ardinger, R. A. Pagon, S. E. Wallace, L. J. H. Bean, G. Mirzaa, et al. Seattle (WA): University of Washington.

Chait, A., and Eckel, R. H. (2019). The Chylomicronemia Syndrome Is Most Often Multifactorial. *Ann. Intern. Med.* 170, 626–634. doi:10.7326/m19-0203

Chen, S., Zhou, Y., Chen, Y., and Gu, J. (2018). Fastp: an Ultra-fast All-In-One FASTQ Preprocessor. *Bioinformatics* 34, i884–i890. doi:10.1093/bioinformatics/bty560

Choi, Y., and Chan, A. P. (2015). PROVEAN Web Server: a Tool to Predict the Functional Effect of Amino Acid Substitutions and Indels. *Bioinformatics* 31, 2745–2747. doi:10.1093/bioinformatics/btv195

Chun, S., and Fay, J. C. (2009). Identification of Deleterious Mutations within Three Human Genomes. *Genome Res.* 19, 1553–1561. doi:10.1101/gr.092619.109

Fu, W., O'Connor, T. D., Jun, G., Kang, H. M., Abecasis, G., Leal, S. M., et al. (2013). Analysis of 6,515 Exomes Reveals the Recent Origin of Most Human Protein-Coding Variants. *Nature* 493, 216–220. doi:10.1038/nature11690

Gagné, C., Brun, L. D., Julien, P., Moorjani, S., and Lupien, P. J. (1989). Primary Lipoprotein-Lipase-Activity Deficiency: Clinical Investigation of a French Canadian Population. *CMAJ* 140, 405–411.

Garg, R., and Rustagi, T. (2018). Management of Hypertriglyceridemia Induced Acute Pancreatitis. *Biomed. Res. Int.* 2018, 4721357. doi:10.1155/2018/4721357

Genomes Project, C., Auton, A., Brooks, L. D., Durbin, R. M., Garrison, E. P., Kang, H. M., et al. (2015). A Global Reference for Human Genetic Variation. *Nature* 526, 68–74. doi:10.1038/nature15393

Jin, J.-L., Sun, D., Cao, Y.-X., Zhang, H.-W., Guo, Y.-L., Wu, N.-Q., et al. (2018). Intensive Genetic Analysis for Chinese Patients with Very High Triglyceride Levels: Relations of Mutations to Triglyceride Levels and Acute Pancreatitis. *EBioMedicine* 38, 171–177. doi:10.1016/j.ebiom.2018.11.001

Karczewski, K. J., Francioli, L. C., Tiao, G., Cummings, B. B., Alföldi, J., Wang, Q., et al. (2020). The Mutational Constraint Spectrum Quantified from Variation in 141,456 Humans. *Nature* 581, 434–443. doi:10.1038/s41586-020-2308-7

Landrum, M. J., Chitipiralla, S., Brown, G. R., Chen, C., Gu, B., Hart, J., et al. (2020). ClinVar: Improvements to Accessing Data. *Nucleic Acids Res.* 48, D835–D844. doi:10.1093/nar/gkz972

Lek, M., Karczewski, K. J., Karczewski, K. J., Minikel, E. V., Samocha, K. E., Banks, E., et al. (2016). Analysis of Protein-Coding Genetic Variation in 60,706 Humans. *Nature* 536, 285–291. doi:10.1038/nature19057

Li, H., and Durbin, R. (2009). Fast and Accurate Short Read Alignment with Burrows-Wheeler Transform. *Bioinformatics* 25, 1754–1760. doi:10.1093/bioinformatics/btp324

Lowenfels, A. B., Maisonneuve, P., and Sullivan, T. (2009). The Changing Character of Acute Pancreatitis: Epidemiology, Etiology, and Prognosis. *Curr. Gastroenterol. Rep.* 11, 97–103. doi:10.1007/s11894-009-0016-4

Lutz, E. P., Merkel, M., Kako, Y., Melford, K., Radner, H., Breslow, J. L., et al. (2001). Heparin-binding Defective Lipoprotein Lipase Is Unstable and Causes Abnormalities in Lipid Delivery to Tissues. *J. Clin. Invest.* 107, 1183–1192. doi:10.1172/jci11774

Ma, Y., Ooi, T. C., Liu, M. S., Zhang, H., Mcpherson, R., Edwards, A. L., et al. (1994). High Frequency of Mutations in the Human Lipoprotein Lipase Gene in Pregnancy-Induced Chylomicronemia: Possible Association with Apolipoprotein E2 Isoform. *J. Lipid Res.* 35, 1066–1075. doi:10.1016/s0022-2275(20)40102-6

Mccoy, M. G., Sun, G.-S., Marchadier, D., Maugeais, C., Glick, J. M., and Rader, D. J. (2002). Characterization of the Lipolytic Activity of Endothelial Lipase. *J. Lipid Res.* 43, 921–929. doi:10.1016/s0022-2275(20)30466-1

Omdal, T., Dale, J., Lie, S. A., Iversen, K. B., Flaatten, H., and Ovrebo, K. (2011). Time Trends in Incidence, Etiology, and Case Fatality Rate of the First Attack of Acute Pancreatitis. *Scand. J. Gastroenterol.* 46, 1389–1398. doi:10.3109/00365521.2011.605464

Pejaver, V., Urresti, J., Lugo-Martinez, J., Pagel, K. A., Lin, G. N., Nam, H.-J., et al. (2020). Inferring the Molecular and Phenotypic Impact of Amino Acid Variants with MutPred2. *Nat. Commun.* 11, 5918. doi:10.1038/s41467-020-19669-x

Pingitore, P., Lepore, S. M., Pirazzi, C., Mancina, R. M., Motta, B. M., Valenti, L., et al. (2016). Identification and Characterization of Two Novel Mutations in the LPL Gene Causing Type I Hyperlipoproteinemia. *J. Clin. Lipidol.* 10, 816–823. doi:10.1016/j.jacl.2016.02.015

Richards, S., Aziz, N., Bale, S., Bick, D., Das, S., Gastier-Foster, J., et al. (2015). Standards and Guidelines for the Interpretation of Sequence Variants: a Joint Consensus Recommendation of the American College of Medical Genetics and Genomics and the Association for Molecular Pathology. *Genet. Med.* 17, 405–424. doi:10.1038/gim.2015.30

Rodrigues, R., Artieda, M., Tejedor, D., Martínez, A., Konstantinova, P., Petry, H., et al. (2016). Pathogenic Classification of LPL Gene Variants Reported to Be Associated with LPL Deficiency. *J. Clin. Lipidol.* 10, 394–409. doi:10.1016/j.jacl.2015.12.015

Schwarz, J. M., Cooper, D. N., Schuelke, M., and Seelow, D. (2014). MutationTaster2: Mutation Prediction for the Deep-Sequencing Age. *Nat. Methods* 11, 361–362. doi:10.1038/nmeth.2890

Shihab, H. A., Gough, J., Cooper, D. N., Stenson, P. D., Barker, G. L. A., Edwards, K. J., et al. (2013). Predicting the Functional, Molecular, and Phenotypic Consequences of Amino Acid Substitutions Using Hidden Markov Models. *Hum. Mutat.* 34, 57–65. doi:10.1002/humu.22225

Sim, N.-L., Kumar, P., Hu, J., Henikoff, S., Schneider, G., and Ng, P. C. (2012). SIFT Web Server: Predicting Effects of Amino Acid Substitutions on Proteins. *Nucleic Acids Res.* 40, W452–W457. doi:10.1093/nar/gks539

Smith, A. J. P., Palmen, J., Putt, W., Talmud, P. J., Humphries, S. E., and Drenos, F. (2010). Application of Statistical and Functional Methodologies for the Investigation of Genetic Determinants of Coronary Heart Disease Biomarkers: Lipoprotein Lipase Genotype and Plasma Triglycerides as an Exemplar. *Hum. Mol. Genet.* 19, 3936–3947. doi:10.1093/hmg/ddq308

Stenson, P. D., Mort, M., Ball, E. V., Evans, K., Hayden, M., Heywood, S., et al. (2017). The Human Gene Mutation Database: towards a Comprehensive Repository of Inherited Mutation Data for Medical Research, Genetic Diagnosis and Next-Generation Sequencing Studies. *Hum. Genet.* 136, 665–677. doi:10.1007/s00439-017-1779-6

Tada, H., Nomura, A., Okada, H., Nakahashi, T., Nozue, T., Hayashi, K., et al. (2019). Clinical Whole Exome Sequencing in Severe Hypertriglyceridemia. *Clinica Chim. Acta* 488, 31–39. doi:10.1016/j.cca.2018.10.041

Van Der Auwera, G. A., Carneiro, M. O., Hartl, C., Poplin, R., Del Angel, G., Levy-Moonshine, A., et al. (2013). From FastQ Data to High Confidence Variant Calls: the Genome Analysis Toolkit Best Practices Pipeline. *Curr. Protoc. Bioinformatics* 43 (11 10 1), 11–33. doi:10.1002/0471250953.bi1110s43

Weinstock, P. H., Bisgaier, C. L., Aalto-Setälä, K., Radner, H., Ramakrishnan, R., Levak-Frank, S., et al. (1995). Severe Hypertriglyceridemia, Reduced High Density Lipoprotein, and Neonatal Death in Lipoprotein Lipase Knockout Mice. Mild Hypertriglyceridemia with Impaired Very Low Density Lipoprotein Clearance in Heterozygotes. *J. Clin. Invest.* 96, 2555–2568. doi:10.1172/jci118319

Conflict of Interest: The author LH is employed by the company Running Gene Inc., Beijing, China.

The remaining authors declare that the research was conducted in the absence of any commercial or financial relationships that could be construed as a potential conflict of interest.

Publisher's Note: All claims expressed in this article are solely those of the authors and do not necessarily represent those of their affiliated organizations, or those of the publisher, the editors and the reviewers. Any product that may be evaluated in this article, or claim that may be made by its manufacturer, is not guaranteed or endorsed by the publisher.

frontiers in Pediatrics

CASE REPORT
published: 10 March 2022
doi: 10.3389/fped.2022.792574

Case Report: Successful Management of a 29-Day-Old Infant With Severe Hyperlipidemia From a Novel Homozygous Variant of *GPIHBP1* Gene

Shu Liu[1†], Zhiqing Wang[2*†], Xianhua Zheng[3], Ye Zhang[1], Sisi Wei[1], Haimei OuYang[1], Jinqun Liang[1], Nuan Chen[1], Weihong Zeng[1] and Jianhui Jiang[1]*

[1] Children Inherited Metabolism and Endocrine Department, Guangdong Women and Children Hospital, Guangzhou, China, [2] Guangdong Provincial Key Laboratory of Gastroenterology, Department of Gastroenterology, Nanfang Hospital, Southern Medical University, Guangzhou, China, [3] Department of Clinical Laboratory, Guangdong Women and Children Hospital, Guangzhou, China

OPEN ACCESS

Edited by:
María L. Couce, Complejo Hospitalario Universitario de Santiago, Spain

Reviewed by:
Patryk Lipiński, Children's Memorial Health Institute (IPCZD), Poland
Urh Groselj, University of Ljubljana, Slovenia

***Correspondence:**
Shu Liu
shmicy@163.com
Zhiqing Wang
wzq2001ing@163.com

[†] *These authors have contributed equally to this work*

Specialty section:
This article was submitted to Genetics of Common and Rare Diseases, a section of the journal Frontiers in Pediatrics

Received: *10 October 2021*
Accepted: *03 February 2022*
Published: *10 March 2022*

Citation:
Liu S, Wang Z, Zheng X, Zhang Y, Wei S, OuYang H, Liang J, Chen N, Zeng W and Jiang J (2022) Case Report: Successful Management of a 29-Day-Old Infant With Severe Hyperlipidemia From a Novel Homozygous Variant of GPIHBP1 Gene. Front. Pediatr. 10:792574. doi: 10.3389/fped.2022.792574

Background: Severe hyperlipidemia is characterized by markedly elevated blood triglyceride levels and severe early-onset cardiovascular diseases, pancreatitis, pancreatic necrosis or persistent multiple organ failure if left untreated. It is a rare autosomal recessive metabolic disorder originated from the variants of lipoprotein lipase gene, and previous studies have demonstrated that most cases with severe hyperlipidemia are closely related to the variants of some key genes for lipolysis, such as *LPL*, *APOC2*, *APOA5*, *LMF1*, and *GPIHBP1*. Meanwhile, other unidentified causes also exist and are equally worthy of attention.

Methods: The 29-day-old infant was diagnosed with severe hyperlipidemia, registering a plasma triglyceride level as high as 25.46 mmol/L. Whole exome sequencing was conducted to explore the possible pathogenic gene variants for this patient.

Results: The infant was put on a low-fat diet combined with pharmacological therapy, which was successful in restraining the level of serum triglyceride and total cholesterol to a low to medium range during the follow-ups. The patient was found to be a rare novel homozygous duplication variant-c.45_48dupGCGG (Pro17Alafs*22) in *GPIHBP1* gene-leading to a frameshift which failed to form the canonical termination codon TGA. The mutant messenger RNA should presumably produce a peptide consisting of 16 amino acids at the N-terminus, with 21 novel amino acids on the heels of the wild-type protein.

Conclusions: Our study expands on the spectrum of *GPIHBP1* variants and contributes to a more comprehensive understanding of the genetic diagnosis, genetic counseling, and multimodality therapy of families with severe hyperlipidemia. Our experience gained in this study is also contributory to a deeper insight into severe hyperlipidemia and highlights the importance of molecular genetic tests.

Keywords: severe hyperlipidemia, whole exome sequencing, *GPIHBP1* gene, novel variant, therapy

INTRODUCTION

Severe hyperlipidemia, with a typical feature of high concentration of lipidemia in fasting state, is primarily attributed to a genetic defect in intravascular lipolysis. Urgent clinical intervention is always required, especially for serious cases in that some severe complications, otherwise, may follow, such as pancreatitis, which contributes to 5–6% of the overall mortality, as well as pancreatic necrosis or persistent multiple organ failure that have been proved to be associated with the highest mortality rate (1). Amongst all the subtypes of severe hyperlipidemia, monogenic forms are the ones linked to the defects in metabolism of triglyceride (TG)-rich lipoproteins, namely lipolytic cascade. These defects may be caused by variants in no less than five different genes, predominantly (about 95%) inherited ones in both alleles of the lipoprotein lipase gene, which, aliased as *LPL* (2), is responsible for encoding of the enzyme lipoprotein lipase (LPL; OMIM #238600). Previous studies have shown that the defects directly related to *LPL* gene variants are also relevant to the majority of severe hyperlipidemia cases (3–6). The rest 5% are the results of variants in other genes involving in LPL functioning, including *APOC2* (encoding apolipoprotein CII, activator of LPL; OMIM #207750) (7, 8), *APOA5* (encoding apolipoprotein AV, activator of LPL; OMIM #144650) (9, 10), *LMF1* (encoding lipase maturation factor 1, a tissue factor triggering the secretion of functional LPL and hepatic lipase; OMIM #611761) (11, 12), and *GPIHBP1* (encoding glycosylphosphatidylinositol-anchored highdensity lipoprotein-binding protein 1, the molecular platform by which LPL is able to interact with TG-rich lipoproteins, apolipoprotein CII, and apolipoprotein AV on the endothelial surface of capillaries; OMIM #612757) (13, 14). Meanwhile, there are also other variants to be identified (3), and all these variants may result in LPL malfunction.

GPIHBP1, categorized as one of the lymphocyte antigen 6 (Ly6) family, is a capillary endothelial cell protein consisting of 184 aa. Being a critical protein for LPL transportation from the subendothelial spaces to capillary lumen, GPIHBP1 can promote lipolysis by working as the main site to bind LPL on endothelial surface (15). So, variants of *GPIHBP1* may disturb lipolysis process and thus result in severe hyperlipidemia. However, although previous studies so far have offered some leads to the lipolytic mechanism of GPIHBP1 and disclosed a handful of case reports concerning *GPIHBP1* variants, our understanding on *GPIHBP1*-deficient diseases is still to be deepened. In this study, we described the clinical features, genetic analysis and our hands-on experience of successful pharmacological management of a 29-day-old baby with abnormally elevated plasma TG (25.46 mmol/L), who was subsequently identified as a rare novel homozygous duplication variant in *GPIHBP1* gene as the cause of her severe hyperlipidemia.

Abbreviations: TG: triglyceride; TC: total cholesterol; HDL-C: high-density lipoprotein cholesterol; LDL-C: low-density lipoprotein cholesterol; LPL: lipoprotein lipase; APOC2: apolipoprotein CII; APOA5: apolipoprotein AV; LMF1: lipase maturation factor 1; GPIHBP1: glycosylphosphatidylinositol-anchored highdensity lipoprotein-binding protein 1; Ly6: lymphocyte antigen 6; MCT: medium chain triglycerides; TPN: total parenteral nutrition; WES: whole exome sequencing; BWA: Burrows-Wheeler Aligner; GATK: Genome Analysis Toolkit; SNVs: single-nucleotide variants; OMIM: Online Mendelian Inheritance in Man; FATHMM: Functional Analysis through Hidden Markov Models; CVD: cardiovascular disease.

MATERIALS AND METHODS

Plasma Lipid Profile Analysis

Blood samples were collected after fasting for 6 h. The levels of serum glucose (Glu), TG, TC, HDL, LDL, APO-A1, and APO-B were measured enzymatically using an automatic analyzer (ADVIA 2400, SIEMENS, Germany).

Genetic Analysis

Enlightened by the abnormal clinical findings, hereditary hyperlipidemia was taken into the pediatricians' consideration for further confirmation using whole exome sequencing (WES, Illumina, San Diego, CA, USA). Details of the experiments, mutation frequency investigation, variant verification, and assessment of the conservation of amino acid residues were displayed in the **Supplementary Material** (shown in **Supplementary Material**-genetic analysis). The pathogenicity of the sequence variants was interpreted according to the American College of Medical Genetics and Genomics/Association for Molecular Pathology (ACMG/AMP) guidelines (16, 17).

The study was approved by the Ethics Committee of Guangdong Women and Children Hospital. Written informed consent was obtained from the patient's legal guardian for the publication of any potentially identifiable images or data included in this article. All the procedures carried out in our study were strictly in accordance with the Declaration of Helsinki.

RETROSPECTIVE ANALYSIS OF PATIENT'S MEDICAL RECORDS CONCERNING DEMOGRAPHICS, CLINICAL SIGNS AND SYMPTOMS, RESULTS OF BIOCHEMICAL, AND GENETIC ANALYSIS

Clinical Information

The patient was a 29-day-old Chinese female infant with a chief complaint of "irritability, fever, vomiting and convulsion for 2 days," who was enrolled in our study after consultation in the pediatric clinic of our hospital. The patient responded poorly to the treatment in previous visits to her local hospitals due to the limited health care resources there, making her condition worsening with the time. Therefore, she was referred to our hospital and finally placed in the pediatric intensive care unit. The infant is the first child of the non-consanguineous parents, with a full-term birth weight of 2,600 g. After admission to hospital, a physical examination was performed in the wake of history collection. The height of this exclusively breastfed infant was 52 cm (22.6th percentile), and the weight 3.7 kg (16.9th percentile). Appearance of low weight, malnutrition, poor response to external stimuli, and somnolence were noticed. Movement range of the joints and muscular tension of the four limbs were normal. Abdominal palpation indicated

normal liver and spleen volume. After aggressive treatment, the infant was stabilized in vital signs, with physical examinations showing normal body temperature (axillary temperature, 37.1 degrees Celsius), normal muscle strength, muscle tension and physiological reflexes.

Unexpected discovery arose from milky blood sample (lactescent plasma) and the results of lipid testing (in fasting state), which revealed abnormally elevated TG (25.46 mmol/L; normal range, 0.46 to 2.28 mmol/L) as well as abnormal cholesterol metabolism-total cholesterol (TC, 14.53 mmol/L; normal range, 3.12 to 5.68 mmol/L), high-density lipoprotein cholesterol (HDL-C, 1.12 mmol/L; normal range, 0.91 to 2.18 mmol/L), and low-density lipoprotein cholesterol (LDL-C, 2.01 mmol/L; normal range, 1.28 to 3.41 mmol/L). The first therapeutic intervention for the infant was oral therapy free of long chain fatty acids, supplemented with high protein, high carbohydrate, and medium chain triglycerides (MCT), which lasted for 5 days but failed to control hyperlipidemia. Due to the potential risk of acute pancreatitis associated with high levels of plasma TG and the signs of hypoproteinemia as demonstrated by her low weight as well as a total serum protein and albumen of 51.2 and 28.8 g/L, respectively, enteral feeding was discontinued at the day when the baby was 1 month and 5 days old, and substituted by multimodality therapy including fasting, nasogastric drainage, total parenteral nutrition (TPN), and anti-infection treatment. After 7 days (1 month and 12 days old), plasma TG level decreased significantly to 1.50 mmol/L and TC to 9.66 mmol/L. Whereas, an evident rise in plasma TG up to 3.77 mmol/L was, again, detected after switching to breastfeeding for 5 days (1 month and 17 days old). So the infant was put on a low-lipid formula diet, mainly STOLLE milk powder (Stolle Milk Biologics International Incorporated, New Zealand), a kind of formula low in fat and high in protein with proper amount of water-soluble vitamins added (the details of dietary interventions was shown in **Supplementary Table 1**). As a result, the plasma TG level declined promptly, ending up at 2.92 mmol/ L when the infant was discharged from the hospital (2 month and 3 days old).

Considering the evidence of lipometabolic disturbance and presumed diagnosis of severe hyperlipidemia, the infant, after discharged, continued to be kept on a low-fat and high-carbohydrate protocol with proper amount of protein diet and supplementation of L-carnitine, coenzyme Q10 as well as water-soluble vitamins (B1, B2, B6, B12, C, and folic acid) during her treatment at home. Individualized dosage was given for her medication protocol and adjusted accordingly based on her clinical manifestation, the level of blood lipid, and other nutritional indicators (shown in **Supplementary Table 2**). Surveillance of her medical condition was also performed to avoid potential complications. Meanwhile, the infant continued to take examinations in our outpatient clinic, irregularly, on and off, because of poor compliance. In the follow-ups, the baby was monitored by serum TG, TC, HDL-C, LDL-C, apoprotein A1 (APO-A1), apoprotein B (APO-B), and glucose every 3 to 6 months (shown in **Supplementary Table 3**). Besides, evaluation of her physical development was conducted at a 3 month interval. The results revealed that the serum TG and TC kept fluctuating from low to medium levels (**Figure 1**), and in the last follow-up when the baby was 9 months old, she was 8.6 kg (42.2th

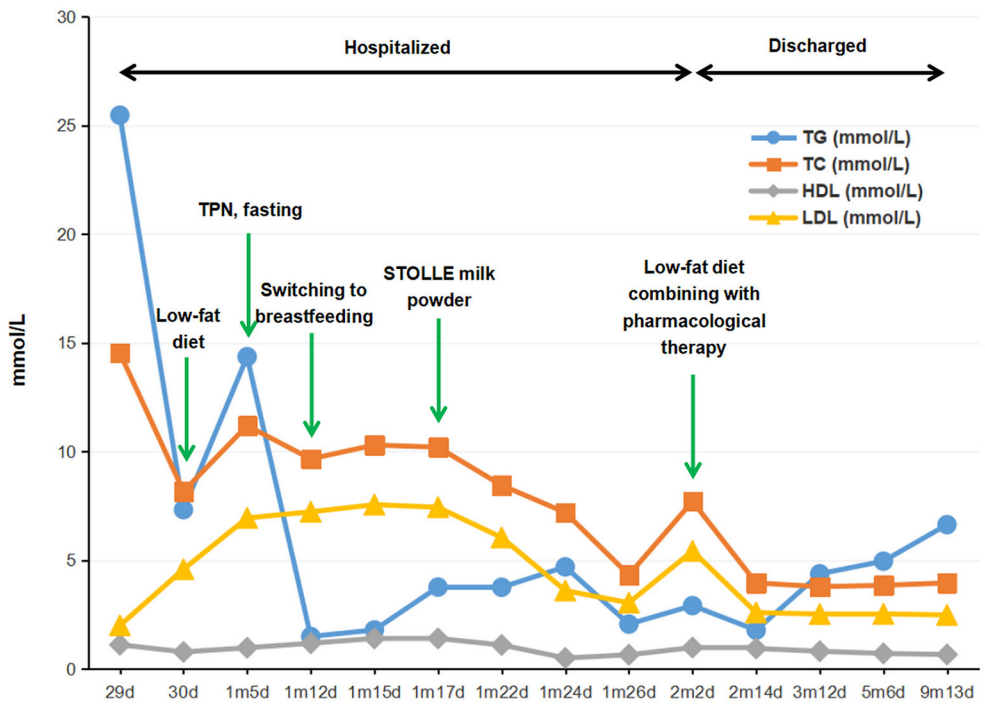

FIGURE 1 | Flow-chart illustrating the management procedure and the serum levels of TG, TC, HDL-C, and LDL-C of the proband. TG, triglyceride; TC, total cholesterol; HDL-C, high-density lipoprotein cholesterol; LDL-C, low-density lipoprotein cholesterol; TPN, total parenteral nutrition.

centile) in weight and 72 cm (56.1th centile) in height, with a head circumference of 44.5 cm (56.9th centile), indicating a good health and normal development. Likewise, laboratory tests also showed dramatic improvement as compared with her first visit, reflecting a sound developmental condition of the patient as well as the beneficial outcomes of this treatment protocol.

Based on the above findings and the latest research consensus (18), the baby was suspected of severe hereditary hyperlipidemia (triglyceride concentration >10 mmol/L), which is likely to have a monogenic cause, despite the fact that the patient's parents were healthy with normal levels of serum lipid and lipoprotein, and that the family history indicated neither hyperlipidemia nor pancreatitis. Therefore, aiming to identify the possible pathogenic gene variants for this infant, we performed this study using genetic analysis tools, with 100 Chinese healthy subjects recruited as the control group.

Genetic Findings

During hospitalization, the WES for this infant revealed the presence of a homozygous duplication variant-c.45_48dupGCGG (Pro17Alafs*22)-in exons 1 of *GPIHBP1* gene (**Figures 2A,B**). However, being heterozygote carriers of the variant, the parents did not show any symptoms of the disorder. This variant was computationally predicted to be deleterious and morbigenous by CADD, PROVEAN, and Mutation Taster. Results of bioinformatic analysis also strongly suggested it a disease-causing variant. Moreover, this variant was not detected in any of the 100 Chinese healthy subjects in the control group, and also had not been disclosed by any public databases as mentioned above, thus ruling out the possibility of a polymorphism and suggesting its novel and rare occurrence. Ultimately, the variant was identified as a pathogenic factor according to the Sherloc/ACMG criteria: it was not recorded in

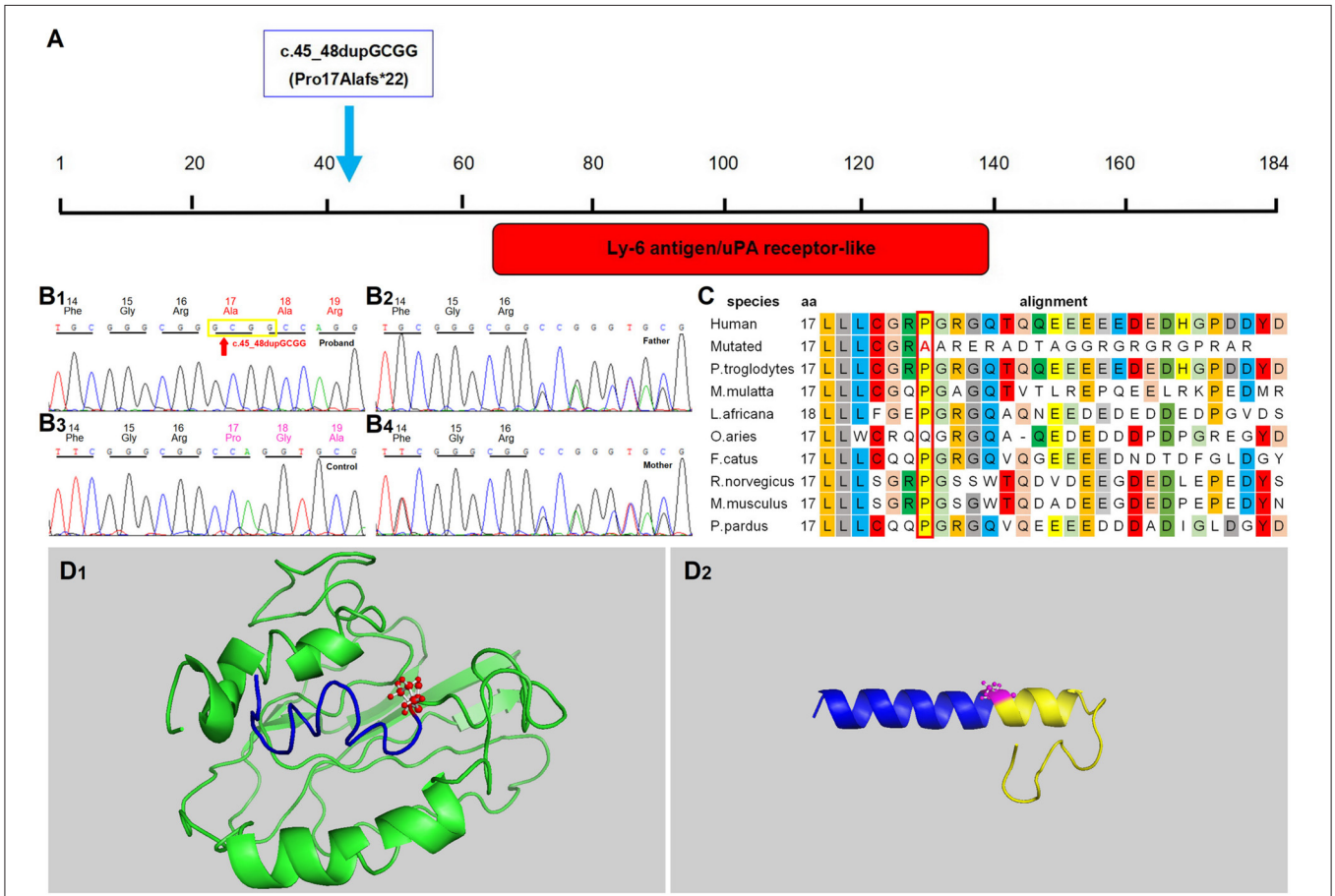

FIGURE 2 | Identification of the variant in *GPIHBP*1 gene. **(A)** Graphical view of the protein domain and structure of *GPIHBP*1. The red box stands for the Ly-6 antigen/uPA receptor-like domain (IPR016054). The homozygous variant c.45_48dupGCGG (p.Pro17Alafs*22) is marked by wathet blue arrow. **(B)** Sequence chromatograms of the *GPIHBP*1 variant. **(B1–B4)** indicates the variant sequences of c.45_48dupGCGG in the proband, his father, mother and normal controls, respectively. The duplication variant site is indicated by red arrow. **(C)** BLAST comparison of the sequence around amino acids 17 in orthologs of GPIHBP1 among various species. The block and colored characters represent highly conserved amino acids among these species, while the white shading stands for inconsistent residues. **(D)** Structural difference between wild-type and C-terminal frameshift GPIHBP1 proteins. Efforts were made to predict the functions of the mutant protein and the wild-type (full-length) GPIHBP1. The full length wild-type protein is exhibited in the left panel **(D1)**, and the mutant protein (p.Pro17Alafs*22) in the right panel **(D2)**. As shown in the mutant GPIHBP1 proteins **(D2)** model, the frameshift originated from p.Pro17Alafs*22 variant is highlighted in yellow, corresponding to the wild-type portion depicted in green **(D1)**. Meanwhile, the consistent part of the N-terminus of the wild-type and the mutant protein is show in blue. It can be seen that the variant compromises the original structure and integrity of the GPIHBP1 protein.

any of the existing population databases, and was assumed to be closely associated with a highly conserved amino acid, and also, to be disease-causing based on *in silico* algorithms used for pathogenicity prediction (17). In this case, the c.45_48dupGCGG duplication variant in exon 1 led to the substitution of the remaining 168 C-terminal amino acid residues with 21 mutant ones (**Figure 2D**), and the Ly-6 antigen/uPA receptor-like domain of this protein was also affected, thus likely to cause a direct impairment on the enzymatic activity of GPIHBP1. Meanwhile, the functional significance of the mutated amino acid is evident considering its high evolutionary conservation from mammals to invertebrates (**Figure 2C**). The outcomes from bioinformatic analysis strongly support that the novel homozygous variant c.45_48dupGCGG(Pro17Alafs*22) is with a disease-causing nature.

As far as we know, this is, in Chinese population, the first report of baby patient with hyperlipidemia due to *GPIHBP1* variant, and also the first case with the variant of c.45_48dupGCGG(Pro17Alafs*22) in *GPIHBP1* gene that was disclosed worldwide among patients with severe hyperlipidemia.

DISCUSSION

Clinical Management

In the present study, we delineated a 29-day-old female baby with incidentally found severe hereditary hyperlipidemia originated from a novel and homozygous *GPIHBP*1 duplication variant. During the treatment, the elevated blood lipid associated with a possible risk of pancreatitis was promptly reduced to a safe level, which, we believe, was attributed to the early detection of the abnormalities in this patient, as well as the timely and effectively clinical intervention. The further administrated low-fat diet combined with pharmacological therapy, a success in constraining the blood lipid within a lower range, was considered a key contributor to the normal and healthy development of the baby over time. As things stand, hereditary hyperlipidemia, being a kind of ultra-rare monogenic disease, was commonly spotted by blood serum screening among the suspects-adults and children with obesity, pancreatitis, or xanthoma. However, even the reported cases of little baby or infant with hereditary hyperlipidemia, which were actually very few, were always with a chief complaint of fever (19, 20), vomiting (21), irritability (20), hemoptysis (22), or jaundice (23) instead of something directly linking to a confirmed diagnosis of hyperlipidemia. Therefore, it was not uncommon that the disease, in some cases, was not even on the suspect list of the pediatricians in the first place. All these facts remind us that we should be more alert and sensitive to the clues (such as the results of lipid tests) hidden behind the common presentations of infancy hyperlipidemia-a disease worthy of higher attention and deeper research. Only in this way can proper diagnostic tools (such as genetic analysis) possibly be recruited for further identification. In this study, our findings from genetic analysis have revealed the key role of genetic defects as a predisposing factor of severe hereditary hyperlipidemia, which also sheds a new light on the complexity underlying the etiology of these phenotypes.

It has been known that there are various ways to treat hyperlipidemia, including low-fat diet, pharmacological therapy, and even plasma exchange. Which one to choose usually depends on the initial diagnosis and the progression of the disease. So far, plasma exchange with direct removal of blood lipid, having been mentioned in the category III of the American Society for Apheresis 2010 guidelines, has been wildly used for hyperlipidemia treatment. However, whether plasma exchange has a beneficial effect on severe hyperlipidemia is still in dispute. In contrast, quite a few single-center clinical studies have shown that the efficacy of conservative treatment is similar to plasma exchange in lowering the serum triglyceride level, and there is no substantial difference between the two approaches in the overall benefit, specifically in terms of morbidity and mortality (24–26). In addition, the blood lipid concentration may return to the pre-apheresis levels after plasma exchange, while low-fat formula diet collocated with pharmacological therapy may be more gentle and sustainable. Moreover, the lack of availability of plasma exchange in most of medical centers as well as its rather high costs also limits its use in clinical settings. As a result, invasive therapeutic options such as plasma exchange were not considered as the first-line treatment in this case.

During hospitalization, since the patient's TG level once raised up to 25.46 mmol/L, putting her at a high risk of pancreatitis, oral medication (low-fat diet) had been suspended and replaced by total parenteral nutrition till her condition was stable, followed by a low-fat diet in combination with pharmacological therapy. This therapeutic option was proved to be sufficient in rapidly reducing the plasma TG to a safe level, and in maintaining the serum TG and TC within a low to medium range, which was also a key factor to ensure the normal growth of the patient in the following months.

Molecular Analysis

As is known that elevated plasma triglyceride may, as an independent risk factor, lead to cardiovascular diseases (CVDs). LPL plays a critical role in lipid metabolism and energy balancing by hydrolyzing the triglyceride in blood circulation. Although it is parenchymal cells that synthesize and secret LPL, it somehow acts on the luminal capillary endothelium, so the mechanism of LPL migrating into the luminal capillary has long been among the list of relevant research (27). According to previous studies, hyperlipidemia was defined as two categories: severe (triglyceride concentration >10 mmol/L) and mild-to-moderate (triglyceride concentration 2–10 mmol/L). The former is more likely to have a monogenic cause triggered by gene variants which consequently cause LPL dysfunction (28–30). It has been understood that multiple factors can interact with LPL, positively or negatively, thus exerting an influence on TG lipolysis. Among them is a recently identified factor GPIHBP1, which is considered indispensible in transportation of LPL to the luminal capillary endothelium as well as in the establishment of the platform for TG hydrolysis (31). Currently, a large amount of evidence supports that GPIHBP1 functions in triglyceride-rich lipoprotein (TRL) metabolism of human in unique and diverse ways (32–34). Recent studies have shown that LPL mislocalization as a result of GPIHBP1 deficiency may cause severe hyperlipidemia (13, 35).

Therefore, the importance of GPIHBP1 in lipolysis is being recognized more widely with more relevant research published.

The human *GPIHBP1* gene consists of 4 exons which encode a 184 amino acid protein. An acidic domain being able to bind LPL and chylomicrons is located in the N-terminus of *GPIHBP1*. Its C-terminus is encoded by exons 3 and 4, including a cysteine-rich lymphocyte antigen 6 (Ly6) motif as well as a carboxylterminal hydrophobic sequence involved in the addition of a GPI anchor (36–39). A bunch of residues in the domain of C-terminus, such as Ser107, Thr124, and Leu135 also play a critical role in LPL binding and its transportation from subendothelial space to luminal capillary (40). Therefore, deleting exons 3 and 4 will produce a crippled protein characterized by the absence of a domain indispensible for LPL binding and translocation as well as for anchoring LPL to the cell surface. This makes sense of the phenotype in cases with severe hyperlipidemia and also explains the lack of circulating LPL and LPL activity in heparin-processed plasma. Since the initial description of hyperlipidemia resulting from the variant of *GPIHBP1* in 2007 (41), only about 50 cases have been reported worldwide (35, 42, 43). Meanwhile, the genotypic spectrum based on HGMD has recorded 47 various pathogenic variants in *GPIHBP1* that can result in severe hyperlipidemia, with most of them (33/47) identified as missense variants. Tendency of these variants toward any ethnicity or racial groups was not observed. Therefore, thorough analysis on these disease-causing variants probably linking to developmental malfunction and phenotypic changes is essential to pathogenesis clarifying and clinical treatment.

The patient in our study predominantly manifested fever, vomiting and convulsion, with unexpected discovery of severe hyperlipidemia and molecular genetic tests revealing the etiology. With the WES method, we found a novel homozygous variant, c.45_48dupGCGG(Pro17Alafs*22), in exons 1 of *GPIHBP1*, which, absent in all of the 100 healthy control samples, was inherited from both of her parents.

The c.45_48dupGCGG duplication variant in exon 1 may lead to the substitution of the remaining 168 C-terminal amino acid residues with 21 mutant ones, at a highly conserved position of this protein. Based on the clinical presentations, serum lipid level and bioinformatics study, an inference stood out from the potential pathogeneses that the disease of the proband was very likely to be attributed to the homozygous duplication variant, which, certainly, needs to be further verified by functional experiments in the future. Fortunately, these unexpected findings, together with timely and proper treatment, have resulted in a good prognosis observed in this patient. Furthermore, this orphan case gave us a lively lesson, and deepened our knowledge of this disease.

CONCLUSIONS

In this study, we presented a comprehensive delineation of the first-reported Chinese infant patient with severe hyperlipidemia whose condition was rooted in a novel homozygous variant of the *GPIHBP*1 gene. Our findings reveal that routine blood biochemical tests are crucial to the diagnosis, and by molecular genetic testing, an integral part of the tools for a confirmed diagnosis, the role of genetic defects as a vital predisposing factor can be identified in severe hereditary hyperlipidemia.

DATA AVAILABILITY STATEMENT

The raw data supporting the conclusions of this article will be made available by the authors, without undue reservation.

ETHICS STATEMENT

Written informed consent was given by the parents for the publication of all associated data and images.

AUTHOR CONTRIBUTIONS

XZ and YZ made a great contribution to the study design and also worked as two of the major participants in genetic analyses and manuscript drafting. SW and HO were responsible for the patient's management and data collection. JL and NC conducted the whole exome sequencing, variant verification, and bioinformatics analysis of the variants. WZ and JJ performed clinical routine biochemistry tests. SL and ZW conceived the study, at the same time worked as coordinators in this study, and assisted in manuscript drafting. All the authors have reviewed, provided comments, and approved the manuscript as the final version.

FUNDING

This research was funded by Natural Science Foundation of Guangdong Province (No. 2021A1515010969) and Research Project of Traditional Chinese Medicine Bureau of Guangdong Province (No. 20211046). The sponsors were not involved in study design, data analyzing or interpreting. Neither did they contribute to developing the report.

ACKNOWLEDGMENTS

We are indebted to all doctors, nurses, and researchers for the follow-up assessment and data collection in the Children Inherited Metabolism and Endocrine Department, Guangdong Women and Children Hospital.

SUPPLEMENTARY MATERIAL

The Supplementary Material for this article can be found online at: https://www.frontiersin.org/articles/10.3389/fped.2022.792574/full#supplementary-material

REFERENCES

1. Hutchison B, Collins J, Makar RS, Dzik W. Retrospective analysis of outcomes in patients with acute hypertriglyceridemic pancreatitis treated without therapeutic plasma exchange. *Transfusion.* (2021) 61:537–45. doi: 10.1111/trf.16214
2. Brahm A, Hegele RA. Hypertriglyceridemia. *Nutrients.* (2013) 5:981–1001. doi: 10.3390/nu5030981
3. Falko JM. Familial chylomicronemia syndrome: a clinical guide for endocrinologists. *Endocr Pract.* (2018) 24:756–63. doi: 10.4158/EP-2018-0157
4. Gotoda T, Shirai K, Ohta T, Research Committee for Primary Hyperlipidemia, Research on Measures against Intractable Diseases by the Ministry of Health, Labour and Welfare in Japan. Diagnosis and management of type I and type V hyperlipoproteinemia. *J Atheroscler Thromb.* (2012) 19:1–12. doi: 10.5551/jat.10702
5. Taghizadeh E, Ghayour-Mobarhan M, Ferns GA, Pasdar A. A novel variant in *LPL* gene is associated with familial combined hyperlipidemia. *Biofactors.* (2020) 46:94–9. doi: 10.1002/biof.1570
6. Péterfy M, Bedoya C, Giacobbe C, Pagano C, Gentile M, Rubba P, et al. Characterization of two novel pathogenic variants at compound heterozygous status in lipase maturation factor 1 gene causing severe hypertriglyceridemia. *J Clin Lipidol.* (2018) 12:1253–9. doi: 10.1016/j.jacl.2018.07.008
7. Okubo M, Toromanovic A, Ebara T, Murase T. Apolipoprotein C-II Tuzla: a novel large deletion in *APOC2* caused by Alu-Alu homologous recombination in an infant with apolipoprotein C-II deficiency. *Clin Chim Acta.* (2015) 438:148–53. doi: 10.1016/j.cca.2014.08.022
8. Xenoulis PG, Tate NM, Bishop MA, Steiner JM, Suchodolski JS, Furrow E. Sequence analysis of the coding regions of the apolipoprotein C2 (APOC2) gene in Miniature Schnauzers with idiopathic hypertriglyceridemia. *Vet J.* (2020) 265:105559. doi: 10.1016/j.tvjl.2020.105559
9. Ariza MJ, Rioja J, Ibarretxe D, Spanish Dyslipidemia Registry. Molecular basis of the familial chylomicronemia syndrome in patients from the National Dyslipidemia Registry of the Spanish Atherosclerosis Society. *J Clin Lipidol.* (2018) 12:1482–92.e3. doi: 10.1016/j.atherosclerosis.2018.06.161
10. Wójcik C, Fazio S, McIntyre AD, Hegele RA. Co-occurrence of heterozygous *CREB3L3* and *APOA5* nonsense variants and polygenic risk in a patient with severe hypertriglyceridemia exacerbated by estrogen administration. *J Clin Lipidol.* (2018) 12:1146–150. doi: 10.1016/j.jacl.2018.05.014
11. Chen WW, Yang Q, Li XY, Shi XL, Pu N, Lu GT, et al. Identification of a novel and heterozygous *LMF1* nonsense mutation in an acute pancreatitis patient with severe hypertriglyceridemia, severe obesity and heavy smoking. *Lipids Health Dis.* (2019) 18:68. doi: 10.1186/s12944-019-1012-9
12. Serveaux Dancer M, Di Filippo M, Marmontel O, Valéro R, Piombo Rivarola MDC, Peretti N, et al. New rare genetic variants of *LMF1* gene identified in severe hypertriglyceridemia. *J Clin Lipidol.* (2018) 12:1244–52. doi: 10.1016/j.jacl.2018.06.018
13. Lima JG, Helena C Nobrega L, Moura Bandeira FT, Pires Sousa AG, Medeiros de Araujo Macedo TB, Cavalcante Nogueira AC, et al. A novel *GPIHBP1* mutation related to familial chylomicronemia syndrome: a series of cases. *Atherosclerosis.* (2021) 322:31–8. doi: 10.1016/j.atherosclerosis.2021.02.020
14. Paquette M, Hegele RA, Paré G, Baass A. A novel mutation in *GPIHBP1* causes familial chylomicronemia syndrome. *J Clin Lipidol.* (2018) 12:506–10. doi: 10.1016/j.jacl.2018.01.011
15. Ioka RX, Kang MJ, Kamiyama S, Kim DH, Magoori K, Kamataki A, et al. Expression cloning and characterization of a novel glycosylphosphatidylinositol-anchored high density lipoprotein-binding protein, GPI-HBP1. *J Biol Chem.* (2003) 278:7344–9. doi: 10.1074/jbc.M211932200
16. Davydov EV, Goode DL, Sirota M, Cooper GM, Sidow A, Batzoglou S. Identifying a high fraction of the human genome to be under selective constraint using GERP++. *PLoS Comput Biol.* (2010) 6:e1001025. doi: 10.1371/journal.pcbi.1001025
17. Richards S, Aziz N, Bale S, ACMG Laboratory Quality Assurance Committee. Standards and guidelines for the interpretation of sequence variants: a joint consensus recommendation of the American College of Medical Genetics and Genomics and the Association for Molecular Pathology. *Genet Med.* (2015) 17:405–24. doi: 10.1038/gim.2015.30
18. Hegele RA, Ginsberg HN, Chapman MJ, Nordestgaard BG, Kuivenhoven JA, Averna M, et al. European Atherosclerosis Society Consensus Panel. The polygenic nature of hypertriglyceridaemia: implications for definition, diagnosis, and management. *Lancet Diabetes Endocrinol.* (2014) 2:655–66. doi: 10.1016/S2213-8587(13)70191-8
19. Ahmad Z, Wilson DP. Familial chylomicronemia syndrome and response to medium-chain triglyceride therapy in an infant with novel mutations in GPIHBP1. *J Clin Lipidol.* (2014) 8:635–9. doi: 10.1016/j.jacl.2014.08.010
20. Jung MK, Jin J, Kim HO, Kwon A, Chae HW, Kang SJ, et al. A 1-month-old infant with chylomicronemia due to GPIHBP1 gene mutation treated by plasmapheresis. *Ann Pediatr Endocrinol Metab.* (2017) 22:68–71. doi: 10.6065/apem.2017.22.1.68
21. Avis HJ, Scheffer HJ, Kastelein JJ, Dallinga-Thie GM, Wijburg FA. Pink-creamy whole blood in a 3-month-old infant with a homozygous deletion in the lipoprotein lipase gene. *Clin Genet.* (2010) 77:430–3. doi: 10.1111/j.1399-0004.2009.01369.x
22. Stefanutti C, Gozzer M, Pisciotta L, D'Eufemia P, Bosco G, Morozzi C, et al. A three month-old infant with severe hyperchylomicronemia: molecular diagnosis and extracorporeal treatment. *Atheroscler Suppl.* (2013) 14:73–6. doi: 10.1016/j.atherosclerosissup.2012.10.020
23. Buonuomo PS, Bartuli A, Rabacchi C, Bertolini S, Calandra S. A 3-day-old neonate with severe hypertriglyceridemia from novel mutations of the GPIHBP1 gene. *J Clin Lipidol.* (2015) 9:265–70. doi: 10.1016/j.jacl.2014.10.003
24. Dichtwald S, Meyer A, Zohar E, Ifrach N, Rotlevi G, Fredman B. Hypertriglyceridemia Induced Pancreatitis: plasmapheresis or conservative management? *J Intensive Care Med.* (2021) 3:1–5. doi: 10.1177/08850666211054365
25. Chen Z, Huang X, Zhang M, Han N, Ning Y. Rapid reduction in triglyceride levels by therapeutic plasma exchange in patients with hypertriglyceridemic pancreatitis. *J Clin Apher.* (2021) 37:82–90. doi: 10.1002/jca.21954
26. Valdivielso P, Ramírez-Bueno A, Ewald N. Current knowledge of hypertriglyceridemic pancreatitis. *Eur J Intern Med.* (2014) 25:689–94. doi: 10.1016/j.ejim.2014.08.008
27. Olivecrona G. Role of lipoprotein lipase in lipid metabolism. *Curr Opin Lipidol.* (2016) 27:233–41. doi: 10.1097/MOL.0000000000000297
28. Gill PK, Dron JS, Dilliott AA, McIntyre AD, Cao H, Wang J, et al. Ancestry-specific profiles of genetic determinants of severe hypertriglyceridemia. *J Clin Lipidol.* (2021) 15:88–96. doi: 10.1016/j.jacl.2020.11.007
29. Yang Q, Pu N, Li XY, Shi XL, Chen WW, Zhang GF, et al. Digenic Inheritance and Gene-Environment Interaction in a Patient With Hypertriglyceridemia and Acute Pancreatitis. *Front Genet.* (2021) 12:640859. doi: 10.3389/fgene.2021.640859
30. Dron JS, Hegele RA. Genetics of hypertriglyceridemia. *Front Endocrinol.* (2020) 11:455. doi: 10.3389/fendo.2020.00455
31. Beigneux AP, Davies BS, Gin P, Weinstein MM, Farber E, Qiao X, et al. Glycosylphosphatidylinositol-anchored high-density lipoprotein-binding protein 1 plays a critical role in the lipolytic processing of chylomicrons. *Cell Metab.* (2007) 5:279–91. doi: 10.1016/j.cmet.2007.02.002
32. Meng X, Zeng W, Young SG, Fong LG. GPIHBP1, a partner protein for lipoprotein lipase, is expressed only in capillary endothelial cells. *J Lipid Res.* (2020) 61:591. doi: 10.1194/jlr.ILR120000735
33. Young SG, Fong LG, Beigneux AP, Allan CM, He C, Jiang H, et al. *GPIHBP1* and lipoprotein lipase, partners in plasma triglyceride metabolism. *Cell Metab.* (2019) 30:51–65. doi: 10.1016/j.cmet.2019.05.023
34. Liu C, Li L, Guo D, Lv Y, Zheng X, Mo Z, et al. Lipoprotein lipase transporter GPIHBP1 and triglyceride-rich lipoprotein metabolism. *Clin Chim Acta.* (2018) 487:33–40. doi: 10.1016/j.cca.2018.09.020
35. Rabacchi C, D'Addato S, Palmisano S, Lucchi T, Bertolini S, Calandra S, et al. Clinical and genetic features of 3 patients with familial chylomicronemia due to mutations in *GPIHBP1* gene. *J Clin Lipidol.* (2016) 10:915–21. doi: 10.1016/j.jacl.2016.03.009
36. Larsson M, Allan CM, Heizer PJ, Tu Y, Sandoval NP, Jung RS, et al. Impaired thermogenesis and sharp increases in plasma triglyceride levels in GPIHBP1-deficient mice during cold exposure. *J Lipid Res.* (2018) 59:706–13. doi: 10.1194/jlr.M083832
37. Surendran RP, Udayyapan SD, Clemente-Postigo M, Havik SR, Schimmel AWM, Tinahones F, et al. Decreased GPIHBP1 protein levels in visceral adipose tissue partly underlie the hypertriglyceridemic phenotype in insulin

resistance. *PLoS ONE.* (2018) 13:e0205858. doi: 10.1371/journal.pone.0205858

38. Allan CM, Jung CJ, Larsson M, Heizer PJ, Tu Y, Sandoval NP, et al. Mutating a conserved cysteine in *GPIHBP1* reduces amounts of GPIHBP1 in capillaries and abolishes LPL binding. *J Lipid Res.* (2017) 58:1453–61. doi: 10.1194/jlr.M076943
39. Birrane G, Beigneux AP, Dwyer B, Strack-Logue B, Kristensen KK, Francone OL, et al. Structure of the lipoprotein lipase-GPIHBP1 complex that mediates plasma triglyceride hydrolysis. *Proc Natl Acad Sci USA.* (2019) 116:1723–32. doi: 10.1073/pnas.1817984116
40. Beigneux AP, Davies BS, Tat S, Chen J, Gin P, Voss CV, et al. Assessing the role of the glycosylphosphatidylinositol-anchored high density lipoprotein-binding protein 1 (*GPIHBP1*) three-finger domain in binding lipoprotein lipase. *J Biol Chem.* (2011) 286:19735–43. doi: 10.1074/jbc.M111.242024
41. Wang J, Hegele RA. Homozygous missense mutation (G56R) in glycosylphosphatidylinositol-anchored high-density lipoprotein-binding protein 1 (*GPI-HBP1*) in two siblings with fasting chylomicronemia (MIM 144650). *Lipids Health Dis.* (2007) 6:23. doi: 10.1186/1476-511X-6-23
42. Hegele RA, Berberich AJ, Ban MR, Wang J, Digenio A, Alexander VJ, et al. Clinical and biochemical features of different molecular etiologies of familial chylomicronemia. *J Clin Lipidol.* (2018) 12:920–7.e4. doi: 10.1016/j.jacl.2018.03.093
43. Ariza MJ, Martínez-Hernández PL, Ibarretxe D, Rabacchi C, Rioja J, Grande-Aragón C, et al. Novel mutations in the *GPIHBP1* gene identified in 2 patients with recurrent acute pancreatitis. *J Clin Lipidol.* (2016) 10:92–100.e1. doi: 10.1016/j.jacl.2015.09.007

Conflict of Interest: The authors declare that the research was conducted in the absence of any commercial or financial relationships that could be construed as a potential conflict of interest.

Publisher's Note: All claims expressed in this article are solely those of the authors and do not necessarily represent those of their affiliated organizations, or those of the publisher, the editors and the reviewers. Any product that may be evaluated in this article, or claim that may be made by its manufacturer, is not guaranteed or endorsed by the publisher.

frontiers in Genetics

CASE REPORT
published: 17 March 2022
doi: 10.3389/fgene.2022.807822

Case Report: Novel Mutations in the *PCCB* Gene Causing Late-Onset Propionic Acidemia

*Guang Ji, Yaling Liu, Xueqin Song and Zhenfei Li**

Department of Neurology, Second Hospital of Hebei Medical University, Shijiazhuang, China

Introduction: Propionic acidemia is an autosomal recessive metabolic disorder and the patients with adult onset are very rare.

Methods: Two PCCB mutations were identified. Clinical data were collected from a patient, and metabolic screening and clinical exome sequencing analysis were performed.

Results: Two novel mutations were identified in the PCCB gene: M1:c.404_406del: p.G135del and M2:c.632C>T:p.T211I.

Conclusion: Late-onset propionic acidemia should be taken into account, and metabolic screening as well as gene analysis should be performed to make a definite diagnosis timely.

Keywords: PCCB gene, novel mutation, late onset, propionic acidemia, clinical exome sequencing

OPEN ACCESS

Edited by:
Emiliano González Vioque, University Clinical Hospital of Santiago, Spain

Reviewed by:
Pawel Swietach, University of Oxford, United Kingdom
Michael V. Osier, Rochester Institute of Technology, United States

****Correspondence:***
Zhenfei Li
54907714@qq.com

Specialty section:
This article was submitted to Genetics of Common and Rare Diseases, a section of the journal Frontiers in Genetics

Received: *02 November 2021*
Accepted: *10 January 2022*
Published: *17 March 2022*

Citation:
Ji G, Liu Y, Song X and Li Z (2022) Case Report: Novel Mutations in the PCCB Gene Causing Late-Onset Propionic Acidemia. Front. Genet. 13:807822. doi: 10.3389/fgene.2022.807822

INTRODUCTION

Propionic acidemia (PA) is an autosomal recessive disorder of organic acid metabolism caused by the accumulation of toxic metabolites. It is due to the deficiency of the mitochondrial enzyme propionyl-CoA carboxylase (PCC), which catalyzes the carboxylation of propionyl-CoA to methylmalonyl-CoA (Wongkittichote et al., 2017). PCC is an α6β6 multimer composed of α and β subunits, encoded by the genes of *PCCA* and *PCCB*, respectively (Campeau et al., 2001). The main function of PCC is to accelerate the conversion of propionyl-CoA to methylmalonyl-CoA.

According to the time of onset, PA can be divided into neonatal onset and late onset. The clinical manifestations are varied and lack of specificity. Neonatal-onset PA is within 1 year old. It is normal at birth and occurs a few days later. The initial symptoms are feeding difficulties, vomiting, dehydration, hypothermia, lethargy, hypotonia, convulsion, and dyspnea. If not treated in time, the condition will aggravate, with ketosis, metabolic acidosis, hyperammonemia, and coma.

Individuals with late-onset PA exhibit significant differences in clinical manifestations, which can occur from 1-year old to adulthood. The common early manifestations are anorexia, growth retardation, convulsion, hypotonia, and abnormal mental behavior. The acute metabolic crisis is often induced by fever, hunger, a high protein diet, and infection. The accumulation of organic acid metabolites, such as propionic acid, often causes bone marrow suppression, anemia, granulocytopenia, and thrombocytopenia, prone to infection and bleeding. Very few patients can also show optic nerve atrophy, hearing loss, chronic renal failure, and premature ovarian failure.

Here we report a patient with PA who was screened by tandem mass spectrometry (MS/MS) and urine gas chromatography MS. Using clinical exome sequencing (CES) analysis, two novel mutations in the *PCCB* gene were found in the patient.

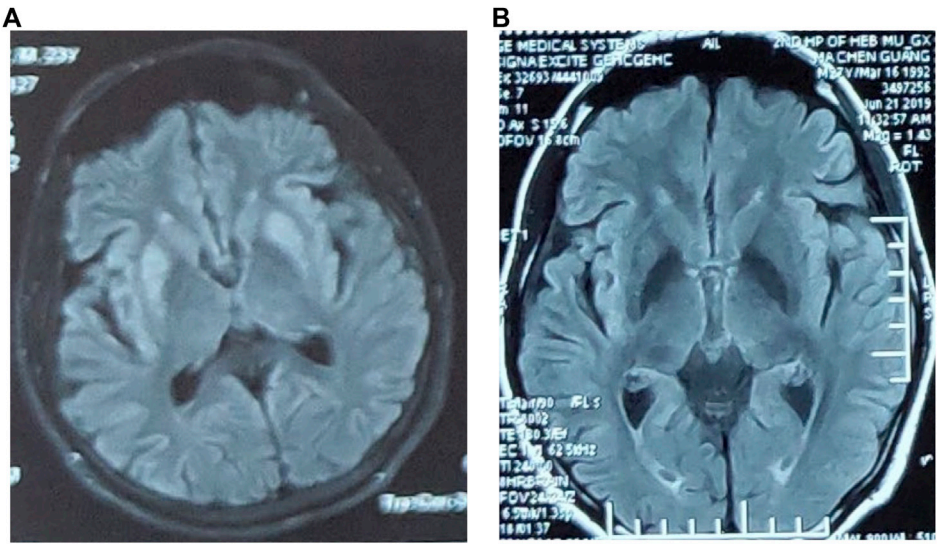

FIGURE 1 | (A) Brain MRI showed symmetrical abnormal signals in bilateral basal ganglia. **(B)** The abnormal signal in the bilateral basal ganglia in the brain MRI disappeared.

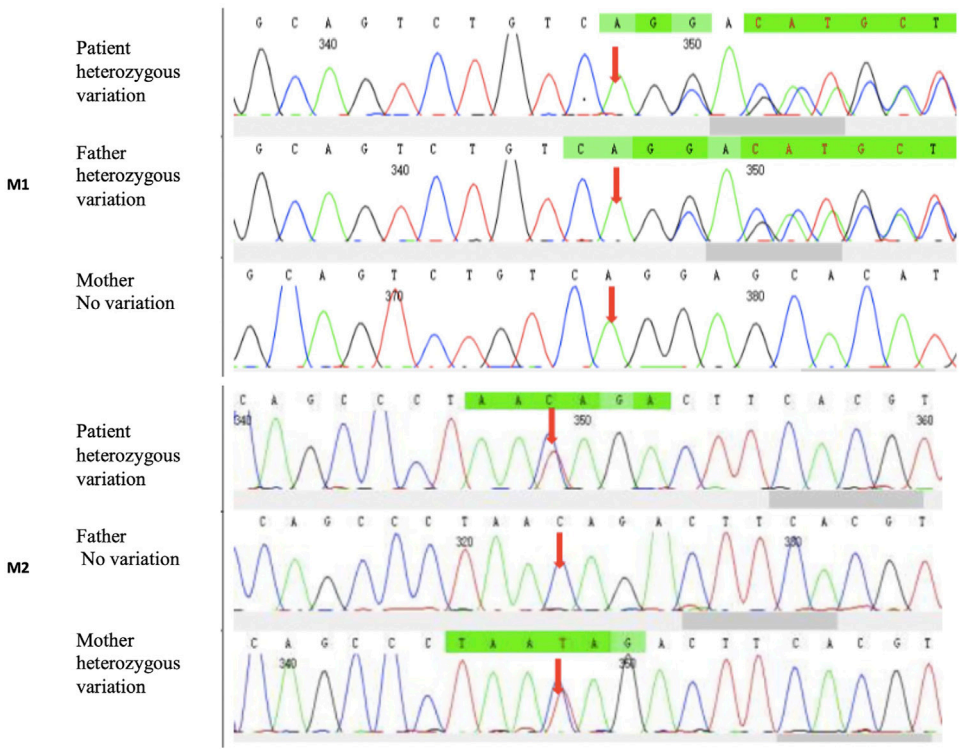

FIGURE 2 | CES identified one heterozygous deletion mutation. M1: c.404_406del:p.G135del and one heterozygous missense mutation. M2: c.632C>T:p.T211I. Sanger sequencing results showed that the mutations M1 and M2 were inherited from the father and mother, respectively.

CASE REPORT

The patient was the only child in the family. The birth and development of the patient were normal. He felt tired in his lower limbs with lumbago after a long-distance walk from the age of 22 years (**Table 1**). After a lot of exercises or a high-protein-diet intake, he developed nausea, vomiting, and, in severe cases, unconsciousness. On physical examination, the

TABLE 1 | The timeline with relevant data from the episode of care.

Time	Episode of care	Treatment and prognosis
2015.12	First onset	Protein-restricted diet and treatment of reducing ammonia; improvement of symptoms
2019.6	Second onset	Reducing-ammonia treatment; symptoms improved again
2019.10	Third onset	Cardiotonic and diuretic treatment; symptoms worsened
2019.11	Metabolic acidosis	Correct acidosis; dead

patient was alert and oriented, and no obvious abnormality was found in the nervous system examination.

The results of liver function showed an increased level of blood ammonia (98.9 μmol/L; normal range, 6–35 μmol/L) and a decreased level of ceruloplasmin (0.144 μmol/L; normal range, 6–35 μmol/L). Cerebrospinal fluid analysis showed normal cell count of 1/mm^3 (normal <5/mm^3), a decreased glucose of 3 mmol/L (normal range, 3.6–4.5 mmol/L), and a normal total protein of 35 mg/dL (normal value, <45 mg/dL). Brain magnetic resonance imaging (MRI) showed symmetrical abnormal signals in bilateral basal ganglia (**Figure 1A**). Electromyogram was normal.

After a protein-restricted diet and treatment of reducing ammonia, the symptoms of weakness in lower limbs and lumbago were once relieved. However, at the age of 26 years, he again developed nausea, vomiting, and diarrhea, followed by numbness and weakness of both lower limbs and transient unconsciousness in severe cases when walking (**Table 1**). The blood ammonia increased to 108 μmol/L, whereas the abnormal signal in bilateral basal ganglia of brain MRI disappeared (**Figure 1B**). The symptoms improved again after reducing-ammonia treatment. Four months later (**Table 1**), the patient developed chest tightness, dyspnea, and general fatigue. The blood gas analysis showed pH 7.438, P_{CO_2} 26.2 mm Hg, and P_{O_2} 105.2 mm Hg. Increased level of troponin (0.51 ng/mL) and brain natriuretic peptide (266 ng/mL) was also detected. Echocardiography showed noncompaction of the myocardium and normal left ventricular systolic function. After admission, the patient's symptoms gradually worsened with unconsciousness and irritability. The blood gas analysis upon admission showed pH 7.007, P_{CO_2} 22.6 mm Hg, and lactate 20.05 mmol/L, which indicated metabolic acidosis. After correction of acidosis and ventilator-assisted respiration, the patient did not respond to the treatment and died at last (**Table 1**).

The level of propionyl carnitine was 8.71 μM (normal range, 0.30–5.00 μM). The ratio of propionyl carnitine to acetyl carnitine was 0.33 (normal range, 0.02–0.20). The increase in these indicators suggested methylmalonic acidemia or PA. By urine organic acid analysis, elevated indicators of hydroxypropionate 23.8 (normal range, 0–4.0 (μ)mol/mol creatinine), propionyl glycine 7.8 (normal range, 0–0.4 (μ)mol/mol creatinine), and methyl citrate 33.9 (normal range, 0.0–0.7 (μ)mol/mol creatinine) were detected, whereas methylmalonic acid (0.0 (μ) mol/mol creatinine) was not present in the urine sample. The above results indicated the diagnosis of PA.

Clinical Exome Sequencing

Peripheral blood was obtained from the patient and his parents. DNA was isolated from peripheral leukocytes using a commercial kit (TIANGEN, China). The quantity/quality of DNA was assessed using Onedrop OD1000 spectrophotometer and by agarose gel electrophoresis. CES analysis was done in Shanghai We-Health Biomedical Technology Co., Ltd.

Two heterozygous mutations of *PCCB* were identified in the patient. According to the ACMG standards and guidelines for the interpretation of sequence variants, the clinical significance of these two mutations was still uncertain. The two *PCCB* mutations were confirmed by Sanger sequencing.

CES identified one heterozygous deletion mutation M1: c.404_406del:p.G135del, which resulted in the deletion of amino acid at position 153 in the *PCCB* gene but did not cause frameshift. Another missense mutation M2: c.632C>T: p.T211I, resulted in the change of codon 211 in the *PCCB* gene from threonine to isoleucine. Both mutations are novel. Sanger sequencing results confirmed that the mutations M1 and M2 were inherited from the father and mother, respectively (**Figure 2**). The results above indicated that the proband's healthy parents were heterozygous carriers. The abnormality of the *PCCB* gene can lead to autosomal recessive PA.

DISCUSSION

The dysfunctions of PCC cause propionyl-CoA accumulation in the body and produce a large number of abnormal metabolites (propionic acid, 3-hydroxypropionate, and methyl citrate) by activating the bypass metabolic pathway. Abnormal metabolites can produce a series of clinical symptoms, including feeding difficulties, vomiting, lethargy, coma, metabolic acidosis, and hyperammonemia.

According to the occurrence of the first symptoms, PA can be divided into early-onset (first symptoms occurred within 28 days of life) and late-onset (symptoms started after the neonatal period). Most PA patients develop symptoms within 1 year of age (Lehnert et al., 1994; Van der Meer et al., 1996). Very few patients have the first symptom after 1-year of age (Nyhan et al., 1999; Perezcerda, 2004). In this case, the first symptoms appeared at the age of 22 years.

The clinical and biochemical picture of late-onset PA is more heterogeneous. Clinical findings, neuroimaging, and neuropathology show a high frequency of basal ganglia lesions in late-onset PA patients (Hamilton et al., 1995; Bergman et al., 1996). While the pathogenesis of the basal ganglia abnormalities is not clear, a possible explanation is that the basal ganglia region is of high energy metabolism, which is more vulnerable to disease than other regions. Hyperammonemia may be one of the causes of basal ganglia damage. Studies have found that organic acids and hyperammonemia can cause brain damage in rats, including

vacuolization, ischemic neurons, and pericellular edema (Viegas et al., 2014). In this case, the abnormal signals in bilateral basal ganglia of brain MRI disappeared after he received reducing-ammonia treatment, which also suggests the close relations between hyperammonemia and the damage of basal ganglia.

Another typical clinical manifestation of the patient was fatigue intolerance. When the patient walked 100 m, he felt tired and needed a rest. This feature is similar to the manifestation of metabolic myopathy. Some studies have found that patients with PA had impaired lipolysis, blunted fatty acid oxidation (FAO), a compensatory increase in carbohydrate utilization, and low work capacity (Storgaard et al., 2020). In normal people, the level of palmitate and free fatty acid (FFA) increased after exercise, but in PA patients, the increase in palmitate and FFA was not obvious. Impaired lipolysis, lack of substrates for FAO, low plasma carnitine concentration, and impaired TCA cycle are most likely to cause the blunted increase in palmitate oxidation and total FAO. As a result, PA patients rely more on carbohydrates as an energy source than healthy people. Similarly, the low work capacity in PA patients may also be ascribed to a shortage of substrates in the TCA cycle. These findings are similar to those reported in a patient with neutral lipid storage disease, which suggests that PA should be added to the list of metabolic myopathies (Laforêt et al., 2012).

PA is a serious, life-threatening metabolic disorder, and several related complications have been described in cases published before. Cardiac complications have been observed in PA including cardiomyopathy and arrhythmias. Cardiomyopathy, dilated usually, has been described in several PA patients, and the age at onset ranged between 4 weeks of age and adulthood, although a portion of the patients were diagnosed during a metabolic crisis (Pena et al., 2012). Echocardiography did not find dilated cardiomyopathy in this patient but showed noncompaction myocardium. Unfortunately, before the results of the metabolic screening and CES analysis, the patient developed cardiac shock during hospitalization and died of circulatory failure within a few days, which may be caused by the myocardial damage involved in the metabolic crisis.

We found two novel compound heterozygous mutations in the PCCB gene causing late-onset PA, including a deletion mutation, which resulted in the deletion of amino acid at position 153 of the *PCCB* gene, but did not shift the frame, and a missense mutation in the *PCCB* gene, which resulted in the change of codon 211 of the *PCCB* gene from threonine to isoleucine. These two novel mutations may be related to mild impairment of PCC function so that clinical symptoms occurred late. Most affected individuals of PA are compound heterozygotes (Pena et al., 2012). The majority of these mutations were missense mutations (40%), followed by small insertions/deletions and splicing mutations. There is a strong relationship between the genotype and phenotype observed in many cases of PA; some were found to affect the protein function and were associated with an early onset and severe clinical phenotype; on the other hand, some were found with mild phenotypes (Zayed, 2015). However, the fact that compound heterozygosity is present in the majority of patients makes it difficult to establish genotype–phenotype correlations; furthermore, population-specific mutations may exist, and it is hard to predict their effect on other ethnic groups with different genetic makeup (Zayed, 2015).

PA at adult onset is very rare. If the patient presents with fatigue intolerance, disturbance of consciousness, hypotonia, seizures, ataxia, vomiting, neutropenia, and thrombocytopenia, this disease should be taken into consideration. Screening of organic acid metabolism in blood and urine as well as gene analysis should be performed to make a definite diagnosis timely.

Statement: The appropriate intervention was not possible as the patient died before the diagnosis could be completed.

DATA AVAILABILITY STATEMENT

The datasets for this article are not publicly available due to concerns regarding participant/patient anonymity. Requests to access the datasets should be directed to the corresponding author.

ETHICS STATEMENT

The studies involving human participants were reviewed and approved by the approved by the Ethics Committee of the second Hospital of HeBei medical university. The patients/participants provided their written informed consent to participate in this study. Written informed consent was obtained from the individual(s) for the publication of any potentially identifiable images or data included in this article.

AUTHOR CONTRIBUTIONS

ZL Collect case data and write papers GJ writer papers XS supervisor to advise on the writing papers YL adviser.

REFERENCES

Bergman, A. J. I. W., Van der Knaap, M. S., Smeitink, J. A. M., Duran, M., Dorland, L., Valk, J., et al. (1996). Magnetic Resonance Imaging and Spectroscopy of the Brain in Propionic Acidemia: Clinical and Biochemical Considerations. *Pediatr. Res.* 40, 404–409. doi:10.1203/00006450-199609000-00007

Campeau, E., Desviat, L. R., Leclerc, D., Wu, X., Pérez, B., Ugarte, M., et al. (2001). Structure of the Pcca Gene and Distribution of Mutations Causing Propionic Acidemia. *Mol. Genet. Metab.* 74, 238–247. doi:10.1006/mgme.2001.3210

Hamilton, R. L., Haas, R. H., Nyhan, W. L., Powell, H. C., and Grafe, M. R. (1995). Neuropathology of Propionic Acidemia: A Report of Two Patients with Basal Ganglia Lesions. *J. Child. Neurol.* 10, 25–30. doi:10.1177/088307389501000107

Laforêt, P., Ørngreen, M., Preisler, N., Andersen, G., and Vissing, J. (2012). Blocked Muscle Fat Oxidation during Exercise in Neutral Lipid Storage Disease. *Arch. Neurol.* 69, 530–533. doi:10.1001/archneurol.2011.631

Lehnert, W., Sperl, W., Suormala, T., and Baumgartner, E. R. (1994). Propionic Acidaemia: Clinical, Biochemical and Therapeutic Aspects. Experience in 30 Patients. *Eur. J. Pediatr.* 153 (Suppl. 1), S68–S80. doi:10.1007/BF02138781

Nyhan, W. L., Bay, C., Beyer, E. W., and Mazi, M. (1999). Neurologic Nonmetabolic Presentation of Propionic Acidemia. *Arch. Neurol.* 56 (9), 1143–1147. doi:10.1001/archneur.56.9.1143

Pena, L., Franks, J., Chapman, K. A., Gropman, A., Ah Mew, N., Chakrapani, A., et al. (2012). Natural History of Propionic Acidemia. *Mol. Genet. Metab.* 105 (1), 5–9. doi:10.1016/j.ymgme.2011.09.022

Perezcerda, C. (2004). Propionic Acidemia: Unusual Course with Late Onset and Fatal Outcome[J]. *Metabolism-clinical Exp.* 53 (6), 809–810.

Storgaard, J. H., Madsen, K. L., Løkken, N., Vissing, J., van Hall, G., Lund, A. M., et al. (2020). Impaired Lipolysis in Propionic Acidemia: A New Metabolic Myopathy? *JIMD Rep.* 53, 16–21. doi:10.1002/jmd2.12113

Van der Meer, S. B., Poggi, F., Spada, M., Bonnefont, J. P., Ogier, H., Hubert, P., et al. (1996). Clinical Outcome and Long-Term Management of 17 Patients with Propionic Acidaemia. *Eur. J. Pediatr.* 155, 205–210. doi:10.1007/bf01953939

Viegas, C. M., Zanatta, Â., Grings, M., Hickmann, F. H., Monteiro, W. O., Soares, L. E., et al. (2014). Disruption of Redox Homeostasis and Brain Damage Caused *In Vivo* by Methylmalonic Acid and Ammonia in Cerebral Cortex and Striatum of Developing Rats. *Free Radic. Res.* 48 (6), 659–669. doi:10.3109/10715762.2014.898842

Wongkittichote, P., Ah Mew, N., and Chapman, K. A. (2017). Propionyl-CoA Carboxylase - A Review. *Mol. Genet. Metab.* 122, 145–152. doi:10.1016/j.ymgme.2017.10.002

Zayed, H. (2015). Propionic Acidemia in the Arab World. *Gene* 564 (2), 119–124. doi:10.1016/j.gene.2015.04.019

Conflict of Interest: The authors declare that the research was conducted in the absence of any commercial or financial relationships that could be construed as a potential conflict of interest.

Publisher's Note: All claims expressed in this article are solely those of the authors and do not necessarily represent those of their affiliated organizations, or those of the publisher, the editors, and the reviewers. Any product that may be evaluated in this article, or claim that may be made by its manufacturer, is not guaranteed or endorsed by the publisher.

frontiers in Genetics

CASE REPORT
published: 29 March 2022
doi: 10.3389/fgene.2022.839212

Case Report: Identification of a Novel Heterozygous Missense Mutation in *COL4A3* Gene Causing Variable Phenotypes in an Autosomal-Dominant Alport Syndrome Family

Yanglin Hu[1†], Wei Li[2†], Lulu Tian[3], Shuai Fu[1], Yonglong Min[1], Jia Liu[1] and Fei Xiong[1*]*

[1]Department of Nephrology, Wuhan No.1 Hospital, Wuhan, China, [2]Department of Endocrinology, Wuhan No.1 Hospital, Wuhan, China, [3]Department of Blood Purification, Central Theater General Hospital, Wuhan, China

Alport syndrome (AS) is a genetic kidney disease of basement membrane collagen disorder accounting for approximately 2% of ESRD patients. Next-generation and whole-exome sequencing methods are increasingly frequently used as an efficient tool not only for the diagnosis of AS but also for the establishment of genotype–phenotype correlation. We herein report the identification of a novel heterozygous missense mutation in *COL4A3* gene (c.G3566A: p.G1189E) causing variable phenotypes in an ADAS Family based on the combination of clinical, histologic, pedigree, and genetic sequencing information. The proband is a 48-year-old Chinese woman suffering from persistent subnephrotic proteinuria and intermittent hematuria without renal function impairment over a 10-year time-span. Renal biopsy showed diffuse thin basement membrane and focal interstitial foam cell infiltration. The proband's mother progressed to end-stage renal failure and the proband's sister presented with subnephrotic proteinuria and intermittent hematuria as well. AS was highly suspected and confirmed by exome sequencing which revealed a novel heterozygous missense mutation in *COL4A3* gene (c.G3566A: p.G1189E) in all the affected family members, although their current medical conditions vary significantly. Our present finding emphasizes the significance of next-generation sequencing technology for genetic screening which gives us an accurate clinical diagnosis of ADAS patients. The identification of c.G3566A as a new ADAS-related mutation contributes to both genetic diagnosis of ADAS and further functional study of *COL4A3*. The variable phenotypes from the same genotype of our case also provide more information to genotype–phenotype correlation study.

Keywords: human genetics, next-generation sequencing, whole-exome sequencing, Alport syndrome, collagen type IV, *COL4A3*, novel variant

OPEN ACCESS

Edited by:
María L. Couce, Complejo Hospitalario Universitario de Santiago, Spain

Reviewed by:
Jinghong Zhao, Xinqiao Hospital, China
Yuki Hitomi, Hoshi University, Japan

***Correspondence:**
Yanglin Hu
yanglin_hu@aliyun.com
Fei Xiong
xiongf23@sina.com

†These authors have contributed equally to this work

Specialty section:
This article was submitted to Genetics of Common and Rare Diseases, a section of the journal Frontiers in Genetics

Received: *19 December 2021*
Accepted: *04 March 2022*
Published: *29 March 2022*

Citation:
Hu Y, Li W, Tian L, Fu S, Min Y, Liu J and Xiong F (2022) Case Report: Identification of a Novel Heterozygous Missense Mutation in COL4A3 Gene Causing Variable Phenotypes in an Autosomal-Dominant Alport Syndrome Family. Front. Genet. 13:839212. doi: 10.3389/fgene.2022.839212

INTRODUCTION

Alport syndrome (AS) is a genetically and phenotypically heterogeneous disorder of glomerular, cochlear, and ocular basement membranes caused by mutations in the genes *COL4A3*, *COL4A4*, and *COL4A5*, which encode type collagen IVα3, α4, and α5 chains, respectively (Kashtan, 2021). It is the second most common cause of genetic kidney disease after autosomal-dominant polycystic kidney disease (Savige et al., 2021). The collagen α3, 4, and 5 are the major components of the mature glomerular basement membrane (GBM) in the kidney, eye, and cochlea. Disruption or alteration of those collagen leads to breakdown of their structure and function. Various clinical manifestations ranging from isolated, asymptomatic hematuria, through hematuria and proteinuria, to progressive renal disease, sensorineural deafness, lenticonus, and retinal flecks may occur (Kashtan et al., 2018).

The disease is transmitted in an X-linked manner in the case of *COL4A5* mutation, in an autosomal manner when mutations are located in the *COL4A3* or *COL4A4* genes, or in a digenic inheritance manner when a combination of two mutations in different genes occurs (Quinlan and Rheault, 2021). X-linked is the major inheritance pattern which accounts for 70–80% of AS patients (Quinlan and Rheault, 2021). It has been increasingly recognized that autosomal-dominant AS (ADAS) accounts for a larger percentage of patients with AS than previously recognized, up to 19–31% of affected patients, which made it the second most common inheritance pattern of AS (Fallerini et al., 2014; Morinière et al., 2014; Quinlan and Rheault, 2021). Increased application of next-generation technology in the evaluation of familial renal disease has led to the confirmed diagnosis of AS patients, especially ADAS, in the molecular level and reveals its correlation with histology and clinical manifestation (Groopman et al., 2019).

In this study, three members of a Chinese AS family with various phenotypes were identified as having the same novel heterozygous missense mutation, c.G3566A: p.G1189E, in the *COL4A3* gene. The result allows us to conclude an accurate diagnosis of the family. More importantly, it expands the mutational spectrum of *COL4A3* gene associated with ADAS family, confirms that heterozygous mutations in *COL4A3* gene are associated with a spectrum of phenotypes ranging from asymptomatic abnormal urine analysis to progressive renal disease, which provides more information about genotype–phenotype correlation, and also highlights the efficiency of high-throughput next-generation sequencing technology for identifying candidate variants.

CASE PRESENTATION

Clinical History and Laboratory Data

A 48-year-old Chinese woman was referred to our nephrology department for consultation regarding persistent sub-nephrotic range proteinuria and intermittent hematuria over a 10-year span. Her mother and her elder sister also had history of kidney disease and, possibly, her maternal grandmother as well. She is not from a consanguineous family and was delivered at full term with normal development (**Figure 1**). 10 years ago, she found herself with binocular edema and the following urine test showed sub-nephrotic–range proteinuria ranging from 1.0 to 2.9 g/g and mild intermittent hematuria with normal serum albumin and creatinine levels. Traditional medical drugs and ACEI (angiotensin-converting enzyme inhibitors)/ARB (angiotensin receptor blocker) were prescribed to her. But there was no significant improvement and she did not take the medications regularly. Renal biopsy was suggested and performed in the year 2018. Only mild mesangial expansion, diffuse thin GBM, and very focal interstitial foam cell infiltration was found. Gene analysis was suggested, but she refused because of financial reasons. Now she agreed to do gene analysis because her urine abnormalities persisted and had the tendency of getting worse, especially proteinuria, and most importantly, her mother reached ESRD and started renal replacement therapy.

Laboratory data when gene analysis was done included UPC of 3.26 g/g, hematuria of + with 70% dysmorphic RBCs, normal serum albumin level 41.1 g/L (34–54 g/L), serum creatinine 62 umol/L (0.7 mg/dl, 44–97 umol/L), and CHOL 7.06 mmol/L (3.38–5.17 mmol/L). Hepatitis C antibody, Hepatitis B surface antigen, HIV, antinuclear antibody (ANA), antineutrophil cytoplasmic antibodies (ANCA), and free light chain were all negative. No high-frequency hearing loss or ocular lesion was found.

The proband's elder sister (52 years old) also suffered from a similar medical history, but shorter and milder. She presented with persistent sub-nephrotic–range (0.5–2.4 g/g) proteinuria and mild intermittent hematuria for 4 years without kidney failure. She was also treated with ACEI/ARB and traditional Chinese medical drugs, but she was not quite compliant.

The proband's mother (80 years old) presented with chronic renal failure (CKD stage 4), sub-nephrotic–range proteinuria and intermittent hematuria for 5 years and reached ESRD this year and started with hemodialysis. Her mother had cataract surgery 8 years ago and intermittent tinnitus for a long time.

The proband's maternal grandmother also may have had proteinuria because of the symptomatic foamy urine, but she had already died and no medical test was done to confirm the suspicion.

The clinical characteristics of the family are summarized in **Table 1**.

Light Microscopy Examination

In multiple levels of section examined with H&E, PAS, trichrome, silver, and elastic tissue stains, up to 20 glomeruli were noted, 30% of which were globally sclerosed. The remaining glomeruli were slightly enlarged. Mesangial regions were segmentally minimally expanded

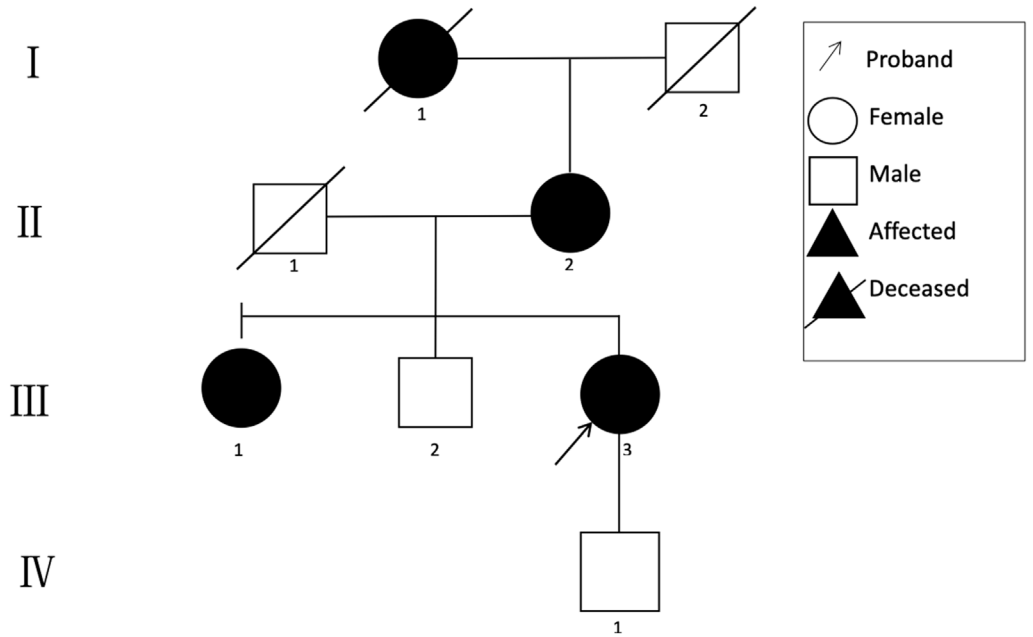

FIGURE 1 | Pedigree of the family.

TABLE 1 | Clinical laboratory and gene data of the family.

Subject	I:1	I:2	II:1	I:2	III:1	III:2	III:3	IV:1
Sex	Female	Male	Male	Female	Female	Male	Female	Male
Age	N/A	N/A	N/A	80	52	55	48	24
Blood pressure	N/A	N/A	N/A	Normal	Normal	Normal	Normal	Normal
Hematuria	N/A	N/A	N/A	Intermittent2+	Intermittent +	Normal	Intermittent+	Normal
Proteinuria	Foamy urine	N/A	N/A	2+–3+	+–2+	Normal	2+	Normal
Alb (g/l)	N/A	N/A	N/A	33.1	43.2	Normal	41.1	Normal
BUN (mmol/l)	N/A	N/A	N/A	24.1	5.8	Normal	6.2	Normal
Scr (mg/dl)	N/A	N/A	N/A	8.19	0.68	Normal	0.7	Normal
Audiological examination	N/A	N/A	N/A	Tinnitus	Normal	Normal	Normal	Normal
Ophthalmic examination	N/A	N/A	N/A	Cataract	Normal	Normal	Normal	Normal
Genotype	N/A	N/A	N/A	Heterozygous	Heterozygous	-	Heterozygous	Wild-type

Alb, serum Albumin; BUN, blood urea nitrogen; Scr, serum creatinine values; N/A, not available; -, no data.

due to matrix deposition. No endocapillary hypercellularity or crescents were found. Chronic changes were noted in the interstitial compartment with focal mild fibrosis and tubular atrophy. Very focal foam cells were found in the interstitium (**Figures 2A,B**). Protein cast and RBC cast could be seen. Arterioles and arteries demonstrated mild hyalinosis.

Immunofluorescence Examination

Immunofluorescence study revealed that the α3 and α5 collagen IV chains were well distributed in the kidney (**Figures 2C,D**). No diagnostic glomerular or extra-glomerular staining was seen with antisera specific for IgG, IgA, IgM, C3, C1q, fibrin, and kappa and lambda light chains.

Electron Microscopy Examination

One glomerulus was examined by electron microscopy. The glomerulus showed diffuse thinning of the glomerular capillary membrane without lamination or splitting and with segmental effacement of overlapping foot processes (**Figures 2E, F**). Endothelial cells were activated. No discrete immune complex electron dense deposits were identified.

Gene-Panel Design Sequencing and Variant Identification

Peripheral blood (5 ml) from the proband (III:3) was collected in EDTA anticoagulant tubes, and DNA samples were obtained using an extraction kit. Gel electrophoresis was

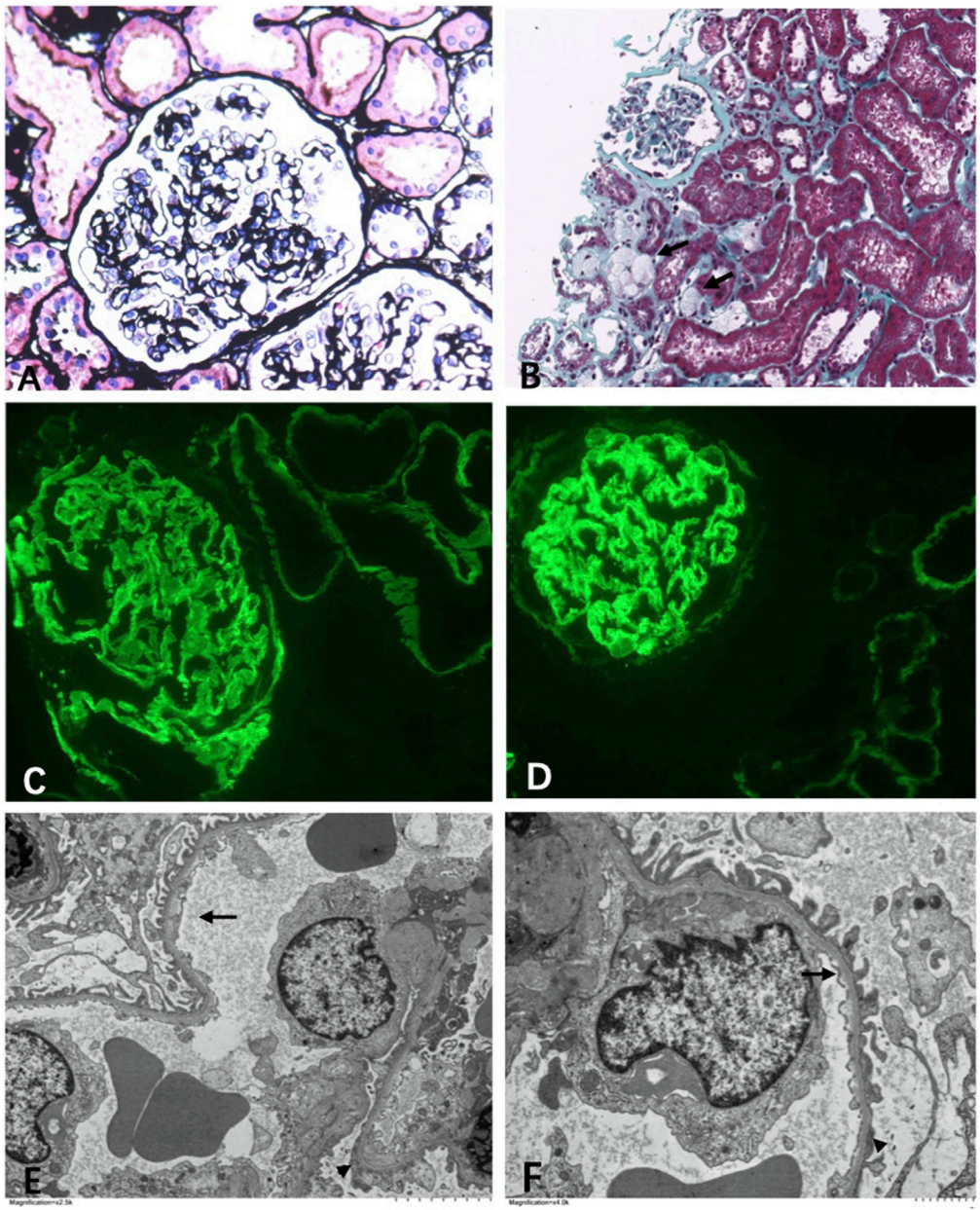

FIGURE 2 | Light microscopy. **(A)** Mild segmental mesangial expansion (Manson's Trichome stain ×400). **(B)** Focal foam cells infiltration (←) (Jones silver stain ×100). Immunofluorescence. **(C)** α3 collagen IV was well distributed in the kidney (×400). **(D)** α5 collagen IV was well distributed in the kidney (×400). Electromicroscopy. **(E,F)** Diffuse thin basement membrane (←) with segmental overlapping podocyte effacement (▲) (×6000).

used to identify, quantify, and purify nucleic acid fragments. The amount of DNA was quantified using a Qubit 3.0 fluorometer. DNA was randomly broken into 250–300 bp long fragments using a Covaris S2 Sonicator (Covaris). The DNA sequencing library was prepared including end-repair, A-tailing, and adapter ligation. After pooling with specific indexes, the DNA library samples were hybridized and captured by streptavidin-coated magnetic beads. Quality assessment was processed after PCR amplification. The target region of genetic kidney disease–related genes (including AS) was enriched, and a total exon library was constructed. Targeted sequences and prepared samples were run on a Illumina NovaSeq PE150 high-throughput sequencing instrument. Average sequencing depth of the target area is 156.57 with 99.54% coverage.

Bioinformatics Analysis

The obtained sequences were compared to those of the human reference genome hg19 (UCSC) using Borrows–Wheeler Aligner software (version 0.7.15 http://bio-bwa.sourceforge.net/) to

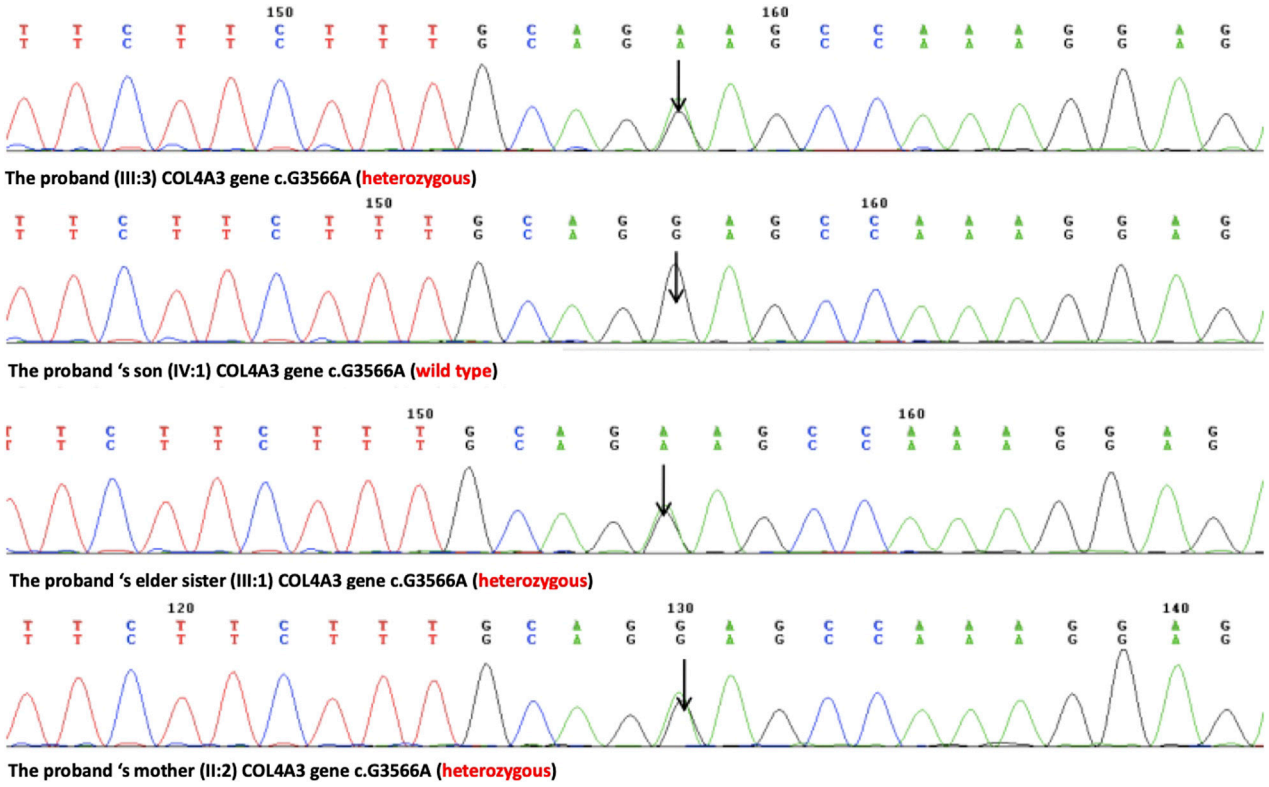

FIGURE 3 | Sanger sequencing results of the c.G3566A (p.G1189E) variant at the 43rd exon of the COL4A3 gene of the proband (III:3), her son (IV:1), her elder sister (III:1), and her mother (II:2).

acquire valid sequences, and variant calling was performed using GATK3.1.1 with HaplotypeCaller. The called variants were annotated using ANNOVAR.

Sanger Sequencing

To validate putative variants, Sanger sequencing was performed using an ABI 3730XL DNA analyzer. Primers flanking the candidate loci were designed based on the reference genomic sequences of the Human Genome from GenBank in NCBI and synthesized by Invitrogen, Shanghai, China. The heterozygous variants identified through targeted next-generation sequencing were verified through Sanger sequencing using the following primers: F:5-ACACTTTAGAGCTTACACCATGCTT-3, R:5-GGTAACATGAGGAGGAGGTTGAAAA-3.

Identification of Novel Variants

A novel heterozygous missense mutation, c.G3566A, has been identified in the *COL4A3* gene (chr2:228162390) in the proband (**Figure 3**). The heterozygous point mutation (c.3566G > A) in exon 42 of *COL4A3* gene causes a codon that codes for a different amino acid which results in a substitution of glycine by glutamic acid at amino acid position 1189 (p.G1189E). It locates in position 1 glycine residues in the Gly-X-Y repeats in the intermediate collagenous domains. The variant was confirmed by Sanger sequencing, and her family members (II:2, III:1, III:3, and IV:1; **Figure 3**) were subsequently assessed. The c.3566G > A (p.G1189E) *COL4A3* variant was not detected in her son (who was also clinically normal), whereas her mother and her sister were both heterozygous (who were both affected by kidney diseases with different phenotypes) (**Figure 3**). This variant was not found in GnomAD, ExAC, or in 1000 Genome Databases. The REVEL computational prediction analysis tool produced a score of 0.974. According to the refining criteria of AS variant interpretation guidelines of the American College of Medical Genetics and Genomics (ACMG) (Richards et al., 2015; Savige et al., 2021), this variant is classified as a "Likely pathogenic" (PM1, PM2, PP3, and PP4). Combing through the clinical, pathology, and pedigree data, we came to the conclusion that this is the novel pathogenic variant for this ADAS family.

Follow Up

Once the diagnosis was made, the patient and her sister were prescribed with ACEI. She and her family were all satisfied because the diagnosis was made and the treatment and prognosis were clear. But unfortunately, she was lost to follow up after the diagnosis.

DISCUSSION

Six genes (*COL4A1–COL4A6*) are arranged in three pairs (*COL4A1–COL4A2*, *COL4A3–COL4A4*, and

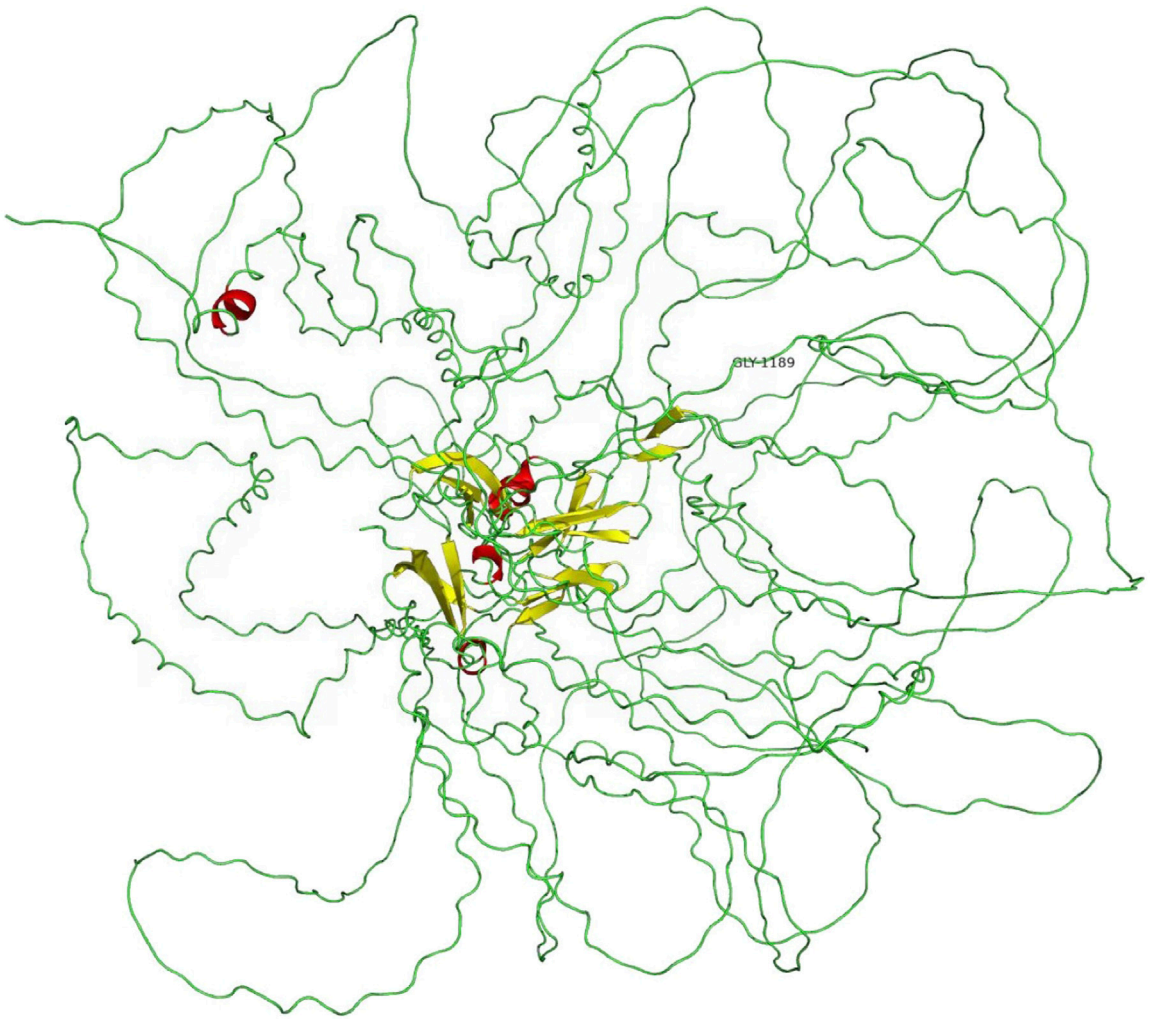

FIGURE 4 | Location of p.G1189E in COL4A3 protein.

COL4A5–COL4A6) and locate on chromosomes 13, 2, and X, respectively. They encode six isoforms, α1 to α6 of type IV collagen, which is the major structural component of all basement membranes (Quinlan and Rheault, 2021). Type IV collagen is a heterotrimer composed of three α chains coiled around one another to form a helical protomer (Timpl, 1989; Jennette, 2015; Savige et al., 2021). Three distinct networks have been recognized: α1.α1.α2-α1.α1.α2, α3.α4.α5-α3.α4.α5, and α1.α1.α2-α5.α5.α6 (Abrahamson et al., 2009; Quinlan and Rheault, 2021). In the mature kidney, the α3α4α5 network is the main component of the GBM, encoded by the *COL4A3*, *COL4A4*, and *COL4A5* genes, respectively (Kashtan et al., 2018; Kashtan, 2021; Quinlan and Rheault, 2021; Savige et al., 2021). Disease-causing mutations in these genes will lead to AS with various phenotypes transmitted in different ways. A milder disorder previously known as "benign familial hematuria" or "thin basement membrane nephropathy" has a common molecular basis and potentially may not be "benign." The entity "benign familial hematuria" or "thin basement membrane nephropathy" has been eliminated by the Classification Working Group in 2018 to avoid the possible harm of classifying a patient with a benign prognosis (Kashtan et al., 2018).

The family we reported here was clinically highly suspected of AS because the proband had hematuria occurring together with a family history of hematuria and renal impairment and an abnormal GBM appearance (Savige et al., 2013). But the intermittent but not persistent hematuria, the increasing proteinuria, no extra-renal symptoms, the foam cells in the kidney biopsy without GBM lamination, the podocyte effacement, and very different clinical phenotypes within the family called for definite gene variant identification to confirm AS diagnosis excluding other hereditary or non-hereditary disease such as podocytopathy, further understanding of phenotype–genotype relationship, and better prediction of prognosis to guide clinical management.

A novel heterozygous missense mutation, c.G3566A, was identified by next-generation sequencing, which locates in exon42 of the *COL4A3* gene on chromosome 2 in which G in the 3566rd position was changed to A (c.G3566A), leading to the amino acid change from glycine to glutamic acid (p.G1189E, **Figure 4**). This variant is absent from all population allele frequency databases (GnomAD, ExAC, and 1000 Genome Databases) and has to our knowledge not been reported in the literature. The normal α3 chain encoded by the *COL4A3* gene is composed of 1,670 amino acids. It has a 28–amino acid leucine-rich signal peptide, followed by a 1,410–amino acid collagenous domain, and a 232–amino acid C-terminal NC1 domain (Mariyama et al., 1994). The collagenous domain begins with a 14–amino acid noncollagenous sequence that includes 4 cysteines, and the collagenous repeat Gly-X-Y is interrupted 23 times by short noncollagenous sequences (Mariyama et al., 1994; Heidet et al., 2001). The collagenous domain is characterized by the repeated Gly-X-Y triplet sequence, in which every third amino acid is a glycine. The presence of glycine is crucial for proper triple-helix formation, because glycine is the only amino acid small enough to fit into the center of the triple helix (Heidet et al., 2001; Jennette, 2015). If glycine is substituted by any other residue, normal folding of the triple-helical collagen molecule would be disrupted and consequently lead to partial or complete absence of these collagens within mature GBM (Yeo et al., 2020). Also, the misfold collagen molecules would also be highly sensitive to proteases and thus prone to degradation (Yeo et al., 2020). The refining ACMG criteria for the molecular diagnostics of AS stated that most glycine residues in the collagenous domain of the collagen IV α5, α3, and α4 chains should be recognized as critical residues equivalent to a functional domain and, therefore, identified position 1 glycine residues in the Gly-X-Y repeats in the intermediate collagenous domains in the collagen IV α5, α3, and α4 chains as "mutational hotspots" (PM1) (Savige et al., 2021). According to the refining criteria, the new variant, c.3566G > A (p.G1189E), locates in the collagenous domain, and PM1 can be applied. The REVEL computational prediction analysis tool produced a score of 0.974, which is above the threshold necessary to apply PP3. All three patients in the family identified with hematuria (PP4). This variant meets criteria to be classified as "likely pathogenic" for AS based on the refining ACMG criteria (Savige et al., 2021). After associating with the clinical, pathology, and pedigree data, we eventually have the final diagnosis of ADAS with this novel heterozygous missense mutation c.G3566A in *COL4A3* gene as the pathogenic variant.

Autosomal-dominant inheritance was mistakenly considered to be very rare previously (Savige et al., 2013; Zhang and Ding, 2018). But as the increasing application of gene sequencing technology, the old narrowed definition of AS was broadened, such as the reclassification of "thin basement membrane nephropathy" and focal segmental glomerulosclerosis with any variant of *COL4A3-5*, as both could be a manifestation of ADAS if the variant located in *COL4A3* and *COL4A4* (Kamiyoshi et al., 2016; Kashtan et al., 2018; Kashtan, 2021; Quinlan and Rheault, 2021; Savige et al., 2021). GBM thinning, which was previously considered to be a very important pathologic finding, can be found in various situations including young male patients with X-linked AS, female patients of any age with X-linked AS, young male and female patients with autosomal recessive AS, and male and female patients with heterozygous mutations in the *COL4A3* and *COL4A4* genes transmitted in an autosomal-dominant pattern who may or may not exhibit progressive renal disease (Kashtan et al., 2018), which is well demonstrated in our case. With a substantial portion of the unrevealed autosomal-dominant inheritance patients with various clinical presentations being identified by NGS (Kamiyoshi et al., 2016; Kashtan et al., 2018; Kashtan, 2021; Quinlan and Rheault, 2021; Savige et al., 2021), ADAS is now considered to account for a larger percentage of patients with AS than previously recognized, which is up to 19–31% (Fallerini et al., 2014; Morinière et al., 2014; Kashtan et al., 2018; Kashtan, 2021; Quinlan and Rheault, 2021).

Accordingly, this makes phenotype–genotype correlation data lag behind for variants in *COL4A3* and *COL4A4* (Rehm et al., 2015). Men with X-linked AS invariably develop kidney failure, and their phenotype is strongly influenced by genotype in that large deletions and nonsense mutations conferred a 90% probability of kidney failure before age 30, compared with a 70% risk with splice site mutations and a 50% risk with missense mutations (Jais et al., 2000; Yamamura et al., 2020). The phenotype of ADAS can vary from isolated hematuria through progressive kidney disease to renal failure, hearing loss, and ocular lesions. What we know now is that renal failure is not common, but recognized increasingly, and hearing loss is unusual, affecting 4–13% of individuals, as are ocular lesions (Kamiyoshi et al., 2016; Kashtan, 2021). But the exact phenotype–genotype correlation has yet to be established. Our case demonstrated that heterozygous missense mutation c.G3566A in *COL4A3* gene can cause various phenotypes in one family. It suggested that the severity of clinical manifestations may not be entirely attributed to the *COL4A3* genetic variant itself in patients. The reasons for this variability of expression/incomplete penetrance are complicated, including modifier genes that ameliorate or exacerbate the effects of mutations on synthesis, assembly, deposition, or function (or a combination of these) of the collagen IV α345 and factors such as smoking, high blood pressure, and dietary levels of salt and animal protein (Kashtan et al., 2018). According to that, an estimated risk of ESRD is given to ADAS patients with 20% or more among those with risk factors, <1% among those without any risk factors including proteinuria, FSGS, GBM thickening and lamination, sensorineural hearing loss, or evidence of progression in patient or family, genetic modifiers (Kashtan et al., 2018). According to the prognosis estimation, the proband and her sister both have more than 20% risk for progression to ESRD because she has the risk factor of proteinuria and family history of ESRD. To delay renal failure,

ACEI should be continuously used. Because although there is no curative treatment for AS, early ACEI therapeutic interventions have been shown to be effective both in AS patients and AS animal models, especially if patients were treated before the occurrence of proteinuria and impaired renal function (Savige et al., 2013; Torra and Furlano, 2019). So early detection of ADAS patients with risk to ESRD is extremely important which could be greatly diagnosed with the help of next-generation and whole-exome sequencing methods. Unfortunately, the cost of the technique is still quite expensive and health insurance cannot cover the cost in China.

In conclusion, the presented case demonstrates how NGS in the combination of bioinformatics analysis strategy, together with clinical, histologic, and pedigree information, provides a specific diagnosis in patients with a family history of kidney disease and illustrates different phenotypes of ADAS family members with the same genotype. More importantly, a novel heterogenous missense *COL4A3* mutation, c.3566G > A (p.G1189E), was identified. Our study showed the importance of application of NGS for early ADAS diagnosis which may potentially improve the prognosis of ADAS population. It also expands the spectrum of *COL4A3* mutations, helps illustrate genotype–phenotype correlation, and contributes to genetic diagnosis and counseling of Alport syndrome.

DATA AVAILABILITY STATEMENT

The datasets for this article are not publicly available due to concerns regarding participant/patient anonymity. Requests to access the datasets should be directed to the corresponding authors.

ETHICS STATEMENT

The studies involving human participants were reviewed and approved by Wuhan No. 1 Hospital. The patients/participants provided their written informed consent to participate in this study. Written informed consent was obtained from the individual(s) for the publication of any potentially identifiable images or data included in this article.

AUTHOR CONTRIBUTIONS

YH: manuscript writing, data collection, and overall instruction. WL: manuscript writing and data collection. LT: clinical data collection and sequencing. SF: light microscope and immunofluorescence examination. YM: pathology materials preparation and electron microscope examination. JL: clinical data collection. FX: manuscript writing and overall instruction.

ACKNOWLEDGMENTS

The authors thank all the patients who participated in this study.

SUPPLEMENTARY MATERIAL

The Supplementary Material for this article can be found online at: https://www.frontiersin.org/articles/10.3389/fgene.2022.839212/full#supplementary-material

REFERENCES

Abrahamson, D. R., Hudson, B. G., Stroganova, L., Borza, D.-B., and St. John, P. L. (2009). Cellular Origins of Type IV Collagen Networks in Developing Glomeruli. *Jasn* 20, 1471–1479. doi:10.1681/ASN.2008101086

Fallerini, C., Dosa, L., Tita, R., Del Prete, D., Feriozzi, S., Gai, G., et al. (2014). Unbiased Next Generation Sequencing Analysis Confirms the Existence of Autosomal Dominant Alport Syndrome in a Relevant Fraction of Cases. *Clin. Genet.* 86, 252–257. doi:10.1111/cge.12258

Groopman, E., Goldstein, D., and Gharavi, A. (2019). Diagnostic Utility of Exome Sequencing for Kidney Disease. Reply. *N. Engl. J. Med.* 380, 2080–2081. doi:10.1056/NEJMoa180689110.1056/NEJMc1903250

Heidet, L., Arrondel, C., Forestier, L., Cohen-solal, L., Mollet, G., Gutierrez, B., et al. (2001). Structure of the Human Type IV Collagen Gene COL4A3 and Mutations in Autosomal Alport Syndrome. *Jasn* 12, 97–106. doi:10.1681/ASN.V12197

Jais, J. P., Knebelmann, B., Giatras, I., Marchi, M. D., Rizzoni, G., Renieri, A., et al. (2000). X-linked Alport Syndrome. *Jasn* 11, 649–657. doi:10.1681/ASN.V114649

Jennette, J. C. O. J. L. S. F. G. D. A. V. D. (2015). *Heptinstall's Pathology of the Kidney* (Lippincott Williams & Wilkins/Wolters Kluwer: Philadelphia).

Kamiyoshi, N., Nozu, K., Fu, X. J., Morisada, N., Nozu, Y., Ye, M. J., et al. (2016). Genetic, Clinical, and Pathologic Backgrounds of Patients with Autosomal Dominant Alport Syndrome. *Cjasn* 11, 1441–1449. doi:10.2215/CJN.01000116

Kashtan, C. E. (2021). Alport Syndrome: Achieving Early Diagnosis and Treatment. *Am. J. Kidney Dis.* 77, 272–279. doi:10.1053/j.ajkd.2020.03.026

Kashtan, C. E., Ding, J., Garosi, G., Heidet, L., Massella, L., Nakanishi, K., et al. (2018). Alport Syndrome: a Unified Classification of Genetic Disorders of Collagen IV α345: a Position Paper of the Alport Syndrome Classification Working Group. *Kidney Int.* 93, 1045–1051. doi:10.1016/j.kint.2017.12.018

Mariyama, M., Leinonen, A., Mochizuki, T., Tryggvason, K., and Reeders, S. T. (1994). Complete Primary Structure of the Human Alpha 3(IV) Collagen Chain. Coexpression of the Alpha 3(IV) and Alpha 4(IV) Collagen Chains in Human Tissues. *J. Biol. Chem.* 269, 23013–23017. doi:10.1016/s0021-9258(17)31612-5

Morinière, V., Dahan, K., Hilbert, P., Lison, M., Lebbah, S., Topa, A., et al. (2014). Improving Mutation Screening in Familial Hematuric Nephropathies through Next Generation Sequencing. *Jasn* 25, 2740–2751. doi:10.1681/ASN.2013080912

Quinlan, C., and Rheault, M. N. (2021). Genetic Basis of Type IV Collagen Disorders of the Kidney. *Cjasn* 16, 1101–1109. doi:10.2215/CJN.19171220

Rehm, H. L., Berg, J. S., Brooks, L. D., Bustamante, C. D., Evans, J. P., Landrum, M. J., et al. (2015). ClinGen - the Clinical Genome Resource. *N. Engl. J. Med.* 372, 2235–2242. doi:10.1056/NEJMsr1406261

Richards, S., Aziz, N., Bale, S., Bick, D., Das, S., Gastier-Foster, J., et al. (2015). Standards and Guidelines for the Interpretation of Sequence Variants: a Joint Consensus Recommendation of the American College of Medical Genetics and Genomics and the Association for Molecular Pathology. *Genet. Med.* 17, 405–424. doi:10.1038/gim.2015.30

Savige, J., Storey, H., Watson, E., Hertz, J. M., Deltas, C., Renieri, A., et al. (2021). Consensus Statement on Standards and Guidelines for the Molecular Diagnostics of Alport Syndrome: Refining the ACMG Criteria. *Eur. J. Hum. Genet.* 29, 1186–1197. doi:10.1038/s41431-021-00858-1

Savige, J., Gregory, M., Gross, O., Kashtan, C., Ding, J., and Flinter, F. (2013). Expert Guidelines for the Management of Alport Syndrome and Thin Basement Membrane Nephropathy. *Jasn* 24, 364–375. doi:10.1681/ASN.2012020148

Timpl, R. (1989). Structure and Biological Activity of Basement Membrane Proteins. *Eur. J. Biochem.* 180, 487–502. doi:10.1111/j.1432-1033.1989.tb14673.x

Torra, R., and Furlano, M. (2019). New Therapeutic Options for Alport Syndrome. *Nephrol. Dial. Transpl.* 34, 1272–1279. doi:10.1093/ndt/gfz131

Yamamura, T., Horinouchi, T., Nagano, C., Omori, T., Sakakibara, N., Aoto, Y., et al. (2020). Genotype-phenotype Correlations Influence the Response to Angiotensin-Targeting Drugs in Japanese Patients with Male X-Linked Alport Syndrome. *Kidney Int.* 98, 1605–1614. doi:10.1016/j.kint.2020.06.038

Yeo, J., Qiu, Y., Jung, G. S., Zhang, Y.-W., Buehler, M. J., and Kaplan, D. L. (2020). Adverse Effects of Alport Syndrome-Related Gly Missense Mutations on Collagen Type IV: Insights from Molecular Simulations and Experiments. *Biomaterials* 240, 119857. doi:10.1016/j.biomaterials.2020.119857

Zhang, Y., and Ding, J. (2018). Renal, Auricular, and Ocular Outcomes of Alport Syndrome and Their Current Management. *Pediatr. Nephrol.* 33, 1309–1316. doi:10.1007/s00467-017-3784-3

Conflict of Interest: The authors declare that the research was conducted in the absence of any commercial or financial relationships that could be construed as a potential conflict of interest.

frontiers | Frontiers in Genetics

CASE REPORT
published: 08 April 2022
doi: 10.3389/fgene.2022.836431

A Novel Mutation of Transferrin Receptor 2 in a Chinese Pedigree With Type 3 Hemochromatosis: A Case Report

Shan Tang[1], Li Bai[1], Yuan Gao[1], Wei Hou[1], Wenyan Song[1], Hui Liu[1], Zhongjie Hu[1], Zhongping Duan[1], Liaoyun Zhang[2] and Sujun Zheng[1]**

[1]Beijing Youan Hospital, Capital Medical University, Beijing, China, [2]The First Hospital of Shanxi Medical University, Taiyuan, China

Type 3 hereditary hemochromatosis (HH) is a rare form of HH characterized by genetic mutation in the *TFR2* gene. Clinical features reported in patients with type 3 HH include abnormal liver function, liver fibrosis, cirrhosis, diabetes, hypogonadism, cardiomyopathy, and skin pigmentation. Since its original description in 2000, 33 pathogenic *TFR2* mutations associated with HH have been described until now. Here, we first reported a Chinese pedigree of *TFR2*-related hemochromatosis with a novel compound heterozygous mutation c.1288G > A (p.G430R)/c.960T > A (p.Y320X). Interestingly, different phenotypes were reported although the proband and his sister shared the same gene mutation. This inconsistency between genotypes and phenotypes indicates multifactorial etiology contributing to the development of HH. Our report broadens the mutation spectrum of the *TFR2* gene associated with HH.

Keywords: case report, TFR2 gene, compound heterozygous mutation, hereditary hemochromatosis, Chinese

OPEN ACCESS

Edited by:
María L. Couce, Complejo Hospitalario Universitario de Santiago, Spain

Reviewed by:
Jinchen Li, Central South University, China
Eduardo Arroyo-Pardo, Complutense University of Madrid, Spain

****Correspondence:***
Sujun Zheng
zhengsujun@ccmu.edu.cn
Liaoyun Zhang
zlysgzy@163.com

Specialty section:
This article was submitted to Genetics of Common and Rare Diseases, a section of the journal Frontiers in Genetics

Received: *17 December 2021*
Accepted: *11 March 2022*
Published: *08 April 2022*

Citation:
Tang S, Bai L, Gao Y, Hou W, Song W, Liu H, Hu Z, Duan Z, Zhang L and Zheng S (2022) A Novel Mutation of Transferrin Receptor 2 in a Chinese Pedigree With Type 3 Hemochromatosis: A Case Report. Front. Genet. 13:836431. doi: 10.3389/fgene.2022.836431

INTRODUCTION

Hereditary hemochromatosis (HH) is defined as an inherited iron overload disorder characterized by excessive absorption of iron (Kowdley et al., 2019). Over time, iron deposits in multiple organs including the liver, pancreas, heart, joints, and pituitary gland, further leading to liver cirrhosis, restrictive cardiomyopathy, heart failure, arthropathy, skin pigmentation, diabetes mellitus, and so on (Bacon et al., 2011). HH can be classified as types 1, 2, 3, and 4. Type 1 HH caused by the *HFE* gene mutation is the most prevalent form of HH in Caucasians (Brissot et al., 2018). Mutations in hemojuvelin BMP co-receptor (*HJV*) and hepcidin antimicrobial peptide (*HAMP*) genes (type 2a and 2b HH, respectively) result in juvenile hemochromatosis, the most severe form of HH (Papanikolaou et al., 2004). Type 4 HH, also known as ferroportin (FPN) disease, is the only autosomal dominant form of hemochromatosis due to the mutations in the solute carrier family 40-member 1(*SLC40A1*) gene (Joshi et al., 2015). Type 3 HH is a rare form of HH characterized by the genetic alterations in the transferrin receptor 2 (*TFR2*) gene, with an estimated allele prevalence between 0.0001 and 0.0004 among European populations (Wallace and Subramaniam, 2016). The human *TFR2* gene is located on chromosome 7q22 and encodes transferrin receptor 2. TFR2 is a type II transmembrane glycoprotein, a member of the TFR family. It provides iron to the cell by internalization of the transferrin iron complex through receptor-mediated endocytosis (Silvestri et al., 2014). Hepcidin is the central regulator of systemic iron homeostasis, which can not only prevent absorption of iron from the gut but also prevent the release of iron from macrophages (Worthen and Enns, 2014). Hepcidin expression at an abnormally low levels leads to iron overload.

TABLE 1 | Laboratory test results of the proband and the proband's family.

	Proband (II-1)	Proband's sister (II-3)	Proband (II-1)	Proband's sister (II-3)	Normal range
			1 year later	1 year later	
Alanine aminotransferase (U/L)	113	19	39	30.7	7–40
Aspartate aminotransferase (U/L)	84	23	56	32.23	13–35
Total bilirubin (μmol/L)	21	6.3	14.3	9.5	5–21
Direct bilirubin (μmol/L)	5.1	1.6	4.3	3.1	0–7
Total bile acid (μmol/L)	52.2	9.8	15.7	—	0–10
Alkaline phosphatase (U/L)	112	116	150	108.1	50–135
γ-glutamyltransferase (U/L)	35	11	25	15.8	7–45
Albumin (g/L)	44.7	41.3	45.7	43.7	40–55
White blood cells (*10⁹/L)	8.63	5.89	6.51	5.76	3.5–9.5
Red blood cells (*10¹²/L)	5.04	4.18	4.52	4.86	4.3–5.8
Hemoglobin (g/L)	157	137	144	156	130–175
Platelets (*10⁹/L)	157	219	136	123	125–350
Hepatitis B virus surface antigen	Negative	Negative	—	—	Negative
Anti-hepatitis C virus	Negative	Negative	—	—	—
Iron (μmol/L)	47	37	48	37.1	<25
Transferrin saturation (%)	97.9	94.9	77.5	83.6	<45%
Ferritin (ng/ml)	>2000	709	>2000	545.8	13–150
Total iron-binding capacity (μmol/L)	48	39	62	44	45–75
HbA1c (%)	9.3	5.6	—	—	4–6

Hemochromatosis, which is associated with mutations in *TFR2,* usually occurs at an earlier age than HFE-related hemochromatosis and usually has a more severe phenotype (Pietrangelo, 2010).

Here, we described a Chinese pedigree presented with typical features of HH. Also, we found a novel compound heterozygous mutation in the *TFR2* gene, namely, c.1288G > A (p.G430R)/c.960T > A (p.Y320X). To the best of our knowledge, this is the first report on a Chinese pedigree of *TFR2*-related hemochromatosis.

CASE PRESENTATION

The patient (**Figure 4**, II-1), a 48-year-old male, was admitted to Beijing YouAn Hospital due to liver cirrhosis. Abdominal ultrasound suggested cirrhosis and splenomegaly 4 months ago even when the patient had no discomfort. In another hospital, he was diagnosed with diabetes and treated with insulin. He hardly ever drank and denied a family history of liver diseases. Physical examination revealed that there are no other abnormalities except for skin pigmentation.

A thorough examination was carried out to find out the cause of cirrhosis. The liver function test showed that the levels of alanine aminotransferase (ALT) and aspartate aminotransferase (AST) were elevated (**Table 1**). Serum markers for viral hepatitis and autoimmune liver diseases were all negative. Notably, the patient had abnormal plasma iron indices: iron, 47 μmol/L; transferrin saturation, 97.9%; and ferritin>2000 ng/ml. HbA1c was significantly elevated. Testosterone was normal (18.26 nmol/L).

Pre-contrast computed tomography (CT) revealed hepatomegaly with an increased attenuation over the liver and spleen, splenomegaly, and collateral circulation formation (**Figure 1A**). Magnetic resonance imaging (MRI) showed a typical decrease in T2-weighted signal intensity over the liver (**Figure 1B**).

A liver biopsy was performed, and the liver histology was evaluated by an experienced pathologist. The findings confirmed established cirrhosis with a marked deposition of iron in the hepatocytes and biliary epithelia, which is consistent with hemochromatosis (**Figures 2A,B**).

We also investigated one of the patient's sisters (**Figure 4**, II-3), and the results showed that she had abnormal plasma iron indices as well: iron, 37 μmol/L; transferrin saturation, 94.9%; and ferritin>709 ng/ml (**Table 1**), while her HbA1c and sex hormones levels were normal (HbA1c 5.6%, estradiol <37 pmol/L, follicle stimulating hormone 58.02 IU/L, luteinizing hormone 25.86 IU/L, progesterone 0.5 nmol/L, prolactin 464.13 mIU/L, and testosterone 0.94 nmol/L). Also, a fine needle aspiration biopsy was performed, which showed iron deposition in the periportal hepatocytes (**Figures 2C,D**).

Genetic Testing Results

Genetic analysis was performed for the patient and his family to explore the genetic factor for hemochromatosis. Panel sequencing was performed for major genes involved in the liver metabolism and carbohydrate metabolism including the common HH-related geness, namely, *HFE*, *HJV*, *HAMP*, *TFR2*, and *SLC40A1*. The SureSelect Human All ExonV6 custom chip was used to capture exons, and the Illumina sequencing platform was used for high-throughput sequencing. BWA (0.7.12-r1039) (Li and Durbin, 2009) was used to compare next-generation sequencing data with the human genome; ANNOVAR ($ Date: 2015-06-17) (Park and Park, 2021) was used to annotate mutation sites according to dbSNP, Clinvar, ExAC, 1,000 Genomes, and other databases. Possible pathogenicity of gene mutation was graded by the ACMG (American Society of Medical Genetics and Genomics) genetic mutation grading system. Then, the target sequence of the suspected pathogenic mutation was amplified by PCR and sequenced *via* an ABI3730xL sequencer (Applied Biosystems,

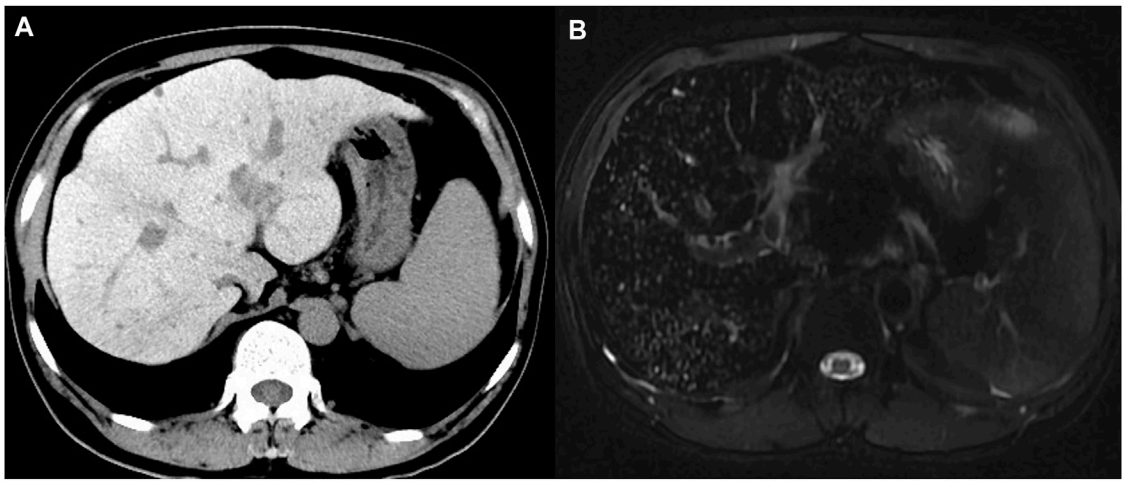

FIGURE 1 | Computed tomography and magnetic resonance imaging of the proband. **(A)** Precontrast CT showed hyper-attenuation of liver parenchyma; **(B)** MRI T2-weighted image showed diffuse low signal intensity of liver parenchyma obviously.

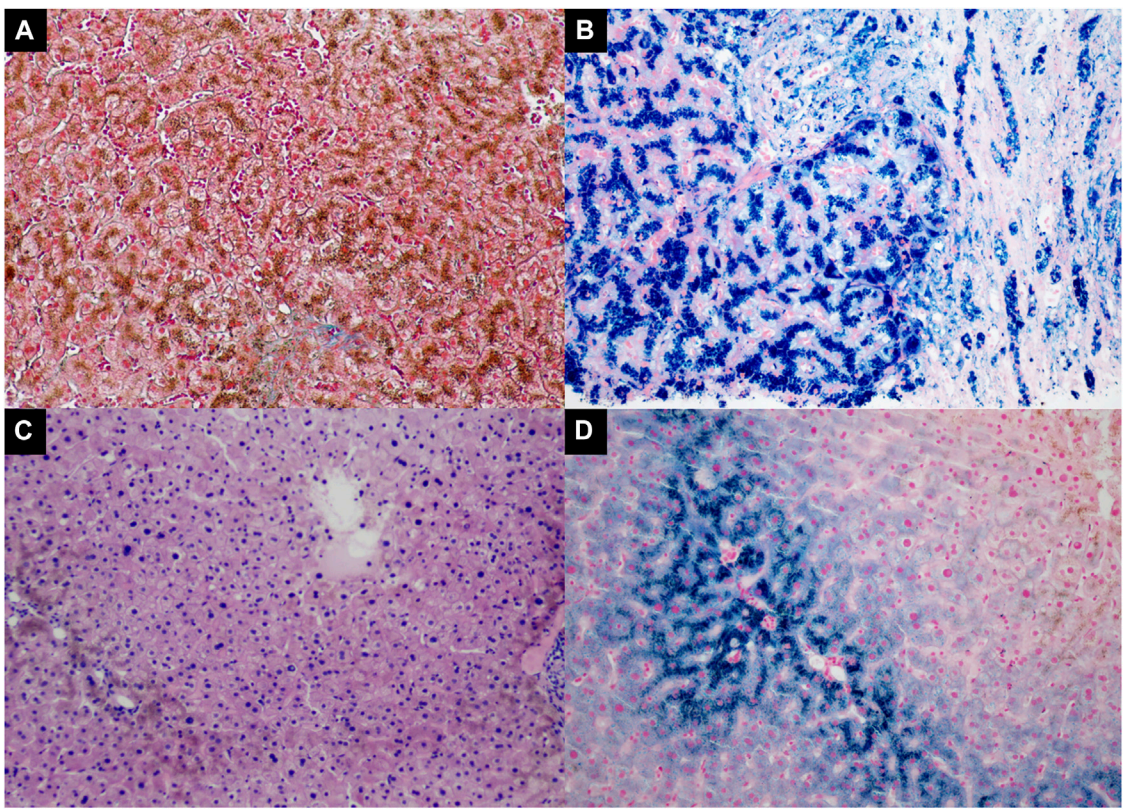

FIGURE 2 | The liver histopathology of the proband [Panel **(A, B)**, II-1] and the proband's sister [Panel **(C, D)**, II-3]. **(A)** Increased collagen fibers stained green by Masson Trichrome stain in the expanded fibrous portal tract with cirrhosis (Masson trichrome, 100×); **(B)** Marked iron deposition in the hepatocytes and biliary epithelium (Prussian blue, 200×); **(C)** Marked deposition of hemosiderin in the hepatocytes (H&E, 100×); **(D)** The proband's sister had iron deposited in the periportal hepatocytes (Prussian blue, 200×).

TABLE 2 | Bioinformatics analysis of the *TFR2* mutations.

Mutation	PolyPhen2		SIFT		PROVEAN		MutationTaster		FATHMM		ACMG
	Score	Prediction	Score	Prediction	Score	Prediction	Score	Prediction	Score	Prediction	Prediction
c.1288G > A p.G430R	1	Probably damaging	0	Deleterious	−6.81	Deleterious	1	Disease causing	0.51	Tolerated	Likely pathogenic
c.960T > A p.Y320X	—	—	—	—	—	—	1	Disease causing	—	—	Pathogenic

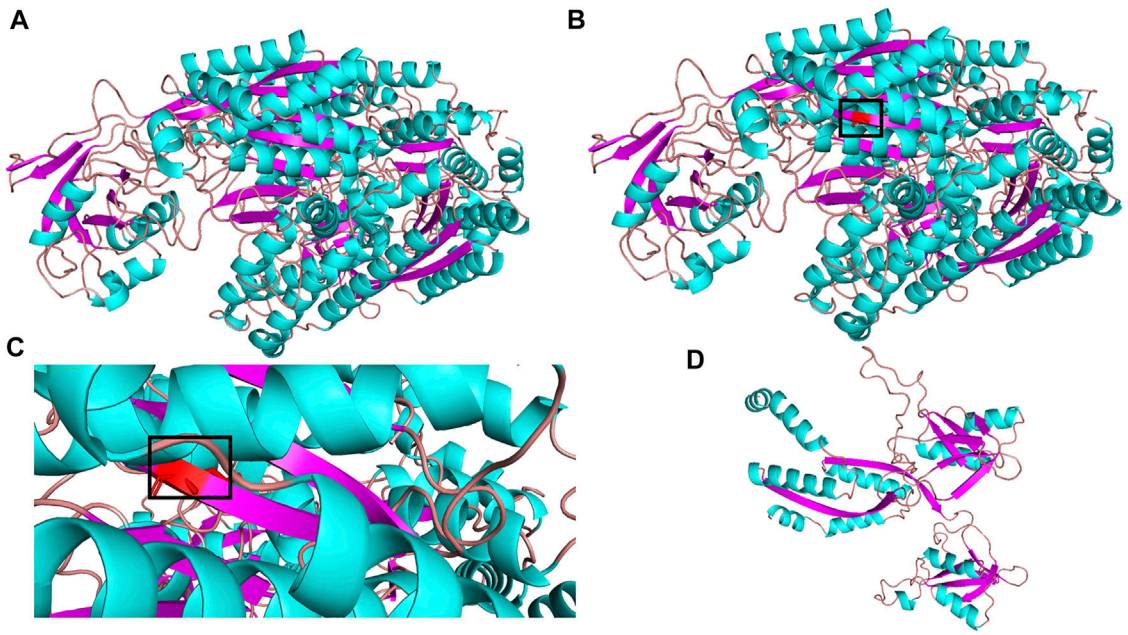

FIGURE 3 | 3D structure of TFR2 protein. **(A)** wild-type; **(B)** mutant type c.G1288A (p.G430R); **(C)** partial mutation graph c.G1288A (p.G430R); **(D)** mutant type c.T960A (p.Y320X).

Foster City, CA, United States). Finally, the comparisons and analysis for Sanger sequencing data were performed by SeqMan (DNASTAR, Madison, Wisconsin, United States). Potential functional effects of detected missense mutations were predicted by PolyPhen-2 (http://genetics.bwh.harvard.edu/pph2/index.shtml), SIFT (http://sift.jcvi.org/), PROVEAN (http://provean.jcvi.org/index.php), MutationTaster (http://mutationtaster.org/), and FATHMM (http://fathmm.biocompute.org.uk/).

The results showed that the patient (II-1) had new heterozygous mutations c.1288G > A (p.G430R)/c.960T > A (p.Y320X) in the *TFR2* gene. These mutations were further confirmed by Sanger sequencing (**Supplementary Figure S1**). As a result, the novel c.960T > A mutation led to a premature stop codon at amino acid 320 (p.Y320X). According to the ACMG guideline, the mutation c.960T > A (p.Y320X) was identified as pathogenic (PVS1: null variant + PM2: absent from controls + PP4: the phenotype of the patient is highly consistent with HH type 3). The mutation c.1288G > A (p.G430R) is a pathogenic mutation that has been reported earlier (Majore et al., 2013). Here, we also predicted its pathogenicity by utilizing six kinds of prediction software. All software programs except for FATHMM showed that the p.G430R mutation was damaging (**Table 2**). The mutation was identified as likely pathogenic according to the ACMG guideline (PM1: the variant is in the domain + PM3: there is a literature suggesting this variant + PM2: absent from controls + PP3: bioinformatics protein function comprehensive prediction software predicts outcomes as harmful + PP4: the phenotype of the patient is highly consistent with HH type 3). The PhastCons scores of these two mutations were both 1, and the corresponding PhyloP values were 4.594 and 4.844, respectively, suggesting the high conservation of these two amino acids. Moreover, amino acid sequence alignments for the corresponding parts in the TFR2 protein in multiple species were studied (**Supplementary Figure S3**). The results showed that the two amino acids at positions 430 and 320 were absolutely conserved.

The molecular structure of *TFR2* was constructed by SWISS-MODEL (https://swissmodel.expasy.org/interactive). Also, molecular graphics were analyzed by PyMOL software. As shown

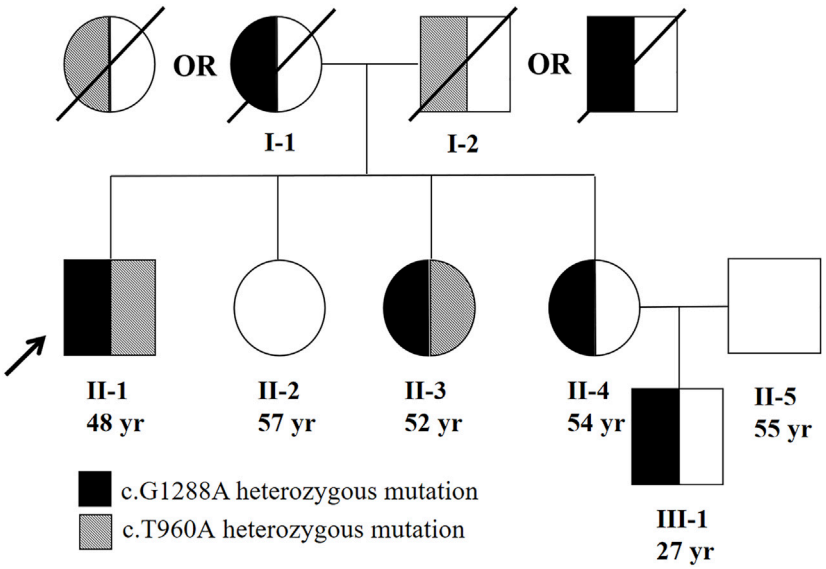

FIGURE 4 | Family pedigree of patient. The parents of the proband should each had a heterozygous mutation (c.960T > A or c.G1288A). The proband's parents were not consanguineous.

in **Figure 3**, the secondary structure of the predicted mutation was not affected by the mutation c.1288G > A (p.G430R) but affected by the mutation c.960T > A (p.Y320X). There is no electricity in the blank space in the model evaluation graph (**Supplementary Figure S2**), indicating that the model quality is acceptable.

Moreover, we tested the mutations in the *TFR2* gene for his family members (**Figure 4**). The same heterozygous mutations were found in one of his sisters (II-3). In addition, one of the patient's sisters (II-4) was found to carry a heterozygous mutation c.1288G > A (p.G430R). However, *TFR2* gene mutation was not found in the other sister (II-2). The patient's parents had passed away, so we cannot perform their genetic sequencing. According to the genetic sequencing results of his sisters, we speculated the mutations in the proband were compound heterozygous. In addition, the nephew (III-1) of the proband was also confirmed to have a heterozygous mutation c.1288G > A (p.G430R).

ETHICAL STATEMENT

All procedures involving human participants were in accordance with the ethical standards of the Institute Ethical Committee of Beijing YouAn Hospital, Capital Medical University, Beijing, China, and with the Helsinki Declaration (as revised in 2013). Written informed consent was obtained from the patient and his family members.

DISCUSSION

In recent years, increasing mutations in the *TFR2* gene which are related to type 3 HH have been documented (Hernández et al., 2021; Joshi et al., 2015). As shown in **Supplementary Table S1**, a total of 33 pathogenic *TFR2* mutations associated with HH have been described in the Human Gene Mutation Database (Stenson et al., 2020). Most patients were Caucasian (27/33, 81.8%), males (17/25, 68.0%). The average age of the patients was 31.4 years, and most of them had liver cirrhosis. The data on the mutations in the *TFR2* gene in Asian patients are relatively rare with only five articles reported.

In the present study, we described a Chinese Han pedigree suffering from type 3 HH with a novel compound heterozygous mutation c.1288G > A (p.G430R)/c.960T > A (p.Y320X) in the *TFR2* gene. The proband exhibits very high plasma transferrin saturation and deposition of iron in the hepatocytes and biliary epithelia, and this phenotype highly suggested hemochromatosis. The gene sequencing results confirm the diagnosis of type 3 hemochromatosis. One of his sisters shares the same *TFR2* gene mutation; however, her liver pathology is milder than that in the proband. Except for the hepatic manifestations, other clinical features including diabetes, hypogonadism, and skin pigmentation have been reported in patients with type 3 hemochromatosis. Given this, we evaluated these symptoms in the proband and his family members. As a result, the proband developed skin pigmentation and diabetes, while his sister showed no other extrahepatic manifestations. We considered that the difference in the phenotype between the proband and his sister can be ascribed to other factors including sex (menstruation), environment (iron intake), or possibly other unknown genetic factors. These factors apart from *TFR2* gene mutation probably contribute to the development of HH. At present, both the proband and his sister have received phlebotomy therapy and resulted in improvement in the laboratory test (**Table 1**).

This case report highlights three important clinical issues. First, our team discovered the *TFR2* gene c.960T > A (p.Y320X)

mutation, which led to a premature stop codon at amino acid 320 (p.Y320X). According to the ACMG genetic mutation grading system, this mutation is pathogenic. We also analyzed the predictive mutation structure and found that the Y320X mutation affects the secondary structure of the *TFR2* protein and may destroy its function. Our report expands the mutation spectrum of the *TFR2* gene associated with HH. Second, this is the first time to report a novel compound heterozygous mutation c. G1288A (p.G430R)/c.T960A (p.Y320X) in the *TFR2* gene in a Chinese pedigree. We analyzed the minor allele frequency (MAF) of the c. G1288A (p.G430R) mutation by utilizing different public databases in different populations (**Supplementary Table S2**). The MAF of c. G1288A (p.G430R) is between 0.000003978 and 0.000008 in different databases, which indicates that the mutation is extremely rare. Third, early diagnosis and treatment for patients with HH have been documented to improve the prognosis as well as decrease mortality. It is helpful to remind even physicians in Asia that where the incidence of HH is low, it is important to keep the diagnosis of HH in mind, when a patient is presented with symptoms such as iron overload, liver fibrosis, diabetes, and so on.

CONCLUSION

In conclusion, we first reported a Chinese pedigree of *TFR2*-related hemochromatosis with a novel compound heterozygous mutation c.1288G > A (p.G430R)/c.960T > A (p.Y320X). Our report broadens the mutation spectrum of the *TFR2* gene associated with HH. On the other hand, our results reveal inconsistency between genotypes and phenotypes, which indicates multifactorial etiology contributing to the development of HH.

DATA AVAILABILITY STATEMENT

The original contributions presented in the study are included in the article/**Supplementary Material**, further inquiries can be directed to the corresponding authors.

ETHICS STATEMENT

The studies involving human participants were reviewed and approved by Beijing You'An Hospital of Capital Medical University and the Declaration of Helsinki (revised in 2013). The patients/participants provided their written informed consent to participate in this study.

AUTHOR CONTRIBUTIONS

All authors listed have made a substantial, direct, and intellectual contribution to the work and approved it for publication.

FUNDING

This work was supported by grants from the Key Medical Professional Development Plan (Sailing plan) of Beijing Hospital Management Center (ZYLX202125), the Beijing Advanced Innovation Center for Big Data-Based Precision Medicine (1212040205), the Beijing Municipal Natural Science Foundation (7202068, 72222093, and 7222094), and the Digestive Medical Coordinated Development Center of Beijing Municipal Administration of Hospitals (XXZ0503). Capital Health Development Research Project (2022-1-2182).

ACKNOWLEDGMENTS

We would like to thank Jing Zhao and LB for their help in polishing the language of our article.

SUPPLEMENTARY MATERIAL

The Supplementary Material for this article can be found online at: https://www.frontiersin.org/articles/10.3389/fgene.2022.836431/full#supplementary-material

REFERENCES

Bacon, B. R., Adams, P. C., Kowdley, K. V., Powell, L. W., and Tavill, A. S. (2011). Diagnosis and Management of Hemochromatosis: 2011 Practice Guideline by the American Association for the Study of Liver Diseases. *Hepatology* 54, 328–343. doi:10.1002/hep.24330

Brissot, P., Pietrangelo, A., Adams, P. C., De Graaff, B., Mclaren, C. E., and Loréal, O. (2018). Haemochromatosis. *Nat. Rev. Dis. Primers* 4, 18016. doi:10.1038/nrdp.2018.16

Hernández, G., Ferrer-Cortès, X., Venturi, V., Musri, M., Pilquil, M. F., Torres, P. M. M., et al. (2021). New Mutations in HFE2 and TFR2 Genes Causing Non HFE-Related Hereditary Hemochromatosis. *Genes* 12, 1980. doi:10.3390/genes12121980

Joshi, R., Shvartsman, M., Morán, E., Lois, S., Aranda, J., Barqué, A., et al. (2015). Functional Consequences of Transferrin Receptor-2 Mutations Causing Hereditary Hemochromatosis Type 3. *Mol. Genet. Genomic Med.* 3, 221–232. doi:10.1002/mgg3.136

Kowdley, K. V., Brown, K. E., Ahn, J., and Sundaram, V. (2019). ACG Clinical Guideline: Hereditary Hemochromatosis. *Am. J. Gastroenterol.* 114, 1202–1218. doi:10.14309/ajg.0000000000000315

Li, H., and Durbin, R. (2009). Fast and Accurate Short Read Alignment with Burrows-Wheeler Transform. *Bioinformatics* 25, 1754–1760. doi:10.1093/bioinformatics/btp324

Majore, S., Ricerca, B. M., Radio, F. C., Binni, F., Cosentino, I., and Gallusi, G. (2013). Type 3 Hereditary Hemochromatosis in a Patient from Sub-Saharan Africa: Is There a Link between African Iron Overload and TFR2 Dysfunction?. *Blood Cells Mol. Dis.* 50 (1), 31–32. doi:10.1016/j.bcmd.2012.08.007

Papanikolaou, G., Samuels, M. E., Ludwig, E. H., Macdonald, M. L. E., Franchini, P. L., Dubé, M.-P., et al. (2004). Mutations in HFE2 Cause Iron Overload in Chromosome 1q-Linked Juvenile Hemochromatosis. *Nat. Genet.* 36, 77–82. doi:10.1038/ng1274

Park, K.-J., and Park, J.-H. (2021). Variations in Nomenclature of Clinical Variants between Annotation Tools. *Lab. Med.* lmab074. doi:10.1093/labmed/lmab074

Pietrangelo, A. (2010). Hereditary Hemochromatosis: Pathogenesis, Diagnosis, and Treatment. *Gastroenterology* 139, 393–408. doi:10.1053/j.gastro.2010.06.013

Silvestri, L., Nai, A., Pagani, A., and Camaschella, C. (2014). The Extrahepatic Role of TFR2 in Iron Homeostasis. *Front. Pharmacol.* 5, 93. doi:10.3389/fphar.2014.00093

Stenson, P. D., Mort, M., Ball, E. V., Chapman, M., Evans, K., Azevedo, L., et al. (2020). The Human Gene Mutation Database (HGMD): Optimizing its Use in a

Clinical Diagnostic or Research Setting. *Hum. Genet.* 139, 1197–1207. doi:10.1007/s00439-020-02199-3

Wallace, D. F., and Subramaniam, V. N. (2016). The Global Prevalence of HFE and Non-HFE Hemochromatosis Estimated from Analysis of Next-Generation Sequencing Data. *Genet. Med.* 18, 618–626. doi:10.1038/gim.2015.140

Worthen, C. A., and Enns, C. A. (2014). The Role of Hepatic Transferrin Receptor 2 in the Regulation of Iron Homeostasis in the Body. *Front. Pharmacol.* 5, 34. doi:10.3389/fphar.2014.00034

Conflict of Interest: The authors declare that the research was conducted in the absence of any commercial or financial relationships that could be construed as a potential conflict of interest.

Publisher's Note: All claims expressed in this article are solely those of the authors and do not necessarily represent those of their affiliated organizations, or those of the publisher, the editors, and the reviewers. Any product that may be evaluated in this article, or claim that may be made by its manufacturer, is not guaranteed or endorsed by the publisher.

frontiers | Frontiers in Genetics

CASE REPORT
published: 13 April 2022
doi: 10.3389/fgene.2022.718853

Case Report: Loss-of-Function *ABCC9* Genetic Variant Associated With Ventricular Fibrillation

Anastasia Zaytseva[1,2], Tatyana Tulintseva[1], Yulya Fomicheva[1], Valeria Mikhailova[1], Tatiana Treshkur[1] and Anna Kostareva[1,3]*

[1]Almazov National Medical Research Centre, St Petersburg, Russia, [2]Sechenov Institute of Evolutionary Physiology and Biochemistry, Russian Academy of Sciences, St Petersburg, Russia, [3]Department of Woman and Child Health, Karolinska Institute, Stockholm, Sweden

Genetic variants in the *ABCC9* gene, encoding the SUR2 auxiliary subunit from K_{ATP} channels, were previously linked with various inherited diseases. This wide range of congenital disorders includes multisystem and cardiovascular pathologies. The gain-of-function mutations result in Cantu syndrome, acromegaloid facial appearance, hypertrichosis, and acromegaloid facial features. The loss-of-function mutations in the *ABCC9* gene were associated with the Brugada syndrome, early repolarization syndrome, and dilated cardiomyopathy. Here, we reported a patient with a loss-of-function variant in the *ABCC9* gene, identified by target high-throughput sequencing. The female proband presented with several episodes of ventricular fibrillation and hypokalemia upon emotional stress. This case sheds light on the consequences of K_{ATP} channel dysfunction in the cardiovascular system and underlines the complexity of the clinical presentation of *ABCC9*-related diseases.

Keywords: *ABCC9*, atrial hypertension, case report, K_{ATP} channels, ventricular fibrillation (VF)

OPEN ACCESS

Edited by:
María L. Couce, Complejo Hospitalario Universitario de Santiago, Spain

Reviewed by:
Prasenjit Mitra, Post Graduate Institute of Medical Education and Research (PGIMER), India
Mark Levin, National Institutes of Health (NIH), United States

****Correspondence:***
Anastasia Zaytseva
zaytseva_ak@almazovcentre.ru

Specialty section:
This article was submitted to Genetics of Common and Rare Diseases, a section of the journal Frontiers in Genetics

Received: *01 June 2021*
Accepted: *15 March 2022*
Published: *13 April 2022*

Citation:
Zaytseva A, Tulintseva T, Fomicheva Y, Mikhailova V, Treshkur T and Kostareva A (2022) Case Report: Loss-of-Function ABCC9 Genetic Variant Associated With Ventricular Fibrillation. Front. Genet. 13:718853. doi: 10.3389/fgene.2022.718853

INTRODUCTION

The *ABCC9* gene encodes a transmembrane protein SUR2 that forms the regulatory part of the ATP-sensitive potassium channel (K_{ATP}) in cardiac, skeletal, vascular, and nonvascular smooth muscle cells (Chutkow et al., 1996). K_{ATP} channels are heterooctamers, which consist of four pore-forming $K_{ir}6.x$ channels, associated with four regulatory SUR (sulfonylurea receptor) subunits. Their main function is to couple the cell metabolic state to its membrane potential, thus adapting the K^+ conductance to the ATP content *via* the ATP-specific channel blockade [for review see (Foster and Coetzee, 2016)]. The subunit composition of K_{ATP} channels depends on the tissue subtype. There are two main types of SUR splice variants (SUR2A and SUR2B), which contribute to the diversity of K_{ATP} channels (Chutkow et al., 1999). There are two main types of $K_{ir}6.x$ channels—$K_{ir}6.1$ and $K_{ir}6.2$—encoded by *KCNJ8* and *KCNJ11* and two SUR proteins—SUR1 and SUR2—encoded by *ABCC8* and *ABCC9* genes, respectively (Aguilar-Bryan et al., 1995; Inagaki et al., 1995; Chutkow et al., 1996).

The gain-of-function (GOF) and loss-of-function (LOF) mutations of all genes encoding K_{ATP} subunits (*ABCC8, KCNJ11*, *ABCC9,* and *KCNJ8*) have been described in patients with completely different and surprisingly opposite phenotypes. The regulatory subunit SUR1 encoded by *ABCC8* and the pore-forming subunit $K_{ir}6.2$ encoded by *KCNJ11* are mainly co-expressed in insulin-secreting tissues. Their GOF mutations are associated with neonatal diabetes, while the LOF mutations cause hyperinsulinism (Galcheva et al., 2019; Pipatpolkai

et al., 2020). No cardiovascular phenotype has been reported for SUR1-and *ABCC8*-associated diseases. The regulatory subunit SUR2 encoded by *ABCC9* and pore-forming subunit $K_{ir}6.1$ encoded by *KCNJ8* are expressed in cardiomyocytes, vascular smooth muscles, endothelial cells, and in many other cells and tissues with different presentations of SUR2A and SUR2B isoforms. *ABCC9* and rarely *KCNJ8* GOF genetic variants are associated with the Cantu syndrome, which often presents with the cardiac phenotype (Grange et al., 2019). Although the most typical and recognized clinical signs of Cantu syndrome include hypertrichosis and a characteristic facial appearance with acromegaloid features, the cardiovascular system's involvement often occurs in the form of cardiomegaly with normal cardiac function, patent ductus arteriosus (PDA), and dilated aortic root (Levin et al., 2016). Additionally, several GOF genetic variants in the *KCNJ8* gene were reported in association with the isolated Brugada syndrome, atrial and ventricular fibrillation, and early repolarization syndrome (Haïssaguerre et al., 2009; Medeiros-Domingo et al., 2010; Barajas-Martínez et al., 2012; Delaney et al., 2012). In contrast, there have been several cases of LOF genetic variants in *ABCC9* and *KCNJ8*. Tester and co-authors described and functionally characterized *KCNJ8* LOF variants in a cohort of sudden infant death syndrome victims in 2011 (Tester et al., 2011). *ABCC9* LOF variants have been reported only twice in a patient with dilated cardiomyopathy and in a case of isolated atrial fibrillation (Bienengraeber et al., 2004; Olson et al., 2007). There were no additional reports on *ABCC9* LOF variants within the next 13 years. The clinical significance and accurate genotype–phenotype correlations of LOF variants in this gene remain unclear. Recently, a homozygous LOF genetic variant in the *ABCC9* gene has been described as a cause of a novel phenotype called intellectual disability and myopathy syndrome (Smeland et al., 2019).

Here, we report another case of a LOF *ABCC9* genetic variant associated with idiopathic ventricular tachycardia and arterial hypertension. The presented case further extends the phenotypic spectrum of *ABCC9*-related disorders and supports the role of K_{ATP} channels in cardiomyocyte and coronary smooth muscle electrophysiology and function.

CLINICAL REPORT

The study was conducted according to the guidelines of the Declaration of Helsinki and approved by the Institutional Ethics Committee of the Almazov National Medical Research Centre. Informed consent was obtained from all subjects involved in the study. Routine clinical examination was performed according to the standard protocols including electrocardiography, Holter monitoring, echocardiography, endomyocardial biopsy, and biochemical and hormonal tests. For genetic testing, a targeted panel of 172 cardiomyopathy-associated genes was analyzed using the SureSelect Target Enrichment System and Illumina MiSeq instrument (Agilent; Waldbronn, Germany). The list of studied genes is presented in **Supplementary Table S1**. The data processing and filter strategy were performed as described earlier (Jorholt et al., 2020).

The proband – 32-year-old female patient with a previously uneventful life history presented with a sudden cardiac death that occurred outside the home after emotional stress. The patient was resuscitated by her husband until the emergency services arrived when ventricular fibrillation (VF) was registered (**Figure 1**). Effective defibrillation led to the recovery of sinus rhythms, but within the next 30 min, in the intensive care unit, several episodes of VF repeatedly occurred registered on the ECG monitoring system, which lead to the deep sopor and clonic seizures. The patient's blood tests revealed hypokalemia (2.9 mmol/L) with additional remarkable changes. There were no alterations in the hormonal state, glucose metabolism, the concentration of electrolytes, and no evidence of endocrine genesis of arrhythmia. Acute cerebrovascular accident and myocardial injury were excluded. On the resting ECG on the first day after VF, changes in repolarization (-) T in I, aVL, and V1-V3 leads were recorded, not subsequently detected. During 15 days of ECG telemonitoring, the sinus rhythm was recorded with an average heart rate of 68 bpm. Single monomorphic ventricular ectopic complexes (n = 3,185) were found mainly in the daytime, and 11 unstable episodes of the monomorphic idioventricular rhythm with an average frequency of 92 bpm were registered for the entire period of telemonitoring (**Figures 2A,B**). There were no changes in the QT interval. Echocardiography demonstrated the slightly increased LV wall thickness (13 mm) and increased myocardium mass (92 g/m2) corresponding to concentric myocardial hypertrophy with a normal ejection fraction (65%). Cardiac MRI revealed no signs of myocarditis or arrhythmogenic dysplasia, normal chamber geometry, normal ejection fraction (62%), and an absence of a late gadolinium enhancement phenomenon.

The patient remained on ventilation support during the next 5 days, followed by successful restoration of spontaneous respiration and consciousness. ECG normalized on the seventh day after hospitalization; the number of single ectopic ventricular complexes reduced to 500 per day, and ventricular tachycardia and QT interval prolongation were not detected. The discharge with bisoprolol 5 mg/day was recommended. Stress echocardiography performed several months later demonstrated high exercise tolerance and no myocardial ischemia, but at the peak of physical activity, single ectopic ventricular complexes were registered (**Figure 3**). The implantation of the implantable cardioverter defibrillator was performed for secondary prevention, and the patient remained stable within the next 2 years on metoprolol therapy (100 mg daily).

According to the anamnesis, the patient developed normally and has an average intelligence. The patient did not have any difficulties in learning at school and demonstrated standard communication skills. The patient had no history of chronic diseases and no family history of sudden cardiac death. Holter monitoring performed during the pregnancy 6 years prior to the episode of abortive sudden death documented 2,683 single ventricular ectopic beats. The

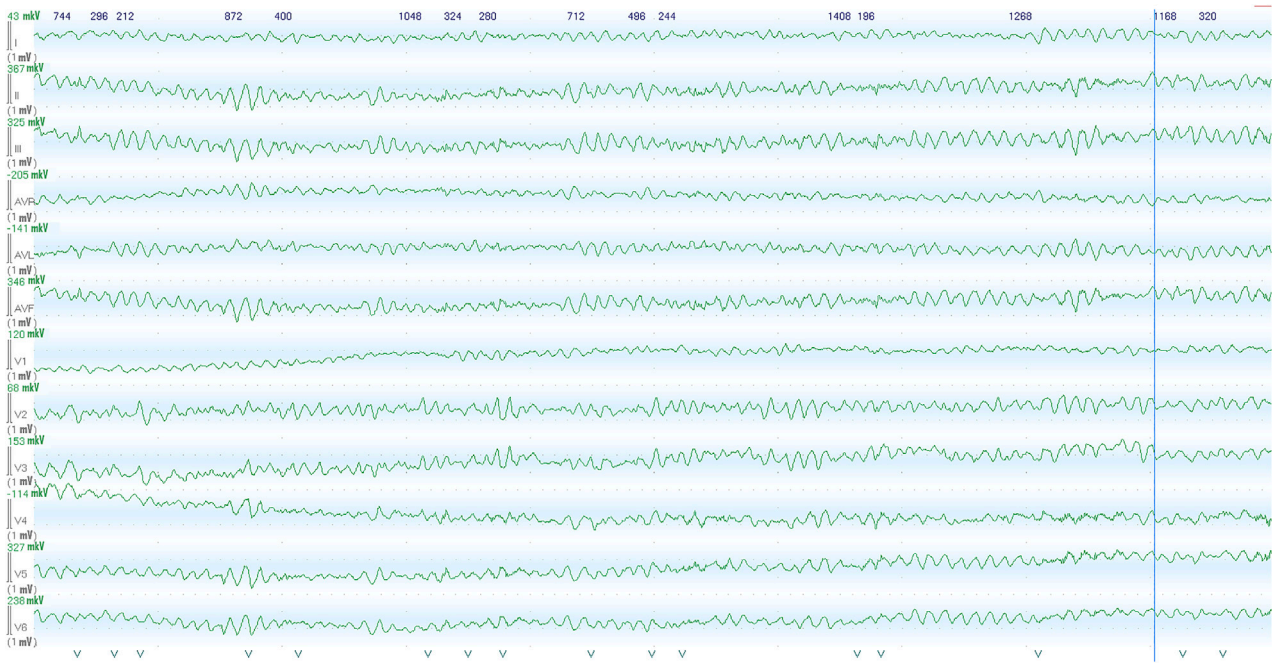

FIGURE 1 | Images recorded by the ECG monitoring system in the intensive care unit within the first hour after the initial out-of-hospital episode of abortive sudden cardiac death. Ventricular fibrillation was recorded from patients, following admission to cardiac ICU.

patient had three natural self-deliveries with preeclampsia (moderate degree) and arterial hypertension (up to 160/100 mmHg) during the third pregnancy, and arterial hypertension retained after the delivery. No causes of the secondary hypertension were found; the patient remained normotensive on ACE inhibitor treatment with rare hypertensive crises upon intensive physical excises or emotional stress.

To exclude the inherited arrhythmic syndromes or early manifestation of cardiomyopathy, the genetic study was performed using a targeted gene panel of 172 cardiomyopathy-associated genes, as previously described (Jorholt et al., 2020). All disease-related genetic variants were confirmed using Sanger sequencing and classified according to the American College of Medical Genetics guidelines (Jorholt et al., 2020). Informed consent was signed prior to the investigation, and the study protocol was approved by the Ethical Committee of the Almazov National Medical Research Centre. All research studies have been performed in accordance with the Declaration of Helsinki.

The target panel sequencing identified a genetic variant in the *ABCC9* gene in the exon 37 *ABCC9* (NM_005,691.3): c.4570_4572delTTAinsAAAT (p.Leu1524LysfsTer5), rs869025349, classified as pathogenic and earlier reported in a family with dilated cardiomyopathy and ventricular arrhythmias. Previous characterization of recombinant K_{ATP} channels including this mutation suggests that the variant causes a decrease in current expression, suggestive of a LOF molecular phenotype (Bienengraeber et al., 2004). This variant was confirmed in proband's father, sister, and young daughter but not in the mother and older daughter (https://varsome.com/variant/hg19/chr12-21958186-TAA-ATTT). The genotype-positive young daughter experienced several syncope episodes at age 12, but no ECG was registered at that time, and the precise link of these episodes to the arrhythmogenic events remains unclear. This variant was previously reported in ClinVar in connection to dilated and arrhythmogenic cardiomyopathy but is currently classified as a variant of unknown significance. However, the absence of this variant in the gnomAd exome or gnomAd genome database together with the loss of function nature and several reported clinical associations prompts to reclassify the variant as pathogenic according to ACMG guidelines. The only reported frequency available for this variant comes from the Kaviar database, where it was reported with relatively high frequency among 454 genomes from the Wellderly study (00,032%), but these data have not been confirmed in other datasets. Therefore taking into account gnomAd exome and genome data, the true frequency of rs869025349 seems to be very low. No other genetic variants, characterized as pathogenic or likely pathogenic, was identified in the proband.

In spite of the fact that the described genetic variant potentially has a LOF mechanism of action different from that in GOF variants linked to the Cantu syndrome, we prompted the deeper clinical phenotyping in order to search for Cantu-related clinical features and excluded the possibility of a mixed clinical phenotype linked to *ABCC9* variants. The patient revealed no signs of hypertrichosis, dysmorphic face, or enlarged acromegaloid features. The patient did not present with

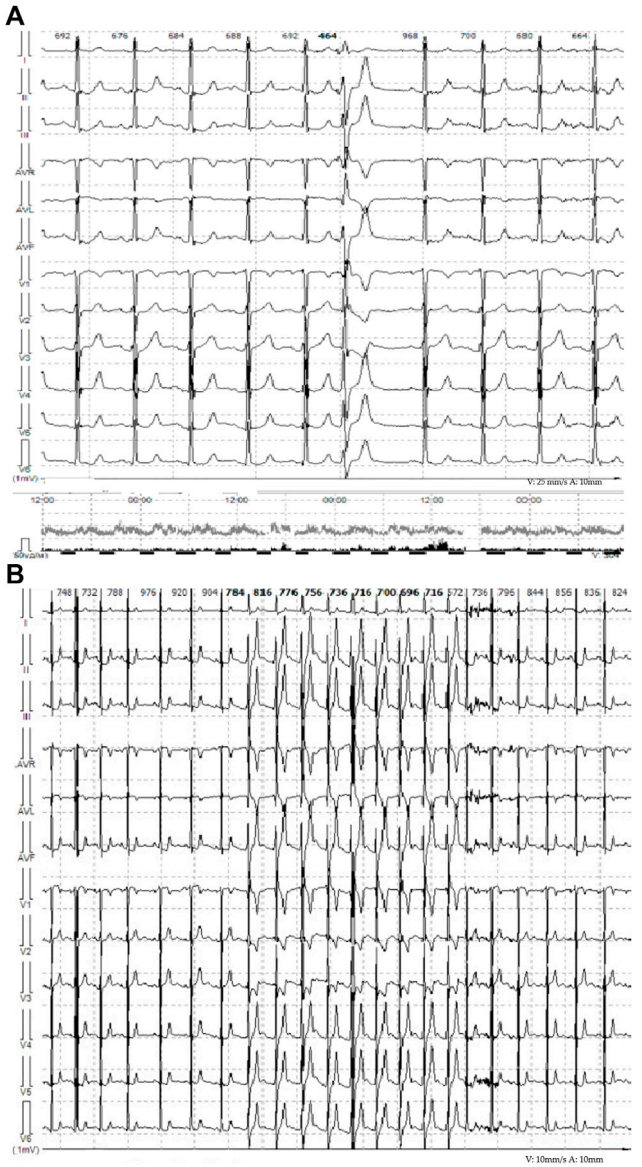

FIGURE 2 | (A) Representative ECG from telemonitoring, single monomorphic ventricular ectopic complexes. **(B)** Representative ECG from telemonitoring. Unstable episodes of the monomorphic idioventricular rhythm with frequency of 81 bpm are observed.

reduced motor skills or delayed development in childhood. Unlike the characteristic features observed in the autosomal recessive SUR2 LOF syndrome, AIMS, no hypotonia, skeletal abnormalities, or scoliosis were noted neither in the proband nor in other carriers of the L1524KfsTer5 variant. The patient did not complain of muscle pain or fatigue after physical exercise. All carriers of the aforementioned genetic variant had an average intelligence and no difficulties in school learning; the patient did not reveal any skin lesions or pathologies and did not complain of sleep apnea. However, no specialized somnological examination has been performed.

DISCUSSION

K_{ATP} channels are of key importance in metabolic stress sensing of the cell. The expression of these channels has been found in various organs and tissues, including the pancreas, nervous system, skeletal and smooth muscle cells, and cardiac myocytes (Miki and Seino, 2005). These channels are composed of pore-forming and regulatory subunits; the latter in the heart is represented by SUR2 protein encoded by the *ABCC9* gene. This gene is a member of the superfamily of the adenosine triphosphate (ATP)-binding cassette (ABC) transporter subfamily C, member 9, which is located on chromosome 12 at 12p12.1[1]. The main isoform of SURs in the cardiac and vascular myocytes, SUR2A, consists of 17 transmembrane segments, organized in three domains: TMD0, TMD1, and TMD2. In addition, there is a highly conserved intracellular region called nucleotide-binding domain 1 (NBD1) with Walker A and Walker B motifs in the linker between TMD1 and TMD2. Another nucleotide-binding site of SUR2A is the NBD2 region localized in the C-terminal part. It is suggested that NBDs are responsible for channel activation (Foster and Coetzee, 2016).

K_{ATP} channel dysfunction leads to the abnormal cellular response to metabolic stress. The growing amount of evidence indicates that K_{ATP} plays an important role in the adaptive cardiac response to systemic metabolic stressors and vascular tone regulation. Numerous cardiac K_{ATP} GOF mutations have been described in the association with Cantu syndrome (Levin et al., 2015) giving a broad range of molecular pathophysiological events linked to K_{ATP} GOF (Huang et al., 2018; McClenaghan et al., 2018). In contrast, LOF mutations in the *ABCC9* gene were only a few times reported in association with quite distinct clinical phenotypes due to different allelic states (heterozygous mutations (Bienengraeber et al., 2004; Olson et al., 2007; Hu et al., 2014) and homozygous mutation reported by Smeland et al. (2019). Therefore, the frequency and clinical consequences of *ABCC9* LOF genetic variants have not been thoroughly characterized until now. Here, we reported a patient with a LOF variant in the *ABCC9* gene (Leu1524LysfsTer5, rs869025349) associated with a complex clinical phenotype, including arterial hypertension and stress-induced ventricular arrhythmia. Despite pvc's at peak exercise, there were no genetic variants in genes responsible for CPVT, such as *RYR2* and *CASQ2*. Importantly, we did not observe any signs of cardiac remodeling in any of the carriers of the genetic variant, and the predominant cardiac phenotype linked to the variant was arrhythmic. However, it leaves the opportunity for the later development of dilated cardiomyopathy, as described previously in association with this genotype. The described case identifies the *ABCC9* gene as a potential causative candidate for inherited arrhythmic syndromes and underscores the significance of the use of broad target genetic panels in patients with cardiac rhythm abnormalities and no structural heart alterations.

The role of ATP-sensitive potassium currents in normal heart physiology has been illustrated by animal studies. Thus, $K_{ir}6.1^{-/-}$ and $SUR2^{-/-}$ mice demonstrated baseline arterial hypertension, coronary artery vasospasm, and predisposition to sudden cardiac

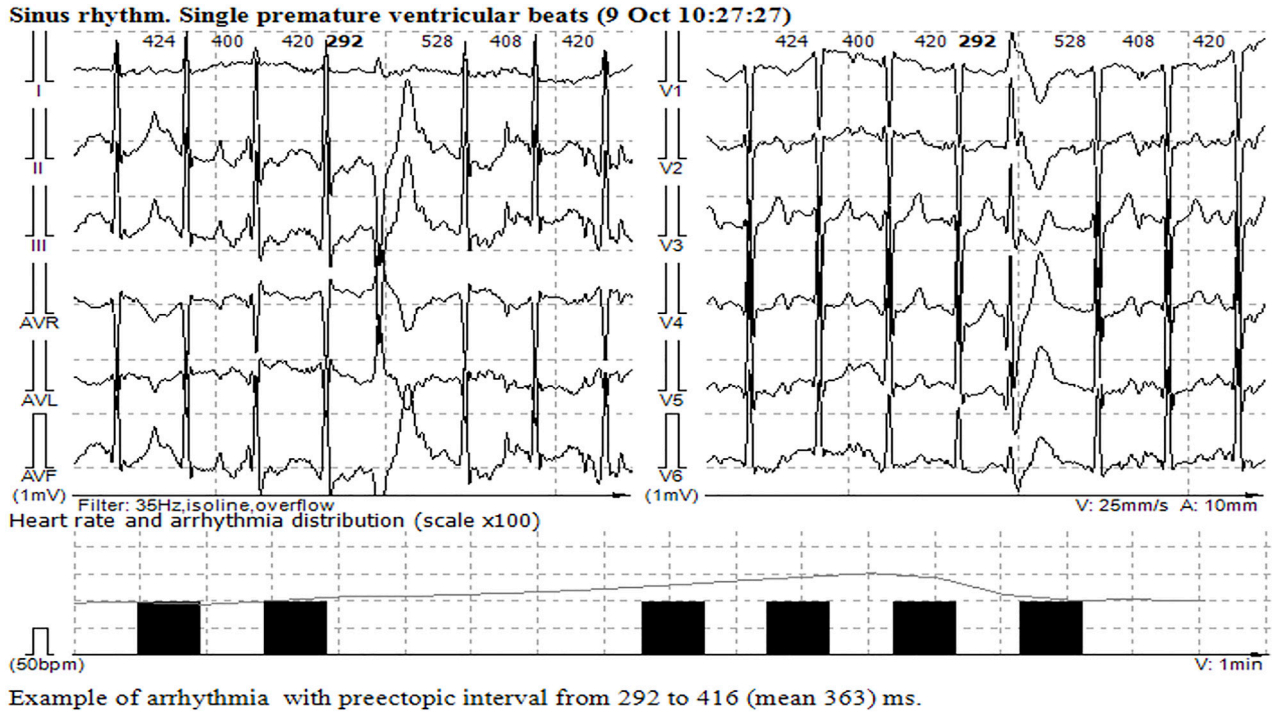

FIGURE 3 | Single monomorphic ventricular ectopic complexes during and at the peak of stress echocardiography.

death (Chutkow et al., 2002). In contrast, in experimental animal models, K_{ATP} GOF resulted in an increased concentration of intracellular calcium and massive cytosolic calcium overload, hypercontractility, and the development of heart failure upon stress (Levin et al., 2016). These data are well in line with the stress-induced nature of the arrhythmogenic episodes in our patient and require deeper molecular studies on *ABCC9* LOF variants to identify the proper anti-arrhythmogenic strategies. There is also a possibility that arterial hypertension, observed in a patient, contributed to the arrhythmic manifestation of the genotype. Importantly, hypertension was also reported in the patient's father carrying the same *ABCC9* variant. A similar observation can be noted for hypokalemia, observed in a patient during acute arrhythmogenic episodes. Due to abnormal K_{ATP} function, patients with *ABCC9* mutations are often reported to have a low potassium serum level which, by itself, can be a severe provocative factor for triggering ventricular fibrillation (Feest and Wrong, 1991).

Our study has several limitations. First, the number of genes tested was limited to 172 which potentially leave the possibility that other genetic causes are not well known or yet described in connection to arrhythmic disorders and cardiomyopathies can be linked to the observed phenotype. The increased number of genes studied, or the use of an exome sequencing approach potentially, will allow in excluding another genetic background linked to the patient's phenotype. Another important limitation is the lack of functional studies for the variant described and the inability to make a strong conclusion regarding the impact of the variant on the phenotype in the genotype-positive family members. Of note, this variant was previously characterized as LOF due to the decrease in the channel expression (Bienengraeber et al., 2004). Finally, the complex effect of *ABCC9* genetic variants should be properly estimated in animal model studies, such as that conducted previously (Chutkow et al., 2002; Miki et al., 2002).

To conclude, we presented the second case of the heterozygous *ABCC9* LOF variant in a patient with arrhythmogenic cardiac phenotype, arterial hypertension, and no signs of structural heart diseases. This case expands the spectrum of *ABCC9*-related disorders and improves our understanding of the clinical consequences of K_{ATP} dysfunction.

DATA AVAILABILITY STATEMENT

The datasets for this article are not publicly available due to concerns regarding participant/patient anonymity. Requests to access the datasets should be directed to the corresponding author.

ETHICS STATEMENT

The studies involving human participants were reviewed and approved by the Local Ethical Committee of the Almazov National Medical Research Centre. Written informed consent to participate in this study was provided by the participants' legal guardian/next of kin.

AUTHOR CONTRIBUTIONS

All authors have read and agreed to the published version of the manuscript. Conceptualization, AK and TTu; methodology, VM; software, YF; validation, AZ and YF; formal analysis, TTu; investigation TTu, TTr and YF; data curation, VM; writing—original draft preparation, AZ; writing—review and editing, AK and TTu; visualization, YF; supervision, AK; project administration, AK; and funding acquisition, AK. All authors have read and agreed to the published version of the manuscript.

FUNDING

This research was funded by the Ministry of Science and Higher Education of the Russian Federation (Agreement No. 075-15-2020-901).

SUPPLEMENTARY MATERIAL

The Supplementary Material for this article can be found online at: https://www.frontiersin.org/articles/10.3389/fgene.2022.718853/full#supplementary-material

REFERENCES

Aguilar-Bryan, L., Nichols, C. G., Wechsler, S. W., Clement, J. P., Boyd, A. E., González, G., et al. (1995). Cloning of the β Cell High-Affinity Sulfonylurea Receptor: a Regulator of Insulin Secretion. *Science* 268, 423–426. doi:10.1126/science.7716547

Barajas-Martínez, H., Hu, D., Ferrer, T., Onetti, C. G., Wu, Y., Burashnikov, E., et al. (2012). Molecular Genetic and Functional Association of Brugada and Early Repolarization Syndromes with S422L Missense Mutation in KCNJ8. *Heart Rhythm* 9, 548–555. doi:10.1016/j.hrthm.2011.10.035

Bienengraeber, M., Olson, T. M., Selivanov, V. A., Kathmann, E. C., O'Cochlain, F., Gao, F., et al. (2004). ABCC9 Mutations Identified in Human Dilated Cardiomyopathy Disrupt Catalytic KATP Channel Gating. *Nat. Genet.* 36, 382–387. doi:10.1038/ng1329

Chutkow, W. A., Makielski, J. C., Nelson, D. J., Burant, C. F., and Fan, Z. (1999). Alternative splicing of sur2 Exon 17 regulates nucleotide sensitivity of the ATP-sensitive potassium channel. *J. Biol. Chem.* 274, 13656–13665. doi:10.1074/jbc.274.19.13656

Chutkow, W. A., Pu, J., Wheeler, M. T., Wada, T., Makielski, J. C., Burant, C. F., et al. (2002). Episodic Coronary Artery Vasospasm and Hypertension Develop in the Absence of Sur2 KATP Channels. *J. Clin. Invest.* 110, 203–208. doi:10.1172/JCI15672

Chutkow, W. A., Simon, M. C., Le Beau, M. M., and Burant, C. F. (1996). Cloning, Tissue Expression, and Chromosomal Localization of SUR2, the Putative Drug-Binding Subunit of Cardiac, Skeletal Muscle, and Vascular KATP Channels. *Diabetes* 45, 1439–1445. doi:10.2337/diab.45.10.1439

Delaney, J. T., Muhammad, R., Blair, M. A., Kor, K., Fish, F. A., Roden, D. M., et al. (2012). A KCNJ8 Mutation Associated with Early Repolarization and Atrial Fibrillation. *Europace* 14, 1428–1432. doi:10.1093/europace/eus150

Feest, T. G., and Wrong, O. (1991). Potassium Deficiency and Sudden Unexplained Nocturnal Death. *The Lancet* 338, 1406. doi:10.1016/0140-6736(91)92290-i

Foster, M. N., and Coetzee, W. A. (2016). KATPChannels in the Cardiovascular System. *Physiol. Rev.* 96, 177–252. doi:10.1152/physrev.00003.2015

Galcheva, S., Demirbilek, H., Al-Khawaga, S., and Hussain, K. (2019). The Genetic and Molecular Mechanisms of Congenital Hyperinsulinism. *Front. Endocrinol.* 10, 111. doi:10.3389/fendo.2019.00111

Grange, D. K., Roessler, H. I., McClenaghan, C., Duran, K., Shields, K., Remedi, M. S., et al. (2019). Cantú Syndrome: Findings from 74 Patients in the International Cantú Syndrome Registry. *Am. J. Med. Genet.* 181, 658–681. doi:10.1002/ajmg.c.31753

Haïssaguerre, M., Chatel, S., Sacher, F., Weerasooriya, R., Probst, V., Loussouarn, G., et al. (2009). Ventricular Fibrillation with Prominent Early Repolarization Associated with a Rare Variant of KCNJ8/KATPChannel. *J. Cardiovasc. Electrophysiol.* 20, 93–98. doi:10.1111/j.1540-8167.2008.01326.x

Hu, D., Barajas-Martínez, H., Terzic, A., Park, S., Pfeiffer, R., Burashnikov, E., et al. (2014). ABCC9 Is a Novel Brugada and Early Repolarization Syndrome Susceptibility Gene. *Int. J. Cardiol.* 171, 431–442. doi:10.1016/j.ijcard.2013.12.084

Huang, Y., McClenaghan, C., Harter, T. M., Hinman, K., Halabi, C. M., Matkovich, S. J., et al. (2018). Cardiovascular Consequences of KATP Overactivity in Cantu Syndrome. *JCI Insight* 3, e121153. doi:10.1172/jci.insight.121153

Inagaki, N., Gonoi, T., Clement, J. P., Namba, N., Inazawa, J., Gonzalez, G., et al. (1995). Reconstitution of I KATP : An Inward Rectifier Subunit Plus the Sulfonylurea Receptor. *Science* 270, 1166–1170. doi:10.1126/science.270.5239.1166

Jorholt, J., Formicheva, Y., Vershinina, T., Kiselev, A., Muravyev, A., Demchenko, E., et al. (2020). Two New Cases of Hypertrophic Cardiomyopathy and Skeletal Muscle Features Associated with ALPK3 Homozygous and Compound Heterozygous Variants. *Genes* 11, 1201. doi:10.3390/genes11101201

Levin, M. D., Singh, G. K., Zhang, H. X., Uchida, K., Kozel, B. A., Stein, P. K., et al. (2016). K ATP Channel Gain-Of-Function Leads to Increased Myocardial L-type Ca 2+ Current and Contractility in Cantu Syndrome. *Proc. Natl. Acad. Sci. U.S.A.* 113, 6773–6778. doi:10.1073/pnas.1606465113

Levin, M. D., Zhang, H., Uchida, K., Grange, D. K., Singh, G. K., and Nichols, C. G. (2015). Electrophysiologic Consequences of KATP Gain of Function in the Heart: Conduction Abnormalities in Cantu Syndrome. *Heart Rhythm* 12, 2316–2324. doi:10.1016/j.hrthm.2015.06.042

McClenaghan, C., Hanson, A., Sala-Rabanal, M., Roessler, H. I., Josifova, D., Grange, D. K., et al. (2018). Cantu Syndrome-Associated SUR2 (ABCC9) Mutations in Distinct Structural Domains Result in KATP Channel Gain-Of-Function by Differential Mechanisms. *J. Biol. Chem.* 293, 2041–2052. doi:10.1074/jbc.RA117.000351

Medeiros-Domingo, A., Tan, B.-H., Crotti, L., Tester, D. J., Eckhardt, L., Cuoretti, A., et al. (2010). Gain-of-function Mutation S422L in the KCNJ8-Encoded Cardiac KATP Channel Kir6.1 as a Pathogenic Substrate for J-Wave Syndromes. *Heart Rhythm* 7, 1466–1471. doi:10.1016/j.hrthm.2010.06.016

Miki, T., and Seino, S. (2005). Roles of K Channels as Metabolic Sensors in Acute Metabolic Changes. *J. Mol. Cell Cardiol.* 38, 917–925. doi:10.1016/j.yjmcc.2004.11.019

Miki, T., Suzuki, M., Shibasaki, T., Uemura, H., Sato, T., Yamaguchi, K., et al. (2002). Mouse Model of Prinzmetal Angina by Disruption of the Inward Rectifier Kir6.1. *Nat. Med.* 8, 466–472. doi:10.1038/nm0502-466

Olson, T. M., Alekseev, A. E., Moreau, C., Liu, X. K., Zingman, L. V., Miki, T., et al. (2007). KATP Channel Mutation Confers Risk for Vein of Marshall Adrenergic Atrial Fibrillation. *Nat. Rev. Cardiol.* 4, 110–116. doi:10.1038/ncpcardio0792

Pipatpolkai, T., Usher, S., Stansfeld, P. J., and Ashcroft, F. M. (2020). New Insights into KATP Channel Gene Mutations and Neonatal Diabetes Mellitus. *Nat. Rev. Endocrinol.* 16, 378–393. doi:10.1038/s41574-020-0351-y

Smeland, M. F., McClenaghan, C., Roessler, H. I., Savelberg, S., Hansen, G. Å. M., Hjellnes, H., et al. (2019). ABCC9-related Intellectual Disability Myopathy Syndrome Is a KATP Channelopathy with Loss-Of-Function Mutations in ABCC9. *Nat. Commun.* 10, 4457. doi:10.1038/s41467-019-12428-7

Tester, D. J., Tan, B.-H., Medeiros-Domingo, A., Song, C., Makielski, J. C., and Ackerman, M. J. (2011). Loss-of-Function Mutations in the KCNJ8 -Encoded Kir6.1 K ATP Channel and Sudden Infant Death Syndrome. *Circ. Cardiovasc. Genet.* 4, 510–515. doi:10.1161/CIRCGENETICS.111.960195

Conflict of Interest: The authors declare that the research was conducted in the absence of any commercial or financial relationships that could be construed as a potential conflict of interest.

Publisher's Note: All claims expressed in this article are solely those of the authors and do not necessarily represent those of their affiliated organizations, or those of the publisher, the editors, and the reviewers. Any product that may be evaluated in this article, or claim that may be made by its manufacturer, is not guaranteed or endorsed by the publisher.

frontiers | Frontiers in Genetics

CASE REPORT
published: 29 April 2022
doi: 10.3389/fgene.2022.810853

Case Report: Two Novel *L1CAM* Mutations in Two Unrelated Chinese Families With X-Linked Hydrocephalus

*Hang Zhou†, Qiuxia Yu†, Yingsi Li, Fang Fu, Ru Li, Guilan Chen, Dan Wang, Yan Lu, Xin Yang, Dongzhi Li and Can Liao**

Department of Prenatal Diagnostic Center, Guangzhou Women and Children's Medical Center, Guangzhou Medical University, Guangzhou, China

L1 cell adhesion molecule is a type I transmembrane glycoprotein belonging to the immunoglobulin superfamily. Pathogenic mutations of *L1CAM* can cause L1 syndrome, referred to as a variety of disease spectrums characterized by hydrocephalus. In the present study, we reported two novel variants of *L1CAM* in two unrelated Chinese families with fetal hydrocephalus history. The woman of family 1, with three consecutive adverse birth histories of male fetuses with hydrocephalus, was identified by an exome sequence with a heterozygous mutation in the *L1CAM* gene, NM_000425.4: c.1696_1703 + 14del (p. S566Vfs*35), which was predicted to be pathogenic. It is predicted to disrupt RNA splicing and likely leads to an absent or disrupted protein product. In family 2, the mother, previously with once a voluntary termination of pregnancy owning to the fetus with hydrocephalus, was pregnant with a fetus with hydrocephalus in her second pregnancy. After fetal blood sampling, a pathogenic deletion of 1511bp in *L1CAM*, chromosome X: 153131395-153132905(hg19/GRCh37)/NM_000425.4: c.2043_2432-121del1511 leading to deletion of fibronectin type-III repeats I-II, was identified in the fetus with hydrocephalus inherited from the mother by an exome sequence. On her third pregnancy, a healthy female fetus was born without the *L1CAM* variant by preimplantation genetic testing for the monogenic disorder. This study emphasizes the importance of ultrasonic manifestation and family history of fetal hydrocephalus for *L1CAM* diagnosis. Our study expands the genotypes of *L1CAM* and aids the genetic counseling of fetal hydrocephalus and even preimplantation genetic testing for the monogenic disorder.

Keywords: *L1CAM*, hydrocephalus, exome sequence, prenatal diagnosis, case report

OPEN ACCESS

Edited by:
María L. Couce, Complejo Hospitalario Universitario de Santiago, Spain

Reviewed by:
Zailong Qin, Maternal and Child Health Hospital of Guangxi Zhuang Autonomous Region, China
Xuan Shang, Southern Medical University, China

****Correspondence:***
Can Liao
canliao@hotmail.com

†These authors have contributed equally to the work

Specialty section:
This article was submitted to Genetics of Common and Rare Diseases, a section of the journal Frontiers in Genetics

Received: *08 November 2021*
Accepted: *04 April 2022*
Published: *29 April 2022*

Citation:
Zhou H, Yu Q, Li Y, Fu F, Li R, Chen G, Wang D, Lu Y, Yang X, Li D and Liao C (2022) Case Report: Two Novel L1CAM Mutations in Two Unrelated Chinese Families With X-Linked Hydrocephalus. Front. Genet. 13:810853. doi: 10.3389/fgene.2022.810853

INTRODUCTION

Hydrocephalus is an important birth defect and not rarely seen in fetuses. The incidence of hydrocephalus is approximately 4.65 per 10,000 live births (Garne et al., 2010). X-linked hydrocephalus due to aqueductal stenosis is the most common genetic cause of fetal hydrocephalus (Schrander-Stumpel and Fryns, 1998). Mutations in L1 cell adhesion molecule (L1CAM) were established as a pathogenic factor in X-linked recessive neural disorders (Rosenthal et al., 1992; Adle-Biassette et al., 2013).

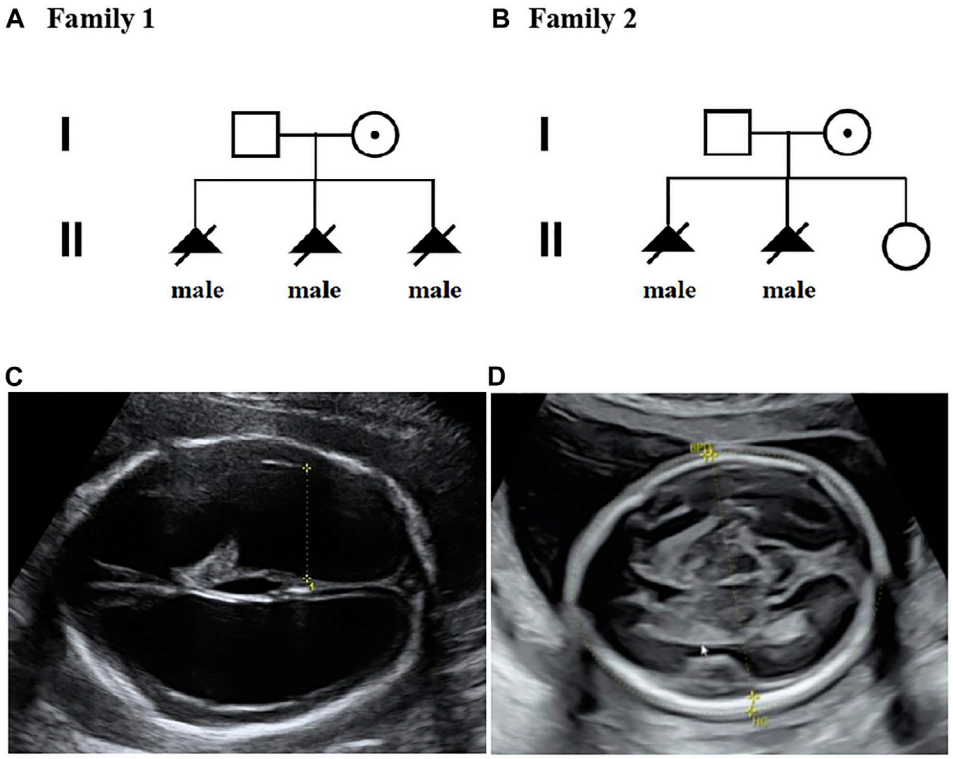

FIGURE 1 | Pedigrees of two families with X-linked hydrocephalus; **(A)** Pedigree of family 1; **(B)** Pedigree of family 2; **(C)** Ultrasound view of the second fetus with severe hydrocephaly from family 2; **(D)** No hydrocephalus was found in II-3 individual with normal anomaly scan of ultrasound from family 2.

L1 cell adhesion molecule (L1CAM) belongs to the immunoglobulin supergene family and plays an essential role in neuronal migration, neuronal cell survival, development, and differentiation (Kenwrick et al., 2000). L1 syndrome is defined as a variety of phenotypes caused by mutations of *L1CAM*, including CRASH syndrome (corpus callosum hypoplasia, retardation, adducted thumbs, spastic paraplegia, and hydrocephalus; OMIM 303350), hydrocephalus due to stenosis of the aqueduct of Sylvius (HSAS; OMIM 307000), and hydrocephalus with Hirschsprung disease (OMIM 307000) (Vos et al., 2010).

To date, 292 pathogenic mutations of L1CAM were identified according to the Human Gene Mutation Database (HGMD). The characteristics of mutations revealed 36.8% missense mutations, 18.6% splice site changes, and 22.3% deletions. The classical phenotypes induced by mutations in *L1CAM* mainly included hydrocephalus, accompanied by other disorders. Here, we described two novel variants of *L1CAM*, which were both unreported previously, including NM_000425.4:c.1696_1703 + 14del (p.S566Vfs*35) and the intragenic base deletion of 1511bp, chromosome X: 153131395-153132905(hg19/GRCh37)/NM_000425.4: c.2043_2432-121del1511, in two unrelated families from the Chinese mainland.

CASE PRESENTATION

Case 1

A non-pregnant woman came to our center of prenatal diagnosis for consultation after three consecutive adverse birth histories of fetuses with hydrocephalus but without image data. All fetuses were male. The pedigree is shown in **Figure 1A**. However, there were no chromosomal or genetic tests for the three fetuses. Karyotype results in this couple did not reveal any abnormality. The couple wanted to find out the etiology of the three consecutive adverse birth histories of hydrocephalus. We offered a whole-exome sequence (**Figure 2A**) for this couple and found a novel pathogenic heterozygous variation in the *L1CAM* gene in the woman, NM_000425.4: c.1696_1703 + 14delAGTGACAAGTGAGGACAGTGAC(p.S566Vfs*35). Sanger sequence results for the couple confirmed this variant (**Figure 3A**). But the variant has yet to be reported or present in population databases (1000 Genome Project, ExAC, EVS, and gnomAD). This variant is a deletion of part of exon 13 (c.1696_1703 + 14del), which may disrupt functions of the Ig-like C2-type 6 domain in the *L1CAM* gene. It is predicted to disrupt RNA splicing and likely leads to an absent or disrupted protein product. It is highly associated with the *L1CAM* gene and the phenotype of three consecutive males with hydrocephalus. Based on the standards and guidelines of the American College of Medical Genetics and Genomics, the variant was predicted to be pathogenic (PVS1+PM2_Supporting + PP4). However, her subsequent fertility condition cannot be acquired by a telephone follow-up.

Case 2

A 36-year-old woman was in her second pregnancy at 24 weeks of gestation (**Figure 1B**). She was referred to our prenatal diagnosis

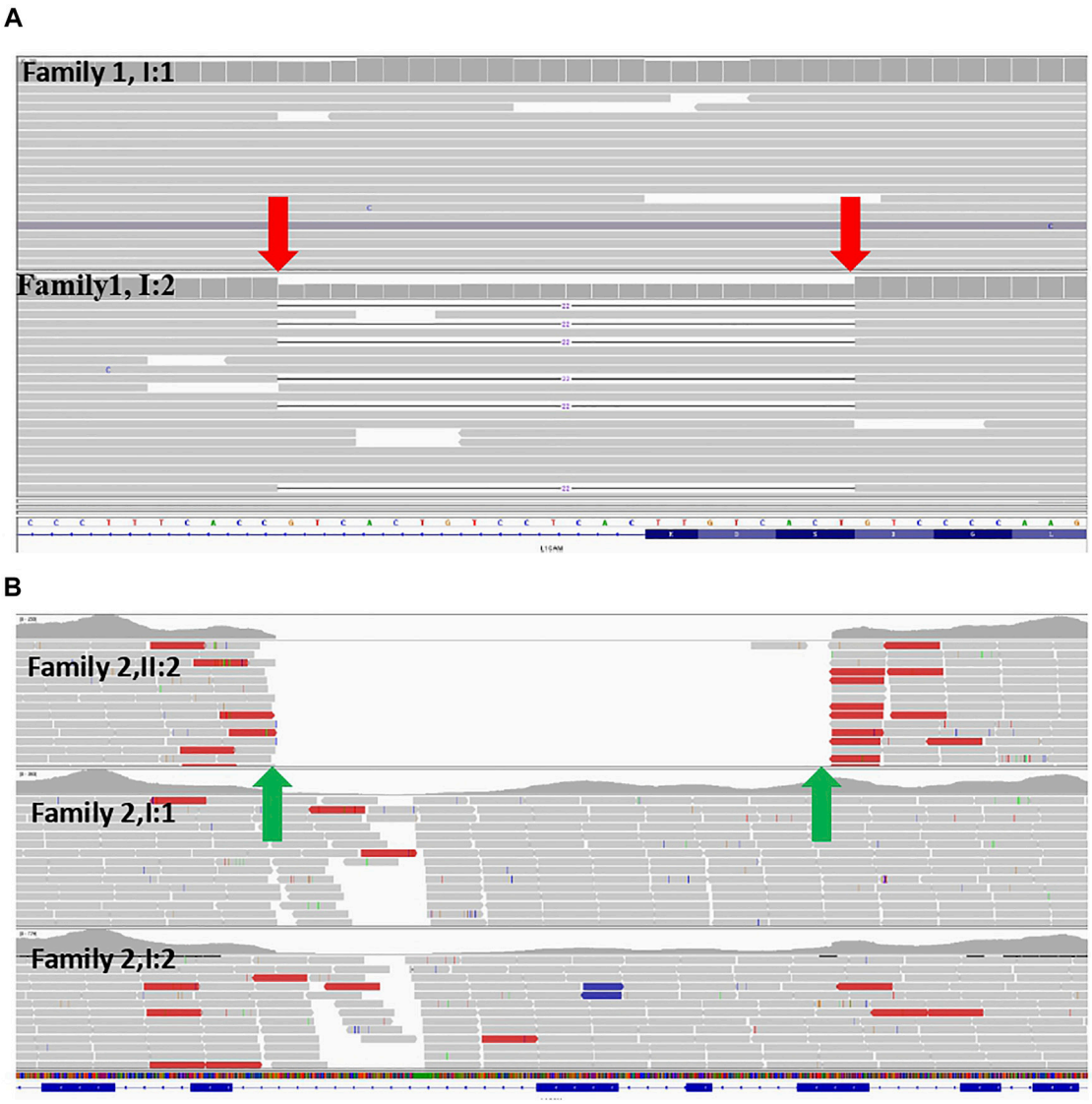

FIGURE 2 | (A) Exome sequence for the couple from family 1 indicated that the woman was a carrier of the variant (NM_000425: c.1696_1703 + 14del) in the *L1CAM* gene (red arrows) **(B)** Exome sequence for family 2 displayed that the deletion of 1511bp in *L1CAM* chromosome X: 153131395 (hg19/GRCh37)/ NM_000425.4:c.2043_2432-121del1511 in the II-2 fetus (green arrows).

department because of fetuses diagnosed with hydrocephalus and invisible cavum septum pellucidum by ultrasound. We confirmed hydrocephalus but did not find invisible cavum septum pellucidum by ultrasound (**Figure 1C**). In the first trimester, there was a normal ultrasound examination, and the nuchal translucency measurement was 1.5 mm. Nevertheless, she previously had one voluntary termination of pregnancy owning to the fetus with hydrocephalus in 24 gestational weeks, but genetic tests were not performed for this fetus. This couple was both healthy and not consanguineous. There were no abnormal karyotype results in the couple. After informed consent, we performed cordocentesis on this woman. The TORCH-IgM and karyotype results were normal. But trio medical exome sequencing identified a copy number variation in *L1CAM* inherited from his mother in this male fetus, chromosome X: 153131395-153132905(hg19/GRCh37)/ NM_000425.4: c.2043_2432-121del1511 (**Figure 2B**); this structural variant was confirmed by Sanger sequence (**Figure 3B**), whereas it has not been previously reported, and it was predicted to cause disruption in partial exon 16 and whole-exons 17 and 18, leading to deletion of fibronectin type-III repeats I-II. The parents requested to terminate the pregnancy but refused autopsy at 25 gestational weeks. After that, she chose preimplantation genetic testing for monogenic disorders (PGT-M) to gain an embryo with an absence of this mutation in her third pregnancy. Amniocentesis was performed in our department at 17 weeks of pregnancy, showing and confirming the absence of this mutation (**Figure 3C**; II-3). Chromosomal

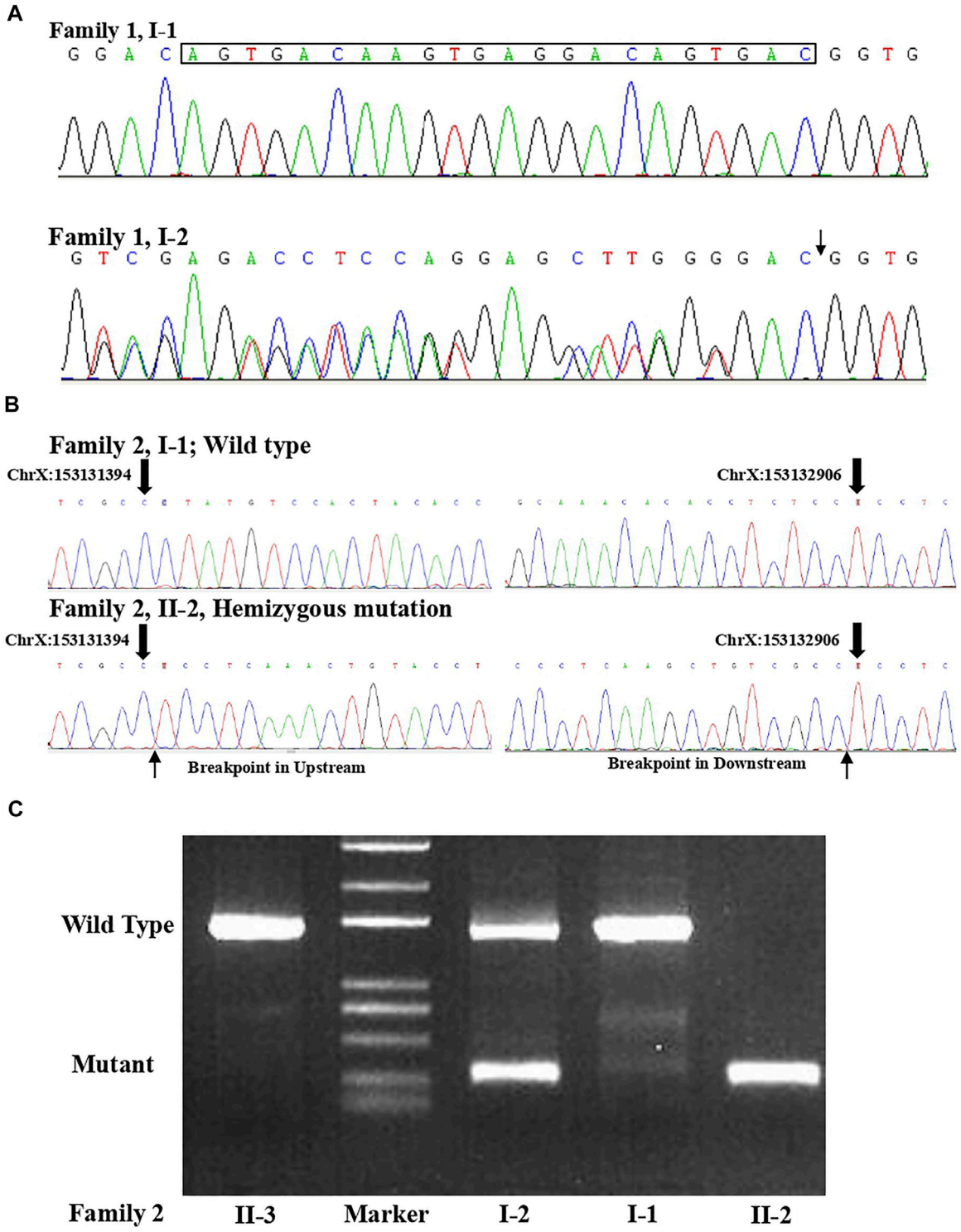

FIGURE 3 | (A) Sanger sequence for the couple from family 1 confirmed that the woman was a carrier of the variant (c.1696_1703 + 14del) in the *L1CAM* gene. **(B)** Sanger sequence result for family 2 validated the deletion (c.2043_2432-121del) in *L1CAM* in II-2 fetus. **(C)** Agarose gel electrophoresis in the *L1CAM* result from family 2.

microarray analysis was normal. This healthy female fetus showed a normal anomaly scan of ultrasound in the second trimester (**Figure 1D**) and was born at 38 weeks of gestation by cesarean section for social reasons. Her birth weight was 3.0 kg, and her head circumference was 33.1 cm. Apgar scores were 9 and 10 at 1 and 5 min after birth, respectively. There was no report of

hydrocephalus and mental disorders through the telephone follow-up.

MATERIAL AND METHODS

Karyotype and Chromosomal Microarray Analysis

To determine the karyotype of fetal cord blood, amniocytes, and peripheral blood, colchicines were used to arrest samples at the metaphase by conventional karyotyping. G-banding karyotype was performed at the 320–400 band level by analyzing 20 split phases. CMA analysis was performed using the Affymetrix CytoScan HD GeneChip Platform (Affymetrix, Santa Clara, CA, United States) with copy number variation (CNV) and single nucleotide polymorphism (SNP) probes, following the manufacturer's instructions. Genomic DNA was isolated from samples by using a QIAamp DNA Blood Midi/Mini kit (QIAGEN GmbH; Hilden, Germany). The CNVs were reported at a 100-kb threshold with a marker count of ≥50.

Exome Sequence

Target enrichment in DNA samples was performed using Agilent SureSelect human exome capture probes (V6, Life Technologies, United States), according to the manufacturer's protocol. The DNA library was sequenced on Hiseq XTen (Illumina, Inc., San Diego, CA, United States) for pair-end 150-bp reads. Raw reads were filtered using Trimmomatic to remove adapter-contaminated reads and low-quality reads. Clean reads were aligned to the human reference genome (hg19/GRCh37) with BWA. BAM files were generated by SNP analysis, duplication marking, indel realignment, and recalibration by GATK and SAMtools. The minor allele frequencies (MAFs) of all known variants were annotated according to dbSNP, the 1000 Genome Project, ExAC, EVS, gnomAD, and our in-house database. Databases such as OMIM, ClinVar, and the Human Gene Mutation Database were used to determine mutation harmfulness and pathogenicity where appropriate. To predict biological effect analysis of candidate variant genes, multiple computational algorithms were used, including SIFT, MutationTaster, PolyPhen2, PROVEAN, CADD, Human Splicing Finder, MaxEntScan, and NNSplice.

DISCUSSION

L1 syndrome is referred to as an X-linked recessive disorder and includes broad phenotypic spectrums dominated by hydrocephalus. The diagnostic yield can become higher when identifying characteristics of the L1 syndrome and family history (Adle-Biassette et al., 2013). The detection rate of the L1 syndrome can reach up to 32% for patients with at least two additional cases (Ochando et al., 2016). Therefore, the clinician should not overlook this syndrome when hydrocephalus in fetuses is recognized by prenatal ultrasound, especially in women with an abnormal reproductive history of a male fetus.

From the mutation characteristics in *L1CAM*, variants of L1CAM seem unique in families, and there is no hotspot mutation. However, recent studies revealed the correlations between genotypes and phenotypes in the *L1CAM* gene. Phenotypic severity primarily depends on the location and type of mutation of *L1CAM* (Fransen et al., 1998). Extracellular mutations resulting in truncation or absence of *L1CAM* lead to a more severe phenotype. Milder to severe phenotype could be caused by missense mutations in the extracellular part. Cytoplasmic mutations tend to generate a milder phenotype which might affect signal transduction or interaction with the cytoskeleton (Sebens Müerköster et al., 2007).

The woman from family 1 carried a novel heterozygous variant NM_000425.4: c.1696_1703 + 14del (p.S566Vfs*35). So we strongly believed that all the three consecutive male fetuses with hydrocephalus were with the hemizygous pathogenic mutation, although samples were unavailable. This variant results in a deletion of part of exon 13 and is predicted to disrupt RNA splicing and likely leads to an absent or disrupted protein product. It might lead to a more severe phenotype from the report of genotype–phenotype correlation in *L1CAM* (Fransen et al., 1998). Although this variant has not been reported in the literature with *L1CAM*-related diseases, it is known that the variant with loss-of-function in *L1CAM* was pathogenic (Vos et al., 2010). A similar variant NM_000425.5: c.1702_1703 + 14del reported from ClinVar (rs1603275315) was classified as likely pathogenic, showing spastic paraplegia. Furthermore, this variant from family 1 affected the integrity of the sixth Ig domain of *L1CAM*. The Ig-like domains of L1CAM play a major role in interactions with several extracellular ligands such as phosphacan and neurocan, integrins, axonin-1/TAG1, Sema 3A, and also itself (Ruppert et al., 1995; Castellani et al., 2000). Another report has also shown that an individual with a variant of splice site change (c. 1704-1G > A) was diagnosed with adducted thumbs, hydrocephalus, and spastic paraplegia, accompanying abnormal karyotype (47, XXY) (Kanemura et al., 2006). A mutation involving the sixth Ig domain of L1CAM (L1-6D) (c.1759 G > C; p. G587R) was previously associated with developmental delay, dysmorphic facies, adducted thumbs, truncated corpus callosum, and periventricular heterotopias associated with polymicrogyria in a 2.5-year-old boy (Shieh et al., 2015). Investigations of the L1-6D knocked-out mice revealed typical hydrocephalus. The L1-6D isoform lost its ability to bind to *L1CAM* in a homophilic manner and α5β1 integrin (Hortsch, 1996). In another report on L1-6D mice, the phenotype exhibited abnormal ensheathment of unmyelinated axons by Schwann cell processes, eventually leading to myelinated multiaxon bundles (Itoh et al., 2005). In conclusion, currently available evidence displays the pathogenicity of this variant, but further study is needed to confirm the observation.

In family 2, we identified a novel large deletion in *L1CAM* in the second fetus and the pregnant woman. First, there are various types of variants in *L1CAM*, which reminds us that besides employing sequencing to detect point mutation, we should consider using proper approaches to identify different variants in *L1CAM*, when one X-linked hydrocephalus is

suspected. Second, there were a few reports of a large deletion in *L1CAM*. To our knowledge, variants of more than 1 kb of deletion were found in our current study, and in addition, three cases of an *L1CAM* whole-gene deletion were previously described in other reports. Knops et al. have reported a 61 kb in size encompassing all of L1CAM, AVPR2, and part of ARHGAP4, leading to L1 syndrome and nephrogenic diabetes insipidus (Knops et al., 2008). This individual was diagnosed to require shunting due to significant hydrocephalus. The second case, identified with an *L1CAM* whole-gene deletion and *PDZD4* gene, was also found with hydrocephalus that needed shunting (Kutsche et al., 2002). Similar to the second case, the third report demonstrated a 4-month-old male with a *de novo L1CAM* whole-gene deletion and *PDZD4* gene (Chidsey et al., 2014). Simultaneous deletions in upstream or downstream were present in all three reports of *L1CAM* whole-gene deletion. Moreover, the variant from family 2 was predicted to cause deletion of fibronectin type-III repeats 1-2 (FN III 1-2). De Angelis et al. demonstrated that mutations located throughout Ig1-Ig6 and Fn2 disrupted both types of interactions by synthesizing L1CAM-Fc fusion proteins of disease-causing variants (De Angelis et al., 1999; De Angelis et al., 2002). One study found that FN III 1-5 in *L1CAM* could interact with the fibroblast growth factor receptor (FGFR), which was essential in neuronal differentiation and FGFR1 phosphorylation. Authors speculated that FN III 2 amino acids (AVNNQGKG) were crucial binding sites (Kulahin et al., 2008). Furthermore, FN III 2 plays an important part in interactions with *L1CAM* and enhances structural stability in the extracellular region (Kunz et al., 1998). Therefore, the variant of family 2 could disturb the interaction with FGFR to cause neural axon malformation, resulting in severe hydrocephalus. Further functional studies of the variant were being conducted in our laboratory.

Preimplantation genetic testing for monogenic disease (PGT-M) is a useful tool for the *in vitro* fertilization (IVF) process (Masset et al., 2019). A biopsy is performed for single or several cells from IVF embryos to exclude the curated disease-causing cells, selectively transferring the unaffected embryos. After the pathogenic variant in *L1CAM* was identified, the couple from family 2 benefited from the PGT technology and eventually delivered a healthy infant without this mutation.

In conclusion, this study described two novel pathogenic variants and phenotypes in two Chinese families, which effectively blocked the transmission of genetic birth defects. These patients presented here may provide insights to better understand the L1 syndrome and probably help genetic counseling and PGT for prenatal X-linked hydrocephalus.

DATA AVAILABILITY STATEMENT

The original contributions presented in the study are included in the article/Supplementary Material, further inquiries can be directed to the corresponding author.

ETHICS STATEMENT

The studies involving human participants were reviewed and approved by The Ethics Committee of Guangzhou Women and Children's Medical Care Center. The patients/participants provided their written informed consent to participate in this study. Written informed consent was obtained from the individual(s) for the publication of any potentially identifiable images or data included in this article.

AUTHOR CONTRIBUTIONS

HZ, QY, YL, FF, RL, and DW analyzed the WES data. GC and YL performed Sanger sequencing. XY and DL provided chromosomal and clinical data. HZ and YL prepared the figures. HZ, QY, and CL wrote the manuscript. All authors read and approved the final manuscript.

FUNDING

This work was supported by the sub-project of the National Key Research and Developmental Program (2021YFC2701002), the National Natural Science Foundation of China (81801461, 81873836, 81771594, 81671474, 81501267), and the Natural Science Foundation of Guangdong Province (2019A1515012034, 2017A030313460), and the General Guide Project of Guangzhou Health Commission (20221A011038).

ACKNOWLEDGMENTS

The authors would like to thank the two families who participated in this study.

REFERENCES

Adle-Biassette, H., Saugier-Veber, P., Fallet-Bianco, C., Delezoide, A.-L., Razavi, F., Drouot, N., et al. (2013). Neuropathological Review of 138 Cases Genetically Tested for X-Linked Hydrocephalus: Evidence for Closely Related Clinical Entities of Unknown Molecular Bases. *Acta Neuropathol.* 126 (3), 427–442. doi:10.1007/s00401-013-1146-1

Castellani, V., Chédotal, A., Schachner, M., Faivre-Sarrailh, C., and Rougon, G. (2000). Analysis of the L1-Deficient Mouse Phenotype Reveals Cross-Talk between Sema3A and L1 Signaling Pathways in Axonal Guidance. *Neuron* 27 (2), 237–249. doi:10.1016/s0896-6273(00)00033-7

Chidsey, B. A., Baldwin, E. E., Toydemir, R., Ahles, L., Hanson, H., and Stevenson, D. A. (2014). L1CAMwhole Gene Deletion in a Child with L1 Syndrome. *Am. J. Med. Genet.* 164 (6), 1555–1558. doi:10.1002/ajmg.a.36474

De Angelis, E., MacFarlane, J., Du, J. S., Yeo, G., Hicks, R., Rathjen, F. G., et al. (1999). Pathological Missense Mutations of Neural Cell Adhesion Molecule L1 Affect Homophilic and Heterophilic Binding Activities. *Embo j* 18 (17), 4744–4753. doi:10.1093/emboj/18.17.4744

De Angelis, E., Watkins, A., Schäfer, M., Brümmendorf, T., and Kenwrick, S. (2002). Disease-associated Mutations in L1 CAM Interfere with Ligand Interactions and Cell-Surface Expression. *Hum. Mol. Genet.* 11 (1), 1–12. doi:10.1093/hmg/11.1.1

Fransen, E., Van Camp, G., D'Hooge, R., Vits, L., and Willems, P. J. (1998). Genotype-phenotype Correlation in L1 Associated Diseases. *J. Med. Genet.* 35 (5), 399–404. doi:10.1136/jmg.35.5.399

Garne, E., Loane, M., Addor, M.-C., Boyd, P. A., Barisic, I., and Dolk, H. (2010). Congenital Hydrocephalus - Prevalence, Prenatal Diagnosis and Outcome of Pregnancy in Four European Regions. *Eur. J. Paediatric Neurol.* 14 (2), 150–155. doi:10.1016/j.ejpn.2009.03.005

Hortsch, M. (1996). The L1 Family of Neural Cell Adhesion Molecules: Old Proteins Performing New Tricks. *Neuron* 17 (4), 587–593. doi:10.1016/s0896-6273(00)80192-0

Itoh, K., Fushiki, S., Kamiguchi, H., Arnold, B., Altevogt, P., and Lemmon, V. (2005). Disrupted Schwann Cell-Axon Interactions in Peripheral Nerves of Mice with Altered L1-Integrin Interactions. *Mol. Cell Neurosci.* 30 (1), 131–136. doi:10.1016/j.mcn.2005.06.006

Kanemura, Y., Okamoto, N., Sakamoto, H., Shofuda, T., Kamiguchi, H., and Yamasaki, M. (2006). Molecular Mechanisms and Neuroimaging Criteria for Severe L1 Syndrome with X-Linked Hydrocephalus. *J. Neurosurg. Pediatr.* 105 (5 Suppl. l), 403–412. doi:10.3171/ped.2006.105.5.403

Kenwrick, S., Watkins, A., and De Angelis, E. (2000). Neural Cell Recognition Molecule L1: Relating Biological Complexity to Human Disease Mutations. *Hum. Mol. Genet.* 9 (6), 879–886. doi:10.1093/hmg/9.6.879

Knops, N. B. B., Bos, K. K., Kerstjens, M., van Dael, K., and Vos, Y. J. (2008). Nephrogenic Diabetes Insipidus in a Patient with L1 Syndrome: A New Report of a Contiguous Gene Deletion Syndrome includingL1CAMandAVPR2. *Am. J. Med. Genet.* 146a (14), 1853–1858. doi:10.1002/ajmg.a.32386

Kulahin, N., Li, S., Hinsby, A., Kiselyov, V., Berezin, V., and Bock, E. (2008). Fibronectin Type III (FN3) Modules of the Neuronal Cell Adhesion Molecule L1 Interact Directly with the Fibroblast Growth Factor (FGF) Receptor. *Mol. Cell Neurosci.* 37 (3), 528–536. doi:10.1016/j.mcn.2007.12.001

Kunz, S., Spirig, M., Ginsburg, C., Buchstaller, A., Berger, P., Lanz, R., et al. (1998). Neurite Fasciculation Mediated by Complexes of Axonin-1 and Ng Cell Adhesion Molecule. *J. Cel Biol* 143 (6), 1673–1690. doi:10.1083/jcb.143.6.1673

Kutsche, K., Ressler, B., Katzera, H.-G., Orth, U., Gillessen-Kaesbach, G., Morlot, S., et al. (2002). Characterization of Breakpoint Sequences of Five Rearrangements inL1CAM andABCD1 (ALD) Genes. *Hum. Mutat.* 19 (5), 526–535. doi:10.1002/humu.10072

Masset, H., Zamani Esteki, M., Dimitriadou, E., Dreesen, J., Debrock, S., Derhaag, J., et al. (2019). Multi-centre Evaluation of a Comprehensive Preimplantation Genetic Test through Haplotyping-By-Sequencing. *Hum. Reprod.* 34 (8), 1608–1619. doi:10.1093/humrep/dez106

Ochando, I., Vidal, V., Gascón, J., Acién, M., Urbano, A., and Rueda, J. (2016). Prenatal Diagnosis of X-Linked Hydrocephalus in a Family with a Novel Mutation inL1CAMgene. *J. Obstet. Gynaecol.* 36 (3), 403–405. doi:10.3109/01443615.2015.1086982

Rosenthal, A., Jouet, M., and Kenwrick, S. (1992). Aberrant Splicing of Neural Cell Adhesion Molecule L1 mRNA in a Family with X-Linked Hydrocephalus. *Nat. Genet.* 2 (2), 107–112. doi:10.1038/ng1092-107

Ruppert, M., Aigner, S., Hubbe, M., Yagita, H., and Altevogt, P. (1995). The L1 Adhesion Molecule Is a Cellular Ligand for VLA-5. *J. Cel Biol* 131 (6 Pt 2), 1881–1891. doi:10.1083/jcb.131.6.1881

Schrander-Stumpel, C., and Fryns, J.-P. (1998). Congenital Hydrocephalus: Nosology and Guidelines for Clinical Approach and Genetic Counselling. *Eur. J. Pediatr.* 157 (5), 355–362. doi:10.1007/s004310050830

Sebens Müerköster, S., Werbing, V., Sipos, B., Debus, M. A., Witt, M., Grossmann, M., et al. (2007). Drug-induced Expression of the Cellular Adhesion Molecule L1CAM Confers Anti-apoptotic protection and Chemoresistance in Pancreatic Ductal Adenocarcinoma Cells. *Oncogene* 26 (19), 2759–2768. doi:10.1038/sj.onc.1210076

Shieh, C., Moser, F., Graham, J. M., Jr., Watiker, V., and Pierson, T. M. (2015). Mutation in the Sixth Immunoglobulin Domain ofL1CAMis Associated with Migrational Brain Anomalies. *Neurol. Genet.* 1 (4), e34. doi:10.1212/nxg.0000000000000034

Vos, Y. J., de Walle, H. E. K., Bos, K. K., Stegeman, J. A., Ten Berge, A. M., Bruining, M., et al. (2010). Genotype-phenotype Correlations in L1 Syndrome: a Guide for Genetic Counselling and Mutation Analysis. *J. Med. Genet.* 47 (3), 169–175. doi:10.1136/jmg.2009.071688

Conflict of Interest: The authors declare that the research was conducted in the absence of any commercial or financial relationships that could be construed as a potential conflict of interest.

Publisher's Note: All claims expressed in this article are solely those of the authors and do not necessarily represent those of their affiliated organizations, or those of the publisher, the editors, and the reviewers. Any product that may be evaluated in this article, or claim that may be made by its manufacturer, is not guaranteed or endorsed by the publisher.

frontiers | Frontiers in Genetics

ORIGINAL RESEARCH
published: 06 June 2022
doi: 10.3389/fgene.2022.824445

Mutant *B3GALT6* in a Multiplex Family: A Dominant Variant Co-Segregated With Moderate Malformations

Fang Shen[1], *Yongjia Yang*[1]*, *Yu Zheng*[1], *Ming Tu*[1], *Liu Zhao*[1], *Zhenqing Luo*[1], *Yuyan Fu*[1] and *Yimin Zhu*[1,2]*

[1]The Laboratory of Genetics and Metabolism, Pediatrics Research Institute of Hunan Province, Hunan Children's Hospital, Hengyang Medical School, University of South China, Changsha, China, [2]Emergency Research Institute of Hunan Province, Hunan People's Hospital, Changsha, China

B3GALT6 is a well-documented disease-related gene. Several *B3GALT6*-recessive variants have been reported to cause Ehlers–Danlos syndrome (EDS). To the best of our knowledge, no dominant *B3GALT6* variant that causes human disease has been reported. In 2012, we reported on a three-generation, autosomal-dominant family with multiple members who suffered from radioulnar joint rotation limitation, scoliosis, thick vermilion of both lips, and others, but the genetic cause was unknown. Here, exome sequencing of the family identified mutant *B3GALT6* as the cause of the multiplex affected family. We observed that, in the compound heterozygous pattern (i.e., c.883C>T:p.R295C and c.510_517del:p.L170fs*268), mutant *B3GALT6* led to severe consequences, and in the dominant pattern, an elongated *B3GALT6* variant co-segregated with moderate phenotypes. The functional experiments were performed *in vitro*. The R295C variant led to subcellular mislocalization, whereas the L170fs*268 showed normal subcellular localization, but it led to an elongated protein. Given that most of the catalytic galactosyltransferase domain was disrupted for the L170fs*268 (it is unlikely that such a protein has activity), we propose that the L170fs*268 occupies the normal *B3GALT6* protein position in the Golgi and exerts a dominant-negative effect.

Keywords: *B3GALT6*, autosomal dominant, heterozygous variant, dominant-negative effect, EDS

OPEN ACCESS

Edited by:
Emiliano González Vioque, University Clinical Hospital of Santiago, Spain

Reviewed by:
Anupriya Kaur, Post Graduate Institute of Medical Education and Research (PGIMER), India
Hongzhou Duan, Peking University, China
Bo Wang, Shanghai Children's Medical Center, China

***Correspondence:**
Yongjia Yang
yongjia727@aliyun.com
Yimin Zhu
xiangeryiym@aliyun.com

Specialty section:
This article was submitted to Genetics of Common and Rare Diseases, a section of the journal Frontiers in Genetics

Received: *29 November 2021*
Accepted: *25 April 2022*
Published: *06 June 2022*

Citation:
Shen F, Yang Y, Zheng Y, Tu M, Zhao L, Luo Z, Fu Y and Zhu Y (2022) Mutant B3GALT6 in a Multiplex Family: A Dominant Variant Co-Segregated With Moderate Malformations. Front. Genet. 13:824445. doi: 10.3389/fgene.2022.824445

INTRODUCTION

Glycosaminoglycan (GAG), a key component of the extracellular matrix, is essential for the development and maintenance of bone, cartilage, skin, and other tissues. GAG synthesis is initiated by the formation of a tetrasaccharide linker region attached to a serine residue in the proteoglycan core protein (Prydz and Dalen, 2000). Synthesis of the linker region involves four successive steps catalyzed by distinctive enzymes: xylosyltransferases I/II (encoded by *XYLT1* and *XYLT2*) (Götting et al., 2000; Bui et al., 2014; Munns et al., 2015; Umair et al., 2018; LaCroix et al., 2019), galactosyltransferase I (β4GalT7, encoded by *B4GALT7*) (Guo et al., 2013; Cartault et al., 2015; Ritelli et al., 2017; Sandler-Wilson et al., 2019), galactosyltransferase II (β3GalT6, encoded by *B3GALT6*) (Malfait et al., 2013; Nakajima et al., 2013), and glucuronosyltransferase I (GlcAT-I, encoded by *B3GAT3*) (Yauy et al., 2018; Colman et al., 2019). Recessive pathogenic variants of any of these four genes lead to severe skeletal deformities and connective tissue disruptions.

B3GALT6 (NM_080605.3) is a single-exon gene on chromosome 1p36.33, which encodes beta-1,3-galactosyltransferase 6 (β3GalT6). The enzyme localizes predominantly in the Golgi apparatus and catalyzes the addition of a third galactose to the second galactose of the GAG linker region. In 2013,

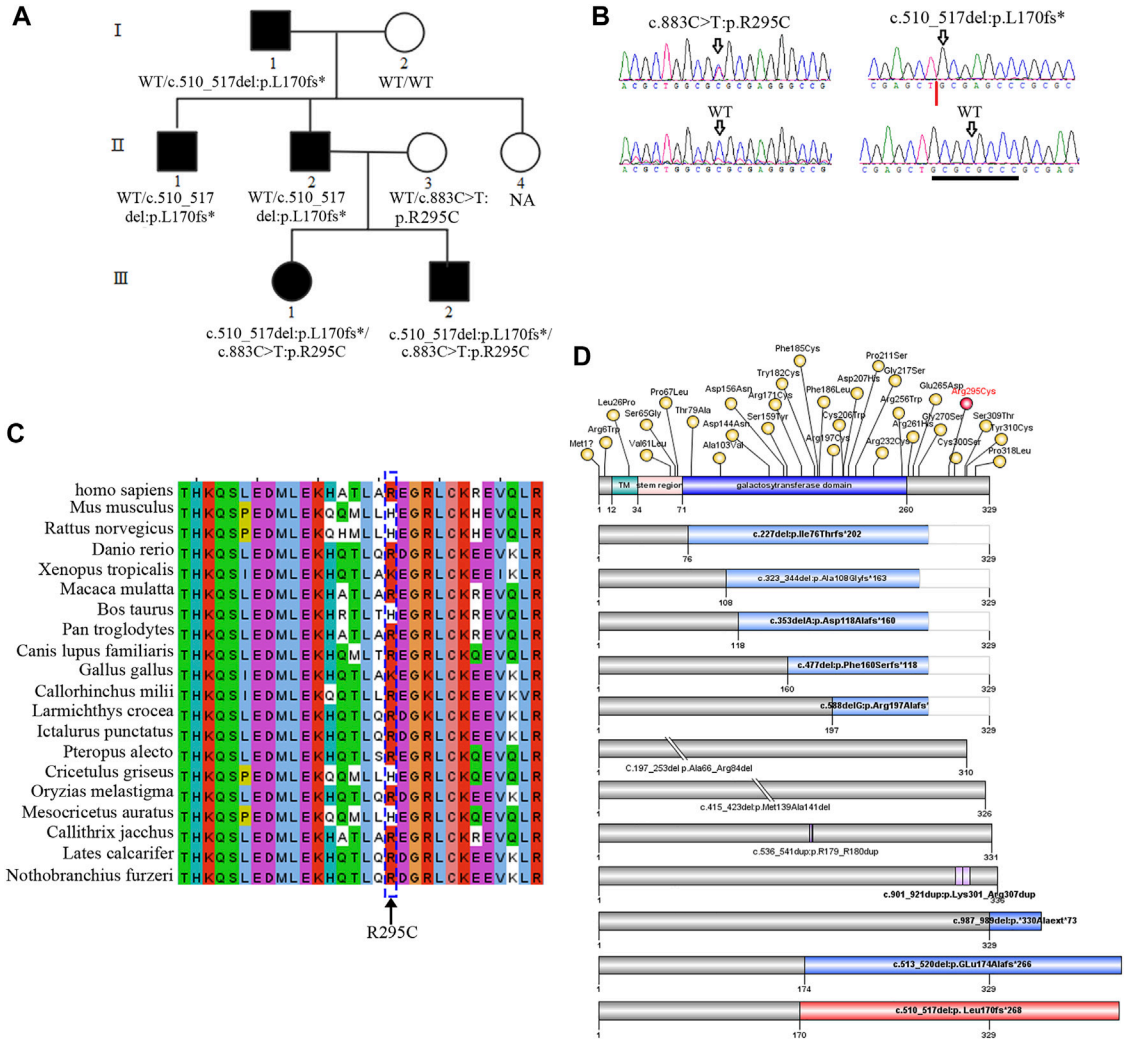

FIGURE 1 | *B3GALT6* mutated in an autosomal-dominant family. **(A)** Pedigree with five affected members. NA, genomic DNA was unavailable. **(B)** Two variants in the family, i.e., c.883C>T:p.R295C and c.510_517del:p. L170fs*268. Note: the trace figure of c.510_517del was identified by Sanger sequencing after the PCR fragment TA-clone experiment. **(C)** Protein sequence alignment of the residue 295 (arginine) across different species. **(D)** Schematic view of β3Galt6 protein and the position of the pathogenic variants reported so far. The upper bar represents the domain structure of wild-type (WT) β3Galt6. Missense variants identified so far were depicted above the WT-β3Galt6, and indel variants were depicted below the WT-β3Galt6. TM, transmembrane region. Note: variants depicted as red were found in this study.

Malfait et al. (2013) and Nakajima et al. (2013) reported *B3GALT6* pathogenic variants in human diseases. Since then, dozens of *B3GALT6* variants in the recessive status have been identified in approximately 40 unrelated families with Ehlers–Danlos syndrome (EDS) (Sellars et al., 2014; Vorster et al., 2015; Alazami et al., 2016; Trejo et al., 2017; Ben-Mahmoud et al., 2018; Van Damme et al., 2018; Caraffi et al., 2019).

In 2012, we reported on an autosomal-dominant (AD), three-generation family with multiple members presenting with radioulnar limitation, scoliosis, thick vermilion of both lips, and a shortened and thickened femur neck (Zhu et al., 2012). Exome sequencing (ES) of the family was performed. Variant analysis and validation tests identified the following: 1) *B3GALT6*-recessive (compound heterozygous) variants led to severe phenotypes (EDS); 2) the frameshift-elongated variant (c.510_517del:p.L170fs*268) segregated with moderate deformities in three members of the family in a dominant manner. Functional experiments confirmed that the R295C variant was loss-of-function, but the elongated variant (p.L170fs*268) may exert a dominant-negative effect. This is the first report on *B3GALT6*-dominant variant leading to disease.

MATERIALS AND METHODS

Study Subjects

The study was approved by the Academic Committee of Hunan Children's Hospital (approval number: HCHLL58, Changsha

TABLE 1 | Manifestations and radiographic findings of the individuals in the family.

Family ID	I:1	II:1	II:2	III:1	III:2
General information					
Gender	Male	Male	Male	Female	Male
Age (years)	67	41	38	14	7
Birth weight (g)	ND	ND	ND	3,030	2,850
Intelligence	Normal	Normal	Normal	Mild deficit in speech	Normal
Height (cm)	169	177	175	139 (158.6)	109 (122)
Weight (kg)	70	76	67	35 (50.5)	18.1 (22.9)
Craniofacial					
Thick vermilion lips	+	+	+	+	+
Flat malar region	+	+	–	+	+
High forehead	–	–	–	+	+
Epicanthal folds	–	–	–	+	+
Prominent eyes	–	–	–	+	+
Blue sclerae	–	–	–	+	+
Protruding ear	–	–	–	+	+
Musculoskeletal					
Scoliosis	+	+	+	++	++
Fifth-finger clinodactyly	+	-	-	+	+
Restricted elbow movement	+	+	+	+	+
Joint hypermobility	–	–	–	++	++
Radiological features					
Radioulnar synostosis	+	–	–	+	+
Shortened and thickened femoral neck	ND	ND	ND	+	+
Others	Aclasis of right humerus and ulna	—	—	Soft, doughy skin	Barrel chest and soft, doughy skin

ND, no data.

City, Hunan Province, China). All family members provided written informed consent to participate in this study.

Exome Sequencing

ES was carried out on seven individuals (I:1, I:2, II:1, II:2, II:3, III:1, and III:2) (**Figure 1A**). The detailed ES pipelines have been reported previously (Yang et al., 2019). Briefly, genomic DNA was fragmented into 180–280 bp segments, libraries were prepared and captured using an Agilent SureSelect Human All Exon V6 kit for each individual, and the effective concentration of each sample was subsequently sequenced on an Illumina HiSeq X Ten Sequencing system (Illumina Inc., San Diego, CA, United States). The raw BCL file was then converted into a raw FASTQ file. Raw reads were filtered using FastQC to remove low-quality reads. Clean reads were then mapped to the reference genome GRCh37 using Bwa. After removing duplications, SNV and InDel were called and annotated using GATK. For each sample, 11.9 G bases were obtained. The average yield was 16.6 Gb with an error rate of <0.1%. Furthermore, >90% bases had a Phred quality score of ≥30 (Q30).

Cell Transfection and Western Blot

The empty vector pCMV-14-3 ×flag or *B3GALT6* expression constructs (WT, R295C, or L170fs*268) were separately transfected into HeLa cells using Lipofectamine 3000 (Invitrogen, L3000-015) for 48 h. Protein extracts were collected and separated by 10% SDS-PAGE, electrotransferred to a polyvinylidene fluoride (PVDF) membrane (0.45 μm, Merck Millipore Ltd.), blocked with buffer containing 5% non-fat milk, and incubated with mouse monoclonal anti-flag antibody (1:2500) (Sigma, F1804) overnight at 4°C and HRP-conjugated secondary antibodies for 1 h at room temperature and developed with an enhanced chemiluminescence HRP substrate kit (Millipore, WBKLS0500). The membrane was visualized using an iBright FL1500 imaging system (Invitrogen).

Cellular Immunofluorescence

HeLa cells were seeded on coverslips in 24-well culture plates. When the cells reached 80% confluence, the *B3GALT6* expression constructs were transfected for 48 h. Cells were blocked with 4% paraformaldehyde for 30 min, permeabilized with 0.2% Triton X-100 for 10 min, and blocked with 5% BSA for 1 h at room temperature. The solution was discarded, and the mouse monoclonal anti-flag antibody (1:500) (Sigma, F1804) and rabbit anti-GOLPH4 antibody (1:400) (Abcam, ab28049) were added onto the coverslips overnight at 4°C in a moist environmental box. The secondary antibody Cy3-conjugated goat anti-mouse IgG (Origene, TA130012) and FITC-conjugated goat anti-rabbit IgG (Origene, TA130021) were incubated for 1 h at room temperature in a dark place, and then DAPI was added onto coverslips for 5 min. Coverslips

were mounted on the slide. Cell images were captured with laser scanning confocal microscopy LSM 800.

RESULTS

B3GALT6 Variants in the Family

As previously reported, an autosomal-dominant family was investigated (**Figure 1A**; **Table 1**), and we suspected that the family was affected by Giuffre–Tsukahara syndrome at that time (Zhu et al., 2012). ES was successfully performed on seven family members (**Figure 1A**). After obtaining the variant list, we first focused on the loss-of-function variants (including canonical splicing variants, indels, or other truncating variants) as well as elongation frameshift variants. Because AD inheritance was observed in the index family (**Figure 1A**), and the disease is extremely rare, we focused on heterozygous, rare, coding variants with AF less than 0.0001 (Exac_eas; gnomAD_eas; 1000G_eas; gomAD_genome all). Then, we only considered the variants (absent in our 700 in-house ES data) that co-segregated with the affected status in the index family; one variant remained, c.510_517del:p. L170fs*268, at *B3GALT6*. Because *B3GALT6* is a known gene for the connective tissue disorder (EDS), we reanalyzed all *B3GALT6* rare variants with AF less than 0.001 (including missense variants) and identified another *B3GALT6* missense variant, i.e., c.883C>T:p.R295C on three family members (II:3, III:1, and III:2). Sanger sequencing validation confirmed that two family members with severe phenotypes (III:1 and III:2) had *B3GALT6* compound heterozygous variants (c.883C>T:p.R295C/c.510_517del:p. L170fs*268) (**Figures 1A,B**; **Table 1**). Unaffected family member II:3 was heterozygous for c.883C>T:p.R295C variant (**Figures 1A,B**; **Table 1**), and family members I:1, II:1, and II:2 with moderate phenotypes suffered by c.510_517del:p.L170fs*268 heterozygous variant (**Figures 1A,B**; **Table 1**).

Functional Characteristics of β3Galt6 Variants

The c.883C>T:p.R295C is not located in the catalytic galactosyltransferase domain (**Figure 1D**). Protein sequence alignment indicated that residue 295 (arginine) was not highly conserved across different species (**Figure 1C**). Meanwhile, in the gnomAD database, there was a very low frequency (AF = 0.0005) in the East Asian population, and 13/23 silico software predicted it to be benign or tolerant (**Supplementary Table S1**). The c.510_517del:p.L170fs*268 variant was not found in the ExAC, 1000G, and gnomAD databases, and it was not observed in 700 exome databases of our in-house datasheet that are unrelated to skeletal diseases (data not shown).

According to the first in-frame ATG in the reference sequence (NM_080605.4), the c.510_517del variant led to a frameshift

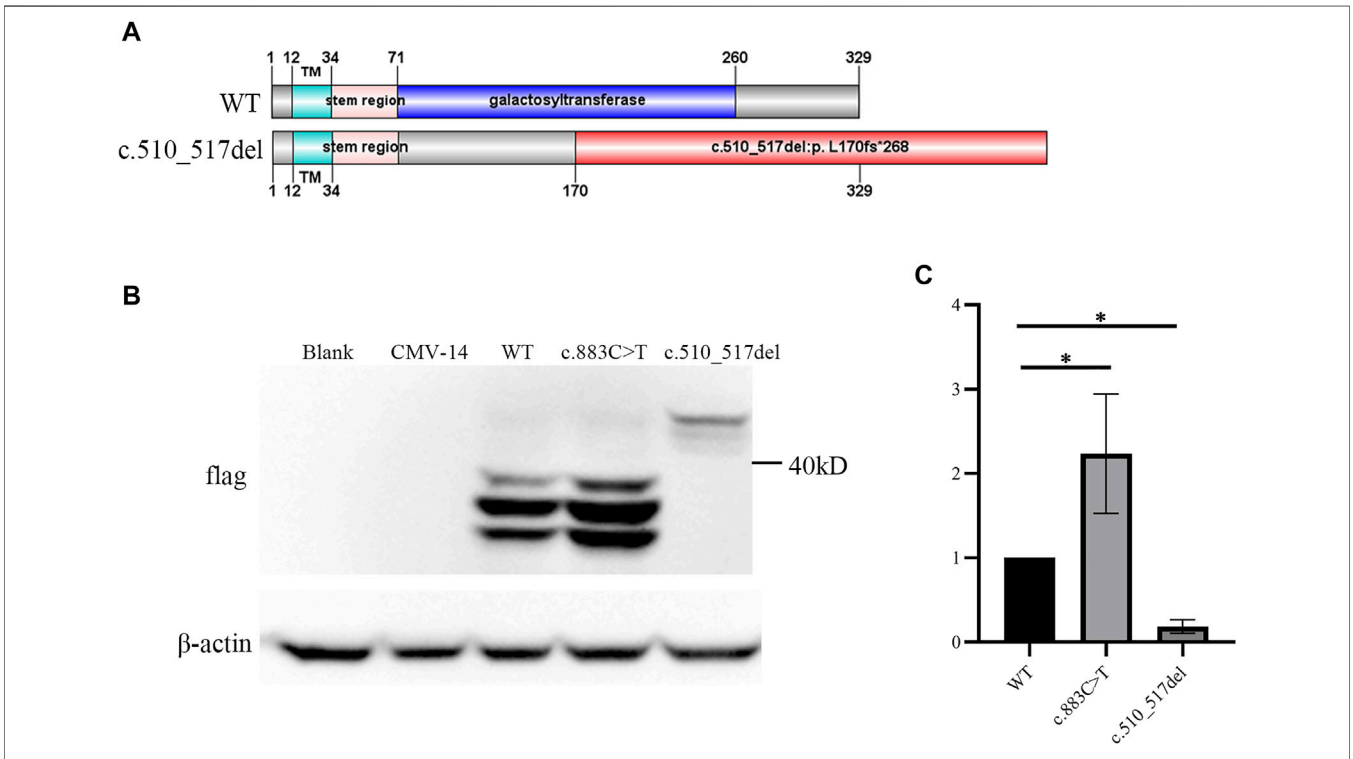

FIGURE 2 | c.510_517del:p. L170fs*268 linked an elongated product. **(A)** Upper panel represents the wild-type (WT) β3Galt6. Lower panel represents the c.510_517del:p. L170fs*268 elongation variant. Note: in wild-type β3Galt6, the catalytic galactosyltransferase domain was depicted in blue; red: frameshift amino acid sequence caused by the deletion. **(B)** Western blot analysis of lysates from HeLa cells expressing WT and mutant *B3GALT6*. CMV-14, empty plasmid. **(C)** Relative density of β3Galt6. $n = 4$ per group, $^*p < 0.05$.

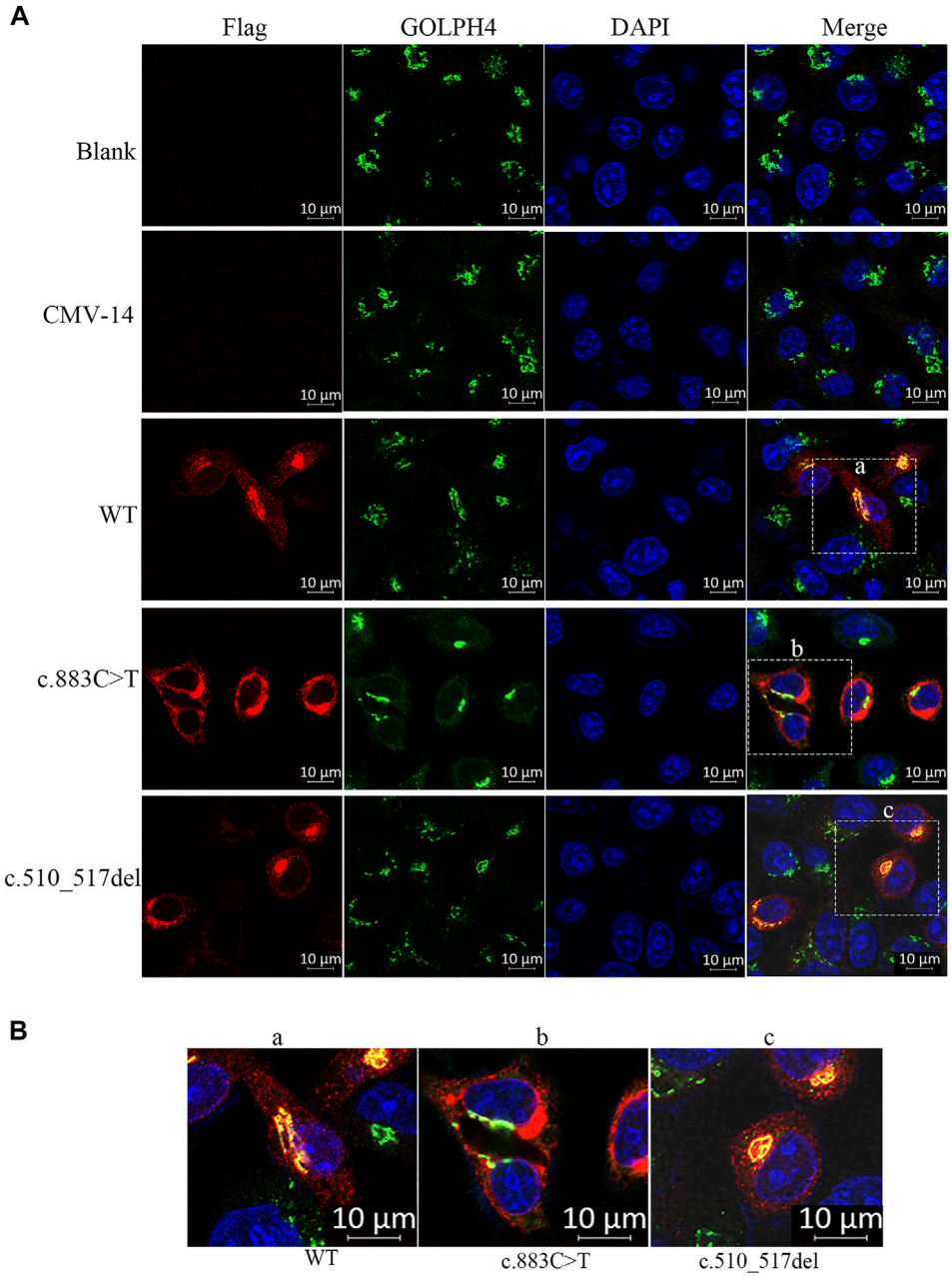

FIGURE 3 | Subcellular localization of β3Galt6. **(A)** HeLa cells were transfected with plasmid carrying the wild-type (WT), the c.883C>T, or the c.510_517del variant. Cells were stained with anti-FLAG (red), anti-GOLPH4 (green), and DAPI (blue). **(B)** Enlarged images of **(a–c)** point of **(A)**.

mutation and introduced a termination codon delay. Consequently, it was predicted that the mutant-elongated protein contained 438 amino acids in contrast to the wild-type protein, which contained 329 amino acids (**Figure 1**; **Supplementary Material S1**).

β3Galt6 mainly functions in the Golgi (Bai et al., 2001). Previous studies have identified *B3GALT6* variants exerting pathogenic effects by subcellular mislocalization or unstable structure of the mutant protein or by the unstable/incomplete transcript at the RNA level (Nakajima et al., 2013; Ben-Mahmoud et al., 2018). We then overexpressed β3Galt6 (WT, R295C, or L170fs*268) in the HeLa cells. Western blot analysis showed that: 1) the size of the R295C protein was the same as that of the wild-type protein, but the expression of R295C was increased significantly (**Figures 2B,C**); 2) in contrast to wild-type β3Galt6, a band with a larger molecular weight was observed for the frameshift mutant protein (L170fs*268), and a significantly reduced expression was observed (**Figures 2B,C**).

Second, we checked the subcellular localization of β3Galt6 (WT, R295C, or L170fs*268). In contrast to WT-β3Galt6

expressed in the Golgi (as it co-localized with GOLPH4, which is a marker of the Golgi) (**Figure 3**), the mutant R295C protein was found in the cytoplasm but not in the Golgi (**Figure 3**), indicating that the mutant R295C protein was functionally null. In contrast, β3Galt6-L170fs*268 was located in the Golgi compartment, as it overlaps with GOLPH4. According to the ACMG/AMP criteria (Richards et al., 2015), both the variants were classified as pathogenic; the evaluation results of the L170fs*268 variant were PVS1, PM1, PM2, PP1, and PP4; and for the R295C variant, the evaluation results were PS3, PM2, PM3, PP1, and PP4.

Heterozygous *B3GALT6*- L170fs*268 Leading to a Moderate Phenotype

The family members III:1 and III:2 exhibited severe phenotypes (which were consistent with EDS). Other individuals in the family (I:1, II:1, and II:2) did not meet the criteria for EDS and clearly exhibited moderate phenotypes (**Table 1** and ref 22). The *in vitro* study identified that a plasmid with c.510_517del:p. L170fs*26 variant can express an elongated protein (**Figure 2**), and the mutant elongated protein can be correctly localized in the Golgi. Given that the L170fs*26 frameshift variant resulted in about half of the catalytic galactosyltransferase domain being disrupted (**Figure 2A**), we propose that the elongated protein (having no catalytic function) occupies the Golgi position disrupting normal GAG production, resulting in a dominant-negative effect.

In brief, the present study identified two novel B3GALT6 pathogenic variants in a multiplex family: 1) in the recessive status, mutant B3GALT6 causing EDS; and 2) in the dominant status, the elongation-mutant β3Galt6 causing moderate phenotypes (although not reaching the level of a typical EDS).

DISCUSSION

As a key enzyme in GAG synthesis, β3Galt6 is encoded by the *B3GALT6* gene (Bai et al., 2001). In an autosomal-recessive manner, pathogenic variants of *B3GALT6* lead to a multisystem disorder mainly comprising bone deformity and connective tissue disruption, that is, spondylodysplastic EDS (Malfait et al., 2013; Nakajima et al., 2013; Van Damme et al., 2018; Caraffi et al., 2019). Approximately, 60 patients from 40 families have been reported to have mutated *B3GALT6* (Malfait et al., 2013; Nakajima et al., 2013; Sellars et al., 2014; Ritelli et al., 2015; Vorster et al., 2015; Alazami et al., 2016; Trejo et al., 2017; Ben-Mahmoud et al., 2018; Van Damme et al., 2018; Caraffi et al., 2019; Zhang et al., 2020; Descartes et al., 2021; Leoni et al., 2021). Among these patients, 41 *B3GALT6* pathogenic variants have been reported (**Figure 1C**), including two start-codon loss (Nakajima et al., 2013; Van Damme et al., 2018), two in-frame deletion variants (Nakajima et al., 2013; Van Damme et al., 2018), two in-frame duplication variants (Alazami et al., 2016; Trejo et al., 2017), five frameshift variants that lead to truncation of the protein (Malfait et al., 2013; Nakajima et al., 2013; Ritelli et al., 2015; Van Damme et al., 2018; Caraffi et al., 2019), two frameshift variants that lead to elongation of the protein (Van Damme et al., 2018; Caraffi et al., 2019), and 28 missense variants (Malfait et al., 2013; Nakajima et al., 2013; Sellars et al., 2014; Ritelli et al., 2015; Vorster et al., 2015; Alazami et al., 2016; Trejo et al., 2017; Ben-Mahmoud et al., 2018; Van Damme et al., 2018; Caraffi et al., 2019; Zhang et al., 2020; Descartes et al., 2021; Leoni et al., 2021). Frameshift variants that lead to protein elongation (combined with other missense variants) have been reported in several severe sporadic patients (Van Damme et al., 2018; Caraffi et al., 2019).

Given that 41 B3GALT6 pathogenic variants (including elongation variants) have been reported on EDS as described previously, none of these variants caused a dominant phenotype. In the present study, we identified two novel *B3GALT6* pathogenic variants, i.e., the c.883C>T: p.R295C and the c.510_517del:p.L170fs*268. The *B3GALT6*-prolonged variant (c.510_517del:p.L170fs*268) was detected in five family members. In two members (who combined with another point R295C variant), severe phenotypes (typical components of EDS) were observed, which is consistent with previous studies, that is, in the recessive status, B3GALT6 variants lead to EDS. The novelty of the present study is that in the other three family patients (I:1, II:1, and II:2), the heterozygous L170fs*268 variant co-segregated with less severe but obvious phenotypes, such as radioulnar joint limitation, "S"-shaped scoliosis, and thick vermilion of the lips.

To test the functional consequences of the elongation variant, we expressed *B3GALT6* L170fs*268 protein in HeLa cells. Western blot analysis identified an apparently elongated band (with a significantly reduced amount), which was consistent with the cell immunofluorescence assay in which the *B3GALT6* L170fs*268 protein could be detected in the cytoplasm. However, in the immunofluorescence assay, we did not observe a reduction in the L170fs*268 protein. Such a difference in protein amount between the Western blot assay and the immunofluorescence assay may contribute to the L170fs*268 proteins having less stability when they are separated from the *in vivo* cells.

Similar to WT-β3Galt6, which is expressed in the Golgi, the β3Galt6-L170fs*268 is also located in the Golgi. Therefore, the previous pathomechanism (subcellular mislocalization or haploinsufficiency) cannot explain the heterozygous β3Galt6-L170fs*268 variant-causing phenotypes. Given that the heterozygous β3Galt6-L170fs*268 variant co-segregated with moderate phenotypes in the family produced an elongated protein, and the mutant protein could localize to the Golgi apparatus, we propose that the disease-causing mechanism for this elongation variant is the L170fs*268 that occupies the Golgi apparatus and disrupts the normal CAG production. Nevertheless, to confirm the novel β3Galt6-pathogenic mechanism, further studies, such as galactosyltransferase activity assay, GAG synthesis assay, and CS and HS chain quantifications, are warranted to elucidate the detailed mechanism.

In conclusion, we identified heterozygous *B3GALT6*-causing phenotypes that implicate a new dominant inheritance pattern of the mutated *B3GALT6* or CAG syntheses.

DATA AVAILABILITY STATEMENT

The datasets presented in this study can be found in online repositories. The names of the repository/repositories and accession number(s) can be found in the article/ **Supplementary Material**.

ETHICS STATEMENT

The studies involving human participants were reviewed and approved by the Academic Committee of Hunan Children's Hospital. Written informed consent to participate in this study was provided by the participants or the participants' legal guardian/next of kin.

AUTHOR CONTRIBUTIONS

YY, FS, and YiZ designed the research, analyzed the experimental data, and wrote the manuscript. YuZ, MT, LZ, ZL, and YF performed the sample collection and research. All authors contributed to the manuscript and approved the submitted version.

FUNDING

This work was supported by grants from the National Natural Science Foundation of China (31501017 to YY and 81271946 to YiZ) and Hunan Health Commission Research Fund (B2019019 to YY).

ACKNOWLEDGMENTS

The authors thank the subjects for their participation in this research study.

SUPPLEMENTARY MATERIAL

The Supplementary Material for this article can be found online at: https://www.frontiersin.org/articles/10.3389/fgene.2022.824445/full#supplementary-material

REFERENCES

Alazami, A. M., Al-Qattan, S. M., Faqeih, E., Alhashem, A., Alshammari, M., Alzahrani, F., et al. (2016). Expanding the Clinical and Genetic Heterogeneity of Hereditary Disorders of Connective Tissue. *Hum. Genet.* 135 (5), 525–540. doi:10.1007/s00439-016-1660-z

Bai, X., Zhou, D., Brown, J. R., Crawford, B. E., Hennet, T., and Esko, J. D. (2001). Biosynthesis of the Linkage Region of Glycosaminoglycans. *J. Biol. Chem.* 276 (51), 48189–48195. doi:10.1074/jbc.M107339200

Ben-Mahmoud, A., Ben-Salem, S., Al-Sorkhy, M., John, A., Ali, B. R., and Al-Gazali, L. (2018). A B3GALT6 Variant in Patient Originally Described as Al-Gazali Syndrome and Implicating the Endoplasmic Reticulum Quality Control in the Mechanism of Some β3GalT6-pathy Mutations. *Clin. Genet.* 93 (6), 1148–1158. doi:10.1111/cge.13236

Bui, C., Huber, C., Tuysuz, B., Alanay, Y., Bole-Feysot, C., Leroy, J. G., et al. (2014). Xylt1 Mutations in Desbuquois Dysplasia Type 2. *Am. J. Hum. Genet.* 94 (3), 405–414. doi:10.1016/j.ajhg.2014.01.020

Caraffi, S. G., Maini, I., Ivanovski, I., Pollazzon, M., Giangiobbe, S., Valli, M., et al. (2019). Severe Peripheral Joint Laxity Is a Distinctive Clinical Feature of Spondylodysplastic-Ehlers-Danlos Syndrome (EDS)-B4GALT7 and Spondylodysplastic-EDS-B3galt6. *Genes* 10, 799. doi:10.3390/genes10100799

Cartault, F., Munier, P., Jacquemont, M.-L., Vellayoudom, J., Doray, B., Payet, C., et al. (2015). Expanding the Clinical Spectrum of B4galt7 Deficiency: Homozygous P.R270c Mutation with Founder Effect Causes Larsen of Reunion Island Syndrome. *Eur. J. Hum. Genet.* 23 (1), 49–53. doi:10.1038/ejhg.2014.60

Colman, M., Van Damme, T., Steichen-Gersdorf, E., Laccone, F., Nampoothiri, S., Syx, D., et al. (2019). The Clinical and Mutational Spectrum of B3gat3 Linkeropathy: Two Case Reports and Literature Review. *Orphanet J. Rare Dis.* 14 (1), 138. doi:10.1186/s13023-019-1110-9

Descartes, M., Melenevsky, Y. V., Rudy, N., Smith, K., Callaway, K., and Parker, J. S. (2021). Keratoconus in a Patient with B3GALT6 -related Disorder. *Clin. Genet.* 99 (6), 849–850. doi:10.1111/cge.13940

Götting, C., Kuhn, J., Zahn, R., Brinkmann, T., and Kleesiek, K. (2000). Molecular Cloning and Expression of Human UDP-D-Xylose:Proteoglycan Core Protein β-d-Xylosyltransferase and its First Isoform XT-II. *J. Mol. Biol.* 304 (4), 517–528. doi:10.1006/jmbi.2000.4261

Guo, M. H., Stoler, J., Lui, J., Nilsson, O., Bianchi, D. W., Hirschhorn, J. N., et al. (2013). Redefining the Progeroid Form of Ehlers-Danlos Syndrome: Report of the Fourth Patient withB4GALT7deficiency and Review of the Literature. *Am. J. Med. Genet.* 161A (10), a–n. doi:10.1002/ajmg.a.36128

LaCroix, A. J., Stabley, D., Sahraoui, R., Adam, M. P., Mehaffey, M., Kernan, K., et al. (2019). Ggc Repeat Expansion and Exon 1 Methylation of Xylt1 Is a Common Pathogenic Variant in Baratela-Scott Syndrome. *Am. J. Hum. Genet.* 104 (1), 35–44. doi:10.1016/j.ajhg.2018.11.005

Leoni, C., Tedesco, M., Radio, F. C., Chillemi, G., Leone, A., Bruselles, A., et al. (2021). Broadening the Phenotypic Spectrum of Beta3GalT6 -associated Phenotypes. *Am. J. Med. Genet.* 185 (10), 3153–3160. doi:10.1002/ajmg.a.62399

Malfait, F., Kariminejad, A., Van Damme, T., Gauche, C., Syx, D., Merhi-Soussi, F., et al. (2013). Defective Initiation of Glycosaminoglycan Synthesis Due to B3galt6 Mutations Causes a Pleiotropic Ehlers-danlos-syndrome-like Connective Tissue Disorder. *Am. J. Hum. Genet.* 92 (6), 935–945. doi:10.1016/j.ajhg.2013.04.016

Munns, C. F., Fahiminiya, S., Poudel, N., Munteanu, M. C., Majewski, J., Sillence, D. O., et al. (2015). Homozygosity for Frameshift Mutations in Xylt2 Result in a Spondylo-Ocular Syndrome with Bone Fragility, Cataracts, and Hearing Defects. *Am. J. Hum. Genet.* 96 (6), 971–978. doi:10.1016/j.ajhg.2015.04.017

Nakajima, M., Mizumoto, S., Miyake, N., Kogawa, R., Iida, A., Ito, H., et al. (2013). Mutations in B3galt6, Which Encodes a Glycosaminoglycan Linker Region Enzyme, Cause a Spectrum of Skeletal and Connective Tissue Disorders. *Am. J. Hum. Genet.* 92 (6), 927–934. doi:10.1016/j.ajhg.2013.04.003

Prydz, K., and Dalen, K. T. (2000). Synthesis and Sorting of Proteoglycans. *J. Cell. Sci.* 113 (Pt 2), 193–205. doi:10.1242/jcs.113.2.193

Richards, S., Aziz, N., Bale, S., Bick, D., Das, S., Gastier-Foster, J., et al. (2015). Standards and Guidelines for the Interpretation of Sequence Variants: a Joint Consensus Recommendation of the American College of Medical Genetics and Genomics and the Association for Molecular Pathology. *Genet. Med.* 17 (5), 405–424. doi:10.1038/gim.2015.30

Ritelli, M., Chiarelli, N., Zoppi, N., Dordoni, C., Quinzani, S., Traversa, M., et al. (2015). Insights in the Etiopathology of Galactosyltransferase Ii (Galt-Ii) Deficiency from Transcriptome-wide Expression Profiling of Skin Fibroblasts of Two Sisters with Compound Heterozygosity for Two Novel B3galt6 Mutations. *Mol. Genet. Metabolism Rep.* 2, 1–15. doi:10.1016/j.ymgmr.2014.11.005

Ritelli, M., Dordoni, C., Cinquina, V., Venturini, M., Calzavara-Pinton, P., and Colombi, M. (2017). Expanding the Clinical and Mutational Spectrum of B4galt7-Spondylodysplastic Ehlers-Danlos Syndrome. *Orphanet J. Rare Dis.* 12 (1), 153. doi:10.1186/s13023-017-0704-3

Sandler-Wilson, C., Wambach, J. A., Marshall, B. A., Wegner, D. J., McAlister, W., Cole, F. S., et al. (2019). Phenotype and Response to Growth Hormone Therapy in Siblings with B4galt7 Deficiency. *Bone* 124, 14–21. doi:10.1016/j.bone.2019.03.029

Sellars, E. A., Bosanko, K. A., Lepard, T., Garnica, A., and Schaefer, G. B. (2014). A Newborn with Complex Skeletal Abnormalities, Joint Contractures, and Bilateral Corneal Clouding with Sclerocornea. *Seminars Pediatr. Neurology* 21 (2), 84–87. doi:10.1016/j.spen.2014.04.007

Trejo, P., Rauch, F., Glorieux, F. H., Ouellet, J., Benaroch, T., and Campeau, P. M. (2017). Spondyloepimetaphysial Dysplasia with Joint Laxity in Three Siblings with B3GALT6 Mutations. *Mol. Syndromol.* 8 (6), 303–307. doi:10.1159/000479672

Umair, M., Eckstein, G., Rudolph, G., Strom, T., Graf, E., Hendig, D., et al. (2018). Homozygous Xylt2 Variants as a Cause of Spondyloocular Syndrome. *Clin. Genet.* 93 (4), 913–918. doi:10.1111/cge.13179

Van Damme, T., Pang, X., Guillemyn, B., Gulberti, S., Syx, D., De Rycke, R., et al. (2018). Biallelic B3galt6 Mutations Cause Spondylodysplastic Ehlers-Danlos Syndrome. *Hum. Mol. Genet.* 27 (20), 3475–3487. doi:10.1093/hmg/ddy234

Vorster, A. A., Beighton, P., and Ramesar, R. S. (2015). Spondyloepimetaphyseal Dysplasia with Joint Laxity (Beighton Type); Mutation Analysis in Eight Affected South African Families. *Clin. Genet.* 87 (5), 492–495. doi:10.1111/cge.12413

Yang, Y., Zheng, Y., Li, W., Li, L., Tu, M., Zhao, L., et al. (2019). Smad6 Is Frequently Mutated in Nonsyndromic Radioulnar Synostosis. *Genet. Med.* 21 (11), 2577–2585. doi:10.1038/s41436-019-0552-8

Yauy, K., Tran Mau-Them, F., Willems, M., Coubes, C., Blanchet, P., Herlin, C., et al. (2018). B3gat3-Related Disorder with Craniosynostosis and Bone Fragility Due to a Unique Mutation. *Genet. Med.* 20 (2), 269–274. doi:10.1038/gim.2017.109

Zhang, J., Huang, K., and Dong, G. (2020). Clinical and Genetic Analysis of a Child with Spondyloepimetaphyseal Dysplasia Type 1 and Joint Laxity. *Zhonghua Yi Xue Yi Chuan Xue Za Zhi* 37 (8), 887–890. doi:10.3760/cma.j.issn.1003-9406.2020.08.020

Zhu, Y., Jin, K., Mei, H., Li, L., Liu, Z., Yang, Y., et al. (2012). A Family with Radio-Ulnar Synostosis, Scoliosis, and Thick Vermilion of Lips: A Novel Syndrome or Variant of Giuffrè-Tsukahara Syndrome? *Am. J. Med. Genet.* 158A (8), 2036–2042. doi:10.1002/ajmg.a.35478

Conflict of Interest: The authors declare that the research was conducted in the absence of any commercial or financial relationships that could be construed as a potential conflict of interest.

Publisher's Note: All claims expressed in this article are solely those of the authors and do not necessarily represent those of their affiliated organizations, or those of the publisher, the editors, and the reviewers. Any product that may be evaluated in this article, or claim that may be made by its manufacturer, is not guaranteed or endorsed by the publisher.

frontiers | Frontiers in Genetics

ORIGINAL RESEARCH
published: 01 July 2022
doi: 10.3389/fgene.2022.808181

Novel Variant Expands the Clinical Spectrum of CUX2-Associated Developmental and Epileptic Encephalopathies

*Feng Zhang[1], Fuwei Li[2], Fujian Chen[1], Jinrong Huang[1], Qiong Luo[1], Xilong Du[2], Jiapeng Zhou[2], Weiyue Gu[2] and Kaishou Xu[3]**

[1]Ganzhou Women and Children's Health Care Hospital, Ganzhou, China, [2]Beijing Chigene Translational Medical Research Center Co. Ltd., Beijing, China, [3]Guangzhou Women and Children's Medical Center, Guangzhou Medical University, Guangzhou, China

OPEN ACCESS

Edited by:
María L. Couce,
Complejo Hospitalario Universitario de Santiago, Spain

Reviewed by:
Carlotta Stipa,
IRCCS Institute of Neurological Sciences of Bologna (ISNB), Italy
Cybel Mehawej,
Lebanese American University, Lebanon
Isabella Peixoto De Barcelos,
Children's Hospital of Philadelphia, United States

***Correspondence:**
Kaishou Xu
xksyi@126.com

Specialty section:
This article was submitted to Genetics of Common and Rare Diseases, a section of the journal Frontiers in Genetics

Received: 03 November 2021
Accepted: 14 June 2022
Published: 01 July 2022

Citation:
Zhang F, Li F, Chen F, Huang J, Luo Q, Du X, Zhou J, Gu W and Xu K (2022) Novel Variant Expands the Clinical Spectrum of CUX2-Associated Developmental and Epileptic Encephalopathies. Front. Genet. 13:808181. doi: 10.3389/fgene.2022.808181

Developmental and epileptic encephalopathies (DEE) caused by heterozygous deleterious variants in Cut Like Homeobox2 (*CUX2*) is rare. To the best of our knowledge the only variant associated with a phenotype in this gene is the *de novo* missense variant c.1768G > A, p.Glu590Lys; however, further additional research is needed to characterize the relationship between disease and variants in this gene. In this study, we reported a patient from a non-consanguineous Chinese family presenting with epilepsy, developmental delay, and speech delay. Additionally, the patient responded well to levetiracetam, and at his last follow-up (5.5 years old), he had discontinued antiepileptic drug treatment and remained seizure-free for 6 months. To identify possible causative variants, trio-whole exome sequencing was performed. We identified a novel *de novo* missense *CUX2* c.2834C > T, p. Thr945Met variant in the patient. Based on clinical and genetics information associated with the bioinformatics analyses, we hypothesized that this variant was the cause of the reported phenotype. AlphaFold and SWISS-MODEL homology modeling servers were used to predict the three-dimensional (3D) structure of CUX2 protein. Predictions based on the 3D-structure modeling indicated that the p.Thr945Met substitution was likely to alter the DNA-binding specificities and affect protein function. On the basis of clinical characteristics and genetic analysis, we presented one case diagnosed with DEE67. Our finding expanded the clinical and molecular spectrum of *CUX2* variants.

Keywords: trio-whole exome sequencing, developmental and epileptic encephalopathy 67, CUX2, levetiracetam treatment, CUX2 clinical phenotype

INTRODUCTION

Developmental and epileptic encephalopathies (DEE) is characterized by onset in infancy/early childhood with refractory seizures, delayed psychomotor development or/and developmental regression. DEE is clinically and genetically heterogeneous, with over 50 genes known to be causative (Specchio and Curatolo, 2021). However, the genotype still has a limited effect on the phenotype. The Cut Like Homeobox 2 (*CUX2*) gene, which encodes a 1426 amino-acids transcription factor, plays an important role in the control of neuronal proliferation and differentiation in the brain (Quaggin et al., 1996). Recently, variants in *CUX2* were found to be

associated with developmental and epileptic encephalopathy 67 (DEE67, OMIM: 618141), an autosomal dominant disorder that typically manifests in infancy and is characterized by refractory seizures, global developmental delay with impaired motor and intellectual development, movement disorders, speech delay, and stereotypic or autistic behavior. To date, only 10 patients carrying recurrent *de novo* heterozygous Glu590-to-Lys (E590K) variant in the CUX2 gene have been reported (Barington et al., 2018; Chatron et al., 2018).

Here, we reported a 5.5 years old boy with epilepsy, developmental delay and speech delay. Trio (parents-proband) whole-exome sequence (WES) analysis revealed a novel *de novo* pathogenic missense variant c.2834C > T (p.Thr945Met) in the CUX2 gene. Our findings expand the genetic and phenotypic spectrum of DEE67 and contribute to our understanding of DEE on a genetic level.

MATERIAL AND METHODS

Patients

The proband was a 5.5-year-old boy, the third child of healthy non-consanguineous parents. He had two unaffected female siblings. The patient visited the hospital after experiencing seizures. A detailed clinical history, including a description of epilepsy, a detailed clinical, and a neurological examination was carried out. The study was approved by the Ethics Committee of Ganzhou Women and Children's Health Care Hospital.

Variant Analysis

After obtaining informed consent, samples were taken from the proband and his parents. The whole-exome capture was carried out (xGen Exome Research Panel v1.0, IDT, IA, United States) according to the manufacturer's protocol. High-throughput sequencing was performed using Illumina NovaSeq 6000 series sequencer (PE150), and at least 99% of the target sequence was sequenced. The sequencing process was performed by the Chigene Translational Medicine Research Center Co., Ltd., 100875, Beijing.

After eliminating adapters and low-quality reads, clean data were obtained and aligned to the Human genome (Hg19/GRC37) using the Burrows-Wheeler Alignment (BWA). The Genome Analysis Toolkit (GATK) was used to identify single nucleotide variants (SNVs) and insertion/deletion (InDel) variants. The Exome Aggregation Consortium ExAC was used to determine the allele frequencies of variants. Pathogenicity of nonsynonymous variants was predicted using the SIFT, Provean, REVEL, varianttaster, PolyPhen, and CADD tools. SNVs/indels were classified according to the standards and guidelines of the American College of Medical Genetics and Genomics (ACMG) and the Association for Molecular Pathology (AMP) (Richards et al., 2015).

Variants were confirmed by Polymerase Chain Reaction (PCR) analysis, followed by Sanger sequencing. *CUX2* was amplified using the following primers: forward primer (5′-CAGCCTGGTACAAGTCCCAAC-3′) and reverse primer (5′-CAGACTTATCCGCTGGTCCC-3′). DNA sequencing was performed using the 3730xl DNA Analyzer (Applied Biosystems, United States). The rare variant identified has been submitted to the ClinVar database (Accession number: SCV001946791) (https://www.ncbi.nlm.nih.gov/clinvar/variation/1296981).

Multiple protein sequence alignments were performed using MEGA X, and the modeling of the 3D structure was analyzed and visualized using Swiss-PdbViewer v4.1.

RESULTS

Clinical Features

The proband (II:1) had the onset of febrile seizure at the age of 2 years with unconsciousness, up-rolling of the eyes, facial twitching, limb stretch, and no visible limb shaking; 6 months later, a second febrile seizure occurred, and 3 months later a third febrile seizure occurred. Each seizure lasted 3 min and was followed by spontaneous remission. At 2 years and 9 months the medical team started levetiracetam (40 mg/kg/day) and patient did not present any other febrile seizure. After 2 years without clinical or electrographic seizures, the boy has discontinued levetiracetam and remained seizure-free until the age of five. At 2 years and 9 months, the electroencephalograph (EEG) revealed a somewhat slower background activity and a small number of bilateral spikes and spike-wave discharges in the central, parietal, and posterior temporal regions during sleep, but subsequent magnetic resonance imaging (1.5T MRI) was normal. EEG performed at the age of 5 years without levetiracetam was normal. He was able to walk alone at 18 months. At the age of 2 years and 9 months, the patient was diagnosed with global developmental delay and he was not able to form three word sentences and just could pronounce few words with correct meaning. The results of the Gesell Development Diagnosis Scale (GDDS) revealed a total development quotient (DQ) of 56 (mild developmental delay). Then the patient has received home-based rehabilitation for 3 years. Now he is 5.5 years in kindergarten and the DQ score has been improved to 75 (borderline deficiency).

Variant Identification and Analysis

Trio-WES was performed and a heterozygous *de novo* missense variant (NM_015267.4: c.2834C > T, p.Thr945Met), in the CUX2 gene was identified in the proband. This c.2834C > T variant was not identified in the 1000 genome project or ExAC. Numerous computational tools, including PolyPhen (probably damaging, 1.0), Provean (deleterious, −4.16), SIFT (damaging, 0.0), mutationtaster (disease_causing, 1), and REVEL (deleterious, 0.582) suggested that the variant was deleterious and had a CADD score of 26.9. The *de novo* missense variant was confirmed by Sanger sequencing, the proband's parents and healthy sisters did not carry the variant (**Figures 1A,B**). Based on these findings, the variant was classified as "Likely pathogenic" by ACMG/AMP guidelines (PS2, PM2, PP2, and PP3) (Richards et al., 2015; Harrison et al., 2019).

Multiple sequence alignment of the protein shows that the Thr-945 residue is highly conserved across species (**Figure 1C**). This variant locates in the second CUT domain of the human homeobox protein CUX2 (Cut-like2) (**Figure 1D**) and results in a threonine to

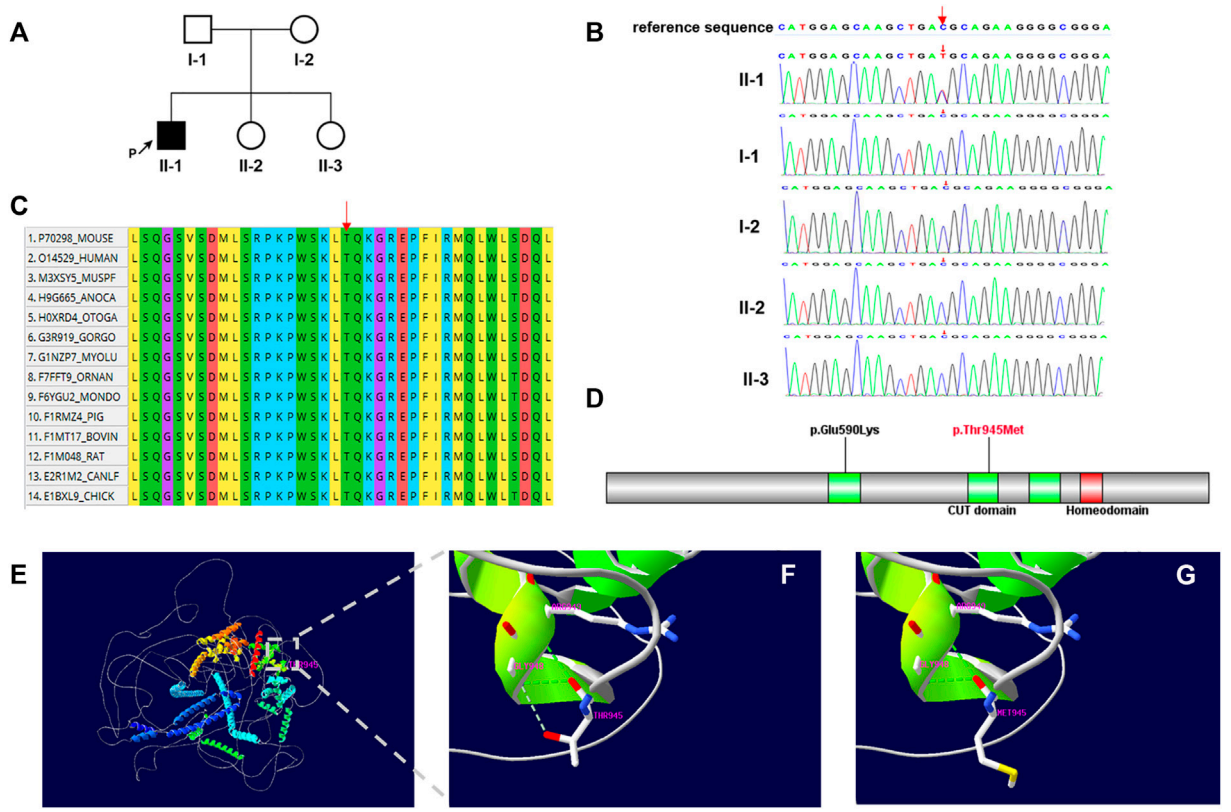

FIGURE 1 | (A) Family pedigree. The black arrow indicates the proband. **(B)** Sanger sequencing of the patient and family members confirmed the *de novo* variant c.2834C > T. **(C)** Multiple-sequence alignment of CUX2 protein among species. Red arrow shows the Thr945 site. **(D)** Domain structure of CUX2 protein (CUT domain, green; Homeodomain, red). Localization of amino acid changes p.Glu590Lys and p.Thr945Met is indicated. **(E–G)** Structural model of the CUX2 protein. Ribbon representations show details of the second CUT domain for wild-type (p.Thr945) **(F)** and mutated (p.Thr945Met) **(G)** CUX2. Noted loss of the weaker hydrogen bond between Thr945 and Gly948. Green dashed lines: hydrogen bonds; grey dashed lines: weaker hydrogen bonds.

methionine amino acid substitution. By substituting a polar and uncharged residue with a non-polar and hydrophobic amino acid, this variant may further affect the formation of a weaker hydrogen bond between Thr 945and Gly948 (**Figures 1E–G**).

DISCUSSION

In this study, we performed trio-whole exome sequencing and characterized a novel missense variant c.2834C > T (p.Thr945Met) in *CUX2* in a Chinese male patient with DEE. In previous studies, all known patients (ten unrelated probands with DEE) presented with a recurrent *de novo* missense variant, c.1768G > A (p.Glu590Lys) (**Table 1**) (Rauch et al., 2012; Allen et al., 2013; Geisheker et al., 2017; Barington et al., 2018; Chatron et al., 2018). The ten patients presented with a variety of epilepsy forms, including myoclonic seizures (3), absence seizures (2), focal, tonic, atonic, and generalized tonic-clonic. The age of onset ranged from 2 months to 9 years. EEG was performed in 9 of 10 patients. All participants had abnormal EEG findings, and 5 individuals presented with generalized spike-wave (GSW) or polyspike-wave (GPSW) patterns. Brain MRI was performed in 9 of 10 patients and was unremarkable in 6 of 9 patients. Cerebellar atrophy, hippocampal asymmetry, thin posterior corpus callosum were observed in some patients. In our case, the EEG revealed bi-parieto-temporal discharges while the MRI was normal. All patients had developmental delays, in addition to a variety of other variable features such as nonverbal (7), movement disorders (6), and autistic features (3). Our patient presented with febrile seizure when 2 years old. Besides, he has developmental delay.

The majority of patients with the p.Glu590Lys variant failed to respond to multiple antiepileptic drugs, including valproate, carbamazepine, clobazam, levetiracetam, and lamotrigine. Only three patients achieved seizure-free status while using valproate or a combination of valproate and lamotrigine. In our case, seizures were controlled after treatment with levetiracetam (Barington et al., 2018; Chatron et al., 2018). At the last follow-up, he had discontinued antiepileptic drug treatment (at age of 5 years) and remained seizure-free for 6 months. Taken together, our patient had a less severe phenotype than previously reported in patients carrying the p.Glu590Lys variant, although the relationship between the reported variant and the described phenotype requires more case reports to be established.

The CUX2 protein consists of three CUT domains and a homeodomain; which are important for DNA binding (Gingras et al., 2005). Additionally, the sequences of all four DNA-binding

TABLE 1 | Clinical features of individuals with the CUX2 variant.

Individual	*De novo* variant	Age	Sex	Type of seizure	Age at seizure onset	Seizure outcome	EEG features	MRI	ID	ASD	Non verbal	Movement disorder	Other features
1 (this study)	c.2834C > T, p.Thr945Met	5.5 years	M	Febrile seizure	2 years	Seizure free	Bi-parieto-temporal discharges	Normal	NA	No	No	No	Speech delay
2 Chatron et al. (2018)	c.1768G > A, p.Glu590Lys	19 years	M	Myoclonic seizures and right occipital seizures with apnea	7 months	Refractory	GSW, sometimes with myoclonic seizures. Right occipital seizure recorded	Normal	Profound	NA	Yes	Yes	Hypotonic at 1 year, then spastic tetraparesis from 12 years with loss of ambulation.
3 Chatron et al. (2018)	c.1768G > A, p.Glu590Lys	21 years	M	Atypical absences with myoclonus	6 months	Refractory	3–4 Hz GSW, GPSW	Cerebellar atrophy	Severe	NA	Yes	NA	No eye contact, inappropriate laughter episodes
4 Chatron et al. (2018)	c.1768G > A, p.Glu590Lys	9 years	F	Myoclonic	6 months	Refractory	GSW, GPSW	Hippocampal asymmetry	Severe	NA	Yes	NA	Decreased reflexes, ataxic gait
5 Chatron et al. (2018)	c.1768G > A, p.Glu590Lys	14 years	F	Absence seizures	12 months	Refractory	3 Hz GSW	Normal	Severe	NA	NA	Yes	NA
6 Chatron et al. (2018)	c.1768G > A, p.Glu590Lys	16 years	M	Myoclonic seizures	5 months	Refractory	GSW, GPSW	Normal	Severe	Yes	Yes	NA	NA
7 Chatron et al. (2018)	c.1768G > A, p.Glu590Lys	6 months	M	Generalized tonic-clonic seizures, atypical absences with apnea and myoclonus, right hemiclonic seizures	2 months	Refractory	Multifocal discharges, mainly independent bi-parieto-temporal	Normal	NA	NA	NA	Yes	NA
8 Barington et al. (2018)	c.1768G > A, p.Glu590Lys	17 years	F	Generalized and myoclonic seizures.	12 months	Seizure free	NA	NA	Severe	Yes	Yes	Yes	Sialorrhea, chronic constipation
9 Rauch et al. (2012)	c.1768G > A, p.Glu590Lys	8 years	M	Focal spasms	6 months	Seizure free	Hypsarrhythmia	Normal	Severe	NA	Yes	Yes	NA
10 Allen et al. (2013)	c.1768G > A ,p.Glu590Lys	12 years	M	Myoclonic seizures	2 months	Refractory	Left temporal spikes/ sharp waves	Normal	Severe	NA	NA	Yes	Ataxic gait, inappropriate laughter episodes
11 Geisheker et al. (2017)	c.1768G > A, p.Glu590Lys	14 years	M	Absence seizures	9 years	Seizure free	Left fronto-central slowing	Thin posterior corpus callosum	Severe	Yes	Yes	NA	NA

EEG, electroencephalograph; MRI, magnetic resonance imaging; ID, intellectual disability; ASD, autistic spectrum disorder; M, male; GSW, generalized spike-wave; NA, not available; GPSW, generalized polyspike-wave; F, female.

domains are highly conserved (Quaggin et al., 1996). The CUT domain 1 is located between amino acids 549 and 627, while the CUT domain 2 is located between amino acids 892 and 967 in CUX2. The previously reported variant p.Glu590Lys, which is located at the CUT domain 1, destabilized the effect in-silico analyses and interfered with DNA binding (Chatron et al., 2018). In this study, we modeled the 3D structure of the wild-type CUX2 protein (1–1486) and examined the potential functional impact of the p.Thr945Met variant (**Figures 1E–G**). Firstly, the variant alters the charge at residue 945 (polar to non-polar) (CUPSAT: $\Delta\Delta G = -6.21$ kcal/mol, I-mutant3.0: $\Delta\Delta G = -0.37$ kcal/mol), potentially disrupting the structure and affecting inter and intramolecular interactions (Chatron et al., 2018). Additionally, the Thr945Met variant affects a highly-conserved threonine residue in the CUT domain 2, which could result in structural changes and alter DNA-binding specificities (Gingras et al., 2005). However, additional molecular functional studies will be required to confirm the potential mechanism of pathogenic variants.

In summary, patients with *de novo* CUX2 variants have developmental and epileptic encephalopathies characterized by developmental delay, speech delay, movement disorders, and autistic behavior. Our findings have further expanded the clinical and molecular spectrum of DEE67.

DATA AVAILABILITY STATEMENT

The datasets presented in this study can be found in online repositories. The names of the repository/repositories and accession number(s) can be found below: https://www.ncbi.nlm.nih.gov/, SCV001946791.

ETHICS STATEMENT

The studies involving human participants were reviewed and approved by the Ethics Committee of Ganzhou Women and Children's Health Care Hospital. Written informed consent to participate in this study was provided by the participants' legal guardian/next of kin. Written informed consent was obtained from the individual(s), and minor(s)' legal guardian/next of kin, for the publication of any potentially identifiable images or data included in this article.

AUTHOR CONTRIBUTIONS

FZ and KX wrote the manuscript. FL, XD, JZ, and WG were responsible for exome sequencing and genetic analysis. FZ, FC, JH, and QL managed the patient and provided clinical information. WG and KX critically reviewed the manuscript. All the authors read and approved the final manuscript.

FUNDING

This study was supported by the Science and Technology Plan Program of the Health Commission of Jiangxi Province (No. 20204662).

ACKNOWLEDGMENTS

We are incredibly thankful to the participants in our study.

REFERENCES

Allen, A. S., Berkovic, S. F., Cossette, P., Delanty, N., Dlugos, D., Eichler, E. E., et al. (2013). De Novo mutations in Epileptic Encephalopathies. *Nature* 501 (7466), 217–221. doi:10.1038/nature12439

Barington, M., Risom, L., Ek, J., Uldall, P., and Ostergaard, E. (2018). A Recurrent De Novo CUX2 Missense Variant Associated with Intellectual Disability, Seizures, and Autism Spectrum Disorder. *Eur. J. Hum. Genet.* 26 (9), 1388–1391. doi:10.1038/s41431-018-0184-5

Chatron, N., Møller, R. S., Champaigne, N. L., Schneider, A. L., Kuechler, A., Labalme, A., et al. (2018). The Epilepsy Phenotypic Spectrum Associated with a Recurrent CUX2 Variant. *Ann. Neurol.* 83 (5), 926–934. doi:10.1002/ana.25222

Geisheker, M. R., Heymann, G., Wang, T., Coe, B. P., Turner, T. N., Stessman, H. A. F., et al. (2017). Hotspots of Missense Mutation Identify Neurodevelopmental Disorder Genes and Functional Domains. *Nat. Neurosci.* 20 (8), 1043–1051. doi:10.1038/nn.4589

Gingras, H., Cases, O., Krasilnikova, M., Bérubé, G., and Nepveu, A. (2005). Biochemical Characterization of the Mammalian Cux2 Protein. *Gene* 344, 273–285. doi:10.1016/j.gene.2004.11.008

Harrison, S. M., Biesecker, L. G., and Rehm, H. L. (2019). Overview of Specifications to the ACMG/AMP Variant Interpretation Guidelines. *Curr. Protoc. Hum. Genet.* 103 (1), 93. doi:10.1002/cphg.93

Quaggin, S. E., Heuvel, G. B. V., Golden, K., Bodmer, R., and Igarashi, P. (1996). Primary Structure, Neural-specific Expression, and Chromosomal Localization of , a Second Murine Homeobox Gene Related to. *J. Biol. Chem.* 271 (37), 22624–22634. doi:10.1074/jbc.271.37.22624

Rauch, A., Wieczorek, D., Graf, E., Wieland, T., Endele, S., Schwarzmayr, T., et al. (2012). Range of Genetic Mutations Associated with Severe Non-syndromic Sporadic Intellectual Disability: an Exome Sequencing Study. *Lancet* 380 (9854), 1674–1682. doi:10.1016/s0140-6736(12)61480-9

Richards, S., Aziz, N., Bale, S., Bick, D., Das, S., Gastier-Foster, J., et al. (2015). Standards and Guidelines for the Interpretation of Sequence Variants: a Joint Consensus Recommendation of the American College of Medical Genetics and Genomics and the Association for Molecular Pathology. *Genet. Med.* 17 (5), 405–424. doi:10.1038/gim.2015.30

Specchio, N., and Curatolo, P. (2021). Developmental and Epileptic Encephalopathies: what We Do and Do Not Know. *Brain* 144 (1), 32–43. doi:10.1093/brain/awaa371

Conflict of Interest: Authors FL, XD, JZ, and WG were employed by Beijing Chigene Translational Medical Research Center Co. Ltd.

The remaining authors declare that the research was conducted in the absence of any commercial or financial relationships that could be construed as a potential conflict of interest.

Publisher's Note: All claims expressed in this article are solely those of the authors and do not necessarily represent those of their affiliated organizations, or those of the publisher, the editors and the reviewers. Any product that may be evaluated in this article, or claim that may be made by its manufacturer, is not guaranteed or endorsed by the publisher.

frontiers | Frontiers in Genetics

ORIGINAL RESEARCH
published: 19 July 2022
doi: 10.3389/fgene.2022.836853

Paternal De Novo Variant of *TAOK1* in a Fetus With Structural Brain Abnormalities

*Lihua Yu[1†], Chaoxiang Yang[2], Ning Shang[3], Hongke Ding[1], Juan Zhu[1], Yuanyuan Zhu[4], Haowen Tan[4] and Yan Zhang[1]**

[1]Medical Genetics Centre, Guangdong Women and Children Hospital, Guangzhou, China, [2]Department of Radiology, Guangdong Women and Children Hospital, Guangzhou, China, [3]Department of Ultrasound, Guangdong Women and Children Hospital, Guangzhou, China, [4]Aegicare (Shenzhen) Technology Co., Ltd., Shenzhen, China

A dilated lateral ventricle is a relatively common finding on prenatal ultrasound, and the causes are complex. We aimed to explore the etiology of a fetus with a dilated lateral ventricle. Trio whole-exome sequencing was performed to detect causative variants. A *de novo* variant of *TAOK1* (NM_020791.2: c.227A>G) was detected in the proband and evaluated for potential functional impacts using a variety of prediction tools. Droplet digital polymerase chain reaction was used to exclude the parental mosaicism and to verify the phasing of the *de novo* variant. Based on peripheral blood analysis, the parents did not exhibit mosaicism at this site, and the *de novo* variant was paternally derived. Here, we describe a fetus with a *de novo* likely pathogenic variant of *TAOK1* who had a dilated lateral ventricle and a series of particular phenotypes. This case expands the clinical spectrum of *TAOK1*-associated disorders. We propose a method for solving genetic disorders in which the responsible genes have not yet gone through ClinGen curation, particularly for prenatal cases.

Keywords: dilated lateral ventricle, *TAOK1*, trio-whole exome sequencing, rare disease, neurodevelopment disorder

OPEN ACCESS

Edited by:
Emiliano González Vioque, University Clinical Hospital of Santiago, Spain

Reviewed by:
Yiran Guo, Children's Hospital of Philadelphia, United States
Victor Wei Zhang, Jiajian Medical Co., Ltd., China

****Correspondence:***
Yan Zhang
zhangyan1981_2003@aliyun.com

†ORCID:
Lihua Yu
orcid.org/0000-0002-8456-9493

Specialty section:
This article was submitted to Genetics of Common and Rare Diseases, a section of the journal Frontiers in Genetics

Received: *16 December 2021*
Accepted: *30 May 2022*
Published: *19 July 2022*

Citation:
Yu L, Yang C, Shang N, Ding H, Zhu J, Zhu Y, Tan H and Zhang Y (2022) Paternal De Novo Variant of TAOK1 in a Fetus With Structural Brain Abnormalities. Front. Genet. 13:836853. doi: 10.3389/fgene.2022.836853

INTRODUCTION

The TAO kinase family consists of three genes, *TAOK1*, *TAOK2*, and *TAOK3*, which encode TAOK1, TAOK2, and TAOK3, respectively (Dan et al., 2001; Miller et al., 2019). TAO kinases play multifunctional roles in many molecular and cellular events and can regulate neuronal survival and development in the nervous system (Fang et al., 2020; Hu et al., 2021). *TAOK1* is highly expressed in the human brain and plays a role in the establishment of neuronal polarity, neuronal differentiation, and early brain development (Biernat et al., 2002; Timm et al., 2006; Draviam et al., 2007; Breuss and Keays, 2014; Poon et al., 2016). Many studies have provided evidence that *TAOK1* dysfunction can result in neurodevelopmental disorders (NDDs) (Cooper et al., 2011; Xie et al., 2016; Deciphering Developmental Disorders Study, 2017; Dulovic-Mahlow et al., 2019; Satterstrom et al., 2020; van Woerden et al., 2021; Hunter et al., 2022). However, dysfunction of this kinase in prenatal cases has not been reported.

Here, we report structural brain abnormalities in a fetus with a *de novo* variant of *TAOK1*. To our knowledge, this is the first report of *TAOK1* dysfunction as a prenatal diagnosis.

Case Presentation

A healthy 32-year-old gravida 3, para 2 (G3P2) woman underwent a prenatal examination at Guangdong Women and Children Hospital. She delivered two normal male infants, in 2013 and 2018, through uncomplicated vaginal deliveries. At 25 weeks of gestation for the current

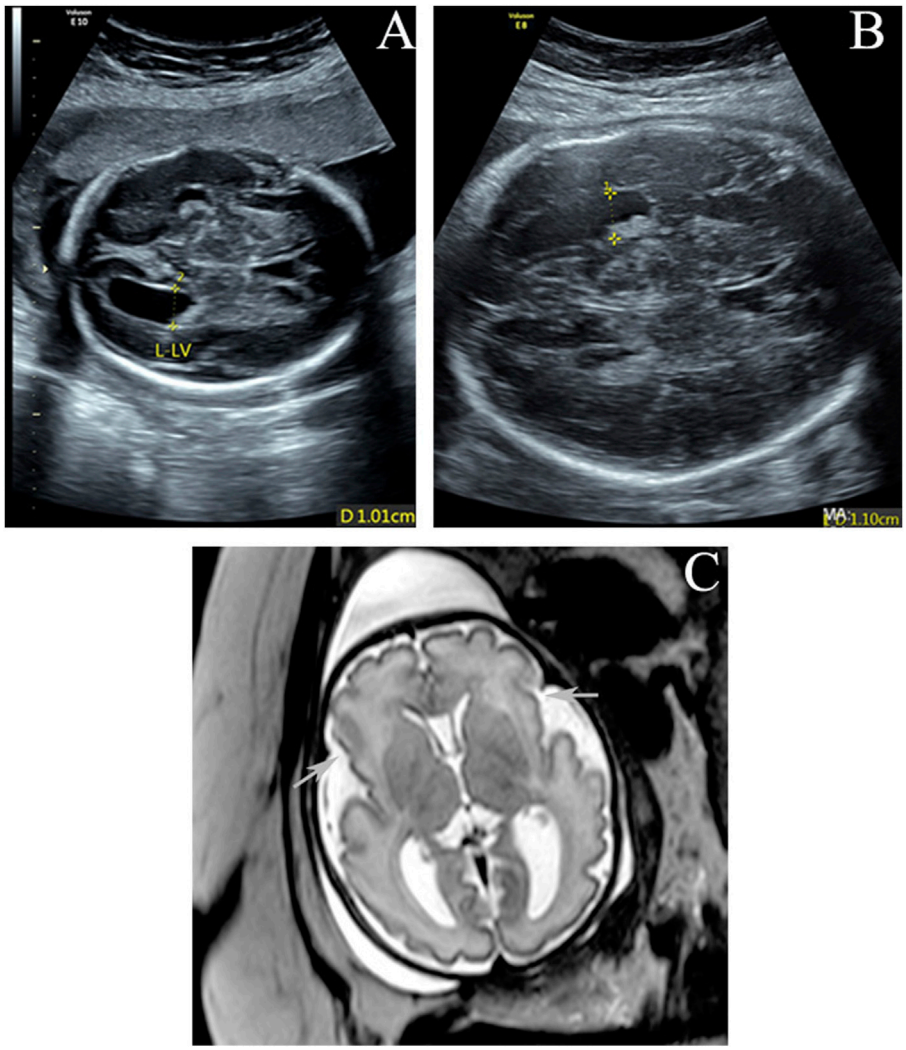

FIGURE 1 | (A,B) Enlarged left lateral ventricle (10.1 and 11 mm) at 25 and 31 gestational weeks. **(C)** Axial T2-weighted imaging at 32 weeks of gestation shows poor bilateral and frontal operculum formation and shallow bilateral lateral fissures (arrows). The left ventricle is slightly wider.

pregnancy, routine ultrasound scanning showed that the left lateral ventricle of the fetus was widened (10.1 mm compared to a reference of <10 mm) (**Figure 1A**). Common factors, such as infection and anemia, were ruled out, and COVID-19 nucleic acid tests were negative. Noninvasive prenatal testing (NIPT) indicated a low risk of fetal trisomy 13, 18, and 21. At 31 weeks of gestation, ultrasound scanning showed slight widening of the left lateral ventricle (11.0 mm compared to reference of <10 mm), with the umbilical cord surrounding the neck, of the fetus (**Figure 1B**). As shown in **Figure 1C**, magnetic resonance imaging (MRI) revealed poor bilateral and frontal operculum formation and shallow bilateral lateral fissures, which were more obvious on the right side. Bilateral polymicrogyria of the lateral fissure area could not be ruled out. The left ventricle was slightly wider. No abnormalities were observed in the corpus callosum, septum pellucidum, cerebellar vermis, or posterior fossa. Due to the abnormal cortical structure detected by MRI, interventional prenatal diagnosis was performed, along with chromosomal microarray analysis (CMA) and trio whole-exome sequencing (trio WES), simultaneously. The CMA result was negative, but trio WES detected a *de novo* missense variant of *TAOK1* in the fetus. Whole-genome sequencing (WGS) and droplet digital polymerase chain reaction (ddPCR) was then performed to identify the source of the variation. Finally, the *de novo* variant of *TAOK1* was found to originate from the paternal allele.

METHODS AND RESULTS

Trio Whole-Exome Sequencing

Genomic DNA was extracted from amniotic fluid and peripheral blood from the fetus and parents, respectively,

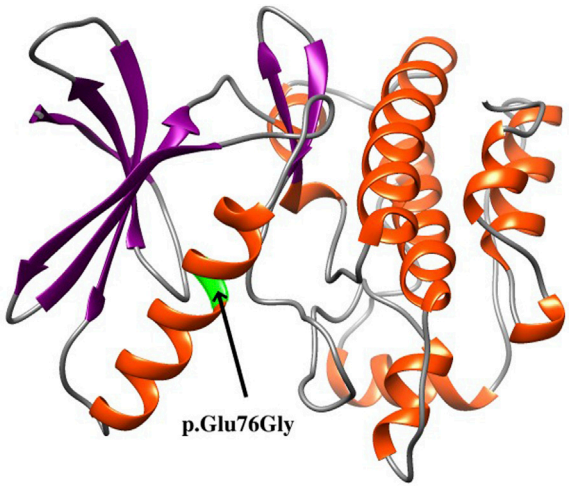

FIGURE 2 | Structure of the kinase domain of the TAOK1 protein from amino acids 28 to 281, showing the localization of the identified variant p.Glu76Gly.

using the QIAamp DNA Mini Kit (Qiagen), following the manufacturer's instructions. Trio WES was performed to detect genetic variants (see **Supplementary Methods**), and a *de novo* variant of *TAOK1* [GRCh37/hg19 chr17: 27802710, NM_020791.2: c.227A>G (p.Glu76Gly)] was found. No other variants were considered to contribute to the phenotype.

The *de novo* variant c.227A>G is absent in the general population according to public databases (gnomAD, 1000 Genomes Project, NHLBI Exome Sequencing Project 6500, and Exome Aggregation Consortium). This variation has not been previously reported in the ClinVar or PubMed databases (retrieved 15 January 2022). A variety of prediction tools (SIFT, DANN, and REVEL) were used to evaluate the possible functional impact of c.227A>G, and it is predicted to be a damaging variation by all three tools. Furthermore, various algorithms (GERP, phyloP, phastCons, and SiPhy) and multiple sequence alignments from the UCSC genome browser predicted that this position is conserved across multiple vertebrate species (from zebrafish to human). The variant p.Glu76Gly is located in the "Protein kinase" domain of TAOK1 (UniProt ID #Q7L7X3) in which benign variants are not found in ClinVar database. Although the protein structure of TAOK1 was not available in the PDB database, the structure of the kinase domain (amino acids 28–281) was predicted with the I-TASSER server, as illustrated in **Figure 2** (Roy et al., 2010). The model with the highest confidence (C-score) and topological similarity (Tm-score) is used. The identified variant p.Glu76Gly is predicted to be located in an alpha-helix of the protein (**Figure 2**).

Whole-Genome Sequencing

To identify the phase of the *de novo* variant, WGS was performed for the proband (see **Supplementary Methods**). A heterozygous variant, c.306+468G>T (GRCh37/hg19 chr17: 27803257G>T), in *TAOK1* was found, which is 547 bp downstream of c.227A>G and was used as the reference for ddPCR analysis.

To validate the *de novo* variant c.227A>G and the reference variant c.306+468G>T, Sanger sequencing was performed for the family (see **Supplementary Methods**). The results showed that the proband carried c.227A>G but that neither parent did (**Figure 3A**); c.306+468G>T was found in the proband and mother but not in the father (**Figure 3B**).

Droplet Digital PCR

ddPCR was used to assess parental mosaicism (see **Supplementary Methods**). As shown in **Figure 4**, the peripheral blood samples of the parents did not show mosaicism at the site of the *de novo* variant of *TAOK1*.

To determine whether the mutant alleles of the variants, c.227A>G and c.306+468G>T, in the proband were located on the same chromosome, ddPCR was used to verify the phase (see **Supplementary Methods**). First, the T allele of c.306+468G>T was used as a reference, and phasing was performed. The results showed that these alleles were not located on the same chromosome (**Figure 5A**). Subsequently, the wild-type allele (G) of c.306+468G>T was used as a reference. The results showed that the G allele of c.306+468G>T and the mutant allele (G) of c.227A>G were located on the same chromosome (**Figure 5B**). The phasing analysis confirmed that the *de novo* variant c.227A>G derived from the paternal chromosome.

DISCUSSION

To the best of our knowledge, only six studies have reported variants of *TAOK1* in 40 patients with NDDs (Xie et al., 2016; Dulovic-Mahlow et al., 2019; Satterstrom et al., 2020; Basel-Salmon et al., 2021; van Woerden et al., 2021; Hunter et al., 2022). The phenotypes of the affected individuals are summarized in **Table 1**. All had NDDs, mainly involving global developmental delay, intellectual disability, hypotonia, and behavior problems, as well as brain MRI abnormalities and eye/visual problems. In this study, the fetus with a variant of *TAOK1* had a dilated left lateral ventricle, and brain MRI imaging in six previously reported postnatal cases revealed dilated lateral ventricles. However, the published studies did not differentiate between unilateral and bilateral ventricular dilation. Therefore, it is uncertain whether variants of *TAOK1* are associated with asymmetric ventricles.

This is the first report of a variant of *TAOK1* in the prenatal stage. We sought to determine whether prenatal *de novo* variants of *TAOK1* can predict the risk of NDDs. To evaluate associations between the *de novo* variant of *TAOK1* we found and phenotypes in the prenatal stage, we compared the pregnancy statuses of the patients with variants of *TAOK1* (**Table 2**). As shown, few abnormal pregnancy statuses were found. MRI abnormalities in the fetus are relatively prevalent in patients with *TAOK1*-associated NDDs. We suggest that fetuses with brain MRI abnormalities accompanied by *de novo* variants of *TAOK1* have a higher risk for NDDs, and should be carefully managed. Our study not only fills the gap between the variant of *TAOK1* and the prenatal phenotypes

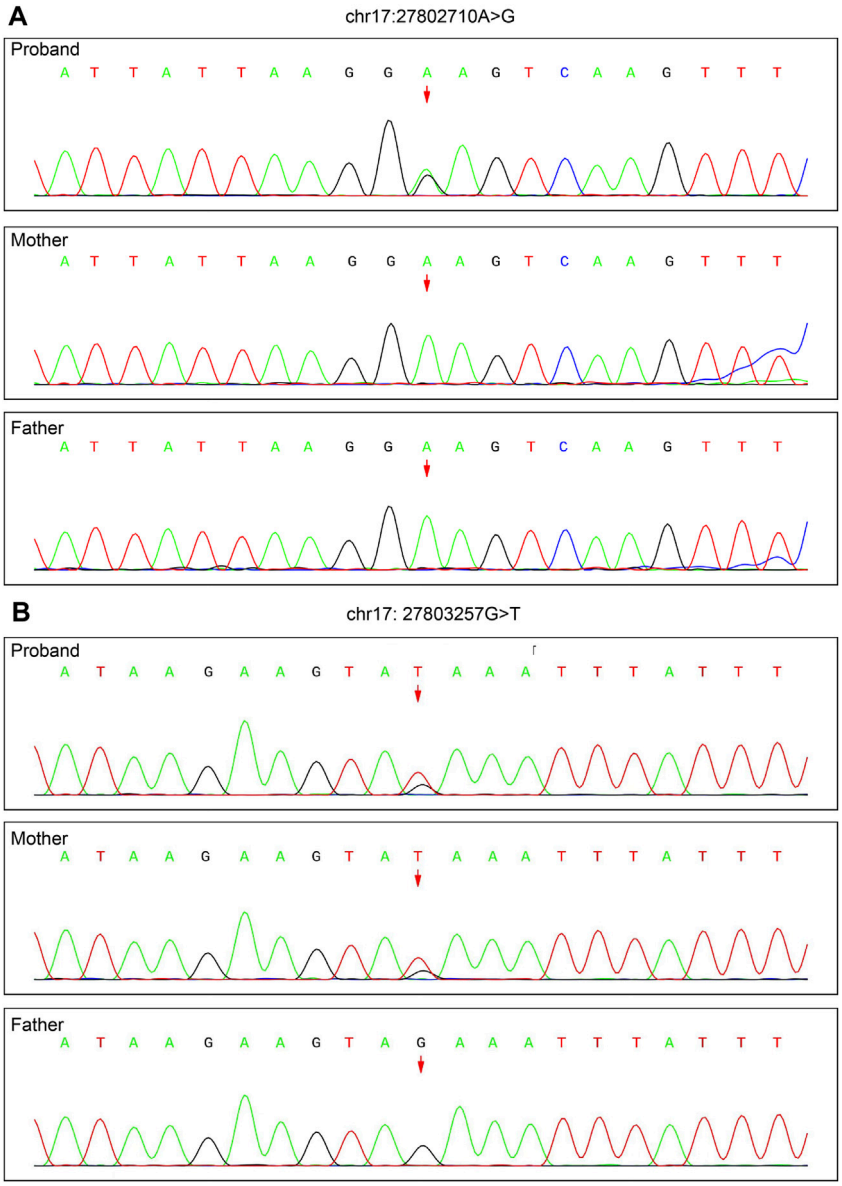

FIGURE 3 | Validation of the *de novo* variant c.227A>G of *TAOK1* (chr17: 27802710) identified by trio WES and the reference variant c.306+468G>T (chr17: 27803257) identified by WGS by Sanger sequencing. **(A)** c.227A>G was found in the proband, but not in either parent. **(B)** c.306+468G>T was detected in the proband and mother, but not in the father.

but also provides valuable information for disease management, prognosis judgment and prenatal consultation.

As shown in **Table 1**, *de novo* variants of *TAOK1* have been found in thirty-one of 40 previously reported patients (77.5%). An additional *de novo* variant of *TAOK1* was detected in the fetus in this study. Variants in five (12.5%) affected individuals, P8, P9, P23, P37, and P38, were considered to be inherited from an affected mother or father (**Table 1**), which are classified as pathogenic herein. The very mild cognitive phenotypes of some affected parents might be explained by incomplete penetrance and variable expressivity (Hunter et al., 2022). Furthermore, no recurrent variants were reported in the region of 17q11.2 (chr17: 27064286-28761847), indicating that *TAOK1* is not prone to hotspot variant, which was also mentioned by van Woerden et al. (2021). The variant identified in this study is located at chr17: 27802710, within the range of previous findings. Based on the protein structure modeling result (**Figure 2**), p.Glu76Gly is predicted to be located in an alpha-helix structure, and glycine is generally considered to destabilize an alpha-helix. Accordingly, we predicted that this novel missense variant affects protein kinase function, though

TABLE 1 | Overview of the identified variants of *TAOK1*.

Patients (Gender)	Chromosome position (GRCh37/hg19)	cDNA change (Amino acid change)	Inheritance	Intellectual disability	Hypotonia	Behavior problems	Brain MRI abnormalities	Eye/ visual problems	Pathogenic (ACMG scoring)	Reference
P1 (F)	chr17: 27064286-28761847 × 1	1.69 Mb	*De novo*	+	NR	NR	NR	NR	P (PVS1, PS2, PM2)	Xie et al. (2016)
P2 (M)	chr17: 27861216	c.2442delG (p.Tyr815Ilefs*31)	*De novo*	+	–	+	–	+	P (PVS1, PS2, PM2)	van Woerden et al. (2021)
P3 (M)	chr17: 27818884	c.831+1dupG (p.?)	*De novo*	+	+	+	+	NR	P (PVS1, PS2, PM2)	van Woerden et al. (2021)
P4 (M)	chr17: 27837949	c.1643T>C (p.Leu548Pro)	*De novo*	+	+	+	+	–	LP (PS2, PM2, PP3)	van Woerden et al. (2021)
P5 (F)	chr17: 27822746	c.999+1dupG (p.?)	*De novo*	+	–	–	+	–	P (PVS1, PS2, PM2)	van Woerden et al. (2021)
P6 (M)	chr17: 27844585	c.1819C>T (p.Gln607Ter)	*De novo*	–	+	+	+	–	P (PVS1, PS2, PM2)	van Woerden et al. (2021)
P7 (F)	chr17: 27818877-27818878	c.825_826insCT (p.Lys277Ter)	*De novo*	–	+	–	NR	NR	P (PVS1, PS2, PM2)	van Woerden et al. (2021)
P8 (M)	chr17: 27816684	c.658G>T (p.Glu220Ter)	Maternal	+	–	+	NR	+	P (PVS1, PM2, PP1)	van Woerden et al. (2021)
P9 (M)	chr17: 27849514	c.2125C > T (p.Arg709Ter)	Paternal	–	–	+	–	+	P (PVS1, PM2, PP1)	van Woerden et al. (2021)
P10 (M)	chr17: 27805365	c.449G>T (p.Arg150Ile)	*De novo*	+	NR	NR	NR	NR	LP (PS2, PM1, PM2, PP3)	van Woerden et al. (2021)
P11 (M)	chr17: 27807436	c.500T>G (p.Leu167Arg)	*De novo*	+	–	+	+	–	LP (PS2, PM1, PM2, PP3)	van Woerden et al. (2021)
P12 (M)	chr17: 27849472	c.2083C>T (p.Arg695Ter)	*De novo*	–	+	–	NR	+	P (PVS1, PS2, PM2)	van Woerden et al. (2021)
P13 (F)	chr17: 27805366	c.449+1G>C (p.?)	*De novo*	–	–	–	NR	–	P (PVS1, PS2, PM2)	van Woerden et al. (2021)
P14 (F)	chr17: 27805309	c.393dupT (p.Thr132Tyrfs*19)	*De novo*	+	-	+	–	–	P (PVS1, PS2, PM2)	van Woerden et al. (2021)
P15 (M)	chr17: 27849493	c.2104C>T (p.Arg702Ter)	Unknown	+	+	+	–	+	LP (PVS1, PM2)	van Woerden et al. (2021)
P16 (M)	chr17: 27822689	c.943C>T (p.Leu315Phe)	*De novo*	–	–	+	NR	+	LP (PS2, PM2, PP3)	van Woerden et al. (2021)
P17 (M)	chr17: 27829690	c.1287delA (p.Lys429Asnfs*42)	*De novo*	+	+	+	–	–	P (PVS1, PS2, PM2)	van Woerden et al. (2021)
P18 (F)	chr17: 27802715-27802716	c.232_233delAA (p.Lys78Valfs*20)	*De novo*	+	+	–	–	–	P (PVS1, PS2, PM2)	van Woerden et al. (2021)
P19 (M)	chr17: 27848992-27849799	c.1909-306_2148+262del (p.? [exon 17 deletion])	*De novo*	+	+	–	–	–	P (PVS1, PS2, PM2)	van Woerden et al. (2021)
P20 (F)	chr17: 27816717	c.691A>G (p.Met231Val)	Unknown	+	–	+	–	–	VUS (PM1, PM2, PP3)	van Woerden et al. (2021)
P21 (F)	chr17: 27844579	c.1813C>T (p.Arg605Ter)	Unknown	+	+	–	–	+	LP (PVS1, PM2)	van Woerden et al. (2021)
P22 (F)	chr17: 27080000-29080000 × 1	2 Mb	Unknown	+	+	–	+	-	LP (PVS1, PM2)	van Woerden et al. (2021)
P23 (M)		264 kb	Maternal	NR	+	+	–	+		

(Continued on following page)

TABLE 1 | (*Continued*) Overview of the identified variants of *TAOK1*.

Patients (Gender)	Chromosome position (GRCh37/hg19)	cDNA change (Amino acid change)	Inheritance	Intellectual disability	Hypotonia	Behavior problems	Brain MRI abnormalities	Eye/ visual problems	Pathogenic (ACMG scoring)	Reference
	chr17: 27670438-27934287 × 1								P (PVS1, PM2, PP1)	van Woerden et al. (2021)
P24 (F)	chr17: 27778616	c.50A>G (p.Glu17Gly)	*De novo*	–	+	+	NR	+	LP (PS2, PM2)	Dulovic-Mahlow et al. (2019)
P25 (M)	chr17: 27822638	c.892A>G (p.Lys298Glu)	*De novo*	–	+	+	NR	–	LP (PS2, PM2, PP3)	Dulovic-Mahlow et al. (2019)
P26 (M)	chr17: 27857617	c.2341G>T (p.Glu781*)	*De novo*	+	–	–	NR	–	P (PVS1, PS2, PM2)	Dulovic-Mahlow et al. (2019)
P27 (F)	chr17: 27822660	c.914A>C (p.Asp305Ala)	*De novo*	+	–	–	NR	–	LP (PS2, PM2, PP3)	Dulovic-Mahlow et al. (2019)
P28 (M)	chr17: 27837936	c.1630C>T (p.Gln544*)	*De novo*	–	+	+	NR	–	P (PVS1, PS2, PM2)	Dulovic-Mahlow et al. (2019)
P29 (F)	chr17: 27804704	c.332C>T (p.Ser111Phe)	*De novo*	+	+	–	NR	–	LP (PS2, PM1, PM2, PP3)	Dulovic-Mahlow et al. (2019)
P30 (M)	chr17: 27861140	c.2366_2367insC (p.Leu790Phefs*3)	*De novo*	+	+	+	NR	–	P (PVS1, PS2, PM2)	Dulovic-Mahlow et al. (2019)
P31 (M)	chr17: 27861262	c.2488G>T (p.Glu830*)	*De novo*	–	+	–	NR	–	P (PVS1, PS2, PM2)	Dulovic-Mahlow et al. (2019)
P32 (NR)	chr17: 27778636	c.70C>A (p.Pro24Thr)	*De novo*	+	NR	NR	NR	NR	LP (PS2, PM2, PP3)	Satterstrom et al. (2020)
P33 (NR)	chr17: 27807436	c.500T>G (p.Leu167Arg)	*De novo*	+	NR	NR	NR	NR	LP (PS2, PM1, PM2, PP3)	Satterstrom et al. (2020)
P34 (NR)	chr17: 27822611	c.865G>A (p.Val289Met)	*De novo*	+	NR	NR	NR	NR	LP (PS2, PM2, PP3)	Satterstrom et al. (2020)
P35 (NR)	chr17: 27816682	c.656C>T (p.Ala219Val)	*De novo*	+	NR	NR	NR	NR	LP (PS2, PM1, PM2, PP3)	Satterstrom et al. (2020)
P36 (F)	chr17: 27857424	c.2149-1G>A (p.?)	*De novo*	NR	NR	NR	NR	NR	P (PVS1, PS2, PM2)	Basel-Salmon et al. (2021)
P37 (M)	chr17: 27857479	c.2203delA (p.Arg735Aspfs*6)	Maternal	NR	+	+	+	NR	P (PVS1, PM2, PP1)	Hunter et al. (2022)
P38* (F)	chr17: 27857479	c.2203delA (p.Arg735Aspfs*6)	Maternal	NR	+	+	+	NR	P (PVS1, PM2, PP1)	Hunter et al. (2022)
P39 (M)	chr17: 27778701-27778704	c.132+3_132+6 delAAGT (p.?)	*De novo*	NR	+	+	+	NR	LP (PS2, PM2, PP3)	Hunter et al. (2022)
P40 (F)	chr17: 2 7829727	c.1324C>T (p.Arg442Trp)	*De novo*	NR	+	+	–	NR	LP (PS2, PM2, PP3)	Hunter et al. (2022)
P41 (NA)	chr17: 27802710	c.227A>G (p.Glu76Gly)	*De novo*	NA	NA	NA	+	NA	LP (PS2, PM1, PM2, PP3)	Current study

*F, female; M, male; NR, not report; NA, not available; p.?, the effect on protein is unknown; +, present; –, absence; P, pathogenic; LP, likely pathogenic; VUS, variant of uncertain significance; *, Patient 38 is the older sibling of patient 37.*

TABLE 2 | Clinical features of patients with *TAOK1* variants.

	Previous Studies	Current Prenatal Case
Gender		
Male	21/36 (58.3%)	NR
Pregnancy status		
Normal	1/22 (4.5%)	Yes
Uncomplicated	13/22 (59.1%)	No
Complicated	1/22 (4.5%)	No
In vitro fertilisation	2/22 (9.1%)	No
Polyhydramnios	5/26 (19.2%)	No
Ventricular dilatation	1/22 (4.5%)	Yes
Preeclampsia	1/22 (4.5%)	No
Oligohydramnios	1/22 (4.5%)	No
Pregnancy-induced hypertension	1/22 (4.5%)	Unknown
No prenatal care	1/22 (4.5%)	No
Neurodevelopmental disorder		
Global developmental delay	29/34 (85.3%)	NA
Intellectual disability	24/34 (70.6%)	NA
Hypotonia	22/33 (66.7%)	NA
Behavior problems	21/33 (63.6%)	NA
Brain MRI abnormalities	9/20 (45.0%)	Yes
Eye/visual problems	9/27 (33.3%)	NA

NR, fetal gender in the current case is not reported; NA, the feature is too early to observe in the prenatal case.

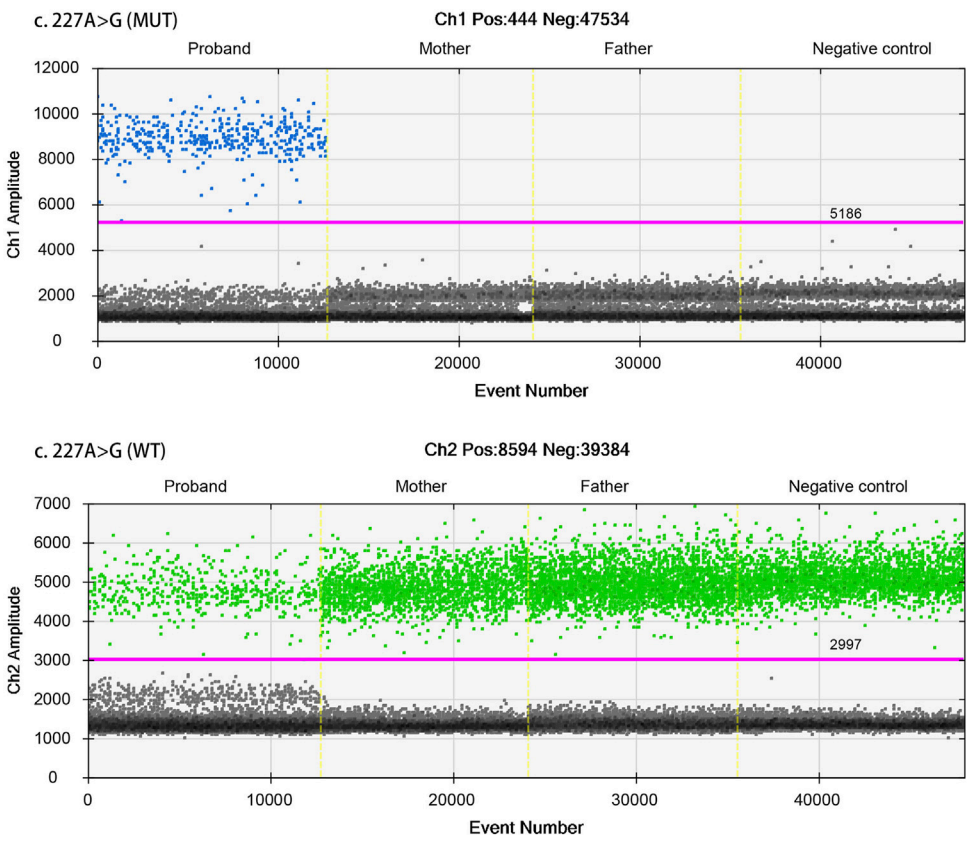

FIGURE 4 | Droplet digital PCR (ddPCR) for mosaic variation detection. The four ddPCRs are divided by vertical dotted yellow lines for the proband, mother, father, and negative control. The pink line is the threshold, above which are positive droplets (blue and green), and below which are negative droplets (gray) without any target DNA. There is no target DNA for the mutant locus c.227A>G in the mother and father (top panel).

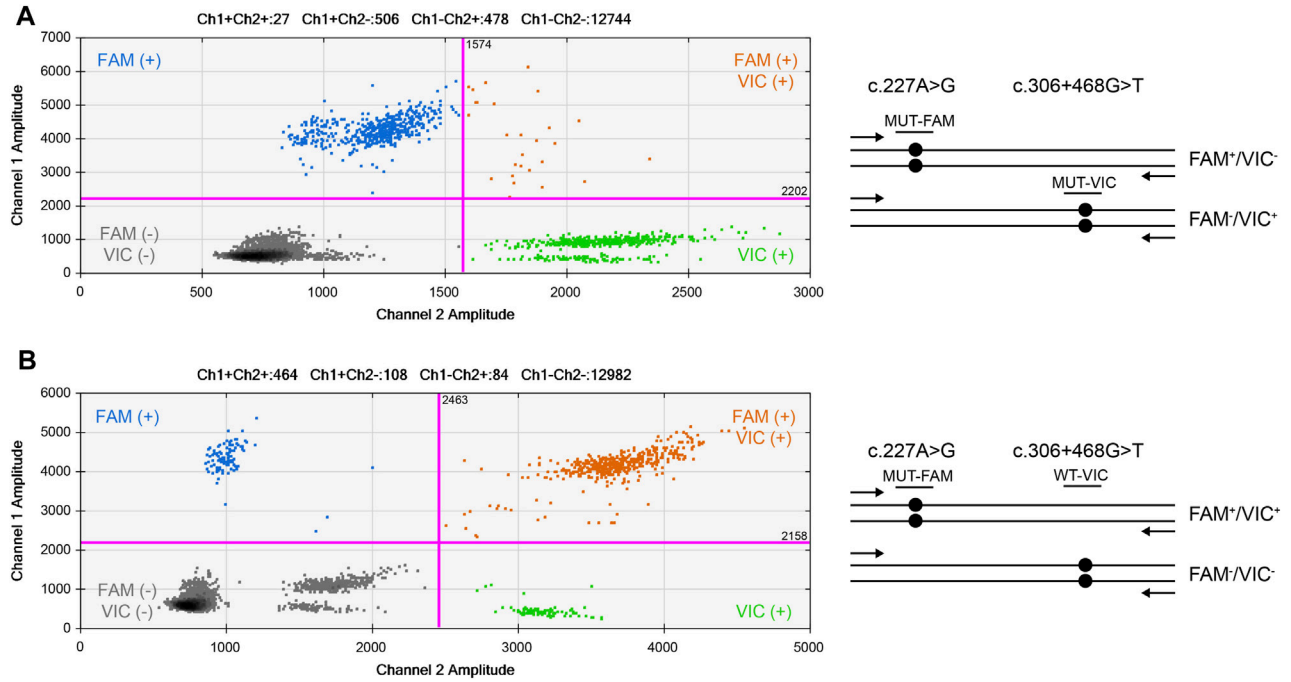

FIGURE 5 | 2D cluster plot of droplet fluorescence for the *de novo* locus and reference locus. **(A)** The result of c.306+468G>T mutant and c.227A>G mutant probes. **(B)** The result of c.306+468G>T wild-type and c.227A>G mutant probes. FAM™ positive (Channel 1, mt–) droplets form the top-left blue cluster, HEX™ positive (Channel 2, mt+) droplets form the bottom-right green cluster, negative droplets for both targets form the bottom-left gray cluster, and positive droplets for both targets form the top-right orange cluster.

more functional experiments are needed to validate this assumption.

In this study, the *de novo* variant was confirmed to originate from the paternal chromosome by a ddPCR phasing strategy, consistent with the findings that *de novo* variants arise more frequently in paternal germ cells than in maternal germ cells (Kong et al., 2012; Goldmann et al., 2016). The primarily *de novo* variants on the paternal chromosome could be explained by fundamental differences in germ cell biology in the female and male lineages. Spermatogenesis requires regular mitotic cell divisions of spermatogonial stem cells throughout male reproductive life (Goriely and Wilkie, 2012). However, the influence of maternal chromosomes on *de novo* variants in offspring cannot be ignored (Gao et al., 2019; Goldmann et al., 2019). In recent years, *de novo* variants have been found to be a prominent cause of NDDs, including intellectual disability (ID), autism, and schizophrenia (SCZ) (Veltman and Brunner, 2012; Acuna-Hidalgo et al., 2016). The relationship between paternal-age-related *de novo* variants and the risk for psychiatric and developmental disorders has been assessed, including for autism spectrum disorder (ASD), congenital heart disease (CHD), NDDs with epilepsy (EPI), ID, and SCZ (Taylor et al., 2019). Recurrent risk of a *de novo* variant should be considered if a germline mosaic variant is detected in parental samples, and the sibling recurrent risk can be as low as 0.5% if absent from samples of both parents by highly sensitive screening technology (Wright et al., 2019).

Variants of a gene of uncertain significance should always be classified as having uncertain significance of pathogenicity (Richards et al., 2015). When we obtained the trio WES results in November 2020, the *TAOK1* gene has not been associated with any Mendelian disorder in the OMIM (Online Mendelian Inheritance in Man) database. We further explored research articles and found that Dulovic-Mahlow et al. (2019) first reported eight patients, all with *de novo* variants considered pathogenic due to loss of function of the TAO kinase family. We then evaluated the gene-disease association following the ClinGen Gene-Disease Validity Standard Operating Procedures (Strande et al., 2017), and curated the *TAOK1* gene to "moderate" grade. Finally, the *de novo* variant c.227A>G of *TAOK1* in our case was classified as likely pathogenic (PS2+PM1+PM2+PP3) based on ACMG guidelines (Zhang et al., 2020). A clear understanding of the clinical validity of the gene-disease relationship is critical for accurate interpretation of variants and successful medical decision-making based on genetic testing results. Because of limitations of the prenatal phenotype, accurate genetic variant classification in prenatal diagnosis is especially important. It would benefit from cross-laboratory data sharing and evaluating the strength of a gene-disease relationship based on the ClinGen Gene-Disease Validity Standard Operating Procedures. During the revision of the manuscript, the definitive classification of the gene-disease relationship between *TAOK1* and syndromic intellectual disability was curated by the ClinGen Intellectual Disability and Autism Gene Curation Expert Panel on 4 August 2021. In addition, the *TAOK1* gene was associated with OMIM disease (developmental delay with or without intellectual impairment or behavioral abnormalities, MIM #619575) starting from 19 October 2021. All of these are essential for future work.

DATA AVAILABILITY STATEMENT

The datasets presented in this study can be found in online repositories. The names of the repository/repositories and accession number(s) can be found below: Genome Sequence Archive (Genomics, Proteomics, and Bioinformatics 2021) in National Genomics Data Center (Nucleic Acids Res 2021), China National Center for Bioinformation/Beijing Institute of Genomics, Chinese Academy of Sciences (GSA-Human: HRA001877) that are publicly accessible at https://ngdc.cncb.ac.cn/gsa-human.

ETHICS STATEMENT

Written informed consent was obtained from the individual(s) for the publication of any potentially identifiable images or data included in this article.

AUTHOR CONTRIBUTIONS

All authors contributed to the study conception and design. Data collection was performed by LY, CY, NS, HD, and JZ. Bioinformatic analysis was performed by YZ and HT. The entire investigation was supervised by YZ. The first draft of the manuscript was written by LY, YZ, HT, and YZ, and all authors revised the manuscript. All authors read and approved the final version.

FUNDING

This work was supported by Guangzhou Municipal Science and Technology Project (202102080358).

ACKNOWLEDGMENTS

We thank the pregnant woman and her family for sharing information.

SUPPLEMENTARY MATERIAL

The Supplementary Material for this article can be found online at: https://www.frontiersin.org/articles/10.3389/fgene.2022.836853/full#supplementary-material

REFERENCES

Acuna-Hidalgo, R., Veltman, J. A., and Hoischen, A. (2016). New Insights into the Generation and Role of De Novo Mutations in Health and Disease. *Genome Biol.* 17, 241. doi:10.1186/s13059-016-1110-1

Basel-Salmon, L., Ruhrman-Shahar, N., Orenstein, N., Goldberg, Y., Gonzaga-Jauregui, C., Shuldiner, A. R., et al. (2021). When Phenotype Does Not Match Genotype: Importance of "Real-time" Refining of Phenotypic Information for Exome Data Interpretation. *Genet. Med.* 23, 215–221. doi:10.1038/s41436-020-00938-5

Biernat, J., Wu, Y.-Z., Timm, T., Zheng-Fischhöfer, Q., Mandelkow, E., Meijer, L., et al. (2002). Protein Kinase MARK/PAR-1 Is Required for Neurite Outgrowth and Establishment of Neuronal Polarity. *Mol. Biol. Cell.* 13, 4013–4028. doi:10.1091/mbc.02-03-0046

Breuss, M., and Keays, D. A. (2014). Microtubules and Neurodevelopmental Disease: the Movers and the Makers. *Adv. Exp. Med. Biol.*, 75–96. doi:10.1007/978-94-007-7687-6_5

Cooper, G. M., Coe, B. P., Girirajan, S., Rosenfeld, J. A., Vu, T. H., Baker, C., et al. (2011). A Copy Number Variation Morbidity Map of Developmental Delay. *Nat. Genet.* 43, 838–846. doi:10.1038/ng.909

Dan, I., Watanabe, N. M., and Kusumi, A. (2001). The Ste20 Group Kinases as Regulators of MAP Kinase Cascades. *Trends Cell. Biol.* 11, 220–230. doi:10.1016/s0962-8924(01)01980-8

Deciphering Developmental Disorders Study (2017). Prevalence and Architecture of De Novo Mutations in Developmental Disorders. *Nature* 542, 433–438. doi:10.1038/nature21062

Draviam, V. M., Stegmeier, F., Nalepa, G., Sowa, M. E., Chen, J., Liang, A., et al. (2007). A Functional Genomic Screen Identifies a Role for TAO1 Kinase in Spindle-Checkpoint Signalling. *Nat. Cell. Biol.* 9, 556–564. doi:10.1038/ncb1569

Dulovic-Mahlow, M., Trinh, J., Kandaswamy, K. K., Braathen, G. J., Di Donato, N., Rahikkala, E., et al. (2019). De Novo Variants in TAOK1 Cause Neurodevelopmental Disorders. *Am. J. Hum. Genet.* 105, 213–220. doi:10.1016/j.ajhg.2019.05.005

Fang, C.-Y., Lai, T.-C., Hsiao, M., and Chang, Y.-C. (2020). The Diverse Roles of TAO Kinases in Health and Diseases. *Int. J. Mol. Sci.* 21, E7463. doi:10.3390/ijms21207463

Gao, Z., Moorjani, P., Sasani, T. A., Pedersen, B. S., Quinlan, A. R., Jorde, L. B., et al. (2019). Overlooked Roles of DNA Damage and Maternal Age in Generating Human Germline Mutations. *Proc. Natl. Acad. Sci. U. S. A.* 116, 9491–9500. doi:10.1073/pnas.1901259116

Goldmann, J. M., Veltman, J. A., and Gilissen, C. (2019). De Novo Mutations Reflect Development and Aging of the Human Germline. *Trends Genet.* 35, 828–839. doi:10.1016/j.tig.2019.08.005

Goldmann, J. M., Wong, W. S. W., Pinelli, M., Farrah, T., Bodian, D., Stittrich, A. B., et al. (2016). Parent-of-origin-specific Signatures of De Novo Mutations. *Nat. Genet.* 48, 935–939. doi:10.1038/ng.3597

Goriely, A., and Wilkie, A. O. M. (2012). Paternal Age Effect Mutations and Selfish Spermatogonial Selection: Causes and Consequences for Human Disease. *Am. J. Hum. Genet.* 90, 175–200. doi:10.1016/j.ajhg.2011.12.017

Hu, C., Feng, P., Yang, Q., and Xiao, L. (2021). Clinical and Neurobiological Aspects of TAO Kinase Family in Neurodevelopmental Disorders. *Front. Mol. Neurosci.* 14, 655037. doi:10.3389/fnmol.2021.655037

Hunter, J. M., Massingham, L. J., Manickam, K., Bartholomew, D., Williamson, R. K., Schwab, J. L., et al. (2022). Inherited and De Novo Variants Extend the Etiology of TAOK1-Associated Neurodevelopmental Disorder. *Cold Spring Harb. Mol. Case Stud.* 8, a006180. doi:10.1101/mcs.a006180

Kong, A., Frigge, M. L., Masson, G., Besenbacher, S., Sulem, P., Magnusson, G., et al. (2012). Rate of De Novo Mutations and the Importance of Father's Age to Disease Risk. *Nature* 488, 471–475. doi:10.1038/nature11396

Miller, C. J., Lou, H. J., Simpson, C., van de Kooij, B., Ha, B. H., Fisher, O. S., et al. (2019). Comprehensive Profiling of the STE20 Kinase Family Defines Features Essential for Selective Substrate Targeting and Signaling Output. *PLoS Biol.* 17, e2006540. doi:10.1371/journal.pbio.2006540

Poon, C. L. C., Mitchell, K. A., Kondo, S., Cheng, L. Y., and Harvey, K. F. (2016). The Hippo Pathway Regulates Neuroblasts and Brain Size in *Drosophila melanogaster*. *Curr. Biol.* 26, 1034–1042. doi:10.1016/j.cub.2016.02.009

Richards, S., Aziz, N., Bale, S., Bick, D., Das, S., Gastier-Foster, J., et al. (2015). Standards and Guidelines for the Interpretation of Sequence Variants: a Joint Consensus Recommendation of the American College of Medical Genetics and Genomics and the Association for Molecular Pathology. *Genet. Med.* 17, 405–424. doi:10.1038/gim.2015.30

Roy, A., Kucukural, A., and Zhang, Y. (2010). I-TASSER: a Unified Platform for Automated Protein Structure and Function Prediction. *Nat. Protoc.* 5, 725–738. doi:10.1038/nprot.2010.5

Satterstrom, F. K., Kosmicki, J. A., Wang, J., Breen, M. S., De Rubeis, S., An, J.-Y., et al. (2020). Large-Scale Exome Sequencing Study Implicates Both Developmental and Functional Changes in the Neurobiology of Autism. *Cell.* 180, 568–584. e23. doi:10.1016/j.cell.2019.12.036

Strande, N. T., Riggs, E. R., Buchanan, A. H., Ceyhan-Birsoy, O., DiStefano, M., Dwight, S. S., et al. (2017). Evaluating the Clinical Validity of Gene-Disease Associations: An Evidence-Based Framework Developed by the Clinical Genome Resource. *Am. J. Hum. Genet.* 100, 895–906. doi:10.1016/j.ajhg.2017.04.015

Taylor, J. L., Debost, J.-C. P. G., Morton, S. U., Wigdor, E. M., Heyne, H. O., Lal, D., et al. (2019). Paternal-age-related De Novo Mutations and Risk for Five Disorders. *Nat. Commun.* 10, 3043. doi:10.1038/s41467-019-11039-6

Timm, T., Matenia, D., Li, X.-Y., Griesshaber, B., and Mandelkow, E.-M. (2006). Signaling from MARK to Tau: Regulation, Cytoskeletal Crosstalk, and Pathological Phosphorylation. *Neurodegener. Dis.* 3, 207–217. doi:10.1159/000095258

van Woerden, G. M., Bos, M., de Konink, C., Distel, B., Avagliano Trezza, R., Shur, N. E., et al. (2021). TAOK1 Is Associated with Neurodevelopmental Disorder and Essential for Neuronal Maturation and Cortical Development. *Hum. Mutat.* 42, 445–459. doi:10.1002/humu.24176

Veltman, J. A., and Brunner, H. G. (2012). De Novo mutations in Human Genetic Disease. *Nat. Rev. Genet.* 13, 565–575. doi:10.1038/nrg3241

Wright, C. F., Prigmore, E., Rajan, D., Handsaker, J., McRae, J., Kaplanis, J., et al. (2019). Clinically-relevant Postzygotic Mosaicism in Parents and Children with Developmental Disorders in Trio Exome Sequencing Data. *Nat. Commun.* 10, 2985. doi:10.1038/s41467-019-11059-2

Xie, B., Fan, X., Lei, Y., Chen, R., Wang, J., Fu, C., et al. (2016). A Novel De Novo Microdeletion at 17q11.2 Adjacent to NF1 Gene Associated with Developmental Delay, Short Stature, Microcephaly and Dysmorphic Features. *Mol. Cytogenet.* 9, 41. doi:10.1186/s13039-016-0251-y

Zhang, J., Yao, Y., He, H., and Shen, J. (2020). Clinical Interpretation of Sequence Variants. *Curr. Protoc. Hum. Genet.* 106, e98. doi:10.1002/cphg.98

Conflict of Interest: YZ and HT are employed by Aegicare (Shenzhen) Technology Co., Ltd., Shenzhen, China.

The remaining authors declare that the research was conducted in the absence of any commercial or financial relationships that could be construed as a potential conflict of interest.

Publisher's Note: All claims expressed in this article are solely those of the authors and do not necessarily represent those of their affiliated organizations, or those of the publisher, the editors and the reviewers. Any product that may be evaluated in this article, or claim that may be made by its manufacturer, is not guaranteed or endorsed by the publisher.

Advantages of publishing in Frontiers

OPEN ACCESS
Articles are free to read for greatest visibility and readership

FAST PUBLICATION
Around 90 days from submission to decision

HIGH QUALITY PEER-REVIEW
Rigorous, collaborative, and constructive peer-review

TRANSPARENT PEER-REVIEW
Editors and reviewers acknowledged by name on published articles

Frontiers
Avenue du Tribunal-Fédéral 34
1005 Lausanne | Switzerland

Visit us: www.frontiersin.org
Contact us: frontiersin.org/about/contact

REPRODUCIBILITY OF RESEARCH
Support open data and methods to enhance research reproducibility

DIGITAL PUBLISHING
Articles designed for optimal readership across devices

FOLLOW US
@frontiersin

IMPACT METRICS
Advanced article metrics track visibility across digital media

EXTENSIVE PROMOTION
Marketing and promotion of impactful research

LOOP RESEARCH NETWORK
Our network increases your article's readership